



The Journal of
Gemmology

2009 / Volume 31 / Nos. 5-8



The Gemmological Association of Great Britain

27 Greville Street, London EC1N 8TN

T: +44 (0)20 7404 3334 **F:** +44 (0)20 7404 8843

E: information@gem-a.com **W:** www.gem-a.com

Registered Charity No. 1109555

Registered office: Palladium House, 1-4 Argyll Street, London W1F 7LD

President: Prof. A.H. Rankin

Vice-Presidents: N.W. Deeks, R.A. Howie, E.A. Jobbins, M.J. O'Donoghue

Honorary Fellows: R.A. Howie, K. Nassau

Honorary Life Members: H. Bank, D.J. Callaghan, T.M.J. Davidson, J.S. Harris, E.A. Jobbins, J.I. Koivula, M.J. O'Donoghue, C.M. Ou Yang, I. Thomson, V.P. Watson, C.H. Winter

Chief Executive Officer: J.M. Ogden

Council: J. Riley – Chairman, A.T. Collins, S. Collins, B. Jackson, C.J.E. Oldershaw, E. Stern, J.F. Williams

Members' Audit Committee: A.J. Allnutt, P. Dwyer-Hickey, J. Greatwood, G.M. Green, B. Jackson, J. Kalischer,

Branch Chairmen: Midlands – P. Phillips, North East – M. Houghton, North West – J. Riley, Scottish – B. Jackson, South East – V. Wetten, South West – R.M. Slater

The Journal of Gemmology

Editor: Dr R.R. Harding

Assistant Editor: M.J. O'Donoghue

Associate Editors: Dr A.J. Allnutt (Chislehurst), Dr C.E.S. Arps (Leiden), G. Bosshart (Horgen), Prof. A.T. Collins (London), J. Finlayson (Stoke on Trent), Dr J.W. Harris (Glasgow), Prof. R.A. Howie (Derbyshire), E.A. Jobbins (Caterham), Dr J.M. Ogden (London), Prof. A.H. Rankin (Kingston upon Thames), Dr K. Schmetzer (Petershausen), Dr J.E. Shigley (Carlsbad), Prof. D.C. Smith (Paris), E. Stern (London), Prof. I. Sunagawa (Tokyo), Dr M. Superchi (Milan)

Production Editor: M.A. Burland

The Editor is glad to consider original articles shedding new light on subjects of gemmological interest for publication in *The Journal of Gemmology*. A Guide to the preparation of typescripts for publication in *The Journal* is given on our website, or contact the Production Editor at the Gemmological Association of Great Britain.

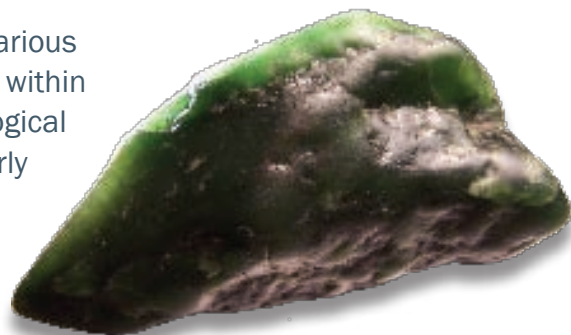
Any opinions expressed in *The Journal of Gemmology* are understood to be the views of the contributors and not necessarily of the publishers.

A signature for nephrite jade using its strontium isotopic composition: some Pacific Rim examples

Dr Christopher J. Adams and Russell J. Beck FGA

Abstract: Geochronological and radiogenic isotope studies of nephrite jade are reviewed, with particular reference to its paragenesis and as an aid to identifying and characterizing various sources around the Pacific Rim. Detailed studies of nephrites within several 'fields' in New Zealand, which fall within distinct geological terranes and within metamorphic belts of differing ages, clearly demonstrate the inheritance of nephrite strontium isotope compositions from their host rocks during metamorphism and metasomatism. The applications and interpretations developed from this approach are also shown to hold for preliminary analyses of nephrite in other localities around the Pacific Rim, in New Caledonia, Australia, Taiwan, Russia and Canada.

Keywords: jade, nephrite, Rb-Sr age, strontium isotopes



Introduction

Jade is a gemstone associated with ultramafic rocks in ophiolite complexes and occasionally in metamorphosed dolomites (Harlow and Sorensen, 2005). It is an almost monomineralic rock, occurring as a tremolite-amphibole type, nephrite (or nephrite jade) or a pyroxene-type, jadeitite (or jadeite jade). Although rare, deposits of nephrite jade are present around the world and especially in countries of the Pacific Rim (New Zealand, Australia, New Caledonia, China, Korea, Japan, Russia (Siberia), USA (Alaska and California) and Canada (British Columbia)) (Figure 1). Almost every culture in these countries prized jade for its beauty and durability, and so it was frequently traded or carried between them, and into Pacific Ocean islands where jade most probably does

not occur naturally. Not surprisingly, considerable interest exists among archaeologists and anthropologists in tracking jade artefacts from place to place and establishing their original source, using mineralogical or chemical characteristics. Unfortunately, such jade 'signatures' may not be completely distinctive, and here we discuss an alternative technique using radiogenic isotopic ratio patterns, as applied to nephrite jades from several Pacific Rim sources.

Characteristics of nephrite jade

Nephrite jade usually comprises >99% microcrystalline amphibole of the tremolite-actinolite series, with the highest quality types close to tremolite $[\text{Ca}_2(\text{Mg,Fe})_5\text{Si}_8\text{O}_{22}(\text{OH})_2]$. It is only moderately hard (6–6.5), but exceedingly tough, and this

toughness arises from the development of an interwoven 'felted' fabric of the tremolite crystals. This toughness can vary slightly with direction of the felted fabric. The lustrous shades of green provide the great beauties of jade and, together with some mesoscopic markings (mm-scale), are the most memorable characteristic.

The specialist can easily recognize distinctive features in jades from different sources around the world, for example in terms of texture, colour and inclusions, but doubts may remain that such features are not entirely diagnostic (see a range of nephrites in Figure 2). Attempts to quantify these features more have included Mossbauer spectroscopy (Wilkins *et al.*, 2003), major element composition and trace element analysis (Nichol, 2000). All these approaches encounter the same problem that the principal jade component

A signature for nephrite jade using its strontium isotopic composition: some Pacific Rim examples



Figure 1: Nephrite jade occurrences in countries around the Pacific Ocean.

is a single, common mineral type with little scope for variation.

Almost invariably, tremolite-actinolites are stable under medium-grade (greenschist facies, 350–450°C) metamorphic conditions at which nephrite jade forms; predictably their major element compositions show little variation, either within a specific locality, or between unrelated localities around the world. Minor and trace element analyses of nephrite jades are potentially more discriminatory because they tend to highlight the chemical distinctiveness of their minor (<1%) mineral impurities, e.g. chromite, spinel, garnet, sulphide, chlorite and chromium-mica (fuchsite). Chromium in particular is widely variable in jade

types, for example between ortho- and para-nephrites and jadeites (Nichol, 2000), but the trace element variability within, and amongst, several nephrite fields remains inadequately investigated. Since minor mineral components have potential for considerable variation at all scales, a purely trace element chemical ‘signature’ remains open to question.

Paragenesis of nephrite jades

Nephrite jades form by recrystallization of original rocks (protoliths) at low to moderate temperatures and pressures (extending from pumpellyite-actinolite to amphibolite facies), either during metamorphism (*in situ* as a closed system)

or by metasomatic reaction (*in situ* as an open system), or, most commonly, by a combination of both. Most nephrites form at greenschist facies (350–450°C, 5–7 kbar) by metasomatic reaction at the boundary between two components:

- (1) serpentinite, itself formed by hydrous alteration of ultramafic (e.g. dunite, harzburgite) and mafic (e.g. dolerite, gabbro) rocks, which contribute Fe, Mg and OH, and
- (2) sedimentary rocks such as greywacke, sandstone and limestone (and in some places volcanic rocks such as basalt and andesite) which essentially contribute SiO₂, Al₂O₃ and Ca (see a typical example in *Figure 3*).

A signature for nephrite jade using its strontium isotopic composition: some Pacific Rim examples

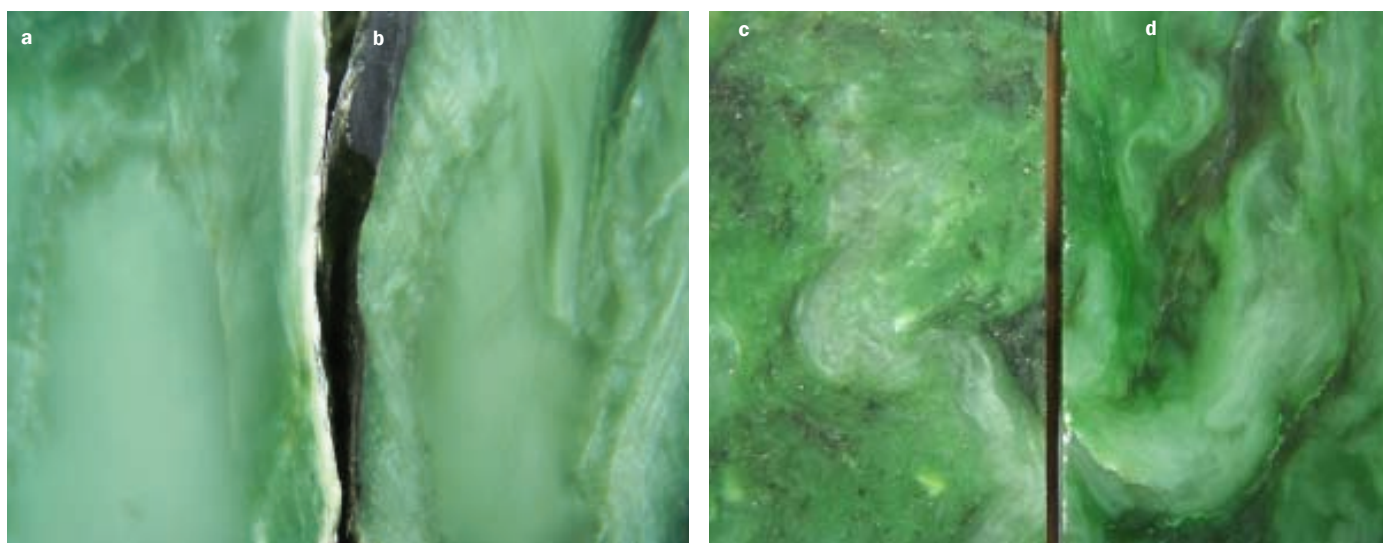


Figure 2: Nephrite jades of similar appearance from the Pacific Rim: (a) East Sayan Mountains, Siberia, Russia, (b) Olderog Creek, North Westland, New Zealand, both with particularly uniform textures; (c) South Westland, New Zealand; (d) Cassiar, British Columbia. These examples do contain microscopic inclusions which are sometimes an aid to source characterization, but they do not necessarily allow a unique distinction. Photos by R.J. Beck.

Metamorphic and metasomatic zones are readily mapped in the field and typical mineral assemblages are established across several geological periods (Coleman, 1966; Cooper and Reay, 1983). For example, in New Zealand, classic, low- to medium-grade metasedimentary successions (Permian to Cretaceous) are grouped into several tectonostratigraphic terranes of differing ancestry, some of which contain small (1–10 km scale) 'fields' of nephrite jade.

Each terrane may contain up to four main metamorphic events: Triassic, 250–240; Jurassic, 210–190; Cretaceous, 150–120; and Miocene, 10–5 Ma (Adams and Graham, 1996, 1997; Adams *et al.*, 1999; Adams and Maas, 2004).

For each terrane and metamorphic event, the ages show a gradual variation, approximately at the 100 m to km-scale, in which mineral ages are inversely related to their original metamorphic crystallization temperature (depth of burial) and the onset of their cooling in response to post-metamorphic uplift. Metamorphic ages within the nephrite fields are therefore site-specific and are to some extent predictable. This region thus provides an excellent starting-point from which to test whether the nephrite jades do properly inherit the age (and associated isotopic ancestry) of their host rocks.

Dating of nephrite jade

Widely used to determine metamorphic mineral ages, the potassium-argon (K-Ar) dating method and the related $^{40}\text{Ar}/^{39}\text{Ar}$ technique rely on the long-lived radioactive decay of isotope ^{40}K to a rare argon isotope ^{40}Ar . Whilst commonly applied to minerals with acceptable K contents $>0.5\%$, such as micas, feldspars and hornblende, for jades with K contents $<0.2\%$ the methods usually do not give

sufficiently precise ages to be useful.

The rubidium-strontium (Rb-Sr) dating method also relies on a radioactive decay with long half-life (c. 50.10^9 years), in this case ^{87}Rb to ^{87}Sr , and it can be applied to a wide range of Rb-bearing minerals (e.g. micas, feldspars) and rocks. The isotopic composition of strontium is thus variable because the minor isotope, ^{87}Sr , is radiogenic, i.e. it is formed by radioactive decay, whilst



Figure 3: Nephrite jade country in New Zealand, in the Dun Mountain-Maitai terrane, Livingstone Mountains, South Island. Serpentinite underlies the grass in the right foreground, the figure is standing on brown rubby metasediments, and there is a pale nephrite lens between the figure and rucksack. The Rb-Sr isochron samples whose data are plotted in Figure 5 were collected from this outcrop. Photo by R.J. Beck.

A signature for nephrite jade using its strontium isotopic composition: some Pacific Rim examples

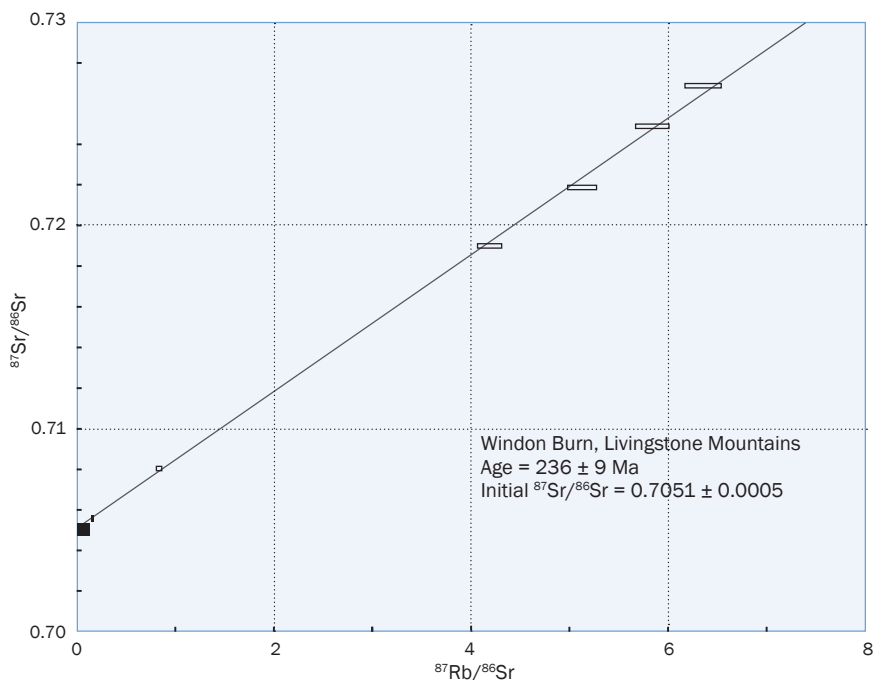


Figure 4: A Rb-Sr isochron diagram of several semi-schist samples (original protolith a graded bed of metasediments) from the outcrop pictured in Figure 3. The original rocks were size-graded sediments and their Sr isotope ratios are assumed to have been homogenized at the time of metamorphism. The analyses thus define an isochron line with slope proportional to the metamorphic age (t), and an intercept at zero $^{87}\text{Rb}/^{86}\text{Sr}$ as the initial $^{87}\text{Sr}/^{86}\text{Sr}$ ratio (i). A nephrite jade from this locality (solid square) lies very close to the initial $^{87}\text{Sr}/^{86}\text{Sr}$ ratio of 0.7051 indicated by the isochron.

its sister strontium isotopes, ^{88}Sr , ^{86}Sr and ^{84}Sr , are all stable. The abundance of ^{87}Sr will thus be higher (as a percentage of total Sr) in rocks and minerals that are old, and/or have high Rb concentrations. Since most minerals and rocks contain some Sr (and thus ^{87}Sr) at their time of formation, then both the age and initial ^{87}Sr present must be determined. This is done using an isochron method, which requires the analysis of several samples of the mineral being dated which have slightly different Rb and Sr contents, but are nonetheless assumed to be coeval and cogenetic. Upon this essential assumption, an isochron diagram (Figure 4) displays the analytical data as the isotopic ratios $^{87}\text{Rb}/^{86}\text{Sr}$ and $^{87}\text{Sr}/^{86}\text{Sr}$, whose array slope is proportional to the age (t) as Ma, and the $^{87}\text{Sr}/^{86}\text{Sr}$ intercept (i) is the initial Sr-isotopic ratio. Naturally, where there is little variation in Rb/Sr ratio of the samples, i.e. they are closely clustered on the isochron line, and/or where the Sr content is high relative to Rb, i.e. the points are close to the intercept, then the resulting age determination will be imprecise. Both possibilities commonly occur with jade analyses. However, a compensatory benefit is that the initial Sr-isotopic ratios (i) can be determined with good precision, and it is this feature, which is related to jade ancestry, that can provide a characteristic signature. This is crucially important in New Zealand, where not only the ages (t) of metamorphic rocks vary in an orderly way, but their terrane ancestry also dictates distinctive ranges of initial $^{87}\text{Sr}/^{86}\text{Sr}$ (i) values. The combined terrane (t)-(i) data for metasedimentary rocks thus occupy specific terrane data-fields (Figure 5) and it would be expected that the nephrite jades formed within them would also follow this pattern.

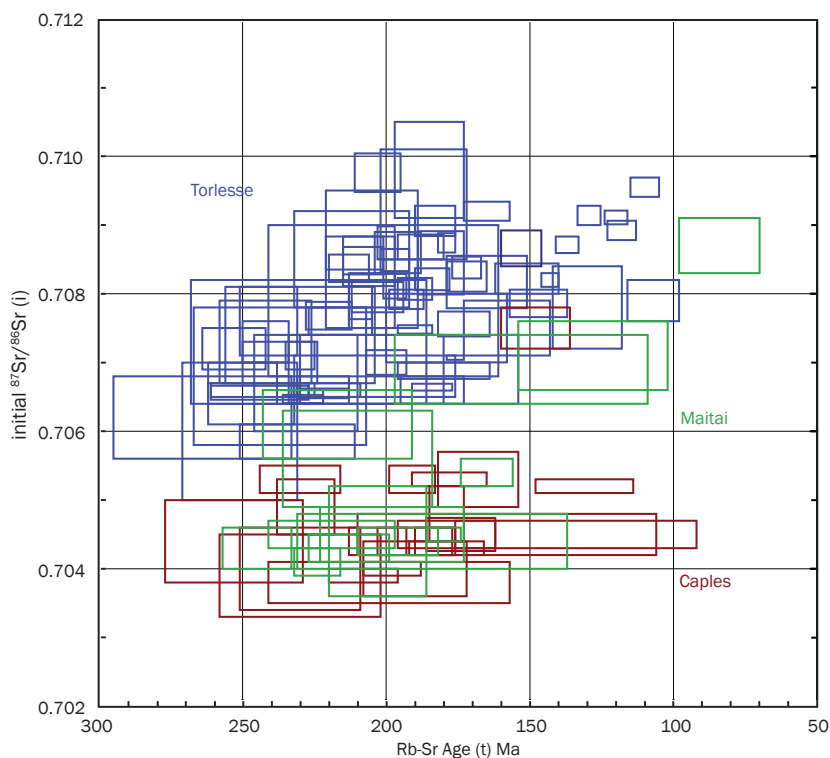


Figure 5: Rb-Sr metamorphic ages, and initial $^{87}\text{Sr}/^{86}\text{Sr}$ ratios at the time of metamorphism of metasediments from Torlesse (Rakaia) (blue line), Dun Mountain-Maitai (green line), and Caples (red line) terranes of New Zealand (data from Adams and Graham 1996, 1997; Adams et al., 1999, 2002; Adams and Maas, 2004).

Nephrite jade could inherit its Sr isotopic composition at the time of formation from either serpentinite or sedimentary rock components (see above). Component (1), serpentinite, is itself produced from protolith rocks of upper mantle origin. The Rb content of the upper mantle is low and fairly uniform, and thus its contribution of ^{87}Sr

A signature for nephrite jade using its strontium isotopic composition: some Pacific Rim examples

over time has been low. Thus the isotopic composition of Sr within the mantle throughout Earth history has always been 'primitive' and it follows only a shallow evolution curve (as expressed by the ratio $^{87}\text{Sr}/^{86}\text{Sr}$) with time. Ultramafic and mafic rocks formed in this region, commonly with elevated Sr contents, 100–1000 ppm, thus inherit similarly primitive Sr isotopic compositions. However, when emplaced into newly-formed lower oceanic crust (e.g. as ophiolite complexes), the common associated process of hydration and serpentinization leads to major loss of Ca, and greatly decreased Sr contents, to 1–10 ppm.

In contrast, the sedimentary rocks of component (2) are overwhelmingly produced by the erosion of continental crust, itself a very complex mixture of igneous (e.g. granite), metamorphic (e.g. schist) and pre-existing sedimentary (e.g. greywacke) rocks. These have widely different ages, Sr contents e.g. 20–200 ppm, and isotopic compositions. Also typically they have Rb contents 50–100 ppm, which are an order of magnitude greater than mantle rocks. For these reasons the Sr isotopic composition of the continental crust, and the sedimentary rocks derived from it, are much more variable and 'evolved', and their $^{87}\text{Sr}/^{86}\text{Sr}$ ratios are higher (more radiogenic). The difference in Sr content between serpentinite (< 1ppm) and sedimentary rock (>100 ppm) components implies that any nephrite tremolite formed in a metasomatic reaction zone would acquire Sr overwhelmingly from the latter, and in doing so largely inherit its strontium isotopic composition. This is well illustrated in data from a New Zealand locality (see Box A).

Strontium isotopes in nephrite jade

New Zealand

Rb-Sr and $^{87}\text{Sr}/^{86}\text{Sr}$ (present-day) isotopic data for New Zealand nephrite jades, summarized from the detailed study of Adams *et al.*, (2007), are listed in Table I and subdivided into the three geological

Box A. Nephrite in South Island, New Zealand

At an isolated nephrite jade locality in a serpentinite melange of the Dun Mountain-Maitai terrane at Windon Burn, Livingstone Mountains, South Island, New Zealand (Adams *et al.*, 2007), a tectonic inclusion comprises dark grey, fine metagreywacke and metasilstones which define a Rb-Sr isochron age, 236 ± 9 Ma (Middle-Late Triassic), and initial $^{87}\text{Sr}/^{86}\text{Sr}$ 0.7051 ± 0.0005 (Figure 4). These data are characteristic of Late Permian, Maitai Group metasediments nearby to the west (Adams *et al.*, 2002). The metamorphism is coeval with a narrow (0.5 m) metasomatic reaction zone at the metasediment/serpentinite boundary, where lenses of nephrite jade have formed (Figure 3). The nephrite at this locality has a present-day $^{87}\text{Sr}/^{86}\text{Sr}$ ratio 0.7057, and the initial $^{87}\text{Sr}/^{86}\text{Sr}$ ratio, calculated at 236 Ma, is 0.7056, coincident with that of the metasediments. Crucially, these data support a model for nephrite formation at a late stage. Its isotopic characteristics could not have been acquired during serpentinization, with its associated metasomatic release of Ca, and Sr of primitive Sr-isotopic composition (0.7032–0.7035), but rather *later* with the metamorphism/shearing that created the tremolite fabric.

terrannes (Dun Mountain-Maitai, Caples and Torlesse) that contain nephrite fields (Beck, 2002). The great majority of these data are from *in situ* jade occurrences, and at many (but not all) of these localities, co-existing host-rock age/isotopic data could also be obtained. However, as discussed above, several limitations frequently preclude useful Rb-Sr nephrite and host-rock age measurements, but rather, since the Rb/Sr ratios are often very low

(<0.1), the present-day $^{87}\text{Sr}/^{86}\text{Sr}$ ratios are sufficiently close to initial $^{87}\text{Sr}/^{86}\text{Sr}$ values to be calculated with good precision. In Figure 6, these data are shown in isochron diagram format, but with a logarithmic $^{87}\text{Rb}/^{86}\text{Sr}$ scale to reveal the fine-scale variation in the lower range of Rb/Sr ratios.

The nephrite data (Figure 6) clearly occupy three fields corresponding to their terrane hosts, and in those localities where independent age evidence is available

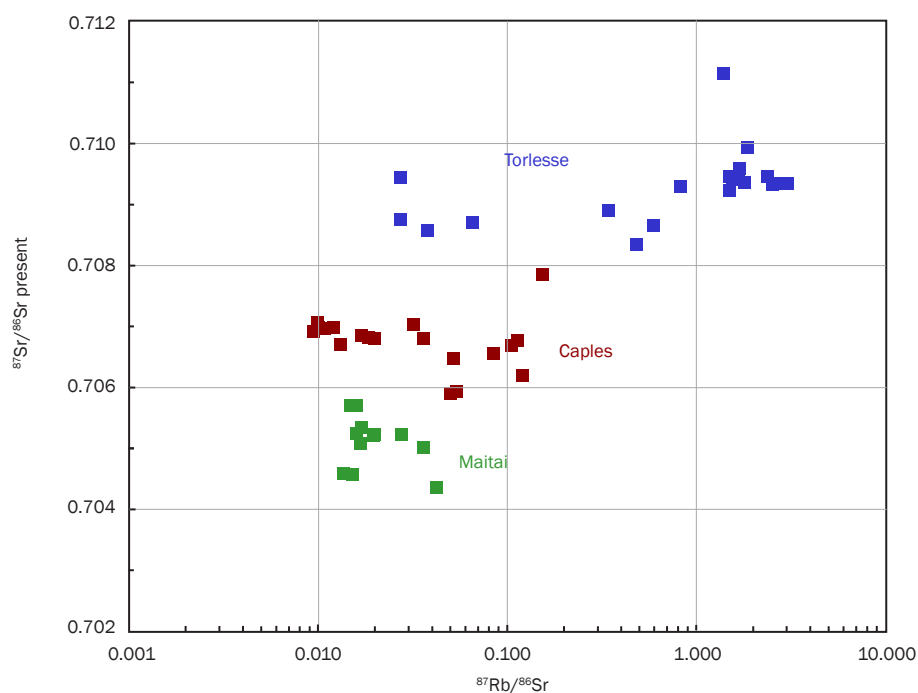


Figure 6: $^{87}\text{Rb}/^{86}\text{Sr}$ and present-day $^{87}\text{Sr}/^{86}\text{Sr}$ ratios of New Zealand nephrite jades from the Dun Mountain-Maitai, Caples and Torlesse terranes. Although the Rb/Sr ratios overlap, their $^{87}\text{Sr}/^{86}\text{Sr}$ ratios are distinct.

A signature for nephrite jade using its strontium isotopic composition: some Pacific Rim examples

Table 1: Rb-Sr isotopic data for Pacific Rim nephrite jades.

Name	Sample type	Formation or location	Rb ppm	Sr ppm	Rb/Sr	⁸⁷ Rb/ ⁸⁶ Sr	⁸⁷ Sr/ ⁸⁶ Sr	e ¹	Metamorphic Age (Ma) ^{2,3}	⁸⁷ Sr/ ⁸⁶ Sr initial	±	e ¹
NEW ZEALAND: DUN MOUNTAIN-MAITAI TERRANE												
BER1	nephrite (not <i>in situ</i>)	Livingstone volcanics?	0.8	52.8	0.015	0.042	0.704366	± 0.000033				
WB	nephrite (not <i>in situ</i>)	Winton melange	0.2	38.9	0.005	0.015	0.705703	± 0.000027	236±9	0.70565	±	0.00003
WB1	nephrite (<i>in situ</i>)	Winton melange	0.2	41.4	0.006	0.016	0.705698	± 0.000027	236±9	0.70564	±	0.00003
LH-1	nephrite (not <i>in situ</i>)	Dun Mountain ophiolite	0.3	23.1	0.013	0.036	0.705017	± 0.000050	236±9	0.70490	±	0.00005
LH-2	nephrite (not <i>in situ</i>)	Dun Mountain ophiolite	0.3	26.0	0.010	0.028	0.705239	± 0.000028	236±9	0.70515	±	0.00003
LV1	nephrite (not <i>in situ</i>)	Winton melange	0.1	18.7	0.006	0.016	0.705240	± 0.000029	236±9	0.70519	±	0.00003
LV2	(multiple analyses, 10×10 mm slice)		0.2	26.3	0.007	0.020	0.705220	± 0.000024	236±9	0.70515	±	0.00002
LV3			0.2	30.5	0.006	0.017	0.705090	± 0.000026	236±9	0.70503	±	0.00003
LV4		(LV1-5)		0.1	22.2	0.006	0.017	0.705340	± 0.000029	236±9	0.70528	±
LV5			0.1	20.7	0.007	0.020	0.705230	± 0.000028	236±9	0.70516	±	0.00003
NEW ZEALAND: CAPLES TERRANE												
ARC-1	nephrite (<i>in situ</i>)	Alpine schist	1.1	31.3	0.036	0.104	0.706689	± 0.000031				
SW-1	nephrite (not <i>in situ</i>)	not known	0.5	12.8	0.039	0.113	0.706765	± 0.000032				
O-1	nephrite (not <i>in situ</i>)	Greenstone melange	0.1	36.3	0.003	0.010	0.707050	± 0.000031	170±18	0.70703	±	0.00003
O-2	(multiple analyses, 10×10 mm slice)		0.1	26.2	0.003	0.009	0.706920	± 0.000034	170±18	0.70690	±	0.00003
O-3			0.1	33.6	0.003	0.010	0.706990	± 0.000032	170±18	0.70697	±	0.00003
O-4		(O1-5)		0.1	35.1	0.004	0.012	0.706990	± 0.000020	170±18	0.70696	±
O-5			0.1	34.6	0.004	0.011	0.706970	± 0.000034	170±18	0.70694	±	0.00003
R1	nephrite (not <i>in situ</i>)	Greenstone melange	0.2	27.9	0.006	0.017	0.706850	± 0.000029	168±11	0.70681	±	0.00003
R2	(multiple analyses, 10×10 mm slice)		0.2	28.3	0.006	0.018	0.706820	± 0.000032	168±11	0.70678	±	0.00003
R3			0.3	28.1	0.011	0.032	0.707030	± 0.000035	168±11	0.70695	±	0.00004
R4		(R1-5)		0.1	32.2	0.005	0.013	0.706690	± 0.000026	168±11	0.70666	±
R5			0.2	30.9	0.007	0.020	0.706800	± 0.000032	168±11	0.70675	±	0.00003
RB	nephrite (not <i>in situ</i>)	Greenstone melange	0.4	34.4	0.013	0.036	0.706807	± 0.000034	168±11	0.70672	±	0.00004
SB	nephrite (not <i>in situ</i>)	Greenstone melange	0.7	22.1	0.029	0.085	0.706550	± 0.000030	168±11	0.70635	±	0.00004
SC5	nephrite (<i>in situ</i>)		0.3	17.3	0.017	0.050	0.705908	± 0.000035	168±11	0.70579	±	0.00004
SC7	nephrite (<i>in situ</i>)		0.5	8.7	0.053	0.153	0.707857	± 0.000032	168±11	0.70749	±	0.00005
BB1	nephrite (<i>in situ</i>)		0.1	6.1	0.016	0.047	0.706116	± 0.000040	150±10	0.70600	±	0.00004
BB2	nephrite (<i>in situ</i>)	Patuki melange	0.1	7.5	0.019	0.054	0.705925	± 0.000100	150±10	0.70579	±	0.00010
EB-1	semi-nephrite ⁴ (<i>in situ</i>)	Croisilles melange	0.1	25.6	0.005	0.014	0.704576	± 0.000038	206±10	0.70453	±	0.00004
EB	semi-nephrite ⁴ (<i>in situ</i>)		0.1	22.9	0.005	0.015	0.704561	± 0.000029	206±10	0.70451	±	0.00003
OB-1	semi-nephrite ⁴ (<i>in situ</i>)	Croisilles melange	0.7	17.3	0.042	0.121	0.706196	± 0.000034	206±10	0.70575	±	0.00040
WR-1	semi-nephrite ⁴ (<i>in situ</i>)	Patuki melange	0.5	28.0	0.018	0.052	0.706468	± 0.000032	160±2	0.70635	±	0.00003
NEW ZEALAND: TORLESSE TERRANE												
J1	nephrite (not <i>in situ</i>)	Pounamu ultramafics	4.0	4.6	0.870	2.518	0.709330	± 0.000029	5.9±6.1	0.70960	±	0.00020
J2	(multiple analyses, 10×10 mm slice)		3.3	4.0	0.822	2.379	0.709460	± 0.000024	5.9±6.1	0.70960	±	0.00020
J3			2.0	3.9	0.519	1.502	0.709450	± 0.000030	5.9±6.1	0.70960	±	0.00020
J4	(J1-5)		4.5	4.3	1.042	3.014	0.709340	± 0.000037	5.9±6.1	0.70960	±	0.00020
J5			5.0	5.4	0.933	2.700	0.709340	± 0.000026	5.9±6.1	0.70960	±	0.00020

A signature for nephrite jade using its strontium isotopic composition: some Pacific Rim examples

Name	Sample type	Formation or location	Rb ppm	Sr ppm	Rb/Sr	⁸⁷ Rb/ ⁸⁶ Sr	⁸⁷ Sr/ ⁸⁶ Sr	e ¹	Metamorphic Age (Ma) ^{2,3}	⁸⁷ Sr/ ⁸⁶ Sr initial	±	e ¹
NEW ZEALAND: TORLESSE TERRANE (continued)												
A1	nephrite (<i>in situ</i>)	Pounamu ultramafics	2.8	4.8	0.581	1.681	0.709420	± 0.000029	5.9±6.1	0.70928	±	0.00014
A2	(multiple analyses, 10×10 mm slice)		3.0	4.7	0.628	1.818	0.709360	± 0.000030	5.9±6.1	0.70921	±	0.00016
A3			3.2	4.9	0.645	1.868	0.709930	± 0.000070	5.9±6.1	0.70977	±	0.00017
A4	(A1-5)		2.7	4.6	0.587	1.698	0.709580	± 0.000028	5.9±6.1	0.70944	±	0.00015
A5			2.7	5.0	0.536	1.550	0.709410	± 0.000033	5.9±6.1	0.70928	±	0.00014
JC-1A	nephrite (not <i>in situ</i>)	Pounamu ultramafics	2.9	5.5	0.516	1.494	0.709220	± 0.000037	5.9±6.1	0.70910	±	0.00014
JC-1	nephrite (not <i>in situ</i>)	Pounamu ultramafics	2.6	5.3	0.481	1.392	0.711156	± 0.000039	5.9±6.1	0.71104	±	0.00013
JC-2	nephrite (not <i>in situ</i>)	Pounamu ultramafics	2.0	7.1	0.284	0.823	0.709297	± 0.000042	5.9±6.1	0.70923	±	0.00008
CR1	semi-nephrite (<i>in situ</i>)		0.2	1.4	0.119	0.343	0.708896	± 0.000063	25±1	0.70877	±	0.00006
MC-1	nephrite (<i>in situ</i>)	Alpine schist	0.2	20.1	0.009	0.027	0.709450	± 0.000040	130±1	0.70856	±	0.00004
MC-2	nephrite (<i>in situ</i>)	Alpine schist	0.3	27.6	0.009	0.027	0.708764	± 0.000032				
J33214C	semi-nephrite ⁴ (not <i>in situ</i>)	Diedrich Ck site B5	0.28	12.40	0.023	0.065	0.708700	± 0.000110				
J33211C	semi-nephrite ⁴ (not <i>in situ</i>)	Kokatahi R, site A4	2.26	11.03	0.205	0.593	0.708648	± 0.000037				
J33216C	semi-nephrite ⁴ (not <i>in situ</i>)	Toaroha R site A3	0.18	13.76	0.013	0.038	0.708575	± 0.000035				
J33217C	semi-nephrite ⁴ (not <i>in situ</i>)	Toaroha R site A3	2.77	16.59	0.167	0.483	0.708336	± 0.000038				
NEW CALEDONIA												
TIKX1	nephrite	Tiwaka River	0.11	13.90	0.008	0.023	0.704334	± 0.000029				
TIWX3	nephrite	Tiwaka River	0.10	15.36	0.007	0.019	0.704460	± 0.000028				
TIWX5	nephrite	Tiwaka River	0.25	67.50	0.004	0.011	0.705297	± 0.000028				
NCP	nephrite	Pombe	0.09	76.79	0.001	0.003	0.704864	± 0.000034				
IDO1	ouenite ⁵	Île d'Ouen	0.27	138.40	0.002	0.006	0.705091	± 0.000044				
IDO2	ouenite ⁵	Île d'Ouen	0.10	22.41	0.004	0.013	0.704530	± 0.000030				
IDO3	ouenite ⁵	Île d'Ouen	0.17	79.89	0.002	0.006	0.704697	± 0.000030				
IDO5D	ouenite ⁵	Île d'Ouen	0.28	165.50	0.002	0.005	0.705732	± 0.000027				
IDO5L	ouenite ⁵	Île d'Ouen	0.14	214.90	0.001	0.002	0.705851	± 0.000029				
COWELL, SOUTH AUSTRALIA												
COW1	nephrite	Cowell	0.69	5.43	0.127	0.368	0.720347	± 0.000031				
COW10	nephrite	Cowell	6.63	5.03	1.318	3.833	0.760777	± 0.000045				
COW20	nephrite	Cowell	2.97	7.71	0.385	1.117	0.728423	± 0.000036				
COW30	nephrite	Cowell	1.35	19.10	0.071	0.205	0.718314	± 0.000031				
CA	nephrite	Cowell	2.40	7.45	0.322	0.934	0.734300	± 0.000033				
BRITISH COLUMBIA, CANADA												
BCC	nephrite	Cassiar	0.22	4.32	0.051	0.147	0.711785	± 0.000042				
TAIWAN												
TH	nephrite	Hualien mine	0.28	3.57	0.078	0.227	0.712853	± 0.000040				
SIBERIA, RUSSIA												
VR	nephrite	Vitim mine	0.50	4.11	0.122	0.352	0.711390	± 0.000031				
SR	nephrite	Sayan mts.	7.06	15.34	0.460	1.332	0.712467	± 0.000036				

NOTES

1. e: 1 standard error
2. Ages in normal type are measured at locality; those in italics are assumed ages from nearby localities
3. Decay constants: Steiger and Jäger (1977)
4. Semi-nephrite is a term used for a tremolite rock in which the felted fabric is only imperfectly developed; it is not as tough as true nephrite.
5. Ouenite is an informal name for a plagioclase-tremolite rock from Île d'Ouen, New Caledonia, locally termed 'jade', and will be described in a forthcoming paper by Beck and Grapes.

A signature for nephrite jade using its strontium isotopic composition: some Pacific Rim examples

(see Adams *et al.*, 2007) to calculate the nephrite initial Sr-isotopic composition, then these fall within the data range of their host-rock terranes as shown in Figure 5.

The Torlesse terrane nephrites have the highest and greatest range of Rb/Sr ratios, a feature of the Torlesse terrane host-rock schists also. They principally form within a metamorphic zone (Alpine Schist) at 5–10 Ma, much younger than their other terrane counterparts, so that the radiogenic strontium corrections required for Sr-initial ratio determination are trivial. The high present-day $^{87}\text{Sr}/^{86}\text{Sr}$ ratios, 0.708–0.711 (Figure 6) of the Torlesse terrane nephrites are thus mainly a consequence of the high initial $^{87}\text{Sr}/^{86}\text{Sr}$ ratios (at time of metamorphism), 0.706–0.710, of their Torlesse Group metasediment host-rocks (Figure 5).

Similarly, present-day $^{87}\text{Sr}/^{86}\text{Sr}$ ratios, 0.704–0.706, for Dun Mountain-Maitai terrane nephrites (Figure 6) fall within the initial $^{87}\text{Sr}/^{86}\text{Sr}$ range for Maitai Group metasediments (Figure 5). In this case,

although the metamorphic ages of the nephrites are much older, *c.* 220–250 Ma, the Rb/Sr ratios, and their range, are 1–2 orders of magnitude lower, and thus the radiogenic isotope correction to calculate the initial $^{87}\text{Sr}/^{86}\text{Sr}$ ratios (at time of metamorphism) remains minimal.

The Caples terrane nephrite present-day $^{87}\text{Sr}/^{86}\text{Sr}$ data (*c.* 0.706–0.707) occupy an intermediate position, between those of Dun Mountain-Maitai and Caples terranes (Figure 6). Here, the metamorphic ages of most of the host Caples Group metasediments are in the range 140–180 Ma and, with $^{87}\text{Rb}/^{86}\text{Sr}$ ratios considerably higher than Dun Mountain-Maitai terrane examples, the calculated nephrite initial $^{87}\text{Sr}/^{86}\text{Sr}$ ratios are *c.* 0.705–0.706. These are significantly lower than present-day values, but just coinciding with uppermost values from the host rocks, *c.* 0.7055 (Figure 5).

Pacific Rim nephrite jades

Preliminary studies have been made of nephrite jades from other countries

around the Pacific Ocean (New Caledonia, Australia, Taiwan, Russia and Canada), and Rb-Sr and Sr-isotopic data are listed in Table I.

All sample collection, processing, analytical and data processing procedures were identical to those described by Adams *et al.*, (2007).

These nephrite jade localities (Figure 1) generally lie within Palaeozoic-Mesozoic mobile belts of the Pacific Rim, but the Australian dataset includes an unusual cratonic, Precambrian, nephrite jade deposit at Cowell, South Australia. Some of these nephrite occurrences are not *in situ*, and hence the original age of both serpentinite and sedimentary host-rock components, and their metamorphic ages, are uncertain. The $^{87}\text{Rb}/^{86}\text{Sr}$ and present-day $^{87}\text{Sr}/^{86}\text{Sr}$ isotopic data are shown in Figure 7, in the same format as the New Zealand data of Figure 6.

New Caledonia

Most nephrite jade deposits in New Caledonia are concentrated in the central, axial mountain ranges, in the Tiwaka River watershed and adjacent rivers that flow east to the Pacific Ocean. The area is dominated by low- to medium-grade metasediments (Central terrane, Triassic-Jurassic), with more local Permian ophiolites with serpentinite complexes (Koh terrane).

At two localities, crucial outcrops show the typical metasomatic reaction zone between serpentinite and fine metagreywackes, with small, 0.2 m lenses of nephrite jade within this zone. A Rb-Sr isochron of the host-rock metasediments yields a very imprecise age of 87 ± 130 Ma, but the initial $^{87}\text{Sr}/^{86}\text{Sr}$ ratio of 0.7049 ± 0.0006 , is concordant with those of nephrites at this locality, 0.7043–0.7051. With Rb/Sr ratios in a slightly lower range of 0.005–0.05, New Caledonia nephrite data lie adjacent to, but slightly overlap, the least radiogenic nephrites from the Dun Mountain-Maitai terrane of New Zealand (Figure 7).

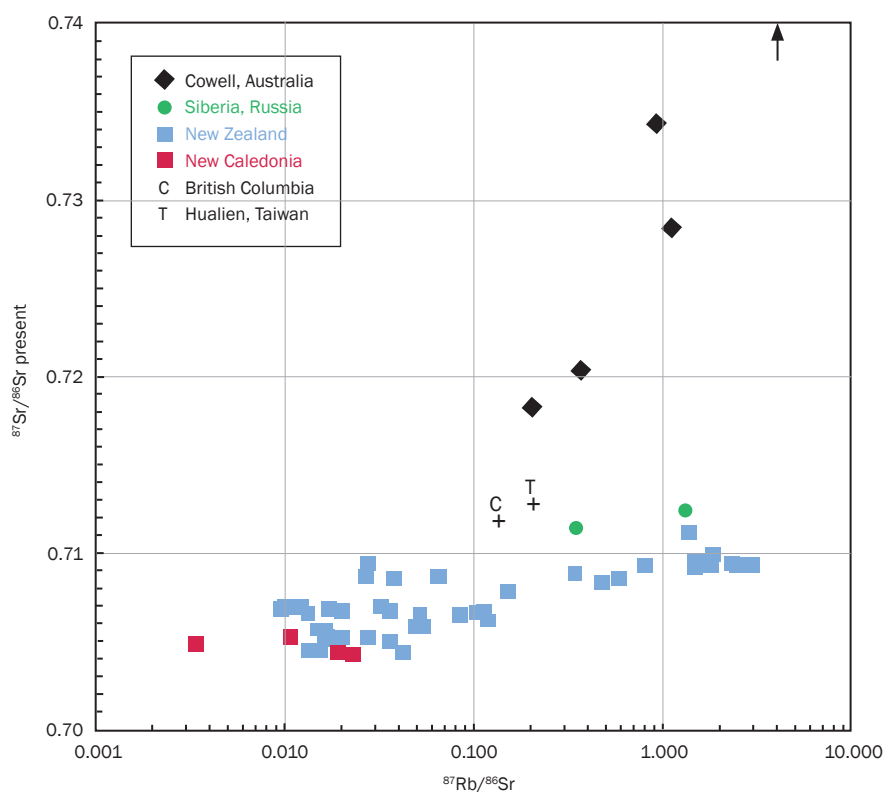


Figure 7: $^{87}\text{Rb}/^{86}\text{Sr}$ and present-day $^{87}\text{Sr}/^{86}\text{Sr}$ ratios of nephrite jades from the Pacific rim. Arrow indicates the position at the $^{87}\text{Rb}/^{86}\text{Sr}$ axis of a Cowell sample analysis that falls above the limit of the diagram. Symbol sizes are larger than the data-point error boxes at 95% confidence limits.

A signature for nephrite jade using its strontium isotopic composition: some Pacific Rim examples

Cowell, South Australia

Nephrite jade occurs west of Cowell, South Australia, in an amphibolite facies metamorphic complex (Cleve Metamorphics) of late Palaeoproterozoic age, *c.* 1600–1700 Ma. A dark green-black jade forms massive (m-scale) lenses in metasomatic reaction zones between granite-gneisses and horizons of metasediment, metavolcanics, talc-schist, dolomitic marble and serpentine marble (Nichol, 1974, 1977). The nephrite jades (Table 1, Figure 7) have distinctive, high present-day $^{87}\text{Sr}/^{86}\text{Sr}$ ratios of 0.720–0.760, presumably reflecting their Precambrian ancestry. Although the several samples come from four separate outcrops, the general slope of the Cowell data array (Figure 7) reflects an Rb-Sr isochron metamorphic age of *c.* 800 Ma (Neoproterozoic), much younger than elsewhere in the Cleve metamorphic complex, but still with distinctively high initial $^{87}\text{Sr}/^{86}\text{Sr}$ ratios of 0.715–0.720.

Taiwan

Nephrite jade is well known in Taiwan; it is found as boulders in several rivers on the east coast of the island, and formerly was mined in the Fengtien area, near the city of Hualien. The Fengtien *in situ* deposits lie within a 3 x 10 km area, where massive jade lenses (m-scale) and diopside-rock intervene between greenschist facies, graphitic mica-schists (Tananao Schist) and serpentinite, which together form part of a late Palaeozoic-Mesozoic basement metamorphic complex (Li-Ping Tan *et al.*, 1978). In Figure 7 the isotopic data for a Fengtien nephrite jade fall between the Cowell and New Zealand data, and the high present-day $^{87}\text{Sr}/^{86}\text{Sr}$ ratio, 0.7128, suggests that the radiogenic strontium contribution to this nephrite would originate from relatively old host-rock metasediments. Unfortunately, their age is not known and an initial $^{87}\text{Sr}/^{86}\text{Sr}$ ratio cannot yet be calculated.

British Columbia, Canada

Numerous nephrite deposits occur along a NW–SE trending belt, 50 km wide, through central British Columbia

(Leaming, 1978). All are associated with late Palaeozoic/early Mesozoic ophiolite complexes, and are concentrated in southern (Lillooet), central (Omineca) and northern (Cassiar) fields. Much of the nephrite is recovered from river and glacial deposits, but *in situ* deposits exist within the Late Devonian to Early Carboniferous Cache Creek Group (ophiolites, chert, argillite and volcanics), at Dease Lake and Cassiar. In Figure 7, a single nephrite analysis from Cassiar appears similar to that of nephrite from Taiwan, and their ages and calculated initial $^{87}\text{Sr}/^{86}\text{Sr}$ ratios are also similar.

Siberia, Russia

Two important nephrite jade fields occur in Siberia. In the Vitim River area nephrite forms at contacts of early Palaeozoic leucocratic granitoids with dolomitic marbles to form distinctive greenish-white jade (Sekerin and Sekerina, 1986a, 1986b; Sekerina, 1992; Sutorin and Zamaletdinov, 1984). In the East Sayan mountains, there is a major nephrite deposit in Late Proterozoic (or possibly Cambrian) ultramafic complexes of the Ospinsk-Kitoy massif. The nephrite lies within metasomatic reaction zones between serpentinite and albitized gabbro and/or albitites (Kolensik, 1970; Prokhor 1991).

Again, the present-day Sr-isotopic ratios of the Siberian nephrites, 0.7113–0.7125 (Figure 7), are similar to those in the nephrites from Taiwan and Canada, but the latter have significantly higher Rb/Sr ratios. Since the host-rocks in this region are probably early Palaeozoic or older, their contents of radiogenic strontium would be significant, and any calculated initial $^{87}\text{Sr}/^{86}\text{Sr}$ ratios substantially lower than these present-day values.

Conclusions

The New Zealand nephrite jade results (Figure 6) clearly show a strong association with the age and isotopic history of their host-rocks. The initial Sr-isotope signatures of each South Island jade field are diagnostic of its terrane and distinctive at least on a 1–10 km scale. At

this level, they thus provide a trustworthy characteristic for identification of nephrite jade sources.

Our preliminary data for other jade provinces around the Pacific Rim appear equally distinctive (Figure 7), with only slight overlap with the New Zealand datafields. Although all the samples are from (or very close to) *in situ* jade occurrences, in many localities the precise relationship to, and age of, the host rocks are unknown or ambiguous, and therefore the initial Sr-isotopic ratios cannot be calculated with precision. Work is now underway to obtain high-quality Rb-Sr isochron age data from host-rock horizons immediately adjacent to the Tiwaka (New Caledonia), Tamworth and Cowell (Australia), and Hualien (Taiwan) jade deposits to improve these Sr-isotope signatures, and to define real Sr-isotope datafields with accuracies similar to those of New Zealand. However, it is clear even from our preliminary New Caledonia nephrite data that the low Rb/Sr and initial $^{87}\text{Sr}/^{86}\text{Sr}$ ratios reflect the relatively young age (possible Late Jurassic) and juvenile sediment material (active volcanic arc) of their host-rocks. In contrast, the much older (Precambrian) and evolved ('continental') host-rocks at Cowell, South Australia, bequeath their distinctively higher radiogenic $^{87}\text{Sr}/^{86}\text{Sr}$ ratios on nephrite jade from this locality.

Acknowledgements

We thank our Ngai Tahu, Mawhera Incorporation and GNS colleagues (especially Simon Cox) in New Zealand, Pierre Maurizot and Christophe Sand (New Caledonia), Robin Offler and Mark Sekerin (Australia), and Tzen-Fu Yui (Taiwan), for sharing their local jade expertise with us. CJA also much appreciates the technical advice and practical assistance of Roland Maas and Graeme Luther at the VIEPS Radiogenic Isotope laboratory, La Trobe University, Melbourne. Simon Cox is also thanked for a preliminary review of this manuscript.

A signature for nephrite jade using its strontium isotopic composition: some Pacific Rim examples

References

- Adams, C.J., and Graham, I.J., 1996. Metamorphic and tectonic geochronology of the Torlesse terrane, Wellington, New Zealand. *New Zealand Journal of Geology and Geophysics*, **39**, 157-80
- Adams, C.J., and Graham, I.J., 1997. Age of metamorphism of Otago Schist in eastern Otago and determination of protoliths from initial strontium isotope characteristics. *New Zealand Journal of Geology and Geophysics*, **40**, 275-86
- Adams, C.J., and Maas, R., 2004. Rb-Sr age and strontium isotopic characterisation of the Torlesse Supergroup in Canterbury, New Zealand, and implications for the status of the Rakaia terrane. *New Zealand Journal of Geology and Geophysics*, **47**, 201-18
- Adams, C.J., Graham, I.J., and Johnston, M.R., 1999. Age and isotopic characterisation of geological terranes in Marlborough Schist, Nelson/Marlborough, New Zealand. *New Zealand Journal of Geology and Geophysics*, **42**, 33-55
- Adams, C.J., Barley, M.E., Maas, R., and Doyle, M.G., 2002. Provenance of Permian-Triassic volcanoclastic sedimentary terranes in New Zealand: evidence from their radiogenic isotope characteristics and detrital mineral age patterns. *New Zealand Journal of Geology and Geophysics*, **45**, 221-42
- Adams, C.J., Beck, R.J., and Campbell, H.J., 2007. Characterisation and origin of New Zealand nephrite jade using its strontium isotopic signature. *Lithos*, **97**, 307-22
- Beck, R.J. (with Mason, M.), 2002. *Mana Pounamu - New Zealand Jade*. Reed, Auckland, 184 pp
- Coleman, R.G., 1966. New serpentinites and associated metasomatic rocks. *New Zealand Geological Survey Bulletin*, **76**, 1-102
- Cooper, A.F., and Reay, A., 1983. Lithology, field relations, and structure of the Pounamu Ultramafics from the Whitcombe and Hokitika Rivers, Westland, New Zealand. *New Zealand Journal of Geology and Geophysics*, **26**, 359-79
- Harlow, G.E., and Sorensen, S.S., 2005. Jade (Nephrite and Jadeitite) and serpentinite:metasomatic connections. *International Geology Review*, **47**, 113-46
- Kolensik, Y.N., 1970. Nephrites of Siberia. *International Geology Review*, **12**, 1-107
- Leaming, S.F., 1978. Jade in Canada. Geological Survey of Canada Paper, **78/19**
- Li-Ping Tan, Chihming Wang Lee, Chi-Chieu Chen, Pei-Lin Tien, Po-Chuan Tsui and Tzen-Fu Yui, 1978. A mineralogical study of the Fengtien nephrite deposits of Hualien, Taiwan. *National Science Council (Taiwan) Special Publication*, **1**, 1-81
- Nichol, D., 1974. Nephrite jade deposits near Cowell, South Australia. *Geological Survey Environment and Resource Division, Department of Mines, South Australia Report*, **74/201**
- Nichol, D., 1977. Nephrite jade deposits near Cowell. *Mineral Resources Review South Australia*, **141**, 11-26
- Nichol, D., 2000. Two contrasting nephrite jade types. *Journal of Gemmology*, **27**(4), 193-200
- Prokhor, S.A., 1991. The genesis of nephrite and emplacement of the nephrite-bearing ultramafic complexes of East Sayan. *International Geology Review*, **33**, 290-300
- Sekerin, A.P., and Sekerina, N.V., 1986a. Genesis of leucocratic nephrites of the central Vitim Highlands. *Doklady Akademii Nauk SSSR*, **284**, 103-5
- Sekerin, A.P., and Sekerina, N.V., 1986b. Petrology of granites in deposits of light-coloured nephrite in the central Vitim Highland country. *Geologiya i Geofisika*, **27**, 36-43
- Sekerina, N.V., 1992. Main regularities of nephrite formation. *Russian Geology and Geophysics*, **33**, 31-6
- Steiger R.H., and Jäger, E., 1977. Subcommittee on Geochronology: Convention on the use of decay constants in geo- and cosmochronology. *Earth and Planetary Science Letters*, **36**, 359-62
- Suturin, A.N., and Zamaletdinov, R.S., 1984. [Nephrites.] Nauka, Novosibirsk (in Russian)
- Wilkins, C.J., Craighead Tennant, W., Williamson, B.E., and McCammon, C.A., 2003. Spectroscopic and related evidence on the colouring and constitution of New Zealand jade. *American Mineralogist*, **88**(8/9), 1336-44

The Authors

Dr Christopher J. Adams

GNS Science, P.O. Box 30368, Lower Hutt, New Zealand

email: argon@gns.cri.nz

Russell J. Beck FGA

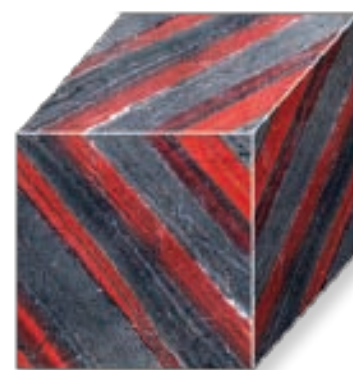
27 Chelmsford Street, Invercargill, New Zealand

email: bex@southnet.co.nz

Jaspilite — the gemstone of Ukraine

P. Baranov, S. Shevchenko, W. Heflik, L. Natkaniec-Nowak and M. Dumańska-Słowik

Abstract: The Ukrainian jaspilites, occurring within Proterozoic sediments of the Krivoy Rog Basin, are an important raw material used in the national metallurgical industry. Some exhibit significant diversity of texture and colour and are suitable as decorative rocks. In a few, the reflective optical effects described as ‘tiger’s-eye’ and ‘falcon’s-eye’ are present. Quartz and iron-ore minerals (hematite, magnetite, goethite) are the main rock-forming minerals of the jaspilites, and carbonates (siderite, ankerite), amphiboles (cummingtonite, grünerite), feldspars and apatite are subordinate phases. In Ukraine, the decorative types of jaspilite are valuable for making fancy goods such as vases and clocks, artistic jewellery, and for the production of facing stone used especially for indoor design.



Keywords: jaspilite, shaping, texture, Ukrainian

Introduction

Jaspilites are iron- and silica-rich metamorphic rocks of volcanic or sedimentary origin, and only occur rarely in nature. Worldwide they appear within Precambrian complexes such as that in the Hamersley Basin in the northwest of Western Australia, Jasper Hill, Marquette Iron Range, Michigan, and Diamond Hill, Chittenden Co., Vermont, in the U.S.A., and the Krivoy Rog Basin, Dnepropetrovsk region, in Ukraine (Trendall, 1975; Morris, 1980; Baranov, 2006; www.mindat.org/min-26407.htm).

Ukrainian jaspilites are an important strategic raw material for the metallurgical industry in Krivoy Rog, Zaporozhe and Komsomolsk (see Dumanska-Słowik *et al.*, 2007). Also many decorative types can be distinguished among these rocks, so some can be used in slab form as facing stones on buildings, while others are fine enough for jewellery (Heflik *et al.*, 2008). The industrial classification of various jaspilite types was presented by

Baranov (2006), and the Gemmological Centre of the National Mining University in Dnepropetrovsk (Ukraine) has promoted jaspilite as the prospective gemstone of Ukraine for some years. The aim of the latter is to show the natural beauty of these stones and their potential use in various contexts. However, the scope of this promotion has been limited since the majority of papers have been published in Ukrainian and Russian (e.g. Baranov, 2002, 2006; Baranov *et al.*, 2006; Heflik *et al.*, 2008).

Geological setting

Of 48 iron ore deposits in Ukraine, only 25 are currently being exploited. The Krivoy Rog iron-ore Basin is the main mining centre and its main geological features are shown in *Figure 1*. It is ca. 100 km long by 2–7 km wide and is elongate south–north. The Krivoy Rog Basin is situated between two large crustal blocks of different age: the Ingulsy block built of Lower Proterozoic

granitoids and metamorphic rocks, and the Srednepridneprovsky block containing Archaean plagiogranites.

The Krivoy Rog Structure contains complexes from both these blocks which have been subjected to extensive and strong folding and faulting. The jaspilites occur within the Proterozoic sedimentary and volcanic rocks (2.5–1.8 Ga) which have been metamorphosed at greenschist and amphibolite facies conditions. The thicknesses of Fe-bearing rocks range from 0.3 to 3.5 km.

Decorative jaspilite varieties

Ukrainian jaspilites exhibit a wide range of textures and colours, mainly red with different tints from bright red to deep-brown, yellow, orange and blue, and some are grey with a metallic lustre. Based on colour, six categories have been distinguished:

- red-banded,
- orange-banded,
- yellow-banded,

Jaspilite — the gemstone of Ukraine

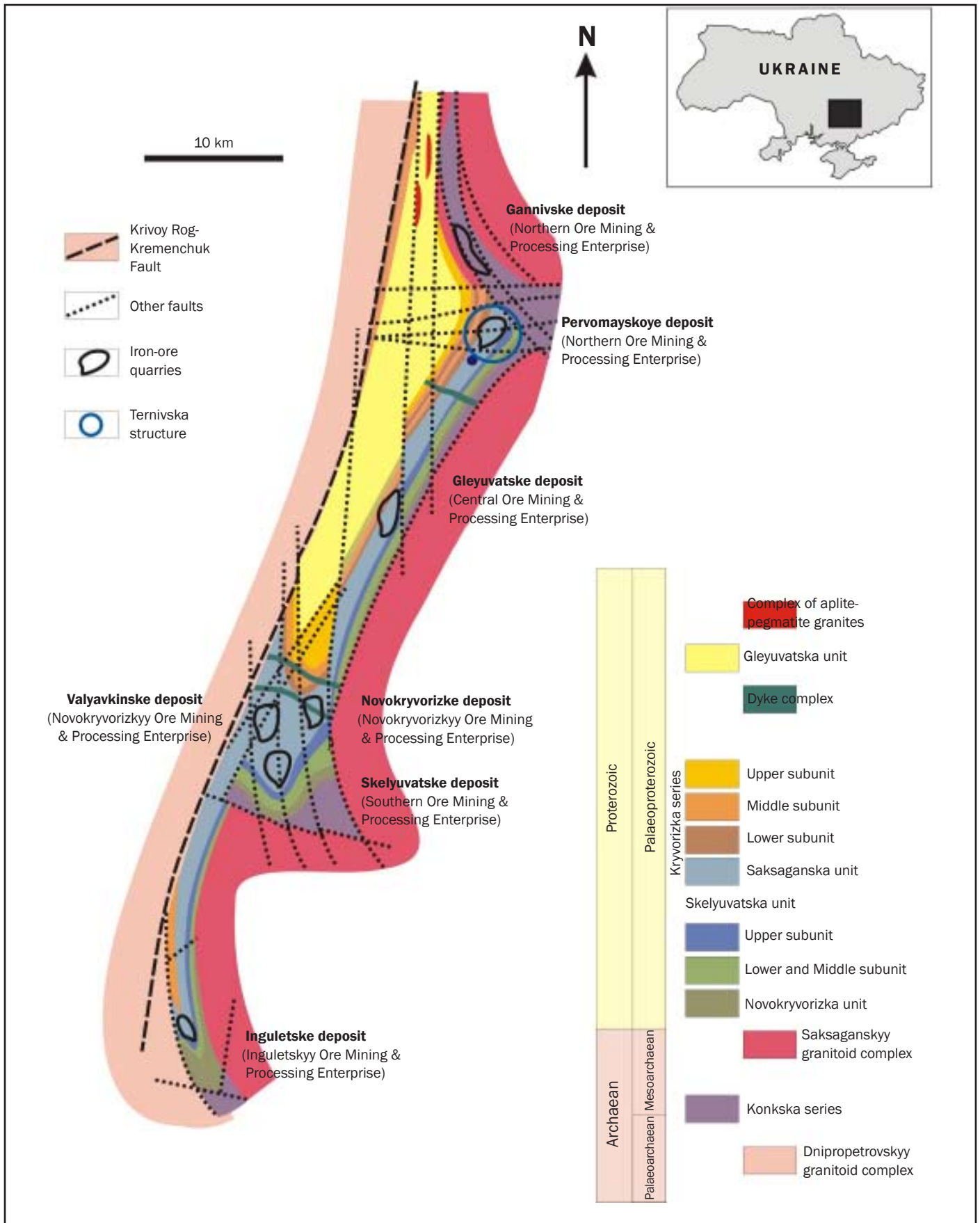


Figure 1: Schematic geological map of the Krivoy Rog Structure, Ukraine.

Jaspilite — the gemstone of Ukraine

- yellow-banded with tiger's-eye,
- blue-banded with falcon's-eye and
- grey-banded.

In addition, the rich diversity of texture has enabled five groups to be distinguished and these are:

- parallel-striated
- wavy-striated
- intensely folded or crumpled on a small scale (plicated),
- breccia-like and
- landscape varieties.

The *parallel-striated jaspilite's* main features are straight parallel stripes of different colour, mineral composition and texture (Figure 2). Wide- and thin-striated varieties can be distinguished, with even and uneven alternation of the layers. According to the location of the stripes, pieces can be cut to create textural pictures with bands parallel or at angles to the edges.

Wavy-striated jaspilite is defined by the presence of uneven wavy-like stripes (Figure 3). Here again, wide- and thin-striated varieties can also occur. The textures may be clear or more diffuse with areas of boudinage or pinched, sausage-like structures. Generally, this variety is decorated by shallow cracks filled with magnetite and hematite of secondary origin.

The *intensely folded or plicated variety* is a kind of parallel-striated jaspilite and/or a wavy-striated type, which has been affected by strong deformation processes. This jaspilite contains traces of various dislocations, breaks and natural cracks filled with quartz, magnetite, hematite or iron-rich mica.

Breccia jaspilite (Figure 4) contains broken fragments, some of different composition, later cemented by siliceous or siliceous-carbonate material. The

broken fragments differ not only in composition but also in their shape (rounded, acute-angled), size and colour (dark grey, light grey, brown red, red, bright red).

Landscape jaspilites are those types with inclusions and structures giving the appearance of scenic landscapes best seen in polished section (Figure 5). The decorative appeal of this variety is determined by the contrast of various colours and healed natural cracks.

The main rock-forming minerals of the jaspilites are quartz, magnetite, hematite, siderite, chlorite, biotite and the amphibole grünerite. Significant amounts of aegirine and riebeckite also occur in jaspilites strongly altered during alkaline metasomatism. Hydrogoethite, albite, rhodosite, ankerite, pyrite, chalcopyrite and apatite appear as secondary

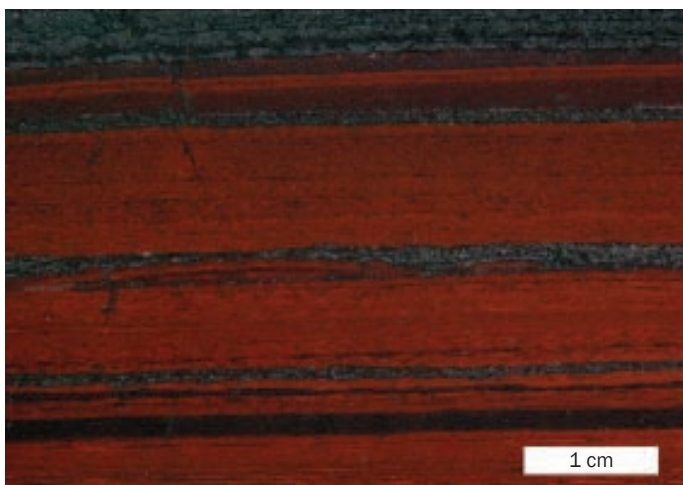


Figure 2: Red, parallel-striated jaspilite.

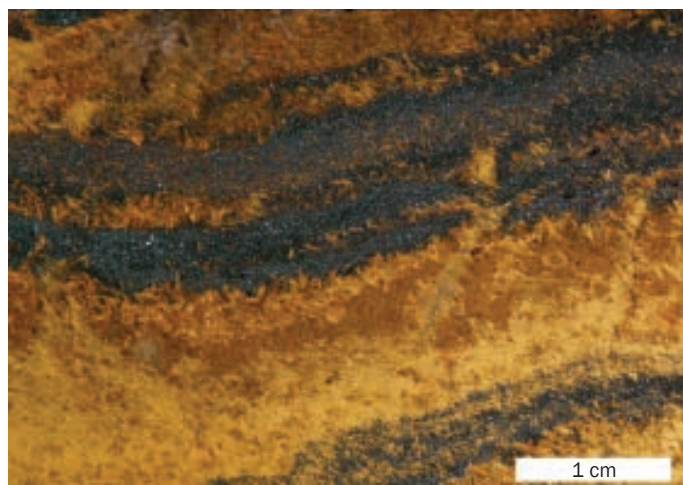


Figure 3: Yellow, wavy-striated jaspilite.

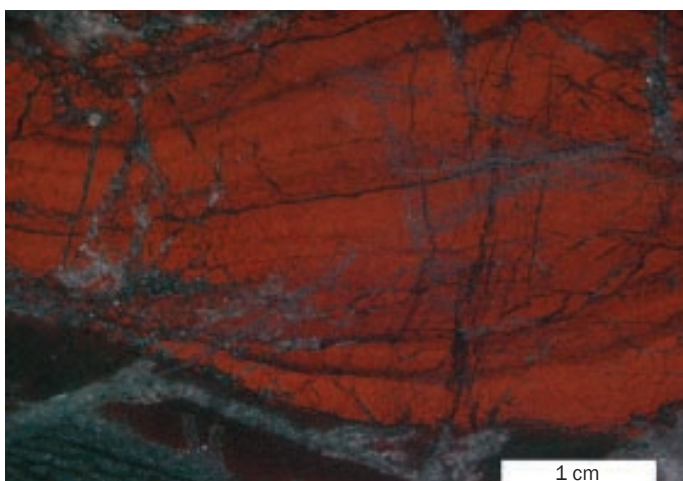


Figure 4: Red, breccia jaspilite.

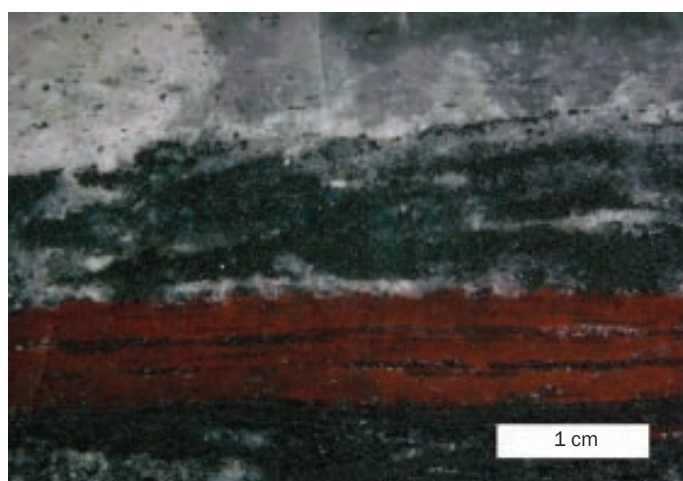


Figure 5: Red, landscape jaspilite.

Jaspilite — the gemstone of Ukraine

and accessory mineral components (Dumanska-Slowik *et al.*, 2007). All the jaspilite varieties contain ≥ 15 wt.% Fe.

The rhythmically banded jaspilites consist of alternate laminae of silica (quartz, chalcedony), iron minerals (magnetite, hematite, siderite or goethite) and amphiboles. Typical red laminae caused by hematite in irregular aggregates are shown in *Figure 6*. Such parallel-striated jaspilites can have alternate red and grey laminae up to 12 cm in thickness. In detail, hematite is responsible for the red colour, and the interstices between the flakes are filled with fine-crystalline quartz and carbonates. The grey laminae consist of magnetite with an admixture of hematite and are commonly accompanied by carbonates (siderite), chlorite and quartz.

Although yellow-banded jaspilites are less common than the red varieties, they exhibit the same textural patterns on polished sections. They consist of golden-yellow and brown-grey laminae up to 12 cm in thickness. Amphiboles (cummingtonite subgroup), forming fibrous and lamellar crystals, are the main constituents of the yellow laminae (*Figure 7*) and the presence of these minerals causes the ‘tiger’s-eye’ effect which is only noticeable in the yellow-bands (*Figure 8*). Also within the yellow laminae, aggregates of Fe-bearing minerals (hematite, goethite) and fine-crystalline quartz can be present (Heflik *et al.*, 2008). The brown-grey bands in the jaspilite may consist of:

- 1) thick layers of micro-crystalline quartz with a small admixture of hematite and goethite;

- 2) thin layers of medium-crystalline quartz (up to 75%) and ore-bearing minerals making up to 25% of the lamina volume; or
- 3) laminae enriched in Fe-bearing minerals (up to 90% of the volume) with quartz as an impurity up to 10%.

The latter layers are in contact with the golden-yellow regions of the jaspilite.

Bands in jaspilites that appear grey overall in detail consist of alternate thin black and grey laminae. The black laminae consist of quartz, hematite and goethite, with chlorites, carbonates (siderite or ankerite), feldspars and apatite as subordinate phases. Grey and grey-green veins up to several cm thick, which intersect the rocks, consist of fibrous crystals of amphiboles (mainly grünerite and subordinate cummingtonite) (*Figure 9*).

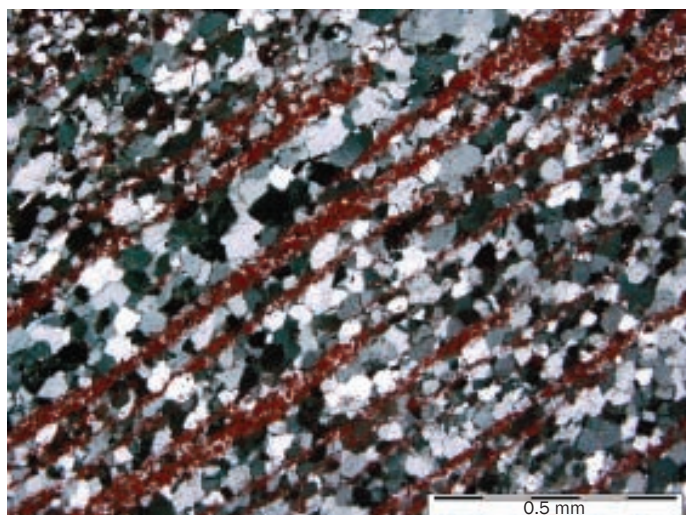


Figure 6: Red hematite in matrix of quartz; detail of texture in parallel-striated jaspilite. Thin section, cross-polarized light.

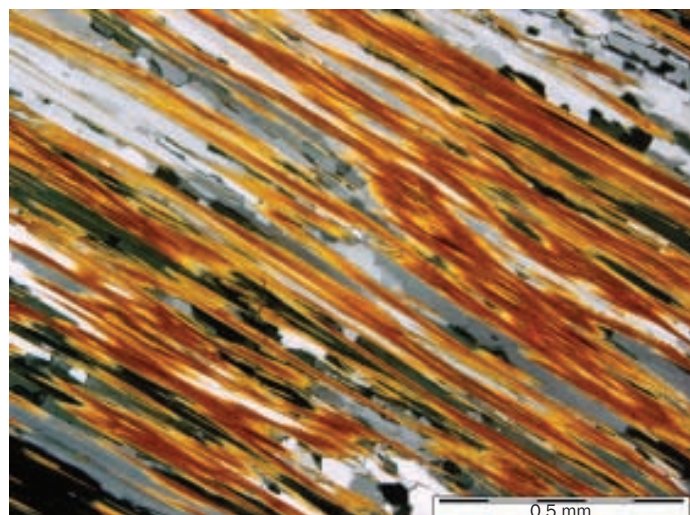


Figure 7: Fibrous crystals of amphibole in quartz matrix in parallel-striated yellow jaspilite. Thin section, cross polarized light.

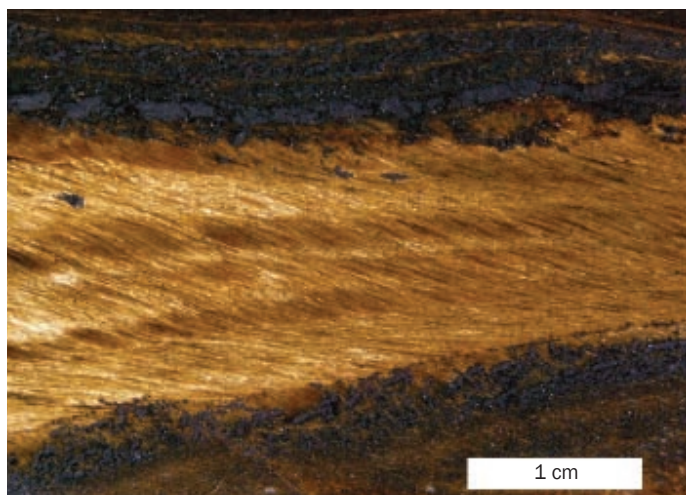


Figure 8: ‘Tiger’s-eye’ effect in yellow, wavy-striated jaspilite.

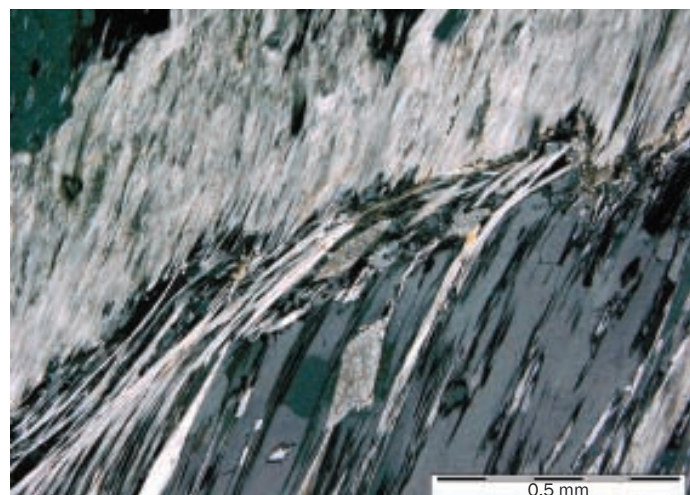


Figure 9: Fibrous crystals of amphiboles in grey jaspilite. Thin section, cross polarized light.

Jaspilite — the gemstone of Ukraine

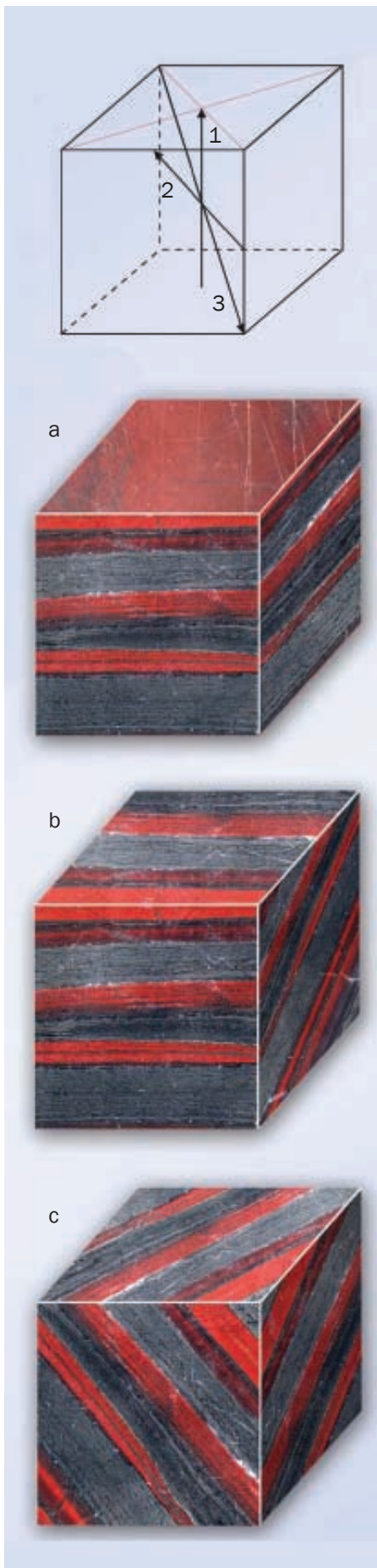


Figure 11: Examples of jaspilite fashioning according to the third principle of stone shaping. In an oval cabochon, it is possible to orientate striated jaspilite to get five different volumetric pictures.

The shaping and manufacture of jaspilite

Based on the study of jaspilite’s decorative properties, three principles of shaping these stones have been established. They guide one in making the most of the textures and colours of the pieces of rough.

The first principle of shaping

The textural picture or pattern depends on the direction of cutting angle (Figure 10).

The second principle of shaping

The textural picture depends on the size of the polished section of the jaspilite. If the surface is large enough, it may contain a mixture of jaspilite varieties.

The third principle of shaping.

The textural picture of the jaspilite depends on its shape. Thus, if one considers cutting striated jaspilite as a cube, it is possible to obtain three different volumetric pictures:

1. Two facets of the cube have a homogeneous picture and four are parallel-striated (Figure 10).

2. Four facets show striation parallel to the edges of the cube and two facets are diagonal-striated.
3. All the facets of the cube exhibit the diagonal-striated picture.

Using striated jaspilite, it is possible to get seven different volumetric pictures out of a parallelepiped, five from a hexagonal prism, five from a tetrahedral pyramid, three from a cone, and three from a cylinder. In an oval cabochon one can reveal five different volumetric pictures of the jaspilite (Figure 11). Examples of plicated and breccia patterns are shown in Figure 12.



Figure 12: Typical patterns shown by plicated (top) and breccia jaspilites.

Figure 10: Examples of jaspilite illustrating the third principle of stone shaping (a cube).
 a. Two facets of the cube appear homogeneous for four have parallel bands.
 b. Four facets have striation parallel to the edges of the cube and two have a diagonal pattern.
 c. All facets have diagonal striations.

Jaspilite — the gemstone of Ukraine



Figure 13: (a) The cameo of Alexander the Great set in jaspilite, silver (made by Peter Baranov and Vladimir Konstantinov). (b) The cameo of Alexander Pole carved in jaspilite and set in silver on a jaspilite stand (designer Irina Buryak, made by Svyatoslav Nikitienko).



Figure 14: Vase 'Geyser' in jaspilite (made by Peter Baranov). Height 20 cm.



15: This box 'The Pearl of Seas' is made of jaspilite, labradorite and silver, and is gilded in places (designer Peter Baranov, made by Maxim Netecha and Vladimir Konstantinov). Length 14 cm.

Jaspilite — the gemstone of Ukraine

The Ukrainian jaspilites provide excellent material for production of functional artistic goods. The two cameos and vase shown in *Figures 13* and *14* are examples of the popular art of glyptography.

Texturation is another technique often applied to jaspilite, in which the coloured parts are polished while the grey or uncoloured areas remain with a ground, matt finish. For special items, the jaspilite may be selectively gilded (*Figure 15*).

Jaspilites can also be used to decorate the interiors of buildings. Some years ago, the idea of the 'Jaspilite Hall' was conceived, being inspired by the Malachite Hall of the Hermitage in St. Petersburg (Russia). Some artistic projects based on this idea, supported by the National Mining University and the Dnepropetrovsk Regional State Administration, have been developed (Baranov *et al.*, 2006).

It is well known that the attractiveness of such decor depends not only on the decorative properties of the stones, but also on the taste and skill employed in their use by the architect. The 'Jaspilite Hall' projects, including 'Cantata about a Gemstone', 'A Stone Flower', 'The Gothic' and 'The Knight Hall', combine these two factors. In 'The Gothic' project, the austere style matches and complements the sober colours of the Ukrainian jaspilites (*Figure 16*).

Conclusion

The attractive decorative properties of Ukrainian jaspilite and the considerable reserves available promise well for the future of this material. A wide range of jaspilite items are already exhibited and sold at the 'World of gemstones' exhibition, held in Dnepropetrovsk every month, and there is potential to expand onto global markets.

Acknowledgements

This work was financially supported by the AGH University of Science and Technology, grant no 11.11.140.158.

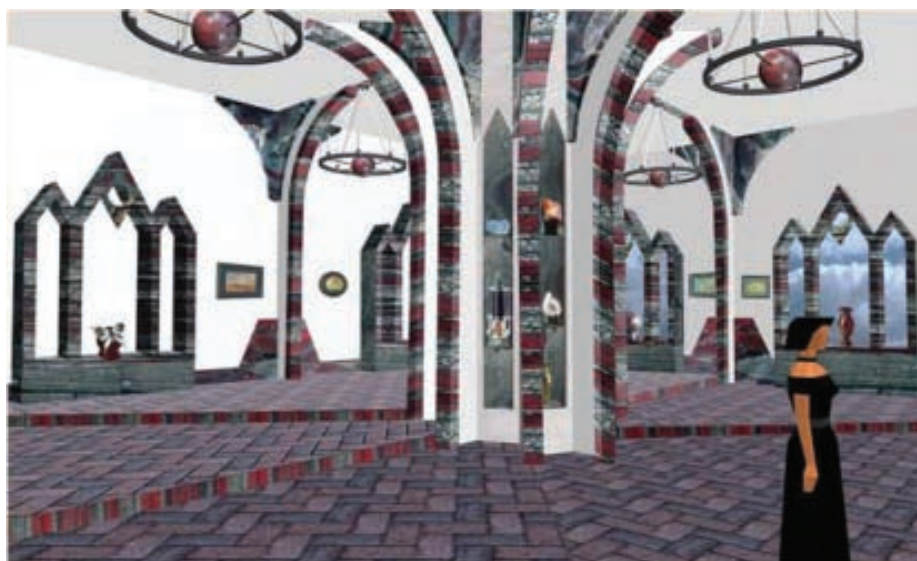


Figure 16: A computer-generated model entitled 'The Gothic' shows a room decorated with jaspilite and depicts a figure to indicate a sense of scale. Project designer Jurij Kolokolov; computer drawer Vadim Karmanov.

References

- Baranov, P., 2002. *Gemmology: diagnostics, design, treatment, estimation of gemstones*. (In Russian.) Dnepropetrovsk. Metall. 208 pp
- Baranov, P., Shevchenko, S., Tsotsko, L., Homenko, U., Karmanov, V., Buryak, I., Almazov, V., Kolokolov, U., Hvylya, I., Kashiya, D., Luzanov, P., Nikitenko, I., Netecha, M., Polischuk, A., and Marchuk, A., 2006. Jaspilite Hall: to be or not to be? (In Russian.) *Herald of Ukrainian Jeweller*, 1, 20–7
- Baranov, P., 2006. *Gemstones of Ukraine Jaspilites*. (In Russian.) Kiev, JewelerPRESS, 100 pp
- Dumanska-Słowik, M., Heflik, W., and Natkaniec-Nowak, L. 2007. Jaspilites — decorative stones of Ukraina. (In Polish.) *Rynek Jubilerski*, 3(3), 10
- Heflik, W., Baranov, P.N., Natkaniec-Nowak, L., Dumanska-Słowik, M., Shevchenko, S.V., and Nikitenko, I.S., 2008. Cat's-eye from Krivoy Rog iron-ore deposits. (In Russian.) *Scientific Herald of National Mining University*, 8, 68–72
- Morris, R.C., 1980. A textural and Mineralogical Study of the relationship of Iron Ore to Banded Iron Formation in the Hamersley Iron Province of Western Australia. *Econ. Geol.*, 75, 184–209
- Trendall, A.F., 1975. Hamersley Basin. *WA Geol. Surv., Mem.* 2, 119–43

The Authors

P. Baranov and S. Shevchenko

The National Mining University, The Gemmological Center, 19 C. Marx Av., Dnepropetrovsk Ukraine, 49005
e-mail: baranov_pn@bk.ru, shevchsergey@gmail.com

W. Heflik, L. Natkaniec-Nowak and M. Dumanska-Słowik

AGH University of Science and Technology, The Faculty of Geology, Geophysics and Environmental Protection, The Department of Mineralogy, Petrography and Geochemistry, 30 Mickiewicza Av., 30-059 Krakow, Poland
e-mail: natkan@uci.agh.edu.pl, dumanska@uci.agh.edu.pl



Gem-A

THE GEMMOLOGICAL ASSOCIATION
OF GREAT BRITAIN

The TravelGem Microscope

Designed for gemmologists,
this compact microscope
is ideal for students,
valuers and gem dealers.



- Fitted aluminium travel case
- Runs on 110 and 220 volts (built in transformer)
- 10x, 20x, 30x and 60x magnification
- Bright field, dark field and top lighting
- Stone holder and darkfield assembly can be removed to examine jewellery

PRICE: £325.00* (Gem-A members and Gem-A registered students £292.50*)

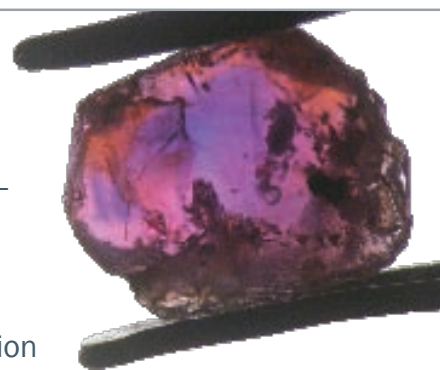
* Prices exclude VAT and shipping

For further details or to order your TravelGem Microscope, contact the Gem-A shop at shop@gem-a.com or call +44 (0)20 7404 3334.

Ruby and sapphire from Marosely, Madagascar

Laurent E. Cartier

Abstract: The Marosely corundum deposit is eluvial and follows in a long line of corundum localities discovered in recent years in Madagascar. Colours range from red to blue, and stones are typically zoned, being purple overall. Thirty-five rough corundum samples of 0.1–2.0 ct in weight were selected for study, and the main aspects of this work focused on spectroscopic and chemical properties of the stones. FTIR spectra show the presence of 3160 cm^{-1} and 3309 cm^{-1} peaks in natural untreated corundums, and the relevance of these to the detection of heat treatment of corundum is discussed. LA-ICP-MS data concerning chromophores in colour-zoned samples are consistent with spectral data. Results for ultra-trace element concentrations proved less revealing, emphasizing the need for a combinatory approach with other analytical methods in advancing corundum origin determination efforts.



Keywords: corundum, FTIR spectra, LA-ICP-MS, Madagascar, origin determination, UV-visible spectra

Introduction

Since the discovery of Andranondambo in 1993, Madagascar has become an increasingly important source of gem corundum for the world market. The past decade and a half has brought about the discovery of a significant number of both large and small ruby and sapphire deposits (Kiefert *et al.*, 1996; Schwarz *et al.*, 1996;

Pezzotta, 2001; Offant, 2005; Ralantoarison, 2006; Giuliani *et al.*, 2007). Considering that much of Madagascar has not yet been thoroughly explored, it is certain that in coming years many more deposits will be found to provide the world market with gem-quality ruby and sapphire (Schwarz *et al.*, 2000; Ramdohr and Milisenda, 2006). The diversity of Madagascar's geological

environment and its different types and origins of corundum deposits (e.g. basaltic, skarn, metasomatic) presents certain challenges for origin determination of corundum. This paper offers a detailed examination of selected samples from a lesser-known corundum deposit at Marosely (Pezzotta, 2007; Cartier, 2008) and is part of a comprehensive study. The results from these natural untreated corundum samples should improve understanding about a range of current gemmological issues such as detection of heat treatment and origin determination.

The Marosely deposit is located in the Ranotsara region (near 47°E , 23°S) of south-central Madagascar and is eluvial. Most of the corundum crystals from this deposit are fragmental; no euhedral crystals have been found, and only a few specimens have crystal faces. Metamorphic corundum deposits have been reported in the region by



Figure 1: Ruby and sapphire from Marosely, Madagascar. From left to right: violetish blue sapphire (0.363 ct), pink sapphire (0.164 ct), ruby (0.208 ct). Note these were not used as specimens for this study and serve merely to illustrate the variation in colour of material from the deposit.

Ruby and sapphire from Marosely, Madagascar



Figure 2 Artisanal mining activity in the Marosely mining area, south Madagascar.

Offant (2005), Ralantoarison (2006) and Ralantoarison *et al.* (2006), but the high-metamorphic Marosely corundums have probably experienced considerable subsequent metasomatic alteration (Cartier 2008). *Figure 1* shows three cut stones typical of this deposit and *Figure 2* mining activity in the area.

Gemmological properties

Table I: Gemmological properties of Marosely corundum samples.

	Range	Mean
SG	3.96–4.05	3.99
RI ω	1.762–1.767	1.764
ϵ	1.769–1.775	1.772
$\omega - \epsilon$	(-0.007)–(-0.010)	-0.008

The recorded values of SG and RI for corundums from Marosely are shown in *Table I*. Their UV-fluorescence ranged as follows:

- 254 nm: none-weak (red)
- 366 nm: none-strong (red)

Nearly all stones are inert to short-wave UV radiation with only one showing weak red fluorescence; this is a Cr-rich sample (1b1). This is also the only stone to show strong fluorescence at 366 nm. Only a few stones show no reaction when

exposed to 366 nm UV light. Generally speaking, the redder, Cr-richer and Fe-poorer the stone, the stronger it fluoresces (which is consistent with the known behaviour of Fe in corundum).

Internal characteristics

Mineral inclusions

A variety of solid mineral inclusions were found in the samples, the main ones being zircon, mica and rutile. Sillimanite, calcite, diaspore, feldspar (Ca-rich plagioclase, colourless) and spinel are also present in some samples. These solid inclusions were identified by means of the microscope and Raman microprobe. Negative crystals are also relatively common.

Typical zircon inclusions and their Raman shift peaks are shown in *Figures 3, 4* and *5*. The differences in peak heights, evident in *Figure 3*, are due to anisotropy in the zircons but their positions correlate well with values reported in literature (e.g. Bruder, 1995; Ostertag, 1996; Waite, 2000).

Colour zoning

Most specimens show patchy colour zoning (*Figures 6* and *7*) and the boundaries between darker bluer colours

Materials and methods

All samples used in this study were acquired at the mining site directly. Thirty-five samples representing a range of colours were selected, and on each two parallel faces were polished. The samples were examined microscopically and mineral inclusions identified using a Renishaw Raman microprobe. FTIR and UV-Vis absorption spectroscopy (using a Varian-Cary 500 spectrometer) and EDXRF measurements were carried out on all samples at the SSEF Swiss Gemmological Institute, and instrumental details are similar to those reported by Krzemnicki *et al.*, (2001) and Krzemnicki (2004). LA-ICP-MS data were obtained from equipment at the University of Berne using an ArF laser of wavelength 193 nm (see Pettke (2006) for more details). Semi-quantitative determination of the oxides in the corundum was obtained using a Tracor X-ray Spectrace 5000 EDXRF model.

and redder colours demark the zones of growth. Although not all stones show colour zoning, the rims of most crystals are redder and more Cr-rich than the centres.

Colour and spectroscopic properties

Marosely corundums range from purplish red (ruby colour) to blue, but the majority are a mixture of both colours, resulting in purple.

Typical UV-Vis absorption spectra for Marosely corundums are shown in *Figure 8*. The six spectra represent a gradual change from a blue sapphire colour to a ruby colour (1d3–1e4–1e1–2a1–2g1–2b1), which can be matched with the shifts in absorption and transmission bands. The 410 nm, 556 nm and 693 nm absorption peaks/bands are all due to Cr³⁺ content (Bosshart, 1981). The peak at 388 nm, which becomes less apparent with increasing Cr³⁺ concentrations, is due to the presence of Fe³⁺ (Kiefert, 1987) and this is near-undetectable in the sample with the lowest Fe/Cr ratio (2.014, 2b1).

Ruby and sapphire from Marosely, Madagascar

Broad absorption bands can be caused by more than one trace element. For example, in the region 550–565 nm, the 556 nm band of Cr³⁺ can be augmented by the band for Fe²⁺/Ti⁴⁺, usually found around 562 nm.

The doublet at 377 nm/388 nm becomes more pronounced with increasing Fe³⁺ concentration and correlates well with the increasing 450 nm peak. This 450 nm peak corresponds to Fe³⁺/Fe³⁺ interactions, whereas the band at 562 nm in *Figure 8*, is caused by Fe²⁺/Ti⁴⁺ inter-valence charge transfer (Schmetzer and Schwarz, 2004).

Colour is very much a product of the combinations of absorption and transmission bands and peaks. Any shift (e.g. 556 nm → 562 nm) of absorption bands in the unpolarized spectrum results in a change of perceived colour.

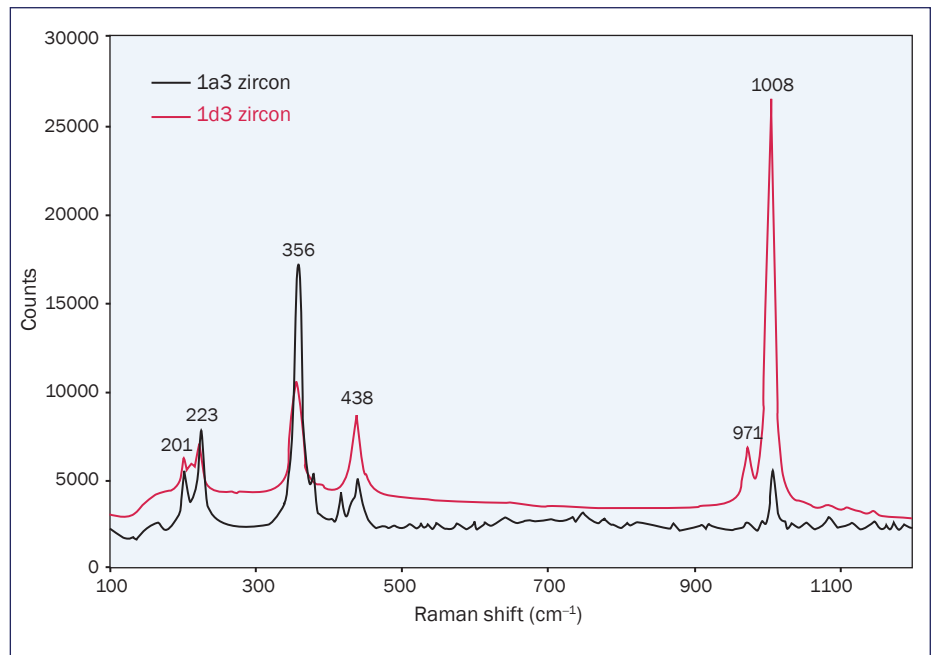


Figure 3: Raman spectra of zircon inclusions in samples 1a3 (blue sapphire) and 1d3 (light purple sapphire)



Figure 4: Zircon inclusion in sample 1d3. 20×

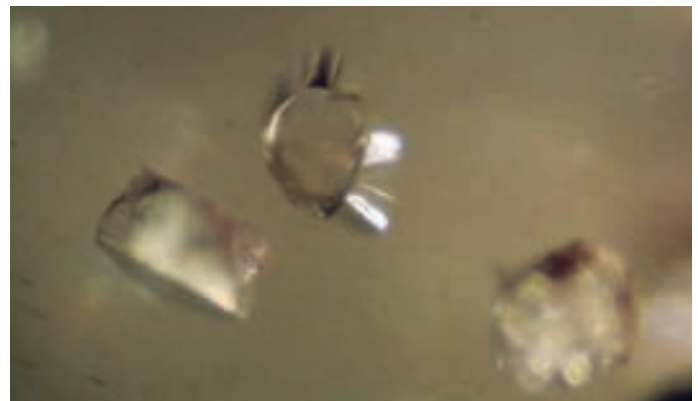


Figure 5: Zircon inclusion in sample 1a3. 20×

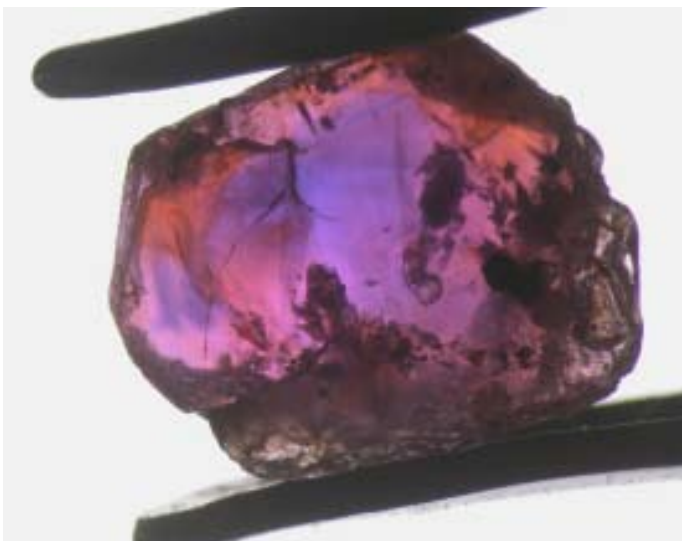


Figure 6: Sample 2c2 (0.663ct) from Marosely showing inhomogeneous or patchy colour zoning and important presence of inclusions. 10×

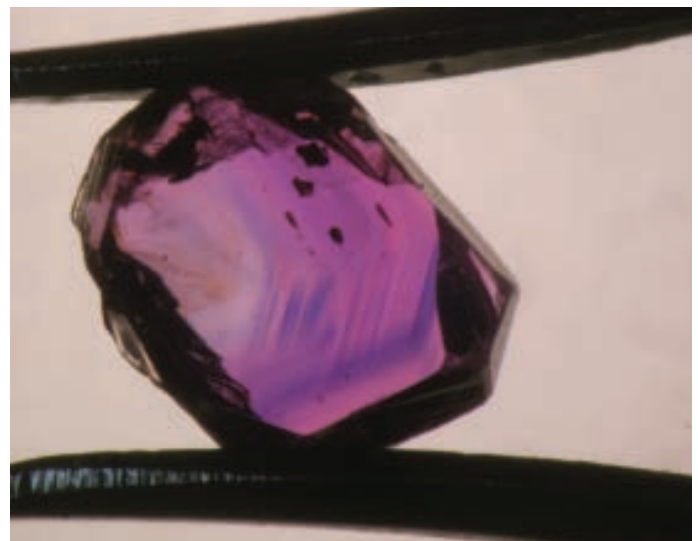


Figure 7: Specimen 2b3 (0.561 ct) showing straight bands of colour.

Ruby and sapphire from Marosely, Madagascar

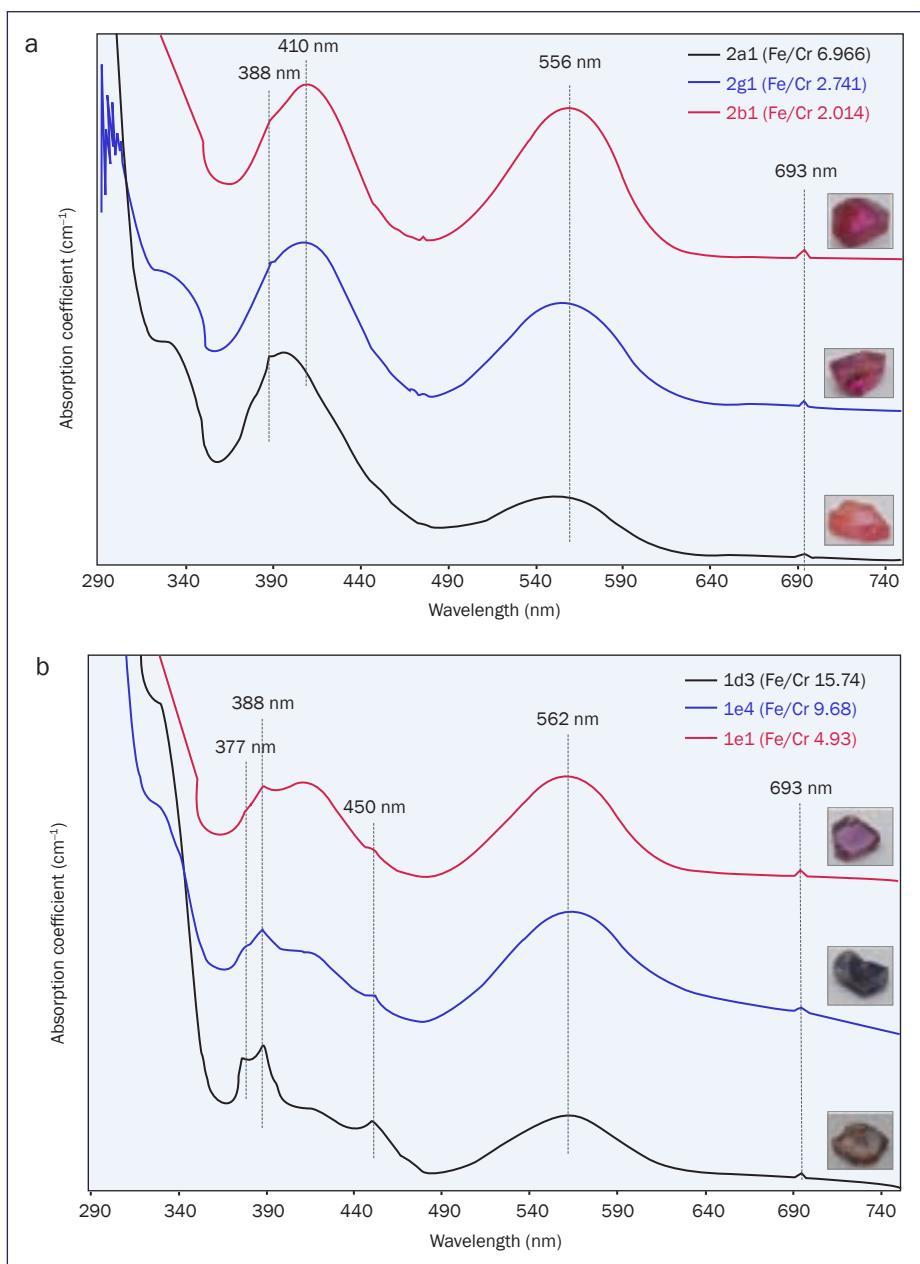


Figure 8a and b: Comparison of different UV-Vis absorption spectra of varyingly coloured Marosely corundum samples. The Fe/Cr ratios are indicated.

Pleochroism

In those stones in which pleochroism was observed, the ordinary ray (ω) colour was purplish red or bluish violet, whereas the extraordinary ray (ϵ) colour was mostly orangey red.

One sample (2a1) demonstrated considerable pleochroism. The ω colour was reddish pink, whilst that for the ϵ

was orangey-pink (see Figure 9). The ordinary ray shows less absorption in the lower parts of the spectrum, but it is more absorbant above 410 nm and its 560 nm band features much more prominently than in the extraordinary ray. The shift in absorption peaks and bands (slightly to the right for ϵ) accounts for the pleochroism and the associated change in colour.

Table II: Frequency of FTIR peak occurrences in 35 Marosely corundums.

	3080 cm ⁻¹	≈3160 cm ⁻¹	3309 cm ⁻¹	≈3390 cm ⁻¹	3619 cm ⁻¹	3650 cm ⁻¹	3695 cm ⁻¹
Number of samples presenting specific peak/band	5	7	27	6	14	5	13

Infrared spectrometry

FTIR has in recent years gained more attention as a potentially useful method for detecting heat treatment of corundum, which is possibly identifiable by the presence of certain peaks (Smith, 1995; Perretti *et al.*, 1995; Balmer *et al.*, 2006; Beran and Rossman, 2006; AGTA, 2007).

All rough stones originally collected from the Marosely deposit and used within the context of this study have neither been heated nor treated. They have been simply cut and polished on two parallel sides. This excludes heat treatment as a possible cause of certain peaks discussed below. The possible influence of specimen orientation on spectral curves suggested by Smith (1995) and Volynets *et al.* (1972) was small or absent. All samples were measured in two directions (i.e. turned 90° for the second measurement), relative to the two parallel faces.

In Figure 10, FTIR spectra of pink and pale purple sapphires are shown. The peaks found at 2854 cm⁻¹, 2922 cm⁻¹ and 2951 cm⁻¹ correspond to oils and fats. This most probably corresponds to contamination from accidental handling or from the substance used for polishing the stones (Epoxide). CO₂ and H₂O bands can vary due to atmospheric fluctuations during and between each measurement and this is evident in the 2300–2600 cm⁻¹ region when comparing Figures 10 and 11. A number of peaks were detected in the region 3600–3700 cm⁻¹. Some are triplets (3619 cm⁻¹, 3650 cm⁻¹, 3695 cm⁻¹), but more often pairs (3619 cm⁻¹, 3695 cm⁻¹) are present and probably indicate the presence of a type of mica or kaolinite (W. Balmer, pers. comm., 2007).

The frequency of occurrence of FTIR peaks in all samples is shown in Table II. The peak at or near 3080 cm⁻¹ is not very common, indicating the scarcity of hydrous aluminium phases (see Smith *et al.*, 1995; Smith, 1995; Peretti *et al.*, 1995). However, neither diaspore nor boehmite

Ruby and sapphire from Marosely, Madagascar

could be clearly identified using Raman microprobe analysis.

Balmer *et al.* (2006) reported a peak at 3160 cm^{-1} in investigations on yellow sapphires, attributing this peak to goethite or an epidote group mineral. As neither could be identified in the seven samples using Raman microprobe analysis, the origin of this peak remains uncertain. Waite (2000) reported that the 3160 cm^{-1} peak was found in powder IR measurements from Tunduru, indicating that it is not due to surface contamination but a phase that is effectively present in corundum.

The peak at 3309 cm^{-1} was found in 27 of the 35 Marosely corundum specimens. Smith *et al.* (1995) believed this peak to be due to the breakdown of hydrous aluminium phases (i.e. diaspore, boehmite), but Balmer *et al.* (2006), in investigations on yellow sapphires, have argued that it may be caused by structurally bonded OH groups, in association with an excess of a certain trace element (see also Volynets *et al.*, 1972). Beran *et al.* (2006) also found that OH bands (e.g. 3309 cm^{-1} , 3160 cm^{-1}) were much more prominent in blue sapphires, hinting at OH associated with oxidation/reduction reactions involving iron. Tetravalent Ti may also play a role (Moon and Phillips, 1994). For the natural, untreated Marosely samples, there is no clear relation between the presence and size of a 3309 cm^{-1} peak and the colour of the crystal, and also its presence is not indicative of artificial heat treatment.

Other recorded peaks in the context of this study on thirty-five Marosely specimens were found at 2345 cm^{-1} , 2428 cm^{-1} , 2514 cm^{-1} , 2532 cm^{-1} , 2732 cm^{-1} and 3012 cm^{-1} .

Chemical composition

Semi-quantitative determinations of the oxides in Marosely corundums were obtained using EDXRF and the results are shown in *Table III*. Total iron is given as Fe_2O_3 since Fe^{2+} and Fe^{3+} cannot be differentiated using this method. Three samples (1b1, 1a5, 2f1) showed especially high Fe concentrations (0.5–0.8 wt%)

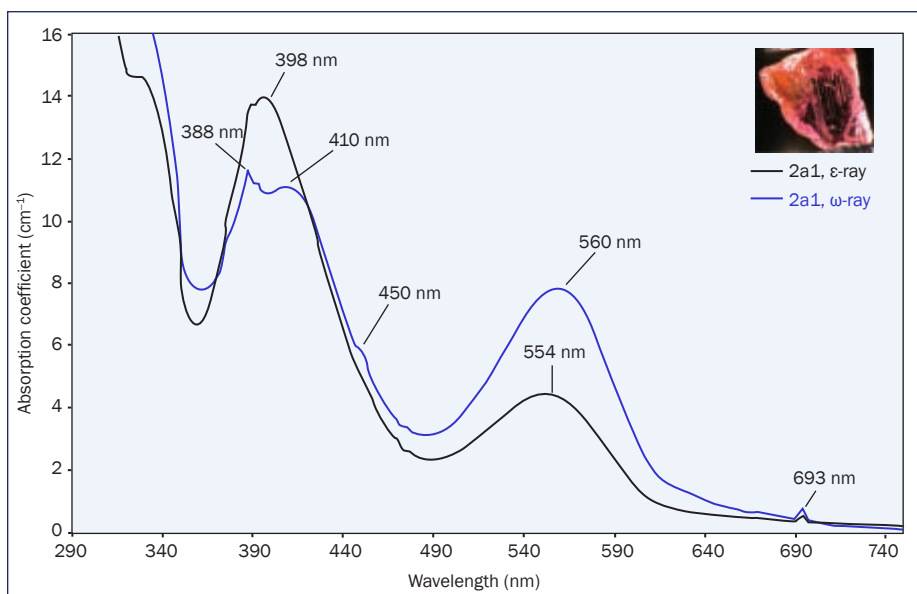


Figure 9: UV-Vis absorption spectra exemplifying pleochroism in sample 2a1.

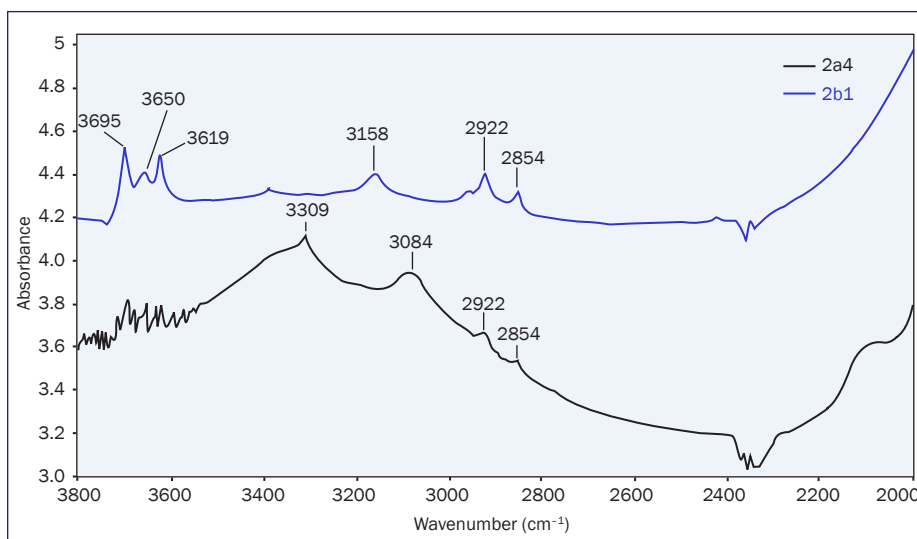


Figure 10: FTIR spectra of pink (2b1) and light purple (2a4) sapphires.

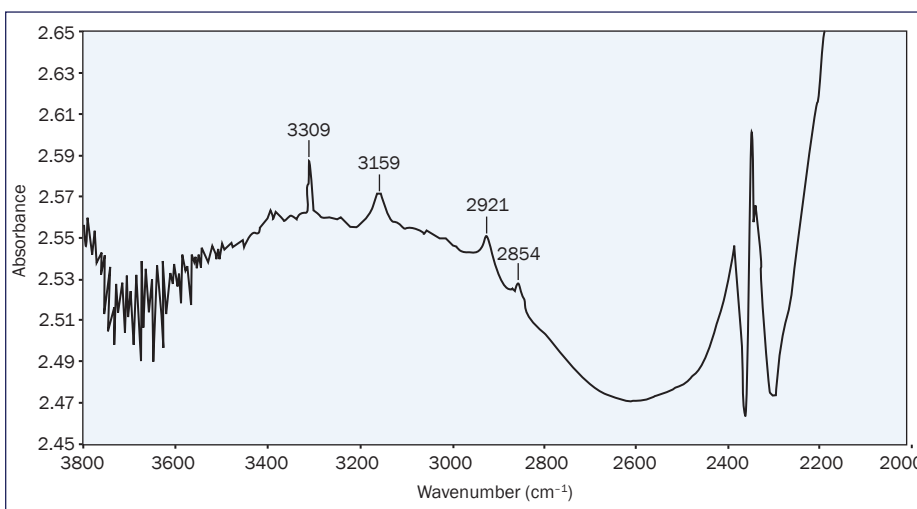


Figure 11: FTIR spectrum of a purple sapphire (2g3). 3159 cm^{-1} and 3309 cm^{-1} are clearly distinct peaks. The varying absorption character of the $2300\text{--}2400\text{ cm}^{-1}$ region is due to atmospheric fluctuations during measurements.

Ruby and sapphire from Marosely, Madagascar

Table III: Compositional range and mean of 35 Marosely corundums determined using EDXRF.

	Concentration range (wt%)	Mean (wt%)	Mean error
Al ₂ O ₃	98.3–99.9	99.39	±0.22
Fe ₂ O ₃	0.086–0.822	0.29	±0.01
Cr ₂ O ₃	0.022–0.19	0.08	±0.008
TiO ₂	0.003–0.098	0.024	±0.002
V ₂ O ₃	0–0.01	0.004	±0.0008
Ga ₂ O ₃	0–0.006	0.003	±0.0003

Fe₂O₃). Chromium was the second most common trace element present, ranging from 0.022–0.19 wt%. It is highly influential in the coloration of corundum from this deposit. The mean concentration of TiO₂ is 0.024 wt%, with higher Ti concentrations generally corresponding to milkier and bluer stones.

The considerable variation of chemical components in different samples makes comparisons to other well-described deposits difficult. This variation is a reflection of the fact that most stones are chemical intermediates between ruby and sapphire.

Trace elements and LA-ICP-MS

The LA-ICP-MS equipment in Berne can be used to analyse areas only 160 µm in diameter, and thus obtain much more detailed data for elements present at trace or ultra-trace levels (Pettke, 2006) than one can using only EDXRF.

Seven corundum samples from Marosely were selected for closer examination. These varied in colour and in chemical composition. For each sample, at least three points were targeted

and measured to ensure accuracy and reproducibility of results.

The stones were measured in two groups of samples:

- 1a2 (violetish blue corundum), 1a3 (blue corundum), 1d1 (light purple corundum)
- 1e2 (purple colour zoned corundum), 2a1 (pink corundum), 2a4 (violetish blue corundum), 2c1 (purple corundum)

and the results in parts per million (ppm) are shown in Table IV.

Recently, research has been conducted using LA-ICP-MS technology on a range of ultra-trace elements in the hope that quantitative results, measured with improving geochemical instrumentation, could deliver more insight into a stone's chemical history, and consequently facilitate origin determination (Hattendorf *et al.*, 2003; Saminpanya *et al.*, 2003; Rankin *et al.*, 2003; Abduriyim *et al.*, 2006). In the Marosely corundums, 40 elements were measured of which

Table IV: Trace element contents of seven Marosely corundums obtained using LA-ICP-MS analysis.

Sample	Group 1				Group 2				
	1a2	1a3	1d1	Standard rsd %	1e2	2a1	2a4	2c1	Standard rsd %
Colour	violetish blue	blue	pale purple		purple (colour- zoned)	pink	violetish blue	purple	
Be	bdl	0.137–0.151	bdl–0.113	0.90	bdl–0.133	bdl	0.097–0.126	bdl–0.029	1.80
Mg	19.42–51.08	106.3–111.4	36.13–61.22	0.70	23.28–26.17	32.87–45.78	150.3–160.7	33.65–53.44	2.10
K	4.03–6.05	0.888–3.06	2.91–7.47	3.70	0.739–2.92	5.37–7.05	5.40–5.89	2.59–7.89	2.50
Ti	40.83–73.00	175.6–184.2	53.07–219.3	0.60	34.13–484.6	23.34–28.01	254.5–263	52.42–74.75	1.10
V	12.77–16.93	23.48–23.95	24.06–33.08	0.50	17–34.5	18.28–20.08	33.3–33.4	21.74–22.02	0.70
Cr	365.8–466.2	232.2–246.4	844.1–1564	0.90	176.3–768.7	742.5–819	650–688.3	724.1–1028	0.80
Mn	0.101–0.124	0.116–0.155	0.108–0.132	0.80	0.078–0.124	0.155–0.163	0.201–0.209	0.101–0.186	0.40
Fe	2184–2285	1959–2037	2005–2778	2.20	1764–1889	1752–1898	3032–3117	1353–1415	2.20
Zn	2.41–3.37	1.92–2.54	4.25–10.92	1.10	1.13–2.18	2.91–3.79	3.94–8.38	2.95–8.88	4.60
Ga	30.58–34.84	80.41–81.90	30.05–36.67	0.50	42.10–59.52	52.24–54.17	56.21–60.89	19.62–21.03	0.40
Ge	0.106–0.116	0.127–0.172	0.084–0.179	0.60	0.169–0.99(*)	0.074–0.139	0.086–0.092	bdl–0.133	1.60
Nb	bdl–0.011	0.002–0.008	0.006– 0.228(*)	1.40	0.015–2.49 (*)	0.002–0.003	0.002–0.006	0.007–0.011	0.40
Sn	0.069–0.086	0.094–0.1	0.085–0.254	0.60	0.111–0.215	0.083–0.105	0.125–0.166	0.123–0.145	1.00
Ta	bdl	bdl	bdl	2.00	bdl–0.81(*)	bdl	bdl	0.003–0.006	1.60
Th	bdl	bdl	bdl–0.006	1.40	bdl–0.118(*)	0.001–0.006	bdl	0.002–0.005	1.00
U	bdl	0.002–0.043	bdl–0.006	0.70	bdl–0.006	0.001–0.004	0.001–0.003	0.008–0.051	1.20

NB: Ranges are in ppm over three or more spots. bdl corresponds to below detection limit. The error margin is expressed as relative standard deviation (rsd). (*): Denotes a maximum value which is too high and probably due to unidentified factors in the raw data.

Ruby and sapphire from Marosely, Madagascar

a relevant 16 are listed in *Tables IV* and *V*. All elements apart from Fe and Cr were present at <1000 ppm. The chromophore element Cr ranges 232–1564 ppm. Titanium, is generally at lower concentrations, but reaches a maximum of 484 ppm in sample 1e2. Mg (19.4–161 ppm), K (0.74–7.9 ppm, most likely from inclusions in the crystal) and Zn (up to 10.9 ppm) concentrations are higher than the figures reported in the literature for other localities (e.g. Abduriyim *et al.*, 2006). There is no correlation between Mg concentration and crystal colour.

Of the only two measured actinides, thorium levels are very near the detection limit, but uranium is higher (maximum 0.051 ppm).

Example of colour and chemical zoning

All selected stones from Marosely range from red to blue, with most stones having an intermediate purple colour. This colour range is largely regulated by variations in Cr³⁺ and Ti⁴⁺ concentrations which can be demonstrated, using LA-ICP-MS technology, through point analysis in the different colour zones.

Three spots in sample 1e2 were ablated and measured (see *Figure 12*):

- 17sbc04 in a pale blue area
- 17sbc05 in a reddish purple area
- 17sbc06 in a dark blue area

The area around 17sbc06 is of a very dark blue colour and this correlated with the higher Ti values (484.6 ppm). The area around 17sbc 05 is of a reddish purple colour and also has the highest Cr values (768.7 ppm). Other element concentrations also showed variations and some may be due to micro-inclusions.

Discussion

The link between colour and the presence of specific chromophores has been confirmed using spectroscopy and chemical analysis. As Cr only exists as Cr³⁺ in corundum, and is not involved in intervalence charge transfer (IVCT) for coloration, the direct relationship between Cr³⁺ and red coloration is more evident and explicable than, for example, the

Table V: Trace element contents of three colour zones in sample 1e2 obtained using LA-ICP-MS analysis.

Spot	17sbc04	17sbc05	17sbc06	standard rsd %
Colour	pale blue	reddish purple	dark blue	
Be	bdl	0.086	0.133	1.80
Mg	26.17	24.49	23.28	2.10
K	0.739	2.71	2.92	2.50
Ti	64.57	34.13	484.6	1.10
V	17	34.5	26.08	0.70
Cr	594.6	768.7	176.3	0.80
Mn	0.124	0.116	0.078	0.40
Fe	1780	1889	1764	2.20
Zn	1.34	1.13	2.18	4.60
Ga	42.10	59.09	59.52	0.40
Ge	0.299	0.169	0.99 (*)	1.60
Nb	0.015	bdl	2.49 (*)	0.40
Sn	0.147	0.111	0.215	1.00
Ta	0.04	bdl	0.81 (*)	1.60
Th	bdl	bdl	0.118 (*)	1.00
U	0.006	bdl	0.005	1.20

NB: Concentrations in ppm. bdl corresponds to below detection limit. The error margin is expressed in relative standard deviation (rsd). (*): Denotes a maximum value, which is too high, and probably due to unidentified factors in the raw data.

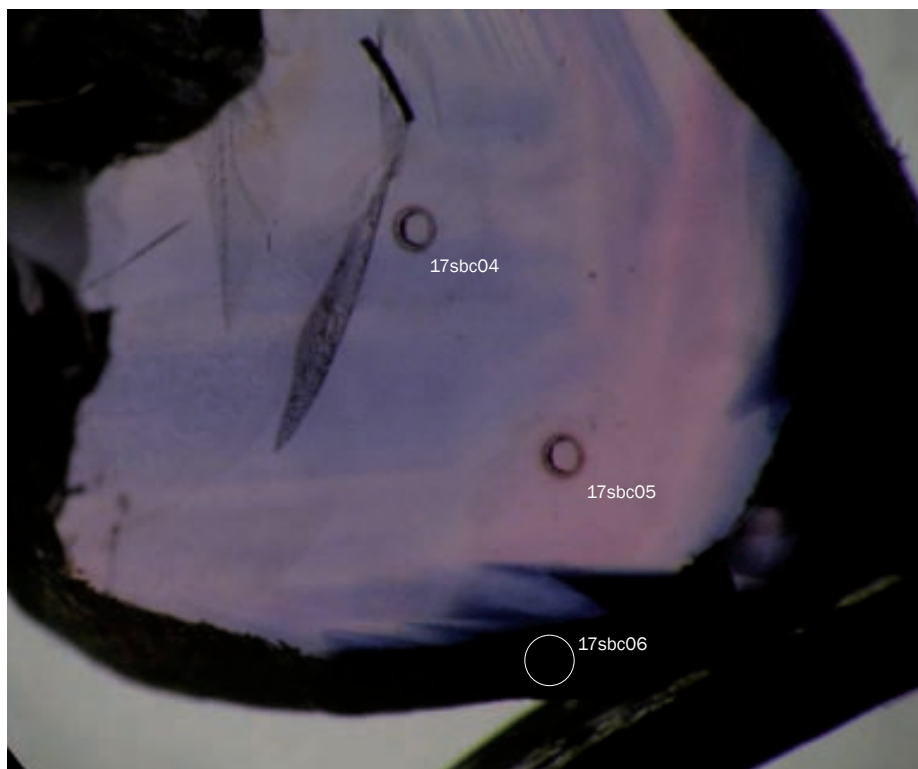


Figure 12: Magnified image of sample 1e2, showing three ablation craters caused by the laser during LA-ICP-MS measurements. The spots are about 0.16 mm across and barely visible to the naked eye.

Ruby and sapphire from Marosely, Madagascar

concentration and role of Ti^{4+} or Fe^{2+}/Fe^{3+} . Generally, Cr and Ti regulate coloration. Fe is present in sufficient quantity and is not the limiting factor, whereas V showed only a very small effect on colour variations.

Apart from Al, Fe and Cr, all other elements in Marosely corundum are present at ultra-trace levels (i.e. <1000 ppm). The LA-ICP-MS method is very useful with the possibility of localized measurement of low quantities of elements. But further calibration and quantification of different deposit types and occurrences is still required to enlarge the dataset and fulfil the potential of LA-ICP-MS as a more potent tool in determining the origin of specific corundum samples.

Quantitative results for elements such as Fe, Cr, Ti, V and Ga have been plotted by many authors (Abduriyim *et al.*, 2006; Muhlmeister *et al.*, 1998; Sutherland *et al.*, 1998; Schwarz *et al.*, 2000) in order to illustrate and search for criteria to distinguish corundum of different origins, based on their chemistry. A commonly used diagram is a logarithmic plot of wt% values Cr_2O_3/Ga_2O_3 vs. Fe_2O_3/TiO_2 . This approach has produced good results when attempting to discern two very different types of corundum; such as when comparing basaltic and non-basaltic sapphires. But considering that the Marosely deposit has been greatly altered by metasomatism and shows no great homogeneity with regard to the above-mentioned elements, this approach, as for many other deposits, is not effective.

The infrared spectral region between 3000 cm^{-1} and 4000 cm^{-1} shows absorption bands due to O-H bonds in the Marosely corundums. The nature of these is still widely debated and uncertain (Volynets *et al.*, 1972; Smith, 1995; Balmer *et al.*, 2006; AGTA, 2006; Beran *et al.*, 2006), but primarily, they are believed to be due to Al-hydroxide phases such as diaspore and boehmite. The three regions around 3160 cm^{-1} , 3309 cm^{-1} and $3600\text{--}3700\text{ cm}^{-1}$ are of most interest. The absence of a 3160 cm^{-1} peak does not imply heat treatment, since it is absent in 28 of the 35 untreated Marosely samples.

The presence of a number of peaks in these stones (e.g. 3160 cm^{-1} and 3309 cm^{-1}) proves that these IR peaks can occur in natural corundum and step-wise heat treatment should be undertaken to understand their evolution and specific nature. The peaks found in some stones between 3600 and 3700 cm^{-1} are probably due to mica and/or kaolinite.

Acknowledgements

The author wishes to thank Prof. Dr Henry A. Hänni and Dr Michael S. Krzemnicki of SSEF for thought-provoking discussions, suggestions to this paper and access to SSEF laboratory facilities. Jean-Pierre Chalain and Pierre Lefèvre are thanked for helpful comments and Luc Phan for help with photographs. Prof. Dr Thomas Pettke is thanked for help with LA-ICP-MS measurements at the university of Berne and Dr Federico Pezzotta for logistical help in Madagascar. Finally, the author is grateful to the Kommission für Reisestipendien der Akademie für Naturwissenschaften Schweiz SCNAT for financial assistance towards the completion of this research project.

References

- Abduriyim, A., and Kitawaki, H., 2006. Determination of the origin of blue sapphire using Laser Ablation Inductively Coupled Plasma Mass Spectrometry (LA-ICP-MS). *Journal of Gemmology*, **30**(1/2), 23–36
- Balmer, W.A., Leelawatanasuk, T., Atichat, W., Wathanakul, P., and Somboon, C., 2006. Update on characteristics of heated yellow sapphires. Poster, Proceedings of the 1st International Gem and Jewelry Conference, 3pp
- Beran, A., and Rossman, G.R., 2006. OH in naturally occurring corundum. *European Journal of Mineralogy*, **18**, 4, 441–7
- Bosshart, G., 1981. Die Unterscheidung von echten und synthetischen Rubinen. *Z. Dt. Gemmologische Gesellschaft*, **30**(3/4), 157–69
- Bruder, B., 1995. *Charakterisierung von Saphiren und Rubinen mit Hilfe von*

- Flüssigkeitseinschlüssen*. Unpublished Master thesis, University of Freiburg i. Br, Germany
- Cartier, L.E., 2008. *Gemmological and mineralogical investigations of corundum from Marosely, Madagascar*. Unpublished Master thesis (part 1), University of Basel, 93 pp
- Giuliani, G., Ohnenstetter, D., Rakotondrazafy, A.F.M., Fallick, A.E., Rakotosamizanany, S., Andriamamonjy, A., Ralantoarison, T., Razanatsheho, M., Dunaigre, C., and Schwarz, D., 2007. Les gisements de corindons gemmes de Madagascar. *Revue de Gemmologie A.F.G.*, **159**, 4–13
- Hattendorf, B., Bleiner, D., Guillon, M., and Horn, I., 2003. Quantitative multi-element analysis of minerals, fluid and melt inclusions by laser-ablation inductively-coupled-plasma mass-spectrometry. *Geochim. Cosmochim. Acta*, **67**(18), 3473–97
- Kiefert, L., 1987. *Mineralogische Untersuchung zur Charakterisierung und Unterscheidung natürlicher und synthetischer Saphire*. Diplomarbeit, Universität Heidelberg, 203 pp
- Kiefert, L., Schmetzer, K., Krzemnicki, M.S., Bernhardt, H.J., and Hänni, H.A., 1996. Sapphires from Andranondambo area, Madagascar. *Journal of Gemmology*, **25**(3), 185–209
- Krzemnicki, M.S., Hänni, H.A., Reusser, E., 2001. Colour-change garnets from Madagascar: comparison of colorimetric with chemical data. *Journal of Gemmology*, **27**(7), 395–408
- Krzemnicki M.S., 2004. Red and green labradorite feldspar from Congo. *Journal of Gemmology*, **29**(1), 15–23
- Moon, A.R., and Phillips, M.R., 1994. Defect clustering and color in Fe,Ti: α - Al_2O_3 . *J. Am. Ceram. Soc.*, **77**, 356–67
- Muhlmeister, S., Fritsch, E., Shigley, J. E., Devouard, B., and Laurs, B. M., 1998. Separating natural and synthetic rubies on the basis of trace-element chemistry. *Gems & Gemology*, **34**(2), 80–101
- Offant Y., 2005. *Charactérisation pétrographique et minéralogique du gisement a saphir de Sabambano*

Ruby and sapphire from Marosely, Madagascar

- (Madagascar). Unpublished Master Thesis, Université Paul Cézanne, Aix-en-Provence, France, 34 pp
- Ostertag, T., 1996. *Spezielle Anwendung der Raman-Spektroskopie in den Gebieten der Mineralogie, Petrologie und Gemmologie*. Unpublished Master thesis, University of Freiburg i.Br, Germany
- Peretti, A., Schmetzer, K., Bernhardt, H.-J., and Mouawad, F., 1995. Rubies from Mong-Hsu. *Gems & Gemology*, **31**(1), 2–26
- Pettke, T., 2006. *In situ laser ablation-ICP-MS chemical analysis of melt inclusions and prospects for constraining subduction zone magmatism*. Mineralogical Association of Canada Short Course, 36, 51–80
- Pezzotta, F., 2001. *Madagascar. A Mineral and Gemstone Paradise*. Extra Lapis, English No 1. Lapis International LLC, East Hampton, CT, 100 pp
- Ralantoarison, L. T., 2006. *Les corindons métamorphiques associés aux zones de cisaillement du sud de Madagascar: Le gisement de saphir de Sabambano (Sud-Est d'Ihoso)*. Unpublished DEA thesis, University of Antananarivo. 102 pp
- Ralantoarison, T., Andriamamonjy, A., Offant, Y., Giuliani, G., Rakotondrazafy, A.F.M., Ohnenstetter, D., Schwarz, D., Dunaigre, C., Fallick, A., Razanatsheho, M., Rakotosamizany, S., Moine, B., and Baillot, P., 2006. Les saphirs multicolores de Sahambano et Zazafotsy, région granulitique d'Ihoso, Madagascar. *Revue de Gemmologie A.F.G.*, **158**, 4–13
- Ramdohr, R., and Milisenda, C.C., 2006. A new find of sapphire placer deposits on Nosy-Bé, Madagascar. *Journal of Gemmology*, **30**(3/4), 144–54
- Rankin, A.H., Greenwood, J., and Hargreaves, D., 2003. Chemical fingerprinting of some East African gem rubies by laser ablation ICP-MS. *Journal of Gemmology*, **28**(8), 473–82
- Saminpanya, S., Manning, D.A.C., Droop, G.T.R., and Henderson, C.M.B., 2003. Trace elements in Thai gem corundums. *Journal of Gemmology*, **28**(7), 399–415
- Schmetzer, K., and Schwarz, D., 2004. The causes of colour in untreated, heat treated and diffusion treated orange and pinkish orange sapphires- a review. *Journal of Gemmology*, **29**(3), 149–82
- Schwarz, D., Petsch, E.J., and Kanis, J., 1996. Sapphires from the Andranondambo Region, Madagascar. *Gems & Gemology*, **32**(2), 80–99
- Schwarz, D., Kanis, J., and Schmetzer, K., 2000. Sapphires from Antsiranana Province, Northern Madagascar. *Gems & Gemology*, **36**(3), 216–33
- Smith, C. P., Kammerling, R.C., Keller, A.C., Peretti, A., Scarratt, K.V., Khoa, N.D., and Repetto, S., 1995. Sapphires from southern Vietnam. *Gems & Gemology*, **31**(3), 168–86
- Smith, C.P., 1995. A contribution to understanding the infrared spectra of rubies from Mong Hsu, Myanmar. *Journal of Gemmology*, **24**(5), 321–35
- Sutherland, F.L., Hoskin, P.W.O., Fanning, C.M., and Coenraads, R.R., 1998. Models of corundum origin from alkali basalt terrains: a reappraisal. *Contributions to Mineralogy and Petrology*, **133**, 356–72
- Volynets, F.K., Vorob'ev, V.G., and Stsepuro, N.A., 1972. Infrared absorption bands in corundum crystals. *Journal of Applied Spectroscopy*, **10**, 981–4
- Waite, K., 2000. *Mineralogical and gemmological analysis of corundum from Tunduru and Songea, Southern Tanzania*. Unpublished Master thesis, University of Basel, 74 pp

Websites

- AGTA Gemstone Update, 2007. FTIR intrigue. <http://www.agta.org/gtc/20070227-ftir.html#ftir> Accessed 10.07.2007
- Pezzotta, F., 2007. New Gem Localities in Madagascar. Accessed 16.10.2007 https://www.gia.edu/gemsandgemology/34468/new_gem_localities_in_madagascar.cfm

The Author

Laurent E. Cartier

Department of Geosciences, University of Basel, Bernoullistrasse 30, 4056 Basel, Switzerland
email: laurent.cartier@unibas.ch

Improve your grading skills by enrolling for the Gem-A

Advanced DIAMOND GRADING Course



This three-day certificated course is taught by a grader with 25 years' experience. Topics covered include:

- Use of the microscope to clarity grade and plot diamonds
- Colour grading and master stones
- Fluorescence grading
- Cut (measurements, proportions, symmetry and polish)

Courses are held at the Gem-A headquarters in Central London. Next course:

Wednesday 21 to Friday 23 April 2010

Fee: £680.00

For further information or to apply for the course, go to www.gem-a.com/education.aspx or contact Paveet Amrit on 020 7404 3334, email paveet.amrit@gem-a.com. Applicants must hold either our Gem Diamond Diploma or our Diamond Practical Certificate.



THE SCOTTISH GEMMOLOGY CONFERENCE

Friday 30 April to
Monday 3 May 2010

The Queen's Hotel, Perth

This popular event attracts speakers and participants from many corners of the world. The well-balanced programme of lectures has something for anyone with an interest in gems.

Speakers will include:

DR DIETMAR SCHWARZ
MARIA ALFEROVA
DAVID CALLAGHAN
GWYN GREEN
ALAN HODGKINSON
DR JACK OGDEN
DR DON HOOVER

Sunday afternoon will be devoted to displays, workshops and demonstrations, and a Field Trip will be held on the Monday morning.

Social events are held each evening, including the Ceilidh (dinner/dance) on the Saturday.

For further information or to book go to www.scotgem.co.uk or call Catriona McInnes on +44 (0)131 667 2199

Identification of dyed jadeite using visible reflection spectra

Yan Liu, Taijin Lu, Manjun Wang, Hua Chen, Meidong Shen, Jie Ke and Beili Zhang

Abstract: Burma jadeites are often dyed to improve their colour. Most dyed jadeites are identified using a microscope or a high resolution digital imaging system. However, when dye-related microscopic features are not clear, their visible reflection spectra can be used for identifying dyed jadeite rapidly and accurately. This visible spectral method can be used to identify both dyed-only jadeite (C type) and the dyed and impregnated jadeites (B+C type), which may otherwise be difficult to distinguish.



Introduction

Low-quality jadeites are often impregnated and/or dyed to improve their transparency and colour. Polymer-impregnated jadeite is classified as B type in the gem trade, and can be identified using FTIR spectroscopy (Fritsch *et al.*, 1992; Lu and Shigley, 2000).

Dyed jadeite is classified as C type, and is usually identified using visual imaging techniques with a microscope or a high resolution imaging system, since the dye is commonly visible in the pores or spaces between the inter-locking crystal fibres. Some dyed materials can be detected using X-ray fluorescence analysis. Hence, in most cases, 'C' jadeite can be easily identified by trained gemmologists. However, when high-quality colourless transparent jadeites with a fine-grained, compact and uniformly distributed texture of fibrous crystal are dyed, the characteristic microscopic features of the dyed jadeite may be unclear or hardly visible using traditional microscopy. Such pieces can be difficult to distinguish from jadeites of natural colour.

Natural green and lavender jadeites commonly display five characteristic spectral absorption lines in the visible wavelength range which are attributed

to their Cr and Fe contents (see Webster, 1994; Nassau, 2001; Zhang, 2006). Although the absorption lines of some transparent jadeites can be recorded with a gemmological spectroscope (GIA, 1990; Zhang, 2006), they generally cannot be easily observed using a hand spectroscope.

Since the spectra of most jadeites cannot be measured using the commercially available visible spectrophotometers generally used in gemmological laboratories due to their size, shape, lack of transparency and other factors, we report here a method to identify dyed jadeite by measuring the visible reflection spectra using a TrueColor spectrometer with dual integrating spheres. By combining reflection spectra in the visible range with IR absorption spectra, dyed-only and impregnated and dyed jadeites can be accurately identified.

Measurement and samples

Although jadeites range from translucent to opaque, only a small proportion of jadeites are transparent enough to yield transmission spectra. But reflection spectra obtained from translucent or opaque stones can be

measured both for colour grading by a colorimetric method and for the spectroscopic study of jadeites.

Reflection spectra of various jadeites were obtained using a new type of visible reflection spectrometer (TrueColor Spectrometer) developed by one author (Y.L.) for spectral measurement and colour grading of coloured diamonds and gemstones. This spectrometer has dual integrating spheres, one for providing illumination and spectral measurement and the other for hosting the sample, as shown in *Figure 1*. A collimating lens is installed in the measurement integrating sphere. The lens is focused on the aperture between the measurement and the sample integrating spheres. The reflected light from a measured jadeite with the transmitted light reflected back by the sample integrating sphere is collected by the lens, and then sent to the spectrometer by an optical fibre cable. A diffraction grating separates the light into a spectrum on a CCD array within the spectrometer. The computer receives the electronic signals generated by the CCD and converts them to a reflection spectrum, and then calculates colour and provides colour grades.

Identification of dyed jadeite using visible reflection spectra

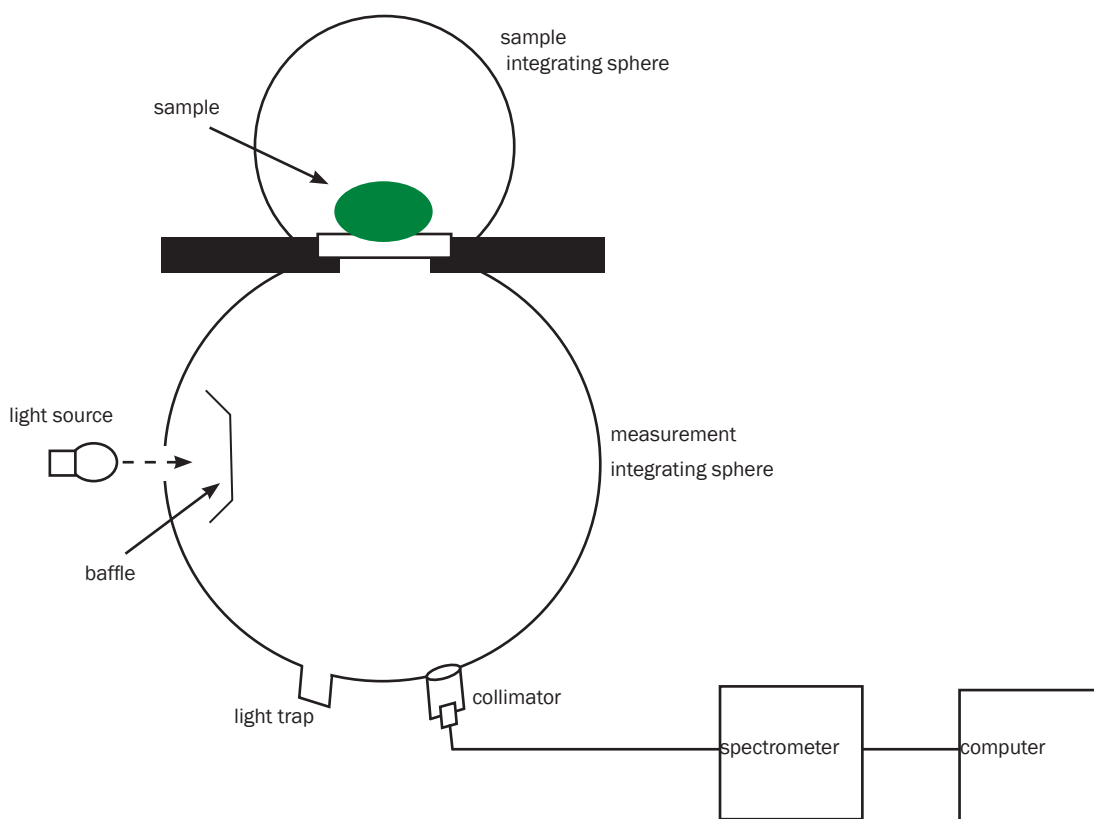


Figure 1: Schematic diagram of the TrueColor reflection spectrometer.

The sample integrating sphere provides an environment similar to that for visual observation of jadeite in the trade. If a jadeite is transparent, a portion of transmitted light is reflected back by the sample integrating sphere and enters the measurement process. Consequently, the

reflection spectrum of a translucent jadeite is significantly higher than that measured without an integrating sphere. More importantly, for the transparent jadeites, the measured reflection spectrum is similar to that observed on a white background in the trade.

Although the visible wavelength ranges only from 400 to 700 nm, the wavelength range of the spectrometer has been established at 380 to 760 nm to aim for more accurate colour measurement and grading. The extended wavelength range also makes it possible to measure the spectral features of gemstones and coloured diamonds in the 380 to 400 nm and 700 to 760 nm ranges for detailed study of such centres as GR1 at 741 nm in green diamonds.

Before taking a measurement, the spectrometer is calibrated by recording three spectra: that of a standard white tile, a standard black tile, and one without a tile. The procedure for measuring the reflection spectrum of jadeites is simple and quick: a jadeite is placed on the aperture between the measurement and sample integrating spheres, the sample integrating sphere is then fitted on the top, the measurement button on the screen of the computer is clicked, and a reflection spectrum will be collected and displayed on the screen. The whole measurement process takes about one



Figure 2: Three B+C type jadeite slabs typical of many hundreds examined.

Identification of dyed jadeite using visible reflection spectra



Figure 4: A carved Buddha pendant of B+C type jadeite.

minute. For many (opaque) jadeites where only reflection is measured, the sample integrating sphere is not necessary, and any size of specimen can be measured as long as it can be put on the spectrometer.

Many hundreds of natural, impregnated, dyed-only, and impregnated and dyed jadeites have been examined. Most samples have been green, but a few were lavender. A natural colourless jadeite slice was measured as a reference spectrum. Several jadeite slabs of B+C type with different colours (obtained from a jadeite factory in Guangdong province, China) were examined in detail using non-destructive imaging and spectroscopic techniques at the National Gemstone Testing Center, China (see Figure 2 for typical samples).

Results

Figure 3 shows typical reflection spectra in the visible wavelength range of naturally-coloured green jadeite and dyed green jadeite. That of the natural jadeite shows the characteristic absorption lines at 433 nm, 437 nm, 630 nm, 655 nm and 691 nm. The strengths of these five lines change significantly depending on the nature and saturation of the colour, but normally the 437 nm line is the strongest. The reflection spectra of many natural jadeites show only the absorption line at 437 nm, with the other four lines being very weak or invisible.

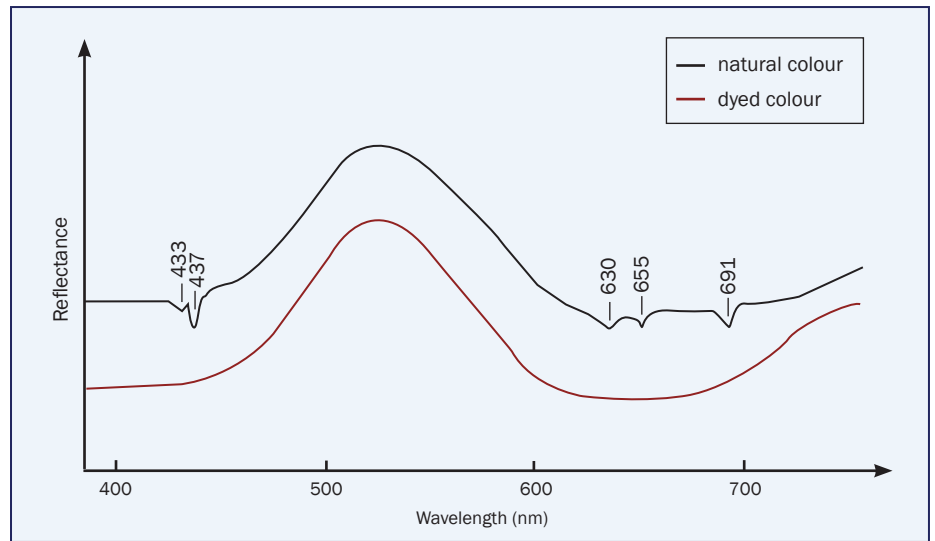


Figure 3: Reflection spectra of a typical natural green jadeite and a dyed green jadeite.

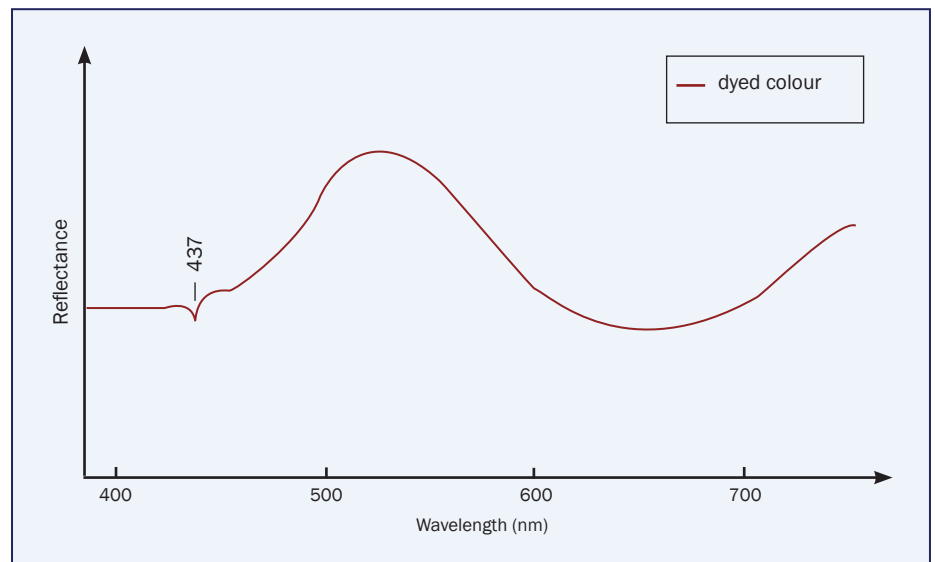


Figure 5: The reflection spectrum of a B+C type green jadeite with a weak 437 nm absorption line.

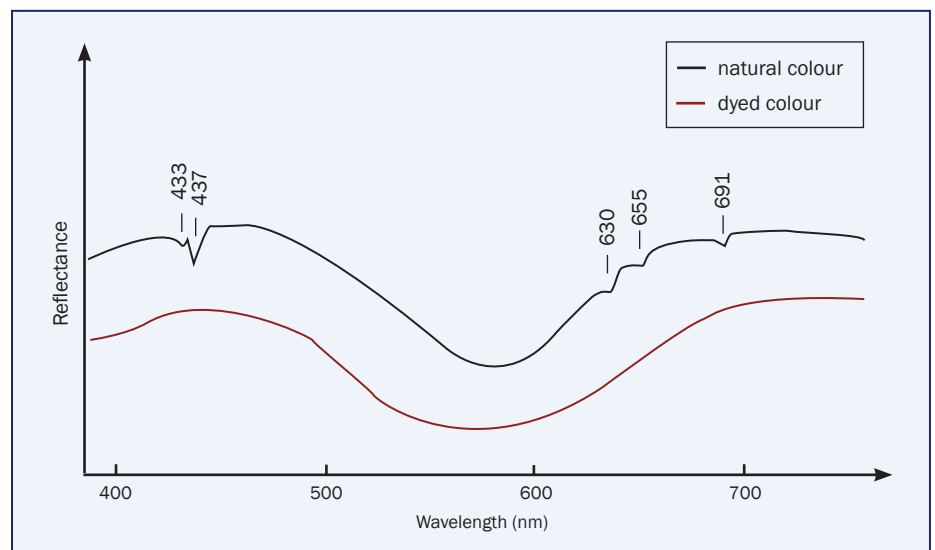


Figure 6: Reflection spectra of natural lavender jadeite and dyed lavender jadeite.

Identification of dyed jadeite using visible reflection spectra

Although the reflection spectrum of dyed green jadeite does not have the five sharp absorption lines (see *Figure 3*), its basic shape is similar to that of the naturally coloured green jadeite, thus appearing similar in colour. Indeed, the two greens cannot be distinguished using only the naked eye.

Figure 4 shows a B+C type of green jadeite Buddha pendant, and its reflection spectrum is the same as the dotted line spectrum shown in *Figure 3*. This is typical of most B+C type green jadeites.

Although only a few of 'B+C' jadeites with an enhanced green colour due to dye treatment show a weak 437 nm absorption line (*Figure 5*), almost all show a relatively strong and broad band at longer wavelengths near 680 nm. In other words, a weak 437 nm absorption line together with a broad absorption band and a long wavelength is a diagnostic feature of a B+C type jadeite. The long wavelength transmittance bands visible in *Figure 5* are probably the reason that such dyed jadeite appears red under the Chelsea Colour filter.

The spectrum of natural colourless jadeite lacks any sharp absorption lines, so when such material is dyed, it too may lack sharp absorption lines and appear similar to the dotted line spectrum in *Figure 3*.

The five characteristic absorption lines in the reflection spectra of naturally coloured green jadeites are also present in naturally coloured lavender jadeites (see *Figure 6*). The dotted line in *Figure 6* shows the typical spectrum with similar broad absorption bands but without the five sharp spectral lines.

Discussion and conclusions

Jadeites are translucent to opaque, and not sufficiently transparent for transmittance spectra to be routinely obtained by the kind of UV-Visible spectrophotometer used in most gemmological laboratories. To study the spectral properties and to measure the colours of jadeites, we have to measure the reflection spectra.

Naturally coloured green jadeites from Burma typically show five absorption lines at 433 nm, 437 nm, 630 nm, 655 nm and 691 nm in their reflection spectra as shown in *Figure 3*.

In contrast, the reflection spectra of most dyed green jadeites do not show these five absorption lines and this absence is an indication that the measured jadeite has been dyed, particularly for those jadeites with vivid green colours. The reflection spectra of both dyed only (C type) and impregnated and dyed (B+C type) jadeites can be identified by this method. Since the 437 nm absorption line is the strongest of the five lines, it may be detected in some of the dyed vivid green jadeites, which suggests that the starting material was a low grade pale green jadeite. The reflection spectra of such dyed green jadeites also show a relatively strong broad absorption band above about 680 nm, which is related to the dye. The existence of both the weak 437 nm absorption line and this broad band at the longer wavelength in vivid green jadeites indicate that they are low saturation jadeites that have been dyed. In fact, any vivid green jadeite with only a weak 437 nm absorption line suggests that it has been dyed, since natural vivid green jadeites should show all five absorption lines.

Identification of some dyed-only green jadeites without clearly visual microscopic features can be a challenge using only traditional microscopic observation and FTIR techniques, but measurement of their reflection spectra by the TrueColor spectrometer with dual integrating spheres can provide a rapid and effective technique for their identification and distinction from natural jadeite.

The reflection spectra of naturally coloured lavender jadeites also show the five narrow absorption lines characteristic of green jadeite, whereas dyed lavender jadeites only show broad absorption bands in their reflection spectra.

Acknowledgement

The authors thank Haibo Li and Jian Zhang of the National Gemstone Testing Center, China, for their valuable comments and comparative data for some examined samples.

References

- Fritsch, E., Wu, S.T., Moses, T., McClure, S.F., and Moon, M., 1992. Identification of bleached and polymer-impregnated jadeite. *Gems & Gemology*, **28**, 176-87
- GIA., 1990. *Gem Reference Guide*. Gemological Institute of America, Santa Monica, California, USA
- Lu, T., and Shigley, J.E., 2000. Non-destructive testing for identifying natural, synthetic, treated, and imitation gem materials. *Materials Evaluation*, **43**, 1204-8
- Nassau K., 2001. *The Physics and Chemistry of Color*, 2nd edn. John Wiley & Sons, New York
- Webster, R., 1994. *Gems, Their Sources, Descriptions and Identification*, 5th edn. Revised by P.G. Read. Butterworth-Heinemann Ltd., Oxford
- Zhang, B. (Ed.), 2006. *Systematic Gemmology*. Geological Publishing House, Beijing, p.550

The Authors

Yan Liu

Liu Research Labs, South El Monte, California, USA

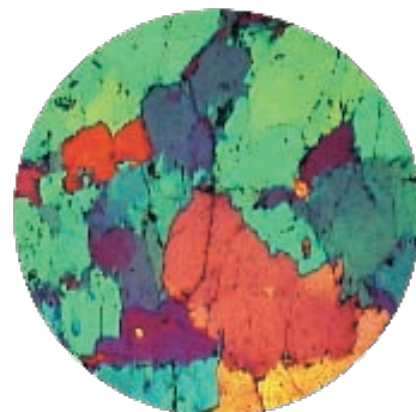
Taijin Lu, Manjun Wang, Hua Chen, Meidong Shen, Jie Ke and Beili Zhang

National Gems & Jewelry Technology Administrative Center, 21-22F, C Building, Global Trade Center, North 3rd Ring, Beijing 100013, P.R. China

Jadeite jade from Myanmar: its texture and gemmological implications

Guanghai Shi, Xia Wang, Bingbing Chu and Wenyan Cui

Abstract: Jadeitites, rocks consisting predominantly of jadeite, are the source of the precious stone known as feitsui by the Chinese. Jadeitites vary greatly in transparency, compactness and toughness due to their diverse textures and microstructures. The authors consider these textures in two major groups: (i) primary and (ii) deformed and recrystallized. In the first group, the rocks are coarse-grained with mosaic, granitoid or radial textures and some crystals are chemically zoned; such rocks can be porous. In the second group are jadeitites of finer grain size, generally formed by metamorphism of the coarse-grained jadeitites, with textures showing variable preferred orientation of crystals, mechanical twinning, shear zones, development of sub-grains, serrated high-angle sutured grain boundaries, or a 'foam' pattern. Texture, compactness and colour variation has generated a large number of trade names. The most precious jadeite jades are described as 'icy' or 'glassy', which relates to the quality of their transparency. Studies of jadeite textures have gemmological applications both in identifying and grading rough material and in the design, fashioning and grading of manufactured articles. Geologically, textures provide evidence of the formation and metamorphism of the whole range of Myanmar jadeitites and it is probable that these processes are linked to the major Sagaing strike-slip faults.



Keywords: classification, gem trade terminology, jadeite, metamorphic textures, Myanmar, petrography

Introduction

The jade which dominantly consists of jadeite crystal aggregates has over the years attracted several names in different countries. The Chinese call jade feitsui (or feicui), which means jadeite jade, with no implications as to its source (e.g., Ouyang, 2003). Westerners simply call it jadeite (e.g., Damour, 1881), which sometimes causes confusion, since jadeite is also the mineral name for sodium-aluminium silicates of the pyroxene group. The Burmese use the term Myanmar jade to

designate jadeite jade from the Jade Tract in Myanmar (e.g., Nyan Thin, 2002). According to current gemmological opinion in China, jade is defined as a natural polycrystalline aggregate with fine compact texture, high toughness, good lustre and a medium to high degree of translucency. Both feitsui and medium- to low-quality jadeite rock are, petrologically, jadeite, composed mainly of jadeite and other sodic- and sodic-calcic clinopyroxenes such as omphacite and kosmochlor. Jadeite is a high pressure

metamorphic rock deposited from jadeitic fluids (Ouyang, 1984; Harlow and Olds, 1987; Hughes et al., 2000; Harlow and Sorensen, 2005; Shi et al., 2003, 2005a, 2008; Yi *et al.*, 2006). However, not all jadeitites have the qualities required of feitsui, because they may have coarse-grained textures which are variably porous and therefore lack the coherence which is desirable for carving materials. Jadeite which has the qualities of precious jade is rarely found even in the best deposits in Myanmar.

Jadeite jade from Myanmar: its texture and gemmological implications

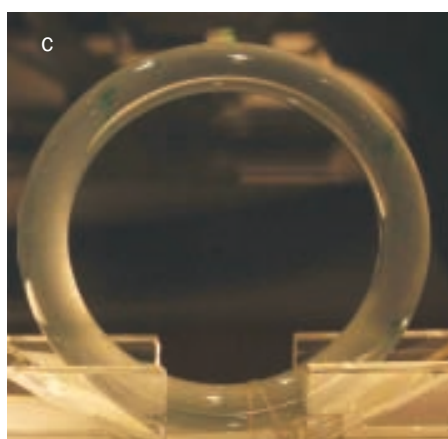


Figure 1: The glassy feitsui (green and colourless jadeite jades) from Myanmar. (a) A necklace of 15 exceptionally bright emerald green oval cabochons; (b) a ring with an imperial green oval cabochon; (c) a colourless bangle.

Having been mined for more than 300 years, the Myanmar jadeite areas, called the Myanmar Jade Tract, still produce the emerald green imperial jadeite jade which is fashioned as cabochons for rings, bracelets, pendants and other jewellery pieces (Figure 1), but on precious jadeite, research has so far been incomplete. Previous mineralogical and gemmological studies on jadeites have dealt with mineral and chemical compositions, fluid inclusions, and with which agents cause colour in jadeite (Gübelin, 1965a,b; Ouyang, 1984; Harder, 1995; Htein Win and Naing Aye Myo, 1994, 1995; Hughes *et al.*, 2000; Johnson and Harlow, 1999; Shi *et al.*, 2003, 2005a, b, 2008). However, there has been little understanding about the primary textures of the Myanmar jadeite materials, and much less about their deformed textures or microstructures, and the relationship of both kinds of texture to jade qualities. Also the process of transformation of coarse-grained to fine, compact jadeite has not been

explained. Although Ouyang (2000) and Shi *et al.*, (2004) have reported on some textures of Myanmar jadeites, the focus has been on their grain sizes, metasomatic textures and brittle deformation, without giving detailed descriptions of the deformed and recrystallized textures and gemmological applications. In this investigation, we present the primary and deformed textures of white jadeite materials (including icy to glassy jades) from Myanmar, attempt to establish correlations between textural features and jade qualities, and discuss the gemmological applications and implications.

Geological setting

Myanmar jadeites occur within the N–S striking Hpakan ophiolite complex which is about 50 km long and 5–10 km wide, situated in the east of the Indo-Myanmar Range and north of the Central Myanmar Basin. The ophiolites straddle a fault which is possibly a branch of the north Sagaing Fault (Figure 2). Geographically, the Indo-Myanmar Range is flanked on the east by the Central Myanmar Basin, and the national border between Myanmar and India generally follows the high points of the Range. Geologically, along the eastern boundary of the Range is a line of discontinuous ophiolite and ophiolite-derived blocks. In this terrain accumulation and deformation of rocks have taken place within a zone where oceanic crust of the Indian plate has been subducted beneath the Burmese plate with intra-oceanic features (Shi *et al.*, 2009). Based on ages of zircon inclusions, this subduction and formation of some jadeite probably took place in Upper Jurassic times (Shi *et al.*, 2008). The Central Myanmar Basin (16°N–25°N, 94°E–97°E), consists of low land between the Indo-Myanmar Range and the China-Myanmar high land. The Sagaing fault is a major strike-slip dextral or right-lateral continental fault that extends over 1200 km and connects to the Andaman spreading centre at its southern end. It has been interpreted by some authors as a plate boundary between India and Indochina (LeDain *et al.*, 1984) and accommodated nearly 60 % of the relative

Jadeite jade from Myanmar: its texture and gemmological implications

motion between the two plates. Two low-angle branch faults connect directly to the main fault at its northern end, and a sub-parallel fault to the west is also a location for jadeitites (Bertrand and Rangin, 2003; Morley, 2004).

The Hpakant ophiolite complex consists mainly of serpentized peridotite, chromite-bearing peridotite, metagabbro and metabasalt. Also within the complex are jadeite veins or blocks, usually separated by sodic- and sodic-calcic-amphibolites, some of which can contain the rare pyroxenes kosmochlor and omphacite (Ouyang, 1984; Harlow and Olds, 1987; Hughes *et al.*, 2000; Shi *et al.*, 2003, 2005a; Yi *et al.*, 2006). The jadeite veins, e.g. the one at the Maw Sit mine near the north end of the Jade Tract, are almost vertical, strike N-S, are 1.5 to 5 m wide, and 5 to 100 m long. These veins are crosscut in some places by thin veins of late-stage albitite, which are commonly less than 5 mm wide. Adjacent to the peridotites, there are high-pressure rocks such as phengite-bearing glaucophane schists, stilpnomelane-bearing quartzites, and amphibolite facies rocks such as garnet-bearing amphibolites and diopside-bearing marbles (Shi *et al.*, 2001).

Primary and deformed textures

A few jadeitites retain an undeformed massive structure, with euhedral to subhedral jadeite prismatic crystals which can exceed 20 mm in length. Most jadeitites, however, have been deformed and are fine-grained. Accordingly, the jadeite samples are described in two textural groups: 1) with primary texture and 2) with deformed, recrystallized texture.

The primary textures

Primary texture is defined as that of jadeite which has formed through deposition from a jadeitic fluid within its host peridotite/serpentine and has undergone little or no ductile deformation. These jadeitites are coarse-grained and to variable degrees, porous; their quality is not considered as precious (see *Figure 3*) but they can be utilized as B-jade materials

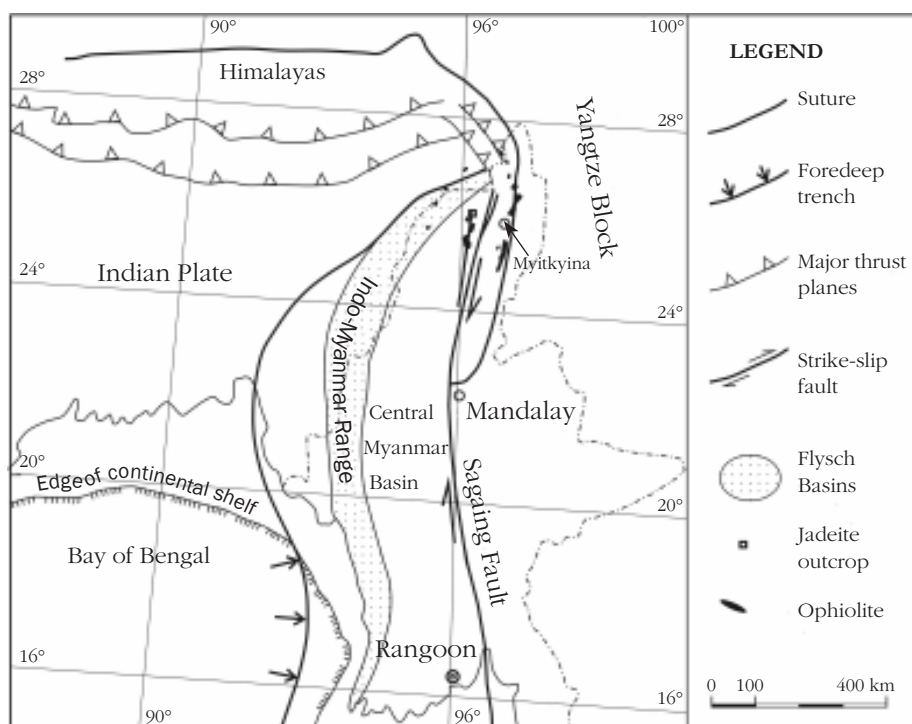


Figure 2: Simplified tectonic map of northern Myanmar. The jadeite deposits straddle a fault adjacent to the northern end of the Sagaing Fault and which is possibly a branch of it. The Fault is active and interpreted by some geologists as a plate boundary between India and Indochina accommodating nearly 60 % of the relative motion between the two plates (modified after Morley, 2004; Chhibber, 1934).

Materials and methods

From more than 150 samples collected in the Myanmar jadeite area, we selected 20 white jadeitites of which four were coarse-grained with granite-like appearance, and 16 were fine-grained and chosen to represent a range of transparencies from translucent to icy and glassy semi-transparency. All samples were prepared as polished thin sections. Microscopes at the Institute of Geology and Geophysics, Chinese Academy of Sciences (IGGCAS) and at the Ruhr-University Bochum (RUB), Germany, were used for extensive textural and microstructural observations on each section and to obtain representative photomicrographs taken in polarized and cross-polarized light. Cathodoluminescence (CL) imaging was also performed on the thin sections and representative images of the undeformed and deformed jadeite materials were acquired.

The chemical compositions of the undeformed and deformed jadeites were obtained using electron probe microanalysis (EPMA) using a CAMECA-SX-51 at the IGGCAS with an operating voltage of 15 kV and a beam current of 12 nA. The microprobe standards comprise synthetic and natural jadeite, chromite, pyrope, amphiboles, feldspar and clinopyroxenes. Backscattered electron (BSE) images, which indicate the spatial distribution of the different elements, were also acquired. All samples were determined to consist of jadeite with more than 90 % of the jadeite molecule (Jd).

The orientations of the jadeite crystals were determined using electron backscatter diffraction (EBSD). The EBSD patterns and the orientation contrast images (OCI) were acquired using a scanning electron microscope (SEM) LEO 1530 at the RUB with field emission gun and forescatter detector, operated at an accelerating voltage of 25 kV, with the section tilted over 70° and a working distance of 25 mm. The EBSD patterns were indexed with the hkl software 'CHANNEL 4'.

Jadeite jade from Myanmar: its texture and gemmological implications

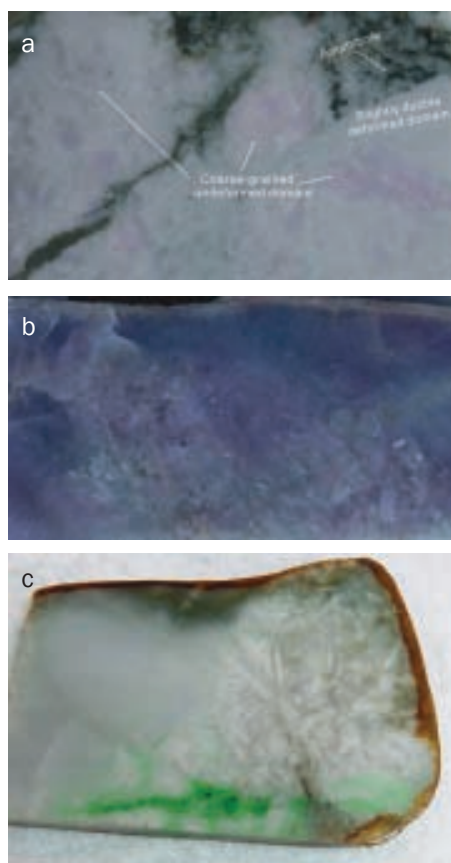


Figure 3: Cut jadeite samples showing undeformed, coarse-grained jadeite domains observed within and/or adjacent to slightly deformed jadeite aggregates. Sample widths (a) 30 cm, (b) 10 cm and (c) 12 cm.

and subject to acid-bleaching and resin-filling. The primary textures consist of zoned semihedral to euhedral jadeite crystals in mosaic and granitoid patterns.

Jadeite crystals in the mosaic and granitoid textures (Figure 4a) can be more than 3 cm long, and can be relatively even-grained (homogranular) or porphyritic. Most crystals are prism-shaped with flat contacts and random orientation. In some rocks, the crystals are in radial clusters. These jadeite crystals probably formed simultaneously with mosaic or granitoid textures. Mostly crystals have zones with slightly different extinction directions under cross-polarized light (Figure 4b) and this indicates some chemical variation. Cathodoluminescence imaging is even more effective in detecting such variation and can show distinct oscillatory zoning in crystals with no obvious optical variation: Figure 4c shows crystals with vivid blue, pink and yellow zones (see also

Harlow, 1994; Sorensen et al., 2006). BSE images of the same area display almost the same oscillatory zoning patterns as the CL images, and are indicative of compositional zoning. With the aid of EPMA, we found that jadeites within the dark CL zones are very pure with more than 98 mol. % Jd, whereas 5-10 mol. % Di (diopside) is present in the bright CL zones (see details in Shi *et al.*, 2005b).

Due to these zonal differences in chemical composition, each jadeite crystal will have zones with variable refractive indices, thus producing optical interfaces or distortion between adjacent zones when light transmits. Therefore, the transparency of a zoned jadeite crystal will be less than that of an unzoned one.

Crystals in primary textured jadeites also have distinct cleavages and fluid inclusions (Shi *et al.*, 2000, 2005b) which will decrease their transparency further.

The deformed, recrystallized textures

These are the textures of jadeites which have experienced shear stress, tectonic movement, apparent ductile deformation and recrystallization of their jadeite grains. The boundaries between the primary and recrystallized textures can be seen by careful examination of some hand specimens (Figure 3), but they are better seen and more distinct under the microscope. As shown in Figure 5, primary jadeite with one large crystal in excess of

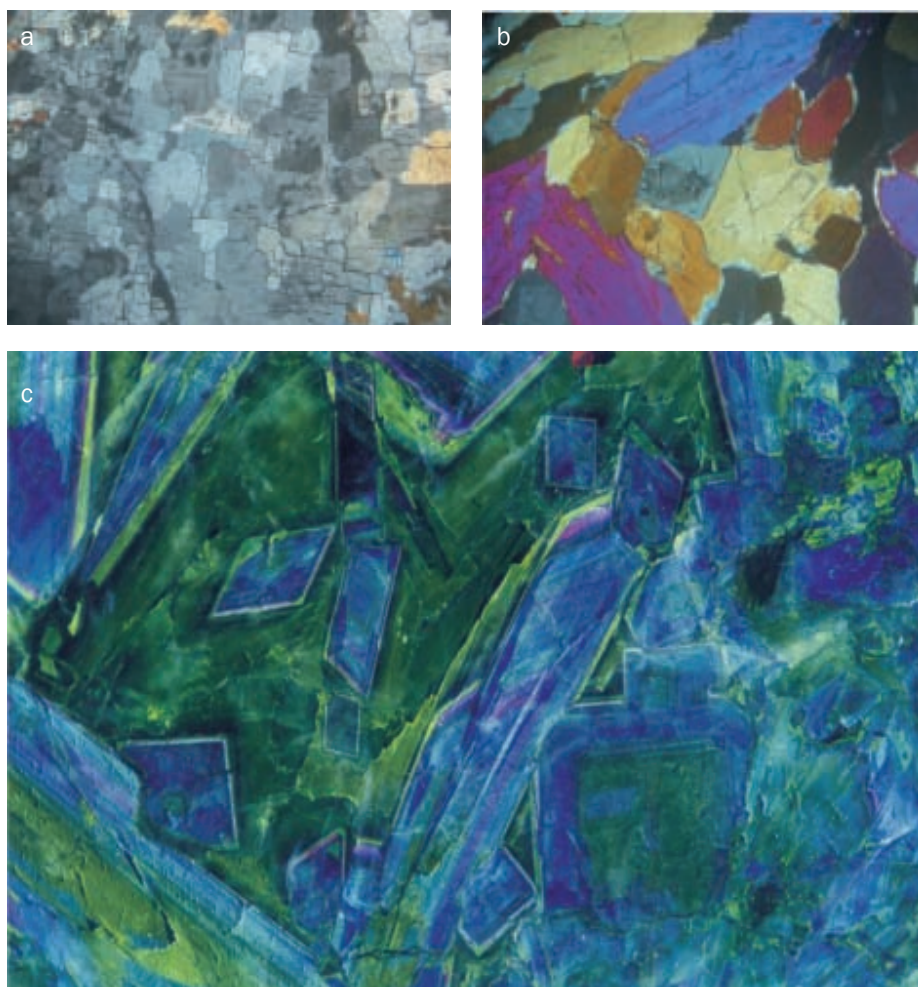


Figure 4: Representative primary textures of undeformed Myanmar jadeites: (a) Thin section photomicrograph of mosaic or granoblastic texture consisting of randomly orientated jadeite crystals with clearly visible cleavage planes (cross-polarized light, section width 2.5 mm); (b) Jadeite crystals intergrown in a hypidiomorphic texture. The pale yellow crystal near the centre has a patchy darker rim representing some compositional zoning (thin section cross-polarized light, section width 2.5 mm); (c) Complex rhythmical zoning patterns in jadeite crystals made apparent by cathodoluminescence imaging (section width 1.25 mm).

Jadeite jade from Myanmar: its texture and gemmological implications

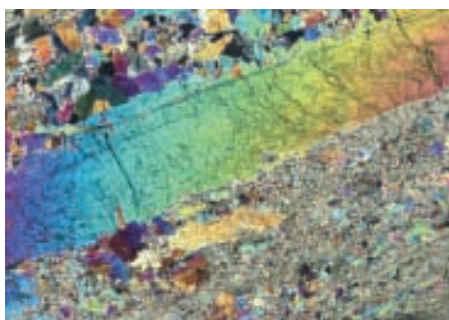


Figure 5: A 20 mm wide section showing the junction between coarse undeformed jadeite (middle and upper left) and fine deformed jadeite domains (lower right). The original undeformed jadeite evidently had a porphyritic texture.

20 mm, is in contact with microcrystalline jadeite containing fragments of primary texture, suggesting that deformation and recrystallization occurred heterogeneously at the expense of the primary texture. With extensive deformation and recrystallization, the jadeites become nearly homogeneous in chemical composition, containing 95-98 mol. % Jd and display no compositional zoning (see detail in Shi *et al.*, 2005b). A number of sub-types of the deformed and recrystallized textures can be recognized, probably related to the deformation mechanism, and these are: textures with different degrees of preferred orientation of elongated crystals; sub-grain; micro-shear; sutured grain boundaries; mechanical twinning; and recovery texture. These are described below.

Textures with preferred orientation

Myanmar jadeites are composed dominantly of elongate jadeite crystals with length/width ratios (aspect ratios) ranging from 2.0 to 20; some are even fibrous. The grain sizes in this sub-group vary greatly, from thin fibres several micrometres wide to prisms more than 20 mm long and several mm wide. Microscope observations and EBSD results show that most of the jadeite aggregates have both shape-preferred orientations (SPO) and crystallographically preferred orientations (CPO). No obvious chemical zoning in jadeite crystals has been found in this texture. Sections of near-glassy jadeite jade (Figure 6a) reveal that their textures consist of very tiny jadeite grains with pronounced SPO and CPO, and



Figure 6: Thin sections showing semi-orientated to preferred orientated jadeite crystals in feitsui from Myanmar: (a) Fine-grained, orientated and compact texture of a near-glassy jade (section width 2.5 mm, cross-polarized light); (b) Semi-orientated grains of intermediate size form a translucent jade (section width 2.5 mm, cross-polarized light).

indistinct grain boundaries; whereas translucent jadeites with an exterior texture reminiscent of cooked sticky rice, have textures with larger grains of lower aspect ratio, more distinct grain boundaries and a lower degree of preferred orientation (Figure 6b). Taking into account previous work on this topic (Ouyang, 2003; Shi *et al.*, 2004), it is concluded that the sizes, shapes, crystallographic orientations and features of the grain boundaries of the jadeite crystals are closely correlated to a jade's transparency; the finer and more preferred the orientation (with a homogeneous extinction direction), and the more indistinct the grain boundaries are, the better the transparency.

Sub-grain

An example of Myanmar jadeite showing development of sub-grain texture is shown in Figure 7. Lines of tiny sub-grains are visible across some of the larger jadeite crystals and mark lines of shear stress and recrystallization. In Figure 7 areas of similar interference colour but consisting of a number of grains represent the original larger jadeite crystals. Most of the boundaries among sub-grains are distinct, but a few are still indistinct. These sub-grains are almost homogranular and tightly interlocking. If there is continued or resumed stress, there can be further generation of sub-grains and reduction in grain size to less than 0.05 mm. When shearing and recrystallization has been prolonged and thorough, textures resembling that in Figure 6a are developed. Generation of sub-grains

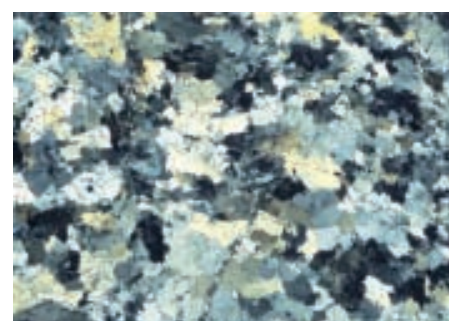


Figure 7: Photomicrograph in cross-polarized light of very compact sub-grain aggregate in Myanmar jadeite (section width 10 mm), in which some precursor grains show sutured boundaries.

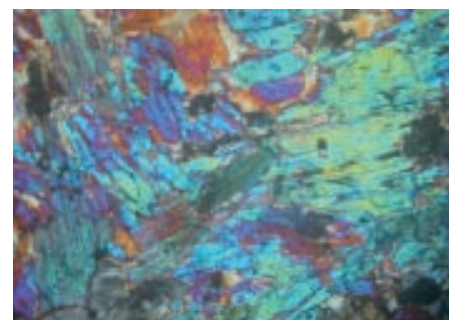


Figure 8: Photomicrograph showing medium to coarse jadeite crystals with cleavage and polysynthetic mechanical twinning in Myanmar jadeite. The presence of twinning is revealed by the parallel bands of alternating interference colours; some are slightly bent. (Section width 2.5 mm, cross-polarized light).

is the main way of reducing grain size in a rock. This takes place by means of dislocation of boundaries and change in the angular mismatch between the two sub-grains. Normally 10-15 degrees misorientation among the newly-generated grains is commonly quoted (e.g., Hirth and Tullis, 1992).

Jadeite jade from Myanmar: its texture and gemmological implications

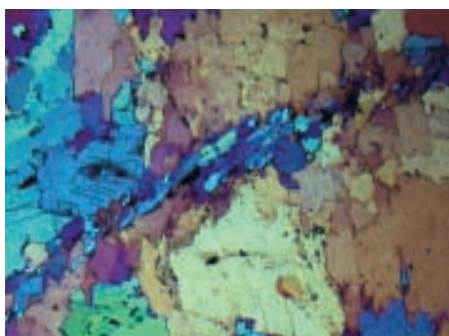


Figure 9: Section of medium to coarse-grained jadeite crossed by a zone of shearing which is marked by smaller more orientated crystals. Section 2 mm across, cross-polarized light with colours enhanced with inserted gypsum plate.

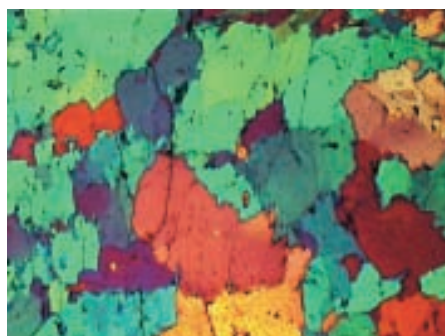


Figure 10: Thin section showing jadeite crystals with serrated high-angle sutured boundaries. Section 2 mm across, cross-polarized light with colours enhanced with inserted gypsum plate.

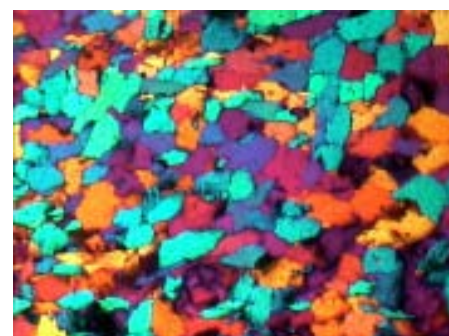


Figure 11: Thin section of jadeite with a recovery texture resembling foam and showing a number of grains in the aggregate with triple junctions close to 120°. Section 2 mm across, cross-polarized light with colours enhanced by inserted gypsum plate.

Mechanical twinning

Generation of mechanical twinning is a stage in the process of grain size reduction; it commonly occurs in calcite, corundum, diamond and feldspar, but seldom in jadeite. So far, natural mechanical jadeite twinning has only been found in ultra-high pressure rocks and is regarded as the result of syn-seismic loading beneath the brittle-

plastic transition conditions for such rocks (Trepman and Stöckhert, 2001; Orzol *et al.*, 2003). In Myanmar, mechanical twinning has occurred in both pure jadeite and in surrounding amphibolite, and some twinned crystals have also been bent (Figure 8). These occurrences are useful for understanding how jadeite jade may form from the coarse-grained jadeite.

Micro-shear zones

In some jadeite jades, veinlets or lines, 10–100 mm long and about 1.0 mm wide, can be distinguished by their different colour and better transparency. They are a kind of deformed and recrystallized texture or microstructure described as micro-shear zones, which have not been distinguished before. They are not cracks, but do resemble ‘healing fractures’ and were formed by means of ductile deformation (e.g. Tullis and Yund, 1985). They are not real repairs, because they are part of an ongoing process of transformation of the rock, and are thus different from a simple healing texture. Micro-shear zones are characterized by tiny elongate jadeite crystals (like stacked tiles) with pronounced orientation (both SPO and CPO) at low angles to the shear zone walls (Figure 9). Some jadeite crystals crossed by a fracture or shear zone have conjugate profiles and crystallographic orientations suggesting that they are from one intact precursor crystal; the newly generated jadeite crystals in the shear zone have formed at the expense of this intact crystal. This is another cause of grain size reduction, of CPO, and ultimately of a tougher more transparent jadeite.



Figure 12: Myanmar jadeite jade showing abrupt changes in appearance. This is usually accompanied by changes in texture which are as important in understanding jades as inclusions are in other gemstones. Note that the appearance of jade in the centre resembles ‘cooked sticky rice’, but in the left of the picture looks like ‘porcelain’. Length of carving 10 cm.

Sutured grain boundaries

Some translucent to transparent jadeites consist of crystals with sutured edges at high angles to adjacent grains and without interstitial spaces (Figure 10). They are the result of an integrated deformation process including dislocation,

Jadeite jade from Myanmar: its texture and gemmological implications

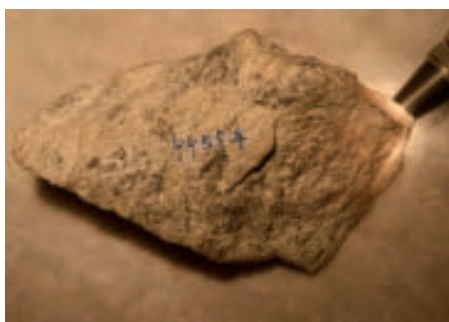


Figure 13: A 'gamble stone' from Myanmar; the small polished window at one end is not sufficient to show the quality of the other part of the stone, but the patchy presence of some orientated crystals in the skin indicate good potential for a valuable piece. Stone length 13 cm.

granular flow and mass transfer (e.g. Tullis and Yund, 1985). The different boundary shapes are the result of different aspects of this process and could influence jade quality. The jades with such intergrown crystal boundaries have excellent toughness, even with grain-sizes up to 1–2 mm.

Recovery textures

The term 'recovery' in this context refers to textures formed through mutual annihilation and/or polygonization during or after the peak deformation, resulting from reduction in the strain produced by the deformation; such textures can show grain dislocation, development of sub-grains, polygonal patterns and recrystallization. Although some of these textures may be confused with the primary fine mosaic texture, they differ by the presence of the following features: the grains are crystallographically orientated, confirmed by EBSD results, they are nearly equal in size, mostly less than 0.08 mm, and have no obvious prismatic habit. The grain boundaries are straight or gently curved (resembling foam), a texture also similar to the quartz grains in mylonitized quartzite (e.g. Tullis and Yund, 1985), but not so far reported in jadeitite. In Myanmar jadeitites with 'foam' texture, a few grains meet at perfect triple junctions with some boundary angles near 120° (Figure 11). The jade with 'foam' texture usually has a high transparency, described as icy or glassy.

Discussion

Gemmological application

The importance of textures to the jadeite jades is comparable with that of inclusions to their host gemstones. Feitsui in Myanmar consists of jadeite aggregates of many different textures. In general, most carvings that appear similar probably have the same texture, whereas the parts and domains of different appearance reflect changes in texture (see Figures 3, 5 and 12). It is clear that the appearance and the transparency of jadeite jade are closely related to texture and if such correlations can be established, we could then predict the texture of a jade based on its appearance. The nature of the aggregate and its relative toughness could then be estimated quickly and non-destructively. Furthermore, if comparable

data were collected from jadeite jades around the world, it may be possible to determine unique features for each locality. By studying textures of rough feitsui it is possible to identify, grade and evaluate them quickly. For instance, although bleached jadeite (B-jadeite) can be identified accurately using ultraviolet luminescence and the infrared spectrometer (see Fritsch *et al.*, 1992), a quick identification can be made using only the naked eye or a 10x lens. In this situation one should look for any damage to texture caused by bleaching (see Tay *et al.*, 1993, 1996). As for grading jadeite jade, toughness is an important factor, and the tougher a jade is, the better its quality. In this respect jadeitites with serrated high-angle sutured and interlocking grain boundaries are probably tougher than other jadeitites of similar grain size.



Figure 15: Another example of correlation between the texture and design in jadeite art; the coarsest part was designed as a rounded base and the 28th Olympics logo was carved in an area of relatively fine quality. Height 15 cm.

Jadeite jade from Myanmar: its texture and gemmological implications



Figure 14: Dragon's head carved in the finest pure white jadeite jade but left unpolished to enhance the atmosphere of the piece: an example of the use of texture and colour in design of the jadeite carving. Height 6.5 cm.



Figure 16: The green parts in two Myanmar jadeite carvings are finer and more transparent than their neighbouring white regions, indicating differences in deformation textures. Lengths of carvings 6 cm.



Figure 17: The green parts in this Myanmar jadeite bangle are finer and more transparent than their adjacent white regions; another example of differences in deformation textures between green and white regions, probably formed under the same P-T and stress conditions. Bangle diameter 5.8 cm.

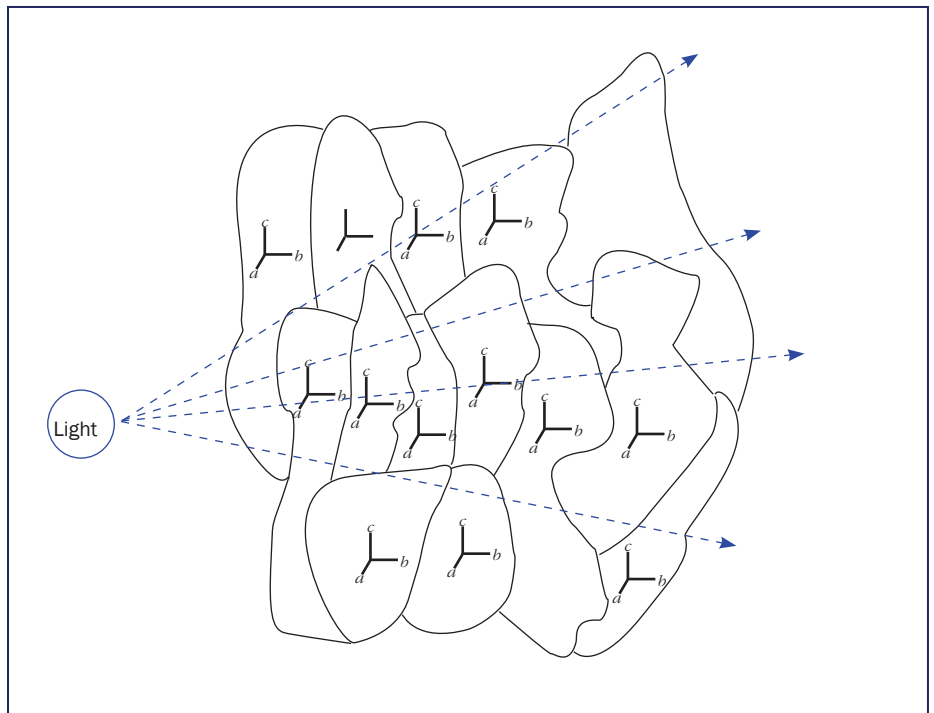


Figure 18: A model of the ideal texture for the best glassy jadeite aggregate. The jadeite crystals are fine-grained, with pronounced crystallographical orientation; they are compactly intergrown with minimal optical interfaces, and there is an absence of any obvious cleavage and chemical zoning; the net optical effect is of one jadeite crystal, allowing transmitted light to pass through without apparent internal reflection or refraction.

Rough jadeite jade normally has an opaque weathered crust (also known as the skin) with a thickness between 1 and 50 mm, thus it is difficult to evaluate without cutting into fresh rock. For the rough stone market, traders sometimes cut and polish a small 'window' through the weathered surface of a stone for a better sale; this is called a 'gamble stone' by the Chinese. In Figure 13 is a good example of such a stone with a 'window' revealing an interior of glassy transparency when illuminated by a torch. A potential buyer would have to evaluate the overall quality of the stone, including the part still covered by the weathered skin, on the basis of this small illuminated area. The indistinct preferred orientation shown by the surface crystals (SPO texture) is a positive indication that the whole stone is of good quality; it turned out to be glassy after the skin was removed, so the initial indications proved positive.

Studies of the textures of feitsui also help a jade manufacturer in deciding on the best way to design and carve a particular piece of jadeite jade. Because

of its textural heterogeneity, jadeite jade enables designers to use their imagination to the best effect, and the best designers know how to make full use of this variability. Two artworks shown in Figures 14 and 15 are good examples; in Figure 14, the dragon's head was carved in the finest pure white area and its unpolished surface gives the art a sense of mystery, whereas in Figure 15, the coarsest part was designed as the base, supporting the 28th Olympics logo which was carved in a relatively fine area of jadeite.

Preliminary investigations indicate that green jadeite jades have slight differences in texture and microstructure from white jadeites under the same pressure and temperature (P-T) and stress conditions. One can even distinguish some textural differences at the colour boundaries: the green areas tend to consist of smaller grains with more pronounced orientation, thus appearing more transparent than neighbouring white areas (Figures 16 and 17). Our studies to date of homogeneous green jadeite jades indicate that they have similar deformation textures to

Jadeite jade from Myanmar: its texture and gemmological implications

those described in the white jades. So, if textural studies of white feitsui can help understand green feitsui, the conclusions could provisionally be extended to the precious imperial green jadeite jade, which currently is too expensive to section for gemmological research!

Textural model of the glassy jadeite jades and how they formed

Its rarity indicates that jadeite cannot easily grow as large transparent crystals in Nature (see Zhang *et al.*, 2002). So far there have been no reports of a single jadeite crystal being cut or otherwise used as a gemstone. But some jadeite aggregates can come surprisingly close to appearing like a single crystal with an icy or glassy transparency nearly as clear as rock crystal. Our observations on the textures and microstructures of Myanmar jadeitites suggest a theoretical textural model for such aggregates. In this model, the individual jadeite crystals are small equant grains or fine fibres too small to develop significant cleavage, which is therefore one factor that will not interfere with transparency. All the grains have preferred orientation, with their crystal and optic axes consistently aligned; therefore they show little, if any, differential refraction between neighbouring grains. This texture is also so compact that there are no spaces at any grain boundaries, so there are no obstructions to the transmitted light; this eliminates any significant internal reflection and refraction (*Figure 18*).

Transformation of coarse jadeitite into the transparent gem-quality jade, i.e. icy to glassy feitsui, should have undergone at least two coupled processes of grain size reduction and crystallographic orientation under conditions of jadeite stability.

The main process causing grain-size reduction is rotation recrystallization, also known as the progressive misorientation of sub-grains. This refers to the formation of sub-grains by the relative rotation of different parts of a crystal and was first identified in such minerals as quartz, feldspar and olivine under conditions of low pressure and high temperature. In jadeites, this phenomenon takes place at high pressure and low temperature



Figure 19: Jadeite from Myanmar described as water-like; the jadeite grains cannot be distinguished with the naked eye. Specimen 5cm across.

in the jadeitites from Myanmar. Other processes causing grain-size reduction include mechanical twinning and shearing along micro-shear zones. In one crystal, such shearing can cause sub-grains that do mismatch but retain overall orientation within 15 degree limits of CPO. CPOs can also be generated from processes including grain-boundary migration (GBM) and diffusion processes (Tullis and Yund, 1985).

From the presence of some elongate jadeite crystals in the Myanmar icy to glassy jadeitites, it is suggested that GBM had occurred during the transformation from coarse-grained jadeitite to fine jadeite jade. Since GBM tends to increase the size of the sub-grains, it is reasonable to include this process as part of the ideal or theoretical texture model. The linked processes of rotation recrystallization and GBM are the main causes of formation of the icy to glassy jades, and since both should have taken place under high pressure low temperature conditions, the conditions of formation for aggregates of jadeite with an icy to glassy appearance are thus very exacting. They are extraordinarily rare, only found so far in Myanmar, and the results are therefore precious.

The undeformed coarse jadeitite and the icy to glassy feitsui are the two end members of the transparency range

of jadeite materials. Most jadeite jades from Myanmar are intermediate, being of moderate grain size, with partially orientated grains, and a translucent appearance.

Jadeite materials representing nearly all degrees of transparency are available on the market, and are sold under the varietal descriptions: 'glassy', 'icy', 'water', 'cooked sticky-rice', 'porcelain' and others (*Figure 19*). These varieties do not take into account colour or impurities – these are other variables that can lead to more commercial varieties.

Formation of the most transparent feitsui has required long-lasting and intensive, localized geological forces, and it is very likely that the source of these was movement along the Sagaing strike-slip faults which have a displacement 150–300 km. Displacement along the faults over a long period of time led to local developments of intense metamorphism inducing ductile deformation and recrystallization, and where coarse-grained jadeitites were caught up in these movements, they were variably recrystallized and transformed.

Gemmological applications will benefit from further related investigations into jadeitite textures and make it possible perhaps to establish an ideal model of how the textures of the glassy jades were formed.

Jadeite jade from Myanmar: its texture and gemmological implications

Conclusions

Jadeitites from Myanmar can be considered in terms of two groups of textures: primary, and deformed and recrystallized. Those with primary textures are coarse-grained, and have mosaic, granitoid or radial textures consisting of chemically zoned jadeite crystals; they are porous to some degree, are not transparent, and are not therefore considered as being of gem quality. The jadeitites which are deformed and recrystallized developed at the expense of primary textures, and are intermediate to fine-grained, with semi-orientated to preferred orientated crystals, some mechanically twinned. They may also contain micro-shear zones, sub-grains, serrated high-angle sutured grain boundaries, and 'foam' textures. These rocks are compact, tough and translucent to transparent, and have the most potential as gems.

One model for the icy and glassy jadeite jades might include the following parameters: the crystals are very small and compact with preferred orientation, they lack obvious chemical zones and cleavages, and the whole rock resembles a single crystal optically. Most jade in the gem market is classed as glassy or coarse. These categories are further subdivided on the basis of three variables: compactness, orientation and grain size, so producing a large number of jadeite varieties.

Studies of the textures have gemmological applications not only in identifying and grading the rough and fashioned jadeite jades, but also in their design and manufacture. Moreover, such studies help understanding of the textural model of the icy and glassy jadeite jades, the textures and microstructures of green and other coloured materials, and how they are formed.

The movements of the Sagaing strike-slip faults, which the Myanmar jadeite deposits straddle, are inferred as the main cause of the formation of the feitsui.

Acknowledgements

This investigation is financially supported by Program for the New Century

Excellent Talents in China (NCET-07-0771) and the National Science Foundation of China (40672046). We thank Prof. B. Stöckhert for assistance with EBSD analyses. Constructive comments by Dr B. Laurs helped to improve the manuscript.

References

- Bertrand, G., and Rangin, C., 2003. Tectonics of the western margin of the Shan plateau (central Myanmar): implication for the India–Indochina oblique convergence since the Oligocene. *Journal of Asian Earth Sciences*, **21**, 1139–57
- Chhibber, H.L., 1934 *The mineral resources of Burma*. Macmillan, London, 320 pp
- Damour, M.A., 1881. Nouvelles analyses sur la jadeite et sur quelques roches sodifères. *Annales de Chimie et de Physique*, 5th ser., **24**, 136–48
- Fritsch, E., Wu S.T., Moses, T., McClure, S.F., and Moon, M., 1992. Identification of bleached and polymer impregnated jadeite. *Gems & Gemology*, **28**, 176–87
- Gübelin, E.J., 1965a. Maw-sit-sit proves to be jade-albite. *Journal of Gemmology*, **9**, 372–9
- Gübelin, E.J., 1965b. Maw-sit-sit: A new decorative gemstone from Burma. *Gems & Gemology*, **11**, 227–38
- Harder, H., 1995. Trace elements as colouring agents in jadeites. *Journal of Gemmology*, **24**, 508–11
- Harlow, G.E., and Olds, E.P., 1987. Observations on terrestrial ureyite and ureyitic pyroxene. *American Mineralogist*, **72**, 126–36
- Harlow, G.E., 1994. Jadeitites, albitites and related rocks from the Motagua fault zone, Guatemala. *Journal of Metamorphic Geology*, **12**, 49–68
- Harlow, G.E., and Sorensen, S.S., 2005. Jade nephrite and jadeite and serpentinite: metasomatic connections. *International Geology Review*, **47**, 113–46
- Hirth, G., Tullis, J., 1992. Dislocation creep regimes in quartz aggregates. *Journal of Structural Geology*, **14**, 145–59
- Hughes, R.W., Galibert, O., Bosshart, G., Ward, F., Oo, T., Smith, M., Tay, T.S., and Harlow, G.E., 2000. Burmese jade: the inscrutable gem. *Gems & Gemology*, **36**(1), 2–26
- Johnson, C.A., and Harlow, G.E., 1999. Guatemala jadeitites and albitites were formed by deuterium-rich serpentinizing fluids deep within a subduction-channel. *Geology*, **27**, 629–32
- LeDain, A.Y., Tapponnier, P., and Molnar, P., 1984. Active faulting and tectonics of Burma and surrounding regions. *Journal of Geophysical Research*, **89**, 453–72
- Morley, C.K., 2004. Nested strike-slip duplexes, and other evidence for Late Cretaceous–Palaeogene transpressional tectonics before and during India–Eurasia collision, in Thailand, Myanmar and Malaysia. *Journal of the Geological Society*, **161**, 799–812
- Nyan Thin, U., 2002. *Myanmar jade*. Mandalay Gem Association, Myanmar, 149 pp
- Orzol, J., Trepmann, C., Stöckhert, B., and Shi, G.H., 2003. Critical shear stress for mechanical twinning of jadeite — an experimental study. *Tectonophysics*, **372**, 135–45
- Ouyang, C.M., 1984. A terrestrial source of ureyite. *American Mineralogist*, **69**, 1180–3
- Ouyang, C.M., 2000. Texture types of jadeite jade and its genetic implications. *Journal of Gems and Gemmology* (in Chinese), **2**(2), 1–5
- Ouyang, C.M., 2003. *Jadeite jade: a stone and a culture*. The Hong Kong Institute of Gemmology, Hong Kong, 184 pp
- Shi, G.H., Cui, W.Y., Wang, C.Q., and Zhang, W.H., 2000. The fluid inclusions in jadeite from Pharkant area, Myanmar. *Chinese Science Bulletin*, **45**, 1896–900
- Shi, G.H., Cui, W.Y., Liu, J., and Yu, H.X., 2001. The petrology of jadeite-bearing serpentinitized peridotite and its country rocks from Northwestern Myanmar (Burma). *Acta Petrologica Sinica*, **17**, 483–90
- Shi, G.H., Cui, W.Y., Tropper, P., Wang, C.Q., Shu, G.M., and Yu, H.X., 2003. The petrology of a complex sodic and sodic–calcic amphibole association and

Jadeite jade from Myanmar: its texture and gemmological implications

- its implications for the metasomatic processes in the jadeitite area in northwestern Myanmar, formerly Burma. *Contributions to Mineralogy and Petrology*, **145**, 355–76
- Shi, G.H., and Cui, W.Y., 2004. Textures and microstructures of the Myanmar jadeitite: implications for formation of jadeitic Feits'ui. *Journal of Gems and Gemmology* (in Chinese), **6**(3), 8–11
- Shi, G.H. *et al.*, 2009. See Web list
- Shi, G.H., Stöckhert, B., and Cui, W.Y., 2005a. Kosmochlor and chromian jadeite aggregates from Myanmar area. *Mineralogical Magazine*, **69**, 1059–75
- Shi, G.H., Tropper, P., Cui, W.Y., Tian, J., and Wang, C.Q., 2005b. Methane (CH₄)-bearing fluid inclusions in Myanmar jadeites. *Geochemical Journal*, **39**, 503–16
- Shi, G.H., Cui, W.Y., Cao, S.M., Jiang, N., Jian, P., Liu, D.Y., Miao, L.C., and Chu, B.B., 2008. Ion microprobe zircon U-Pb age and geochemistry of the Myanmar jadeitite. *Journal of Geological Society*, **165**, 221–34
- Sorensen, S., Harlow, G.E., and Rumble III, D., 2006. The origin of jadeitite-forming subduction-zone fluids: CL-guided SIMS oxygen-isotope and trace-element evidence. *American Mineralogist*, **91**, 979–96
- Tay, T.S., Liew, S.P., and Puah, C.M., 1996. Scanning electron microscope studies on bleaching jadeite. *Australian Gemmol.*, **19**(7), 310–4
- Tay, T.S., Paul, S., and Puah, C.M., 1993. SEM studies of bleached and polymer-impregnated jadeite. *Australian Gemmol.*, **18**(8), 257–61
- Trepmann, C., and Stöckhert, B., 2001. Mechanical twinning of jadeite: an indication of synseismic loading beneath the brittle-plastic transition. *International Journal of Earth Sciences*, **90**, 4–14
- Tullis, J., and Yund, R.A., 1985. Dynamic recrystallization of feldspar: A mechanism for ductile shear zone formation. *Geology*, **13**, 238–41
- Win Htein and Aye Myo Naing, 1994. Mineral and chemical composition of jadeite jade of Myanmar. *Journal of Gemmology*, **24**, 269–76
- Win Htein and Aye Myo Naing, 1995. Studies on kosmochlor jadeite and associated minerals in jade of Myanmar. *Journal of Gemmology*, **24**, 315–20
- Yi, X., Shi, G.H., and He, M.Y., 2006. Jadeitized omphacitite from Myanmar jadeite area. *Acta Petrologica Sinica*, **22**, 971–6
- Zhang, L.F., Ellis, D.J., Williams, S., and Jiang, W.B., 2002. Ultra-high pressure metamorphism in western Tianshan, China: Part II. Evidence from magnesite in eclogite. *American Mineralogist*, **87**, 861–6

Web list

Shi, G.H., Jiang, N., Liu, Y., Wang, X., Zhang, Z.Y., and Xu, Y. J., 2009. Zircon Hf isotope signature of the depleted mantle in the Myanmar jadeitite: implications for Mesozoic intra-oceanic subduction between the Eastern Indian Plate and the Burmese Platelet. *Lithos*, doi: 10.1016/j.lithos.2009.03.011

All photos and photomicrographs by G.H. Shi.

The Authors

Professor Dr Guanghai Shi

Laboratory Director at the School of Gemology, China University of Geosciences, Beijing 100083. China. email shiguanghai@263.net.cn

Miss Xia Wang and Miss Bingbing Chu

Postgraduates at the China University of Geosciences, Beijing 100083. China.

Professor Wenyuan Cui

School of Space and Earth Sciences, Peking University, Beijing 100871, China.

A description and history of one of the largest nacreous pearls in the world

J.C. (Hanco) Zwaan and Herman A. Dommissie

Abstract: A large pearl, weighing approximately 2385 grains, is described. This pearl is one of the largest nacreous pearls ever found. Although the first known owner, Sir H.C. Sander, left this pearl to be auctioned in Amsterdam in 1778, and the pearl has been part of a Dutch private collection, at least from the nineteenth century onwards, it has never been described before. Its properties indicate a freshwater origin. Supported by an eighteenth century print and historical references, its properties point to the Far East as its most likely provenance. The weight of the pearl is slightly less than the recorded weight of the Pearl of Asia, as described in the literature.

Based on its shape, it had been suggested previously by the present owner that this pearl could actually be the disappeared Arco Valley Pearl, which until recently had been owned by one Italian family since 1700. After the sudden announcement that the Arco Valley Pearl had been put up for auction in Abu Dhabi in 2007, and the recent discovery that the pearl described herein had been sold in Amsterdam in 1778, the suggested Italian link could be refuted and a strong Dutch link confirmed.



Introduction

In 1979, a large baroque pearl was brought to the Netherlands Gemmological Laboratory for identification, by L.W. van Kooten, the Dutch owner at the time. Professor Dr P.C. Zwaan, the director of the Laboratory at the time, confirmed its natural identity in a letter written on 7 June 1979 and immediately recognized its uniqueness. For that reason, he stated that the pearl deserved to be shown to the public. However, no publicity was generated around the discovery, and the pearl stayed locked away after a change of ownership in the same year. However, in 1998 it was shown to the public for the first time during the Christmas period, right after the opening of the new exhibition halls and depot of the National Museum

of Natural History, 'Naturalis', in Leiden. Now, after more than ten years out of the public eye, the pearl is described in detail for the first time and compared with other large pearls that have been reported in the literature.

History and lore

Only very recently, a print of an 'Oosterse Paarel' (oriental pearl) dated 1778, was found in the city archive of Amsterdam (Lakmaker, 2009). It was accompanied by a note stating: "A large pearl, of 578 carats, visualizing a sleeping lion, left by H.C. Sander, has been sold in 'the Munt' on 26th August 1778." A separate note stated that the pearl was sold for 2100 Dutch guilders (Muller, 1876-77). Comparing this drawing with the

described pearl (*Figure 1*), we can confirm that it is the same pearl. It means that this illustration is the first account of this pearl that has been found so far.

Another note mentioned that the pearl was actually a 'well known Royal Cabinet piece' and gave more information on the first known owner. Sir Hendrik Coenraad Sander was an agent of the 'Duke of Tweebrugge'. He not only left the pearl, but also an "extremely beautiful brilliant, weighing c. 58 grains". Accordingly, the stone was sold at the same time for 17500 Dutch guilders.

The second known owner of the pearl was a Polish ship-owner named Plonsky, from Danzig (now known as Gdansk). Around 1865 Plonsky sent one of his daughters to Paris and to Rome, to sell the



Figure 1: The first record of the described pearl is a print dated 1778. The marginal note, written in Dutch, translates as: "An Oriental pearl, weighing 578 carats." A photo of the described pearl in the same orientation shows that it is identical to the pearl on the drawing.

pearl (L.W. (Louk) Van Kooten, 1994, pers. comm.). At the time Gdansk was besieged by Russian troops trying to seize this German harbour on Polish territory. This might have been the reason that Plonsky urgently needed money.

At the same time in Rome, the jewellers Castellani were working on the crown jewels of Victor Emmanuel II (1820-1878, the first king of united Italy). The old royal regalia had been stolen by the French troops and had to be replaced. On behalf of the monarch they were looking for special pearls and gemstones for the crown, sceptre, orb and sword. The crown was finished first; it contained a pearl of around 500 grains. It is possible that Castellani advised the King to buy the pearl from Plonsky, to be used

for the sceptre. At the time the young goldsmith Lodewijk Willem van Kooten from Amsterdam worked at Castellani. Van Kooten helped to manufacture the crown and was involved in preparations to make the other jewels. But these other jewels were not finished because the King needed money to fight Garibaldi and his troops. To prevent the King from losing face, Pope Pius IX advised him to present the crown as a gift to the Church of the Holy Sepulchre in Jerusalem (Kunz and Stevenson, 1908, p.468) but with no prospect of completing the other regalia, the unused pearl was sold privately to Lodewijk van Kooten (Figure 2), who returned to Amsterdam around 1868.

Tradition has it that the pearl made a single journey to Fabergé, the

royal jeweller of Tsar Nicolas II, in St. Petersburg (L.W. (Louk) Van Kooten, pers. comm.). Louis Van Kooten, Lodewijk's son, and Fabergé knew each other from the 1910 World Exhibition in Brussels. At this event, the firm Van Kooten won a prize for manufacturing gold and enamel jewellery, after designs of Lambert Nienhuis (Van Diedenhoven, 1911), which is still present at the Rijksmuseum in Amsterdam (Anonymous, 1980).

Thereafter Van Kooten represented Fabergé in The Netherlands and its colonies. Van Kooten sent the pearl to St. Petersburg to be mounted in one of the spectacular and famous 'eggs' for the Russian monarch, but the pearl had to be brought back unsold from Russia because revolutionaries and a shaky throne had prevented a sale.

In 1914, Fabergé closed its doors. Between 1914 and 1979, the pearl stayed in a safe of the Van Kooten family, unseen and unnoticed. The Van Kooten jewellery firm ceased to exist in 1951, exactly 90 years after its foundation. In 1979 the pearl was sold, and from that time it has been in the hands of a well-known art collector from Amsterdam.

In 1992, the pearl was set in a mount designed by Jean Lemmens, a goldsmith based in Antwerp. He chose to design a



Figure 2: The young Amsterdam jeweller Lodewijk Willem van Kooten (1842-1900), pictured in Paris, August 1865, just after the purchase of the giant pearl in Rome.

A description and history of one of the largest nacreous pearls in the world



Figure 3 (left): The described baroque pearl with an estimated weight of around 2385 grains, was set in this mount in 1992. The design is a stylized Lotus bud with the pearl in the centre, surrounded by golden 'stamens' which are decorated with ruby, sapphire and emerald beads at the upper ends, and mounted on a pedestal of lapis lazuli. Photo © Amsterdam Pearl Society

Figure 4 (above): Surface growth lines on the reverse side of the pearl indicate that parts were attached to the shell.

stylized Lotus bud with the pearl in the centre, protected by 'stamens' (Figure 3). The 'stamens' consist of gold, with ruby, sapphire and emerald beads at the upper ends, and are mounted with a gold rod on a pedestal of lapis lazuli, which contains a gold frame set with various small coloured gemstones.

Properties

The pearl, measuring approximately 70 x 43 x 39 mm, has an irregular pear shape described as baroque, and is creamy white with a slightly brownish tint in some areas at the back (Figures 3 and 4). The weight of the pearl is estimated to be approximately 2385 grains (119.25 g, see under 'weight estimation').

The pearl shows a good lustre and a subtle play-of-colour or 'orient' over much

of its surface. Under magnification, the surface of the pearl shows characteristic irregular relief lines, which correspond to the borderlines of aragonite platelets, marking extremely thin layers of mother-of-pearl, stacked on each other. A part of the reverse side of the pearl reveals surface growth lines, indicating an area of the pearl originally attached to the shell (Figure 4).

X-radiographs and computer tomography (CT) scans taken perpendicular to the direction of the X-radiographs, revealed a layered growth structure, which confirms that the pearl was naturally formed (Figures 5 and 6) and that it is solid; it does not contain any substantial cavities.

Under long wave UV radiation, the pearl showed a strong bluish to slightly

Table I: Trace element contents in the described pearl.

Oxide	Spot analyses (wt.%)				
	1	2	3	4	5
MnO	0.21	0.22	0.26	0.26	0.30
SrO	0.03	0.03	0.03	0.07	0.06

NB: Measurements were done with micro-EDXRF. MnO and SrO values were corrected for the presence of CO₂ (carbon cannot be measured by this analytical technique).

greenish-white fluorescence. Under X-rays, the pearl distinctly fluoresced a slightly creamy white. Micro-EDXRF analyses on five selected spots (each of 300 µm diameter) on the pearl surface, revealed Ca as the main element and traces of Mn and Sr (Table I). The fluorescence under X-ray combined with the relatively high concentrations of

A description and history of one of the largest nacreous pearls in the world

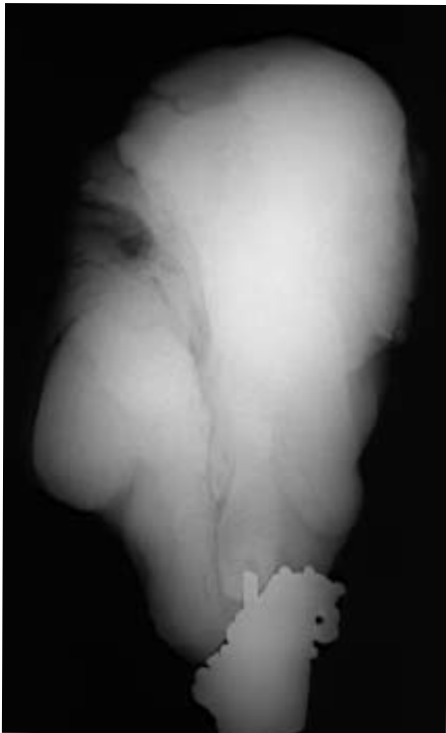


Figure 5: X-radiograph of the pearl, showing a layered growth structure, which confirms its natural identity.

manganese and low concentrations of strontium, point to a freshwater origin for this pearl (compare, e.g., Farn, 1986; Wada and Fujinuki, 1988; Gutmannsbauer and Hänni, 1994; Kennedy *et al.*, 1994).

Weight estimation

Ideally, a loose pearl should be weighed on an accurate balance to establish its exact weight. However, the pearl was tightly mounted on a gold rod, which would have to be drilled out to obtain an accurate weight, a procedure likely to cause damage and loss of weight. But by comparing the gross weight of the pearl with the sizes and weights of different gold rods, an approximate weight of the loose pearl could be calculated.

Based on X-radiographs, CT-scans and the length of the rod sticking out, the total length of the gold rod was estimated to be 22 mm. The designer of the mount, J. Lemmens, kindly provided a gold rod of identical thickness and a length of 11 mm,

which weighed 0.2782 g. This means that the identical rod of 22 mm attached to the pearl should weigh 0.5564 g.

The pearl, including the gold rod, weighed 119.87 g. Based on the weight of the 22 mm gold rod, the weight of the loose pearl would be $119.87 - 0.5564 = 119.3136$ g, that is rounded to 2386 grains. The uncertainty in this calculation mainly lies in the estimation of the length of the golden rod inside the pearl, which is partly hidden by a gold frame that covers the back of the pearl (unfortunately there was no opportunity to make radiographs of the pearl without the frame). Therefore it is possible that the rod could be up to 2 mm longer than estimated. In that case, the calculation would give 2385 grains and we have used this most conservative calculation as the approximate weight of the pearl.



Figure 7: A box made specifically to hold the pearl is made of gilded copper. The box appears to be of Asian origin.

Metal box

A metal box that came with the pearl (Figure 7) was originally made for it, as it fits around the pearl perfectly. It has been made of gilded copper, and measures approximately 74 x 54 x 47 mm. The construction of the box is unusual. The lid is larger than the base which only has low rims no more than 5 mm in height. Thus by removing the lid, the pearl could be displayed on its base. The box contained a piece of paper with hand-written notes (in Dutch and French), “Concrétion perlière de *Maleagrina margaritifera*” on one side and the address of Madame Plonsky in Rome and the weight of the pearl in grams on the other.

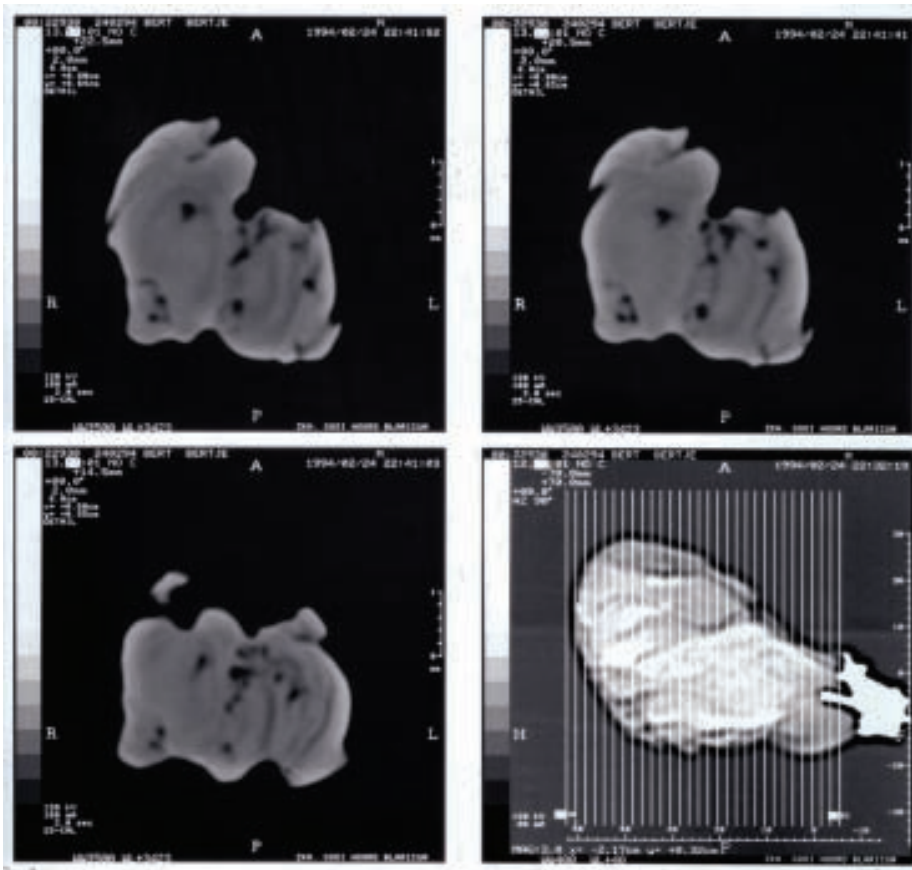


Figure 6: CT-scans also confirm the natural identity of the pearl, showing concentric layered growth structure in parallel sections, taken perpendicular to the direction of the X-radiograph. In total, 19 sections were scanned, three examples of which are shown here.

A description and history of one of the largest nacreous pearls in the world

The box is probably made in east Asia, possibly in China. This view is independently confirmed by specialists in antique metal objects. It is uncertain when it was made, but it may be significantly earlier than the nineteenth century.

Discussion

The first account of the pearl

The detailed print of the pearl made in 1778 clearly represents the same pearl as described. However, the mentioned weight, 578 ct (i.e. 2312 grains) deviates considerably from the approximate weight of 2385 grains as stated above. This difference can be understood, when realizing that the metric carat weight of 200 mg (0.2 g) was only standardized in the early twentieth century. Until that time the carat weight varied considerably in different parts of the world; with a range between 0.1885 and 0.2160 g (Lenzen, 1970, p.100). The value of 0.204304 grams was that defined for the old English carat, but never a legal weight, and only mentioned for the first time in 1878 (O'Donoghue, 2006). When comparing the 578 ct mentioned on the drawing with our approximate weight of 2385 grains (119.25 g), the carat weight used at the time must have been around 0.206 g. This is consistent with the value of the Amsterdam carat of 0.2057 g at the end of the nineteenth century, as given by Lenzen (op. cit.). After the pearl was sold in Amsterdam in 1778, the pearl's history is not known until 1865, when the second known owner from Poland appeared. The return of the pearl to Amsterdam around 1868 only appears to confirm strong ties between the pearl, Amsterdam and The Netherlands.

Origin

Which pearl-producing mollusc would have been capable of producing a pearl this size? Previous owners thought that the pearl was produced by a marine bivalve mollusc of the genus *Pinctada*, this being the main producer of natural pearls in the Persian Gulf/Red Sea region. There is a hand-written note with the pearl (see above) that states "concrétion

perlière de *Maleagrina margaritifera*". The *Pinctada* genus was often referred to as *Maleagrina* from 1819 until the middle of the nineteenth century (Strack, 2006). Thus *Maleagrina margaritifera* can be read as a synonym of *Pinctada margaritifera*. This attribution was most probably based on the colour and iridescence ('orient') of this pearl, which closely resembles the appearance of natural pearls formed in salt water.

However, there is general consensus that marine pearls do not fluoresce under x-rays, although marine pearls coming from river deltas may show a weak fluorescence. The mother-of-pearl of especially American, Chinese and Japanese freshwater shells normally has a distinct fluorescence (see Strack, 2006). As concluded above, the distinct fluorescence and high manganese content of the described pearl indicate strongly a freshwater origin. However, most of the pearl-producing freshwater molluscs appear simply too small to produce such a huge pearl. The largest freshwater molluscs are part of the extensive family of Unionidae; purely based on size, species that could have produced a pearl this large may be pond 'mussels' like *Anodonta cygnea* and *Anodonta anatina*, which can reach lengths up to 22 cm and are widely distributed from Europe to Eastern Siberia. *Anodonta woodiana* can grow up to 19 cm in length, and occurs in China and Japan. Other possible sources are *Hyriopsis cumingii* or, less likely because of the size, *Hyriopsis schlegelii*. *Hyriopsis cumingii* can grow up to 25 cm in length and 20 cm in width, and occurs in rivers and lakes of China; *Hyriopsis schlegelii* may reach a size of 20 x10 cm and is found in Japan. *Cristaria plicata* can reach a length of 30 cm and is found in East and Southeast Asia. Finally, *Megaloniaias gigantea*, the 'washboard' (up to 30 cm or more in length), and *Lasmigona (P.) complanata* (up to 20 cm) occur in North America (data from Strack, 2006; Sweaney and Latendresse, 1984, Williams *et al.*, 2008).

From descriptions in Williams *et al.* (2008), it appears that *Lasmigona (P.) complanata* has really white nacre, either

going in the bluish or pinkish direction, and bears no resemblance to the nacre of the described pearl. Also *Megaloniaias gigantea* usually produces white nacre, and rarely pale pink. In fact, most North American species produce white nacre, although many other colours also occur, including pink, orange, lavender and purple. White is the most prevalent body colour of freshwater pearls in America. Cream colours are commonly seen in freshwater pearls of Japan and China (Sweaney and Latendresse, 1984).

Although *Anodonta* has produced pearls in China and Japan for centuries, their sizes have not been exceptional (Strack, 2006). Kunz and Stevenson (1908) mentioned earlier that *Anodonta* produced pearly concretions that are less lustrous and not brilliant in colour.

Based on the size, colour and properties of the pearl, it seems to be most probable that this pearl grew in either *Hyriopsis cumingii*, *Cristaria plicata* or *Hyriopsis schlegelii*, with China or Japan as most likely sources. Statements in the (historical) literature do not appear to contradict this view, and also mention large pearls that came from these areas. Farn (1986) and Landman *et al.* (2001) confirmed that even in remote antiquity China had access to significant quantities of freshwater pearls from pearl mussels (*Cristaria* and *Hyriopsis*) native to the Yangtse delta and nearby rivers in central eastern China. Strack (2006) stated that the majority of Chinese natural freshwater pearls which are known since the third millennium BC have probably originated from *Hyriopsis cumingii*.

Marco Polo reported on the trade in pearls in China and mentioned a lake near 'Kain-du' (the north western part of Yunnan), where many pearls were found "of a white colour, but not round" (Polo, 1298, in Penzer, 1929). Kunz and Stevenson (1908) wrote that it appeared from ancient Chinese literature that pearl fisheries of considerable extent and importance have existed in the rivers and lakes of China for several thousand years. They reported that in about 200 BC a pearl dealer at Shao-hing, an ancient city (now Shao-xing, NE Zhejiang province, East

A description and history of one of the largest nacreous pearls in the world

Table II: Comparison of the described pearl with the largest reported nacreous pearls.

Largest pearls	Approximate size (mm)	Weight	
		grains	grams
Pearl described in this article	70 x 43 x 39	2385	119.25
<i>Historic pearls</i>			
Pearl of Asia	76 x 50 x 28	2420	121
Arco Valley Pearl	Length 75, width 52.5	2300	115
Hope Pearl	Length 90, width 30-40	1800	90
<i>Recent discoveries</i>			
Centaur Pearl	69 x 49 x 35	3426	171.30
Myanmar Pearl	62 x 53 x 30	3380	169

Pearl of Asia data: Boutan (1925); Hope pearl data: Kunz and Stevenson (1908), Kennedy (1994); Arco Valley Pearl data: Taburiaux (1985); Centaur Pearl data: Scarratt (2001); Myanmar Pearl: Hlaing (2001).

China), furnished to the Empress a pearl of one inch in diameter, and to an envious princess the same dealer sold a "four-inch pearl". Kunz and Stevenson (1908) also indicated that numerous pearls were found in Manchuria, where they have long been exploited for the account of the Emperor of China. They further stated that many superb pearls were among the precious objects in the Yuen-Min-Yuen or Summer Palace in Beijing at the time of its capture by the European forces in 1860. Some of these pearls found their way to Europe, and were of "good size and lustre and were mostly yellowish in colour". Earlier on, Tavernier (1676) had seen some of the pearls the Dutch brought from Japan: "They were of very beautiful water, and some of them of large size, but all baroques." It is unclear though whether these pearls originated from coastal areas or lakes. Summarizing, historical sources indicate that since antiquity, large pearls, including freshwater pearls, were known to come from the Far East, in particular China and Japan, and were finding their way to Europe.

Comparison with other large pearls

The size and weight of the described pearl is compared with the largest pearls known so far (Table II). Compared with the historic pearls, the pearl appears to weigh slightly less than the Pearl of Asia, which according to Boutan (1925) weighs 605 ct (2420 grains). However, Boutan did not report on weighing it himself and showed a drawing of a mounted pearl.

The Pearl of Asia is still mounted in the same setting as became apparent when temporarily exhibited by the Smithsonian Institution in 2005. Consequently, as the Pearl of Asia has been known for around 300 years (Strack, 2006) and taking into account the variation in carat weight used at the time, as discussed above, the exact weight of this pearl could lie somewhere between 2280 and 2580 grains.

It was previously suggested by the present owner that the pearl described here could be the similarly-shaped Arco Valley Pearl which was in the possession of the Italian d'Arco family for a long time, at least since 1700 (Taburiaux, 1985). This family originally came from Arco village; the Count Carlo d'Arco (1799–1872), painter and art-historian, lived in Mantova, northern Italy. Until recently, the whereabouts of the Arco Valley Pearl were unclear. However, on 8 May 2007 it was announced that the Arco Valley Pearl would be put up for auction in Abu Dhabi. A picture of the pearl was shown, which closely resembled a drawing of the Arco Valley Pearl published by Taburiaux (1985). A death in the Emirates royal family postponed the auction (2007, <http://abcnews.go.com/International>). Since then, it is unclear whether this pearl has been offered at auction again, or perhaps secretly sold. Nevertheless, from the released information and photographs it appears that there is no link between the pearl described in this article and the Arco Valley Pearl. Additionally, the discovery that the described pearl

was sold in Amsterdam in 1778 is not consistent with one family having owned the pearl since 1700.

Comparing origins for the Pearl of Asia, the Hope Pearl, the Myanmar Pearl and the Centaur Pearl, a marine origin is indicated or implied. For the Hope Pearl, the *Pinctada margaritifera* is the most likely source (Kennedy *et al.*, 1994). The Myanmar Pearl was found in a *Pinctada maxima* (gold-lipped pearl oyster; Hlaing, 2001). The Pearl of Asia is supposed to have come from *Pinctada maxima* as well (Strack, 2006). So far, the origin of the Arco Valley pearl remains unknown. Consequently, the described pearl could have the status of being the largest freshwater pearl found to date.

Conclusion

The pearl described, measuring 70 x 43 x 39 mm and weighing 2385 grains, is one of the largest nacreous pearls that have been documented. In contrast to the other few very large baroque pearls, the properties of this pearl suggest a freshwater origin. Taking into account its size and colour, it appears to be likely that the pearl was formed in a large freshwater mussel of the family Unionidae, somewhere in East Asia (China or Japan). The eighteenth-century print with the subscript 'Oosterse parel' appears to support a Far East origin. Historical references also confirm that from early times, large pearls were known to come from China and Japan.

Acknowledgements

Dr P. Marsman is thanked for producing the CT scans of the pearl. Dirk van der Marel is thanked for making X-radiographs and for general technical assistance.

A description and history of one of the largest nacreous pearls in the world

References

- Boutan, L., 1925. *La Perle*. Libraire Octave Doin, Paris, 421 pp
- Farn, A.E., 1986. *Pearls, Natural, Cultured and Imitation*. Butterworths, London, 150 pp
- Gutmansbauer, W. and Hänni, H.A., 1994. Structural and chemical investigations on shells and pearls of nacre forming salt- and fresh-water bivalve molluscs. *Journal of Gemmology*, **24**(4), 241–52
- Hlaing, U.T., 2001. World's largest pearl. *Australian Gemmologist*, **21**(3), 135
- Kennedy, S., Akamatsu, S., and Iwahashi, Y., 1994. The Hope Pearl. *Journal of Gemmology*, **24**(4), 235–40
- Anonymous, 1980. Keuze uit de aanwinsten (choice of acquisitions). *Bulletin van het Rijksmuseum*, **28**(3), 134
- Kunz, G.F., and Stevenson, C.H., 1908. *The Book of the Pearl*. The Century Co., New York, 548 pp
- Lakmaker, J., 2009. Amsterdamse reuzeparel maakte veel mee. *Ons Amsterdam*, **61**(2), 52–5
- Landman, N.H., Mikkelsen, P.M., Bieler, R., and Bronson, B., 2001. *Pearls: a Natural History*. Harry N. Abrams, Inc., New York, 232 pp
- Lenzen, G., 1970. *The history of diamond production and the diamond trade*. Transl. By F. Bradley. Barrie and Jenkins, London, 230 pp
- Muller, F., 1876–77. *De Nederlandse geschiedenis in platen. Beredeneerde beschrijving van Nederlandsche Historieplaten, Zinneprenten en Historische kaarten, tweede deel (1702–1795)*. F. Muller & Co., Amsterdam, No. 4327
- O'Donoghue, M., 2006. *Gems*. 6th edn. Butterworth-Heinemann, Oxford, 873 pp
- Penzer, N.M. (Ed.), 1929. *The most noble and famous travels of Marco Polo. Edited from the Elizabethan translation of John Frampton, London, 1579*. The Argonaut Press, London
- Scarratt, K., 2001. A statuette containing a large blister pearl. *Gems & Gemology*, **37**(3), 231–2
- Strack, E., 2006. *Pearls* (English translation of 'Perlen', publ. in 2001). Rühle-Diebener-Verlag, Stuttgart. 707 pp
- Sweaney, J.L. and Latendresse, J.R., 1984. Freshwater pearls of North America. *Gems & Gemology*, **20**(3), 125–40
- Taburiaux, J., 1985. *Pearls – their Origin, Treatment and Identification*. NAG Press, Ipswich. 247 pp
- Tavernier, J.B., 1676. *Travels in India*. Translation by V. Ball, Volume II, 1889. Macmillan and Co., London
- Van Dienenhoven, W., 1911. Een woordje bij enige bijoux van Bert Nienhuis. *Onze Kunst*, **19**, 89–93
- Wada, K. and Fujinuki, T., 1988. Factors controlling amounts of minor elements in pearls. (In Japanese.) *Journal of the Gemmological Society of Japan*, **13**(1–4), 3–12
- Williams, J.D., Bogan, A.E., and Garner, J.T., 2008. *Freshwater mussels of Alabama and the Mobile basin in Georgia, Mississippi and Tennessee*. The University of Alabama Press, 908 pp

Web list

- 2007, <http://abcnews.go.com/International/wireStory?id=3136801> (The Associated Press, Dubai, 3rd May, 2007)

The Authors

Dr J.C. (Hanco) Zwaan

Netherlands Gemmological Laboratory and
National Museum of Natural History Naturalis, Leiden, The Netherlands
email: zwaan@naturalis.nl

Herman A. Dommissie

Amsterdam Pearl Society, Amsterdam, The Netherlands

Geographic typing of gem corundum: a test case from Australia

F. Lin Sutherland and Ahmadjan Abduriyim

Abstract: A group of analysed sapphires attributed to the rather broad source region of New South Wales was investigated by comparison of their trace element contents with those of sapphires from known Australian fields. Both groups of sapphires were analysed using laser ablation inductively coupled plasma mass spectrometry (LA-ICP-MS) at the same Japanese laboratory. Blue sapphires from Anakie, Queensland, were included for comparison as these are also sold in New South Wales. Comparisons of Fe, Ti, Mg, Cr, Ga and other trace element contents suggest that the vaguely located group of sapphires came from the Inverell gem field in New England. The results give encouragement for more studies on geographic typing of gem corundum.

Keywords: Australia, gem sourcing, LA-ICP-MS analysis, sapphire, trace elements



Faceted blue sapphire, typical of Inverell area, New England, New South Wales, 3.56 ct, Australian Museum Collection (D48268). Photo Stuart Humphreys.

Dedication

This paper is dedicated to the memory of the late Professor Akira Chikayama, who donated a collection of New South Wales sapphires to the GAAJ-Zenhokyo Laboratory in Tokyo and provided many valuable services to gemmological studies during his career.

Introduction

Laser ablation inductively coupled plasma mass spectrometry (LA-ICP-MS) analysis is a useful geochemical technique for 'fingerprinting' an array of trace elements in gemstones (Günther and Kane, 1999; Shigley, 2008). Gem corundum, with colours related to trace element substitutions in the Al_2O_3 structure makes a particularly suitable target for LA-ICP-MS characterization (Gulliong and Günther, 2001; Rankin *et al.*, 2003; Abduriyim and Kitawaki, 2006; Khin Zaw *et al.*, 2006; Peucat *et al.*, 2007; Graham *et al.*, 2008; Sutherland *et al.*, 2008a,b). The Abduriyim and Kitawaki (2006) study on blue sapphires included a group of

faceted stones with a reported source only as New South Wales, Australia. In New South Wales, however, several basaltic sapphire fields have supplied rough and faceted sapphire to the gem market from the late 1800s to present times (Coldham, 1992; Hughes, 1997). The main Inverell-Glen Innes-Tenterfield fields, in the New England area are 300–400 km north of Sydney, but faceted sapphires also come from intermittent small-scale mining elsewhere at Barrington Tops, near Gloucester, 150–200 km north of Sydney and Vulcan State Forest, near Oberon, 130 km west of Sydney (Sutherland and Graham, 2003; Sutherland and Webb, 2007). The New South Wales stones

analysed by Abduriyim and Kitawaki (2006) came to the GAAJ-Zenhokyo Laboratory in Tokyo in the early 1990s from the late Professor A. Chikayama, so unfortunately the means of tracking the exact source of these stones through their trading history is denied us. That they may not even be New South Wales stones is possible because sapphires from the Anakie-Rubyvale gem fields in central Queensland are sold there also. These latter stones are supplied to New South Wales gem merchants, particularly by companies that operate sapphire fields in both states.

This paper aims to identify the source of the 'unsourced' New South

Geographic typing of gem corundum: a test case from Australia



Figure 1: Sapphire-ruby fields, East Australia, including localities discussed in this study. The dash-dot line represents the western exposure of the New England Fold Belt.

Wales sapphires (termed here the Unsourced NSW Group) by comparing their previously published trace element contents with similar LA-ICP-MS analyses on sapphires of documented origin from specific gemfields (made using the same instruments in the same laboratory

and with the same operator). Recent LA-ICP-MS analyses of gem corundum from several New South Wales localities were reported at a recent Applied Mineralogy Congress (Sutherland *et al.*, 2008b) and these are incorporated with new LA-ICP-MS analyses in this paper.

Few LA-ICP-MS analyses of sapphires of known geographical origin from the main commercial New South Wales and Queensland fields have been available prior to this study. Sapphires from magmatic or metamorphic sources are now readily distinguishable in most cases using detailed trace element plots (Abduriyim and Kitawaki, 2006; Peucat *et al.*, 2007; Sutherland *et al.*, 2008b). The distribution of the main gem corundum fields in Australia including those used in this study are shown in Figure 1 and examples of faceted sapphires from the main Australian gem fields are shown in Figure 2. Geological settings and locations for the analysed sapphire localities, summarized from referenced descriptions in Sutherland *et al.* (2009), are given in Appendix I.

Materials and analytical methods

The same methodology described by and instrumentation illustrated by Abduriyim and Kitawaki (2006) were used again in this study. The documented sapphires for this test case included faceted stones, polished wafers and grains held in the Australian Museum collection, viz:

- Two cut blue stones, and one blue and yellow, Inverell, NSW (0.984–1.022 ct, D.A. Porter collection)
- Two cut green stones, Inverell, NSW (1.890–2.229 ct, T. Coldham collection)
- Two cut purple stones, New England, NSW (0.154–0.340 ct, D. Cupit collection)
- One cut green-blue stone, Vulcan State Forest, NSW (1.514 ct, I. Hall collection)
- Three cut blue stones, two purple and one green, Barrington, NSW (0.10–0.16 ct, A. Chubb collection)
- Three cut blue stones, Anakie, Qld (1.538–2.163 ct, A. Wirth collection)

Analyses were made using an Agilent model ICP-MS 7500a with New Wave UP-213 laser ablation sampling system (Abduriyim and Kitawaki, 2006, pp 28–30). Two random sites on the table facet of each stone were analysed using a laser ablation spot 80 μm in diameter and the data were processed using Al_2O_3

Geographic typing of gem corundum: a test case from Australia

98 wt% (Al 51.8 wt %) as an internal standard. The chemical concentration was calibrated using NIST glass 612 and 610. The detected trace elements in the samples include Mg, Sc, Ti, Cr, Mn, Fe, Ni, Ga, Sn and Ta and values are reported in *Table I*, apart from Sc and Mn, which were below detection limit or had negligible value for most analyses. The advantage in using this analytical technique for cut gem stones is its almost non-destructive nature (Rankin *et al.*, 2003).

Results

Main elements

The elemental ranges are grouped by colour of the sapphire from each locality along with an average for each colour group (*Table I*). The blue Inverell and green Inverell groups both show relatively high Ga (> 120 ppm), low Mg (< 18 ppm) and low Cr (< 10 ppm), features that typify magmatic sapphires (Khin Zaw *et al.*, 2006; Peucat *et al.*, 2007). The blue Inverell group, however, shows lower Fe, V and Mg and higher Ti than does the green group. The purple sapphires from this general New England region differ from the Inverell stones in having higher Cr (>290 ppm), but still retain magmatic-like features such as high Ga (>170 ppm) and moderate Mg (< 43 ppm) contents.

The Vulcan State Forest blue sapphire, like the Inverell blue and green stones has high Ga (> 113 ppm) and low Mg (< 14 ppm), but has much more Fe (> 9600 cf < 8300 ppm). The Barrington Tops blue group in contrast mostly shows metamorphic signatures, with relatively low Ga (< 45 ppm) and high Mg (> 262 ppm), with a pale blue zoned stone (Ga 101–102; Mg 45–50 ppm) having intermediate values and distinctly lower Fe (< 2750 cf > 3745 ppm). The yellow green Barrington Tops sapphire shows both low Ga (< 26 ppm) and Mg (< 35 ppm) and is unrelated to the other groups.

The Queensland Anakie blue group differs marginally from the Inverell blue group, with higher Fe (av. 5300 cf 4000 ppm) and lower Ti (av. 67 cf 116 ppm) and noticeably lower Mg (av. < 1 cf 7 ppm).

Other elements

Some stones show noticeable V, Ni and Sn. The highest V values appear in the New England purple and Barrington Tops blue, purple and green sapphires (4–187 ppm), with lesser amounts in Inverell blue (1–7 ppm) and green (9–13 ppm), Vulcan State Forest blue (9–10 ppm) and Anakie blue (1–8 ppm) groups. The highest Ni is found in the Barrington Tops blue and purple sapphires (0–10 ppm) and is < 2 ppm in other sapphires. The Sn values have sporadic higher levels in a few Barrington Tops blue and purple sapphires (226–330 ppm) and are < 2 ppm or below detection in the other sapphires. Minor Ta values in the stones are mostly < 3 ppm.

Discussion

The results from the sapphire groups are plotted in three trace element variation diagrams for comparison with the Unsourced NSW Group analyses. A Cr/Ga-Fe/Ti diagram (*Figure 3*) shows only partial separation of the analysed groups. The Inverell, Vulcan State Forest and Anakie blue and Inverell green groups all fall decisively into the magmatic field. The analysed Barrington blue and purple groups in contrast mostly show metamorphic affinities, even though magmatic Barrington blue sapphires are known (Sutherland *et al.*, 2008b). To overcome this sampling problem, a Barrington magmatic field from that work is depicted on the diagram (BAR). Overall, this discrimination diagram shows overlaps between the Inverell, Vulcan State Forest, Barrington and Anakie magmatic fields, so does not provide good discrimination. Consequently, the Unsourced NSW Group is not clearly linked to a specific field, although it lies near the Inverell and Barrington magmatic blue groups.

The Fe (ppm) – Ga/Mg diagram (*Figure 4*) shows better separation of the analysed groups, with the Barrington blue, purple and green groups all lying in the metamorphic screen (Ga/Mg < 3) suggested by Peucat *et al.* (2007). That screen was based on blue sapphires only, but further data for other coloured corundum show this screen to be generally applicable (Sutherland *et al.*, 2008a,b).

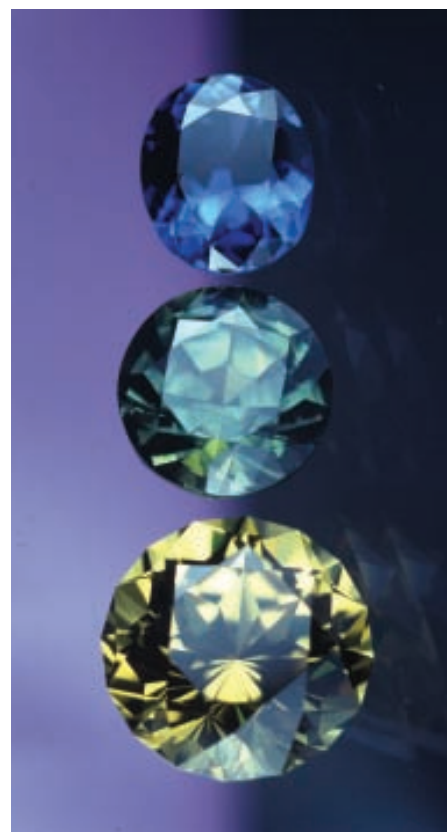


Figure 2: Faceted sapphires, from the main Australian gem fields. The golden yellow stone (12.2 ct) is from Tommahawk Creek, central Queensland, while the green (7.2 ct) and blue (3.5 ct) stones are from the Inverell area, New South Wales. Photo Australian Museum.

In this diagram, the average plot for the Unsourced NSW Group lies within the Inverell blue group and well apart from the other magmatic groups, which have higher Fe contents.

The triangular Fe–Ti (x10) – Mg (x100) diagram (*Figure 5*) is scaled after factors used by Peucat *et al.* (2007). They used this relationship to separate magmatic and metamorphic blue sapphires (Fe–Mg x 100 ratio = 0.64). This diagram largely separates the Inverell, Vulcan State Forest and Anakie blue and Inverell green groups, apart from some overlap with the Barrington magmatic blue group at the Fe-rich end (Fe/Mg x 100 > 0.70). The Inverell blue and New England purple groups overlap the magmatic–metamorphic boundary, suggesting some transitional features. The average for the Unsourced NSW Group plots near the Fe-poor end of the Inverell blue group and well apart from the other magmatic groups.

Geographic typing of gem corundum: a test case from Australia

Table 1: Trace element contents in ppm of East Australian sapphires determined using LA-ICP-MS.

Location	Sample	Colour (ct wt)	Number of spot analyses	ppm range										
				Fe	Ti	Cr	V	Ga	Mg	Ni	Sn	Ta		
Inverell, NSW	D15778a	blue (1.022)	2	2927-3054	55.5-119.2	3.1-9.1	3.6-6.5	127.2-135.9	17.5-30.0	bdl-1.3	bdl	0.9		
	D15778b	blue (1.940)	2	3391-3541	196.9-227.2	bdl	6.6	117.1-120.5	0.5-1.3	0.2-0.4	0.9-1.2	bdl		
	D15778c	yellow blue (0.984)	2	5223-5729	26.3-69.4	0.1-0.3	1.5	137.3-149.2	9.9-13.1	bdl-0.2	bdl	0.1-0.7		
	Average	blue	6	3978	115.8	<2.1	4.4	131.2	7.1	<0.4	<0.4	<0.4		
	D46824	green (1.890)	3	6787-6898	24.0-30.4	0.7-4.3	12.4-12.9	137.0-139.8	10.3-12.1	bdl	0.3-0.9	bdl		
	D46825	green (2.229)	2	6898-8260	32.8-35.4	1.7-4.9	9.3-9.6	132.4-134.7	10.2-12.1	bdl	0.1-0.2	bdl		
New England, NSW	Average	green	5	7321	30.5	2.5	11.4	136.6	11.4	bdl	0.4	bdl		
	D53903	purple (0.340)	2	4642-4966	42.4-62.7	290.2-291.2	37.3-37.6	169.8-173.1	20.0-24.1	bdl-1.4	bdl	bdl		
	D53902	purple (0.154)	2	7841-8260	69.7-73.4	723.2-694.7	4.7-4.8	207.6-209.6	39.9-42.6	bdl-0.2	bdl	0.4-0.9		
	Average	purple	4	6427	62.1	499.8	21.1	190.0	31.6	<0.4	bdl	<0.3		
	D53007	green-blue (1.514)	2	9626-9982	150.3-157.1	2.8-3.2	9.0-9.6	113.8-115.3	9.7-13.8	bdl	bdl	0.5-1.6		
	Average	green-blue	2	9804	153.7	3.0	9.3	114.6	11.8	bdl	bdl	1.1		
Vulcan State Forest, NSW	D54487a	blue (zoned) (0.160)	2	2390-2747	27.2-203.2	3.0-3.3	4.1-4.2	101.4-101.8	45.3-49.9	0.6-2.6	bdl-329.6	bdl		
	Average	blue (zoned)	2	2569	115.2	3.2	4.2	101.6	47.6	1.6	164.8	bdl		
	D54487b	blue (0.104)	2	4379-4721	436.4-467.4	12.4-13.7	182.6-186.6	42.1-44.4	265.7-293.3	3.7-4.6	bdl-324.6	bdl		
	D54487c	blue (0.099)	2	3747-4265	408.7-426.4	187.9-203.0	80.0-86.2	29.7-33.3	262.5-271.8	0.6-2.6	bdl	bdl		
	Average	blue	6	4278	434.7	104.3	133.9	37.4	273.3	2.9	<81.2	bdl		
	D54487d	purple (0.105)	2	2852-2953	339.3-344.5	491.4-495.2	39.2-39.9	26.1-28.1	236.0-262.6	4.4-5.9	bdl-266.3	bdl		
Barrington Tops, NSW	D54487e	purple (0.241)	2	2450-2466	303.5-324.6	1626-1700	33.4-33.6	31.5-32.5	104.9-212.8	9.4-9.6	bdl	bdl		
	Average	purple	4	2680	328.0	1078	36.5	29.6	204.1	7.3	<66.6	bdl		
	EA BAR	green (0.211)	1	6811	61.1	2.8	10.6	25.6	34.8	bdl	bdl	bdl		
	D42708a	blue (1.899)	2	5128-5396	29.6-38.8	6.1-6.6	6.2	120.8-122.1	bdl-3.3	bdl-0.2	0.3-0.5	bdl		
	D42708b	blue (1.852)	2	4518-4625	41.1-119.3	1.7-2.7	5.8-7.3	114.7-115.5	bdl	bdl	bdl	bdl		
	D42708c	blue (1.538)	2	5723-6426	41.3-131.8	0.8-1.1	7.6-9.2	160.5-176.3	bdl-1.5	bdl	bdl-1.0	bdl-0.5		
Average	blue	6	5303	67.0	3.2	7.1	135.0	<0.8	<0.0	<0.3	<0.1			

NB: bdl means below detection limit

Geographic typing of gem corundum: a test case from Australia

Assessment of chemical comparisons

The results from the sourced sapphires and Unsourced NSW Group are plotted on three trace element variation diagrams (Figures 3, 4 and 5) that are commonly used to characterize gem sapphires. The Unsourced NSW Group field touches the edges of the Inverell and Barrington magmatic blue fields in Figure 3, falls in the Inverell blue group field in Figure 4 and overlaps the Inverell blue group more closely than the other magmatic groups in Figure 5. Although in general this would suggest an up to 83% probability that the Unsourced NSW Group came from the Inverell sapphire field, the results in the three variation diagrams are subject to differences in errors related to the different plotting processes, which need assessment. The plus or minus errors for the chemical fields can either reinforce each other and favour closer overlaps or negate each other and favour greater separations. This will affect the extent of any overlaps in the plotted fields and needs consideration in assigning potential correlations.

The element ratios and values are plotted on a log-log scale in Figure 3, a linear-log scale in Figure 4 and linear scales in Figure 5. The log-log plot errors will be relatively constant at about 10% for element abundances above 50 ppm, although analytical uncertainties will increase for element abundances below 50 ppm. Thus, the analytical uncertainty for a single element axis on a log scale would be about 0.1 of a log cycle and for element ratios would be about 0.2 of a log cycle. So over a whole ratio-ratio diagram (Figure 3), the uncertainty in a ratio is 0.2 of a log cycle, perhaps increasing to 0.5 of a log cycle where element abundances under one ppm are involved. The uncertainties become harder to assess where a linear axis is used with a logarithmic axis (Figure 4) and even more so in triangular plots where axes are variously scaled (Figure 5), so that potential correlations may be reduced to probabilities as little as 17%.

For further assessment of probable correlations between the sourced and unsourced sapphires, an additional ratio-

KEY		
Inverell blue (IB)	New England purple (NEP)	Barrington green (BG)
Inverell green (IG)	Barrington blue (BB)	Anakie blue (AB)
Vulcan Forest blue (VB)	Barrington purple (BP)	Unsourced blue (NSW)

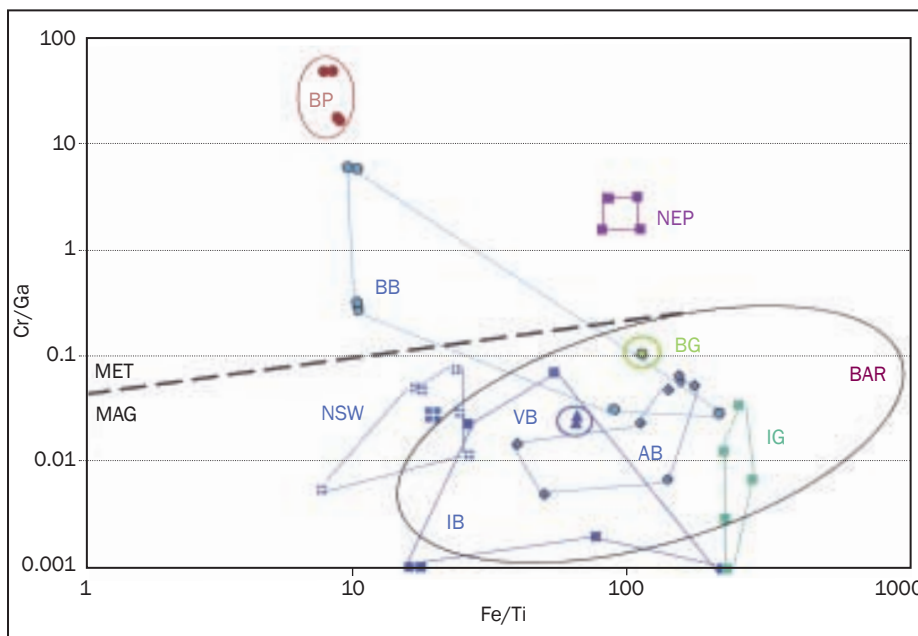


Figure 3: Cr/Ga and Fe/Ti log-log plots of sapphires analysed in this study and an average plot from data in Abduriyim and Kitawaki (2006). BAR is the oval area marking the Barrington magmatic sapphire field using data from Sutherland et al. (2008b, 2009).

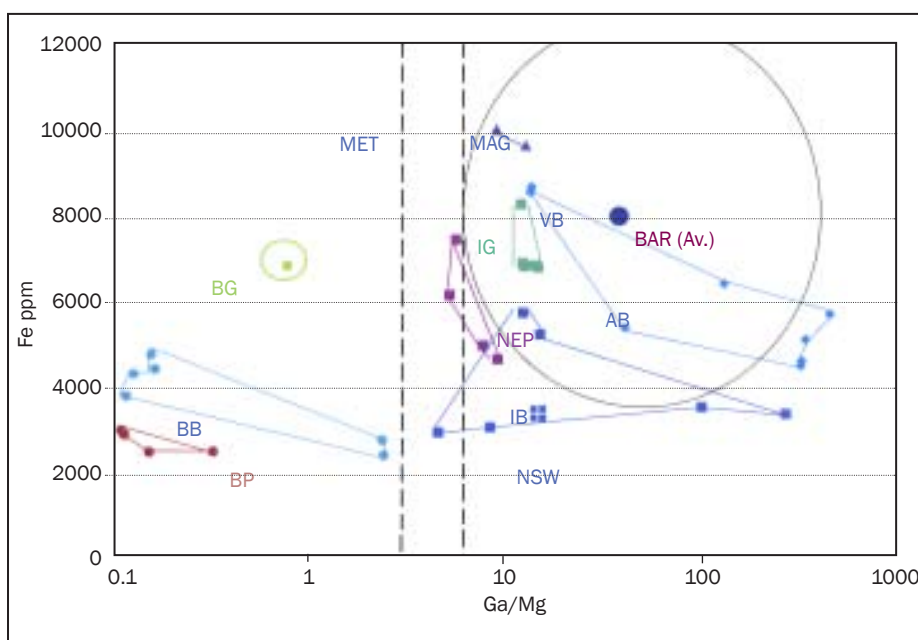


Figure 4: Fe (ppm) contents (linear scale) and Ga/Mg ratios (log scale) of sapphires analysed in this study and averaged from data in Abduriyim and Kitawaki (2006). BAR (av.) is the position of the average Barrington magmatic sapphire data in the near-circular field.

Geographic typing of gem corundum: a test case from Australia

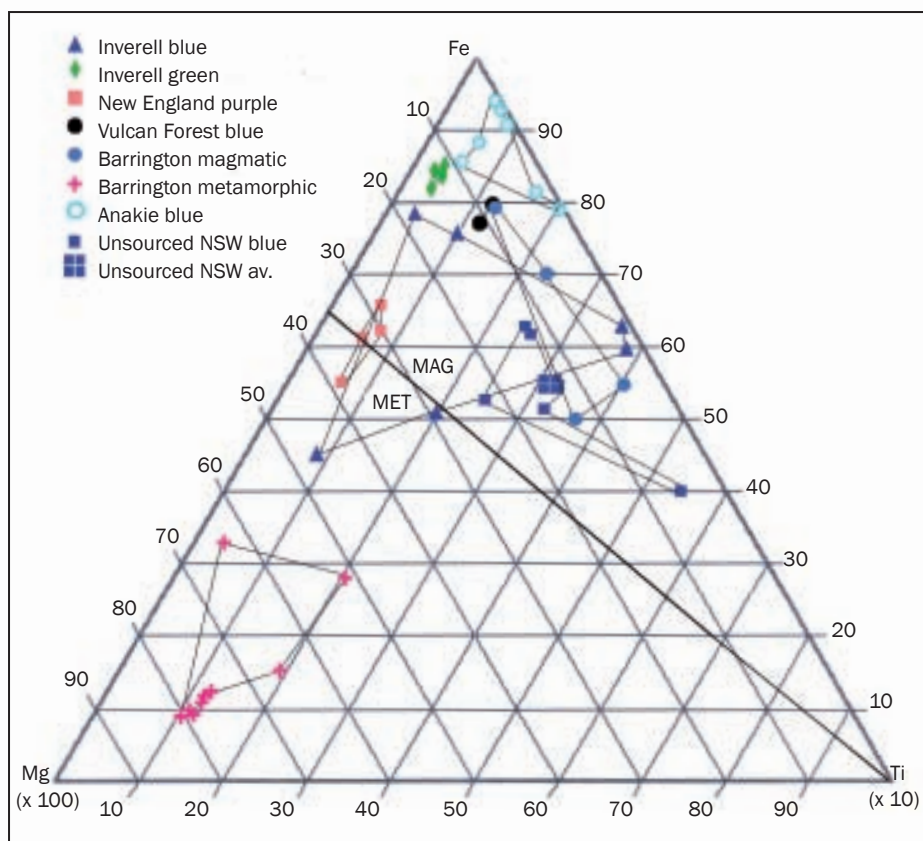


Figure 5: Trace element Fe- Ti × 10 - Mg × 100 diagram, with plots of analyses from this study; Barrington Tops magmatic blue sapphire plots are from Sutherland et al. (2009) and NSW data are from Abduriyim and Kitawaki (2006).

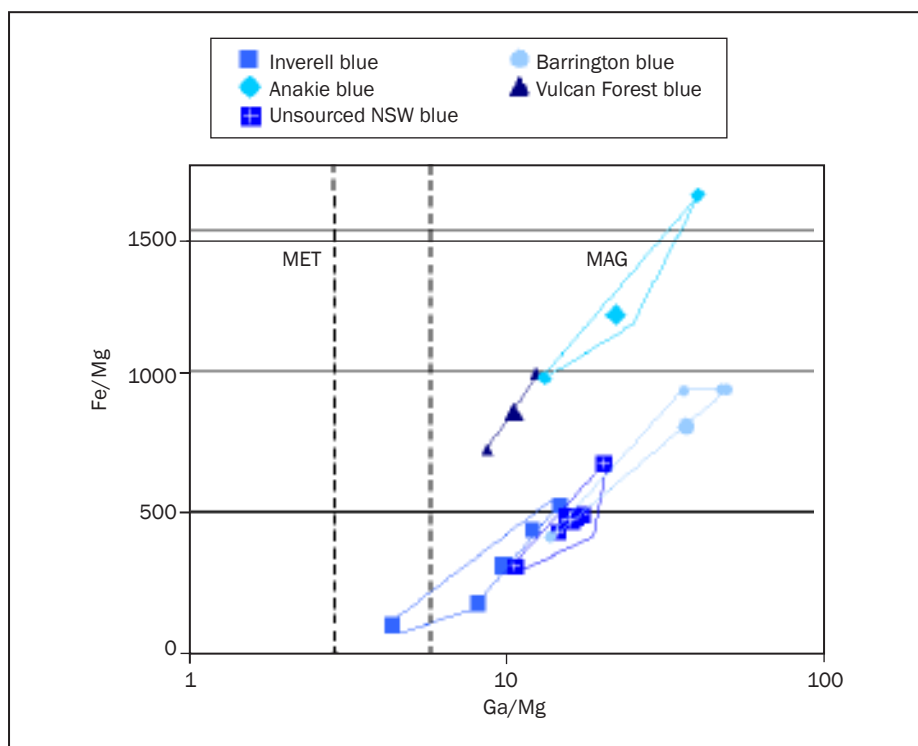


Figure 6: Trace element ratios Fe/Mg-Ga/Mg plotted for magmatic blue sapphires from this study, from Abduriyim and Kitawaki (2006) and from Sutherland et al. (2009).

ratio plot could provide tighter control on relative uncertainties. The results from the sourced sapphires in this study show that Ga and Mg are the two best indicators of origin (magmatic/metamorphic) and that Fe and Mg form another discriminating pair. So, a Fe/Mg-Ga/Mg diagram showing the different magmatic group plots is presented in Figure 6, for comparison with the other diagrams. An average (LA-ICP-MS) plot of magmatic blue Barrington Tops stones (4 analyses) is included from Sutherland *et al.* (2009) in this comparison. The results from the Unsourced NSW Group marginally overlap the Inverell blue field and the Barrington Tops magmatic blue average is farther away. The Vulcan State Forest and the Anakie blue results lie significantly apart from these localities. The average Fe/Mg and Ga/Mg ratios for the groups (excluding the extreme outlying Inverell plots) are respectively Unsourced NSW Group (477±201; 14.9±4.8), Inverell blue group (309±212; 9.35±5.1), Barrington Tops magmatic blue group (802±395; 34.0±11.3), Vulcan State Forest blue group (858±134; 9.7±1.7) and Anakie blue group (1197±437; 49.4±30.0). The two excluded Inverell blue plots show quite different ratios (off-scale) to the other Inverell blue and unsourced NSW blue plots and are regarded as representing a separate subsidiary magmatic source. Thus, the probabilities favour a likely correlation of the Unsourced NSW with the Inverell blue stones, rather than with any of the other groups. This assessment is consistent with a good match for the Inverell green group and analyses of green sapphires in the unsourced New South Wales donation (A. Abduriyim, unpublished analyses).

Other aspects

This study also highlights the unusual geochemistry of the New England purple group, which come from a zoned sapphire-ruby association (Webb, 2007; Sutherland and Webb, 2008). Unlike most known ruby, which has metamorphic associations, the New England ruby shows high Ga levels more typical of magmatic sources. In this, they resemble zoned

Geographic typing of gem corundum: a test case from Australia

sapphire-ruby from Rio Mayo alluvial deposits, Colombia, South America, attributed to a transitional magmatic–metamorphic origin (Sutherland *et al.*, 2008a).

The sporadic high Sn values in some Barrington metamorphic/metasomatic sapphires is another curious feature. Elevated Sn is known in sapphires elsewhere, including Australian sapphires (Khin Zaw *et al.*, 2006). Introduction during polishing using Sn paste is a possibility for faceted stones from collections, although rough, unpolished sapphires from some localities contain significant Sn (I.T. Graham and F.L. Sutherland, unpublished data). Having taken extreme care to avoid any Sn contamination during polishing, high Sn values have still been found by Sutherland *et al.* (2008b) using LA-ICP-MS. In magmatic sapphires, this Sn accompanies elevated Be, Ta and Nb contents and cloudy fluid inclusions are present, so the sapphires may incorporate a mobile volatile component.

Debate exists whether locality of origin for gemstones is important for the gem trade and whether modern gem laboratories can distinguish gems from different localities (McClure *et al.*, 2006). For gem corundum, the geological source can now be specified with some certainty (McClure, 2006 and this paper) and identifying the source can affect the values of stones (Rossman, 2009). The next step of exactly pin pointing precise gem localities or regional deposits is more problematic. The results from this study, however, provide a guide and encouragement towards this future feasibility.

Conclusions

Comparative trace element studies on gem corundum of unknown and known sources, as in this Australian case study, may guide geographical sourcing of unlocalized gemstones. Trace elements in the studied Australian sapphires, including Fe, Cr, Ga and Mg and their ratios, have proved useful in characterizing sapphire localities. In particular, Fe/Mg and Ga/

Mg ratios plotted on a mutual diagram have provided good separations. Faceted sapphires labelled broadly from New South Wales in a previous LA-ICP-MS study are now related to an Inverell, New England gem field source.

Acknowledgements

Thanks are due to Ross Pogson and Gayle Webb, Mineralogy, Australian Museum, Sydney for arranging samples from the collection for study and for help with computer plotting programs. The University of Western Sydney, The Australian Museum, Sydney, and the Gemmological Association of All Japan Research Laboratory, Tokyo, provided facilities to pursue this study. Francesca Kelly, St Peters, Sydney, and Jacqueline Timms, University of Western Sydney, helped with script preparation. Constructive comments on the work were made by Dr Larry Barron, Research Associate, Australian Museum, and Dr Ian Graham, School of Biological, Earth and Environmental Sciences, University of New South Wales, Sydney. An anonymous referee suggested constructive improvements to the paper.

References

- Abduriyim, A., and Kitawaki, H., 2006. Determination of the origin of blue sapphire using Laser Ablation Inductively Coupled Plasma Mass Spectrometry (LA-ICP-MS). *J. Gemmol.*, **30**(1/2), 23–6
- Abduriyim, A., Kiefert, L., Larson, W., Molina, A.J., Smith, C., and Roskin, G., 2006. Locality Origin: Does it really matter? *Gems & Gemol.*, **42**(3), 74–5
- Coldham, T., 1992. The Australian sapphire industry. *Austral. Gemmol.*, **18**(2), 104–8
- Graham, I. T., Sutherland, F.L., Zaw, K., Nechaev, V., and Khanchuk, A., 2008. Advances in our understanding of the gem corundum deposits of the West Pacific continental margins intraplate basalt fields. *Ore Geology Reviews*, **34**, 200–15

- Gulliong, M., and Günther, D., 2001. Quasi 'non-destructive' laser ablation-inductively coupled plasma-mass spectrometry fingerprinting of sapphire. *Spectrochimica Acta B*, **56**(7), 1219–31
- Günther, D., and Kane, R.E., 1999. Laser ablation-inductively coupled plasma-mass spectrometry: a new way of analyzing gemstones. *Gems & Gemol.*, **35**(3), 160–6
- Hughes, R.W., 1997. *Ruby and Sapphire*. RWH Publishing, Boulder, 511 pp
- Khin Zaw, Sutherland, F.L., Dellapasqua, F., Ryan, C.G., Yui, T-F., Mernagh, T.P., and Duncan, D., 2006. Contrasts in gem corundum characteristics, eastern Australian basaltic fields: trace elements, fluid/melt inclusions and oxygen isotopes. *Mineral. Mag.*, **70**(6), 669–87
- McClure, S.F., 2006. Source type classification of gemstones. *Gems & Gemol.*, **42**(3), 102
- Peucat, J.J., Ruffault, P., Fritsch, E., Bouhnik-Le, E., Simonet, C., and Lasnier, B., 2007. Ga/Mg ratio as a new geochemical tool to differentiate magmatic from metamorphic blue sapphires. *Litbos*, **98**, 261–74
- Rankin, A.H., Greenwood, J., and Hargreaves, D., 2003. Chemical fingerprinting of some East African gem rubies by Laser Ablation ICP-MS. *J. Gemmol.*, **28**(8), 473–82
- Rossman, G.R., 2009. The geochemistry of gems and its relevance to gemology: Different traces, different prices. *Elements*, **5**, 159–62
- Shigley, J.E., 2008. A review of current challenges for the identification of gemstones. *Geologija*, **50**(4), 227–36
- Sutherland, L., and Graham, I., 2003. *Geology of the Barrington Tops Plateau. Its Rocks, Minerals and Gemstones, New South Wales, Australia*. The Australian Museum Society, Sydney, 56 pp
- Sutherland, F.L., and Webb, G.B., 2007. Australian sapphires and rubies. *Rocks & Minerals*, **82**(2), 116–25
- Sutherland, F.L., Duroc-Danner, J.M., and Meffre, S., 2008a. Age and origin of

Geographic typing of gem corundum: a test case from Australia

- gem corundum and zircon megacrysts from the Mercaderes-Rio Mayo area, South-west Colombia, South America. *Ore Geology Reviews*, **34**, 155–68
- Sutherland, F.L., Zaw, K., Meffre, S., Giuliani, G., Fallick, A.E., and Graham, I.T., 2008b. Applied mineralogy in characterising origins of natural sapphire and ruby. *Ninth International Congress for Applied Mineralogy Proceedings, 8-10th September, 2008, Brisbane*. AUSIMM, Melbourne, 561–5
- Sutherland, F.L., Zaw, K., Meffre, S., Giuliani, G., Fallick, A.E., Graham, I.T., and Webb, G.B., 2009. Gem corundum megacrysts from East Australian basalt fields: Trace elements, O isotopes and origins. *Austral. J. Earth Sci.*, **56**, 1003–20
- Webb, G., 2007. Ruby suites from New South Wales. *Austral. Gemmol.*, **23**(3), 99–117

Appendix I: Geological settings of analysed sapphire localities

Inverell field, New South Wales

This long established mining field includes some of the highest grade sapphire placer deposits known. It is particularly renowned for its dark blue sapphire, while ruby and fancy-coloured sapphire are recovered as a minor component. The sapphires are recovered from basaltic volcanoclastic, sub-basaltic palaeo-alluvial and recent alluvial deposits associated with extensive alkali basaltic eruptive rocks most of which are between 85 and 30 Ma old (from K-Ar whole-rock basalt and reset zircon fission track ages). The rocks overlie Devonian to Carboniferous folded sequences and Late Carboniferous to Early Permian granites and volcanics that make up the New England Orogen and are unconformably overlain by less folded Permian to Triassic beds of the Sydney Basin sequence. Dating of syngenetic zircon included in the sapphires suggest there were several ages of gem-formation, particularly between 36 and 33 Ma.

Vulcan State Forest, New South Wales

An intermittently mined sapphire placer field in the Oberon area lies within folded Silurian to Devonian sedimentary and volcanic beds and Carboniferous granites of the Lachlan Orogen, which are overlain by Late Cenozoic alkali basalt remnants. Associated zircon megacrysts in the placers give fission track ages of 157 to 154, 24 to 20, 16 to 15 and 9 Ma and U-Pb dating of these zircons indicates several episodes of Late Cenozoic gem formation, but no zircon included in sapphire is as yet dated.

Barrington Tops, New South Wales

This field is noted for near-equal amounts of ruby, fancy coloured and blue metamorphic sapphire and blue magmatic sapphire. Recent mining, now ceased, was in placers shed from the adjacent basalt plateau, dominated by alkali basalts. Dating of basalts, a rare gem-bearing diatreme and associated zircon megacrysts suggest multiple eruptive discharges of gem materials between 61 and 4 Ma ago. The underlying rocks consist of folded Late Palaeozoic sequences, a Late Permian granodiorite pluton and minor Early Mesozoic dykes and tuffs within the New England Orogen. At least two ages of magmatic gem-formation are suggested by U-Pb dating of separate zircon megacryst types at 60 and 45 Ma, while the metamorphic sapphire and ruby was probably formed prior to initial basaltic eruption.

Anakie field, Queensland

This major sapphire mining field is made up of several alluvial fields lying within an eroded alkali basaltic province now largely represented by numerous plugs and rare lavas (dated from 58 to 14 Ma). The sapphires are recovered from multi-recycled alluvial deposits and rare volcanoclastic remnants, while rare sapphire xenocrysts and sapphire-bearing syenite xenoliths are found in a few plugs. The field is noted for its large yellow, orange and black star sapphires among the prevailing blue and green sapphires. The basalts intruded the Anakie Inlier, a basement feature that incorporates Neoproterozoic to Early Palaeozoic metamorphic rocks, a Middle Devonian granite pluton and overlying Late Devonian to Carboniferous sedimentary and volcanic beds. Sapphire formation extends to ages at least greater than 58 Ma.

The Authors

Dr F. Lin Sutherland

School of Natural Sciences, BCRI Campus, University of Western Sydney, Locked Bag 1797, Penrith South DC, NSW 1797, Australia
Email: L.Sutherland@uws.edu.au
Mineralogy, Australian Museum, 6 College Street, NSW 2010, Australia

Dr Ahmadjan Abduriyim

Research Laboratory, Gemmological Association of All Japan (GAAJ)-ZENHOKYO, 5-25-11 Uneo Taitoku, Tokyo, 110-0005 Japan
Email: Ahmadjan@gaaj-zenhokyo.co.jp

Dickite: a gem material for carving from Thailand

Seriwat Saminpanya, Chaichart Dharmgrongartama and Namrawee Susawee

Abstract: Dickite ($\text{Al}_2\text{Si}_2\text{O}_5(\text{OH})_4$) from Saraburi, Thailand, is a raw material for the ceramics industries. It is also an ornamental gem material and its physical and gemmological properties are reported. In the gem trade, three grades are distinguished: grade A (cream and red with Al_2O_3 ~41 wt% and SiO_2 ~43 wt%), grade B (grey); and grade C (dull red) (Al_2O_3 ~15-16 wt% and SiO_2 ~79 wt%). The XRD results indicate that the samples of grades B and C contain quartz. The dickite occurs as cryptocrystalline aggregates and SEM images indicate that these are pseudo-hexagonal plates stacked like books. Even though dickite has a hardness of only 1½–2 on Mohs' scale, it is quite coherent and easily carved. A survey indicates that carvers prefer the unique colours and textures of grade A samples to produce animal figurines. The rough stones should be chosen with care in order to match the appearance and size of the expected product.

Keywords: carving, dickite, ornamental gem material, properties, spectroscopy, Thailand



Introduction

The demand for ornamental gem materials in the form of carvings is increasing in various markets. Some raw materials other than expensive mainstream and traditional materials such as jadeite and nephrite, have become a choice for some carvers and consumers. Indeed, several soft materials such as steatite, gypsum, marble, calcite and fluorite can be carved and sold in the market. These materials can be more easily carved and entail lower costs and less time than harder and tougher ones. The quality and the fascinating appearance of the products are dependent on factors such as the unique properties of the material itself, the design, and the skill and experience of the carver. Although less durable than tougher materials, their beauty and rarity make

them interesting for consumers. Carvings are generally used for decoration or showcase display, therefore the hardness and toughness of the items are less important than their beauty.

Dickite, described here, is one of the soft materials in the mineral kingdom which can make fascinating products. A highly pure variety (red breccia-like appearance) has been used as a raw material for a long time. However, the products are still locally marketed as, for example, the decorations on some temples (*Figure 1*). Carved dickite items can take various forms, for example Buddha statuettes, tables, jars and animal figurines. For industry, dickites can be used as a raw material for refractory products, tiles and white cement. Dickite ($\text{Al}_2\text{Si}_2\text{O}_5(\text{OH})_4$) is a clay mineral with a low hardness on Mohs'

scale of 1½–2 and occurs in fine-grained masses in a range of colours: generally cream, greyish green, pale greyish blue, white, pale green, yellow or dark blue (Khuentak, 1988b: 28-9). However, the owner of a mine in Thailand revealed that there are also red, pink and yellowish cream varieties with a waxy lustre. Khuentak (1988b: 29) classified dickites in the Thai deposits into three broad grades: i.e. grade A (high purity) grade B (less pure and contaminated by other minerals) and grade C (low quality and similar to rhyolite in appearance).

Originally, dickite in Thailand was thought to be pyrophyllite and this name appeared in the concessions for mining from the government (Yaemniyom, 1988: 27), so this is how it was sold. The two minerals are similar in appearance

Dickite: a gem material for carving from Thailand

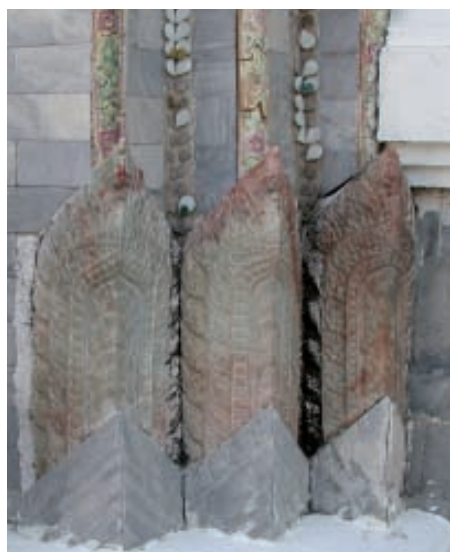


Figure 1: (Left) Three pieces of carved dickite (cream+red) are used to renovate parts of the throne-hall in the Phra Maha Monthien, a group of buildings in the Grand Palace, Bangkok. (Below) Phra Mondob (pavilion) of the footprint of Lord Buddha at Wat (temple) Phra Buddhabat in Saraburi Province, decorated with the carved dickite pieces (marked with arrows).



and some of their physical properties are very close to each other. However, misidentification of dickite may cause trading at unrealistic prices. Some mine operators sell their crushed dickite for 300–1000 Thai Baht (~ US\$9–\$30) per ton to the ceramics industry, while some Taiwanese customers may buy grade-A blocks of dickite for 10,000 Baht (~US\$300) per ton specifically for carving (based on information from

a mine operator). In this way dickite from Thailand may appear in Taiwanese markets as carved gem products.

The Department of Mineral Resources of Thailand (Yaemniyom, 1988: 27, Khuentak, 1988a: 67, 69; and Khuentak, 1988b: 28-9) reported that the reserves of dickite in Thailand total approximately 20,000 tons. Moreover, grade-A dickite is rare, so the reserves of this variety may be the largest in the world.

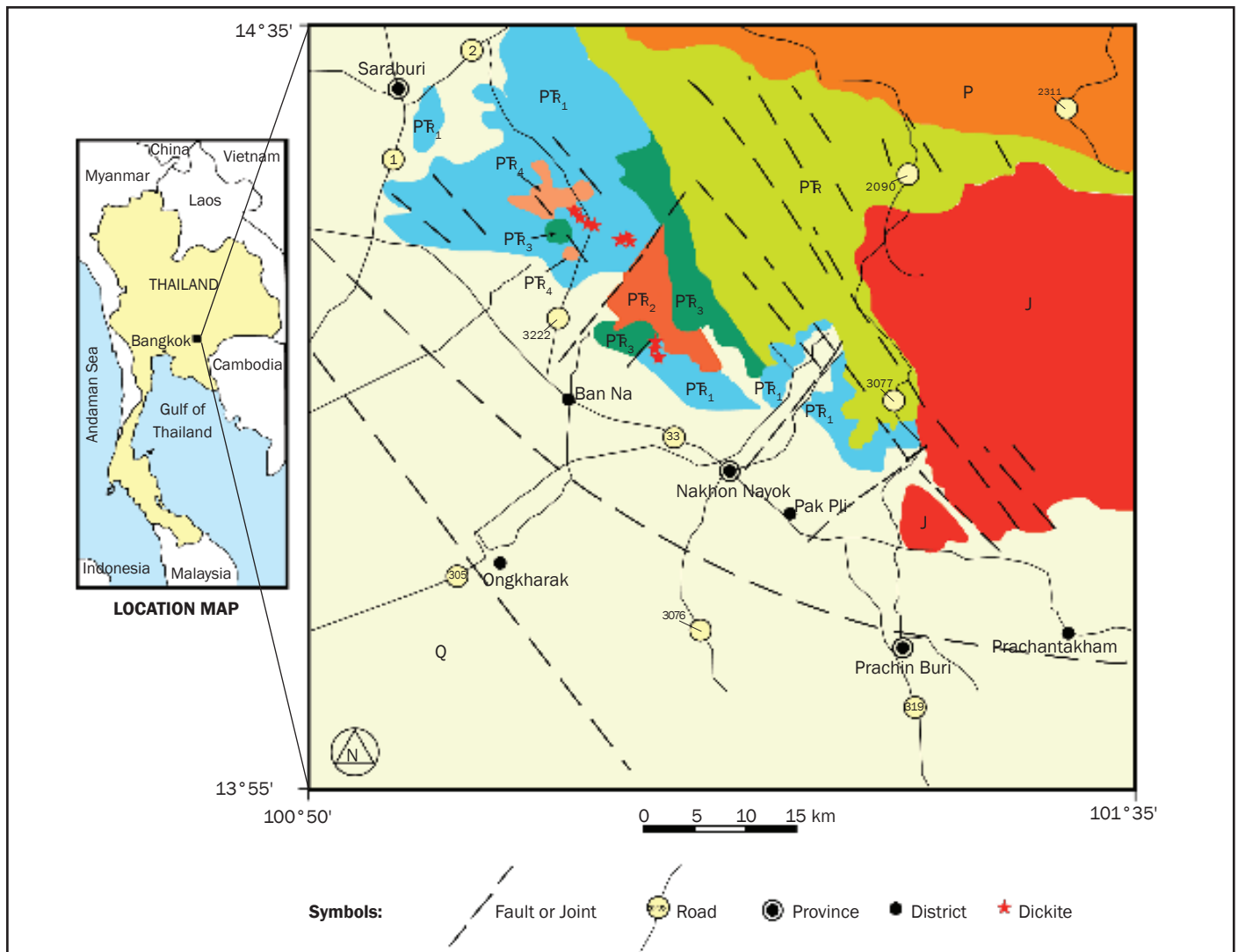
Dickite has been studied in many aspects by several authors. Spectroscopy and structure were investigated by e.g. Brindley *et al.* (1986), Johnston *et al.* (1998), Beaufort *et al.* (1998), Zamama and Knidiri (2000), Balan *et al.* (2002) and Johnston *et al.* (2002). Works on heat treatment of dickite include Kerr and Kulp (1948), Frost and Vassallo (1996) and Shoal *et al.* (2001). Marumo (1989) studied the origins of dickite, and isotope geochemistry has been reported by Girard and Savin (1996). However, dickite has not yet been reported in any gemmological literature.

Although carved dickite cannot be used to substitute for the much harder carving materials such as jadeite or nephrite, it has the advantages of low price, a unique beauty and ease in carving due to its low hardness and low brittleness. This paper will present a brief geology of the dickite deposits in the study area and the subjective points of view obtained from carvers will be compared. Finally, the physical, chemical, gemmological and spectroscopic properties of dickite will be discussed and compared with other carvable stones.

Location and brief geology of deposits

There are two known dickite deposits in Thailand. The larger is located near the border of Nakhon Nayok and Saraburi provinces and the other is in the Muang district of Nakhon Nayok province. Dickite occurs in Permo-Triassic volcanic rocks (Salayaphong, 1996) (Figure 2). Khuentak (1998b) reported that at these localities mineral solutions and volatiles seeped into fractures and cavities in the host rocks, rhyolites and tuffs, and transformed them hydrothermally to dickite. This is consistent with its paragenesis in other world localities where the dickite is formed by replacement of volcanic rocks and fracture-filling (Choo and Kim, 2004; Viorica *et al.*, 2004; Deyell *et al.*, 2005). Alumina and H₂O are added by means of the hydrothermal process while CaO, Na₂O and K₂O are reduced. In the Khoa Cha-Om mine, Saraburi, this process resulted in

Dickite: a gem material for carving from Thailand



Explanation of Geological Map

<p>Q</p>	<p>Clastics</p>	<p>Clay, silt, sand and gravel</p>	<p>Quaternary</p>	
Unconformity				
<p>J</p>	<p>Clastic rocks</p>	<p>White to brown quartzitic sandstone underlain by maroon micaceous and calcareous siltstone and sandstone with basal conglomerite.</p>	<p>Jurassic</p>	
Unconformity				
<p>PR</p> <p>Volcanic rocks</p> <p>Unclassified quartz-feldspar flow tuff overlain by lapilli flow tuff and volcanic breccia.</p>	<p>PR₄</p>	<p>Lava flow and shallow intrusive</p>	<p>Permo-Triassic</p>	
	<p>PR₃</p>	<p>Pyroclastic rocks and dyke rocks</p>		<p>Deep green, medium- to fine-grained, locally vesicular, porphyritic andesites and equigranular basaltic andesites.</p>
	<p>PR₂</p>	<p>Pyroclastic rocks</p>		<p>Pink and greyish green, massive, medium- to coarse-grained quartz-feldspar flow tuff with flow orientation of rock fragments and local dykes of porphyritic andesites and basaltic andesites.</p>
	<p>PR₁</p>	<p>Pyroclastic rocks, dyke rock and volcanic plug</p>		<p>Maroon, pink and green, massive, fine- to medium-grained plagioclase flow tuff with some oriented rock fragments.</p>
Unconformity				
<p>P</p>	<p>Chemical and clastic rocks</p>	<p>Limestone, chert, shale, siltstone, sandstone and shale.</p>	<p>Permian</p>	

Figure 2: Geological map of Saraburi and Nakhon Nayok provinces showing locations of dickite deposits (modified from Salayaphong, 1996: 18).

Dickite: a gem material for carving from Thailand

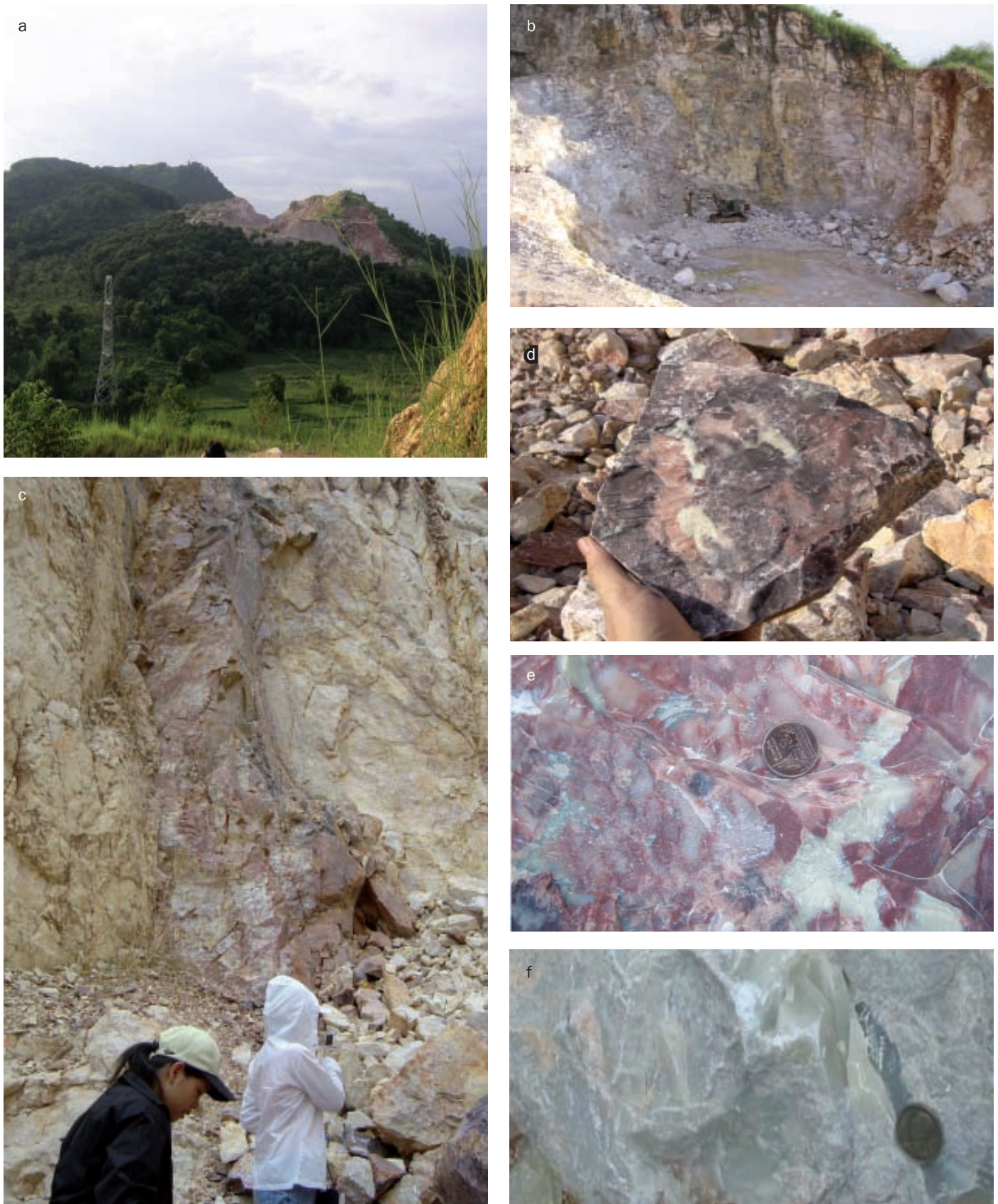


Figure 3: (a) The mine at Khoa Cha-Om, Tambon Cha-Om, Amphoe Kaeng Khoi, Saraburi province, picture taken from 21 km post on route No. 3222. (b) The quarry at the mine. (c) Cream and red grade A dickite occurs in the dark red vein near the centre of the picture.

(d) Block of cream and red dickite from the vein visible in (c). (e) The detailed texture of cream and red dickite. (f) The high quality, cream variety of dickite exists as veinlets in grey dickite of lower grade, but this cream grade is not abundant.

Dickite: a gem material for carving from Thailand

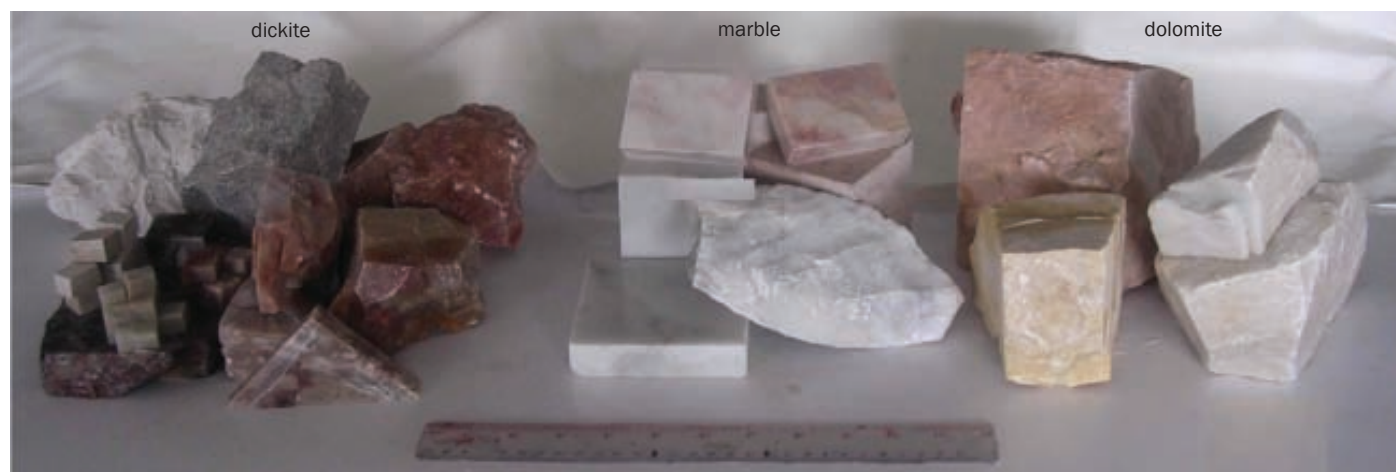


Figure 4: The rough materials used in this study showing the range of their colours.

small scale or vein-like ore bodies (Figure 3). The distribution of the ore bodies is dependent on the structure (cavities or fractures) of the host rocks and may appear random. Some domains in the host rocks are completely converted to dickite while others have only been partially replaced. Small crystals of pyrite can be found disseminated in some zones.

Materials and methods

The dickite samples for the present study were collected from Suthakit Mining Co. Ltd, located in the area of Khao Cha-Om, Cha-Om subdistrict, Kaeng Khoi district, Saraburi province. Two low-durability materials which are actively mined and available in Thailand were also collected for comparison: first, marble from Na Phra Laan, Saraburi province (the quarries are located to the northwest and approximately 50 km away from the dickite deposit) and second, dolomite from P&S Pand's Group Co. Ltd., Kanchanaburi province (located to the west and about 300 km away from the dickite deposit) (Figure 4). The marble and dolomite are commonly used for carving decorative items in Thailand. Dickite samples were sorted on the basis of different colours and textures (Figure 5).

Carving dickite

According to chemical compositions presented later (Table IV), dickite samples DA (cream) and DB (cream+red) are both of high purity. Therefore they are grouped in this study as grade A. Samples DC (grey-

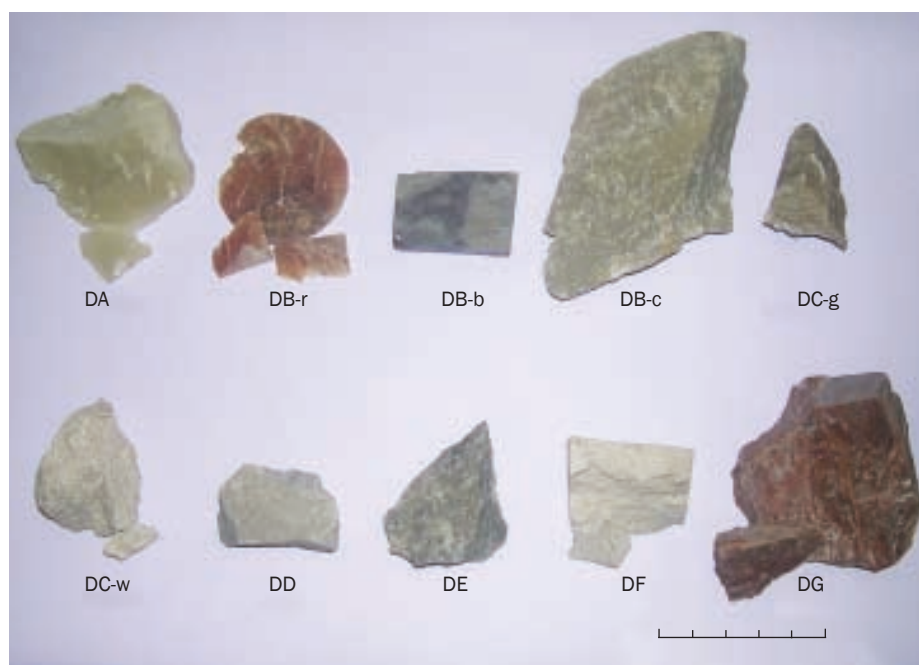


Figure 5: The varieties of dickite studied: samples DA, DB-r and DB-b were treated as the top-quality group (Grade A) for gem ornamental material due to their translucency, waxy appearance and beautiful colour and texture. The rest are dull, subtranslucent to opaque and more brittle. Sample DF is dull white and brittle with high porosity while DG is dark red, fine-grained and massive, harder and more brittle; these two samples are probably only partly converted to dickite from tuff and rhyolite respectively.

yellow), DD (grey), DE (dark grey) and DF (dull white) are grouped as grade B because of similarity in composition and significant impurity. The samples of DB (cream+red) with breccia-like appearance were selected to be carved in this study as they are available in relatively large amounts in the mine and the colours of the samples are more beautiful than the rest. Moreover, this variety is popular for carving in Thailand. The DA variety is too rare to be used in this carving survey and

the DC and grade C varieties are either too dull or brittle — making them unsuitable as carving material.

The equipment used for carving includes rock saw, table, hose, foredom (flexible shaft) and mounted abrasive point, sanding paper, goggles, mask, etc. The DB samples with the fewest and least fractures were selected and sawn or trimmed to the required size. Then they were carved according to the following procedures (Wertz and Wertz, 1994: 12–42):

Dickite: a gem material for carving from Thailand



Figure 6: A selection of carvings made from dickite DB (cream and red). (a) Image of Buddha. (b) Chinese Buddha ('laughing Buddha'). (c) Cameo portrait of a lady. (d) Horse.

1. drawing an outline on the rough (designing);
2. pre-forming with a saw;
3. grinding the outline;
4. grinding the features;
5. sanding; and
6. polishing.

This job was done by nine carvers who have been working on carving rocks and minerals for more than five years, and the questions in this survey sought their opinions on carving dickite compared to marble and dolomite.

Physical gemmological and spectroscopic studies of samples













Grade A (DA and DB) and grade B (DC) dickites were investigated. Samples DD, DE and DF were also studied but not chemically analysed. The specific gravity (SG) was measured by the hydrostatic method using an electrical balance. The refractive index (RI) of dickite samples could not be obtained accurately using a standard refractometer with a glass table and attempts to measure RI by the use of a reflectance meter only gave unreliable results. However, the Becke Line method can give a single RI value regardless of birefringence. Hardness pencils were used to obtain Mohs' hardness values. Polarizing microscopy and scanning electron microscopy (SEM) were employed to study the habits of dickite crystals. Infrared and Raman spectra were obtained, and the mineral species present in the samples were identified using X-ray diffractometry (XRD). Chemical compositions of dickite

Table I: Summary of opinions of nine carvers on the rough samples of dickite, marble and dolomite prepared for carving.

Property	Dickite (cream+red)	Marbles (white-grey; pink; black)	Dolomite (yellow)
Colour and texture	Uneven colour and texture: can be used for carvings but the rough samples should be chosen carefully; not suitable for portrait but good for animal figurines.	Even colour: suitable for carving portraits, spiritual images and animal figures.	Even colour: suitable for carving as portraits and animal figurines.
Hardness	Lowest	Low	Low but harder than dickite and marble.
Toughness	Higher than marble and dolomite, less risky for breakage than marble and dolomite, suitable for both cameos and round work (three-dimensional items).	Less tough and more brittle than dickite: more suitable for cameos than round work.	The brittleness is intermediate between dickite and marble but it contains abundant fractures: more suitable for cameos than for round work.

Dickite: a gem material for carving from Thailand

Table II: Dickite, marble and dolomite carvings used in the survey of the nine carvers, and the summarized opinions of the carvers.

Carving form	Dickite (cream+red)	Marbles (white-grey; pink; black)	Dolomite (yellow)
Horse	 <p data-bbox="304 656 667 763">Easier than marble due to higher toughness but care is needed, then the trunk may be carved to support horse's body.</p>	 <p data-bbox="730 656 1054 763">The trunk must be carved to support the horse as the legs of the horse would not be tough or strong enough.</p>	 <p data-bbox="1129 656 1465 763">The trunk must be carved to support the horse as the legs have too many fractures and are too brittle.</p>
Deer	 <p data-bbox="316 1104 655 1155">Easier than marble and dolomite as dickite is tougher.</p>	 <p data-bbox="742 1104 1043 1155">The product has some cracks due to brittleness.</p>	 <p data-bbox="1107 1104 1485 1211">The rock can be carved as a cameo. It is brittle probably because explosives were used to extract the ore.</p>
Bear	 <p data-bbox="308 1552 662 1659">The carving was easier than those of marble and dolomite because dickite is tougher and the object has fewer sharp edges.</p>	 <p data-bbox="743 1552 1038 1603">Though the sample is brittle, no cracks have developed.</p>	 <p data-bbox="1141 1552 1449 1632">The product is good because the rock is hard and beautiful colour.</p>
Boxers	 <p data-bbox="296 2000 675 2107">The sample can be carved in round work but special care must be taken because the object has some thin and long components.</p>	 <p data-bbox="730 2000 1054 2051">The rock sample is not suitable for this form of carving.</p>	 <p data-bbox="1118 2000 1474 2051">The sample is not suitable for this form of carving.</p>

Dickite: a gem material for carving from Thailand

Table II (continued)

Carving form	Dickite (cream+red)	Marbles (white-grey; pink; black)	Dolomite (yellow)
Lady with a bowl	 <p>Can be carved as round work but uneven colour in the sample is not suitable for the this form of carving.</p>	 <p>Can be carved in this form but the colour is too pale; the pink marble would be more suitable.</p>	 <p>Can be carved but the raw material should be free of fractures.</p>
Lady portrait cameo	 <p>Higher toughness but unevenness of cream and red colours in the sample can make the product less beautiful.</p>	 <p>Suitable for this form of carving as cameos are less fragile than the round work and the even colour is not a drawback to the beauty of product.</p>	 <p>Suitable for this carving form because the cameo is less fragile than round work and its even colour does not affect its beauty. Heavy fractures in the sample are difficult to avoid.</p>

were analysed by wavelength dispersive-X-ray fluorescence (WD-XRF) for the major elements with the use of the standards SY-2 and SY-3 from CCRMP (Canadian Certified Reference Materials Project). The traces were analysed with an atomic absorption spectrophotometer (AAS) using the standard solutions with calibration curves. The H_2O^- data were obtained by heating the samples at the temperatures of 105–110°C and at 900–1050°C the values of loss on ignition (LOI) were collected. Details of these techniques can be found in, for example, Potts (1987), Skoog and Leary (1992), Reed (1996, 1997), Hibbard (2002) and http://www.crrp.cnrs-nancy.fr/Geostandards/GGR_ms.v03/ms072.html.

Results and discussion

It should be noted that in some parts of this paper the authors report or focus mainly on the properties of dickite samples

DA, DB and DC since the rest are not important in terms of unsuitable conditions for carving and their properties are more likely to be the same as DC. The results for an experiment on carvings, physical and gemmological properties and XRD, FTIR and Raman microprobe, will be discussed as follows.

The results of a study on carving different subjects in different materials

Some examples of the dickite carvings studied are shown in *Figure 6*. Samples of dickite, marble and dolomite have their own unique blend of colour and texture as well as different hardnesses and strengths. For example, marble and dolomite are harder, but are more brittle than dickite and have a higher tendency to break if the carved object has a sharp corner or a long thin component. The evaluation information on the rough materials used

in this work supplied by the carvers is summarized in *Table I*.

This study has concerned the carving of such subjects as a horse, a deer, a bear, boxers, a lady with bowl and a cameo of a lady. The images of the carved items and the opinions of nine carvers while they were carving them are summarized in *Table II*.

Physical and gemmological properties

The appearance and characteristics of dickite compared to marble and dolomite samples are shown in *Figure 4* and *Table III*. The crystal habit of dickite in polished section viewed under the polarizing microscope is not decipherable because of its intergranular texture; red inclusions can be clearly seen in sample DB (*Figure 7*). Under the SEM, there are good images of polycrystalline habit in which the crystals show granular texture

Dickite: a gem material for carving from Thailand

Table III: Some physical and gemmological properties of dickite, marble and dolomite used for carving.

Property\Material	Dickite	Marble	Dolomite
Chemical formula	$\text{Al}_2\text{Si}_2\text{O}_5(\text{OH})_4$	CaCO_3	$\text{CaMg}(\text{CO}_3)_2$
Crystal system	Monoclinic	Trigonal	Trigonal
Locality in Thailand	Cha-Om subdistrict, Kaengkhoi district, Saraburi province	Khao Ngob (for white-grey and pink varieties) and Khao Khaow (for black variety), Na Phra Laan subdistrict, Chalermphrakiat district, Saraburi province	Wang Dong subdistrict, Muang district, Kanchanaburi province
Crystal habit	Polycrystalline-massive	Polycrystalline-massive	Polycrystalline-massive
Colour	Cream, red, grey, white	White-grey, pink, black	Grey, light yellow, pink
Hardness (Mohs) scale*	1½–2	3	3½–4
Lustre of polished surface	Waxy	Subvitreous	Waxy to subvitreous
Transparency	Translucent to opaque	Translucent to opaque	Translucent to opaque
SG	DA = 2.58–2.66 (av. = 2.61, n=33)	2.58–2.75 ^a	2.84–2.86 ^a
	DB = 2.56–2.62 (av. = 2.61, n=33)		
	DC = 2.58–2.64 (av. = 2.61, n=33)		
RI	1.560 ^b ; 1.561–1.570 ^a	1.486–1.660 ^a	1.500–1.681 ^a

a. Data from <http://www.mindat.org/min-1287.html> (the RI of marble is from calcite).

b. Tested by the Becke Line method under the transmitted light microscope.

Note: Other tests for gemmological properties, e.g. ultraviolet, Chelsea colour filter and spectroscope, do not give any useful result.

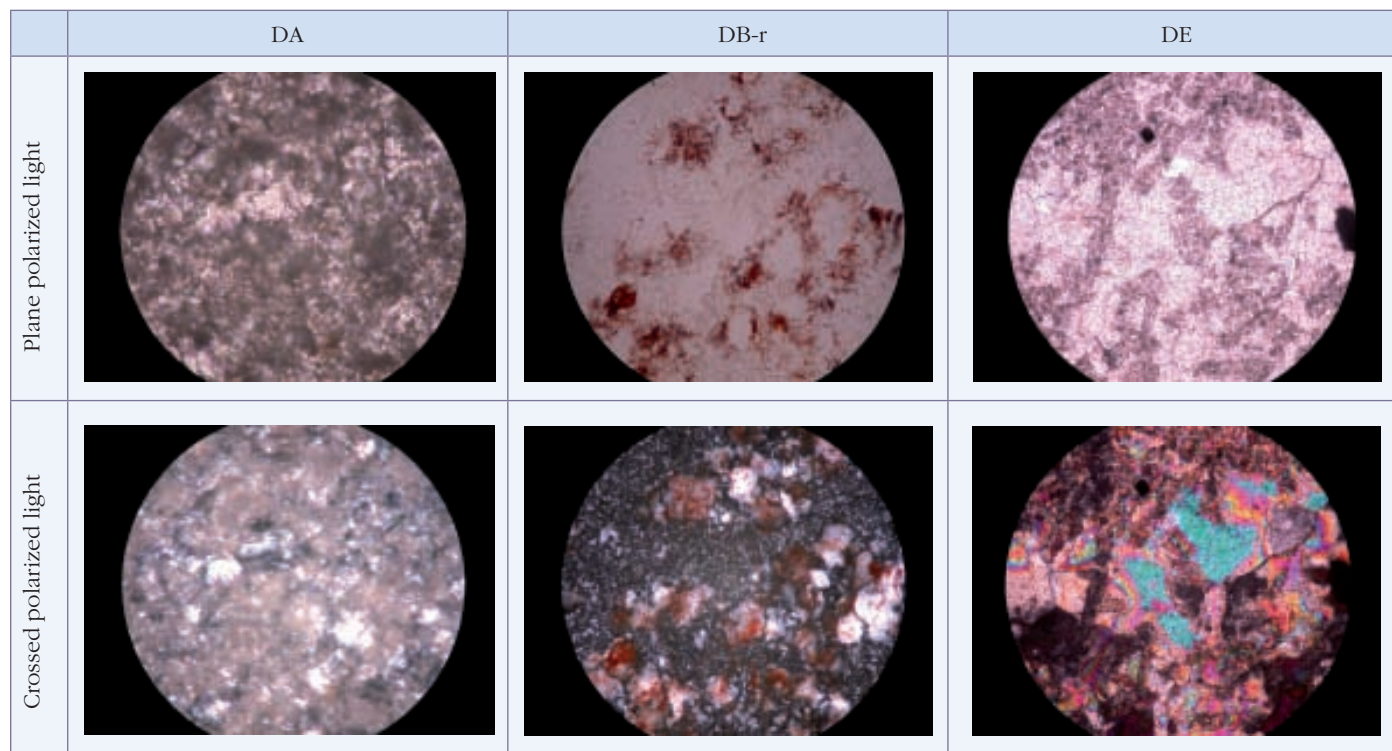


Figure 7: Photomicrographs of dickite thin sections from samples DA, DB-r and DE under a polarizing microscope. At these magnifications, all samples exhibit granular textures. Compositional and spectral information for DA are given in Tables IV, V and VI. The red area of the cream and red variety sample DB-r shows red platelet inclusions which are probably hematite. The DE sample contains some larger grains which show the uniaxial interference figure typical of quartz. The high birefringent colours on this slide are due to it being thicker than the normal 0.03 mm. Magnification 400x.

Dickite: a gem material for carving from Thailand

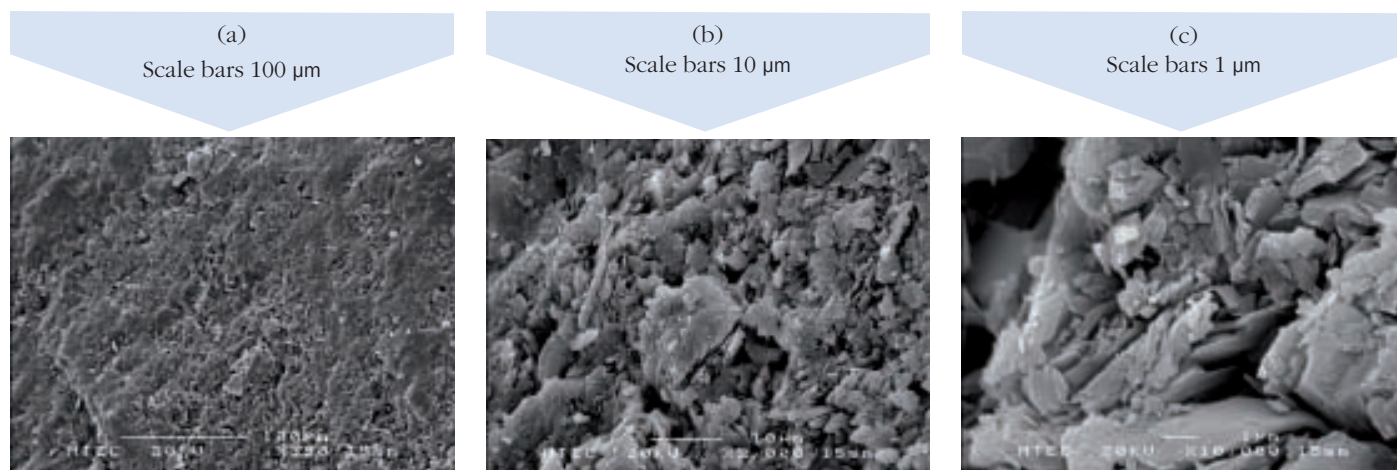


Figure 8: SEM images of cream dickite (DA). The plate-like crystals are tightly intergrown and very narrow spaces between crystals mean that porosity is low.

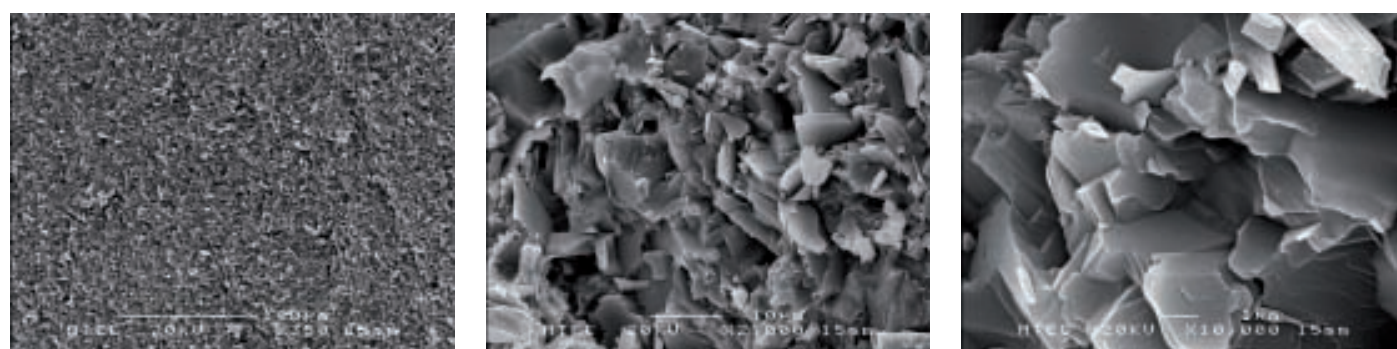


Figure 9: SEM images of dickite sample DB-r (cream and red). In c, the bright crystals at the top-right corner are probably hematite. The crystals are tightly packed, massive and porosity is low.

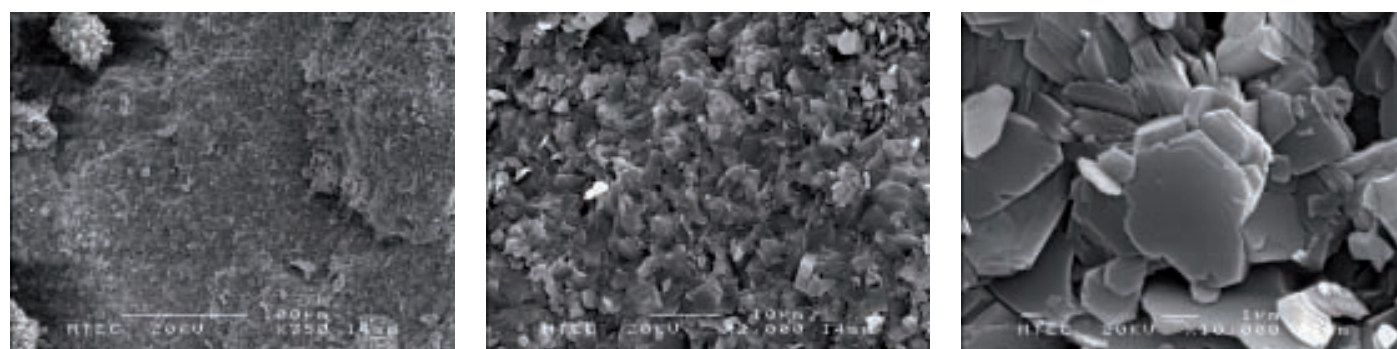


Figure 10: SEM images of white-grey dickite (DC-w). There are more spaces between grain boundaries in this sample and it has higher porosity than DA and DB. The image (c) clearly shows stacks of pseudo-hexagonal platy crystals. Note that the crystal habit of samples DD, DE and DF are similar to that of DC.

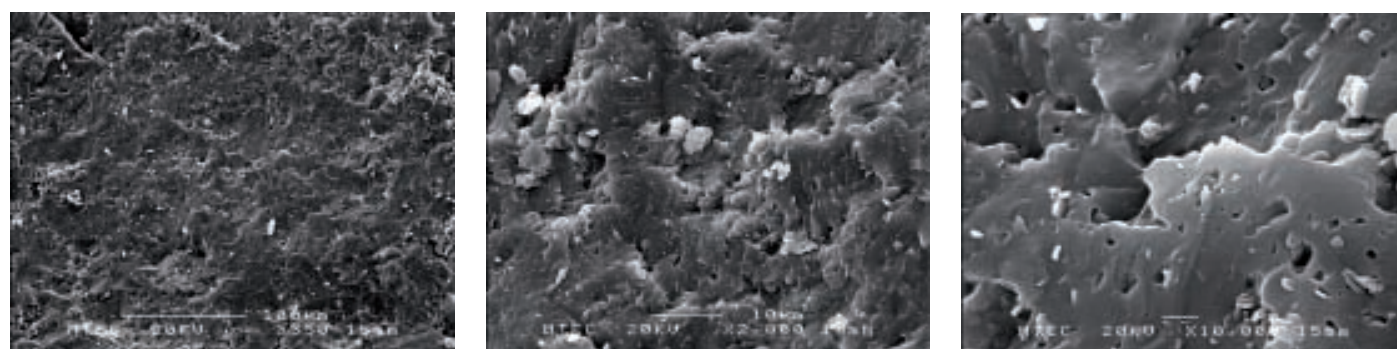


Figure 11: SEM images of dull-red sample DG (rhyolite?). Even at high magnification, the sample is very fine-grained (glass?) although it contains some pits which give it some degree of porosity. Some of the individual pits contain a platy or tabular crystal.

Dickite: a gem material for carving from Thailand

Table IV: The chemical compositions of dickite, marble and dolomite from Thailand.

Sample	Dickite						Marble ^a	Dolomite ^b	
	DA 1-3 (cream)	DB 1-3 (cream+red)	DC 1-3 (white grey)	DD 1-3 (dark grey)	DE 1-3 (dark grey)	DF 1-3 (dull white)	White-grey	White	Pink-yellow
Major element (wt%):									
SiO ₂	43.39	42.85	76.12	79.37	75.52	78.18	0.65	0.15	0.32
TiO ₂	<0.05	<0.05	0.12	0.11	0.16	0.13	n/a	n/a	n/a
Al ₂ O ₃	41.39	41.73	16.89	14.60	17.21	15.41	0.03	n/a	n/a
Fe ₂ O ₃	<0.10	0.10	0.43	0.34	0.45	0.22	0.10	0.20	0.24
MnO	<0.05	<0.05	0.06	0.05	0.05	<0.05	n/a	n/a	n/a
CaO	<0.10	<0.10	<0.10	<0.10	<0.10	<0.10	54.93	31.23	31.31
MgO	<0.10	<0.10	<0.10	<0.10	<0.10	<0.10	0.43	21.41	21.14
Na ₂ O	<0.10	<0.10	<0.10	<0.10	<0.10	<0.10	n/a	n/a	n/a
K ₂ O	<0.05	<0.05	<0.05	<0.05	<0.05	<0.05	n/a	n/a	n/a
P ₂ O ₅	<0.05	0.16	<0.05	<0.05	<0.05	<0.05	n/a	0.01	0.01
LOI	14.15	14.20	5.63	4.83	5.90	5.32	43.55	n/a	n/a
H ₂ O ⁻	0.50	0.46	0.27	0.21	0.22	0.22	0.28	n/a	n/a
Trace element (ppm):									
Co	<3	<3	<3	<3	<3	<3	n/a	n/a	n/a
Cr	5	5	13	9	12	6	n/a	n/a	n/a
Cu	6	3	6	4	13	15	n/a	n/a	n/a
Ni	<2	<2	2	<2	3	<2	n/a	n/a	n/a
Sr	93	920	61	25	18	30	n/a	n/a	n/a
Zn	3	8	2	2	2	2	n/a	n/a	n/a

a. An analysis of marble from Khao Ngob, Na Phra Laan, Saraburi province, provided by Thai Marble Corp (TMC).

b. Analyses of dolomite from Wang Dong subdistrict, Muang district, Kanchanaburi province, provided by P&S Pand's Group Co. Ltd.

n/a = data are not available.

Table V: Absorption peaks, bands and shoulders in the infrared spectra of dickite samples, DA, DB and DC (in cm⁻¹).

Sample	Position																	
	1	2	3	4	5	6(B)	7	8(Sh)	9(Sh)	10	11	12	13(B)	14(B)	15	16	17	18
DA (Cream)	2140	2216	2678	2686	2706	3400-3900	4196	4353	4435	4529	4587	4732	5230	5553	7072	-	7231	7354
DB (Cream+Red)	2138	2216	2673	2686	2706	3000-4000	4194	4353	4435	4530	4585	4731	5222	5557	7070	7194	7246	7356
DC (Grey)	2135	2234	2672	2686	2705	3300-3800	4194	4353	4435	4528	4590	4732	5239	5564	7069	-	-	-
Average	2138	2222	2674	2686	2706	-	4194.7	4353	4435	4529	4587	4731.7	5230.3	5558	7070	7194	7239	7355

B=Band; Sh=Shoulder

Table VI: Raman peak positions in wave numbers (cm⁻¹) of three dickite samples (DA, DB and DC).

Sample	Position																
	1	2	3	4	5	6	7	8	9	10	11	12	13	14*	15	16	17
DA (cream)	133	-	-	242	269	334	434	-	460	748	793	914	1123	-	3624	3645	3687
DB (cream)	131	197	-	244	269	335	434	451	460	747	792	919	1123	2840-2940	3622	3646	3686
DB (red)	131	196	-	247	270	336	434	450	460	749	793	915	-	2840-2940	3622	3654	3690
DC (grey)	-	-	204	-	266	-	-	-	465	-	-	-	-	-	-	-	-
Average	132	197	204	244	269	335	434	450	461	748	793	916	1123	2840-2940	3623	3648	3687

* Plateau

Dickite: a gem material for carving from Thailand

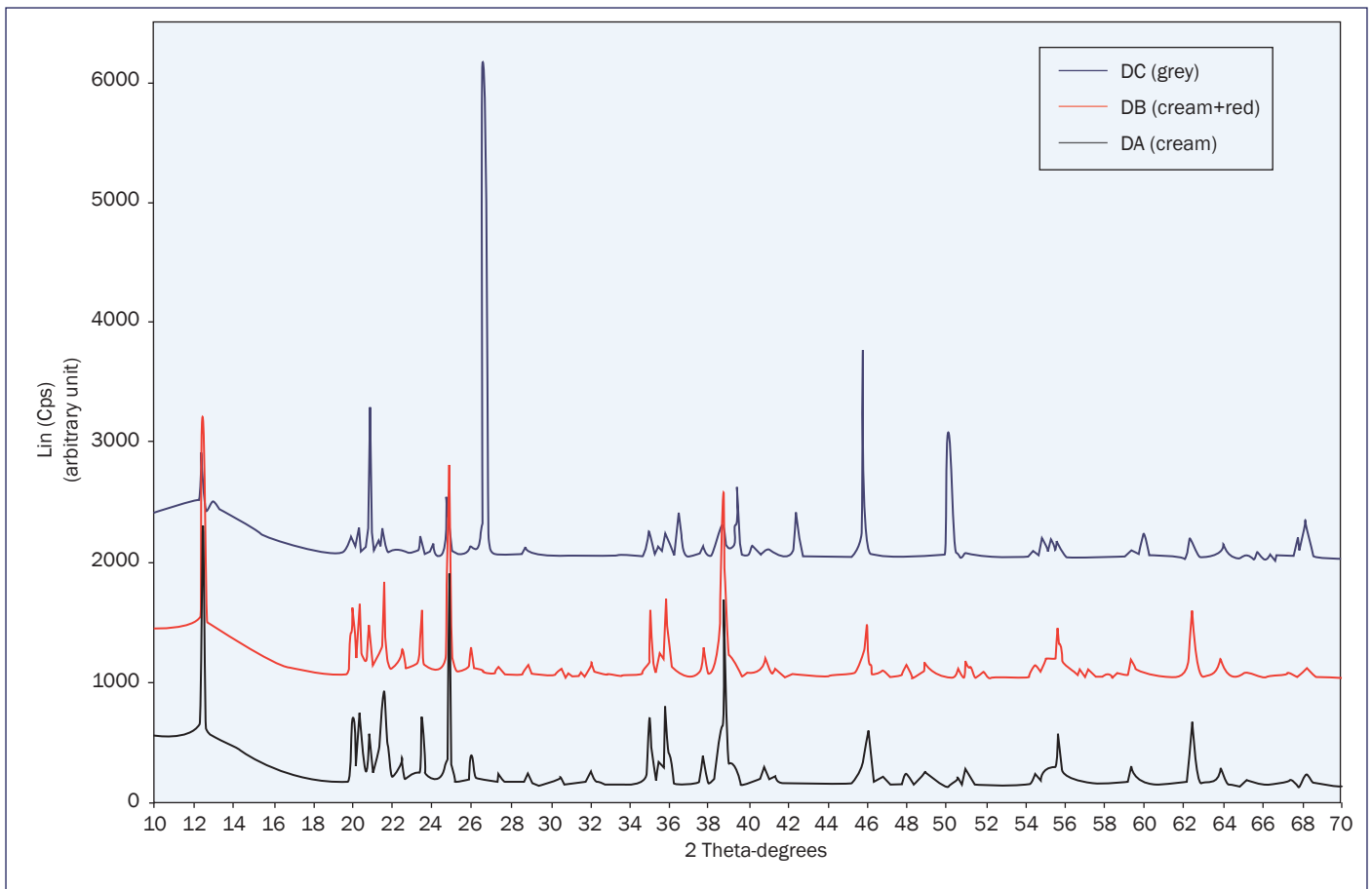


Figure 12: Diffractograms of samples DA, DB and DC. Sample DC contains both dickite and quartz. The major peaks of dickite are at 2 theta angles of 12.40, 21.56, 23.48, 24.88, 35.06, 35.86, 38.72, 45.96, 55.66 and 62.42, while those of quartz are at 20.86, 26.64, 39.46, 42.44 and 50.14.

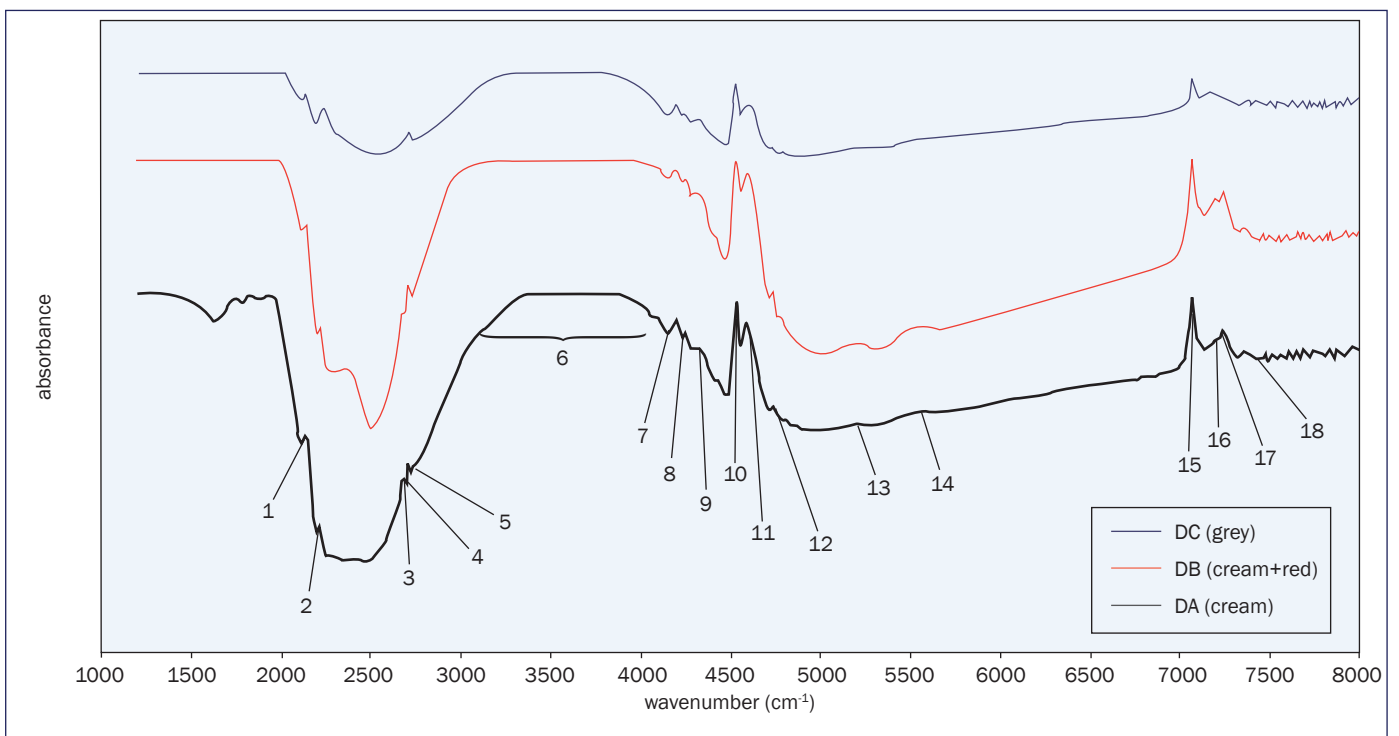


Figure 13: Infrared spectra of dickites DA, DB and DC. The peaks of sample DC are not as strong as those of DA and DB, probably because it is more opaque. The absorption wave numbers of the 18 indicator lines in spectrum DA are in Table V.

Dickite: a gem material for carving from Thailand

at low magnification but these are better resolved at high magnification where pseudo-hexagonal plates 1–10 μm across are stacked together like books (Figures 8, 9 and 10). In contrast, sample DG (grade C dickite) is a dull red, resembling rhyolitic rock, and under the SEM it shows a different, very fine grained texture with tiny holes, some of which contain tabular crystals (Figure 11).

Images frSEM illustrate the crystal habits of dickite samples under low and high magnifications (a and c images respectively in Figures 8, 9 and 10). Under low magnification (see 100 μm scale bars), samples DA and DB and DC look massive and granular. Under high magnification (see 1 μm scale bars), tabular or plate-like crystals approximately 3–5 microns across are apparent (Figures 8c, 9c and 10c).

The compositions of dickite obtained using wavelength dispersive XRF are given in Table IV. The higher quality (grade A) cream and red samples have

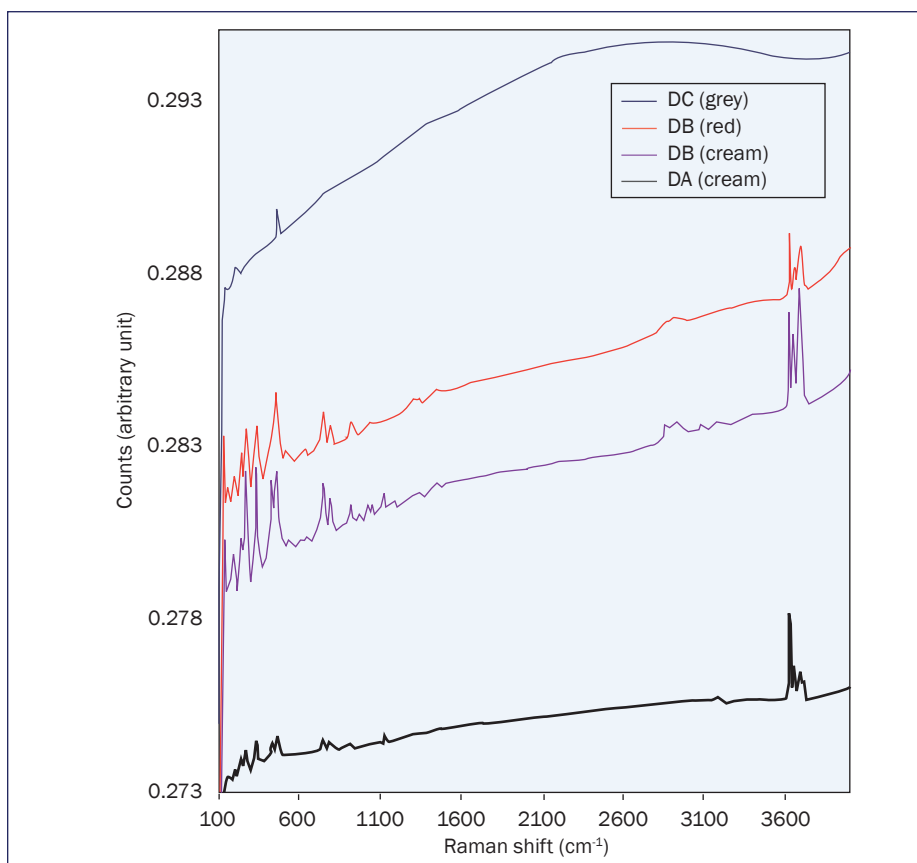


Figure 14: Raman spectra of dickites DA, DB and DC. Two spectra from DB represent the two different colours (cream and red) in the dickite. The significant Raman wave numbers are listed in Table VI).

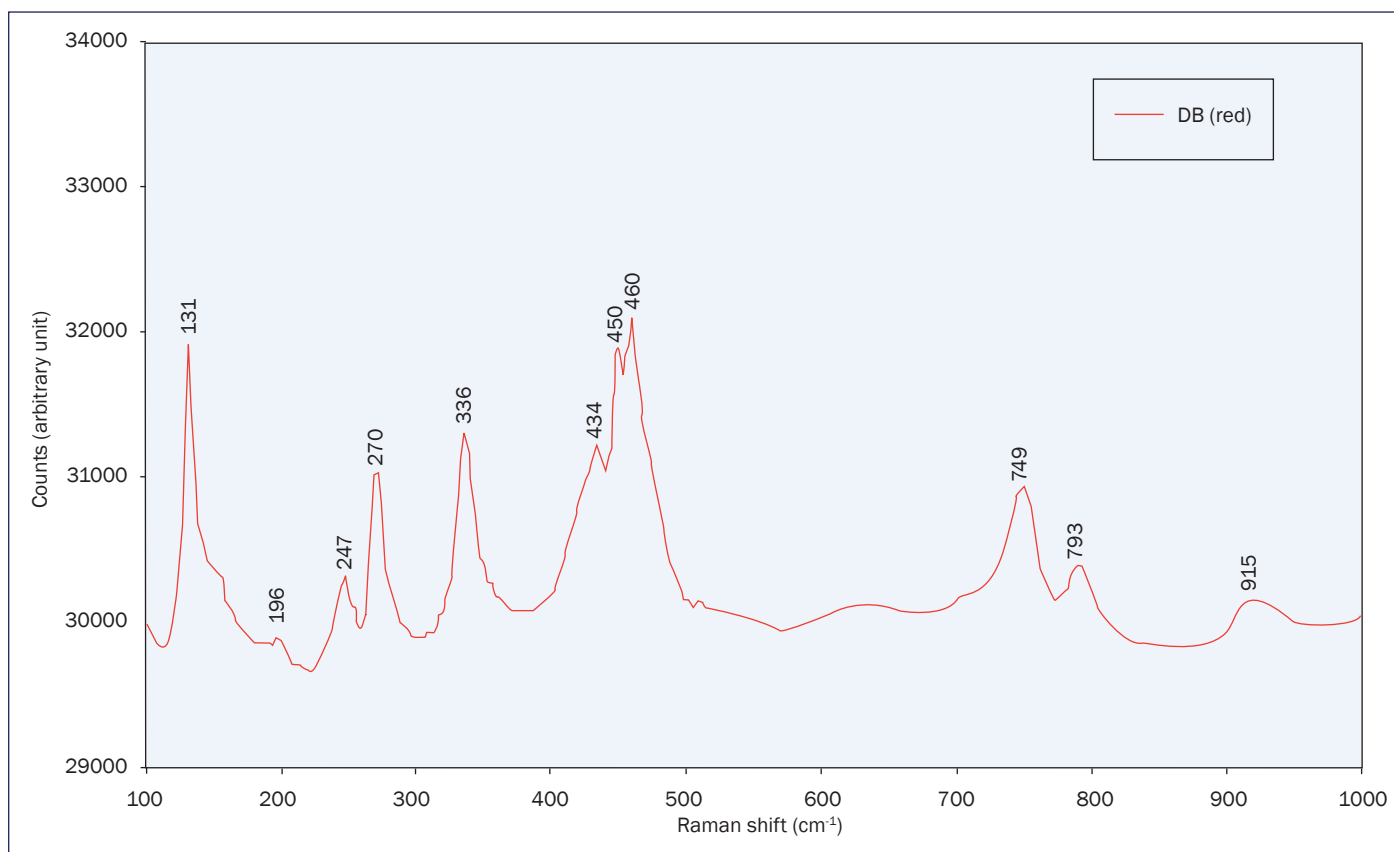


Figure 15: Raman peaks of dickite sample DB (red) in the region of 100–1000 cm^{-1} showing the detail of most typical peaks.

Dickite: a gem material for carving from Thailand

higher Al₂O₃ contents (41.39–41.73 wt%) and lower SiO₂ contents (42.85–43.39 wt%) than the grade B samples (DC–DF). Sample DB contains relatively high Sr (up to 920 ppm) and P, but not Ca, so it may contain unusual impurities.

The XRD results indicate that the DA (cream) and DB (cream+red) samples match the reference 72–1163 (Newnham and Brindley, 1965) for dickite and the major peak positions in terms of 2 theta are shown in *Figure 12*. The strong peak positions of DA and DB are at 2 theta angles of 12.40, 21.56, 23.48, 24.88, 35.06, 35.86, 38.72, 45.96, 55.66 and 62.42. In the DC (grey) sample, the presence of quartz peaks particularly at 26.64 and 50.14 2 theta (reference 79–1906, Dubrovinskii and Nozik, 1989) agrees well with the results from chemical analysis which indicate that this sample has nearly twice as much SiO₂ as DA or DB. The peak patterns of DE, DF, and DG, not shown here, are similar to that of DC.

Infrared absorption spectra of DA, DB and DC are presented in *Figure 13* and the positions of their most prominent wave numbers listed in *Table V*. The purest and most transparent dickite, DA, gives the clearest and most pronounced spectrum.

Raman spectra were collected from the surface of each sample and the cream and the red areas were measured separately on the DB sample (*Figure 14*). The range of 100–1000 cm⁻¹ is enlarged to clarify the peak positions in this region (*Figure 15*).

Brindley *et al.* (1986) and Balan *et al.* (2002) studied phyllosilicate minerals and found that the OH stretching vibrations in dickite produced absorption bands at 3710, 3655 and 3620 cm⁻¹. Unfortunately our samples show only a single high and broad absorption band from 3000–4000 cm⁻¹ but in the Raman spectra, there are three major peaks at 3623, 3648 and 3687 cm⁻¹ (positions 15, 16 and 17 in *Table VI*).

Conclusions

Dickite, marble and dolomite each have their own unique colour, texture hardness and toughness. Marble and dolomite are harder but less tough than

dickite. In terms of brittleness, they have a higher tendency to break if the carved object has a sharp corner or thin or long components. In comparison with marble and dolomite, carvers believe that dickite can be carved more easily and it can also have a distinctive range of colours and textures. For example, dickite with an uneven red colour should be used to carve animal figurines in the form of round work. Such carvings should ideally be from 75 mm to 150 mm across for reasons of packaging and transport but of course this depends on the original size of the rough.

The dickite deposits in Thailand are classed in three quality grades, A, B and C. To maximize the potential of the deposit, grade A dickite should be extracted from the mine by sawing without use of explosives, which can cause severe strain and fractures in the mineral. Dickite grades B and C, however, can be removed from the mine using explosives and then sold to the ceramics industries.

Dickite samples in the present study have a polycrystalline texture. Their crystal form cannot be seen by the naked eye and an optical microscope can help resolve some textures. SEM images of dickite show that it consists of pseudo-hexagonal plates stacked together like books.

However, standard gemmological instruments may not be sufficient to identify dickite. Advanced techniques may be needed: especially WD-XRF, XRD, FTIR and Raman spectroscopy. In particular, the Raman microprobe can give useful results, especially for grade A dickite.

Acknowledgements

The authors would like to thank Srinakharinwirot University for funding this research, the mining companies named in the text for providing samples, the Department of Mineral Resources for chemical analysis, and the Gem and Jewelry Institute of Thailand for the Raman microprobe analyses.

We are also indebted to Pornchalai Maneeratpairoj, Angsana Himasuttidach,

Sernsuke Radreng, Pek Phaoduang, Niphon Saminpanya, Rattapol Thanakit, Khom Kannirand, Thasanu Kitchalong, Patiwat Laemkhunawat, Phornthep Punthavanit and Pitthayut Saminpanya for their help, which ranged from collecting samples to the analysis of samples and reading the manuscript. Thanks also go to Tom Sigurdson who proofed this article. Finally, we thank the anonymous referee for comments.

References

- Balan, E., Allard, T., Morin, G., and Calas G., 2002. Incorporation of Cr³⁺ in dickite: a spectroscopic study. *Phys. Chem. Miner.*, **29**(4), 273–9
- Beaufort, D., Cassagnabere, A., Petit, S., Lanson, B., Berger, G., Lacharpagne, J.C., and Johansen, H., 1998. Kaolinite-to-dickite reaction in sandstone reservoirs. *Clay Minerals*, **33**(2), 297–316
- Brindley, G.W., Chih-Chun Kao, Harrison, J.L., Lipsicas, M., and Raythatha, R., 1986. Relation between structural disorder and other characteristics of kaolinites and dickites. *Clays and Clay Minerals*, **34**(3), 239–49
- Chang Oh Choo and Soo Jin Kim, 2004. Dickite and other kaolin polymorphs from an Al-rich clay deposit formed in volcanic tuff, southeastern Korea. *Clays and Clay Minerals*, **52**(6), 749–59
- Deyell, C. L., Leonardson, R., Rye, R.O., Thompson, J.F.H., Bissig T., and Cooke, D.R., 2005. Alunite in the Pascua-Lama high-sulfidation deposit: Constraints on alteration and ore deposition using stable isotope geochemistry. *Econ. Geol.*, **100**(1), 131–48
- Dubrovinskii, L. S., and Nozik, Y.Z., 1989. Calculation of the anisotropic thermal parameters of the atoms of α -quartz. *Sov. Phys. Dokl.*, **34**, 484–5
- Frost, R.L., and Vassallo, M., 1996. The dehydroxylation of the kaolinite clay minerals using infrared emission spectroscopy. *Clays and Clay Minerals*, **44**(5), 635–51
- Girard, J.P., and Savin, S. M., 1996. Intracrystalline fractionation of oxygen isotopes between hydroxyl and non-

Dickite: a gem material for carving from Thailand

- hydroxyl sites in kaolinite measured by thermal dehydroxylation and partial fluorination. *Geochim. Cosmochim. Acta*, **60**(3), 469–87
- Hibbard, M.J., 2002. *Mineralogy: a geologist's point of view*. McGraw-Hill Higher Education, Boston Burr Ridge. 562 pp
- Johnston C.T., Wang, S.L., Bish, D.L., Dera, P., Agnew, S.F., and Kenney III, J.W., 2002. Novel pressure-induced phase transformations in hydrous-layered materials. *Geophys. Res. Lett.*, **29**(16), 1770
- Johnston, C. T., Helsen, J., Schoonheydt, R.A., Bish, D.L., and Agnew, A.F., 1998. Single-crystal Raman spectroscopic study of dickite. *Am. Mineral.*, **83**(1/2), 75–84
- Kerr, P. F., and Kulp, J. L., 1948. Multiple differential thermal analysis. *Am. Mineral.*, **33**(7/8), 387–419
- Khuentak, C., 1988a. *Clay mineral deposits in Thailand. Proceedings of annual meeting of mining 1988*. Mitcharoen Karnphim Partnership, Bangkok. 63–9
- Khuentak, C., 1988b. Valuable resources: The sources of minerals and rocks for industries. In: *Treasures in soils of Saraburi*. Department of Mineral Resources, Bangkok. 23–9
- Marumo, K., 1989. Genesis of kaolin minerals and pyrophyllite in kuroko deposits of Japan; implication for the origins of the hydrothermal fluids from mineralogical and stable isotope data. *Geochim. Cosmochim. Acta*, **53**(11), 2915–24
- Newnham, R.E., and Brindley, G.W., 1956. The crystal structure of dickite. *Acta Crystallogr., Sect. A: Found. Crystallogr.*, **9**(9), 759–64
- Potts, P.J., 1987. *A handbook of silicate rock analysis*. Blackie, London. 621 pp
- Reed, S.J.B., 1996. *Electron microprobe analysis and scanning electron microscopy in geology*. Cambridge University Press, Cambridge. 201 pp
- Reed, S.J.B., 1997. *Electron microprobe analysis, 2nd edn*. Cambridge University Press, Cambridge. 326 pp
- Salayaphong, S., 1996. Rocks in Nakhon Nayok and vicinity. In: *Environmental geology of Changwat Nakhon Nayok and vicinity*. Samaphan Publishing Co. Ltd, Bangkok. 15–37
- Shoval, S., Boudeulle, M., Yariv, S., Lapidès, I., and Panczer, G., 2001. Micro-Raman and FT-IR spectroscopy study of the thermal transformations of St. Claire dickite. *Opt. Mater.*, **16**(1/2), 319–27
- Skoog, D.A. and Leary, J.J., 1992. *Principles of instrumental analysis, 4th edn*. Saunders College Pub, Fort Worth. 700 pp
- Viorica, M., Jean-Pierre, M., and Jacques, L., 2004. Rosia Poieni copper deposit, Apuseni Mountains, Romania: advanced argillic overprint of a porphyry system. *Miner. Deposita*, **39**(2), 173–88
- Wertz, E., and Wertz, L., 1994. *Handbook of gemstone carving*. Gems Guides Book Company, Suite F Baldwin Park, CA. 47 pp
- Yaemniyom, 1988. *Mineral resources in Thailand*. A document of the Department of Mineral Resources. Prachachon Co. Ltd, Bangkok. 51 pp
- Zamama, M., and Knidiri, M., 2000. IR study of dickite-formamide intercalate, $\text{Al}_2\text{Si}_2\text{O}_5(\text{OH})_4 - \text{H}_2\text{NCOH}$. *Spectrochim. Acta, Part A*, **56**(6), 1139–47

Web

- http://www.crbg.cnrs-nancy.fr/Geostandards/GGR_ms.v03/ms072.html (accessed on 20 May 2007)
- <http://www.mindat.org/min-1287.html> (accessed on 11 May 2008)

The Authors

Seriwat Saminpanya* and Chaichart Dharmgrongartama

Department of General Science, Faculty of Science, Srinakharinwirot University, Sukhumvit 23, Watthana, Bangkok 10110, Thailand.
E-mails: seriwat@hotmail.com; seriwat@swu.ac.th

Namrawee Susawee

The Gem and Jewelry Institute of Thailand (Public Organization), Gemmological Research and Testing Building, Faculty of Science, Chulalongkorn University, Phayathai Road, Patumwan, Bangkok 10330, Thailand

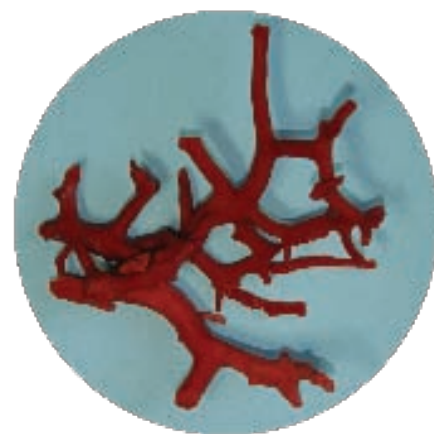
* Corresponding author

Application of mineralogical methods to the investigation of some gem-quality corals

Lucyna Natkaniec-Nowak, Magdalena Dumańska-Słowik, Jerzy Fijał and Anna Krawczyk

Abstract: Infrared spectroscopy, microscopy, cathodoluminescence and X-ray analysis have been used to investigate corals from various sources. The red, pink and white corals are composed mainly of magnesian calcite with a poorly ordered structure; a lack of cathodoluminescence indicates that they are rather young. The organic corals consist mainly of biopolymers of collagen type with subordinate magnesian calcite. Their FTIR spectra contain bands attributed to vibrations of OH, H₂O, C-H and N-H in molecules occurring in the protein structures of collagen. Infrared spectra were also used to detect wax or resin treatment of red coral.

Keywords: coral, calcite, collagen, protein, FTIR, gem treatment



Introduction

Corals are marine Coelenterates most often found in warm, tropical or subtropical waters where they form colourful ecosystems which are especially appreciated by scuba divers. Today, global warming and environmental pollution are responsible for the extinction of many coral species, so in recent years the different corals have been the subject of various scientific investigations. Under pressure from biologists and ecologists all over the world, action to preserve corals was taken some years ago through the Convention on International Trade in Endangered Species of Wild Fauna and Flora (CITES), agreed in Washington in 1973, and EU Wildlife Trade Regulation (Council Regulation (EC) no 338/97) of 9 December 1996. These were designed to regulate and supervise the

international trade in corals and products derived from them.

Currently about 6500 coral species are known; some of them exist in waters down to 7000 m. The groups of contemporary living corals can be subdivided into two subclasses: i.e. *Octocorallia* and *Hexacorallia* (Cairns, 2007). Each coral is a tiny polyp with a stomach and a mouth surrounded by retractable, stinging tentacles. Corallum is a characteristic hard calcium carbonate shell that protects the polyp and has been used for adornment since prehistoric times. The oldest coral ornaments have been dated to the Upper Palaeolithic (Sobczak and Sobczak, 1995). Nowadays, in spite of very limited supply, the interest in coral products is still intense. Black coral (*Antipatharia*), blue coral (*Heliopora coerulea*) and yellow-brown

coral (*Meliithaea ochracea*) have appeared on the jewellery market (Henn, 2006). However, coral imitations are commonly offered to customers as natural gems these days and distinguishing them from natural and treated coral can be a significant problem. For this purpose spectroscopic investigations seem to be the most effective way to solve such problems.

The bibliography on corals, especially concerning mineral corals, is very rich, since scientists active in biology, ecology and mineralogy as well as gemmology have been interested in these beautiful objects for many years. Special attention has been paid to horny corals by Brown (1977; 1988), Kim *et al.* (1992) and Hänni (2004). All results obtained with modern analytical techniques are aimed at better recognition of these organic gems.

Application of mineralogical methods to the investigation of some gem-quality corals

The natural corals and their classification in the gem trade

In gemmology and the jewellery trade, colour and shape are the criteria used to classify and name the corals. Henn (2006) distinguished red coral (noble coral), white, black, blue, golden, sponge, yellow (bamboo coral), yellow-brown (tiger coral), yellow-red (apple coral), organ-pipe and stony coral. In southern Europe, especially in Mediterranean countries, the classification used in Italy is more popular. There, the colour of coral is also the main criterion for its description. In the Italian classification, white coral (*bianco*), pale pink (*pelle d'angelo*), pink (*rosa palido*), vivid pink (*rosa vivo*), pink-red (*secondo coloro*), red (*rosso*), dark red (*rosso scurro*) and vivid red (*arciscuro lub carbonetto*) are distinguished. The extent of coral's development in terms of the thickness of its branches is another variable parameter. Here four subgroups are used: *Capo testa*, noble coral; *Barbaresco*, coral with twig fragments; *Terragila*, thin coral with twigs; and *Raspatelli*, coral shred.

In addition to colour, it is important in the jewellery trade that coral is as durable as possible and on this basis three subgroups are used:

- Corals with a homogeneous and massive structure. These include red, pink and white corals (*Corallium rubrum*, *Corallium japonicum*, *Corallium elatius*, *Corallium konojoi*, *Corallium secundum*), golden (*Gerardia sp.*, *Narella sp.*, *Callogorgia gilberti* and *Calyptrophora sp.*) and black corals (*Antipathes grandis*, *Antipathes dichotoma* and *Cirripathes sp.*).
- Corals with a heterogeneous or porous structure. These include bamboo coral (*Lepidid sp.*, *Keratosid sp.*, *Isidella sp.*, *Acanella sp.*), blue coral (*Heliopora coerulea*) and yellow-brown corals (e.g. *Millepora alcicornis*). These corals are less popular than those in (a) above.
- Fossil corals

In recent years, corals have also been considered as mineral or organic. Here the main constituent (mineral phase or

Samples and methods

Samples of white, red, pink, black and golden coral were obtained from gem trade sources and subjected to gemmological examination. Investigations were carried out at the laboratories of the Department of Mineralogy, Petrography and Geochemistry, Faculty of Geology, Geophysics and Environmental Protection, AGH-UST in Krakow, Poland. They included hand specimen and optical observations with the use of a 10x triplet lens, a binocular microscope and a standard polarizing microscope Olympus BX 51 with camera DP12. The bulk density of all corals was determined applying the hydrostatic method.

Scanning electron microscope (SEM) observations were performed on polished sections and natural surfaces of the corals with a FEI Quanta 200 FEG scanning electron microscope equipped with an Energy Dispersive Spectroscopy (EDS) detector. The system was operated at 15 kV accelerating voltage, high-vacuum mode.

The X-ray diffraction (XRD) analyses were done with a Philips APD PW 3020 X'Pert diffractometer in the angular range 5–75° 2 θ applying CuK α radiation, a graphite monochromator, voltage 35 kV, lamp current 30 mA.

Absorption infrared spectra were recorded with a BIO-RAD model FTS 165 spectrometer in the range 400–4000 cm⁻¹. The specimens were powdered, mixed with KBr, and pressed as pellets.

Contents of collagen in coral were estimated from residues after dissolution of carbonate minerals in 1M HCl solution.

Cathodoluminescence (CL) studies were carried out at the Polish Geological Institute in Warsaw. A Cambridge Image Technology 8200 mk3 device (cold cathode) linked to a Nikon Optiphot 2 polarizing microscope was used.

organic substance) determines how the coral is named. White, red, pink and blue corals belong to the mineral group, while, black and golden corals are organic.

Somewhat apart from the general ideas expressed above, there are also a few corals that have a distinctive colour and come from a particular locality, and these features determine their value on the gem market (Henn, 2006).

Results

Mineral corals

White coral

The sample of white coral *Corallium konojoi* comes from the South China sea (either from the Japanese coast or from Hainan Island, China). The coral's bulk density is ca. 2.66 g/cm³.

The surface of the coral is smooth apart from tiny pinholes or pits which occur only locally and its whiteness may be interrupted by numerous pink spots (*Figure 1*). The lustre of the polished coral

is strong pearly. Under UV radiation the white coral fluoresces purple-red under short-wave and blue under long-wave.

Under the polarizing microscope, a section of coral shows complex structure. The growth zones are arranged concentrically around the core, but the main components of these corals (carbonates) have different optical orientations within the individual growth zones – indicated by their different interference colours (*Figure 2*). The sizes of crystallites are bigger near the core than in the outer parts of the coral. In some places, deformation of the concentric-sector structure (so called 'nodes') can be observed.

XRD investigations revealed that calcite is the only mineral phase present in the coral. The location (i.e. the movement of the main calcite peaks to lower 2 theta values) and intensity of the recorded diffraction peaks, indicate that the calcium carbonate is characterized by low crystallinity index, and this is consistent

Application of mineralogical methods to the investigation of some gem-quality corals



Figure 1: White coral typical of that tested.

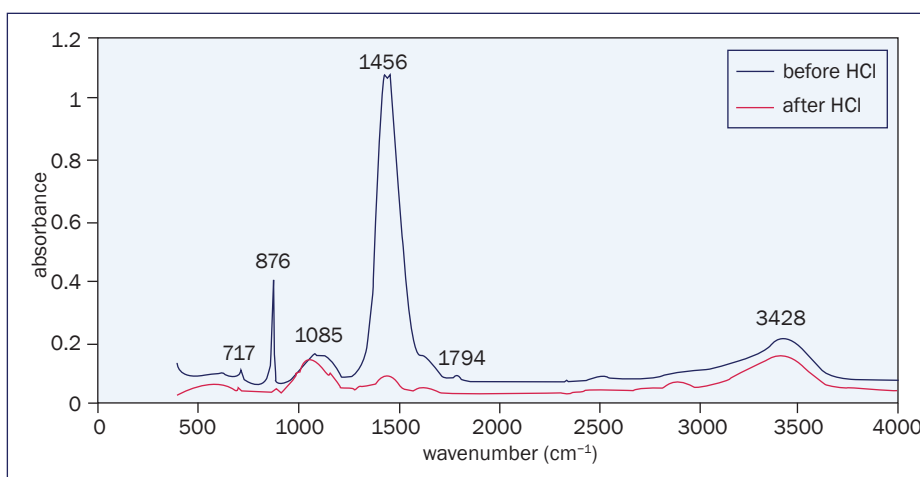
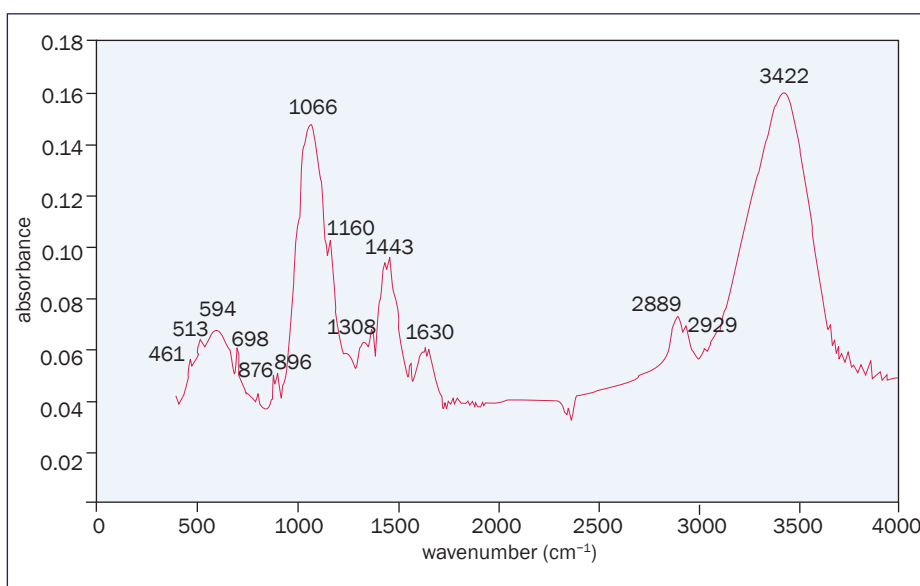


Figure 3a: Comparison of infrared absorption band intensities recorded for white coral before and after its treatment with HCl.



3b. Detail of infrared spectrum of white coral residue obtained after HCl treatment .

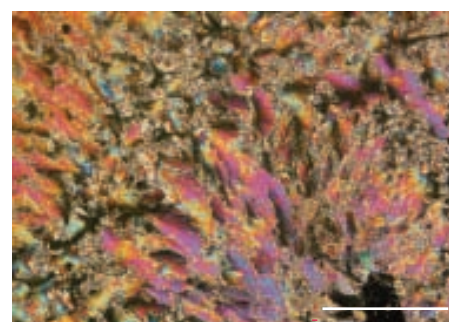


Figure 2: Magnesian calcite showing high birefringence in zones in the internal part of the white coral. Thin section, crossed polars. Bar 0.2 mm.

with the lack of cathodoluminescence. No cathodoluminescence indicates that the coral studied is rather young and has a poorly ordered structure.

In the SEM the white coral appears relatively homogeneous, with some porous structure. SEM-EDS analyses indicate that some Mg is present with the Ca and that there is also some sulphate.

Fourier transform infrared spectroscopy (FTIR) investigations of natural and HCl-treated samples of coral give detailed information on the character and composition of the coral skeleton. After treatment of white coral with 1M HCl solution, the proportion of residue remaining is 0.03 wt.%. Mineral coral consists of carbonates with traces of silicates. The bands at 1456, 876 and 717 cm^{-1} can be attributed to calcite which contains some magnesium (Figure 3A). The substitution of Mg^{2+} for Ca^{2+} is responsible for the movement of the $\nu_4(\text{CO}_3^{2-})$ band in the IR spectrum from 712 cm^{-1} to 717 cm^{-1} . In the FTIR spectrum of an unprocessed white coral there is also a band at 900–1150 cm^{-1} which is attributed to a silicate admixture. After treating the coral with HCl, the carbonates were almost completely removed; in the FTIR spectrum the intensities of bands at 1450 and 876 cm^{-1} are visibly reduced. The bands at 950–1200 cm^{-1} and 400–800 cm^{-1} may be connected with quartz and poorly ordered silicate phases. Traces of organic substance in the white coral are indicated by the presence of bands at 2889 and 2929 cm^{-1} attributed to the CH_3 and CH_2 vibrations (Figure 3B). These absorption

Application of mineralogical methods to the investigation of some gem-quality corals

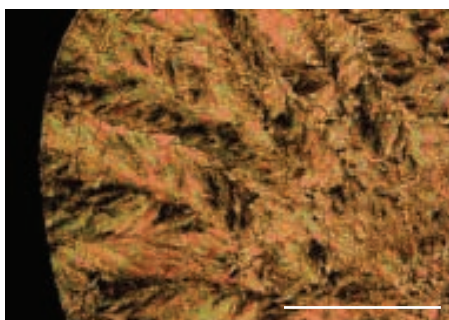


Figure 5: Radial and segment structure in red coral. Thin section, crossed polarized light. Bar 0.5 mm.

maxima, as well as the bands assigned to amide group vibrations may confirm the presence of collagen group substances.

Red coral

The fragments of red coral (*Corallium rubrum*) that were tested come from waters near the Sardinian coast in the Mediterranean Sea. The dark red colour of the coral skeletons is quite homogeneous (Figure 4), but their surface is rather rough and lustre is dull; numerous pits are filled with secondary calcite. Its bulk density is ca. 2.43 g/cm³.

In cross section, the red coral exhibits a structure of concentric growth rings. Under UV radiation it fluoresces dark red. Microscopic observations revealed three zones in the structure: an outer zone of several mm thickness, a thick internal zone and an elliptical core. In thin section, the interference colours and polysynthetic twinning both indicate that calcite is the main constituent of this mineral matrix. The calcite crystals vary in size and locally overlap to form characteristic cone-shaped patterns (Figure 5). The deformation of the red coral's concentric-sector structure ('nodes') can be observed in each zone.

The XRD patterns indicate that calcite in the red coral has a poorly ordered structure, and the lack of any cathodoluminescence colours is consistent with recent formation.

The red coral appears to be completely homogeneous in the SEM. The analyses indicate that the coral consists of calcium carbonate with some magnesium, and traces of S, Si and P were also detected.

After treatment of the red coral with HCl, the residue makes up only 0.3 wt.%



Figure 4: Red coral.

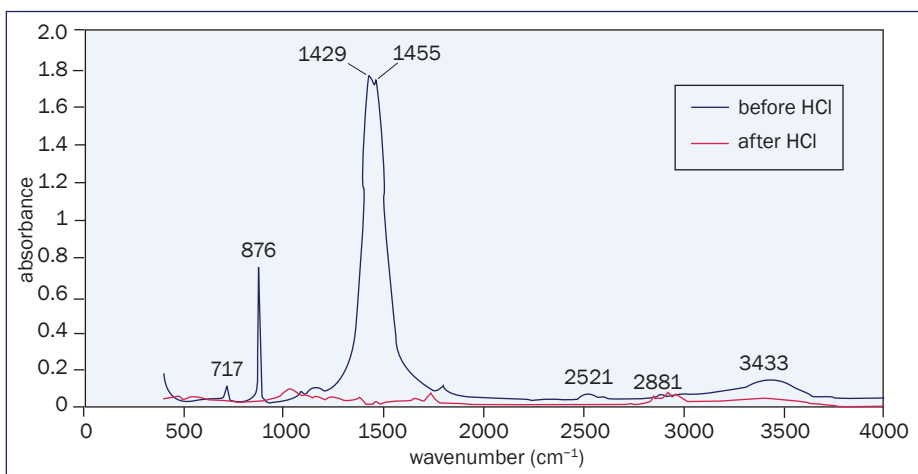


Figure 6a: Comparison of infrared absorption band intensities recorded for red coral before and after its treatment with HCl.

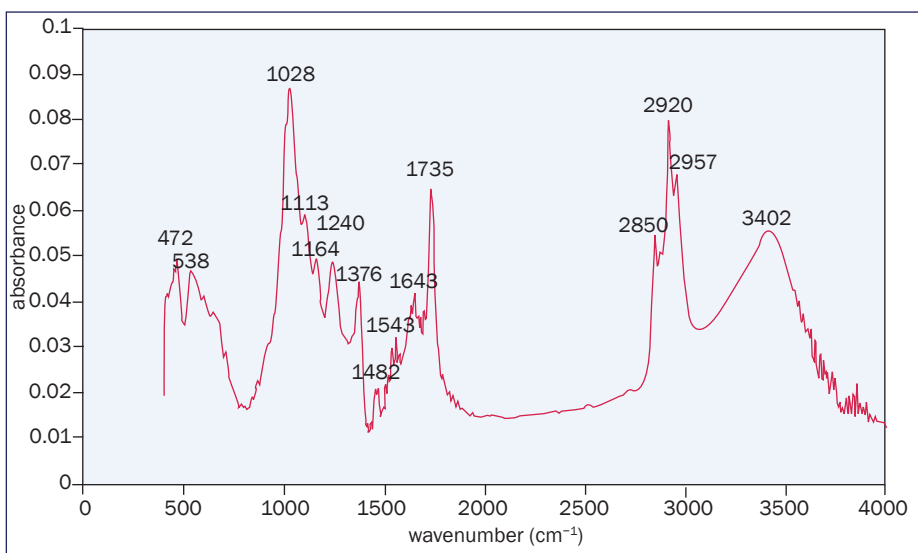


Figure 6b: Detail of infrared spectrum of red coral residue obtained after HCl treatment.

Application of mineralogical methods to the investigation of some gem-quality corals



Figure 7: Pink coral.

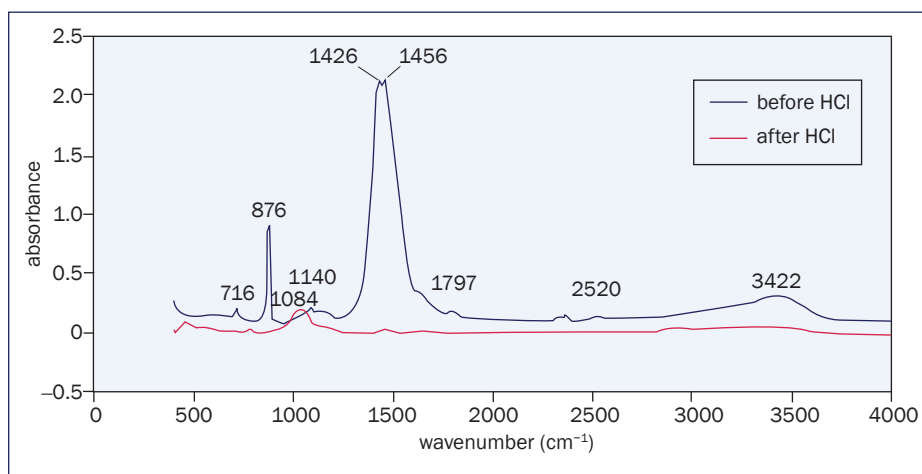


Figure 9a: Comparison of infrared absorption band intensities recorded for pink coral before and after its treatment with HCl.

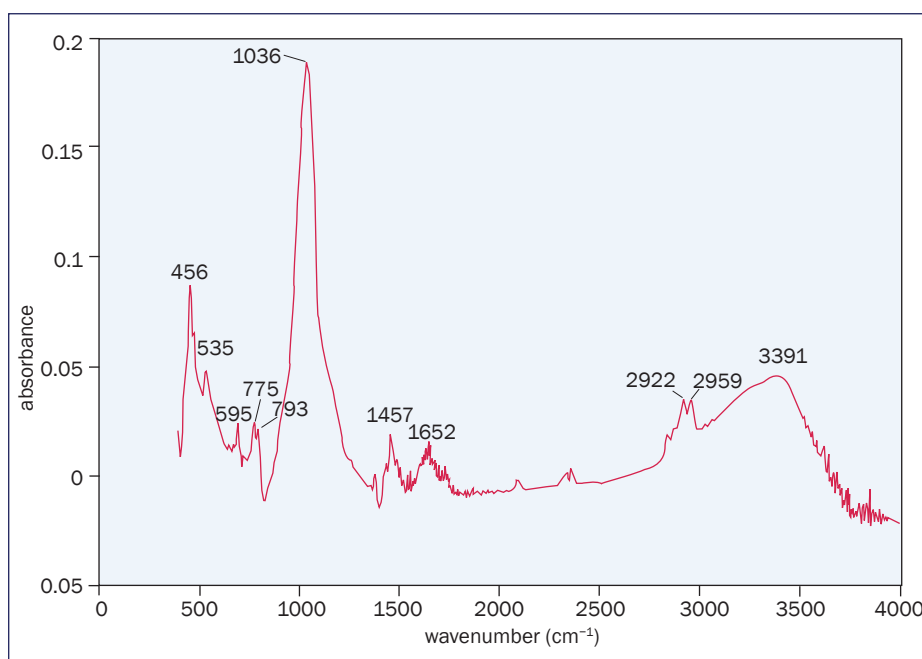


Figure 9b: Detail of infrared spectrum of pink coral residue obtained after HCl treatment.

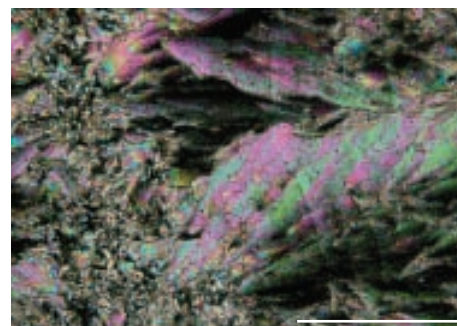


Figure 8: Segment structure in the centre of the pink coral showing calcite grain-size variation and characteristic 'nodes'. Thin section, crossed polarized light. Bar 0.5 mm.

of the original. The FTIR studies of natural and HCl-treated red corals confirmed that calcite is the main component; silicate minerals and organic substances are subordinate (Figure 6a). Maxima in the range 2800–3000 cm⁻¹ indicate the presence of organic material containing CH₃, CH₂ and COOH groups (Figure 6b). In the spectrum of the HCl-treated sample the organic components predominate. The appearance of group frequencies coming from the strong –CH₂ and –CH₃ stretchings (2800–3000 cm⁻¹) and carboxyl –COOH groups (with strong C=O stretching vibrations at 1735 cm⁻¹ and νC–O vibrations at 1240 cm⁻¹) may indicate that some foreign substances, such as resin and/or wax were used to impregnate a porous gem material to improve its colour and coherence. The natural collagen group substances are subordinate components of the HCl-treated sample and a weak absorption peak at 1543 cm⁻¹ could be the Amide II band of collagen.

Pink coral

The sample of pink coral examined comes from the South China Sea, near the coast of Vietnam. In the trade it is known as *pelle d'angelo* (angel's skin). Its colour is heterogeneous with numerous red spots in a pink background and its surface is relatively smooth with pearly lustre (Figure 7). Its bulk density is ca. 2.79 g/cm³. The coral is pale purple-red under short and long wave ultraviolet light but CL is absent — indicating its recent origin.

Under the polarizing microscope, a thin section of the coral shows that three zones of calcite can be distinguished: an

Application of mineralogical methods to the investigation of some gem-quality corals

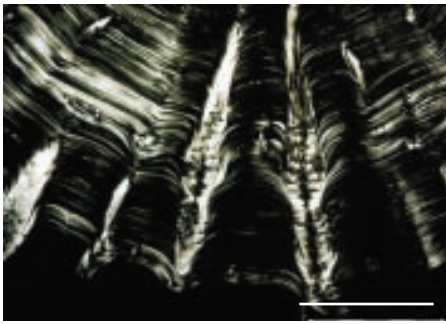


Figure 11: The segment structure of black coral. Bar 1 mm.

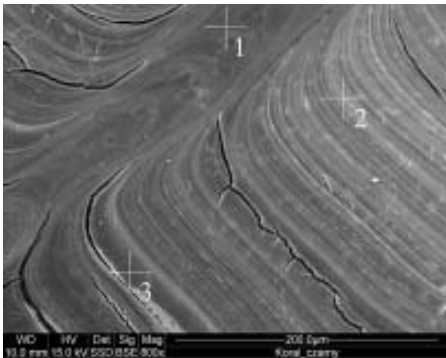


Figure 12: Back-scattered electron image of black coral showing its structure and three analysis points.

outer, an intermediate zone and a core. All the zones differ in their crystal size and structure. The outer layer mainly consists of small crystals about 0.02 mm long which form a massive and chaotic matrix. In the intermediate layer the calcite crystals range from 0.1 to 0.5 mm long and two autonomous segments can be observed within this zone. One is coarsely-crystalline with elongated crystals, often overlapping, while the other has a much smaller grain size. The elliptically shaped core is composed of the largest calcite crystals which radiate from its centre. In this zone the deformation of the pink coral's concentric-sector structure ('nodes') is most apparent (Figure 8).

The pink coral appears quite homogeneous in the SEM, although crystal nuclei (CN) can be observed within the calcite matrix and they are associated with numerous pores of 1-5 µm across. SEM-EDS analyses revealed the presence of calcium carbonate with magnesium and the admixture of S- and Si-bearing phases.

The infrared spectrum recorded for the pink coral is very similar to those of



Figure 10: Two specimens of black coral.

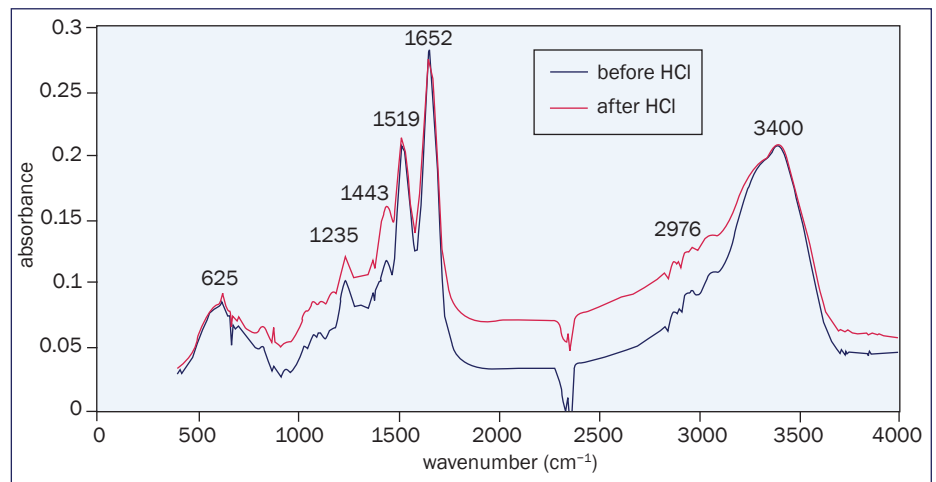


Figure 13a: Comparison of infrared absorption band intensities recorded for black coral before and after its treatment with HCl.

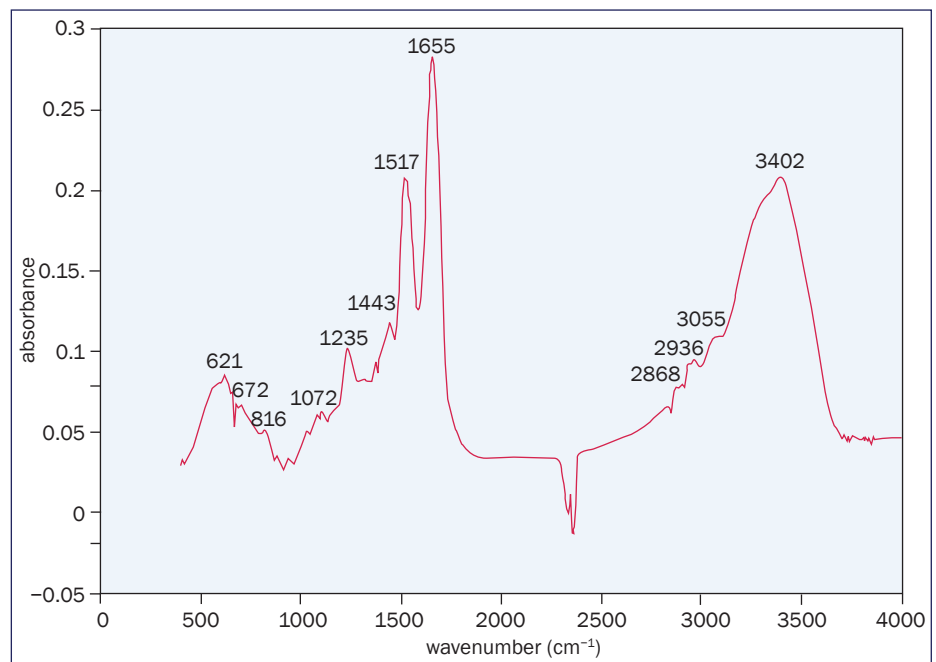


Figure 13b: Detail of infrared spectrum of the black coral residue obtained after HCl treatment.

Application of mineralogical methods to the investigation of some gem-quality corals



Figure 14: Golden coral.

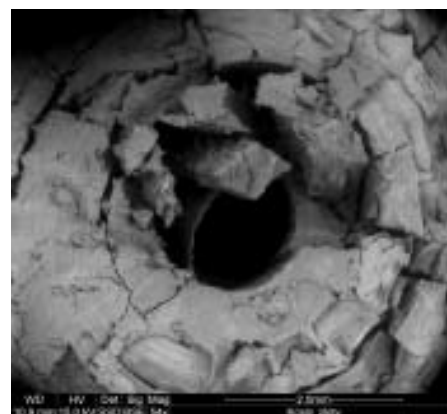


Figure 15: The concentric and segment structure of golden coral, back-scattered electron (BSE) image.

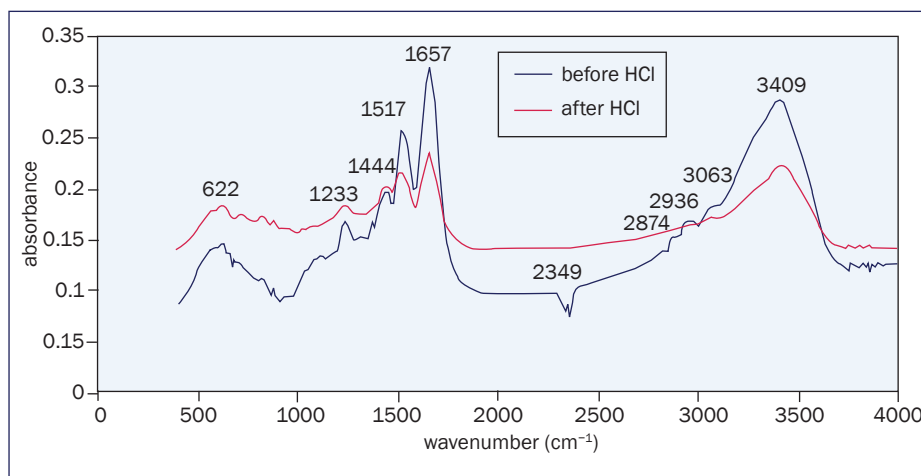


Figure 17a: Comparison of infrared absorption band intensities recorded of golden coral before and after its treatment with HCl.

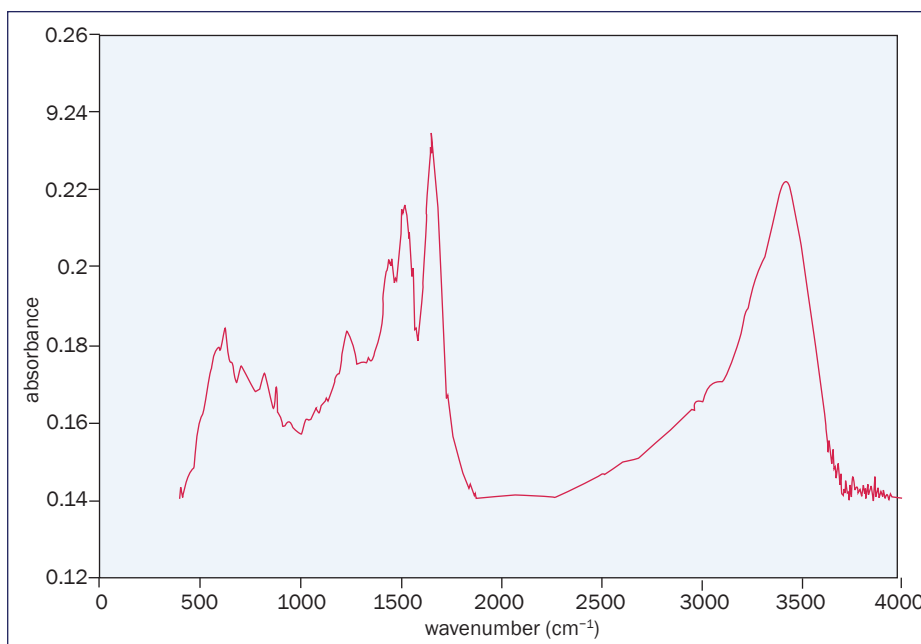


Figure 17b: Detail of infrared spectrum of golden coral residue obtained after HCl treatment.

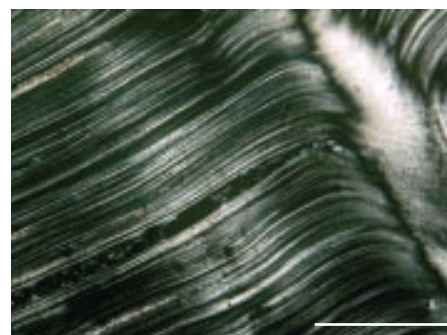


Figure 16: The wavy-shaped zone within an individual segment of the golden coral. Thin section, crossed polarized light. Bar 0.2 mm.

the white and red corals described above. It indicates that calcite is a dominant component, while silicates appear as traces (Figure 9a). After treatment of the pink coral sample with 1 M HCl solution, the residue makes up 0.017 wt.%. In the spectrum of the HCl-treated skeleton, the doublet at 775 and 793 cm^{-1} indicates the presence of quartz, while bands occurring in the range 2800–3000 cm^{-1} indicate the presence of an organic component (Figure 9b).

Organic corals

Black coral

The specimens of black coral (*Antipathes*) come from tropical and subtropical reefs at depths of 30–40 m, in the waters of the Malay Peninsula. This coral is also found around Indonesia, the Philippines, Hawaii, Australia, and in the Caribbean and the Red Seas (Henn, 2006).

The smaller sample of black coral (Figure 10) has a rough and pitted

Application of mineralogical methods to the investigation of some gem-quality corals

surface, dull lustre and a homogeneous colour, and in cross section its concentric-sector structure can be observed (*Figure 11*). The larger fragment has a rougher surface with numerous spines. Its bulk density is *ca.* 1.40 g/cm³. It shows pale blue fluorescence under long wave ultraviolet light, but under short wave UV it is inert. The CL colour of the black coral is dark brown. In cross section typical growth ring structure is visible, the borders between the growth zones being emphasized by thin layers composed of carbonates. The core is filled with secondary carbonates.

Thin section observations revealed that the main component of the coral is anisotropic with first order interference colours (*Figure 11*) and XRD investigations confirmed that the black skeleton is largely amorphous or a substance which is poorly crystalline.

The ring-sector structure of the black coral is well shown in SEM photos (*Figure 12*). The elongated structural elements, like furrows, are often disrupted and dislocated, and some of them appear on the surface of the coral skeleton as spines. The wavy-shaped zones occur between these 'furrows' (Dumanska-Słowik *et al.*, 2008). Black coral is more porous than the mineral corals described above. Some pores are empty while others are filled with calcium carbonates.

SEM-EDS analyses were done in three characteristic areas, marked 1, 2 and 3 in *Figure 12*. The 'furrows' (1) are built mainly of organic molecules enriched in Cl, I and S, and subordinate magnesian CaCO₃. Wavy-shaped zones occurring among the elongated structural elements exhibit a similar composition (3). Preliminary work indicates that the light grey laminae (2) contain more iodine than the dark grey laminae (3).

It took longer to etch a powdered sample of black coral with 1 M HCl than it did for the mineral corals and organic residue weighs about 80 % of the original. FTIR investigations indicate that the black skeleton of this coral is built mainly of biopolymers of collagen type mixed with some magnesian calcite (*Figure 13a*). The wide band at 2800–3700 cm⁻¹ is

attributed to O-H vibrations in the proteins in collagen. Weak maxima at 2868 and 2936 cm⁻¹ are probably caused by C-H vibrations in CH₃ and CH₂ groups (*Figure 13b*). The bands associated with N-H stretching vibrations in amino and amido (NH₂) groups in the collagen structures (Doyle Brodsky *et al.*, 1975; Twardowski and Anzenbacher, 1988; Kamińska and Sionkowska, 1998) overlap peaks caused by O-H stretching in water molecules. The band at 1655 cm⁻¹ probably results from the coincidence of absorption caused by H₂O bending vibrations and C=O stretching vibrations in amido groups in the collagen ('the Amide I band'), and the weaker band at 1517 cm⁻¹ is associated with N-H bending vibrations ('the Amide II band'). C-N stretching vibrations in amido groups probably cause the band at 1443 cm⁻¹, while the coupling of N-H bending vibrations and C-N stretching vibrations probably cause the band at 1235 cm⁻¹. Absorption in the region 550–850 cm⁻¹ with a maximum at 621 cm⁻¹ is probably due to N-H out-of-plane oscillation.

Golden coral

The origin of this golden coral is unknown. Its colour is homogeneous with dull lustre. The presence of characteristic nodules (the remains of spikes) indicates that it is black coral, probably treated by oxidation with hydrogen peroxide (*Figure 14*). Its bulk density is *ca.* 1.26 g/cm³. Under UV the coral is strong blue in long wave; its CL colour is brown.

In cross section, the golden coral is similar in structure to black coral (*Figure 15*) and the borders between the growth rings are emphasized by thin laminae of carbonates (*Figure 16*). SEM-EDS analyses indicate that secondary magnesian calcites are also present in numerous fissures in this coral. Even so, their total volume is low because after treatment with 1M HCl solution, the collagen content of the original coral was estimated at about 99 wt.%.

FTIR spectra of both raw and HCl-treated samples of golden coral are shown in *Figure 17a–b*. These spectra are comparable to those recorded for black coral in *Figure 13a–b*.

Conclusions

In all the corals studied, growth zones round the core are clearly visible with the unaided eye or under the microscope. The mineral corals (white, pink and red) consist mainly of calcite which has a poorly ordered structure. The concentric structure of these corals is emphasized by size variation of the calcite crystals — the nearer the centre of the coral, the larger the calcite. The SEM-EDS analyses revealed that the carbonate is a magnesian calcite, and FTIR spectra indicate that silicate minerals and organic matter are present only in traces. The black and golden organic corals are composed mainly of biopolymers of collagen type with subordinate carbonate and also show a concentric-radial structure despite being composed of a different building material.

In this study spectroscopic analyses have proved to be most effective in distinguishing natural from treated corals: i.e. red coral containing wax or resin and 'golden coral' with the same structure and composition as black coral.

Acknowledgements

Magdalena Sikorska, Adam Gawel and Stanisław Olkiewicz are gratefully acknowledged for performing CL observations, SEM-EDS and XRD investigations and FTIR analyses respectively. Thorough review by an anonymous reviewer helped to improve the paper considerably. This work was financially supported by the AGH-University of Science and Technology (Krakow, Poland), through research project no 11.11.140.158.

References

- Brown, G., 1977. Black coral — true or false. *Austral. Gemmol.*, **13**(2), 35–41
- Brown, G., 1988. Gold coral re-evaluated. *Austral. Gemmol.*, **16**(12), 473–6
- Cairns, S.D., 2007. Deep-water corals: an overview with special reference to diversity and distribution of deep-water scleractinian corals. *Bulletin of Marine Science*, **81**(3), 311–22

Application of mineralogical methods to the investigation of some gem-quality corals

- Doyle Brodsky, B., Bendit, E.G., and Blout, E.R., 1975. Infrared spectroscopy of collagen and collagen-like polypeptides. *Biopolymers*, **14**, 937–57
- Dumańska-Słowik, M., Natkaniec-Nowak, L., and Krawczyk, A., 2008. Perishing biocen – the mineralogical characterization of some coral varieties In: *Transformation in natural environment and sustainable development* (in Polish with English summary). M.J. Kotarba [Ed]. TBPS Geosfera, 207–16
- Hänni, H.A., 2004. Black horn coral coated with artificial resin. Gem News International. *Gems & Gemology*, **40**(1), 78–9
- Heflik, W., Mrozek, A., Natkaniec-Nowak L., and Szczepanowicz B., 2005. *The atlas of biblical gems and decorative stones* (in Polish). WAM, Krakow, Poland, 184 pp
- Henn, U., 2006. Corals in the gem and jewellery trade (in German with English abstract). *Gemmologie. Z. Dt. Gemmol. Ges.*, **55**(3/4), 77–104
- Kamińska, A., and Sionkowska, A., 1998. Application of FTIR spectroscopy in estimation of changes of collagen structure under influence of UV radiation. In: M. Handke and Cz. Paluszkiewicz [Eds]. *Methods and techniques in vibrational spectroscopy* (in Polish). Akapit, Kraków, 159 pp
- Kim, K., Goldberg, W.M., and Taylor, G.T., 1992. Architectural and mechanical properties of the black coral skeleton (Coelenterata: Antipatharia): A comparison of two species. *Biol. Bull.*, **182**, 195–209
- Łapot, W., 2006. *Corals as jewellery stones* (in Polish). LabGem, Sosnowiec. p.124.
- Sobczak, N., and Sobczak, T., 1995. *Ivory. Corals* (in Polish). Tomasz Sobczak, Warszawa. 106 pp
- Twardowski, J., and Anzenbacher, P., 1988. *Raman and IR spectroscopy in biology* (in Polish). PWN, Warszawa, 94 pp

The Authors

Lucyna Natkaniec-Nowak, Magdalena Dumańska-Słowik, Jerzy Fijał and Anna Krawczyk

The Department of Mineralogy, Petrography and Geochemistry, The Faculty of Geology, Geophysics and Environmental Protection, AGH University of Science and Technology, 30 Mickiewicza Av. 30-059 Krakow, Poland
e-mail: natkan@agh.edu.pl, dumanska@agh.edu.pl

Colour-change garnets from Madagascar: variation of chemical, spectroscopic and colorimetric properties

K. Schmetzer, H.-J. Bernhardt, G. Bosshart and T. Hainschwang

Abstract: A detailed account is given of the chemical composition and chromatic characteristics of a suite of 52 faceted colour-change garnets from Bekily, Madagascar. Microprobe results show them to be pyrope-spessartines with minor amounts of uvarovite (Cr) and goldmanite (V). All samples reveal absorption spectra with a dominant maximum in the visible range between 569 and 584 nm, which correlates with the chromium and vanadium contents of the garnets. From these considerations, it is concluded that the ratio spessartine : (goldmanite + uvarovite) is the key feature to understand the colour and colour changes of these samples.

Colorimetric parameters for all garnet samples were calculated for daylight and incandescent light for the CIE 1931 chromaticity diagram and for the CIELAB 1976 uniform colour space, which are described in detail and illustrated.

The three effects discussed are colour difference, hue angle difference, and chroma difference. The extent of colour change is described as a function of two fundamental parameters, colour difference and hue angle difference, and correlated with simple categories such as faint, moderate, strong and very strong.

Keywords: CIE, CIELAB, colorimetry, Cr-V-Mn content, garnet, Madagascar, UV-Vis spectra



Introduction

Gemstones revealing special light effects such as chatoyancy, asterism or colour change are much appreciated. The latter quality is the subject of this paper, and was first described for alexandrite, the chromium-bearing variety of chrysoberyl originating from the Tokovaya river area in the Urals, Russia (von Pott, 1842). Its property of appearing green in daylight and red in incandescent light was

subsequently named the 'alexandrite effect' in gemmological literature. Other minerals showing an 'alexandrite effect', i.e. a colour change ranging from blue green in daylight to violet or purplish red in incandescent light, were only rarely described in the nineteenth and the first part of the twentieth century, but more species have been discovered in the second half of the twentieth century. As a first example, a chromium-rich

colour-change tourmaline variety was mentioned by Cossa and Arzruni (1883), also originating from the Ural mountains. A century later in the 1980s, several alexandrite-like gem materials such as sapphire, spinel, garnet, fluorite, monazite,

Above: Colour-change garnet from Bekily, Madagascar, in daylight (top) and incandescent light; size of sample 4.7 x 6.8 mm, weight 0.74 ct.

Colour-change garnets from Madagascar: variation of chemical, spectroscopic and colorimetric properties



Figure 1: A striking example of colour-change in a garnet from Bekily, Madagascar; in daylight it is blue green and in incandescent light purple; diameter of sample 7.4 mm, weight 1.78 ct.

kyanite, and diaspore became known and their compositions and spectra reported (Schmetzer *et al.*, 1980; Schmetzer and Gübelin, 1980; Gübelin and Schmetzer, 1982; Bosshart *et al.*, 1982; Hänni, 1983).

Gem-quality garnets with an alexandrite-like colour change have been known for about three decades from Umba, Tanzania, and Sri Lanka. Chemical, spectroscopic and colorimetric data were published by Schmetzer and Ottemann (1979) and Schmetzer *et al.* (1980). The garnets were members of the pyrope-spessartine solid solution series with minor iron (almandine), vanadium (goldmanite) and chromium (uvarovite) contents. Additional chemical and spectroscopic data of colour-change pyrope-spessartine garnets were published in the 1980s by Stockton (1982), Manson and Stockton (1984) and Stockton and Manson (1985). In the subsequent decades, new occurrences of colour-change garnets have been reported in Sri Lanka (Johnson and Koivula, 1996; Zoysa 1999/2000), the Tundururu-Songea area in Tanzania (Henn and Milisenda, 1997) and from a Nigerian source (Milisenda, 2003).

Different types of colour-change in garnets from Madagascar including samples which are blue green in daylight and purple in incandescent light, or yellowish green or greenish yellow in daylight changing to an intense pink in incandescent light, have been reported by Johnson and Koivula (1998) and Schmetzer and Bernhardt (1999). Also, and in contrast, samples with high chromium contents showing a colour change from brownish purple red in

daylight to purplish red in incandescent light were reported by Schmetzer *et al.* (2002).

The first colorimetric data of alexandrite-like gemstones were evaluated for chrysoberyl, corundum, garnet and fluorite. Chromaticity coordinates were calculated for daylight and incandescent light and presented graphically in the CIE 1931 chromaticity diagram which was traditionally used at that time (Schmetzer *et al.*, 1980). In the CIE 1931 colour space, the so-called dominant wavelength, which can be determined by graphical or by mathematical methods, was used to represent the observed colour in each of the four colour-change mineral species mentioned above (see also Boguth, 1990).

The more recent CIELAB 1976 colour space has been used to graphically demonstrate the colorimetric properties of colour-change gem materials by Liu *et al.* (1994, 1999 a,b). In these papers the term 'alexandrite effect' was no longer limited to the traditional alexandrite-like colour change but expanded and applied to all types of colour change between different pairs of illuminants, and even a 'reverse alexandrite effect' has been described in tourmaline by Liu and Fry (2006) and in zircon by Bosshart and Balmer (2006).

This expansion, however, did not include the pyrope-spessartine garnets (designated as malaya garnets in the gem trade), which can also show a colour variation from daylight to incandescent light; for them, the general term 'colour shift' has been and is used (Schmetzer *et al.*, 2001). There has been a tendency to use the term colour-change for gemstones with

different colour behaviour under various illuminations when this behaviour is not typical for this gem variety as a whole, and to describe the behaviour as a colour shift when all samples of a certain gem variety show varying colours under different light sources (Liu *et al.*, 1999a). More confusingly still, the term 'colour shift' has been applied to garnets showing different colours in transmitted and reflected light (Manson and Stockton, 1984).

A detailed correlation of colorimetric with chemical data of 24 colour-change garnets from Madagascar by Krzemnicki *et al.* (2001) used the CIELAB 1976 colour space to demonstrate also that the extent of colour change was correlated with the hue angle difference for specific pairs of illuminants in the colour circle. The influence of the thickness of a sample on the saturation of colour was discussed by Liu *et al.* (1999b), and Krzemnicki *et al.* (2001) emphasized the influence of different saturation on the visually observed colour changes in a gemstone between different pairs of illuminants.

The vanadium and chromium contents of the garnets, which were correlated with the extent of colour change by Krzemnicki *et al.* (2001), are certainly two relevant properties in explaining colour-change behaviour, but they do not explain all the colorimetric data, and especially not the various types of colour change observed. Thus, the present authors decided to collect additional chemical, spectroscopic and colorimetric data from colour-change garnets of Madagascar, to compare with and augment the work of Krzemnicki *et al.* (2001).

The present study is based on 52 garnet samples (see example in Figure 1) from Madagascar which were chemically analysed by electron microprobe and spectroscopically measured with two different spectrophotometers. The samples have been collected within the last decade by two of the present authors (KS and TH). At first sight, some of our specimens obviously did not fit into any of the five groups described by Krzemnicki *et al.* (2001) indicating that there could be more groups or that we should subdivide some groups into specific subgroups in order

Colour-change garnets from Madagascar: variation of chemical, spectroscopic and colorimetric properties

to investigate and explain their observed colour changes.

For clarity of terminology, the expression ‘colour change’ is used for minerals and gemstones which reveal a different coloration to the human observer under different pairs of illuminants (traditionally daylight and incandescent light, today also artificial daylight and other light sources). The expression ‘colour change’, however, is not to be used for samples with colours altered by various types of treatment, such as heat treatment or irradiation. These are best termed colour alterations. In other words, colour change is not a description of different states of coloration before and after the gemstone has undergone a specific treatment. Colour change should also not be used to describe a variation of colour due to bleaching, fading or other types of alteration involving colour centres (e.g. by heat treatment, irradiation, exposure to sunlight or even in darkness). Furthermore, colour change should neither be confused with pleochroism which describes different colours in different orientations of a stone (caused by optical anisotropy) nor with variation of colour caused by variation in thickness (caused by different path lengths of light, the Usambara effect, see Liu *et al.*, 1999b, Halvorsen, 2006).

As the number and variety of different light sources available on the market increase, it is becoming more important to be able to describe the colours in gems and how they may change precisely. Consequently, it is important to outline the background to and the basis for the authors’ choice of colorimetric systems in this research. The two systems selected, i.e. the CIE 1931 and the CIELAB 1976 system, are the most commonly used colour spaces applied in the twentieth century, and a few gemmological texts have already applied one or both systems. Since, however, there is no readily available gemmological text which explains the background of both systems, an outline is given below, and those readers already well-versed in the CIE and CIELAB colour concepts may like to skip the ‘Colorimetric systems’ and move to ‘Materials and Methods’.

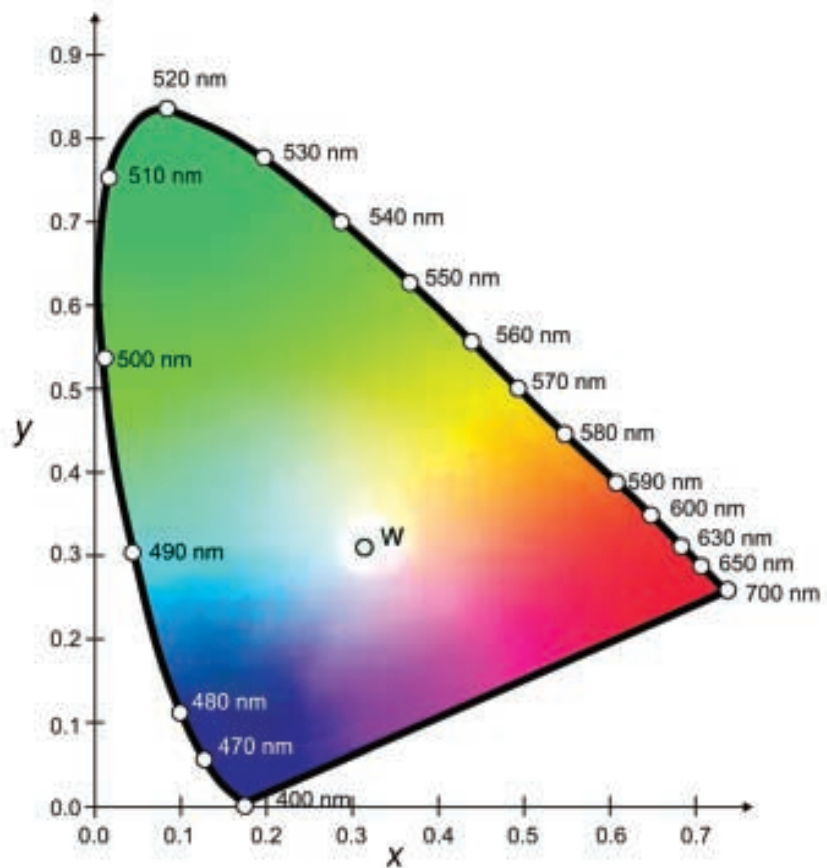


Figure 2: Colour distribution in the CIE 1931 chromaticity diagram. Copyright GretagMacbeth, Regensdorf, Switzerland (reproduced by permission).

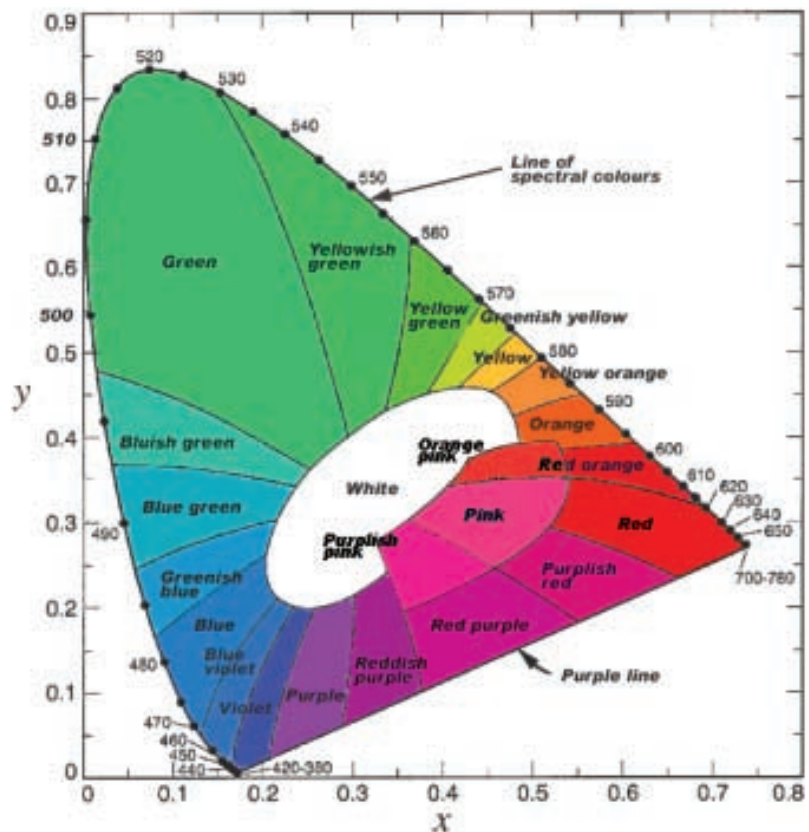


Figure 3: Colour regions in the CIE 1931 chromaticity diagram, prepared according to the black-and-white line drawing of Kelly (1943).

Colour-change garnets from Madagascar: variation of chemical, spectroscopic and colorimetric properties

Table I: Spectral hue names, wavelength in the CIE 1931 chromaticity diagram and hue angle in the CIELAB 1976 colour circle.

Hue name	CIE 1931 chromaticity diagram, centre (nm) ^a	CIE 1931 chromaticity diagram, range (nm) ^b	Hue angle in the CIELAB 1976 colour circle ^c
Red	c493	620 – c495	25° (u c494 nm)
Red orange	606	595 – 620	42°
Orange	592	585 – 595	59°
Yellow orange	583	580 – 585	76°
Yellow	578	575 – 580	92° (u 574 nm)
Greenish yellow	573	570 – 575	110°
Yellow green	565	560 – 570	127°
Yellowish green	545	530 – 560	145°
Green	508	498 – 530	162° (u 503 nm)
Bluish green	495	492 – 498	190°
Blue green	490	486 – 492	217°
Greenish blue	485	482 – 486	244°
Blue	476	465 – 482	272° (u 475 nm)
Blue violet	454	420 – 465	286° (*)
Violet	c566	c565 – 420	300°
Violet purple			315° (*)
Purple	c560	c550 – c565	329°
Reddish purple	c545	c530 – c550	345° (*)
Red purple	c506	c500 – c530	357°
Purplish red	c496	c495 – c500	11° (*)

^a Kelly (1943) for daylight C

^b MacEvoy (2008) derived after Hunt (2004), based on Kelly (1943)

^c hue angles based on the 16 hue colour circle of Richter (2008), intermediate hue angles (*) were calculated for this paper, hue names were adapted from Kelly (1943)

c before a wavelength indicates 'complement of' and is used in the line of purples (between red and violet)

u indicates the four unique hues, characteristic wavelength after Richter (1996)

Colorimetric systems

Colorimetric systems are used for the quantitative description and prediction of colour phenomena. For the description of colour, special colour coordinate systems (colour spaces) were developed, and two of the most practically used systems shall be described in this section. These colour systems were developed and published by the Commission Internationale de l'Éclairage (CIE, International Commission on Illumination, Internationale Beaufchtungskommission) in 1931 and 1976. Using special tristimulus functions, which were empirically determined to define the sensitivity of the red, green and blue colour receptors of the human eye, a

given colour is represented by a vector in the XYZ colour space. Colour coordinates (chromaticity values, e.g., x,y or u',v' or a*,b*) of a sample, e.g. a faceted gemstone, within one of these different colour spaces can be calculated from the visible absorption spectrum of the sample which leads to the X, Y and Z values (tristimulus parameters) of the gemstone. These parameters are transformed into the relevant coordinates in different colour spaces. For further details, especially for the detailed mathematical algorithms needed for the calculation of coordinates in various colour spaces from spectroscopic data, the reader is referred to standard textbooks or treatises on

colour and colorimetry, e.g. Wyszecki and Stiles (1982), CIE (1986, 2004), Richter (1996), Kuehni (1997), Nassau (1998), Hunt (2004), Ohta and Robertson (2005) and MacEvoy (2005), and to the recent article by Liu and Hurwit (2008).

The CIE 1931 system

A specific colour locus in the three-dimensional CIE 1931 colour space, which was developed in 1931 by the Commission Internationale de l'Éclairage (CIE), is conventionally represented by its projection onto a two dimensional x,y plane. The x and y coordinates are designated as chromaticity components or chromaticity coordinates. The x,y plane of the CIE 1931 colour space is represented by the CIE standard chromaticity diagram (Figure 2). In this diagram, the spectral colours of maximum purity within the visible range (from red to violet) are located on a horseshoe-shaped curve which is also called the line of spectral colours. The non-spectral colours between red and violet are located on a straight line, the so-called purple line. Figure 3 shows the chromaticity diagram subdivided into regions of various colours after Kelly (1943). The spectral hue names and the corresponding wavelengths for the pure spectral colours located on this line are listed in Table I. Colours located on the purple line between red and violet are conventionally represented by their complementary wavelengths which are located on the opposite side of the purple line within the chromaticity diagram. A complementary wavelength is found at the intersection point of the line of spectral colours with a straight line starting at a point on the purple line and running through the neutral point representing the light source towards the horseshoe-shaped line.

The colour of a sample located in the chromaticity diagram with specific chromaticity coordinates x,y is represented by its dominant wavelength λ_d . This characteristic parameter is obtained by drawing a line from the x,y coordinates of the light source through the sample point (see Figures 4 and 5). The dominant wavelength is found at the intersection

Colour-change garnets from Madagascar: variation of chemical, spectroscopic and colorimetric properties

of this line with the horseshoe-shaped line of spectral colours. Again, non-spectral colours on the purple line are represented by their complementary wavelengths. Consequently the position of a complementary wavelength on the purple line varies according to the point of the illuminant used in the chromaticity diagram. The line between the coordinates of the light source and the point representing the dominant wavelength is subdivided into two fractions by the sample point (*Figures 4 and 5*). The purity of a sample colour is the fraction of this line between the sample point and the locus of the illuminant and, consequently, a purity of 100% represents the pure spectral colour.

The CIE 1931 chromaticity diagram is a good representation for the colours of samples, but it is difficult to obtain a colour difference value in this colour space. Therefore the development of uniform colour spaces with improved representation of colour and colour differences was desirable.

Different solutions for colour spaces with uniform chromaticity spacing were obtained directly from tristimulus functions and XYZ values. They were designed by the CIE and designated as CIE L u v colour space (1960) or as CIE L* u* v* colour space (1976). The CIE L* u* v* colour space incorporates the u'v' chromaticity diagram, which is a projective transformation of the CIE (1931) x,y chromaticity diagram (*Figure 6*; Wyszecki and Stiles, 1982).

The CIELAB 1976 system

Many colour systems used today correlate with the uniform CIE L* a* b* colour space (CIELAB colour space), published first by the Commission Internationale de l'Éclairage (CIE) in 1976. The CIELAB colour space is the most complete colour model used conventionally to describe colours and colour differences visible to the human eye (*Figure 7 a,b*). The term 'uniform' indicates that equally measured distances in the colour space ideally equate to equally perceived colour differences as seen by the standard observer. The three-

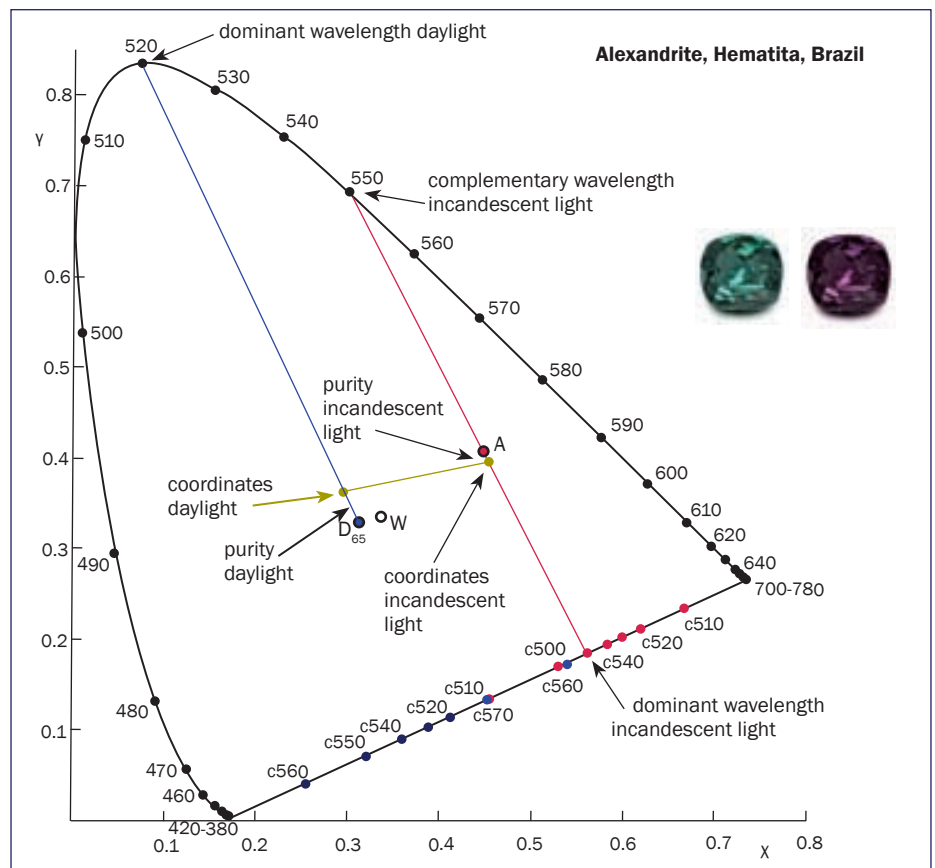


Figure 4: Colorimetric parameters of an alexandrite from Hematita, Brazil, in the CIE 1931 chromaticity diagram.

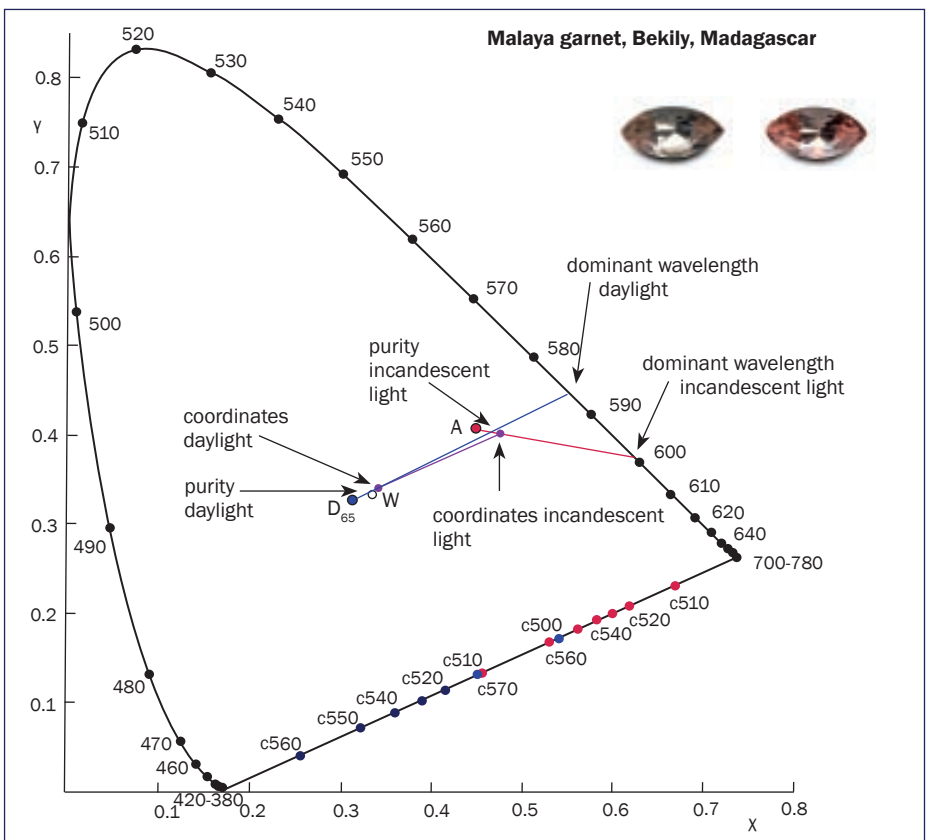


Figure 5: Colorimetric parameters of a malaya garnet from Bekily, Madagascar, in the CIE 1931 chromaticity diagram.

Colour-change garnets from Madagascar: variation of chemical, spectroscopic and colorimetric properties

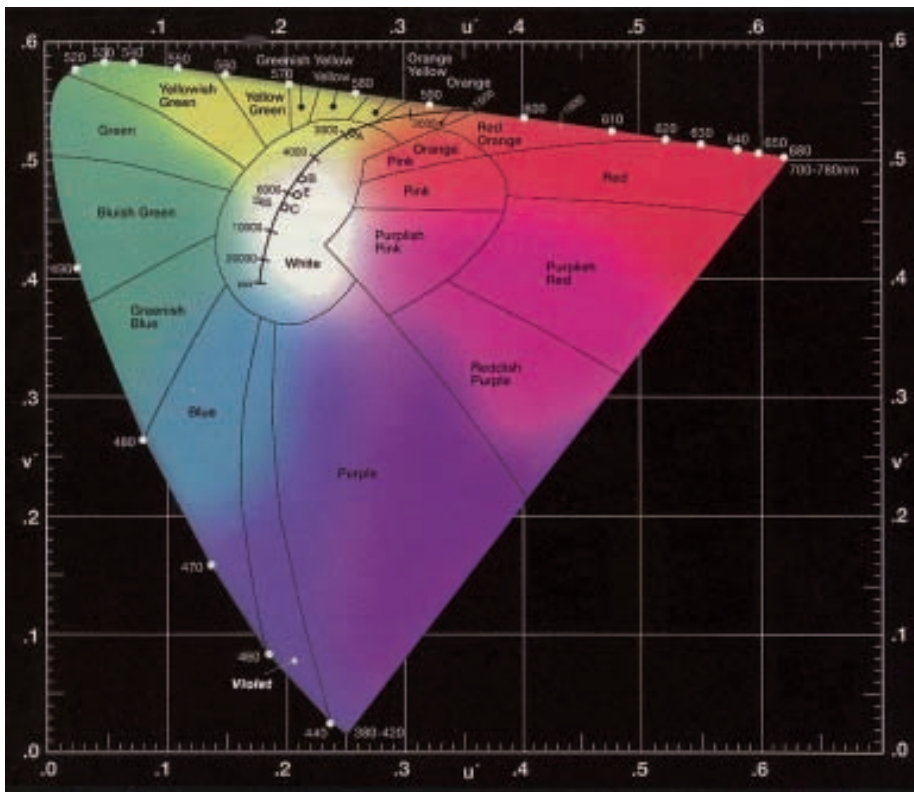


Figure 6: Colour distribution in the $u'v'$ 1976 chromaticity diagram; this diagram is based on a transformation from the CIE 1931 chromaticity diagram. The CIE $L^*a^*b^*$ colour space (which incorporates the $u'v'$ chromaticity diagram) is one of the commonly used uniform colour spaces; the distance between two points on the diagram is approximately proportional to the perceived colour difference. Copyright HyperPhysics by Rod Nave, Georgia State University, USA (reproduced by permission).

dimensional colour space shows lightness/darkness along the vertical axis (L^*) and colours in a two-dimensional plane with redness/greenness along a first horizontal axis (a^*) and blueness/yellowness along a second horizontal axis (b^*). The colours related to this rectangular coordinate system are:

- + a^* axis: red purple
- + b^* axis: yellow
- a^* axis: bluish green
- b^* axis: blue

The orientation of the CIELAB a^*b^* coordinate system in relation to the CIE 1931 chromaticity diagram is given in Figure 8.

Changing the first parameter L (lightness) in this colour space is like changing the brightness setting in a TV. Therefore only a few representations with various slices or projections (i.e. different cross sections) perpendicular to the lightness axis are used to visualize the CIELAB colour space (see again Figure 7 a, b).

The parameters a^* and b^* are also expressed as hue angle h_{ab} and chroma C_{ab}^* , which sometimes is also designated as saturation (Figure 9). The hue angle h_{ab} is measured in degrees and ranges from 0° to 360° starting with $h_{ab} = 0^\circ$ at the + a^* axis and increasing counterclockwise. Chroma C_{ab}^* represents the distance of a sample locus from the origin of the a^*b^* plane. Hue angle h_{ab} and chroma C_{ab}^* are calculated from a^* and b^* values as follows: $h_{ab} = \arctan(b^*/a^*)$ and $C_{ab}^* = (a^{*2} + b^{*2})^{1/2}$.

Two examples are given in Figures 10 and 11.

Quantitative data for colour difference, hue angle difference and chroma difference between two sample loci P_1 , P_2 in the CIELAB colour space are easily obtainable as follows:

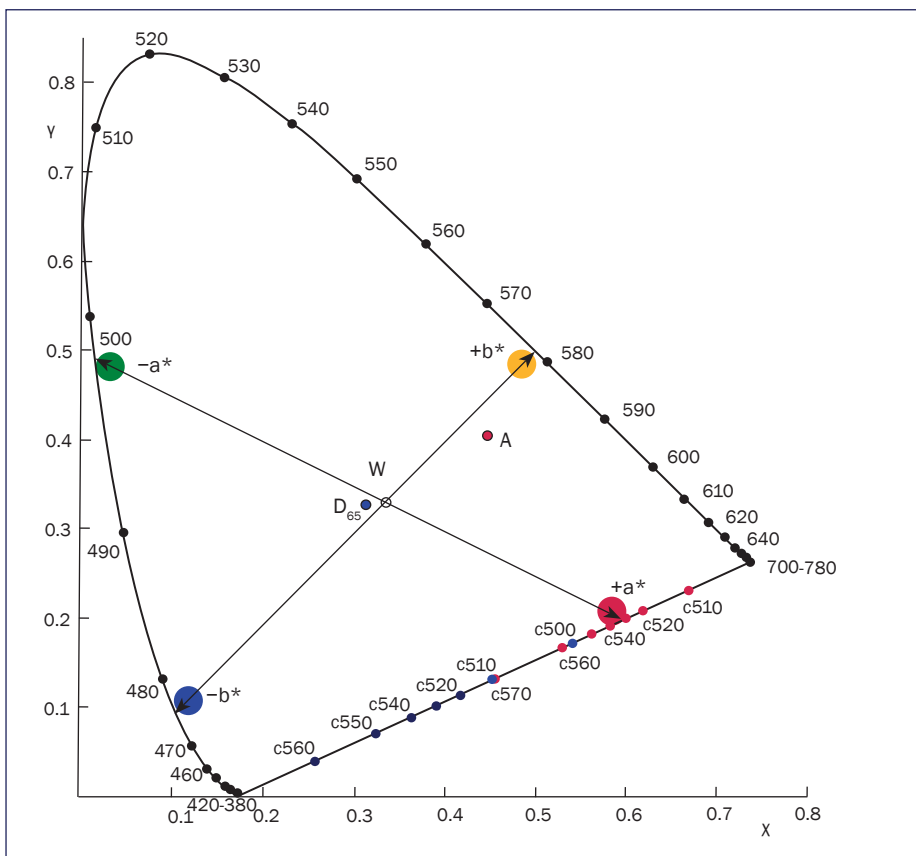


Figure 8: Orientation of the CIELAB a^*b^* plane relative to the CIE 1931 chromaticity diagram; the a^* and b^* axes intersect the line of spectral colours and the line of purples of the CIE chromaticity diagram at red purple (+ a^*), bluish green (- a^*), yellow (+ b^*) and blue (- b^*).

Colour-change garnets from Madagascar: variation of chemical, spectroscopic and colorimetric properties

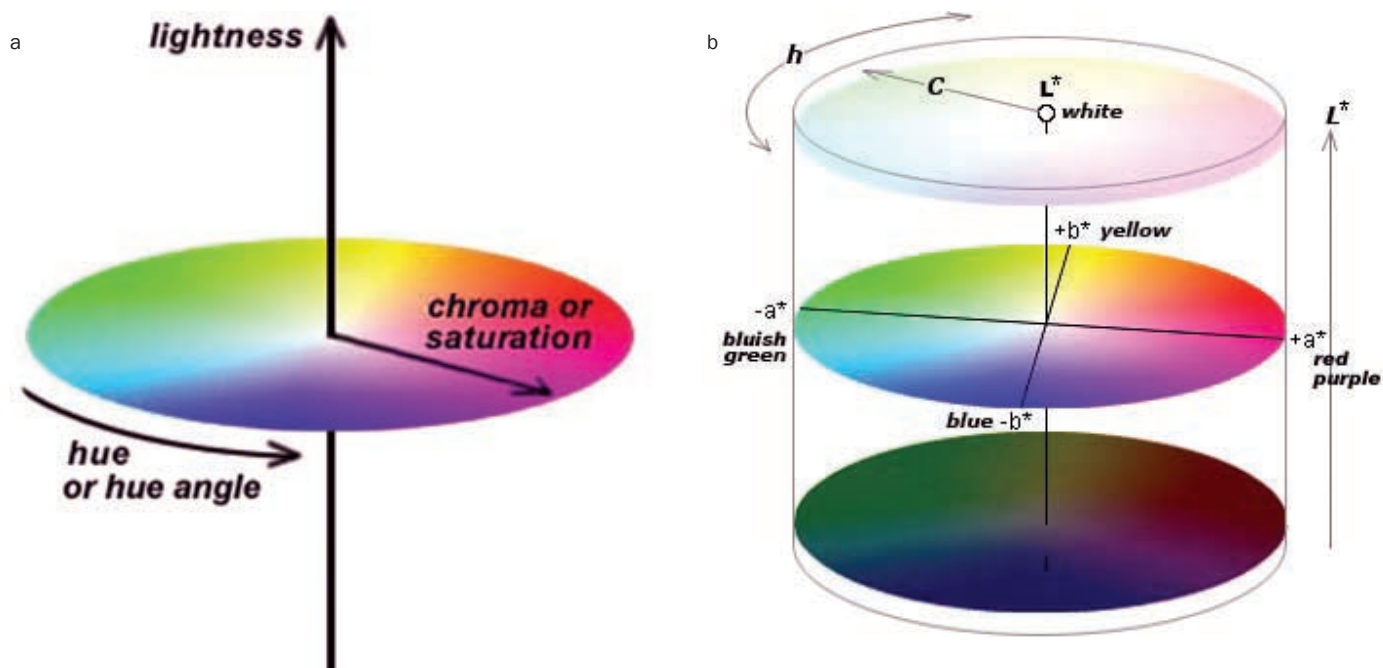


Figure 7a,b: Schematic outline of the three-dimensional CIELAB 1976 colour space; the principal parameters representing a specific colour are hue or hue angle (h_{ab}), chroma or saturation (C_{ab}^*) and lightness (L^*). Copyright handprint media by Bruce MacEvoy (reproduced by permission).

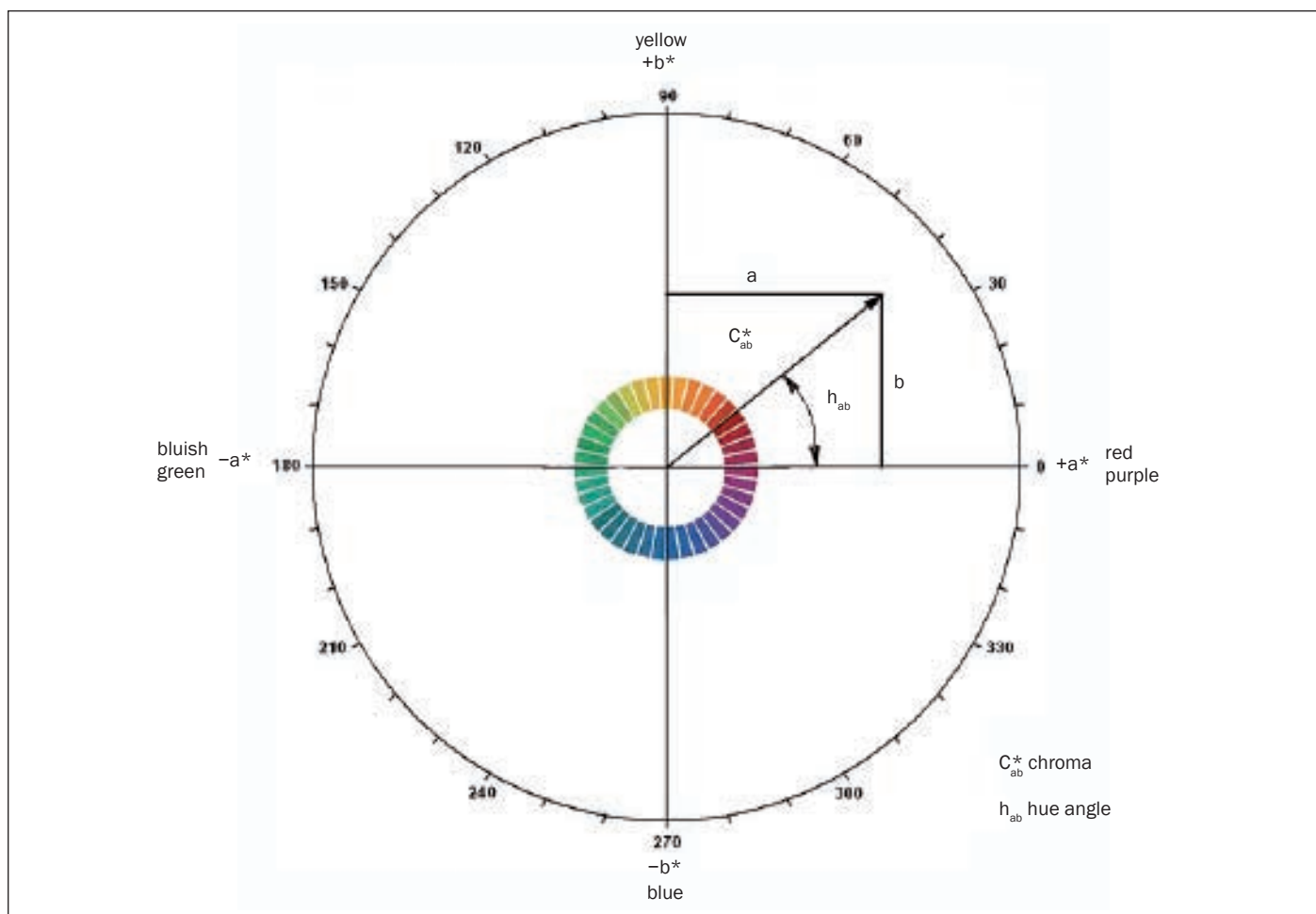


Figure 9: Geometric representation of hue angle and chroma relative to the a^*b^* plane (the rectangular a^*b^* coordinate system) of the three-dimensional CIELAB colour space; the third parameter lightness L^* is perpendicular to the a^*b^* plane; a and b are the coordinates of the sample locus.

Colour-change garnets from Madagascar: variation of chemical, spectroscopic and colorimetric properties

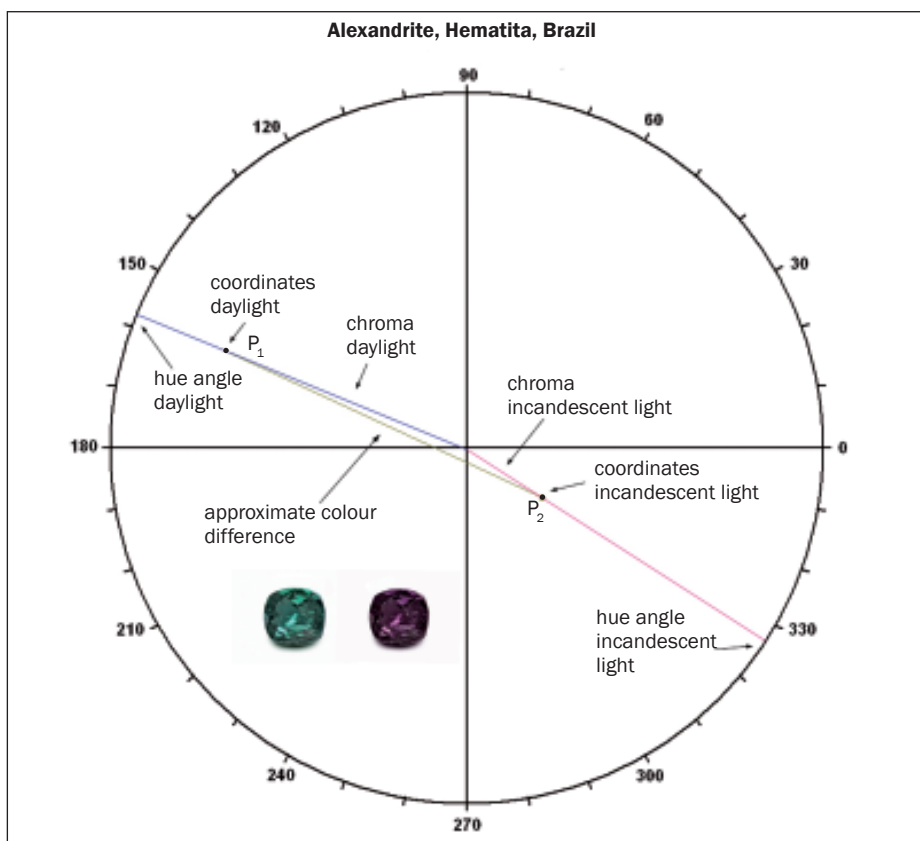


Figure 10: Colorimetric parameters of an alexandrite from Hematita, Brazil, in the CIELAB 1976 colour space.

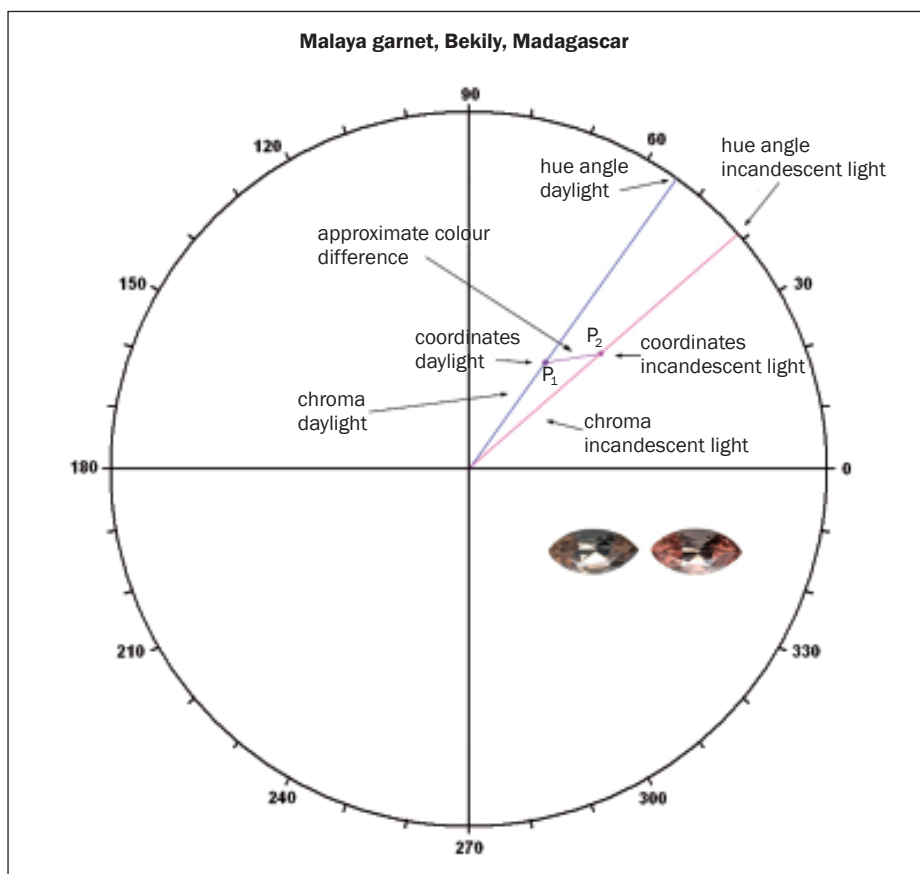


Figure 11: Colorimetric parameters of a malaya garnet from Bekily, Madagascar, in the CIELAB 1976 colour space.

- a) The colour difference ΔE_{ab}^* is calculated as $\Delta E_{ab}^* = [(\Delta L^*)^2 + (\Delta a^*)^2 + (\Delta b^*)^2]^{1/2}$ where ΔL^* , Δa^* and Δb^* represent the difference between the L^* , a^* and b^* values of the two points P_1 and P_2 . This indicates, that colour difference is represented by the distance of two sample loci in the three dimensional colour space from each other.
- b) The hue angle difference Δh_{ab} is calculated as $\Delta h_{ab} = h_{ab}(\text{point } P_1) - h_{ab}(\text{point } P_2)$.
- c) Chroma difference differs from the parameter ΔE_{ab}^* (colour difference) and is calculated as $\Delta C_{ab}^* = C_{ab}^*(\text{point } P_1) - C_{ab}^*(\text{point } P_2)$. Chroma difference is represented by the different distances of two sample loci from the origin of the a^*b^* coordinate system of the CIELAB colour space.

Colour differences ΔE_{ab}^* of less than 1 CIELAB unit are practically invisible, differences more than 3 CIELAB units are clearly visible.

The German RAL DESIGN system was specially developed for the visualization of the CIELAB 1976 colour space and can help to further illuminate details of this colour space. The individual colours were arranged according to hue, chroma and lightness (Figure 12). The central non-chromatic axis of the colour space starts at black (minimum lightness) and runs through lighter shades of grey to white (maximum lightness, Figure 13). A specially developed colour wheel can illustrate the interdependency of hue angles and colours (Figure 14). For this illustrative colour wheel, colours with high chroma were arranged at hue angle distances of 10° each (for practical use it was desirable to have intermediate colours at hue angle differences of 5° available for the yellow to orange range).

A good impression of the variability of colour for a given hue angle, with different chroma and lightness is illustrated in Figure 15. A very useful continuous colour wheel showing also the colours with different hue angle and chroma in the CIELAB colour space was developed by GretagMachbeth and is illustrated in Figure 16.

Colour-change garnets from Madagascar: variation of chemical, spectroscopic and colorimetric properties

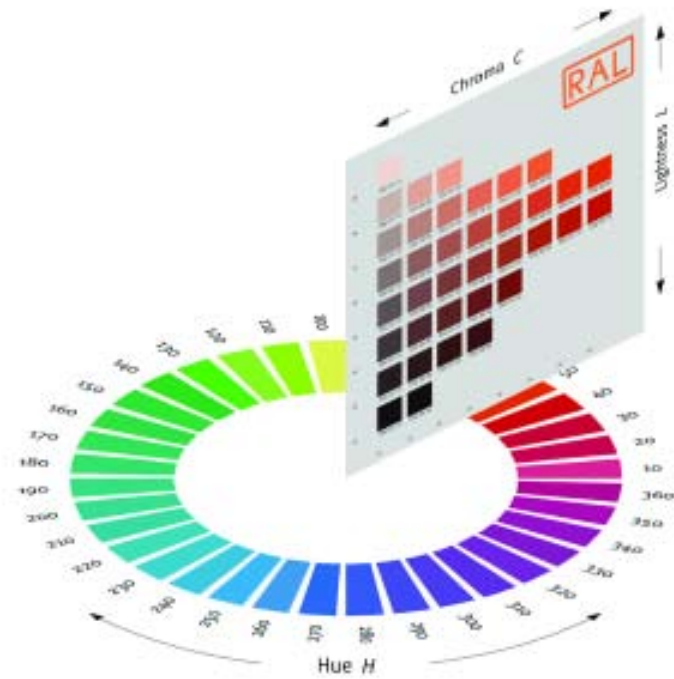


Figure 12: Outline of the RAL colour design system within the three-dimensional CIELAB colour space; the colour charts are systematically organized according to different hue angles, chroma and lightness; the printed colour chart represents an example of red orange at a hue angle of 50°. Copyright dtp studio Oldenburg and RAL gGmbH, Sankt Augustin, Germany (reproduced by permission).



Figure 13: Model of the three-dimensional CIELAB colour space, model of the colour solid, section parallel to the non-chromatic (black to white) lightness axis. Copyright dtp studio Oldenburg and RAL gGmbH, Sankt Augustin, Germany (reproduced by permission).



Figure 14: Hue circle (colour wheel) of CIELAB colour space representing examples of colours at different hue angles of the three-dimensional colour solid at high chroma and lightness 50. Copyright dtp studio Oldenburg and RAL gGmbH, Sankt Augustin, Germany (reproduced by permission).

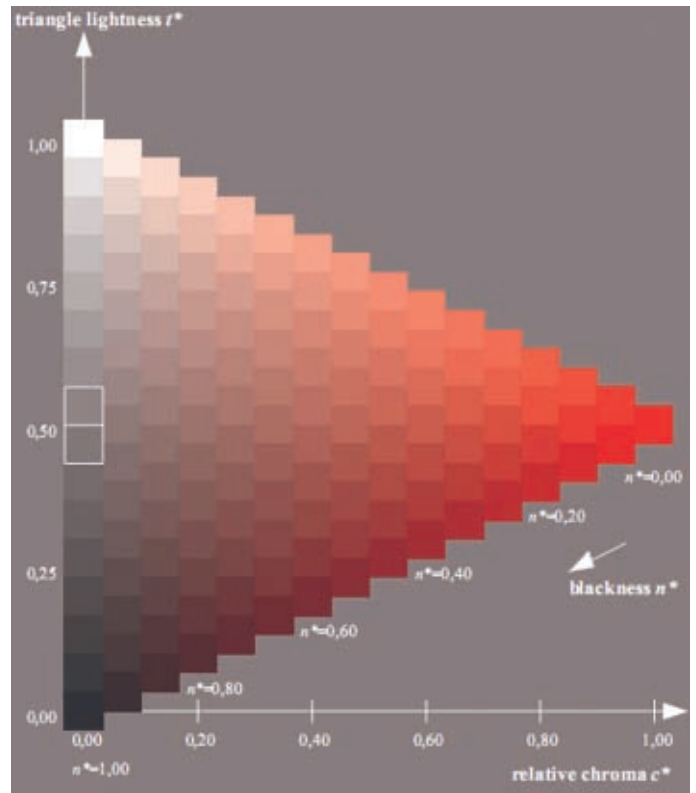


Fig. 15: Colour variation of red orange in the three dimensional CIELAB colour space at hue angle of 42° with varying lightness and chroma; at left the L* axis of the CIELAB colour space from black to white is shown; with increasing chroma, more saturated, 'bright' colours are obtained. Copyright Relative Elementary Colour System (RECS) by K. Richter (reproduced by permission).

Colour-change garnets from Madagascar: variation of chemical, spectroscopic and colorimetric properties

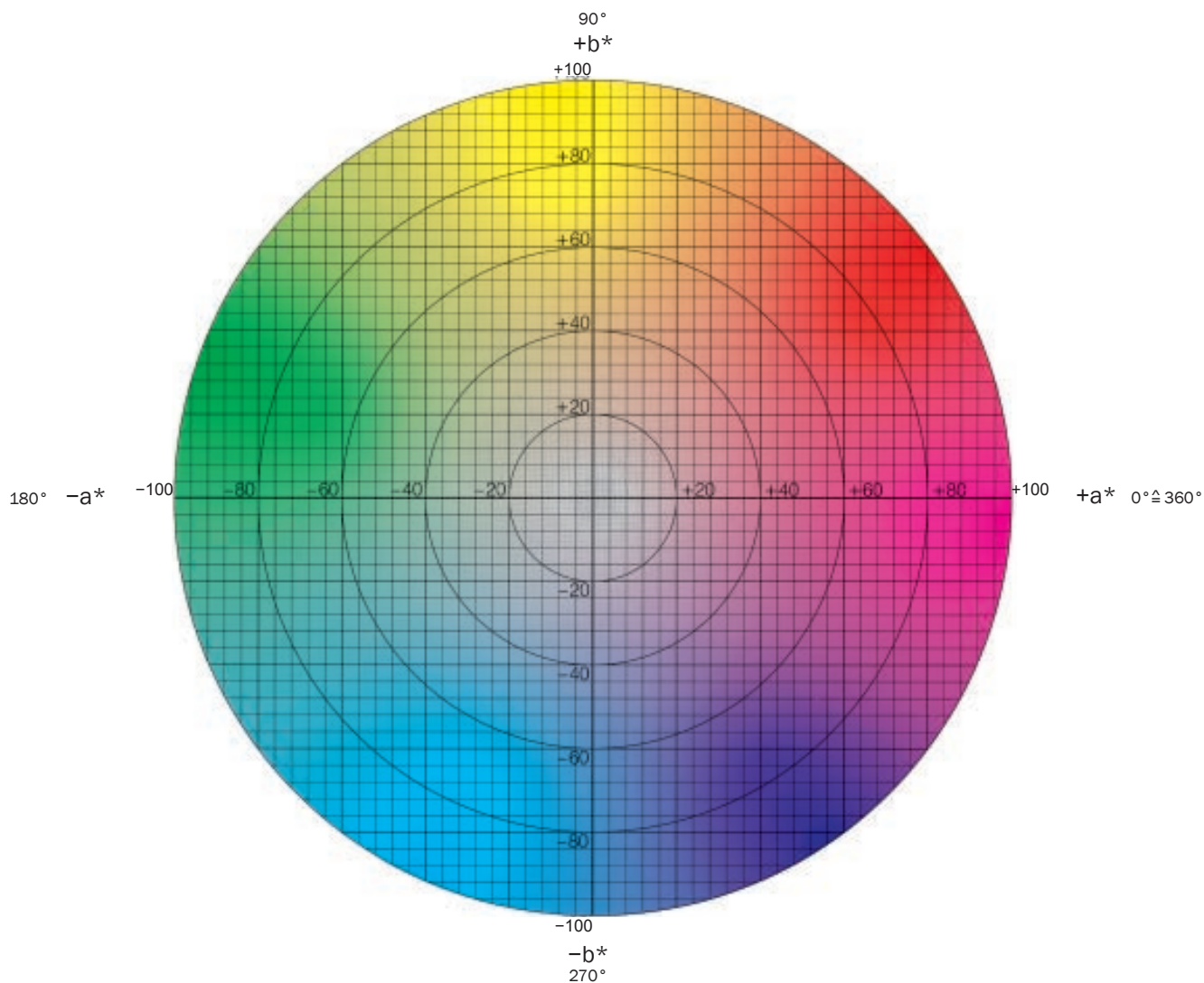


Fig. 16: Colour distribution in the CIELAB 1976 colour circle at various hue angles and chroma. Copyright GretagMacbeth, Regensdorf, Switzerland (reproduced by permission).

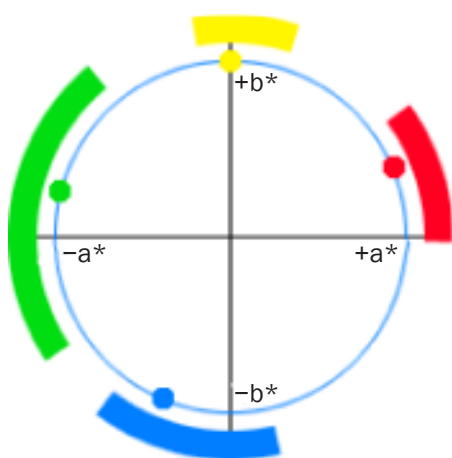


Figure 17: Variable location of the four 'unique' hues red, yellow, green and blue in the CIELAB colour circle; these are the hue angle ranges of 'unique' hues chosen by individuals in different colour studies. Copyright handprint media by Bruce MacEvoy (reproduced by permission).

There is, however, no 'correct' standardization and correlation of hue names related to hue angles in the CIELAB colour circle (see, e.g., Robertson, 1994; Liu, 2007; Liu and Hurwit, 2008). In particular the designation and selection of the four 'unique' colours red, yellow, green and blue is problematic as discussed in detail by Kuehni (2004) and MacEvoy (2005). The variability of the location of red, yellow, green and blue relative to the CIELAB colour circle is given in Figure 17.

For the present paper the authors decided to use the following scheme:

The hue angles for red, yellow, green, and blue were taken from Richter (1996, 2008b). These were calculated from the spectral data for the four test-colour samples red, yellow, blue and green as

published by the CIE (1995) (K. Richter, pers. comm. 2008; for further information see Richter, 2007, 2008a; DIN 33872, 2007). The hue angles for the three equidistant colours between each of the four colours red, yellow, green, and blue were also taken from Richter (2008b). For illustration, this colour wheel is shown in Figure 18, with the names of colours assigned by the present authors, e.g. bluish green, blue green, greenish blue for the three colours between green and blue. Finally, the loci of intermediate colours, e.g. blue violet or reddish purple, were calculated by the present authors as desirable for the designation of colours in the present paper. The location of all these colours relative to the CIELAB colour circle and their designation in the present paper is given in Table I and Figure 19.

Colour-change garnets from Madagascar: variation of chemical, spectroscopic and colorimetric properties

Examples: Natural alexandrite from Hematita, Brazil, and malaya garnet from Bekily, Madagascar

To demonstrate application of the above principles, the authors also examined two natural and two synthetic alexandrites and four malaya garnets from Bekily, Madagascar. The parameters calculated from the absorption spectrum of one example from each group are listed below and plotted in *Figures 4, 5, 10* and *11*.

Alexandrite, Hematita, Brazil

CIE 1931 system (*Figure 4*):

Chromaticity coordinates for daylight

D_{65} : $x = 0.2974$; $y = 0.3622$;

Dominant wavelength $\lambda_d = 520$ nm;

purity $p = 6.6$ %; colour: green;

Chromaticity coordinates for

incandescent light A: $x = 0.4536$; $y =$

0.3951 ;

Dominant wavelength $\lambda_d = 551$ nm;

purity $p = 5.5$ %; colour: purple.

CIELAB 1976 colour space (*Figure 10*):

Coordinates for daylight D_{65} : $L^* =$

56.82 ; $a^* = -14.95$; $b^* = 6.01$;

Further parameters for daylight D_{65} :

chroma $C_{ab}^* = 16.11$; hue angle $h_{ab} =$

158° ; colour: green;

Coordinates for incandescent light A:

$L^* = 55.54$; $a^* = 4.58$; $b^* = -3.07$;

Further parameters for incandescent

light A: chroma $C_{ab} = 5.51$; hue angle

$h_{ab} = 326^\circ$; colour: purple;

Colour difference $\Delta E_{ab}^* = 21.56$; hue

angle difference $\Delta h_{ab} = 168^\circ$.

Malaya garnet, Bekily, Madagascar

CIE 1931 system (*Figure 5*):

Chromaticity coordinates for daylight

D_{65} : $x = 0.3379$; $y = 0.3412$;

Dominant wavelength $\lambda_d = 586$ nm;

purity $p = 10.4$ %; colour: orange;

Chromaticity coordinates for

incandescent light A: $x = 0.4744$; $y =$

0.4031 ;

Dominant wavelength $\lambda_d = 598$ nm;

purity $p = 15.3$ %; colour: red orange.

CIELAB 1976 colour space (*Figure 11*):

Coordinates for daylight D_{65} : $L^* =$

63.62 ; $a^* = 4.72$; $b^* = 6.56$;

Further parameters for daylight D_{65} :

chroma $C_{ab}^* = 8.08$; hue angle $h_{ab} =$

54° ; colour: orange;



Figure 18: Colour circle in the CIELAB colour space with four unique colours and twelve (4 x 3) intermediate, equidistant colours; the verbal designation of colours was chosen by the present authors. Copyright Relative Elementary Colour System (RECS) by K. Richter (reproduced by permission).

Coordinates for incandescent light A:

$L^* = 64.49$; $a^* = 8.07$; $b^* = 7.09$;

Further parameters for incandescent

light A: chroma $C_{ab}^* = 10.74$; hue angle

$h_{ab} = 41^\circ$; colour: red orange;

Colour difference $\Delta E_{ab}^* = 3.51$; hue

angle difference $\Delta h_{ab} = 13^\circ$.

Materials and methods

Two authors (KS and TH) collected 52 garnet samples showing clear colour changes, i.e. visually discernible colour changes upon changes of illuminant. Subsequent to earlier work on colour-change garnets from Bekily, Madagascar (Schmetzer and Bernhardt, 1999), which described mainly bluish green garnets with one yellow sample, the first author (KS) obtained garnets from Madagascar with a wider range of coloration from a German dealer who had purchased

the garnets on local gem markets in Madagascar between 2000 and 2007. Most garnets were stated to come from Bekily, the classic locality mentioned in our previous paper, but it is possible that a few originate from other localities in Madagascar, e.g. from Ilakaka (where there are also many different gem varieties of garnets). However, we are confident that our samples have not originated from other countries. Most of the remaining samples studied come from the private collection of one author (TH), with specific colours that were rare or absent from the range in the first lot collected. For this second group, the history of the samples also points to Bekily as the source. Most samples are faceted, but a few rough garnets available to the authors were cut in Germany in order to study all samples under similar conditions.

Colour-change garnets from Madagascar: variation of chemical, spectroscopic and colorimetric properties



Figure 19: Examples of the verbal designation of colours in the present paper are shown in the RAL colour wheel, which is based on the three-dimensional CIELAB colour space (see also Table I and Figure 14, copyright dtp studio Oldenburg and RAL gGmbH, Sankt Augustin, Germany (reproduced by permission).

For comparison, the authors also examined four vanadium- and chromium-free pyrope-spessartine garnets (malaya garnets) from Bekily (see Schmetzer *et al.*, 2001), two natural alexandrites from Hematita, Brazil, and two synthetic flux-grown alexandrites produced in Novosibirsk, Russia.

The chemical compositions of all 52 garnets were obtained using a Cameca

Camebax SX 50 electron microprobe, and at least 10 point analyses from traverses across the table facet of each sample were recorded.

Colorimetric and spectroscopic data were obtained in transmission mode with a Zeiss multi-channel colour spectrometer, version MCS 311, and a Gemprobe GP 311 integration sphere. The MCS 311 is a double-beam colorimeter equipped with

a pulsed Xenon lamp housed in a BaSO_4 -lined integration sphere of 60 mm internal diameter providing diffuse, indirect illumination, Schott quartz-type fibre-light guides, two identical dispersive modules, each with a concave holographic grating and a 512-channel photodiode array, and a BaSO_4 -lined sample platform with a central 3 mm mask hole for light transmission through the sample.

Colour-change garnets from Madagascar: variation of chemical, spectroscopic and colorimetric properties

The instrument is designed for (nearly) simultaneous light intensity measurement of the sample beam and the reference beam and for colorimetric data processing.

The UV-Vis-NIR spectra of the garnets were also recorded on a second type of spectrophotometer, especially for the evaluation of absorption maxima of the main vanadium-chromium absorption band between 569 and 584 nm. This spectrometer system was designed and assembled by one of the authors (TH) using a BaSO₄-covered integration sphere, a 100 Watt Xenon light source and a high resolution spectrometer with a 2048 pixel CCD detector; the system had a resolution of 0.5 nm and covered the range of 245 to 1050 nm. Spectra were recorded with 200 to 500 sample scans to obtain a good signal to noise (S/N) ratio.

The spectra recorded using both spectrometer systems are closely comparable. The differences obtained for the vanadium-chromium maxima were mostly in the range of ± 1 nm, with a few extending up to ± 2 nm between both spectrophotometers. The differences in band positions of manganese and iron absorption maxima are also in the range of ± 1 nm.

Colorimetric data processing was performed using the Zeiss MCS 311 system including the Zeiss DIAMOCR software which instantly provides the CIE 1931 chromaticity values x , y , Y and the CIELAB parameters L^* , a^* , b^* , hue

angle h_{ab} , and chroma C^*_{ab} for the two illuminants D₆₅ and A in the present study. These values are based on the absorbance spectrum recorded from 375 to 774 nm at 10 ms integration time, 0.8 nm spectral pixel spacing, 2.4 nm spectral resolution, and ≤ 0.1 nm wavelength accuracy and reproducibility. Characteristic parameters such as dominant wavelengths for different light sources which were not available automatically from the Zeiss system, were calculated by a computer program written by one author (HJB).

The distance between the two loci of one sample with different illumination in the three-dimensional CIELAB colour space is represented by the parameter ΔE^*_{ab} , which represents the exact colour difference for the specific pair of illuminants used.

Visual determination of body and reflection colours of gemstones

It was desirable to compare the colorimetric results with visual determinations. The observed colours of these colour-change garnets are dependent not only on a major change of illuminants (from daylight to incandescent light), but also on more subtly different types of natural light such as direct sunlight, diffuse light from cloudy skies, or morning, noon or evening light. The colour temperature of daylight is mostly in the range 5500 to 6500 K but depends in detail on geographical location, time, date and atmospheric conditions.

The colours of many of the garnets in the suite changed in different types of daylight. Therefore, the visual estimation of colour was performed in a dark room using a daylight-equivalent fluorescent light source (Eickhorst, Hamburg, Germany) with 6400 K colour temperature (close to CIE standard illuminant D₆₅). For incandescent light, a tungsten bulb was used. D₆₅ is an artificial daylight with an ultraviolet component which is also designated 'standard noon daylight'. Its colour temperature is approximately 6500 K. Illuminant A is tungsten light with a colour temperature of 2856 K. According to their spectral power distribution, both illuminants are the best suited, standardized substitutes of the traditional, natural light sources, diffuse daylight (not direct sunlight) and candle light. D₆₅ is produced by xenon lamps (sometimes with UV filters) and is widely used in simultaneously recording spectrometric systems. Illuminant A is generated by tungsten-halogen lamps and is used in sequentially recording spectrometers. Illuminants D₆₅ and A are widespread in the industry, e.g. in GretagMacbeth colour viewing booths.

The garnets were placed face-up on a white (neutral) background under 0° illumination and 0° observation (0°/0° geometry) as well as under 0° illumination and 45° observation (0°/45° geometry). The illuminated samples were visually compared in reflection with a printed

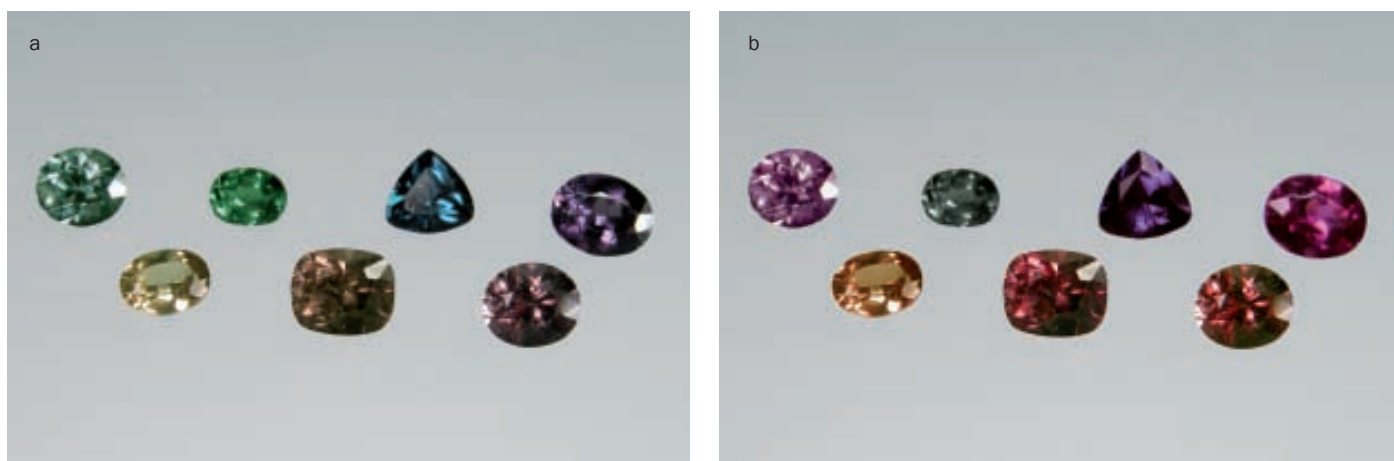


Figure 20 a,b: Colour-change garnets from Madagascar representing the seven groups of samples described in this paper in daylight (left) and incandescent light, upper row from left to right: Groups 1 to 4, lower row from left to right: Groups 5 to 7. Size of the garnet at the upper right 5.2 x 6.8 mm, weight 0.89 ct.

Colour-change garnets from Madagascar: variation of chemical, spectroscopic and colorimetric properties

Table II: Physical properties, chemical compositions and colorimetric data of seven groups of colour-change garnets from Madagascar.

Group	1	2	3	4	5	6	7
Sample numbers	1/1–1/10	2/1–2/9	3/1–3/7	4/1–4/3	5/1–5/14	6/1–6/7	7/1–7/2
Colour in daylight	green to slightly yellowish green or greenish yellowish grey	green to slightly yellowish green	bluish green or greenish blue	purple or violet or purplish red	yellow green to yellow or yellowish grey to greenish yellowish grey	orange to yellow orange	red
Colour in incandescent light	red purple to reddish purple or purple	red purple or yellowish grey to greenish yellowish grey or greyish bluish green	violet purple to purple or blue violet or blue green	reddish purple to red purple	orange to red purple	red	red or purplish red
Mol.% end members ^a							
Goldmanite	1.10–3.41	3.63–4.92	2.29–5.13	1.63–2.70	0.92–2.18	0.64–1.50	0.37–0.55
Uvarovite	0.34–0.73	0.19–2.02	0.44–1.86	1.03–1.61	0.15–0.74	0.61–1.06	0.34
Almandine ^b	2.87–7.24	6.09–10.57	3.21–9.29	7.45–14.95	3.18–5.15	5.61–7.85	10.02–16.35
Spessartine	24.95–45.73	54.69–62.03	33.41–41.29	29.24–36.62	27.09–73.83	48.75–61.87	22.96–26.24
Pyrope	42.42–62.42	22.41–31.20	38.29–55.04	44.06–58.08	14.49–59.57	28.99–39.54	55.43–59.27
Grossular	2.18–11.88	0.24–6.09	1.11–13.30	2.07–3.47	3.02–10.45	1.44–2.43	3.75–3.76
Goldmanite + Uvarovite	1.50–4.14	4.23–6.94	2.78–6.75	3.16–4.31	1.17–2.92	1.66–2.26	0.71–0.89
Spessartine : (Goldmanite + Uvarovite)	9.7–16.9	8.6–12.9	6.1–12.2	8.5–9.9	17.2–33.1	23.1–30.2	25.8–37.0
Absorption maximum (nm)	572–576	578–583	574–584	571–573	570–573	569–571	570–571
Colorimetric data CIE 1931 ^c							
λ_D (nm) for daylight D ₆₅	513–552	517–548	484–501	635–c563	567–577	581–587	598–608
Purity p for daylight D ₆₅	1.0–5.0	7.6–11.4	1.1–17.1	4.5–7.1	2.1–34.2	9.0–15.6	9.9–12.5
λ_D (nm) for incandescent light A	c509–c550	c507 or 504–576	c540–495	c510–c531	586–c511	609–633	619–c504
Purity p for incandescent light A	3.8–7.1	1.6–6.1	5.2–21.3	20.0–27.9	4.8–38.0	11.4–20.7	17.1–19.9
Colorimetric data CIELAB 1976 ^d							
C* _{ab} for daylight D ₆₅	1.52–8.24	10.92–17.90	1.92–21.57	3.41–6.83	1.16–17.88	5.70–8.60	9.37–9.91
h _{ab} (°) for daylight D ₆₅	141.5–161.8	144.4–159.4	173.4–238.5	307.9–14.2	79.4–119.1	51.6–69.4	22.2–30.7
C* _{ab} for incandescent light A	3.07–6.37	1.21–4.13	5.41–14.30	15.27–17.98	4.54–18.16	10.42–15.11	13.59–15.66
h _{ab} (°) for incandescent light A	326.6–357.3	4.3 or 105.9–193.9	223.3–332.5	336.5–355.8	353.8–65.4	19.2–28.7	14.6–23.2
Δh_{ab} (°)	144.3–176.2	147.8 or 0.6–34.5	48.9–159.1	13.0–29.4	30.7–119.7	28.8–48.9	7.5–7.6
ΔE^*_{ab}	6.8–12.4	8.9–16.1	7.3–17.1	11.4–12.4	5.1–11.2	7.8–9.8	4.6–6.1

^a Formulae of garnet end members:

goldmanite $\text{Ca}_3\text{V}_2\text{Si}_3\text{O}_{12}$; uvarovite $\text{Ca}_3\text{Cr}_2\text{Si}_3\text{O}_{12}$; grossular $\text{Ca}_3\text{Al}_2\text{Si}_3\text{O}_{12}$

almandine $\text{Fe}_3\text{Al}_2\text{Si}_3\text{O}_{12}$; spessartine $\text{Mn}_3\text{Al}_2\text{Si}_3\text{O}_{12}$; pyrope $\text{Mg}_3\text{Al}_2\text{Si}_3\text{O}_{12}$

^b Total iron calculated as FeO in almandine

^c λ_D = dominant wavelength, c indicates 'complement of'

^d C*_{ab} = chroma; h_{ab} = hue angle

Δh_{ab} = hue angle difference between daylight and incandescent light

ΔE^*_{ab} = colour difference between daylight and incandescent light in the three dimensional CIELAB colour space

Colour-change garnets from Madagascar: variation of chemical, spectroscopic and colorimetric properties

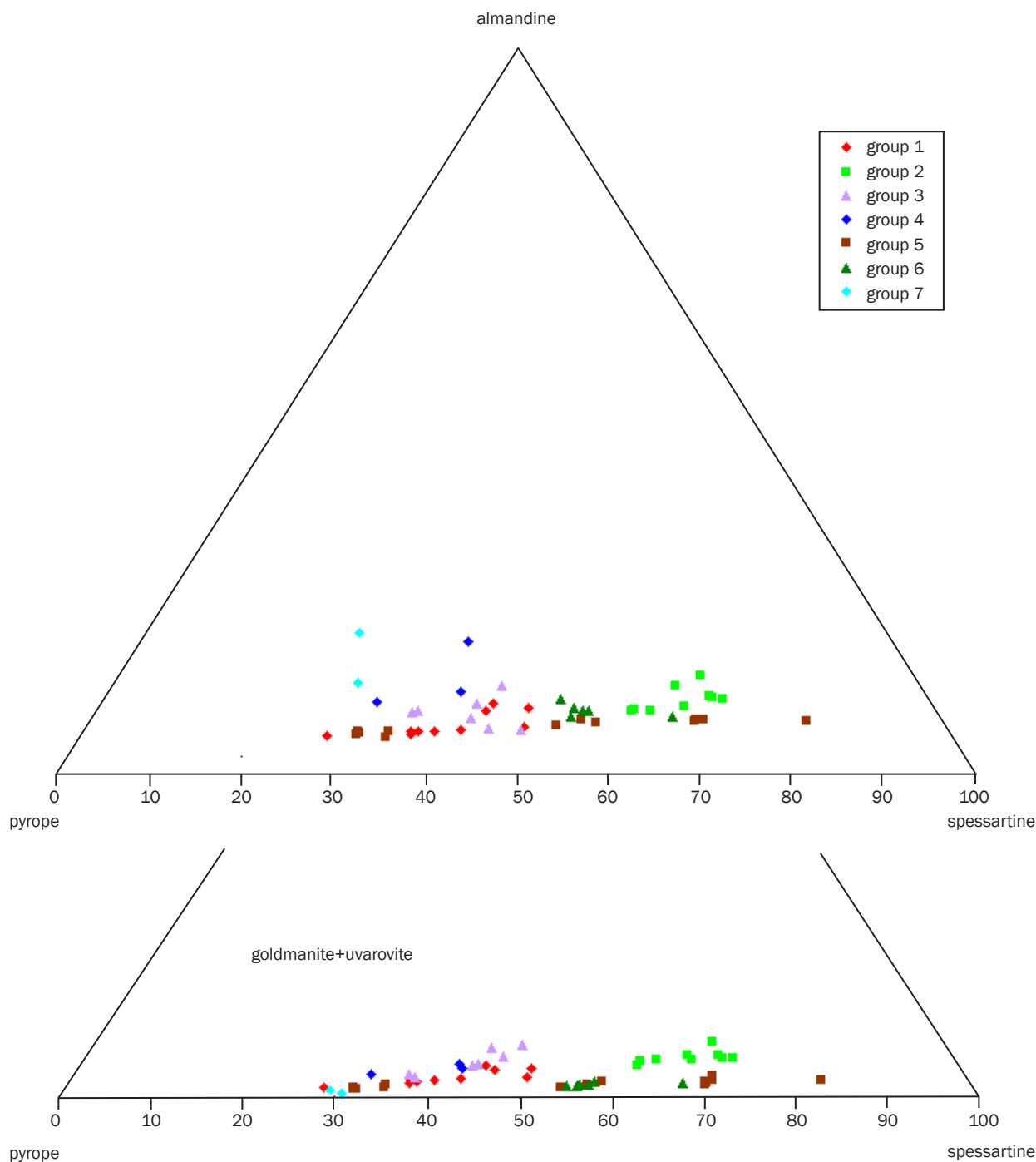


Figure 21: Compositions of colour-change garnets normalized to end-members (pyrope + spessartine + goldmanite + uvarovite) = 100 (below) and to (pyrope + spessartine + almandine) = 100 (above) and shown on triangular diagrams.

version of the CIE 1931 chromaticity diagram (the ‘horseshoe’) and a printed version of the CIELAB 1976 colour circle as well as with the diagrams published by Richter (2008b). Alternatively one could use Figures 2, 16 and 19. Using this procedure, it was confirmed that the visually estimated colour was identical

or nearly identical with the colour coordinates of the sample calculated from spectroscopic data for the different colour spaces (see above).

For the designation of colours we use the hue names for highly saturated colours as summarized in Table I. In order to avoid numerous fantasy names which

could lead to a great deal of confusion, we do not add special modifiers to these names and comment only if there is a relatively low or high chroma (saturation) measured for the colour of a specific garnet. Each garnet colour observed under standard illumination was compared with its computer screen colour of the

Colour-change garnets from Madagascar: variation of chemical, spectroscopic and colorimetric properties

digitally photographed samples and, if necessary, the latter was adjusted to the closest match using Photoshop Elements 6.0 software. However, we are aware that these colours could look slightly different on other screens or in print.

Results

Presentation of data

The 52 garnets were divided into seven main groups based on their colour in daylight as determined (measured and calculated) in the CIE 1931 and the CIELAB 1976 colour spaces and confirmed by visual impression (*Figure 20 a,b*). In the three-dimensional CIELAB colour space, the hue, represented by hue angle, was considered as the most important factor in grouping the garnets. This brings together those garnets with similar colour in daylight and with similar chemical and spectroscopic properties as well as a similar colour change, but such a group may also include samples with different spectra, composition and colour change.

Chemical properties

The composition of each garnet is more or less homogeneous without any significant chemical zoning; this is consistent with the absence of any significant colour zoning. All samples

Table III: Assignment of iron- and manganese-absorption bands in pyrope-spessartine garnets from Madagascar^a.

Absorption maximum (nm)	Fe ²⁺	Mn ²⁺	Fe ³⁺
410		✓	
421		✓	
430		✓	✓
459	✓	✓	
483		✓	
503	✓		
525	✓	✓	
569	✓		
610	✓		
687	✓		

^a after Schmetzer *et al.* (2001)

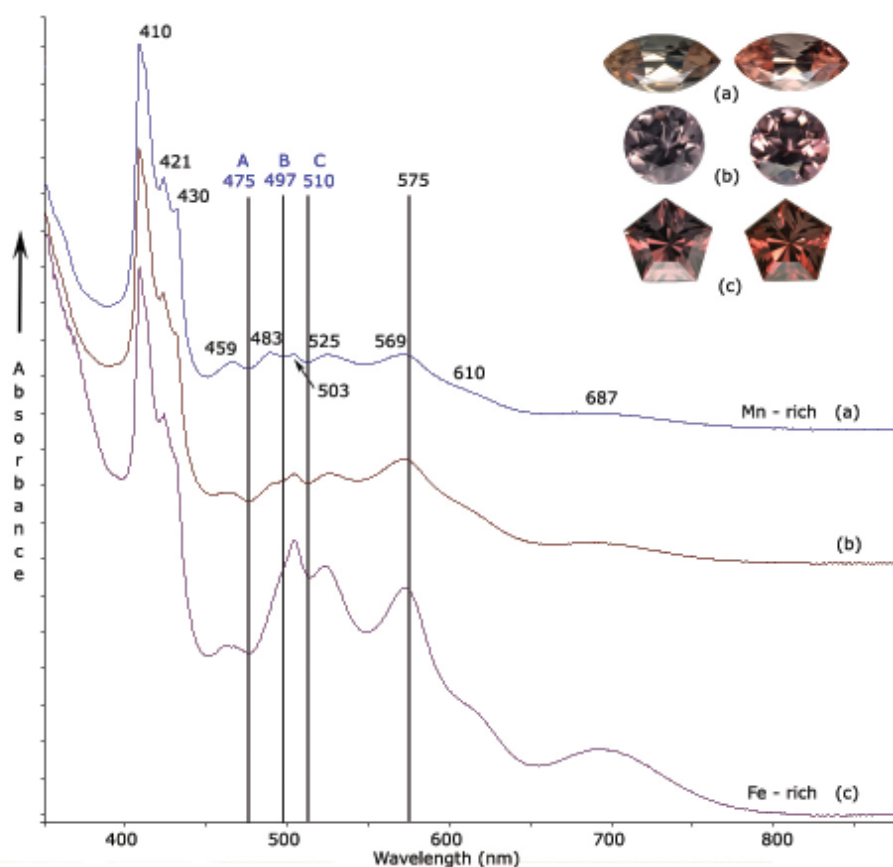


Figure 22: Absorption spectra of three vanadium- and chromium-free malaya garnets from Bekily, Madagascar, with different manganese and iron contents; the samples are shown in daylight (left) and incandescent light (right).

are members of the pyrope-spessartine solid solution series with minor to major contents of iron (almandine) and minor contents of vanadium and chromium. Formally, the vanadium and chromium contents are calculated as minor percentages of the goldmanite and uvarovite molecules. In addition, a range of percentages of grossular is present. The compositional range of all 52 analysed samples is as follows:

pyrope $Mg_3Al_2Si_3O_{12}$ 14.49–62.42 mol.%
 spessartine $Mn_3Al_2Si_3O_{12}$ 22.96–73.83 mol.%
 almandine $Fe_3Al_2Si_3O_{12}$ 2.87–16.35 mol.%
 grossular $Ca_3Al_2Si_3O_{12}$ 0.24–13.30 mol.%
 goldmanite $Ca_3V_2Si_3O_{12}$ 0.37–4.92 mol.%
 uvarovite $Ca_3Cr_2Si_3O_{12}$ 0.19–2.02 mol.%

The compositions of the differently coloured seven basic groups are given in *Table II* and shown graphically in *Figure 21*. It is evident that there is no clear correlation between the different colours

of the groups and their compositions, nor with low, medium or high spessartine (manganese) contents. However, comparison of the composition of samples with a daylight colour from green, bluish green or greenish blue (Groups 1 to 3) indicates that they tend to have higher goldmanite (vanadium) and uvarovite (chromium) contents than garnets with a daylight colour from yellow to reddish orange (Groups 5 and 6). The few samples with violet, purple and purplish red coloration in daylight (Group 4) have relatively high goldmanite and uvarovite contents, but also contain high amounts of the almandine (iron) molecule. The two samples with red coloration in daylight (Group 7) are the garnets with the smallest vanadium and chromium contents, but have high or extremely high iron (almandine) values.

Colour-change garnets from Madagascar: variation of chemical, spectroscopic and colorimetric properties

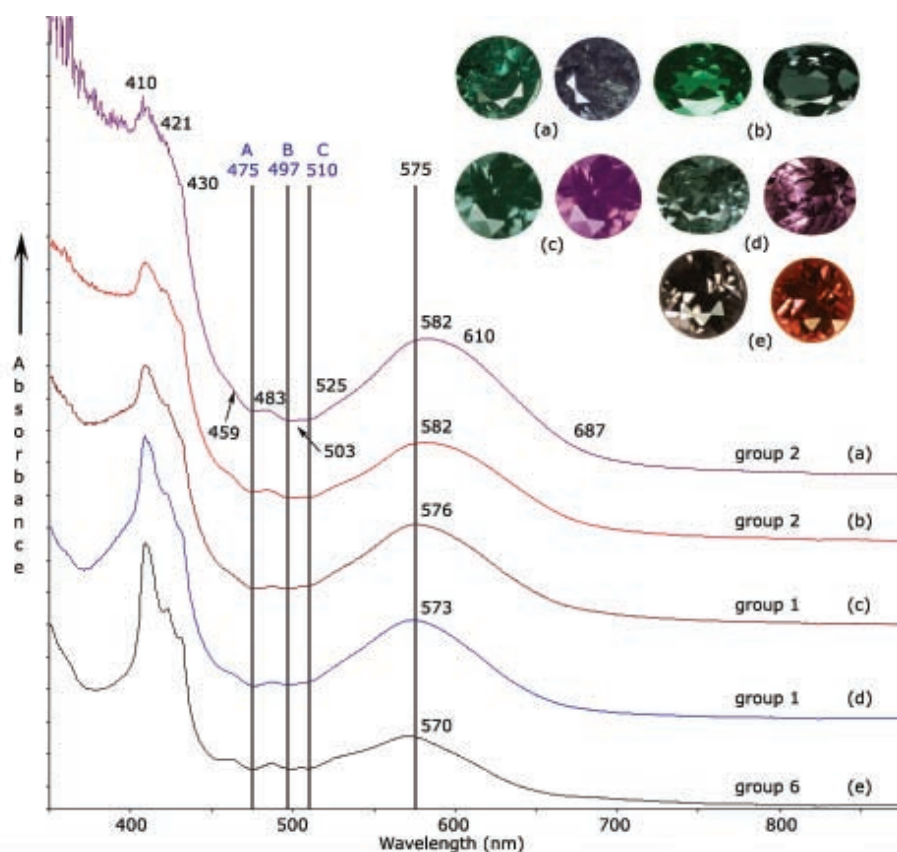


Figure 23: Absorption spectra of vanadium- and chromium-bearing colour-change garnets from Madagascar showing the variation of the position of the dominant vanadium-chromium absorption band in the yellow range of the visible; the daylight colour is shown on the left and incandescent light colour on the right in each pair of images of samples a-e.

Spectroscopic properties

Assignment and positions of absorption maxima

The chemical compositions of the colour-change garnets indicate that we should consider mainly the transition elements vanadium, chromium, iron and manganese for the assignment of peaks in the absorption spectra and in finding the causes of their colour. A general problem with the assignment of absorption bands in garnet spectra is the overlap of several bands with identical or almost identical absorption maxima which have different causes. In previous work by Schmetzer *et al.* (2001) some absorption bands in the spectra of iron-bearing pyrope-spessartine garnets (malaya garnets from Bekily, Madagascar) were assigned to manganese and iron (Table III). Three spectra of this type with varying iron : manganese ratios are shown in Figure 22. For a more

detailed discussion and additional spectra with varying iron : manganese ratios the reader is referred to the paper of Schmetzer *et al.* (2001) and the references cited therein.

The spectra of all the colour-change garnets in this study show the typical iron and manganese bands of malaya garnets with an additional dominant absorption band in the greenish yellow, yellow or yellow orange area of the visible range. In detail, the position of this absorption maximum shifts between 569 and 584 nm (Figure 23).

The positions of iron and manganese absorption bands in pyrope-almandine-spessartine garnets are constant or almost constant, while the vanadium and chromium peak positions in these garnets do vary to a certain degree (Amthauer, 1976; Schmetzer and Ottemann, 1979). In general, both vanadium and chromium show two strong absorption bands in the

yellow and in the blue to near ultraviolet range which are designated $\nu 1$ and $\nu 2$, respectively; their wavelength positions in garnets of various compositions are given in Table IV.

In garnets with strong manganese absorption bands, the position of $\nu 2$ of vanadium and/or chromium cannot be accurately determined because of overlap. However, from the spectra of manganese-free samples, especially synthetic garnets, the positions of both absorption maxima can be estimated. But even then, since the positions of $\nu 1$ and $\nu 2$ of chromium and vanadium lie in the same spectral range, when both elements are present in a garnet, their absorption maxima overlap and cannot be separated satisfactorily.

All the colour-change garnets in this study contain a distinct amount of the almandine end member. Iron has a strong absorption band at about 569 nm which cannot be distinguished from the vanadium and chromium absorption band in this area (Figures 22 and 23). Therefore, the exact peak position and width of this absorption band may be influenced by the iron content of the samples, especially in samples with relatively low vanadium and chromium and high iron contents.

The variation of the absorption maxima of chromium and vanadium in natural garnets with the general composition $X_3Y_2(SiO_4)_3$ is caused by structural expansion (in literature also designated as lattice expansion) due to isomorphic replacement on the X- and Y-sites in the garnet structure. The three main replacements are:

- Starting with pure pyrope in pyrope-almandine-spessartine garnets, structural expansion is caused by replacement of aluminium on Y-sites by various amounts of vanadium and chromium or, to a smaller extent, by replacement of magnesium by various amounts of manganese and iron (as Fe^{2+}) on X-sites.
- In calcium-bearing garnets (grossular, goldmanite, uvarovite, andradite), expansion is caused by an isomorphic replacement of aluminium on Y-sites by vanadium, chromium or iron (as Fe^{3+}).

Colour-change garnets from Madagascar: variation of chemical, spectroscopic and colorimetric properties

Table IV: Wavelengths in nm of vanadium and chromium absorption bands in natural and synthetic garnets.

Vanadium-bearing garnets	$\nu 1$ (V^{3+})	$\nu 2$ (V^{3+})	Ref.	Chromium-bearing garnets	$\nu 1$ (Cr^{3+})	$\nu 2$ (Cr^{3+})	Ref.
				synthetic pyrope	560	408	4
				pyrope	556–574	410–416	3
				Cr-rich pyrope (colour-change)	576	416	3
pyrope-spessartine (colour-change)	568–576		1	pyrope-spessartine (colour-change)	570–575		1
				synthetic knorringite (colour-change)	579	411	4
synthetic pyrope ^a	581	407	2				
Ca-Mg-spessartine	588		1				
grossular	606–610	425–427	1	grossular	606	435	3
Mn-goldmanite	621	446	1				
				uvarovite	615	440	3
goldmanite	625	444	1				
				andradite	621		3

References: 1. Schmetzer and Ottemann (1979); 2. Taran *et al.* (2002); 3. Anthauer (1976);

4. Taran *et al.* (2004).

^a Containing V^{3+} and V^{4+}

- There is also a difference of absorption maxima between vanadium- and/or chromium-bearing pyrope and/or vanadium- or chromium-bearing grossular, which is caused by structural expansion following replacement of magnesium by calcium on X-sites.

As a result of one or more of these replacements, the absorption maxima of vanadium and/or chromium are shifted to higher wavelengths, and the effects may overlap.

Using this generally accepted background for interpreting measurements from our samples, we have to examine the effect of replacement of aluminium by vanadium and chromium and the effect of replacement of magnesium and/or manganese and/or iron by calcium. Any expansion in the structure due to the replacement of magnesium by manganese and/or iron has such a small influence on the position of the absorption maximum that it can be neglected in this discussion.

A graph of the absorption maxima in all the colour-change garnets versus the

sum of their goldmanite and uvarovite contents is shown in *Figure 24* and indicates a positive correlation. The main shift of the absorption maximum from 569–584 nm is correlated with increasing isomorphic replacement of aluminium on Y-sites by vanadium and chromium, but we have to consider also the influence of other chemical components of the garnets, e.g. iron and calcium.

Considering the expansion of the structure caused by replacement of magnesium by calcium, the influence of the calcium content of our samples on the position of the dominant vanadium and chromium absorption maximum cannot be neglected. If the samples are now considered in terms of their calcium contents (represented by the sum of goldmanite + uvarovite + grossular), the line of correlation in *Figure 25* (representing samples with intermediate calcium contents) separates most of the low calcium-bearing samples below from most of the high calcium-bearing samples above. This means

that the contents of magnesium and calcium are influencing the position of the vanadium-chromium maximum. With increasing calcium contents, there is a shift of the vanadium-chromium maximum to higher wavelengths. This is consistent with the peak positions of vanadium- and chromium-bearing garnets as summarized in *Table IV*. Consequently, the replacement of magnesium by calcium is also influencing the colour of the garnets, although magnesium and calcium themselves are not colour-causing elements.

In summary, the absorption maxima in colour-change garnets from Madagascar are assigned to vanadium and chromium on Y-sites and to manganese and iron on X-sites of the garnet structure. A general outline in *Figure 26* shows the wavelengths of maxima (peaks) and minima with the elements that caused them. The exact position of this maximum, however, is also slightly influenced by substitution of magnesium by calcium and by the overlap with an iron absorption band at 569 nm. The second strong absorption band of chromium and vanadium occurs in the range of the strong manganese triplet in the violet and cannot be separated from the three strong manganese bands in this range. Any possible shift of this second vanadium-chromium maximum is masked by the Mn peaks, so it is labelled 'shift?' in the figure.

Position of absorption minima

To discuss the causes of colour and colour change in garnets in this study, the areas of the spectra with high transparency in the visible range must be examined. In the spectra of all samples (see *Figure 23*) there are two areas of high transparency, one in the red to orange and the other in the yellowish green to blue violet. It is clear that transparency in the red to orange range is mainly dependent on the position and intensity of the vanadium-chromium band with a maximum measured between 569 and 584 nm (see above).

In the yellowish green to blue violet

Colour-change garnets from Madagascar: variation of chemical, spectroscopic and colorimetric properties

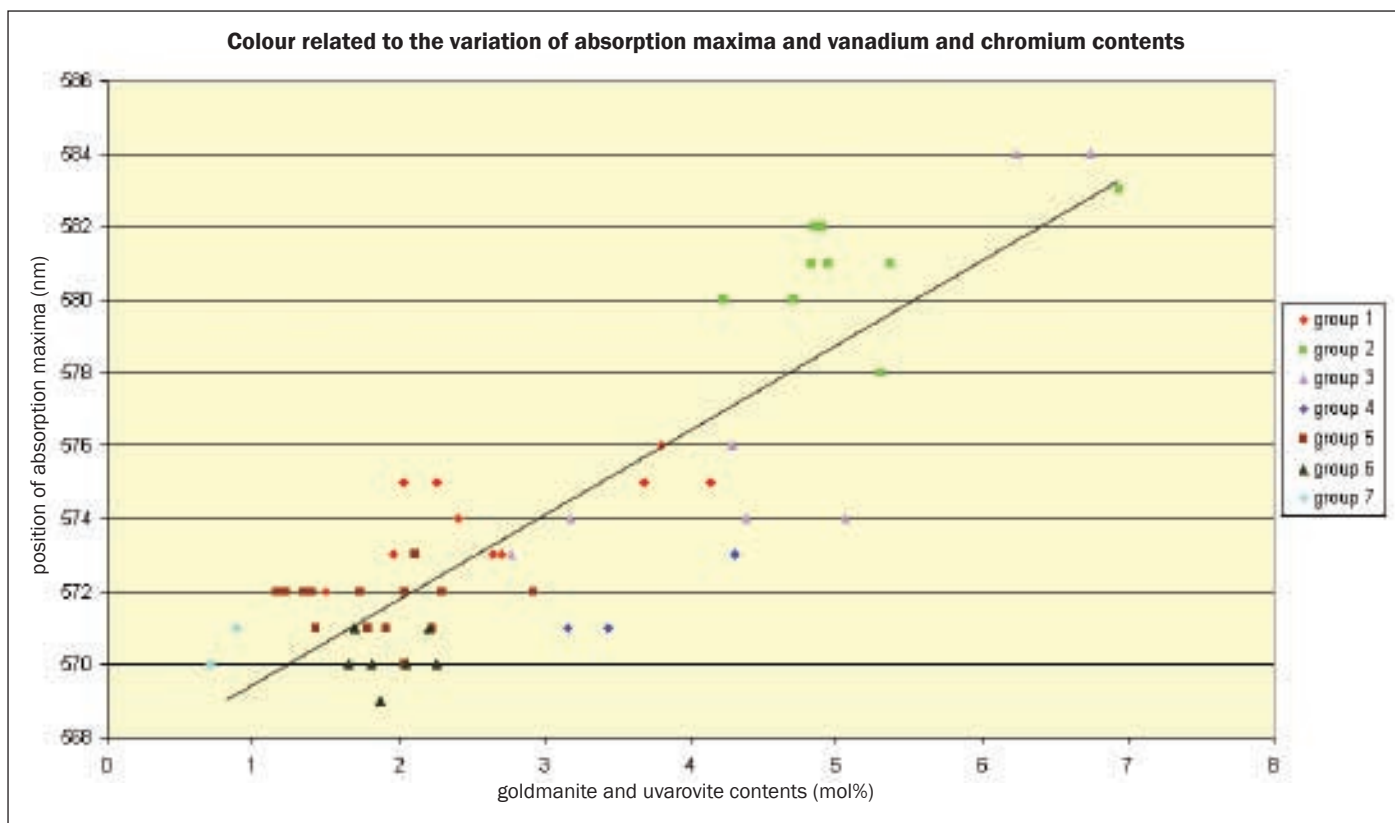


Figure 24: Correlation of the position of the absorption maximum of the vanadium-chromium absorption band in the yellow range of the visible and the vanadium+chromium contents within the seven groups of colour-change garnets.

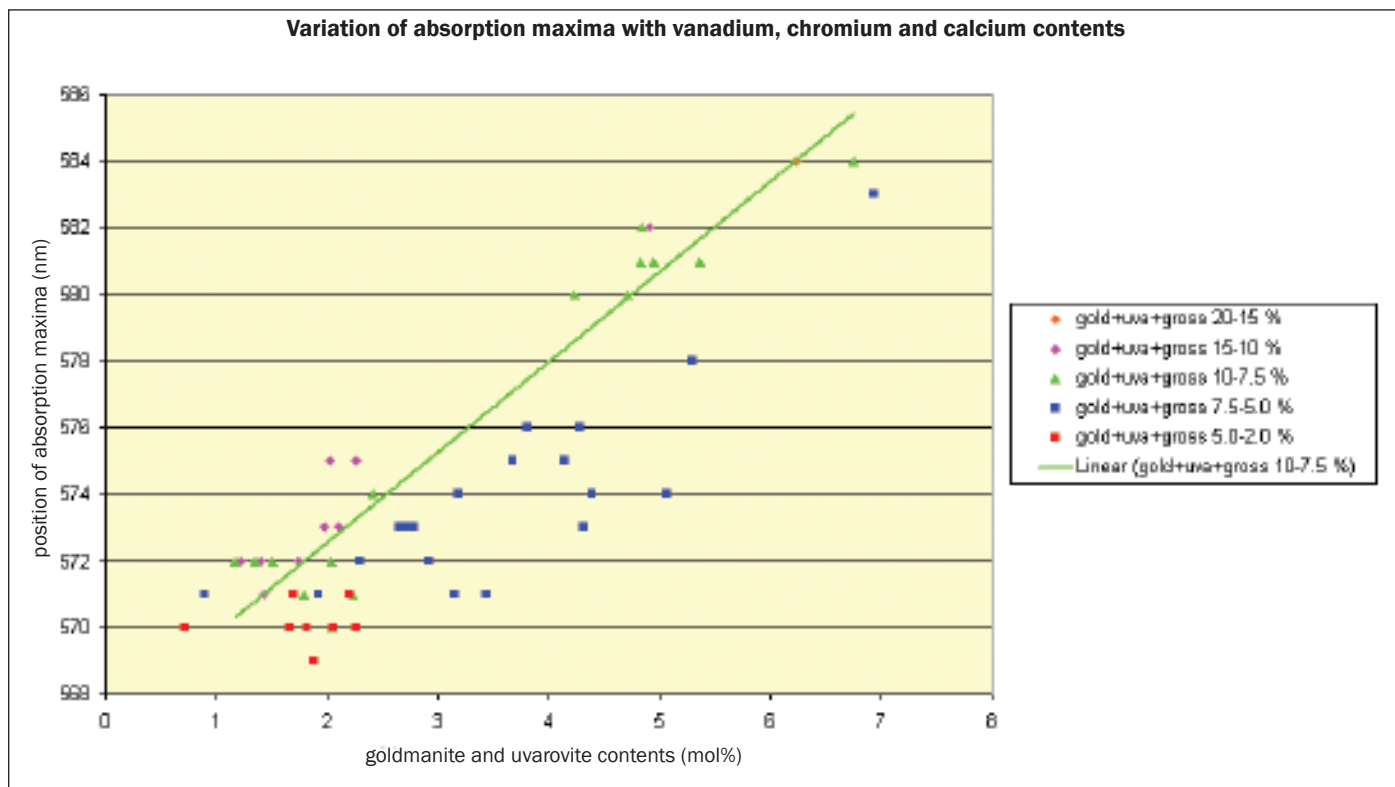


Figure 25: Correlation of the position of the absorption maximum of the vanadium-chromium absorption band in the yellow range of the visible and the vanadium+chromium contents of the garnets, with symbol identification of the different calcium contents (represented by goldmanite+uvarovite+grossular molecular percentages) of the samples.

Colour-change garnets from Madagascar: variation of chemical, spectroscopic and colorimetric properties

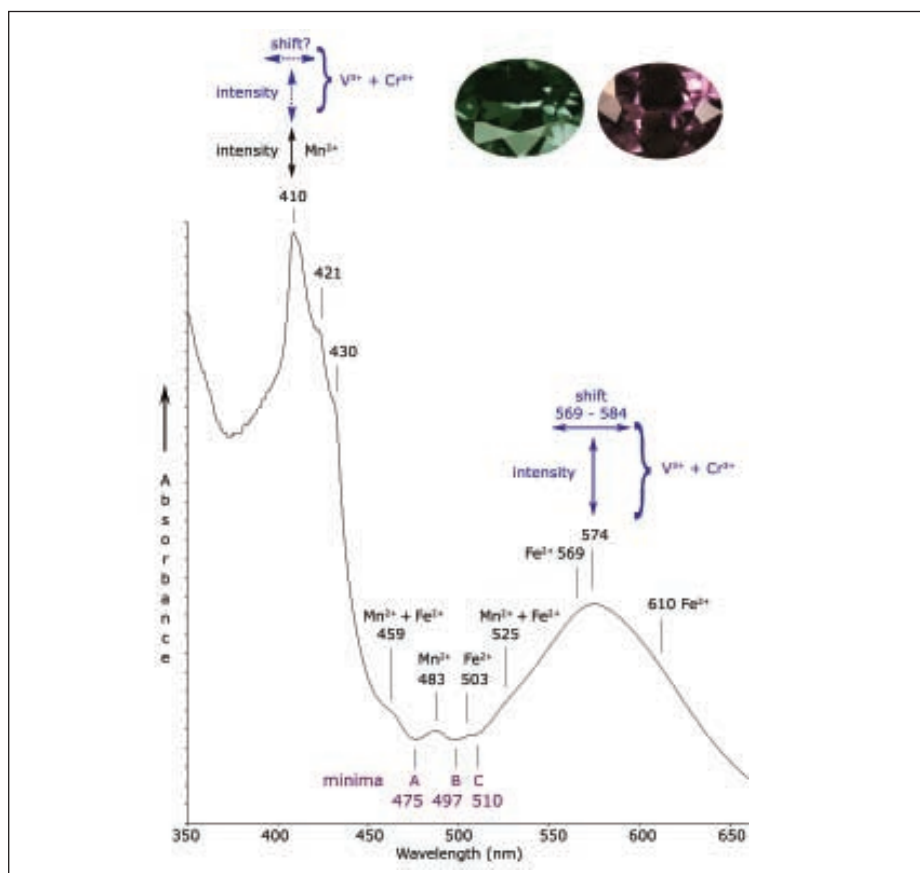


Figure 26: Schematic outline of the different parameters influencing the absorption spectra of vanadium- and chromium-bearing garnets within the pyrope-spessartine-almandine-grossular solid solution series; one such typical garnet is shown in daylight (left) and incandescent light (right), the spectrum of the same sample is also drawn.

range there are four manganese and/or iron absorption bands of low intensity at 525, 503, 483 and 459 nm (see Table III). Between these four absorption bands, three individual minima are located, which are designated as A = 475 nm (blue), B = 497 nm (bluish green), and C = 510 nm (green). The balance between these three minima can be used to estimate the area with highest transmission, i.e. the position of the centre of the absorption minimum. Together, the absorption minimum in the orange to red region, and that in the blue-green determines the colour and colour change of the garnet.

Table V: V, Cr and Mn contents and associated absorption maxima and minima in spectra of colour-change garnets from Madagascar.

Group	Sample	Goldmanite + uvarovite (mol.%)	Almandine (mol.%)	Spessartine (mol.%)	Ratio spessartine : (goldmanite + uvarovite)	Maxima (nm)	Minima*	
Groups with differently coloured garnets						<i>Figure 23</i>		
2	2/7	4.85	6.09	56.39	11.6	582	B>C>>A	(a)
2	2/3	4.23	6.21	54.69	12.9	580	B>C>>A	(b)
1	1/4	3.80	6.64	44.96	11.8	576	A≈B>C	(c)
1	1/6	2.65	3.74	38.82	14.6	573	A≈B>C	(d)
6	6/1	2.26	6.34	52.16	23.1	570	A≈B≈C	(e)
Green to greenish blue groups (1–3) and violet to purplish red group (4)						<i>Figure 27</i>		
3	3/5	6.24	3.21	38.96	6.2	584	B	(a)
2	2/4	5.37	7.90	61.68	11.5	581	B>C>>A	(b)
1	1/8	1.97	3.29	31.77	16.1	573	A≈B>C	(c)
3	3/1	2.78	6.34	33.86	12.2	573	A>B>C	(d)
4	4/1	3.16	7.45	29.24	9.2	571	A>B>C	(e)
Yellow green to orange groups (5–6) and red group (7)						<i>Figure 28</i>		
7	7/2	0.71	10.02	26.24	36.9	570	A>>C	(a)
6	6/7	1.66	7.85	48.75	30.4	570	A≈B≈C	(b)
5	5/4	2.04	4.81	60.78	29.8	570	B≈C>A	(c)
5	5/9	1.35	2.76	30.86	22.9	572	A≈B≈C	(d)
5	5/10	1.74	3.29	30.00	17.2	572	A≈B>C	(e)

* Minima: A = 475 nm blue, B = 497 nm bluish green, C = 510 nm green; A>C means that transmission is higher at the A wavelength, B>C higher at the B wavelength, etc..

Colour-change garnets from Madagascar: variation of chemical, spectroscopic and colorimetric properties

Since the region in the blue-green with the highest transparency is mainly dependent on the position and intensity of the vanadium-chromium absorption and on the intensity of the manganese triplet in the violet at 430, 421 and 410 nm, the ratio spessartine : (goldmanite + uvarovite), calculated from analytical data, could provide a parameter of help in understanding the colour behaviour of these garnets. This parameter is abbreviated s:(g+u) in the following text.

Chemical and spectroscopic parameters of selected samples with characteristic spectra (Figures 23, 27 and 28) are summarized in Table V. The first samples to be considered are those with s:(g+u) ratios smaller than 17 and a colour in daylight varying from green to greenish blue (Groups 1, 2 and 3) or from violet to purplish red (Group 4).

If we start with a sample of Group 1 (a group which shows the strongest change in hue angle between daylight and incandescent light and a colour change from green to purple, reddish purple or red purple), in Figure 27c it is apparent that there is almost equal transparency at minimum A (blue) and B (bluish green) and a somewhat weaker transparency at minimum C (green). The parameter s:(g+u) of this garnet is 16.1. For samples with smaller s:(g+u) parameters, there are two situations:

- The absorption maximum lies at wavelengths above 576 nm and although the relative intensity of the vanadium-chromium absorption band is high, the highest transparency occurs at minimum B (bluish green) with high transparency also at minimum C (green) (Figure 27 a,b).
- The absorption maximum is at 576 nm or lower wavelengths, and the highest transparency is at minimum A (blue) (Figure 27 d,e).

The second collection of samples (Groups 5, 6 and 7) to be considered consists of those with s:(g+u) ratios larger than 17 and a colour in daylight between yellow and red. All these garnets have absorption maxima at 572 nm or below. A garnet sample with a s:(g+u) ratio slightly above 17 has a spectrum with almost

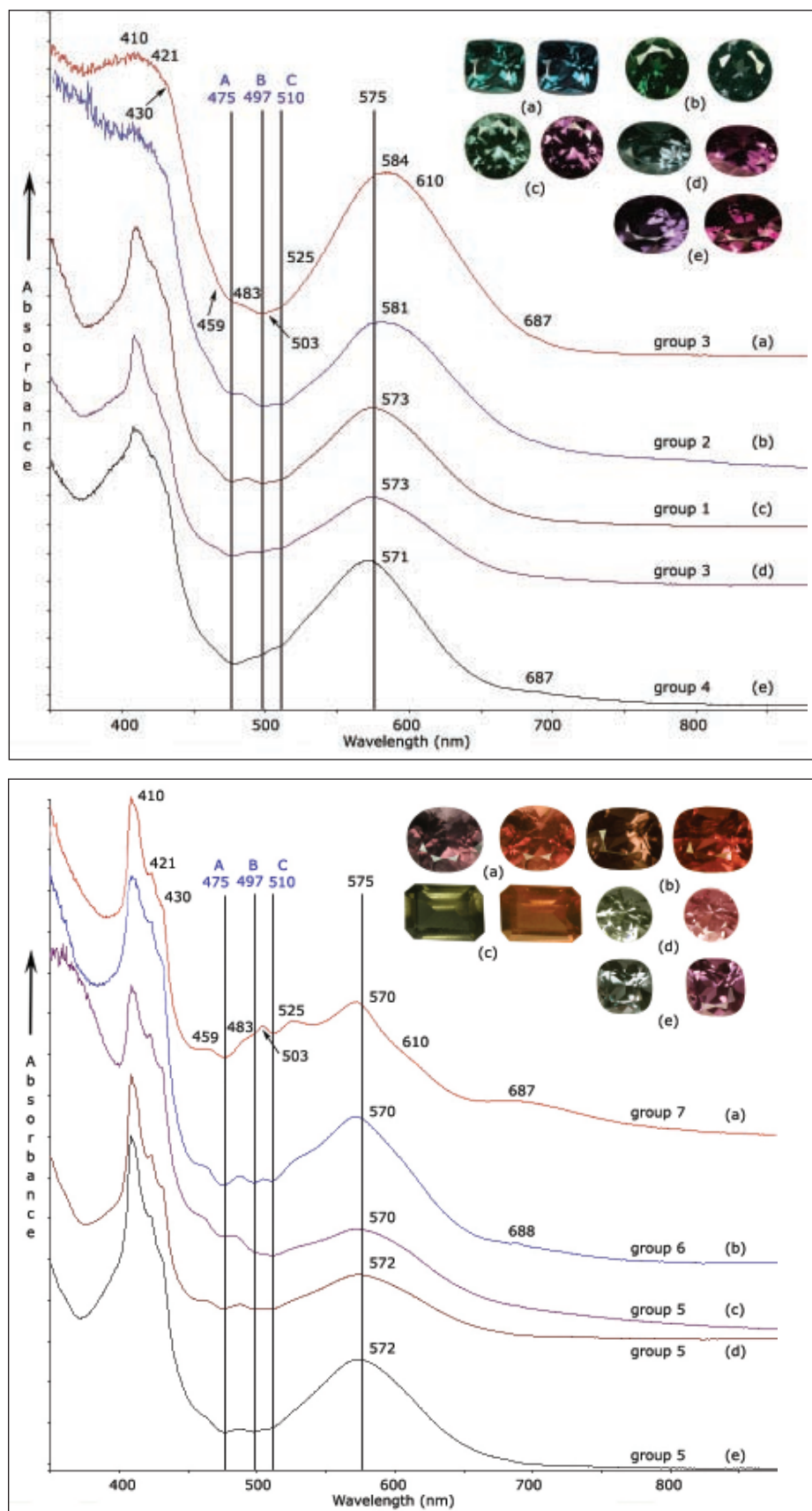


Figure 27 (top) and 28: Absorption spectra of vanadium- and chromium-bearing colour-change garnets from Madagascar showing the variation of the position of absorption maxima of the dominant vanadium-chromium absorption band in the yellow region and the variation of the position of absorption minima in the blue to green region; each sample pair is shown in daylight (left) and incandescent light (right).

Colour-change garnets from Madagascar: variation of chemical, spectroscopic and colorimetric properties

Table VIa. Physical, chemical and colorimetric data of individual colour-change garnets from Madagascar

Group	1			2			3				
	1/2	1/8	1/10	2/1	2/6	2/9	3/3	3/4	3/5	3/6	3/7
Colour in daylight	green	slightly yellowish green	greenish yellowish grey	green	green	green	bluish green	bluish green	bluish green	bluish green	greenish blue
Colour in incandescent light	red purple	red purple	reddish purple	red purple	greenish yellowish grey	greyish bluish green	violet purple	blue violet	blue green	blue violet	violet purple
Microprobe analyses (wt.%) ^a											
SiO ₂	39.46	40.61	41.32	37.28	37.90	37.45	39.97	37.87	39.08	39.51	38.87
TiO ₂	0.06	0.07	0.03	0.14	0.08	0.10	0.03	0.05	0.07	0.05	0.05
Al ₂ O ₃	27.07	22.47	23.06	20.20	21.08	20.69	22.71	21.83	20.57	21.05	21.16
V ₂ O ₃	1.08	0.47	0.39	1.57	1.42	1.46	0.94	1.24	1.65	1.61	1.12
Cr ₂ O ₃	0.16	0.19	0.15	0.65	0.11	0.12	0.15	0.19	0.36	0.62	0.52
FeO ^b	3.45	1.62	1.44	4.79	2.89	3.48	2.98	2.56	1.49	1.84	4.45
MnO	19.22	15.39	12.31	26.74	24.98	27.58	16.06	18.60	17.85	19.41	19.04
MgO	12.17	14.31	17.49	5.69	8.06	5.70	15.04	13.05	9.98	12.55	11.63
CaO	2.34	4.94	3.81	2.54	2.72	2.70	2.06	2.61	7.08	2.92	2.68
Total	100.02	100.06	99.99	99.60	99.23	99.28	99.95	100.01	98.12	99.58	99.52
Cations ^c											
Si	2.972	2.992	2.990	2.963	2.963	2.973	2.958	2.985	3.008	2.985	2.966
Ti	0.004	0.004	0.002	0.008	0.005	0.006	0.002	0.003	0.004	0.003	0.003
Al	1.960	1.951	1.966	1.892	1.942	1.936	1.981	1.926	1.866	1.875	1.903
V	0.065	0.028	0.022	0.100	0.089	0.093	0.056	0.075	0.102	0.098	0.069
Cr	0.010	0.011	0.008	0.041	0.007	0.008	0.009	0.011	0.022	0.037	0.031
Fe	0.217	0.100	0.087	0.318	0.189	0.231	0.185	0.160	0.096	0.117	0.284
Mn	1.226	0.960	0.754	1.800	1.654	1.854	1.007	1.180	1.164	1.243	1.231
Mg	1.366	1.573	1.886	0.674	0.939	0.675	1.659	1.457	1.144	1.414	1.324
Ca	0.189	0.390	0.295	0.216	0.228	0.229	0.163	0.209	0.584	0.237	0.219
Mol.% end members											
Goldmanite	3.19	1.41	1.10	4.92	4.37	4.56	2.74	3.73	5.13	4.89	3.48
Uvarovite	0.49	0.56	0.40	2.02	0.34	0.39	0.44	0.56	1.11	1.86	1.59
Almandine	7.24	3.29	2.87	10.57	6.28	7.73	6.14	5.32	3.21	3.87	9.29
Spessartine	40.89	31.77	24.95	59.84	54.95	62.03	33.41	39.25	38.96	41.29	40.26
Pyrope	45.56	52.03	62.42	22.41	31.20	22.58	55.04	48.47	38.29	46.98	43.29

Colour-change garnets from Madagascar: variation of chemical, spectroscopic and colorimetric properties

Grossular	2.63	10.94	8.21	0.24	2.86	2.71	2.23	2.67	13.30	1.11	2.09
Spessartine : (goldmanite + uvarovite)	11.1	16.1	16.6	8.6	11.7	12.5	10.5	9.1	6.2	6.1	7.9
Absorption maximum (nm)	575	573	572	583	581	581	574	576	584	584	574
Colorimetric data CIE 1931 ^d											
λ_b (nm) for daylight D ₆₅	541	552	550	538	538	517	494	493	500	491	484
Purity p for daylight D ₆₅	3.0	5.0	1.0	9.4	7.7	11.4	2.1	11.1	16.8	17.1	10.3
λ_b (nm) for incandescent light A	c514	c509	c520	c507	567	504	c557	c575	495	437	c558
Purity p for incandescent light A	3.8	6.5	5.0	6.1	2.5	2.2	5.2	6.8	8.8	7.1	21.3
Colorimetric data CIELAB 1976 ^e											
C* _{ab} for daylight D ₆₅	4.99	6.62	1.52	11.60	12.61	17.9	2.50	10.44	21.57	13.59	4.57
h_{ab} (°) for daylight D ₆₅	149.0	141.5	143.9	150.0	150.3	159.4	189.0	190.9	174.4	199.0	238.5
C* _{ab} for incandescent light A	3.39	6.14	5.32	4.13	1.59	2.31	5.41	9.10	9.38	12.34	14.30
h_{ab} (°) for incandescent light A	349.6	357.3	342.4	4.3	128.5	193.9	321.4	291.6	223..3	279.7	322.1
Δh_{ab} (°)	159.4	144.3	161.6	145.7	21.8	34.5	132.4	100.7	48.9	80.8	83.6
ΔE^*_{ab}	8.3	12.1	6.8	15.2	11.2	16.1	7.3	15.1	17.1	16.9	14.5

^a Average composition of 10 analyses each

^b Total iron as FeO

^c Calculated on the basis of 12 oxygens

^d λ_b = dominant wavelength, c indicates 'complement of

^e C*_{ab} = chroma; h_{ab} = hue angle

Δh_{ab} = hue angle difference between daylight and incandescent light

ΔE^*_{ab} = colour difference between daylight and incandescent light in the three dimensional CIELAB colour space

Colour-change garnets from Madagascar: variation of chemical, spectroscopic and colorimetric properties

Table 17b: Physical, chemical and colorimetric data of individual colour-change garnets from Madagascar

Group	4			5			6			7	
	4/1	4/2	4/3	5/6	5/9	5/10	5/11	5/13	6/1		6/7
Sample	purple	violet	purplish red	yellow	greenish yellow	yellow green	yellow	yellowish grey	yellow orange	orange	red
Colour in daylight	reddish purple	reddish purple	red purple	red orange	red	red purple	red	red purple	red	red	red
Colour in incandescent light	reddish purple	reddish purple	red purple	red orange	red	red purple	red	red purple	red	red	red
Microprobe analyses (wt.%) ^a											
SiO ₂	40.83	39.67	39.06	37.58	40.81	40.70	38.00	40.89	38.32	39.55	40.50
TiO ₂	0.07	0.08	0.06	0.16	0.06	0.05	0.05	0.01	0.03	0.03	0.05
Al ₂ O ₃	22.91	21.73	21.94	21.03	22.99	22.89	21.62	22.79	21.86	22.51	23.19
V ₂ O ₃	0.56	0.89	0.80	0.69	0.35	0.40	0.40	0.35	0.33	0.35	0.13
Cr ₂ O ₃	0.53	0.54	0.30	0.24	0.11	0.20	0.22	0.13	0.22	0.21	0.12
FeO ^b	3.69	4.14	7.11	2.35	1.36	1.62	2.88	1.69	2.95	3.71	4.90
MnO	14.27	17.36	15.99	28.65	14.98	14.51	23.69	13.22	24.37	22.77	12.66
MgO	16.10	12.97	11.74	6.46	15.61	15.06	9.93	16.04	9.79	10.50	16.25
CaO	2.02	2.48	2.55	2.11	3.75	4.57	1.56	4.49	1.59	1.42	1.70
Total	100.98	99.86	99.60	99.27	100.02	100.01	98.36	99.61	99.46	101.05	99.50
Cations ^c											
Si	2.972	2.980	2.966	2.971	2.986	2.985	2.961	2.992	2.956	2.982	2.977
Ti	0.004	0.005	0.004	0.009	0.003	0.003	0.003	0.001	0.005	0.002	0.003
Al	1.965	1.924	1.963	1.959	1.982	1.979	1.985	1.966	1.976	2.000	2.016
V	0.033	0.054	0.049	0.044	0.021	0.023	0.025	0.020	0.030	0.021	0.008
Cr	0.031	0.032	0.021	0.015	0.006	0.012	0.014	0.008	0.015	0.012	0.007
Fe	0.224	0.260	0.451	0.155	0.083	0.099	0.188	0.103	0.190	0.234	0.301
Mn	0.879	1.105	1.028	1.918	0.928	0.902	1.564	0.819	1.590	1.454	0.788
Mg	1.746	1.452	1.329	0.761	1.702	1.647	1.154	1.750	1.129	1.180	1.781
Ca	0.157	0.199	0.208	0.179	0.294	0.359	0.130	0.352	0.139	0.115	0.134

Colour-change garnets from Madagascar: variation of chemical, spectroscopic and colorimetric properties

Mol.% end members													
Goldmanite	1.63	2.70	2.41	2.18	1.05	1.14	1.24	1.02	1.50	1.05	0.37		
Uvarovite	1.53	1.61	1.03	0.74	0.30	0.60	0.68	0.38	0.76	0.61	0.34		
Almandine	7.45	8.63	14.95	5.14	2.76	3.29	5.15	3.42	6.24	7.85	10.02		
Spessartine	29.24	36.62	34.08	63.66	30.86	30.00	51.51	27.09	52.16	48.75	26.24		
Pyrope	58.08	48.15	44.06	25.26	56.60	54.77	38.02	57.86	37.04	39.54	59.27		
Grossular	2.06	2.29	3.47	3.02	8.43	10.20	3.40	10.23	2.30	2.20	3.76		
Spessartine : (goldmanite + uvarovite)	9.2	8.5	9.9	21.8	22.9	17.2	26.8	19.3	23.1	30.4	36.9		
Absorption maximum (nm)	571	573	571	572	572	572	571	572	570	570	570		
Colorimetric data CIE 1931 ^d													
λ_b (nm) for daylight D ₆₅	c550	c563	635	576	568	567	576	572	581	587	598		
Purity p for daylight D ₆₅	7.1	5.8	4.5	30.0	6.0	5.0	9.0	2.2	9.0	14.4	12.5		
λ_b (nm) for incandescent light A	c531	c530	c510	595	608	c506	616	c509	625	621	619		
Purity p for incandescent light A	20.0	27.9	22.1	34.9	5.8	6.4	11.4	4.8	11.4	19.7	19.3		
Colorimetric data CIE LAB 1976e													
C* _{ab} for daylight D ₆₅	6.83	3.41	5.01	13.80	5.00	3.96	6.21	1.49	5.70	7.99	9.37		
h_{ab} (°) for daylight D ₆₅	323.5	307.9	14.2	90.5	115.3	119.1	88.6	102.4	69.4	51.6	30.7		
C* _{ab} for incandescent light A	17.98	15.27	16.07	15.34	4.83	6.16	9.76	4.54	10.42	13.95	13.59		
h_{ab} (°) for incandescent light A	336.5	337.3	355.8	49.9	27.9	5.9	23.6	358.7	20.5	22.8	23.2		
Δh_{ab} (°)	13.0	29.4	18.4	40.5	87.5	113.3	65.1	103.8	48.9	28.8	7.6		
ΔE^*_{ab}	11.4	12.4	11.4	10.2	6.8	8.5	9.1	5.1	7.9	8.0	4.6		

^a Average composition of 10 analyses each

^b Total iron as FeO

^c Calculated on the basis of 12 oxygens

^d λ_b = dominant wavelength, c indicates 'complement of'

^e C*_{ab} = chroma; h_{ab} = hue angle

Δh_{ab} = hue angle difference between daylight and incandescent light

ΔE^*_{ab} = colour difference between daylight and incandescent light in the three dimensional CIE LAB colour space

Colour-change garnets from Madagascar: variation of chemical, spectroscopic and colorimetric properties

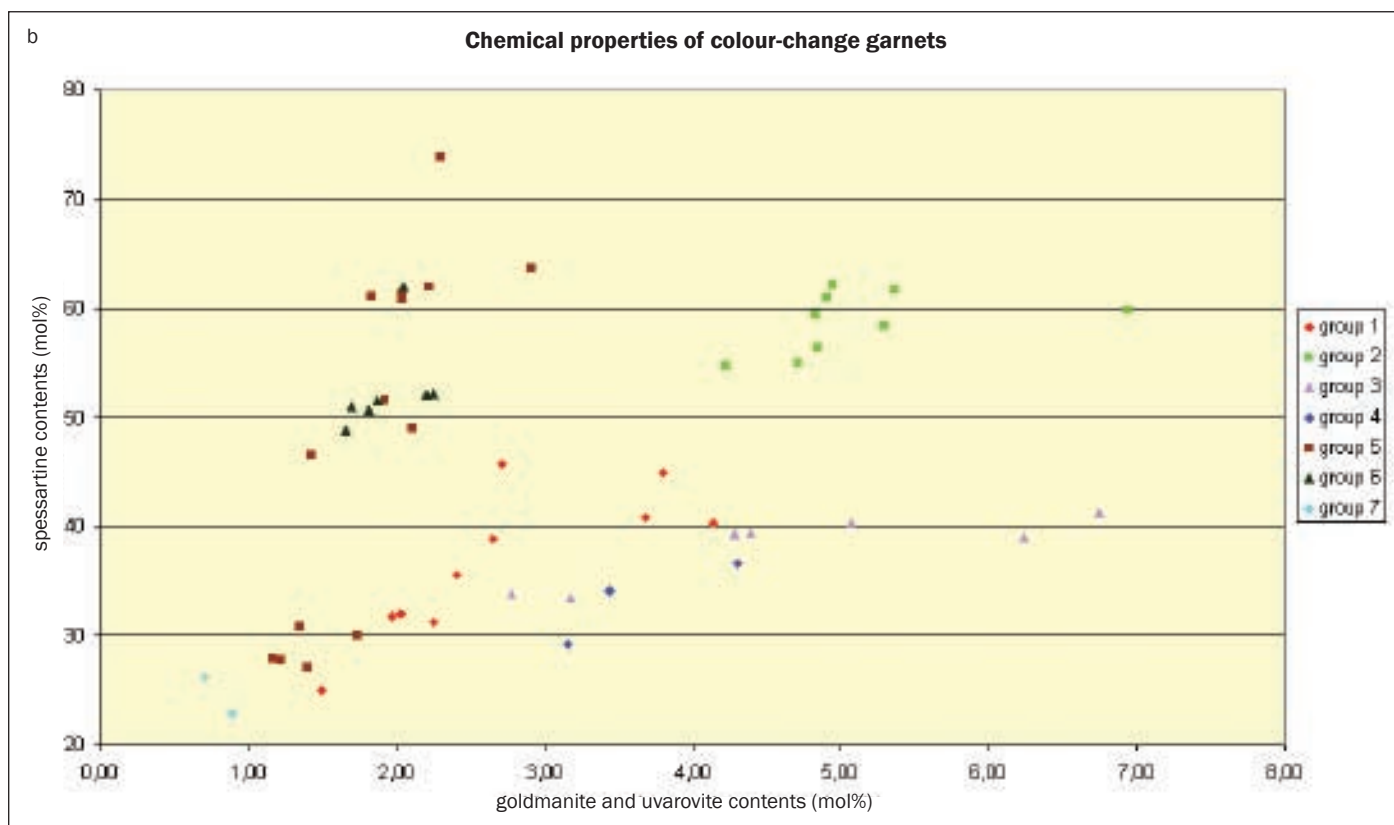
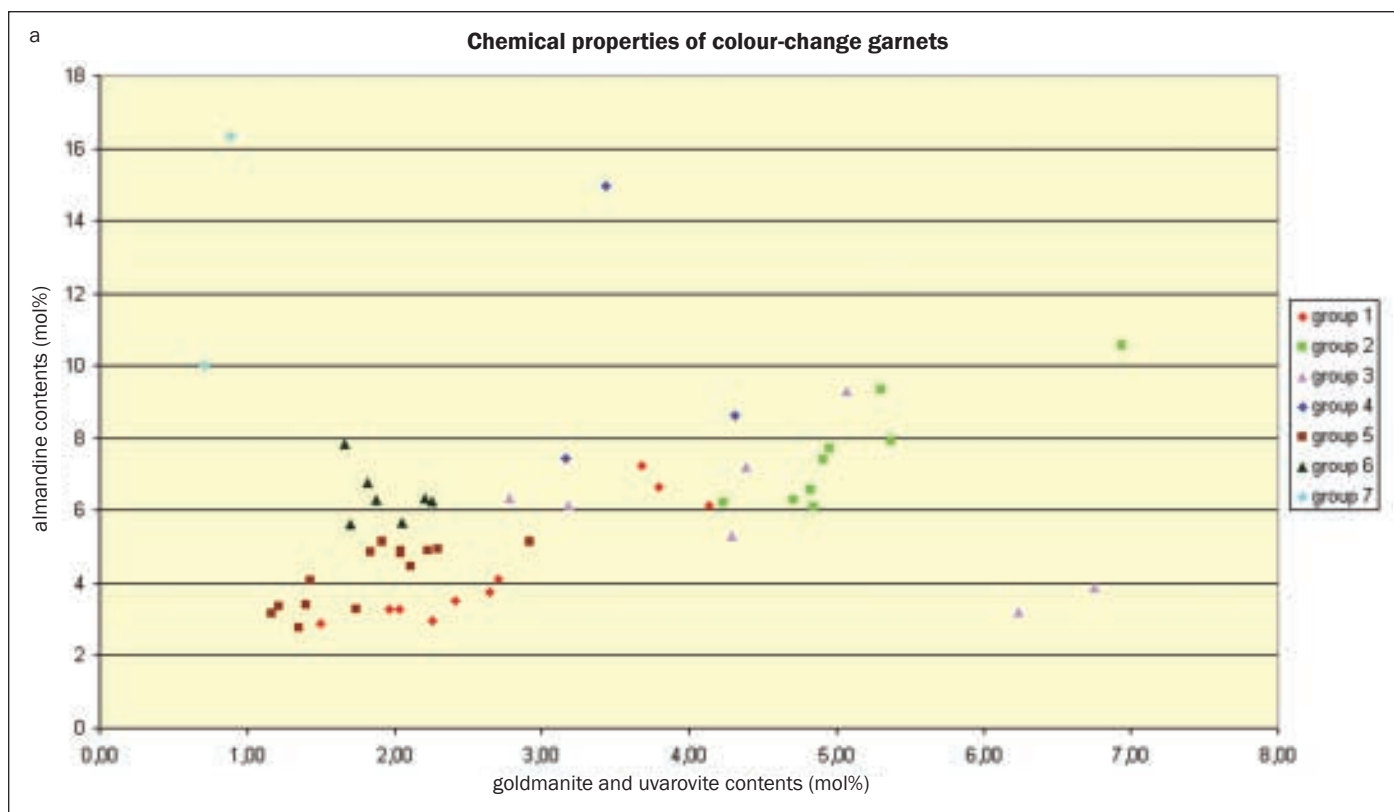


Figure 29: Compositional range of garnet; (a) range of goldmanite (vanadium) and uvarovite (chromium) contents versus almandine (iron) contents; (b) range of goldmanite (vanadium) and uvarovite (chromium) contents versus spessartine (manganese) contents in colour-change garnets from Madagascar.

Colour-change garnets from Madagascar: variation of chemical, spectroscopic and colorimetric properties

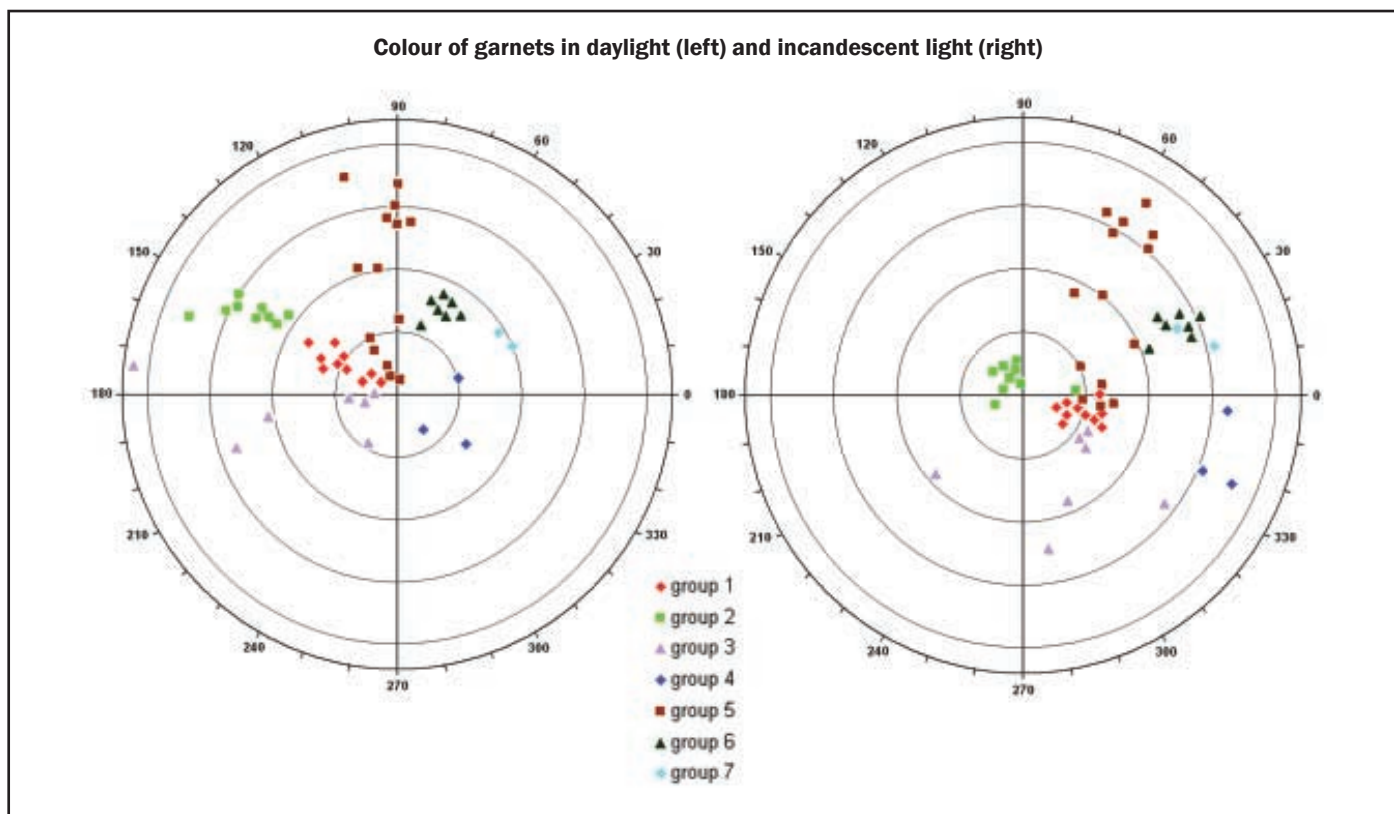


Figure 30: Colorimetric parameters of seven groups of colour-change garnets in the CIELAB colour circle showing the ranges of hue angle h_{ab} and chroma C_{ab}^* in daylight (left) and incandescent light. The hue angles can be read around the outer circles; chroma is represented by the radial distance of a colour locus from the centre of the coordinate system, the circles represent chroma differences of 5, with the outer circle at chroma 22.

equal transparency at minimum A and minimum B and a weaker transparency at minimum C (a 'balanced' spectrum; Figure 28e). With decreasing vanadium and chromium contents, i.e. with increasing s:(g+u) ratios, spectra with almost equal transparencies at minima A (blue), B (bluish green) and C (green) are present (Figure 28d). For garnets with even higher s:(g+u) ratios, there are three situations:

- For samples with relatively low iron contents, the transparency at minima B (bluish green) and C (green) is almost equal, and higher than at A (blue) (Figure 28c).
- For samples with moderate iron contents, the transparencies at A, B and C are comparable (Figure 28b).
- For samples with high iron contents, the influence of the vanadium-chromium band on the transparencies at minima A, B and C is negligible and the spectrum is dominated by the known iron and manganese bands (Figure 28a).

Description of garnet groups and individual samples

Chemical, spectroscopic and colorimetric data of all seven groups are summarized in Table II, the properties of individual samples are given in Tables VIa and VIb. The goldmanite, uvarovite, spessartine and almandine contents are plotted in Figure 29, and colorimetric data for the CIELAB 1976 colour space (hue angle h_{ab} and chroma C_{ab}^*) are pictured in Figure 30. In the following text the term 'daylight' refers to standard illumination D_{65} , and the term 'incandescent light' refers to standard illumination A. The main colour-causing components will be abbreviated as follows:

- gold = goldmanite (indicating the vanadium contents)
- uva = uvarovite (indicating the chromium contents)
- spess = spessartine (indicating the manganese contents)
- alm = almandine (indicating the iron contents)

Group 1

- These ten garnets form the most homogeneous group (Figure 31 a-d). Nine are green to slightly yellowish green in daylight and purple, reddish purple or red purple in incandescent light. One sample (1/10) is greenish yellowish grey in daylight with a colour change to reddish purple in incandescent light. Their chemical properties show a wide variation for (gold + uva) from 1.50 to 4.41 %, for spess from 24.95 to 45.73 % and for alm from 2.87 to 7.24 %. Sample 1/10 had the lowest (gold + uva) content of 1.50 %.

Group 2

- Within this group are samples with higher vanadium and chromium (gold + uva from 4.23 to 6.09 %) and higher manganese contents (spess from 54.69 to 62.03 %). The iron contents vary between alm 6.09 and alm 10.57 %. All nine samples are green to slightly

Colour-change garnets from Madagascar: variation of chemical, spectroscopic and colorimetric properties

Group 1 colour-change garnets

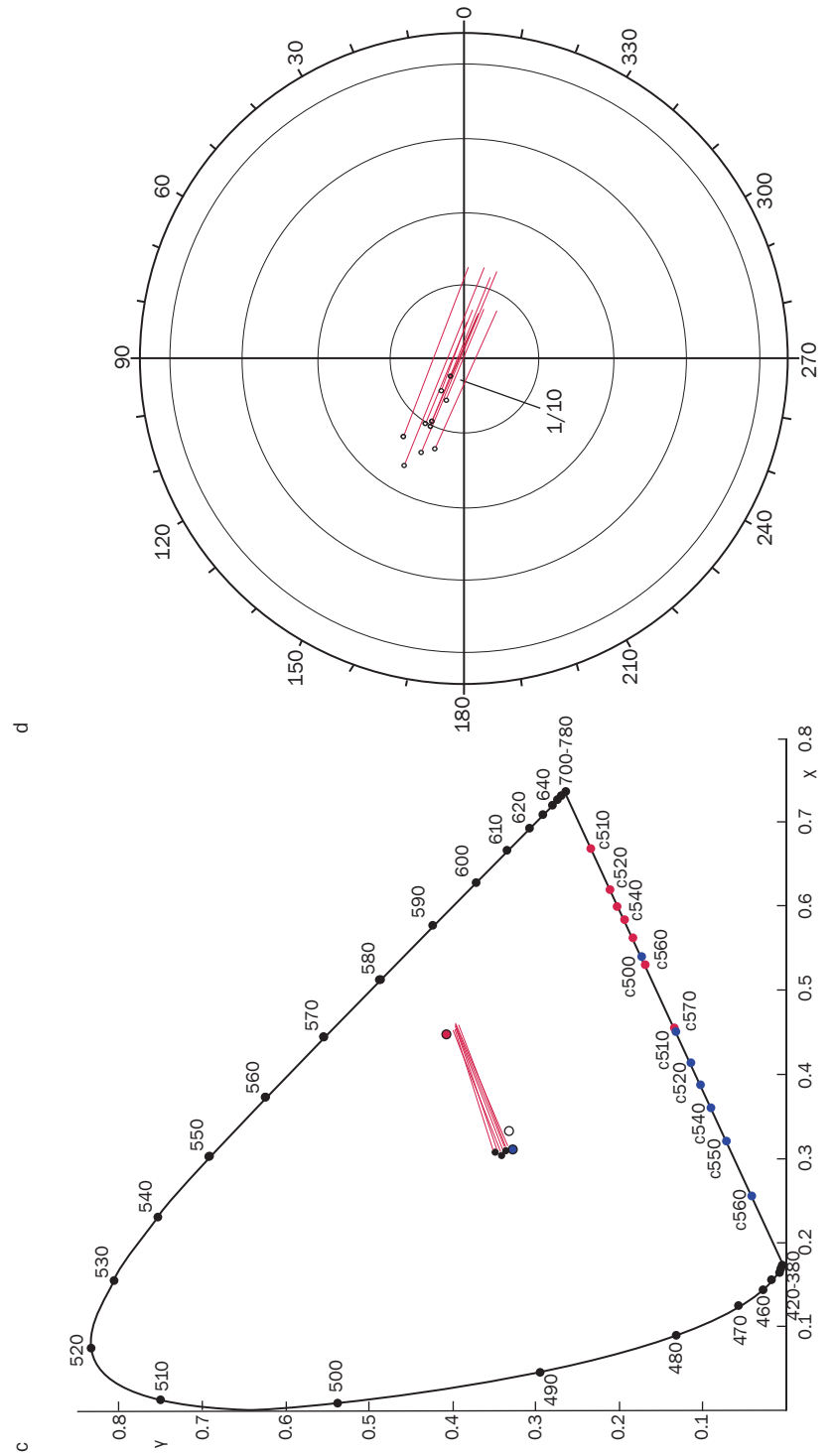


Figure 31: Colour-change garnets of Group 1 in daylight (a) and incandescent light (b); diameter of the sample on the right 7.4 mm, weight 1.78 ct; the garnet at the left (sample 1/10) had the lowest contents of chromium and vanadium. Colorimetric parameters in the CIE 1931 chromaticity diagram (c); the blue circle represents the position of daylight D_{65} , the red circle, that of tungsten light A, and the open circle is the neutral point (white point); the small black circles represent the coordinates for the garnets in daylight D_{65} and the ends of the differently coloured bars represent their coordinates for tungsten light A. Colorimetric parameters in the CIELAB 1976 colour circle (d); the neutral point (white point) is in the centre of the a^*b^* coordinate system; the small black circles represent the coordinates for the garnets in daylight D_{65} and the ends of the differently coloured bars represent their coordinates for tungsten light A; the circles represent chroma differences of 5, with the outer circle at chroma 22. The colour change from daylight to incandescent light is evident.

Colour-change garnets from Madagascar: variation of chemical, spectroscopic and colorimetric properties

Group 2 colour-change garnets

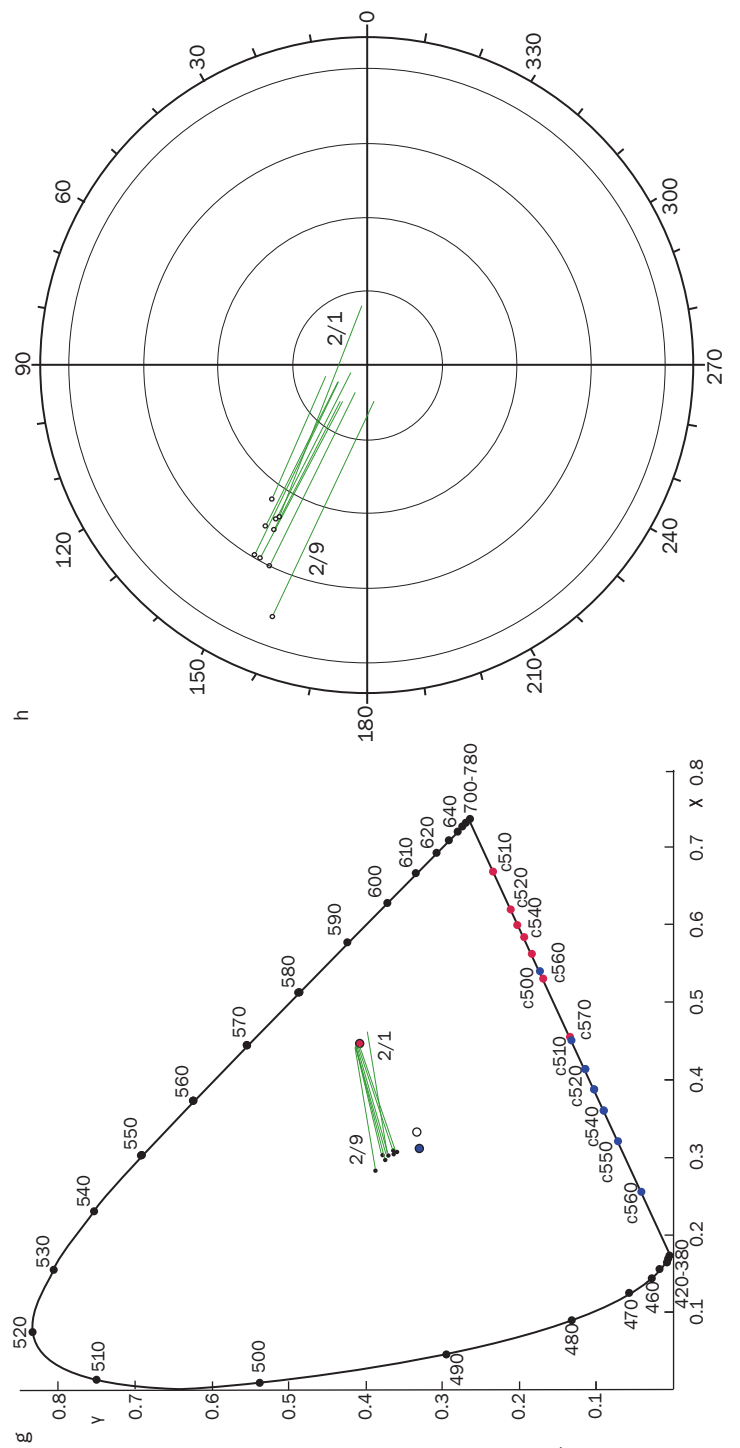


Figure 32: Colour-change garnets of Group 2 in daylight (a,c,e) and incandescent light (b,d,f); most are green in daylight and grey in incandescent light (a,b), diameter of the sample at the upper right 4.6 mm, weight 0.47 ct.; sample 2/1 changes from green to red purple (c,d; size 5.1 x 6.4 mm) and sample 2/9 (e,f; size 6.0 x 8.3 mm) varies from green to greyish bluish green. Colorimetric parameters are shown in the CIE 1931 chromaticity diagram (g), with notation as in Figure 31. Colorimetric parameters in the CIELAB 1976 colour circle are shown in (h), with notation as in Figure 31.

Colour-change garnets from Madagascar: variation of chemical, spectroscopic and colorimetric properties

Group 3 colour-change garnets

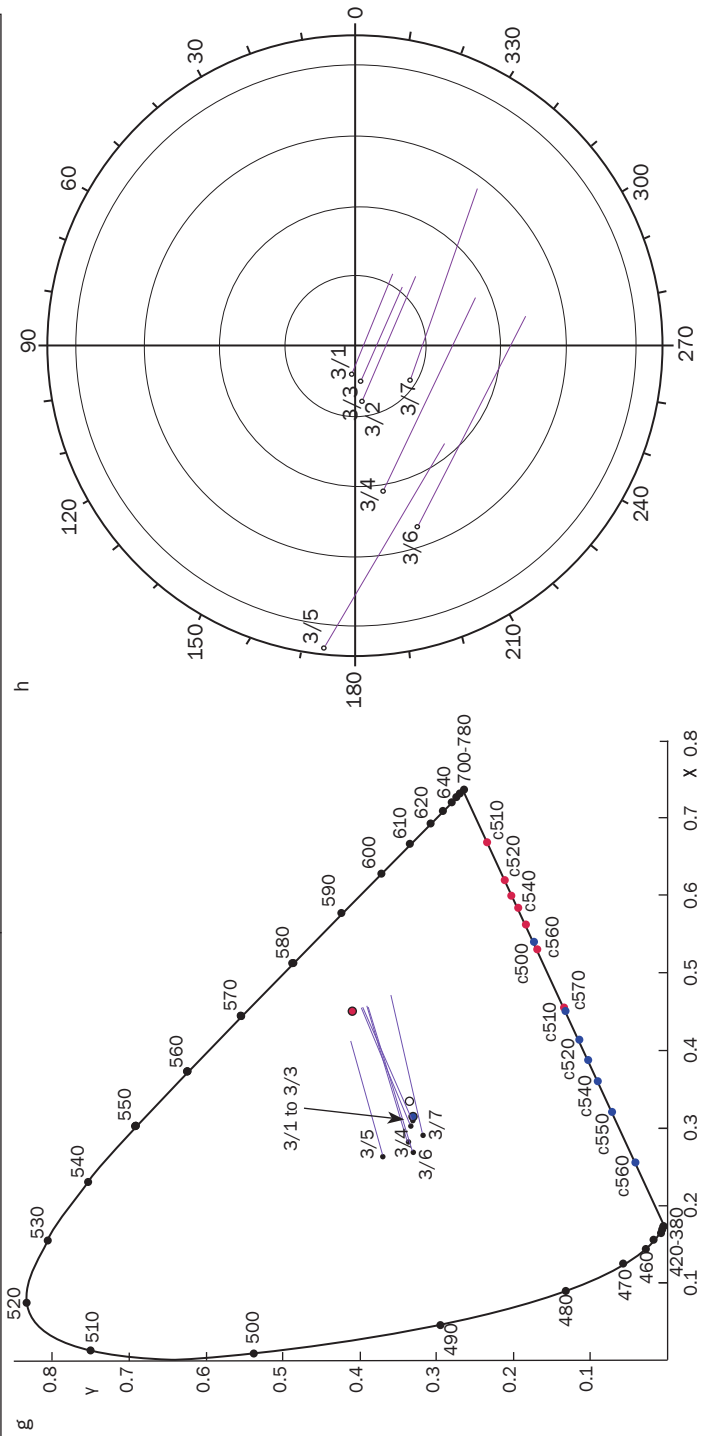
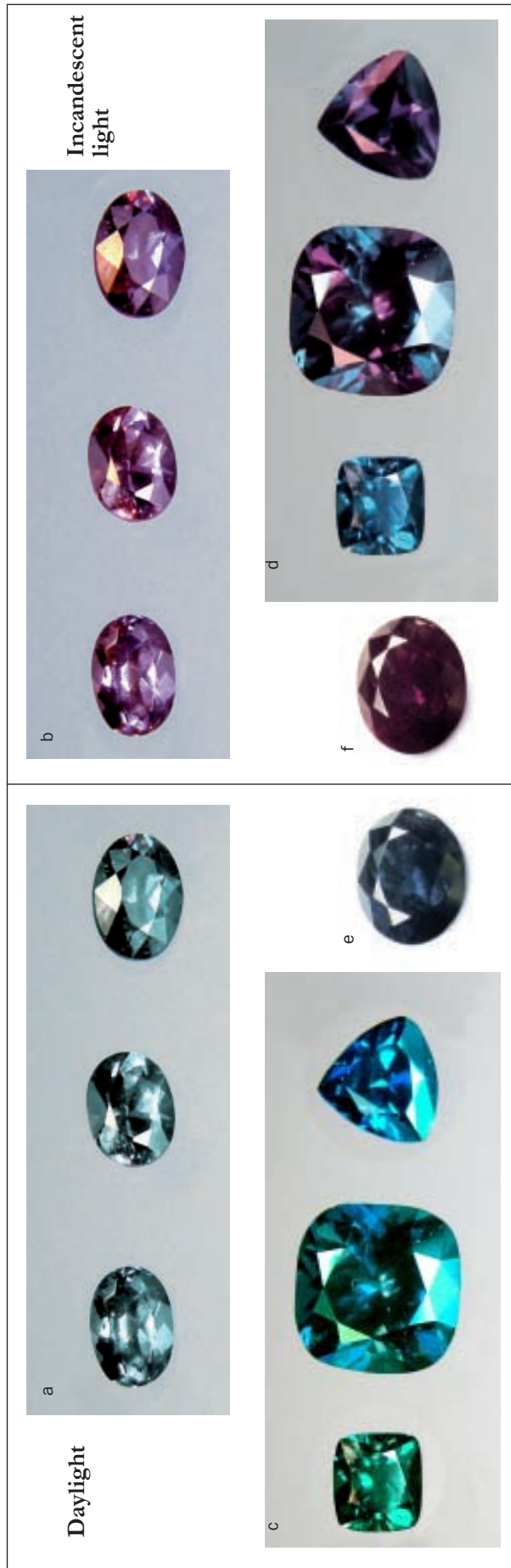


Figure 33: Colour-change garnets of Group 3 in daylight (a,c,e) and incandescent light (b,d,f); samples 3/1 to 3/3 (a,b) are bluish green in daylight and violet purple in incandescent light, size of the right sample 3.8 x 5.4 mm, weight 0.49 ct.; samples 3/5 (left), 3/4 (centre) and 3/6 (right, 5.5 x 5.8 mm, weight 0.59 ct) are bluish green in daylight but variable in incandescent light (c,d); sample 3/7 (e,f, 6.6 x 8.1 mm) is the only garnet which is greenish blue in daylight. Colorimetric parameters are shown in the CIE 1931 chromaticity diagram (g) with notation as in Figure 31. Colorimetric parameters in the CIELAB 1976 colour circle are shown in (h), with notation as in Figure 31. The colour change from daylight to incandescent light is evident.

Colour-change garnets from Madagascar: variation of chemical, spectroscopic and colorimetric properties

Group 4 colour-change garnets

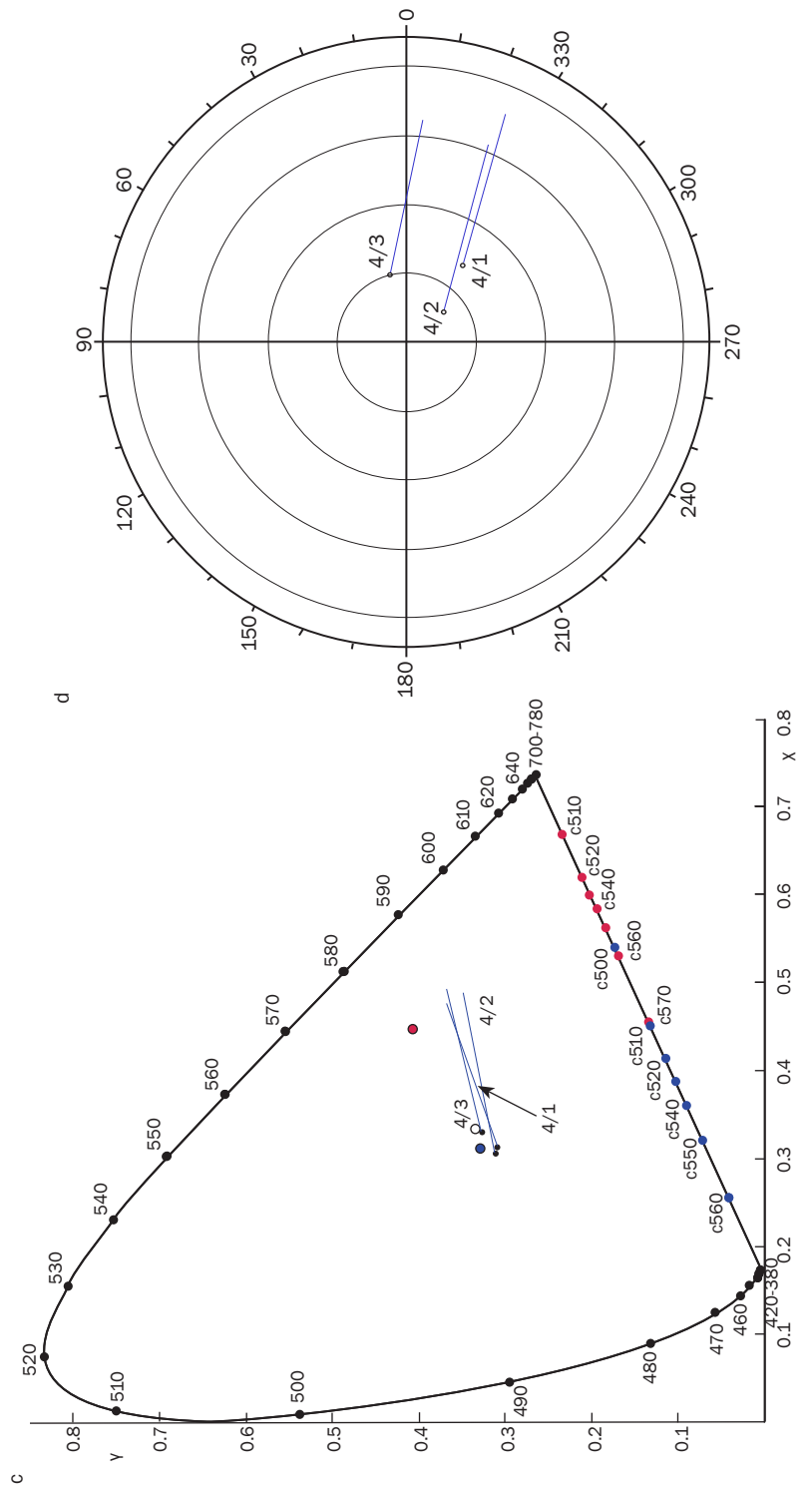
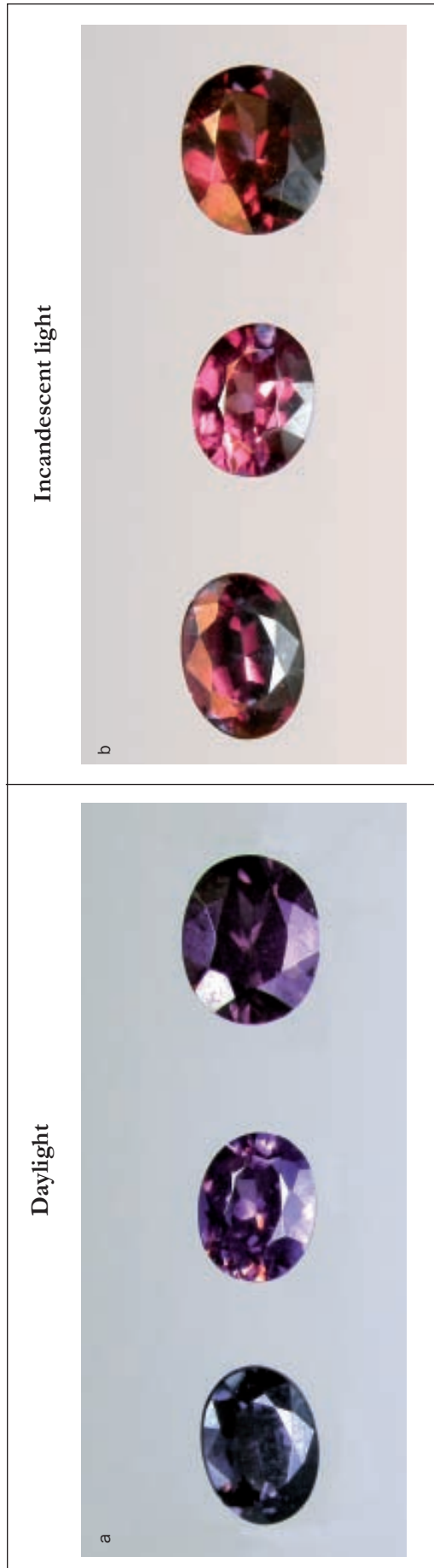


Figure 34: Colour-change garnets of Group 4 in daylight (a) and incandescent light (b), samples 4/2 (left), 4/1 (centre) and 4/3 (right), size 6.2 x 7.7 mm, weight 1.46 ct) are violet, purple or purplish red in daylight and reddish purple or red purple in incandescent light. Colorimetric parameters in the CIE 1931 chromaticity diagram are shown in (c); see Figure 31 for notation. Colorimetric parameters in the CIELAB 1976 colour circle are in (d); see Figure 31 for notation. The colour change from daylight to incandescent light is evident.

Colour-change garnets from Madagascar: variation of chemical, spectroscopic and colorimetric properties

Group 5 colour-change garnets

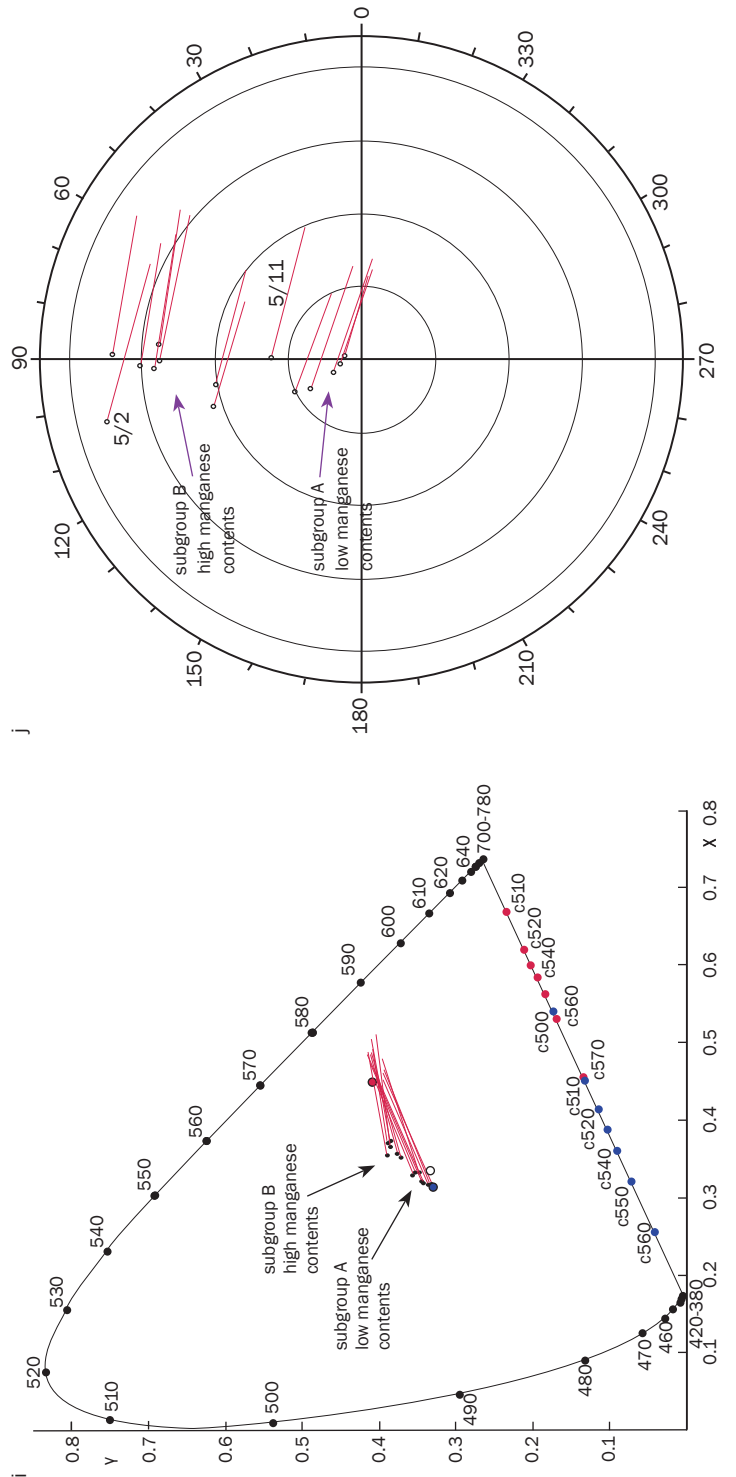
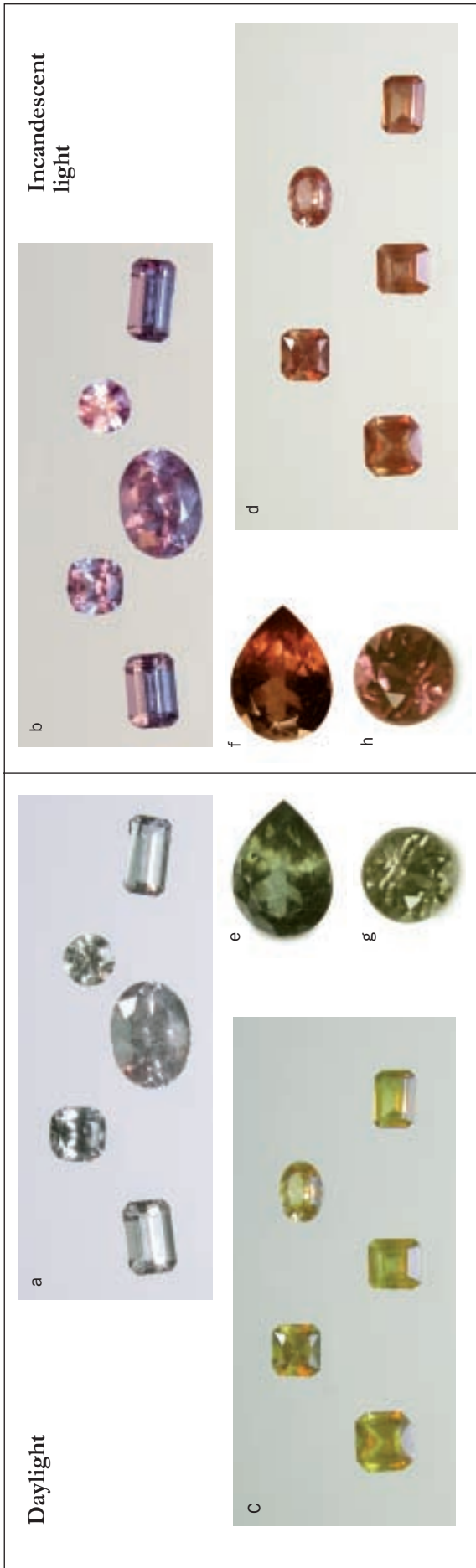


Figure 35: Colour-change garnets of Group 5 in daylight (a,c,e,g) and incandescent light (b,d,f,h); samples with low manganese contents (subgroup A) are almost colourless in daylight (a, size of the lower right sample 4.7 x 6.8 mm, weight 0.74 ct); samples with higher manganese contents (subgroup B) are yellow (c, size of the lower right sample 3.6 x 5.0 mm, weight 0.41 ct) or greenish yellow (e, sample 5/2, 6.4 x 8.8 mm) in daylight; the samples are red orange or orange in incandescent light, or rarely red (h, sample 5/11, diameter 3.7 mm). Colorimetric parameters are plotted on the CIE 1931 chromaticity diagram (i), and on the CIE LAB 1976 colour circle (j); the notations are as in Figure 31. The colour change from daylight to incandescent light is evident.

Colour-change garnets from Madagascar: variation of chemical, spectroscopic and colorimetric properties

Group 6 colour-change garnets

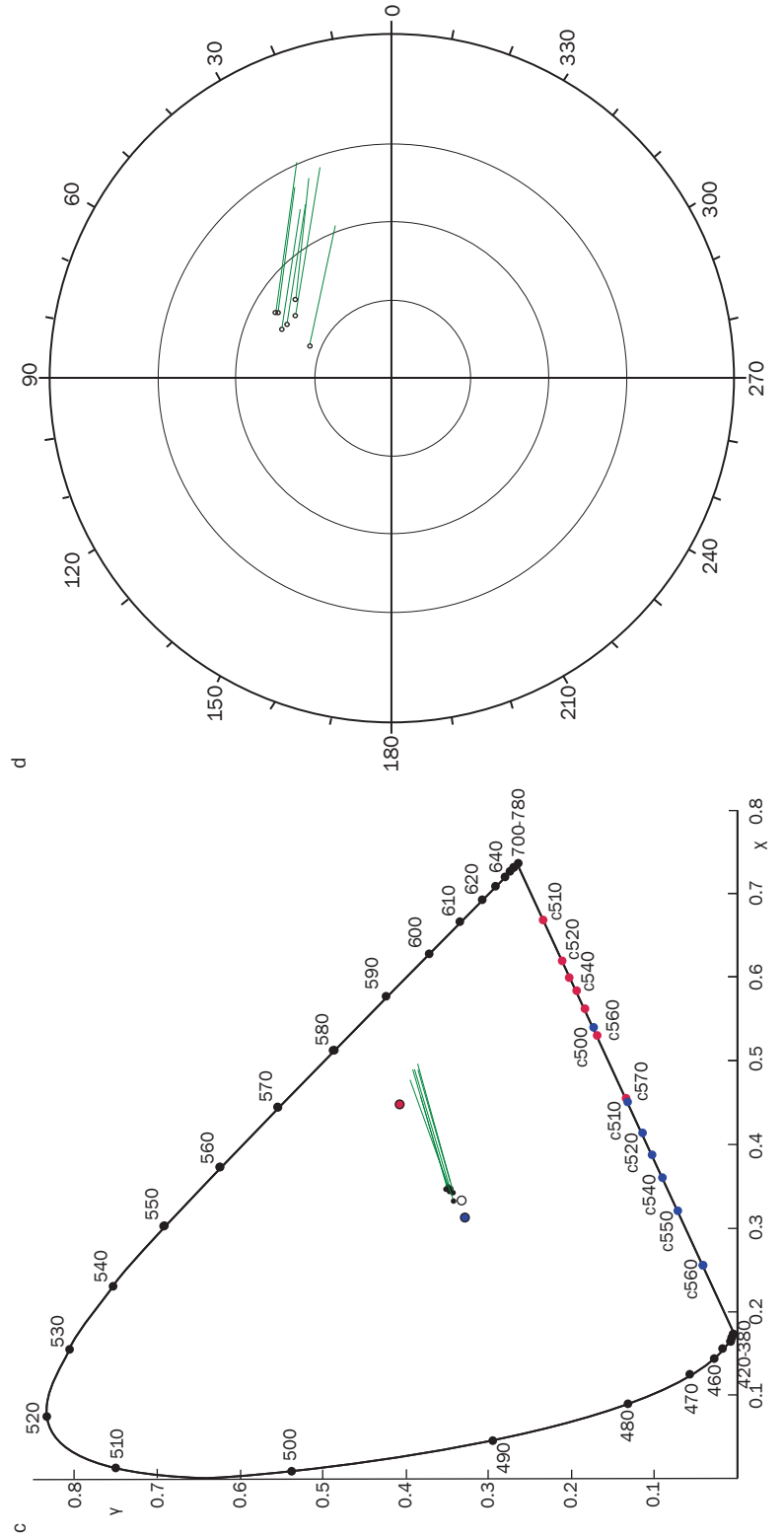
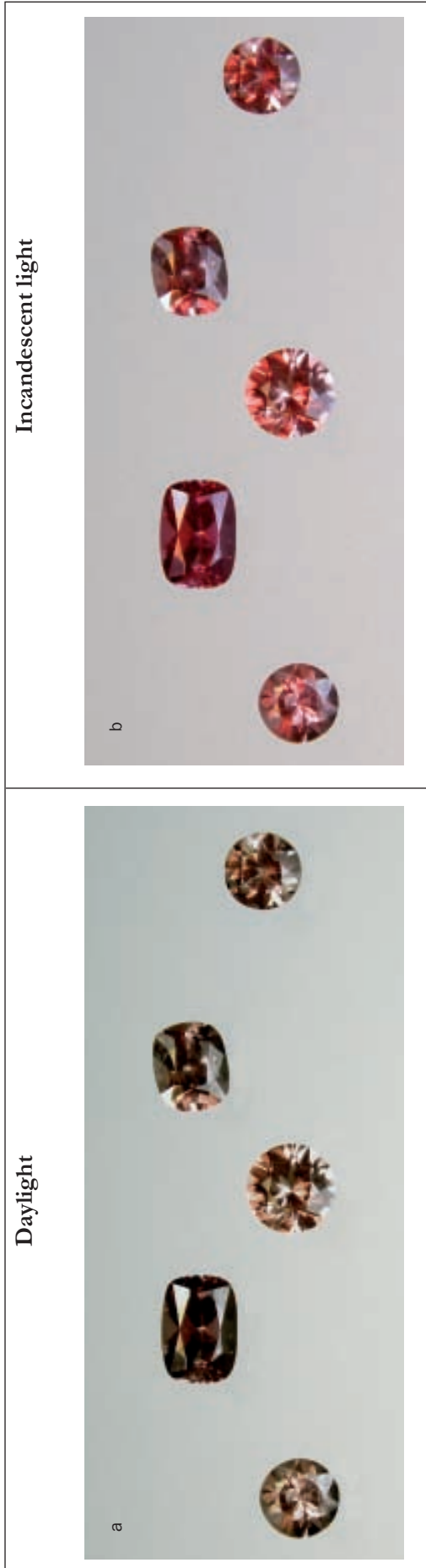


Figure 36: Colour-change garnets of Group 6 in daylight (a) and incandescent light (b), diameter of the lower right sample 5.2 mm, weight 0.73 ct. Colorimetric parameters are plotted on the CIE 1931 chromaticity diagram (c) and on the CIELAB 1976 colour circle (d); notations are as in Figure 31. The colour change from daylight to incandescent light is evident.

Colour-change garnets from Madagascar: variation of chemical, spectroscopic and colorimetric properties

Group 7 colour-change garnets

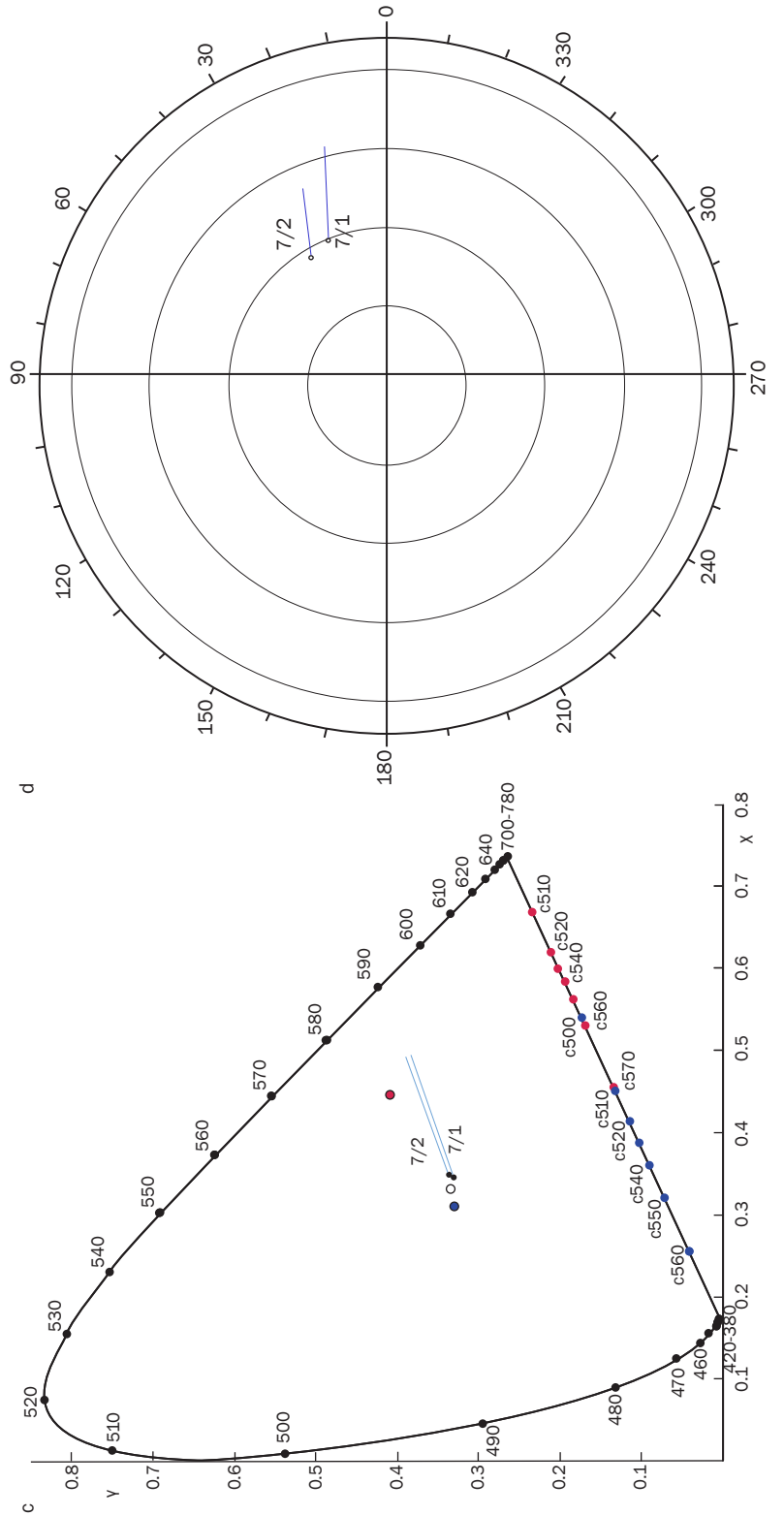
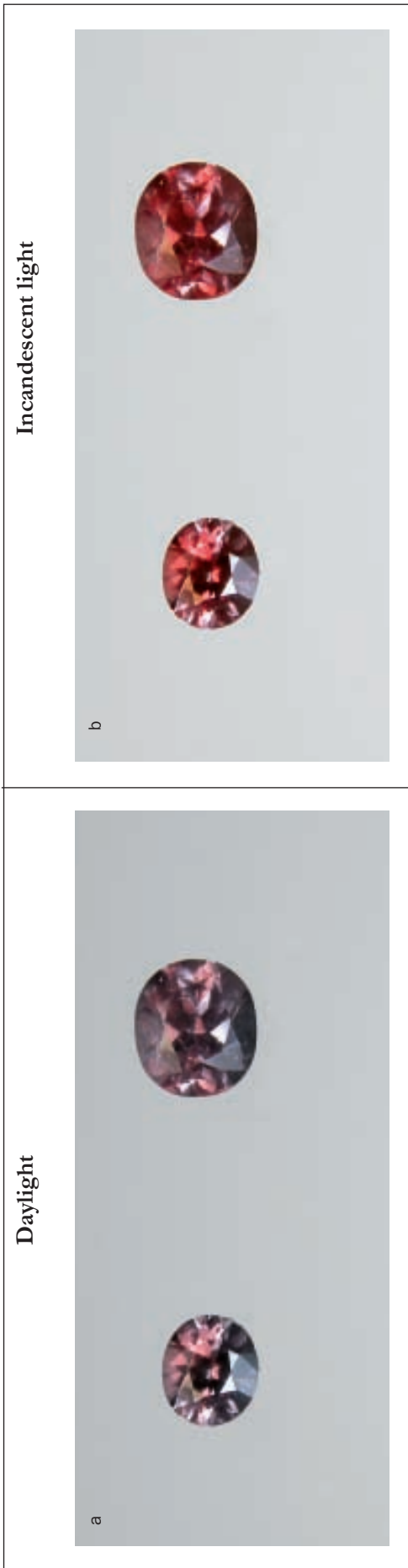


Figure 37: Colour-change garnets of Group 7 in daylight (a) and incandescent light (b), samples 7/1 (left) and 7/2 (right, 6.7 x 7.6 mm, weight 1.72 ct). Colorimetric parameters are shown on the CIE 1931 chromaticity diagram (c) and on the CIELAB 1976 colour circle (d); notations are as in Figure 31. The colour variation from daylight to incandescent light is evident.

Colour-change garnets from Madagascar: variation of chemical, spectroscopic and colorimetric properties

Malaya garnets

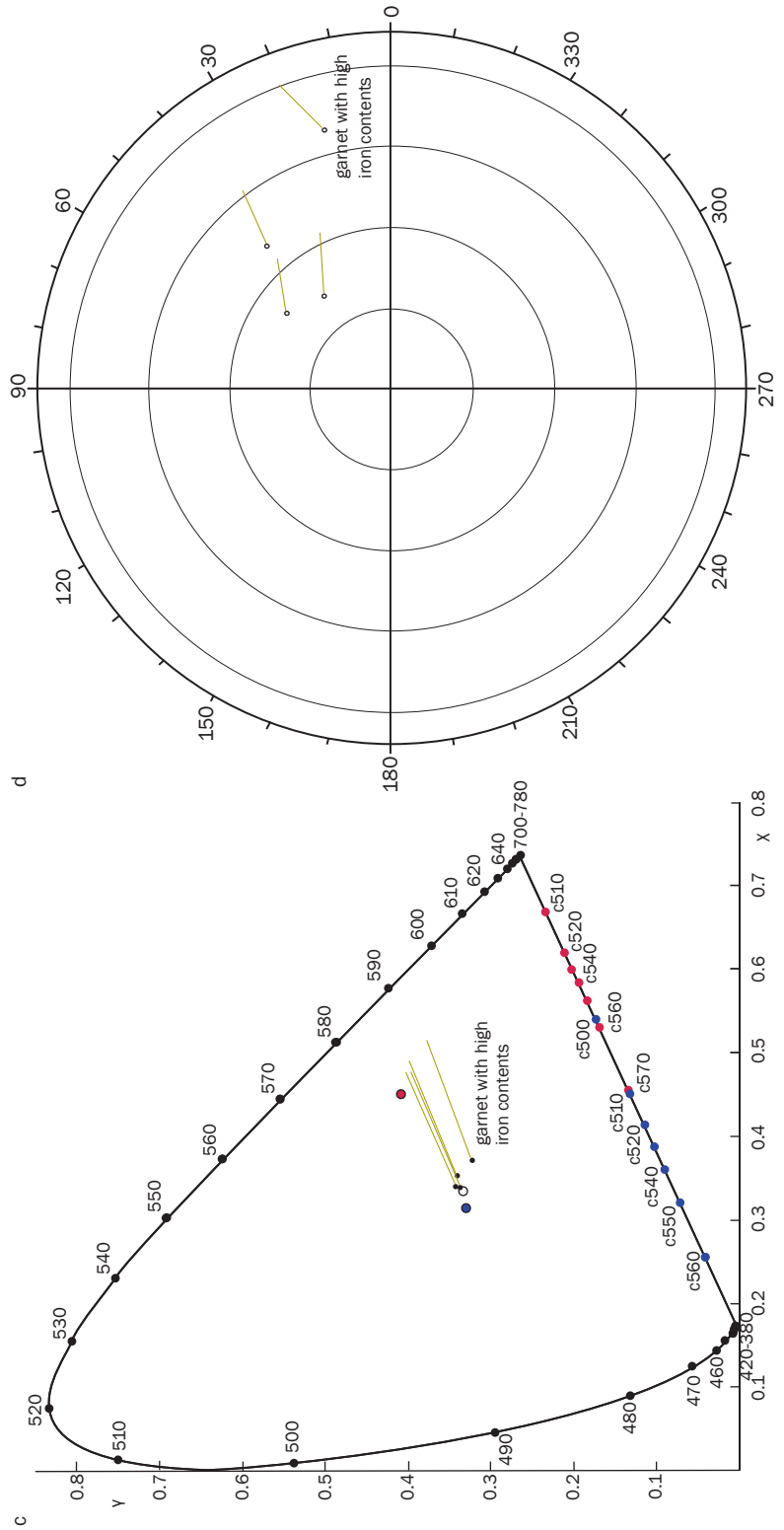


Figure 38: Malaya garnets in daylight (a) and incandescent light (b); the garnet with the highest iron content (right, diameter 6.8 mm, weight 1.40 ct) shows an increase of yellowness in incandescent light. Colorimetric parameters are shown on the CIE 1931 chromaticity diagram (c) and on the CIELAB 1976 colour circle (d); notations are as in Figure 31. The colour variation from daylight to incandescent light is evident.

Colour-change garnets from Madagascar: variation of chemical, spectroscopic and colorimetric properties

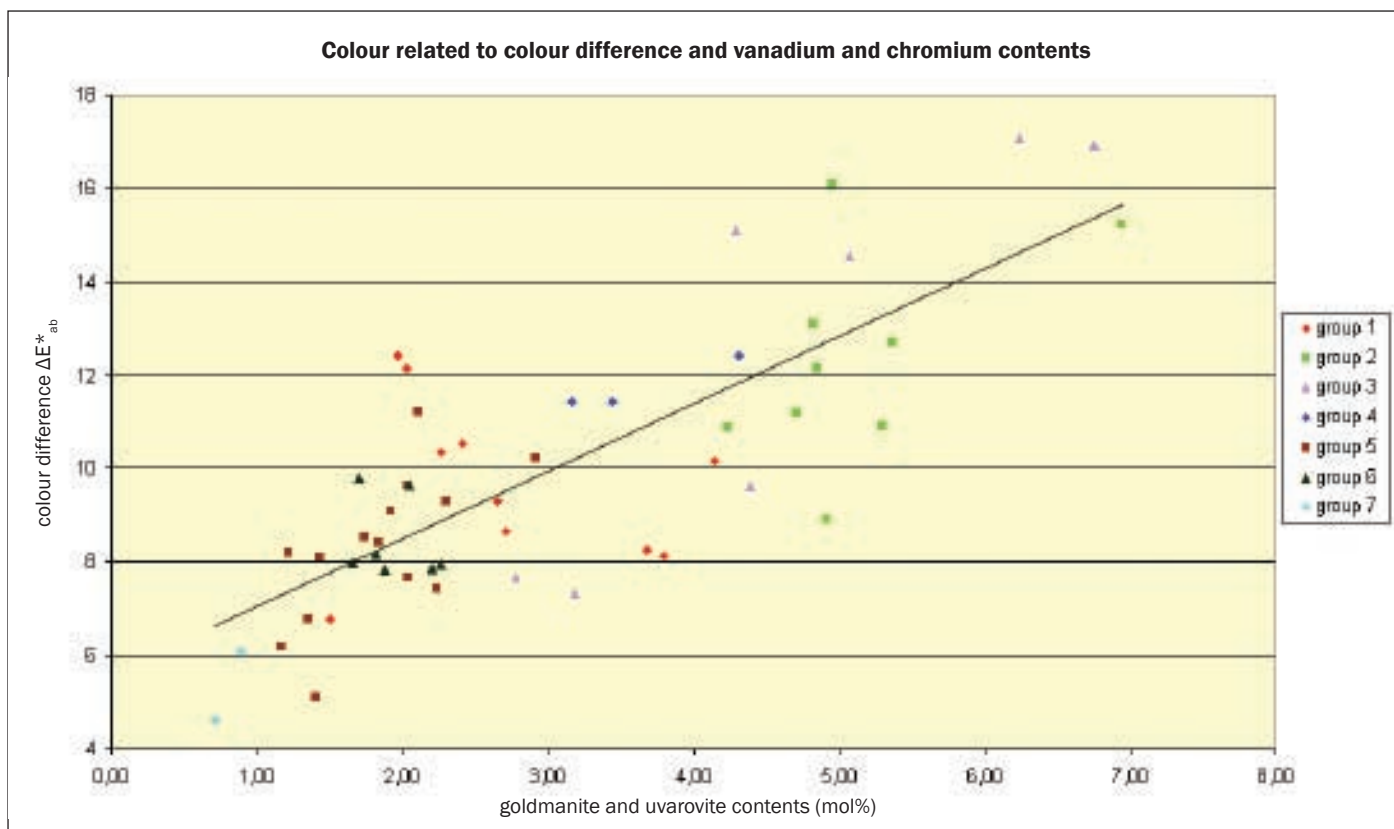


Figure 39: Correlation of vanadium and chromium contents within the seven groups of colour-change garnets with their colour differences ΔE^*_{ab} in the three-dimensional CIELAB colour space.

yellowish green in daylight (Figure 32 a–b). Seven garnets are very slightly yellowish grey or greenish yellowish grey, and almost colourless in incandescent light. Sample 2/1 with the highest vanadium and chromium contents within this group (gold + uva 6.94 %) is green in daylight and red purple in incandescent light, and sample 2/9 with the highest manganese content (spess 62.03 %) is greyish bluish green in incandescent light.

Group 3

- This group contains seven samples which are bluish green or greenish blue in daylight (Figure 33 a–b), but with otherwise varying chemical, spectroscopic and colorimetric properties. Vanadium and chromium contents vary widely (between gold + uva 2.78 and 6.75 %), and the spessartine and almandine ranges are 33.41 to 41.29 % and 3.21 to 9.29 % respectively. Three garnets (Figure 33

a, b) are slightly bluish green in daylight and somewhat more intense violet purple in incandescent light. Sample 3/4 (Figure 33 c, d, centre stone, gold + uva 4.29 %) is bluish green in daylight and blue violet in incandescent light. The remaining three garnets in this group have very high vanadium and chromium contents (Figure 33 c to f; gold + uva above 5 %), they range from bluish green in daylight and blue green in incandescent light (sample 3/5) to greenish blue in daylight and violet purple in incandescent light (sample 3/7).

Group 4

- This group consists of three garnets which are violet, purple or purplish red in daylight and reddish purple or red purple in incandescent light (Figure 34 a–d). Vanadium and chromium contents vary between 3.61 and 4.31 % gold + uva. Spessartine contents lie between 29.24 and 36.62 %, and almandine contents are relatively high

(7.45 or 8.63 %) or extremely high in garnet 4/3 (14.95 % alm).

Group 5

- The 14 garnets in this group (Figure 35 a–j) show relatively low vanadium and chromium contents (gold + uva from 1.17 to 2.92 %) and low iron percentages (alm 3.18 to 5.15 %). The manganese contents, on the other hand, vary within a wide range (spess 27.09 – 73.83 %). Five samples with the lower manganese contents (Figure 35 a, b; subgroup A, spess 27.09 to 30.86 %) are yellowish grey or greenish yellowish grey, almost colourless or greenish yellow to yellow green in daylight and red purple to red in incandescent light. The nine samples with higher spessartine percentages (Figure 35 c–h, subgroup B, between 46.55 and 73.83 %) are yellow or greenish yellow in daylight and red orange or orange in incandescent light (Figure 35 c–f) and rarely red (Figure 35 g, h).

Colour-change garnets from Madagascar: variation of chemical, spectroscopic and colorimetric properties

Group 6

- The seven garnets in this group (Figure 36 a-d) have manganese, vanadium and chromium contents which are comparable to those of subgroup B of Group 5, i.e. goldmanite plus uvarovite percentages of 1.66 to 2.26 % and spessartine contents of 48.75 to 61.87. Iron contents, on the other hand are somewhat higher (alm 5.61 – 7.85 %). Their colours are orange or yellow orange in daylight to red in incandescent light.

Group 7

- The two garnets (Figure 37 a-d) in this group have the lowest vanadium and chromium contents of all the samples (gold + uva 0.71 and 0.89 %) and also have very low spessartine contents (22.96 and 26.24 %). Iron contents, on the other hand, are high or extremely high (10.02 and 16.35 % alm). They are red in daylight and red or purplish red in incandescent light.

Malaya garnets

- The four vanadium- and chromium-free malaya garnets examined for comparison are orange, red orange or red in daylight and red orange to red in incandescent light (Figure 38 a-d). The garnet with the highest iron content showed a remarkable increase of yellowness in incandescent light, i.e. a reaction different from the vanadium-bearing garnets examined in this study. Colour difference and hue angle change in the CIELAB system for these four garnets are respectively ΔE^*_{ab} 3.51–4.43, and Δh_{ab} 4–13°, and these parameters will be referred to later when colour change is discussed.

Colorimetry

An evaluation of different chemical properties of the garnets and a possible relationship between chemical and colorimetric properties indicates that there is a clear correlation of the colour difference ΔE^*_{ab} with the contents of vanadium and chromium (Figure 39).

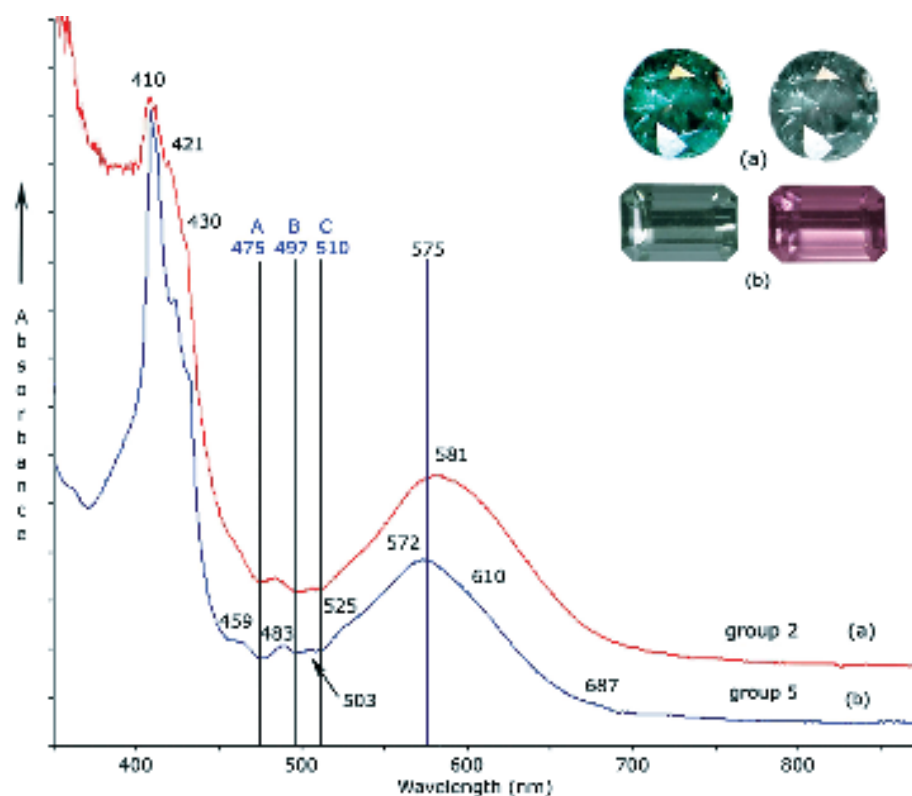


Figure 40: Absorption spectra of colour-change garnets from Madagascar which are light grey, almost colourless in incandescent light (a) or in daylight (b). Both garnets have the same type of absorption spectrum with only slight differences in the position of the vanadium-chromium absorption maximum; each sample pair is shown in daylight (left) and incandescent light (right).

This is consistent with conclusions from the garnet spectra because the contents of vanadium and chromium are directly responsible for the intensity of the dominant absorption maximum between 569 and 584 nm.

Furthermore, since the colorimetric parameters calculated for all 52 garnets in this study show only a minimal change of lightness for different illuminations, the graphical representations in the a^*b^* plane of the CIELAB colour circle in Figures 30 to 37 are close approximations to the characteristic changes in three-dimensional CIELAB colour space. In other words: the length and direction of the line connecting the two loci of one sample in the a^*b^* plane give a good graphic representation of the colour difference.

As described above, the 52 garnets have absorption spectra with a dominant vanadium-chromium absorption maximum in the greenish yellow, yellow or yellow orange region of the visible range and

two regions with high transparency — the red to orange and the yellowish green to blue violet. With a change of illuminants from daylight D_{65} to incandescent light A, all garnets in Groups 1 to 6 with this type of absorption spectrum show an increase of redness and blueness. The two garnets in Group 7 with the smallest vanadium and chromium contents show only an increase in redness, with minimal increase in blueness.

In most of the garnets studied, spectral purity p (in the CIE 1931 colour space) or chroma C^*_{ab} (in the CIELAB colour space) is relatively low. This indicates that even samples with distinct absorption maxima and minima in the visible range, may appear grey or almost colourless in daylight or in incandescent light (see Figure 40). The spectra in Figure 40 do not provide a clear reason for such distinct colour changes so these are related to the complexities of colour perception by the human eye.

Colour-change garnets from Madagascar: variation of chemical, spectroscopic and colorimetric properties

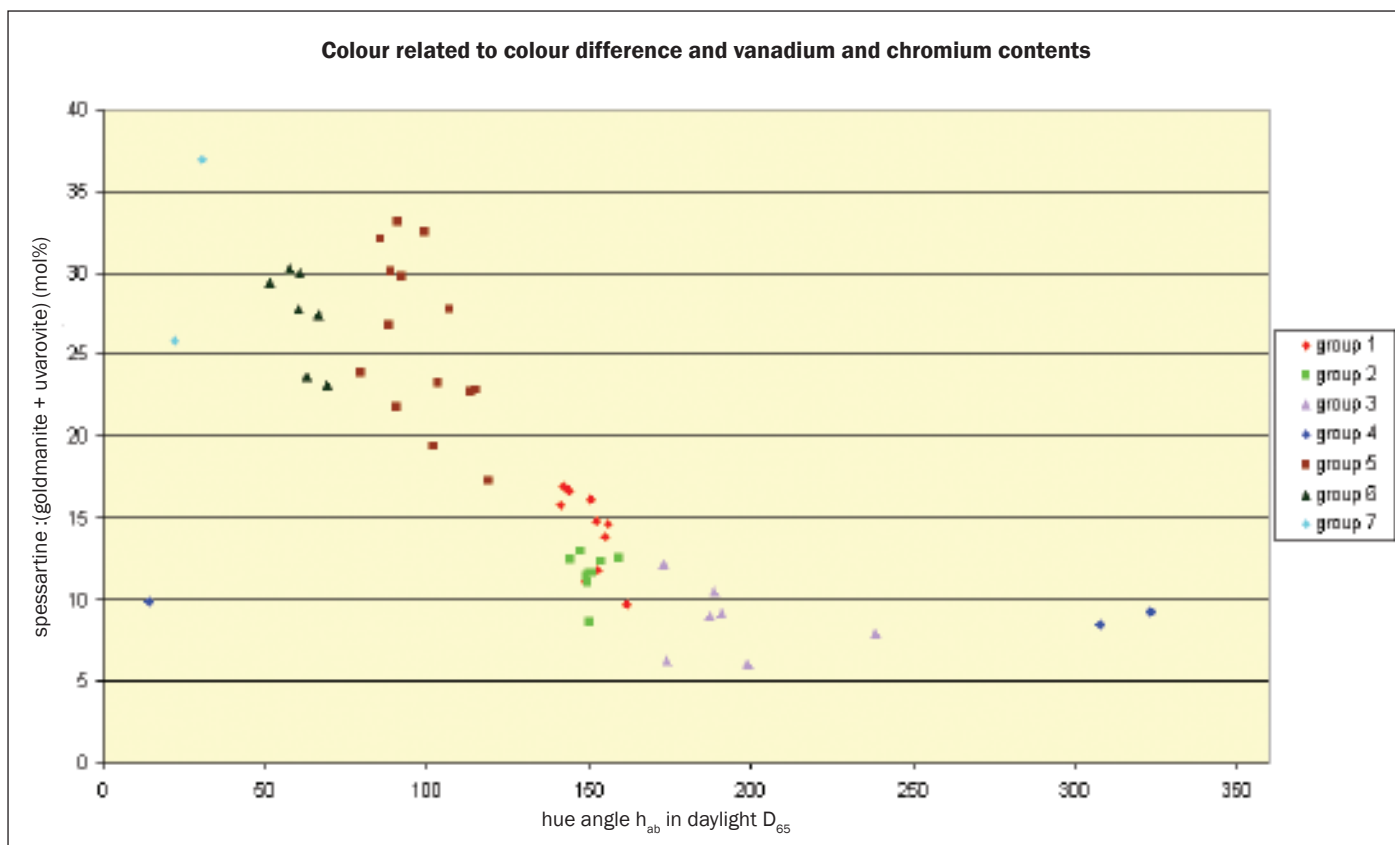


Figure 41: Variation of colour in daylight, represented by the hue angle h_{ab} , with the ratio spessartine : (goldmanite + uvarovite) in the colour-change garnets; the differently coloured groups are clearly separated.

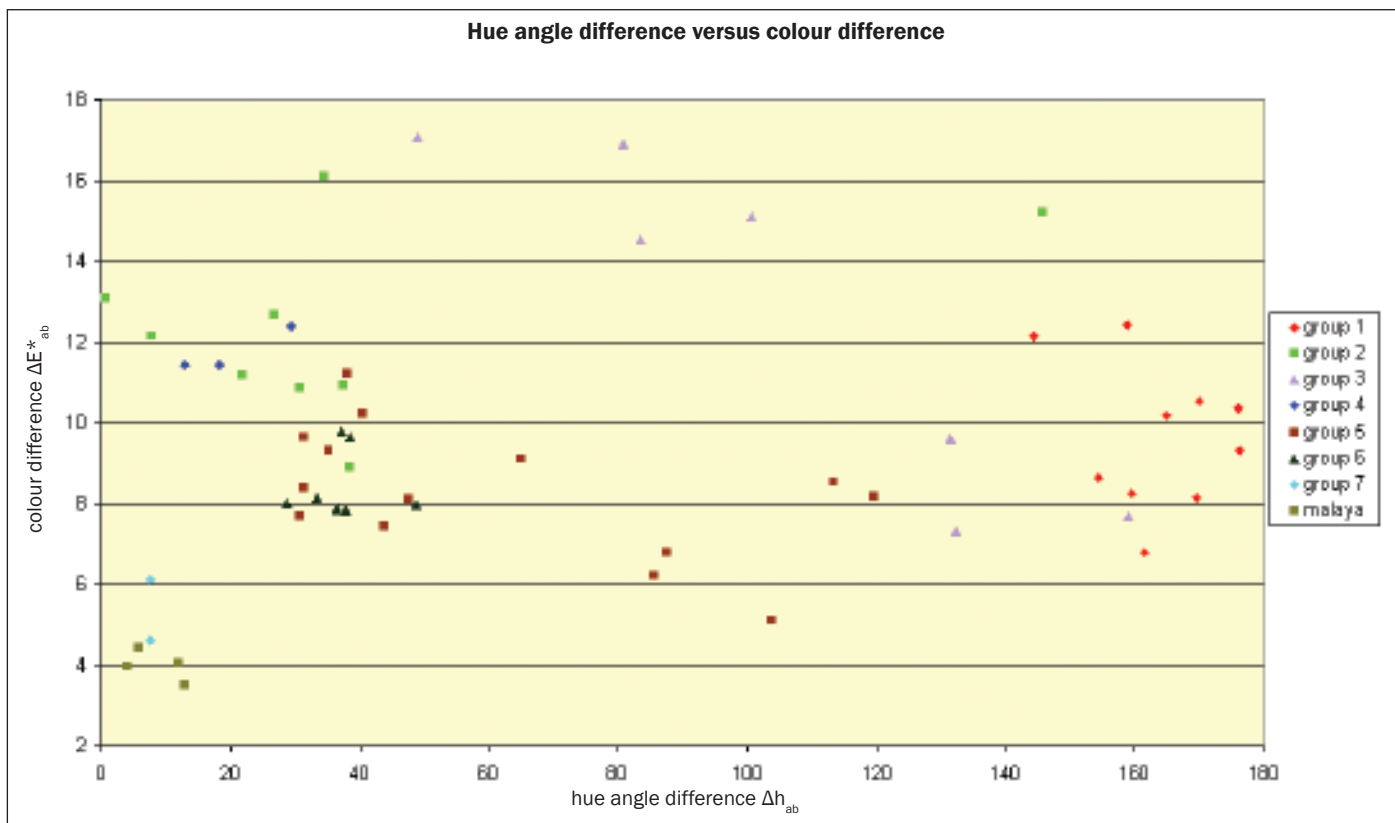


Figure 42: Variation of the main colorimetric parameters hue angle difference and colour difference of colour-change garnets from Madagascar.

Colour-change garnets from Madagascar: variation of chemical, spectroscopic and colorimetric properties

Causes of colour: correlation of chemical, spectroscopic and colorimetric data

Important features of the chemistry of our garnets are plotted on *Figure 29* and their colours in daylight and incandescent light are plotted on *Figure 30*. In the section on spectra the various intensities of the (vanadium + chromium), manganese and iron absorption bands and the shift of the position of the dominant vanadium-chromium absorption maximum from 569 to 584 nm were discussed. The two regions in the spectra of low absorption (the red to orange and yellowish green to blue-violet ranges) and their ratios should play a major role in determining the colour of the garnets. The balance between these two regions of high transparency depends on the intensity of the first vanadium-chromium absorption maximum in the greenish yellow, yellow or yellow orange compared with that of the manganese triplet in the violet, on which is superimposed the second vanadium-chromium absorption band (see *Figure 26*).

On the basis of daylight colour, represented by hue angle h_{ab} , the seven groups of colour-change garnets can be plotted against the spessartine : (goldmanite + uvarovite) ratio (*Figure 41*), and they can be subdivided further into

- garnets with a daylight colour of green to greenish blue and lower spessartine : (goldmanite + uvarovite) ratios (Groups 1, 2 and 3);
- garnets with a daylight colour of yellow green to orange and higher spessartine : (goldmanite + uvarovite) ratios (Groups 5 and 6);
- garnets of Group 4 with daylight colour violet, purple or purplish red with low spessartine : (goldmanite + uvarovite) ratios and very high iron contents; and
- garnets of Group 7, red in daylight with high spessartine : (goldmanite + uvarovite) ratios and very high iron contents.

In addition to these compositional factors, to understand the colour variations in the garnets, the intensity and position of the absorption maximum of the dominant vanadium-chromium band (*Figure 26*) and the intensity of the manganese triplet in the violet must be considered. As general background we know that standard daylight D_{65} has high percentages of blue and green compared with incandescent light A, which has higher amounts of red and orange. So, typical vanadium- and chromium-bearing pyrope-spessartine garnets show an increase of redness and blueness under light source A. The colour difference as measured by ΔE_{ab}^* in three-dimensional colour space is, in general, correlated with the vanadium and chromium contents (*Figure 39*). The relationship between colour difference ΔE_{ab}^* and hue angle difference Δh_{ab} is shown in *Figure 42*.

Group 1 (see *Figure 31*):

- Garnets in this group are colorimetrically homogeneous with a colour change from green to slightly yellowish green in daylight to red purple, reddish purple or purple in incandescent light. They have an absorption maximum in the range 572 to 576 nm, and the absorption minima in the blue to green range are A (blue) \approx B (bluish green) > C (green) (see *Table V* and *Figures 23* and *27*). The spessartine : (goldmanite + uvarovite) ratios vary between 9.7 and 16.9. These garnets have almost identical chroma in daylight and incandescent light lying equidistant from the centre of the CIELAB colour space. The hue angle differences vary between 144.3 and 176.2°. In order to better understand how these colours and colour changes vary from those of other groups, we may designate a typical spectrum of a Group 1 garnet as a 'balanced spectrum'.

The differences shown by other groups of garnets may then be summarized as follows:

Group 2 (see *Figure 32*):

- Garnets in this group have higher goldmanite, uvarovite and spessartine contents than Group 1 garnets, but the spessartine : (goldmanite + uvarovite) ratios are within the same range (*Figure 41*).
- The absorption maxima of eight samples lie between 578 and 582 nm (*Figure 27, 40a*). Thus the absorption minima in the blue to green become broader with B (bluish green) > C (green) \gg A (blue) and the absorption in the red to orange is somewhat stronger. Consequently the chroma in daylight and the intensity of the green coloration in daylight is strong. However, the stronger absorption in the red to orange range means that under incandescent light most samples are still yellowish grey, greenish yellowish grey or greyish bluish green (almost colourless) and not red or purple (see *Figure 32b*).
- The absorption maximum of sample 2/1, which is green in daylight and red purple in incandescent light, lies at 583 nm. The percentage of goldmanite + uvarovite is 6.94 and the spessartine : (goldmanite + uvarovite) ratio is 8.6. Thus, the effect of the shift of the absorption maximum to higher wavelength is compensated by a somewhat higher vanadium and chromium content and the structure of the absorption minimum is similar to that of samples in Group 1. This higher transmission at A is the cause of the red purple coloration in incandescent light.

Group 3 (see *Figure 33*):

- Four garnets in this group have absorption maxima between 573 and 576 nm, i.e. in the range of the maxima measured for samples of Group 1 (*Figure 27*). However, these garnets have somewhat smaller spessartine : (goldmanite + uvarovite) ratios. Thus the minimum in the blue to green is shifted to lower wavelength with A (blue) > B (bluish green) > C (green). Their colour in daylight is bluish green (samples 3/3 and 3/4),

Colour-change garnets from Madagascar: variation of chemical, spectroscopic and colorimetric properties

and under incandescent light this changes to violet purple (sample 3/3) or blue violet (sample 3/4).

- The same type of spectrum with a maximum at 574 nm and minima according to the scheme A (blue) >B (bluish green) >C (green) is shown by sample 3/7. However, due to the higher contents of vanadium and chromium (gold + uva 5.07 %) the intensity of the absorption maximum is higher and the resulting colour in daylight is greenish blue. This is the bluest of the 52 studied garnets, and in incandescent light it is violet purple.
- Garnets 3/5 and 3/6 have extremely high vanadium and chromium contents, and their absorption maxima were measured at 584 nm (Figure 27). This shift of absorption to a higher wavelength and the resulting structure of the minimum where B (bluish green) > C (bluish green) > A (blue), results in a daylight colour of bluish green. With the increase of blueness and redness in incandescent light, the blueness remains strong and 3/5 is blue green in this light and 3/6 is blue violet.

Group 4 (see Figure 34):

- The garnets in this group have somewhat lower spessartine : (goldmanite + uvarovite) ratios than comparable samples of Group 3 (Figure 41). The vanadium-chromium maximum lies at 571–573 nm (Figure 27) and the transmission pattern in the blue is A (blue) >B (bluish green) >C (green). The intensity of the vanadium-chromium absorption band is probably enhanced by the high to extremely high iron contents of the garnets, and due to the position of this band at 571 nm, the red in daylight has more influence resulting in violet, purple or purplish red. The garnet with the highest almandine content (sample 4/3) is purplish red in daylight.
- Upon change of illuminant to incandescent light, the increase of blueness and redness result in a reddish purple or red purple coloration of the three garnets.

Group 5 (see Figure 35):

- Within this group, the three garnets with the lowest manganese contents (spess 27.09 – 27.90 %) and a vanadium-chromium absorption maximum at 572 nm (see Figure 40b) are slightly yellowish grey, almost colourless. The structure in the blue transmission region is A > B ≈ C. Although these samples reveal pronounced absorption spectra in the visible range, their chromas are extremely low (1.2 to 2.1). The resulting colour is only understandable in terms of the mechanism of human colour perception, but it proves the results of chromaticity calculation in the CIELAB colour space to be correct. In incandescent light, these stones are red purple.
- Two samples have somewhat higher spessartine contents and similar vanadium and chromium contents. The structure of the absorption minimum (see Figure 28) is A ≈ B > C (sample 5/10) or A ≈ B ≈ C (sample 5/9) and in daylight they are greenish yellow or yellow green; consequently, these two samples are closest to those of Group 1. In incandescent light redness and blueness are increased and the colour shifts to red or red purple.
- The remaining nine samples have distinctly higher manganese contents between 46.44 and 73.83 % spess. The ratio spess : (gold + uva) varies accordingly from 21.8 to 33.1 (Figure 41). The structure of the absorption minimum (see again Figure 28) is B ≈ C > A or C > B > A and the daylight colour is greenish yellow or yellow. In incandescent light they are orange to red.

Group 6 (see Figure 36):

- The seven garnets in this group have similar manganese, vanadium and chromium but higher iron contents than the first three garnets mentioned in Group 5. The absorption maximum, which is influenced by the high iron contents, lies between 569 and 571 nm (Figure 28) and the structure at the

absorption minimum is A ≈ B ≈ C. The resulting colour in daylight is orange or yellow orange. In incandescent light, the increase of blueness is weak or extremely weak, and the stones are red.

Group 7 (see Figure 37):

- The two garnets in this group show the smallest vanadium and chromium contents of the whole garnet series, and they also have high iron contents (alm 10.02 or 16.35 %). The spectra (Figure 28) are comparable with the spectra of iron-rich malaya garnets (Figure 22) which show a somewhat increased intensity of the absorption band at 569 nm. The structure at the absorption minimum is A >> B ≈ C and is not influenced by the vanadium-chromium band. The stones are red in daylight, and a somewhat more intense red or purplish red in incandescent light.

In comparing our groups with those of Krzemnicki *et al.* (2001) we can note the following similarities:

This paper:	Krzemnicki <i>et al.</i> :
Two samples of Group 3	Compare with Group 1
Groups 1, 3, 4	Compare with Group 2
Group 5, low manganese contents	Compare with Group 3
Group 5, high manganese contents	Compare with Group 4

Krzemnicki and his co-workers did not examine samples comparable with our Groups 2, 6 and 7, and the single garnet in their Group 5 has a particular combination of properties not represented among our 52 samples.

Most probably, according to the spectrum, this garnet specimen reveals — in addition to the ‘normal’ absorption bands of manganese, iron, vanadium and chromium discussed in detail in this paper — a continuously increasing absorption from red to violet. A similar spectroscopic feature was observed in samples from

Colour-change garnets from Madagascar: variation of chemical, spectroscopic and colorimetric properties

Tranaroa, Madagascar (Schmetzer *et al.*, 2002), but such garnets are not included in the present study.

Evaluation of the extent of colour change

According to the colorimetric data obtained from our samples it is evident that the wide variety of colours in daylight and incandescent light relates to different spectroscopic properties. The data are presented in *Tables II, VIa* and *VIb*, and shown in *Figures 31 to 38*.

The colorimetric parameters of colour-change garnets in the CIE 1931 chromaticity diagram are useful to characterize stone colours in daylight and incandescent light. But if we want to characterize colour differences and especially to quantify the extent of any colour change, we have to refer to a uniform colour space such as CIELAB.

Upon measurement of 18 colour-change gem materials, Liu *et al.* (1994, 1999a) suggested a criterion for recognition and description of colour change, which is based on a hue angle difference Δh_{ab} of 20° or above (for gemstones with relatively saturated colour, i.e. with chroma higher than 5 CIELAB units). In these papers, they used a general, non-restricted definition of colour such as “colour in gemstones is the colour appearance that a person sees” (Liu *et al.*, 1999a, p.372) and “colour is described in words by means of three attributes – hue, ... saturation, ... and lightness” (op.cit. p.373).

While investigating the 52 colour-change garnets and four malaya garnets, the proposed 20° hue angle difference was assessed. Among these samples, there are six vanadium- and chromium-bearing garnets (*Figure 43 a,b; Table VII*) from Groups 2, 4 and 7, and four vanadium- and chromium-free malaya garnets (*Figure 38 a,b*) which, although having hue angle differences below 20°, show a clearly visible colour variation between daylight and incandescent light. This is understandable because the human eye is unable to distinguish clearly between various colorimetric parameters such as



Figure 43 a,b: Colour-change garnets from Madagascar with hue angle differences between daylight (a) and incandescent light of below 20°; two samples of Group 4 (left), two of Group 7 (centre) and two of Group 2 (right) are pictured; diameter of the garnet in the lower right 3.9 mm, weight 0.28 ct.

Table VII: Colorimetric data of six samples with hue angle differences < 20°.

Group	2	2	4	4	7	7
Sample	2/7	2/8	4/1	4/3	7/2	7/1
Colorimetric data CIE 1931 ^a						
λ_D (nm) for daylight D ₆₅	537	530	c550	635	598	608
Purity p for daylight D ₆₅	9.2	9.4	7.1	4.5	12.5	9.9
λ_D (nm) for incandescent light A	555	538	c531	c510	619	c504
Purity p for incandescent light A	3.0	1.6	20.0	22.1	19.3	17.1
Colorimetric data CIELAB 1976 ^b						
C* _{ab} for daylight D ₆₅	14.90	14.98	6.83	5.01	9.37	9.91
h _{ab} (°) for daylight D ₆₅	151.0	153.8	323.5	14.2	30.7	22.16
C* _{ab} for incandescent light A	2.83	1.93	17.98	16.07	13.59	15.66
h _{ab} (°) for incandescent light A	143.3	153.2	336.5	355.8	23.2	14.62
Δh_{ab} (°)	7.7	0.6	13.0	18.4	7.6	7.5
ΔE^*_{ab}	12.1	13.1	11.4	11.4	4.6	6.1

^a λ_D = dominant wavelength, c indicates ‘complement of’

^b C*_{ab} = chroma; h_{ab} = hue angle

Δh_{ab} = hue angle difference between daylight and incandescent light

ΔE^*_{ab} = colour difference between daylight and incandescent light in the three dimensional CIELAB colour space

Colour-change garnets from Madagascar: variation of chemical, spectroscopic and colorimetric properties

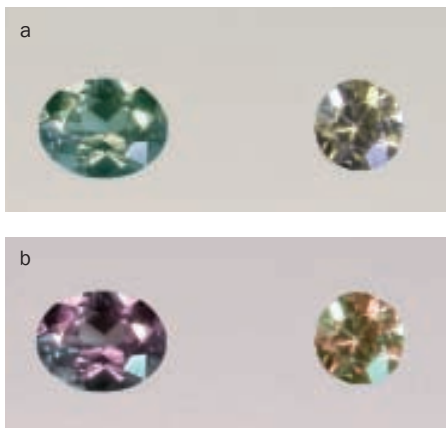


Figure 44 a,b: Two colour-change garnets from Madagascar with chroma below 5 CIELAB units for daylight (a) and incandescent light; samples from Group 1 (left) and Group 5 (right); diameter of the right garnet 4.7 mm, weight 0.47 ct.

hue and chroma (saturation) and only an overall colour impression is observed. Therefore, the hue angle change Δh_{ab} cannot be the only parameter important in understanding colour change.

In addition to a hue colour change above 20°, Liu *et al.* (1994, 1999a), also mentioned that the method seemed

best suited to gems whose chroma C_{ab}^* is above 5 CIELAB units (i.e. for clearly observable colour change). This suggestion was tested with the 10 samples mentioned above and only two garnets from Group 2 have chroma below 5 in incandescent light (see again *Table VII*). However, these garnets still showed a clear colour change, and within the range of our 52 garnets there are numerous stones with low chroma C_{ab}^* for both daylight D_{65} and incandescent light A (*Tables II, VIa, VIb*). Of these, there are two samples with both chroma values below 5 or close to 5 (*Figure 44 a,b*). Since all our studied garnets show clearly observable colour changes, this indicates that the value of chroma has to be considered in the context of other criteria.

In the uniform CIELAB colour space, three parameters should be considered:

- The colour difference ΔE_{ab}^* which represents the distance between two sample loci in the three-dimensional colour space. Because the differences of lightness L^* are so small in the

range of samples under different illuminants, the lengths of the bars in the CIELAB graphics of *Figures 31 to 38* are graphical representations of this parameter projected into the a^*b^* plane.

- The hue angle difference Δh_{ab} , i.e. the hue angle h_{ab} representing the spectral point in daylight minus the hue angle h_{ab} representing the spectral point in incandescent light, is also shown in these graphics and summarized in *Figure 42*.
- The chroma C_{ab}^* under different illumination. Graphically C_{ab}^* is represented by the radial distance of the spectral point from the origin of the CIELAB a^*b^* plane (see *Figures 31 to 38* and especially *Figure 30*). So chroma difference in a stone under two light sources can be represented by the difference between two radial distances.

Because there is a large variation of hue angle differences Δh_{ab} from almost 0° to almost 180°, the hue difference

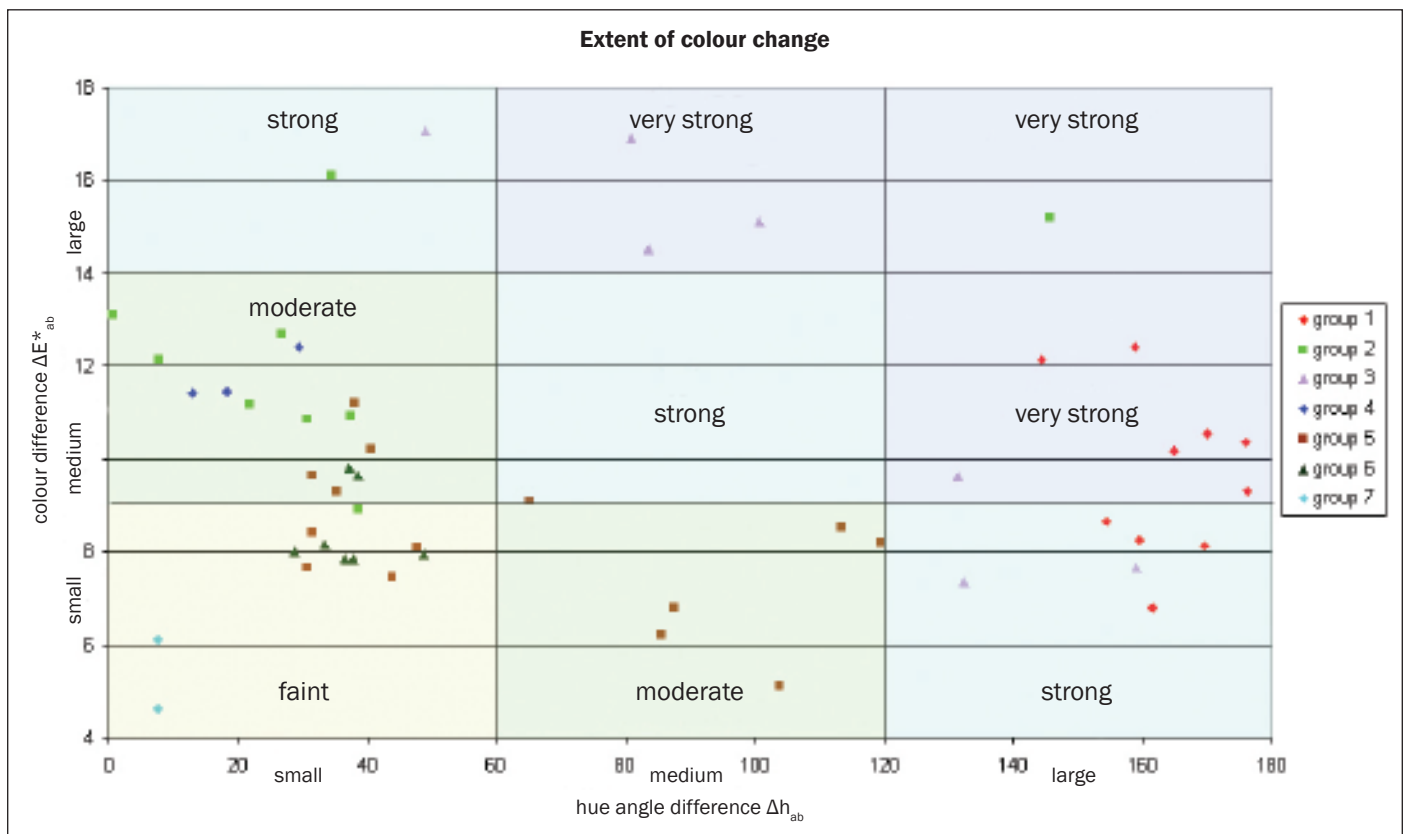


Figure 45: Correlation of the main colorimetric parameters hue angle difference and colour difference of colour-change garnets from Madagascar with the extent of colour change which is represented by broad categories such as faint, moderate, strong and very strong.

Colour-change garnets from Madagascar: variation of chemical, spectroscopic and colorimetric properties

(which can be calculated from lightness difference ΔL^* , colour difference ΔE_{ab}^* and chroma difference ΔC_{ab}^*) is not used in our discussion. In general, hue difference is only used for investigating samples with smaller hue angle differences (see colorimetric textbooks).

The colour differences ΔE_{ab}^* and the hue angle differences Δh_{ab} of the garnets are plotted in *Figure 42*.

On the basis of hue angle difference Δh_{ab} we can separate the garnet points into three groups with small (0° – 60°), medium (60° – 120°) and large (120° – 180°) hue angle differences (*Figure 45*). Only some of the garnets (all of Group 1, one of Group 2 and three of Group 3) show a colour change from green or bluish green in daylight to violet purple, purple, reddish purple or red purple in incandescent light and can be designated as garnets with an alexandrite-like colour change; this category has large hue angle differences above 120° . The second category with hue angle differences between 60° and 120° consists of six samples of Group 5 and three of Group 3. The remainder with hue angle differences below 60° consists of numerous garnets from different groups.

For garnets with both small and large hue angle differences there is an almost continuous range of colour difference ΔE_{ab}^* values. Thus it is difficult to categorize the samples on this basis. Furthermore, there is a clear gap in the centre of *Figure 45* for garnets with medium hue angle differences, i.e. we measured no garnets with these colorimetric parameters. The effect of various colour differences on samples with similar hue angle differences, i.e. on samples with small, medium or large hue angle differences, is demonstrated in *Figure 46 a–b*. From the samples selected it is evident that there is stronger colour change with increasing colour differences. Therefore the extent of colour change, especially for faceted gemstones, is not only dependent on Δh_{ab} variation but also on ΔE_{ab}^* .

For practical communication in the gem trade and use in gemmological laboratories it is highly desirable to

translate the numerical values of colour change, as measured by Δh_{ab} and ΔE_{ab}^* , into easily understandable terminology. One way of doing this is to subdivide the range of each parameter into three categories, called respectively small, medium and large (*Figure 45*). This produces nine areas containing four strengths of colour change, i.e. faint, moderate, strong and very strong. A second way is to subdivide the hue angle difference Δh_{ab} versus colour difference ΔE_{ab}^* diagram by diagonal northwest-southeast lines into four diagonal zones depicting faint, moderate, strong and very strong colour changes. This scheme would change the categories of a few borderline samples, but would not change the general scope and usefulness of the diagram; two options for different boundary positions are shown in *Figure 47 a,b*.

The parameters of the four vanadium- and chromium-free malaya garnets measured for comparison are located close to the values of low vanadium- and chromium-bearing garnets and lie in the 'faint' zone of colour change. Consequently, there is no physical basis for distinguishing samples with faint colour change from those with 'colour shift'.

For the four alexandrites with 'good' colour change examined for comparison, we obtained colour differences ΔE_{ab}^* from 15.2 to 21.6 and hue angle differences Δh_{ab} between 97° and 168° . Consequently, these four samples would be classified according to the scheme described above as alexandrites with very strong extent of colour change. Although the system needs testing further for alexandrites and other pleochroic gemstones to establish a standard procedure, provisionally it seems to be an adequate solution for describing the extent of colour change and for the clear separation and designation of these samples in laboratory practice.

Although many may not have thought of, let alone expressed, the concept, it is very desirable that gemstones have good colour or colours in both daylight and incandescent light. This depends on the respective chroma of the samples under different illuminants (*Figure 30*). The greater the chroma, the purer is the colour

observed. Good examples are garnets of Groups 1 and 2, with similar ranges of hue angles but different chroma, i.e. lower chromas in Group 1 and higher in Group 2 (*Figures 20a, 30, 31a and 32a*).

Most Group 1 garnets have equal or almost equal chroma in daylight and incandescent light as do some garnets in Groups 3 and 5. Garnets with high chroma in daylight and low chroma in incandescent light are represented by most of the samples in Group 2, while those with smaller chroma in daylight and higher chroma in incandescent light are in Groups 4, 6 and 7.

Samples with a significant colour change and high chromas for both daylight and incandescent light are considered as most attractive gems in the trade and by the consumer.

Our data focus on quantifying colour change behaviour in garnets and the colour parameters discussed are not yet adequate to predict colour behaviour in other gem species. In order to predict behaviour, the colour-change data will have to be augmented by data from a wide range of other gems in order to precisely locate the important factors in colour change.

In the gem trade, the designation 'colour-change' is frequently used as an attribute of quality. Another widely-accepted attribute of gemstones is rarity, and to maintain this concept we suggest the use of the attribute 'colour-change' only for gemstones with moderate, strong or very strong colour-change according to *Figures 45 and 47*. Furthermore, we suggest that stones falling in the faint category of colour change, which is common in some gem materials, should be described as having colour variation, and not to be labelled 'colour-change' stones. This would, for example, lead to a clear separation between alexandrites and those pale green or yellowish green chrysoberyls which show only a slight variation of colour upon change of illuminants. However, we must emphasize that — especially for the garnets examined in this paper — there is an almost continuous variability of both hue angle difference and colour difference.

Colour-change garnets from Madagascar: variation of chemical, spectroscopic and colorimetric properties

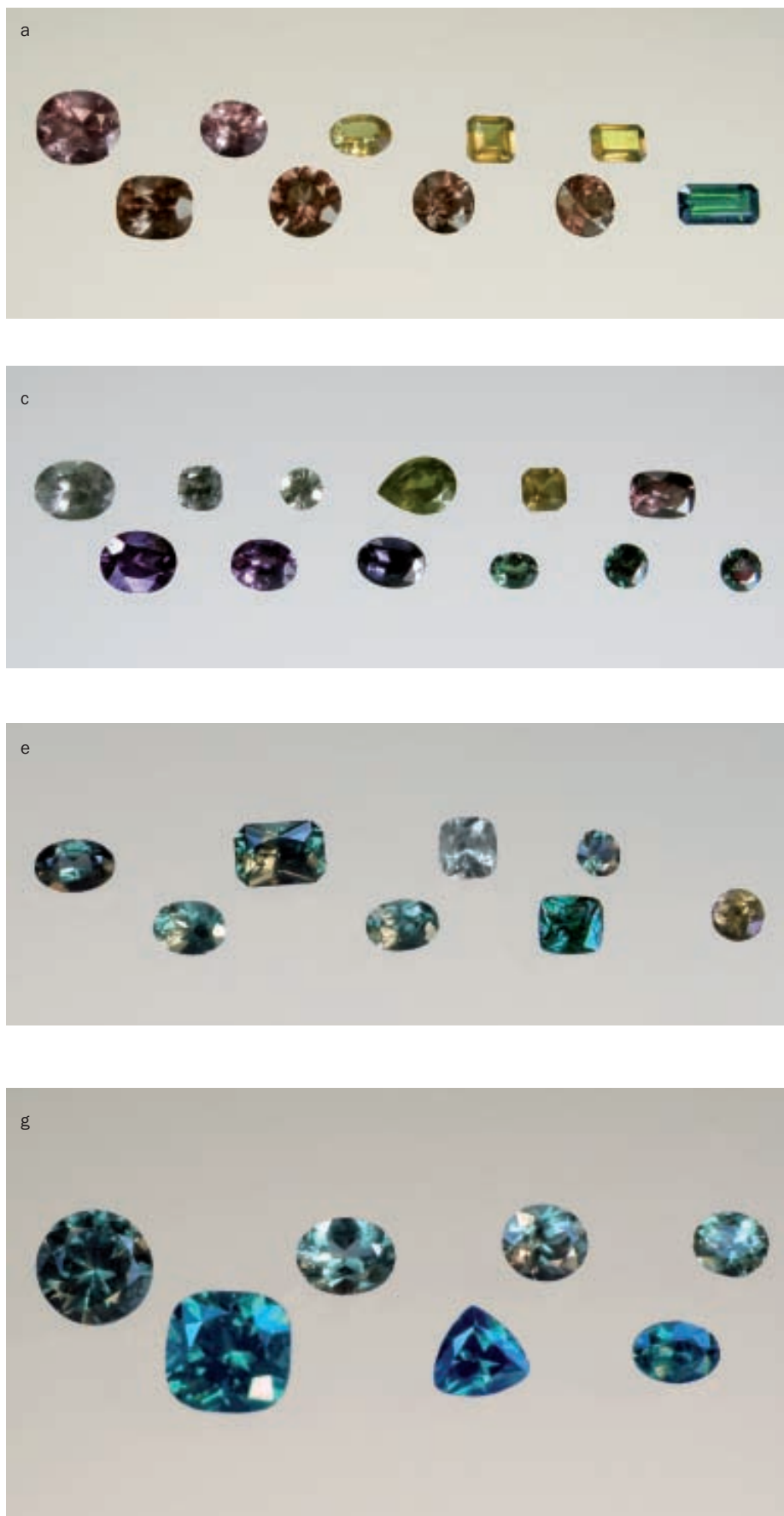
Figure 46: Colour change garnets assembled to demonstrate the faint, moderate, strong and very strong categories shown in Figure 45. Daylight colours are in a, c, e and g, and colours in incandescent light are in b, d, f and h. Garnets with faint colour change (a) and (b), upper row from left, two samples of Group 7, three of Group 5, lower row from left, four of Group 6, one of Group 2; size of the lower right sample 3.5 x 7.0 mm, weight 0.69 ct. Samples with moderate colour change (c) and (d), upper row from left, five samples of Group 5, one of Group 6, lower row from left, three of Group 4, three of Group 2; diameter of the lower right sample 4.5 mm, weight 0.44 ct. Garnets with strong colour change (e) and (f), upper row four samples of Group 1, lower row from left, four of Group 3, one of Group 5; diameter of the lower right sample 3.7 mm, weight 0.27 ct. Samples with very strong colour change (g) and (h), upper row four samples of Group 1, lower row three of Group 3; size of the upper right sample 4.4 x 5.0 mm, weight 0.48 ct.

We are also unable to predict for which general type of absorption spectrum in gem materials colour change is observable. Furthermore, it is outside the scope of this article to discuss the mechanism of colour change under illuminants other than D₆₅ and A and in all these materials in general.

In the absence of analytical equipment such as a colour spectrometers or spectrophotometers, values like colour difference or hue angle difference are not directly obtainable. Nevertheless, colorimetric parameters in daylight and incandescent light as well as the type and extent of colour change of gemstones can be determined by visual comparison with colorimetric standards. Some commercially available colorimetric standard sets (compare Figures 12 to 19) are based on the uniform CIELAB colour space. So, by visual estimation, the CIELAB coordinates a*, b* and L* are directly obtainable, and the chroma, hue angle, hue angle difference and colour difference may be calculated by simple mathematical equations. Only simple facilities are necessary:

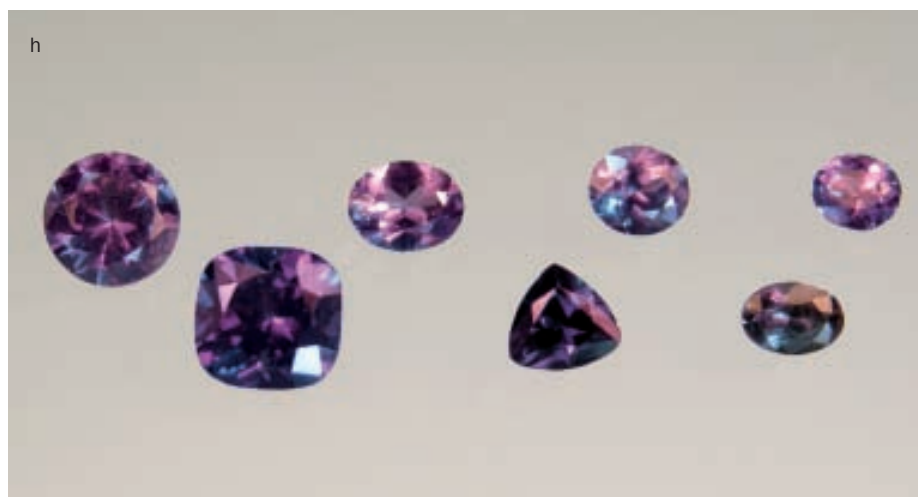
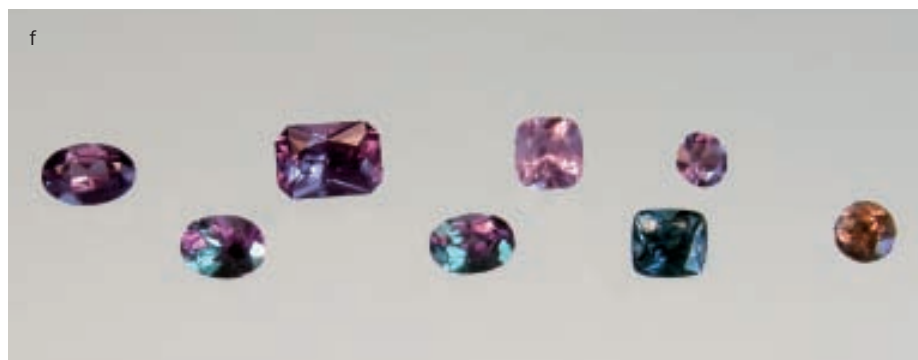
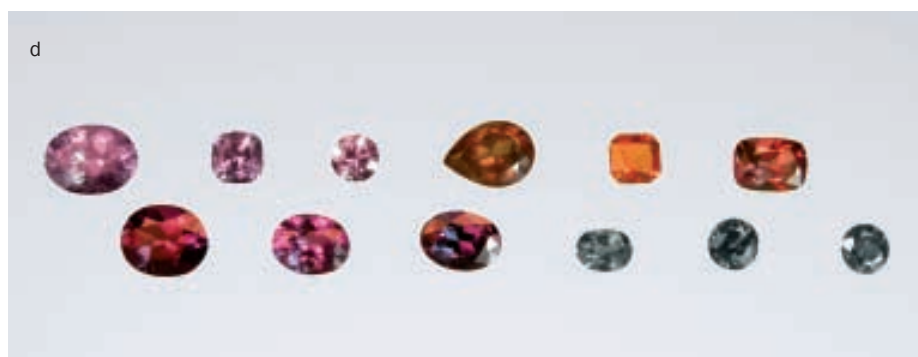
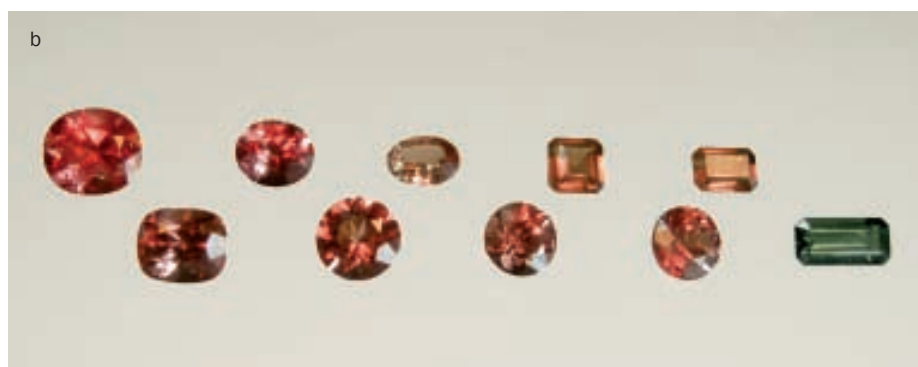
- Colour viewing box with light to medium grey walls.
- Bright but diffuse daylight-equivalent

Daylight



Colour-change garnets from Madagascar: variation of chemical, spectroscopic and colorimetric properties

Incandescent light



and incandescent light sources, mounted in the top of the viewing box, alternately switched on and off or alternately shielded, best used in a darkened room.

- Complete and uniform set of spectral reference colours for comparison with the gemstone being tested.
- If possible colour-change reference stones with known colorimetric parameters would be helpful.

A computer-based system for the determination of CIELAB parameters of gemstones has recently been described by Liu (2007) and Liu and Hurwit (2008).

Conclusions

The results presented lead to a more detailed understanding of the complex relationship of chemical composition and spectra with parameters describing colour and colour change for 52 colour-change garnets. However, no simple parameters were found that could enable one to predict colour and colour change over the whole group of samples.

The ratio spessartine : (goldmanite + uvarovite), which can be calculated easily from analytical data, provides a parameter which can be helpful in understanding the causes of colour and colour change and was useful to subdivide the garnets into two larger groups: the green to greenish blue, and the yellow green to orange in daylight. The colour differences for the garnets between daylight and incandescent light are generally correlated with their vanadium and chromium contents.

However, a wide range of minor elements in the garnets can cause very subtle differences in the absorption spectra of visually similar samples, and must be taken into account.

If the results of this study are applied in the gem trade and for practical work in the laboratory it is clear that colour change in gemstones should not be described without further specification. Although, in practice, a combination of effects is observed, an effort should be made to distinguish between

- a hue difference represented by the difference of the hue angle Δh_{ab} or

Colour-change garnets from Madagascar: variation of chemical, spectroscopic and colorimetric properties

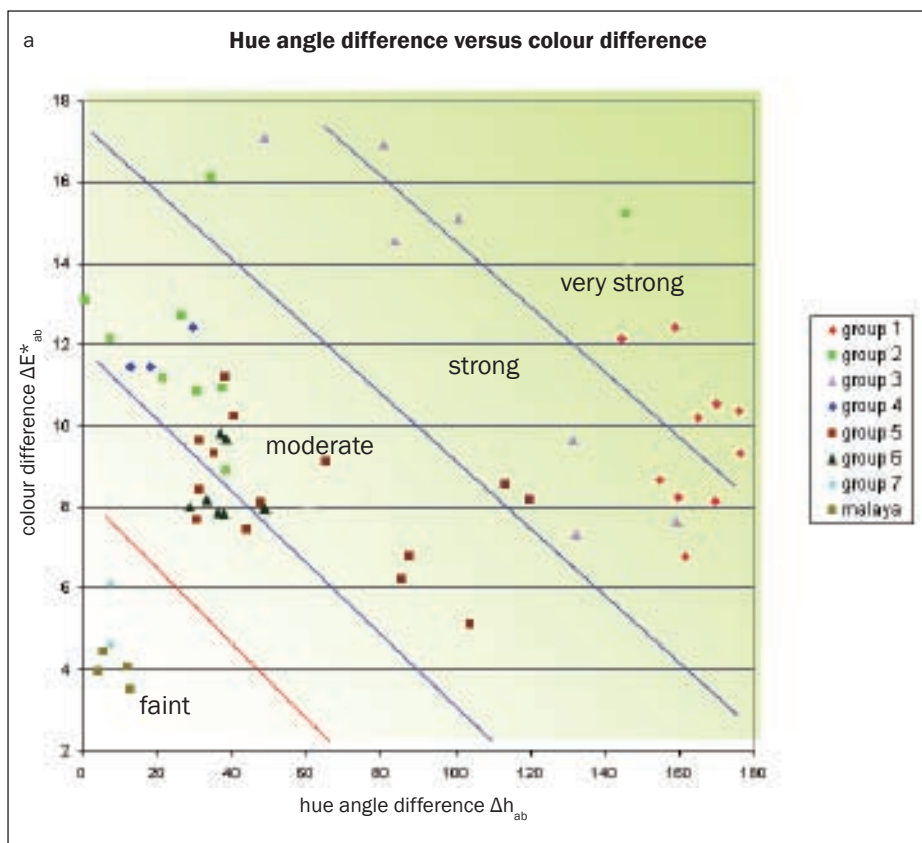


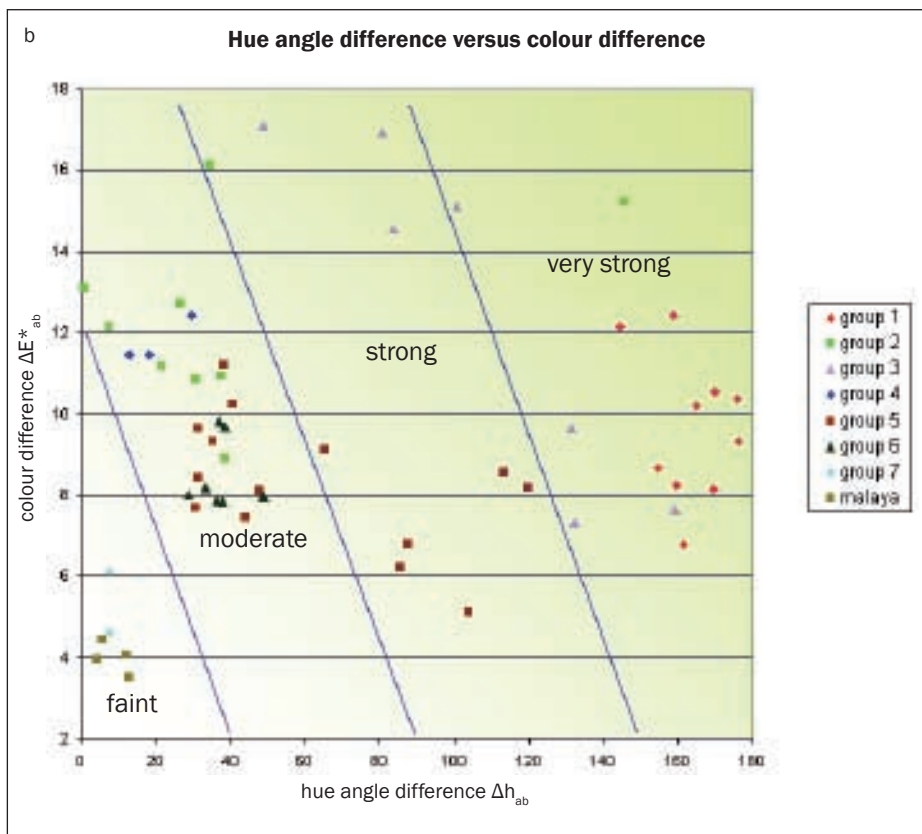
Figure 47 a,b: Graphs showing the correlation of the hue angle difference and colour difference of colour-change garnets from Madagascar with other possible groupings of the colour change behaviour into faint, moderate, strong and very strong. (a) This graph is almost consistent with Figure 45, i.e. only a few garnets grouped according to Figures 45 and 46 lie in neighbouring categories; according to the red line in this plot, the 'faint-moderate' boundary is shifted to include only garnets of Group 7 and malaya garnets (see Figures 37 and 38) in the 'faint' category, and most garnets of Groups 2, 4, 5 and 6 are 'moderate'. (b) Here, again, only samples of Group 7 and malaya garnets are 'faint', most samples of Groups 2, 4 and 6 are 'moderate', and half of Group 5 are 'moderate', and all samples of Groups 1 and 3 and half the samples of Group 5 are 'strong' or 'very strong'

- a colour change represented by the colour difference ΔE^*_{ab} or
- a chroma difference represented by different chroma C^*_{ab} under different illuminants.

Without this type of specification, the description of a gemstone as having a 'good' colour change is almost meaningless. Furthermore, the recent introduction of many more kinds of lights under which gems may be seen, only strengthens the case for a more precise description of colour behaviour using colorimetric parameters.

The terms 'alexandrite-effect' and 'alexandrite-like colour change' should only be used for stones with a hue change in the range of natural alexandrite (as historically described), i.e. from green, bluish green or blue green in daylight to violet purple, purple, reddish purple, red purple, purplish red or red in incandescent light. For other colours the approximate hues and chromas under both illuminants should be given. This information (hue and chroma under both illuminants, see Figure 30) contains the necessary information about hue angle difference Δh_{ab} and colour difference ΔE^*_{ab} (see also Figures 42, 45 and 47).

Semi-quantitative measures of colour change can be specified as faint, moderate, strong or very strong according



Colour-change garnets from Madagascar: variation of chemical, spectroscopic and colorimetric properties

to a combination of two fundamental parameters, i.e. hue angle difference and colour difference. But in the gem trade we suggest that the faint category stones are referred to as showing 'colour variation' not 'colour change' and that the term 'colour shift' be abandoned.

References

- Amthauer, G., 1976. Kristallchemie und Farbe chromhaltiger Granate. *Neues Jahrbuch für Mineralogie Abhandlungen*, **126**(2), 158–86
- Boguth, W., 1990. Microscopic colour measurement on mineral sections and precious stones. *Zeiss Information*, **30**(100E), 12–15
- Bosshart, G., and Balmer, W.A., 2006. Rare reverse color change in a blue zircon from Myanmar (Burma). *Gems & Gemology*, **42**(3), 94–5
- Bosshart, G., Frank, E., Hänni, H.A., and Barot, N., 1982. Blue colour-change kyanite from East Africa. *Journal of Gemmology*, **18**(3), 205–12
- CIE Commission Internationale de l'Éclairage, 1986. *Colorimetry*. 2nd edn, Publication CIE No. 15.2 (1986); Vienna, Austria
- CIE Commission Internationale de l'Éclairage, 1995. Technical Report. Method of measuring and specifying colour rendering properties of light sources. CIE 13.3-1995; Vienna, Austria
- CIE Commission Internationale de l'Éclairage, 2004. Technical Report. Colorimetry. 3rd edn, CIE 15: 2004; Vienna, Austria
- Cossa, A., and Arzruni, A., 1883. Ein Chromturmalin aus den Chromeisenlagern des Urals. *Zeitschrift für Krystallographie und Mineralogie*, **7**, 1–16
- DIN 33872-1 to 33872-6, 2007. Verfahren zur Kennzeichnung der relativen Farbwiedergabe mit JA/NEIN Kriterien. Parts 1 to 6, Berlin, November 2007
- Gübelin, E., and Schmetzer, K., 1982. Gemstones with alexandrite effect. *Gems & Gemology*, **18**(4), 197–203
- Halvorsen, A., 2006. The Usambara effect and its interaction with other colour change phenomena. *Journal of Gemmology*, **30**(1/2), 1–21
- Hänni, H.A., 1983. Weitere Untersuchungen an einigen farbwechselnden Edelsteinen. *Zeitschrift der Deutschen Gemmologischen Gesellschaft*, **32**(2/3), 99–106
- Henn, U., and Milisenda, C.C., 1997. Neue Edelsteinvorkommen in Tansania: Die Region Tundura-Songea. *Zeitschrift der Deutschen Gemmologischen Gesellschaft*, **46**(1), 29–43
- Hunt, R.G.W., 2004. *The reproduction of colour*. 6th edn. John Wiley & Sons, Chichester, UK
- Johnson, M.L., and Koivula, J.I. (Eds), 1996. Gem News: A second Sri Lankan locality for color-change garnet. *Gems & Gemology*, **32**(4), 285–6
- Johnson, M.L., and Koivula, J.I. (Eds), 1998. Gem News: Color-change pyrope-spessartine garnet, also from Madagascar. *Gems & Gemology*, **34**(3), 222–3
- Kelly, K.L., 1943. Color designations for lights. *Journal of the optical society of America*, **33**(11), 627–32
- Krzemnicki, M.S., Hänni, H.A., and Reusser, E., 2001. Colour-change garnets from Madagascar: comparison of colorimetric with chemical data. *Journal of Gemmology*, **27**(7), 395–408
- Kuehni, R.G., 1997. *Color: an introduction to practice and principles*. John Wiley & Sons New York, USA
- Kuehni, R.G., 2004. Variability in unique hue selection: a surprising phenomenon. *Color research and application*, **29**(2), 158–62
- Liu, Y., 2007. *Method and system for color grading of gemstones*. United States Patent Application Publication US 2007/0153256 A1, published 5 July 2007
- Liu, Y., and Fry, B.A., 2006. A colorimetric study of a tourmaline from Mozambique which shows a reverse alexandrite effect. *Journal of Gemmology*, **30**(3/4), 201–6
- Liu, Y., and Hurwit, K.N., 2008. The TrueGemColor system: a new computer color imaging system based on a uniform CIELAB color space for color grading of gemstones. *Gemmologie. Zeitschrift der Deutschen Gemmologischen Gesellschaft*, **57**(3–4), 133–42
- Liu, Y., Shigley, J., Fritsch, E., and Hemphill, S., 1994. The 'alexandrite effect' in gemstones. *Color research and application*, **19**(3), 186–91
- Liu, Y., Shigley, J.E., Fritsch, E., and Hemphill, S., 1999a. A colorimetric study of the alexandrite effect in gemstones. *Journal of Gemmology*, **26**(6), 371–85
- Liu, Y., Shigley, J.E., and Halvorsen, A., 1999b. Colour hue change of a gem tourmaline from Umba Valley, Tanzania. *Journal of Gemmology*, **26**(6), 386–96
- MacEvoy, B. 2005. See Web list p.282
- Manson, D.V., and Stockton, C.M., 1984. Pyrope-spessartine garnets with unusual color behavior. *Gems & Gemology*, **20**(4), 200–7
- Milisenda, C.C., 2003. Changierende Granate aus Nigeria. *Zeitschrift der Deutschen Gemmologischen Gesellschaft*, **52**(1), 3–5
- Nassau, K. (Ed.), 1998. *Color for science, art and technology*. Elsevier, Amsterdam, The Netherlands
- Ohta, N., and Robertson, A.R., 2005. *Colorimetry: fundamentals and applications*. John Wiley & Sons, Chichester, England
- von Pott, H.A.G., 1842. Geschichte und wissenschaftliche Beschäftigungen der in St. Petersburg gestifteten russisch-kaiserlichen Gesellschaft für die gesamte Mineralogie von 1817 bis 1842. *Schriften der in St. Petersburg gestifteten russisch-kaiserlichen Gesellschaft für die gesamte Mineralogie*, I. Band, I. Abteilung, 116–26
- Richter, K., 1996. *Computergrafik und Farbmatrik*. VDE-Verlag, Berlin und Offenbach, Germany
- Richter, K., 2007. See Web list p.282

Colour-change garnets from Madagascar: variation of chemical, spectroscopic and colorimetric properties

- Richter, K., 2008a. See Web list
- Richter, K., 2008b. *Relative Elementary Colour System (RECS)*. Eigenverlag, Berlin, Germany
- Robertson, A.R., 1994. Color order systems – diversity and congruence. *Vision*, **6**, 165–8
- Schmetzer, K., Bank, H., and Gübelin, E., 1980. The alexandrite effect in minerals: chrysoberyl, garnet, corundum, fluorite. *Neues Jahrbuch für Mineralogie Abhandlungen*, **138**(2), 147–64
- Schmetzer, K., and Gübelin, E., 1980. Alexandrite-like natural spinel from Sri Lanka. *Neues Jahrbuch für Mineralogie Monatshefte*, **1980**(9), 428–32
- Schmetzer, K., and Ottemann, J., 1979. Kristallchemie und Farbe Vanadiumhaltiger Granate. *Neues Jahrbuch für Mineralogie Abhandlungen*, **136**(2), 146–68
- Schmetzer, K., Hainschwang, T., Kiefert, L., and Bernhardt, H.-J., 2001. Pink to pinkish orange malaya garnets from Bekily, Madagascar. *Gems & Gemology*, **37**(4), 296–308
- Schmetzer, K., Hainschwang, T., Bernhardt, H.-J., and Kiefert, L., 2002. New chromium- and vanadium-bearing garnets from Tranoroa, Madagascar. *Gems & Gemology*, **38**(2), 148–55
- Schmetzer, K., and Bernhardt, H.-J., 1999. Garnets from Madagascar with a color change of blue-green to purple. *Gems & Gemology*, **35**(4), 196–201
- Stockton, C.M., 1982. Two notable color-change garnets. *Gems & Gemology*, **18**(2), 100–1
- Stockton, C.M., and Manson, D.V., 1985. Unusual color-change garnet. *Gems & Gemology*, **21**(2), 116–17
- Taran, M.N., Langer, K., Abs-Wurmbach, I., Frost, D.J., and Platonov, A.N., 2004. Local relaxation around $^{60}\text{Cr}^{3+}$ in synthetic pyrope-knorringite garnets, $^{80}\text{Mg}_3^{60}(\text{Al}_{1-x}\text{Cr}_x^{3+})_2^{64}\text{Si}_3\text{O}_{12}$, from electronic absorption spectra. *Physics and Chemistry of Minerals*, **31**, 650–7
- Taran, M.N., Langer, K., and Geiger, C.A., 2002. Single-crystal electronic absorption spectroscopy of synthetic chromium-, cobalt-, and vanadium-bearing pyropes at different temperatures and pressures. *Physics and Chemistry of Minerals*, **29**, 362–8
- Wyszecki, G., and Stiles, W.S., 1982. *Color Science: concepts and methods, quantitative data and formulae*. 2nd Edn. John Wiley & Sons, New York, USA
- Zoysa, E.G., 1999/2000. Gem deposits in Sri Lanka with special emphasis on unusual types of gems (part 3). *Journal of the Gemmological Association of Hong Kong*, **21**, 38–43

Web list

- MacEvoy, B., 2005. Handprint: color vision. <http://handprint.com/LS/CVS/color.html> (different chapters updated and revised at different times)
- Richter, K., 2007. Colour definition and workflow for relative affini colour image reproduction in offices. <http://www.ps.bam.de/BAMWS07E.PDF>
- Richter, K., 2008a. Colorimetric supplement for DIN 33872–1 to –6. <http://www.ps.bam.de/D33872-AE.PDF>

Illustrations

Unless otherwise stated in the captions, all figures (photographs and diagrams) were produced by and are the copyright of the authors.

The Authors**K. Schmetzer**

D–85238 Petershausen, Germany
email: SchmetzerKarl@hotmail.com

H.-J. Bernhardt

ZEM, Institut für Geologie, Mineralogie und Geophysik, Ruhr-University,
D–44780 Bochum, Germany
email: Heinz-Juergen.Bernhardt@rub.de

G. Bosshart

CH–8810 Horgen, Switzerland
email: george.bosshart@swissonline.ch

T. Hainschwang

GEMLAB Gemmological Laboratory, FL–9496 Balzers, Liechtenstein
email: thomas.hainschwang@gemlab.net

The characteristics of red andesine from the Himalaya Highland, Tibet

Ahmadjan Abduriyim

Abstract: Natural-coloured Tibetan andesine has been mined using simple hand tools from an alluvial deposit at Bainang County in the Xigazê area of Tibet. The gem-quality andesine is derived from Tertiary–Quaternary volcanogenic sediments related to Jurassic–Cretaceous volcanic rocks. Weathering and alluvial transport have resulted in round detrital crystals, most of which have an orangy-red body colour; a few stones have bicoloured zones of red and green. Top-quality stones in deep red are characterized by fine granular inclusions and some twin lamellae. Poorer qualities of andesine in orange-red and reddish-orange generally contain abundant turbid irregular colour patches, irregular dislocations, tubes and parallel lath-like hollow channels and a few tiny platelets of native copper. EPMA chemical analyses indicate a composition range of $(K_{0.03}Na_{0.46-0.49})Ca_{0.46-0.49}Al_{1.43-1.48}Si_{2.51-2.53}O_8$, the equivalent ratios of albite:anorthite:orthoclase being $Ab_{46.96-49.79}:An_{46.72-49.94}:Or_{3.03-3.50}$, which indicates andesine near the andesine-labradorite border. The lattice parameters are $a_0=8.161-8.193 \text{ \AA}$, $b_0=12.849-12.919 \text{ \AA}$, $c_0=7.105-7.126 \text{ \AA}$, $\alpha=93.26^\circ-93.74^\circ$, $\beta=116.27^\circ-116.38^\circ$, $\gamma=89.93^\circ-90.16^\circ$, and the RIs are $\alpha=1.550-1.551$, $\beta=1.555-1.556$, $\gamma=1.560-1.561$. LA-ICP-MS analysis indicates the presence of the trace elements; Li, Mg, K, Sc, Ti, Mn, Fe, Cu, Ga, Sr and Ba. An estimate of the degree of structural ordering of Al in tetrahedral sites in Tibetan andesine was made by measuring the parameters $\Delta=2\theta(1\bar{3}1) - 2\theta(131)$ and γ , from the X-ray powder diffraction pattern. Both Δ and γ values are plotted as a function of mole percent anorthite (An), and indicate that Tibetan andesine has a low degree of Al/Si ordering with only 22–29 percent of Al lying in the tetrahedral T1(o) site; this indicates that it formed at about 800 °C in a volcanic environment. By plotting Ba/Sr versus Ba/Li ratios Tibetan red andesine can be differentiated from andesines of Inner Mongolia.

Keywords: andesine, EPMA, Inner Mongolia, labradorite, LA-ICP-MS, Tertiary–Quaternary, volcanogenic sediment



The characteristics of red andesine from the Himalaya Highland, Tibet



Figure 1: Since 2007, natural-coloured orange-red and red-green pleochroic andesines have been recovered from a deposit in the Xigazê area. The faceted stones are up to 5 ct; rough samples (not shown) are up to 30 ct. Courtesy of King Star Jewellery Co. and M. P. Gem Corp. Photo by M. Kobayashi.

Introduction

A natural gem-quality plagioclase feldspar (andesine) has become available recently from Tibet. Orange-red or intense red andesine straight from the ground is a brilliant and treasured gemstone due to its rarity and colour, and the green variety is even rarer. In late 2005, a red andesine called 'Tibetan sunstone' was supplied by Do Win Development Co. Ltd of Tianjin, China, which reported its origin as Nyima in central Tibet (Laurs, 2005). Later, at the February 2007 Tucson gem shows, King Star Jewellery Co. (Hong Kong) and M.P. Gem Corp. (Kofu, Japan) introduced a similar red andesine from Tibet called 'Lazasine' and raised again the gem value of plagioclase sunstone (Figure 1). However, a large supply of red andesine allegedly from China, was offered for sale as the official gemstone of the 2008 Summer Olympic Games in Beijing. Despite claims to the contrary, there has been widespread suspicion that the red Chinese andesines are diffusion-treated. In the light of this, the author investigated the mine in Tibet and also localities in the Inner Mongolian Autonomous Region in October–November 2008, to confirm the authenticity of the sources stated for

the andesine (Abduriyim, 2008). The visit to Tibet was made possible with the cooperation of the mine owner Li Tong in Tibet, of the mine investors of Wong Ming (King Star Jewellery Co.) and of Christina

Iu (M.P. Gem Corp.). Also participating in the expedition were Masaki Furuya of the Japan Germany Gemmological Laboratory, Kofu, Japan, David Chiang of BBJ Bangkok Ltd, Bangkok, and Marco Cheung of Litto Gems Co. Ltd, Hong Kong. This paper focuses on describing the geographical location of the andesine in Tibet, its recovery and its properties which are of interest to the gem industry.

Location and access

The Tibetan andesine mine is located at Bainang County (29.03984°N, 89.38791°E), 70 km south-east of the region's second largest city, Xigazê (or Shigatse), in southern Tibet (Qin Zang Gao Yuan) (Figure 2). From the capital city of Lhasa, a well-paved road leads 280 km to Xigazê city, five hours drive in a van, and the road lies at an elevation between 4000 and 5000 m. During the winter season, the road is frozen and it is difficult to reach this city. It is another one to two hours from Xigazê on a mixture of paved and dirt roads to the mining area. The mine is located at an elevation of more than 4000 m, in freezing temperatures with thin oxygen.



Figure 2: The andesine mine, marked with crossed hammers, is in the south of Bainang County, southern Tibet, close to the border with Bhutan, and at around 4000 m elevation.

The characteristics of red andesine from the Himalaya Highland, Tibet

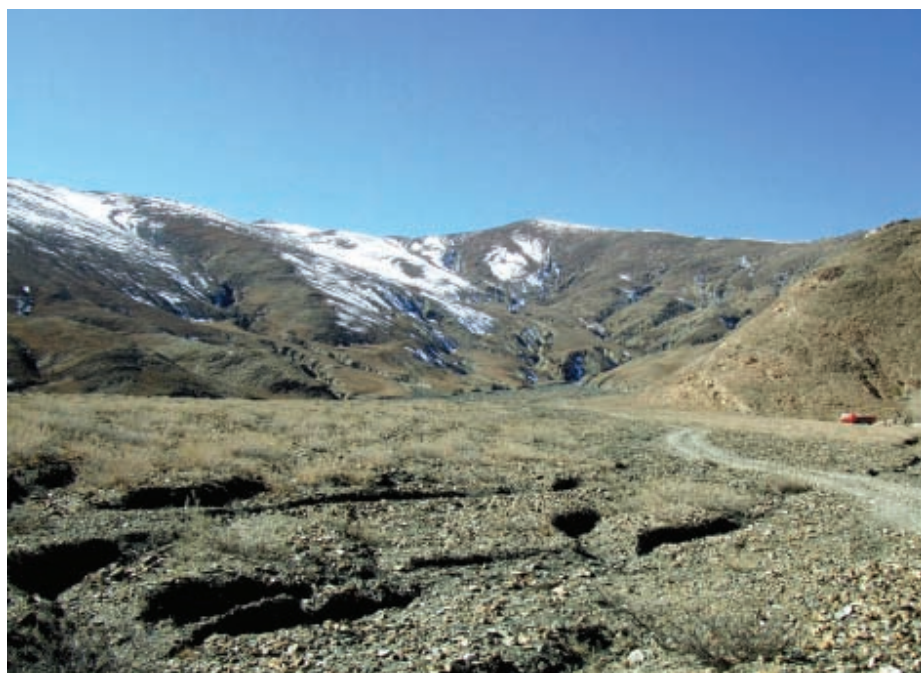


Figure 3: Red andesine is recovered from secondary deposits located at the base of the mountain on the far right and left (here, looking west). The mine site is divided into north and south areas. Photo by A. Abduriyim.

Twenty to thirty local Tibetan families live there, and fewer than ten miners were digging pits near a riverbed when we visited. Without authorization from the Chinese government and without local permission, foreigners are not permitted to visit this area. According to the miners, red andesine was originally found in this area in the 1970s, and beads of this material appeared in Lhasa's largest bazaar — Bakuo Street — in 2003. However, andesine was not mined officially until 2006 when commercial mining began in January under the supervision of Li Tong. The work is not mechanized and is done by hand from April to November.

Geological setting and mining

The andesine mine is located in the alluvium of a riverbed at the foot of a mountain. This terrain may derive from an ice sheet. The site is divided into north and south areas with a total coverage spanning 3–4 km east west and 5–7 km north south (Figure 3). The surface layer is weathered and consists of humic soil 0.5–3 m thick. Beneath this is greenish grey or dark grey sand/gravel in the southern area, and yellowish-red or greenish-grey

soil in the northern area which contain the andesine (Figure 4a and b). The andesine-bearing layers are apparently derived from Quaternary and Tertiary volcano-sedimentary deposits. The Chengdu Institute of Multipurpose Utilization of Mineral Resources, China Geological Survey, has recently carried out regional geological mapping in the Qin Zang Gao Yuan (Tibet highland) area (Figure 5), but unfortunately the scale was not appropriate for any detail to be recorded for the mine area of Bainang County. A visit to the summit in the mining area revealed large quantities of late Jurassic to early Cretaceous detrital (clastic) and mixed with volcanic rocks (Figure 6), and observations on these indicated that andesine crystals may grow to some size underground and then be carried to the surface with magma during eruption of the volcano. However, the author did not find any such crystals in the volcanic rock at the time of visiting. Weathering and ice transport of the primary deposits has resulted in secondary alluvial deposits on the lower parts of the mountain. These accumulations appear to have been concentrated across a wide area by water from seasonal snowmelt. In the southern area, mining activities are limited to a few small tunnels penetrating



Figure 4: (a) Tibetan andesines are found in dark grey sand and gravel or soil in the southern mine area. (b) Andesine-bearing yellowish-red or greenish-grey soil in the northern area of the mine. A shaft was sunk several metres deep but mining there was discontinued after the devastating Chengdu earthquake. Photos by A. Abduriyim and M. Furuya.



Figure 6: Near the summit above the southern area of the mine area there is a contact (on the extreme left of the photo) between the main weathered sediment and massive clastic rock mixed with volcanic rock. Photo by M. Furuya.

The characteristics of red andesine from the Himalaya Highland, Tibet

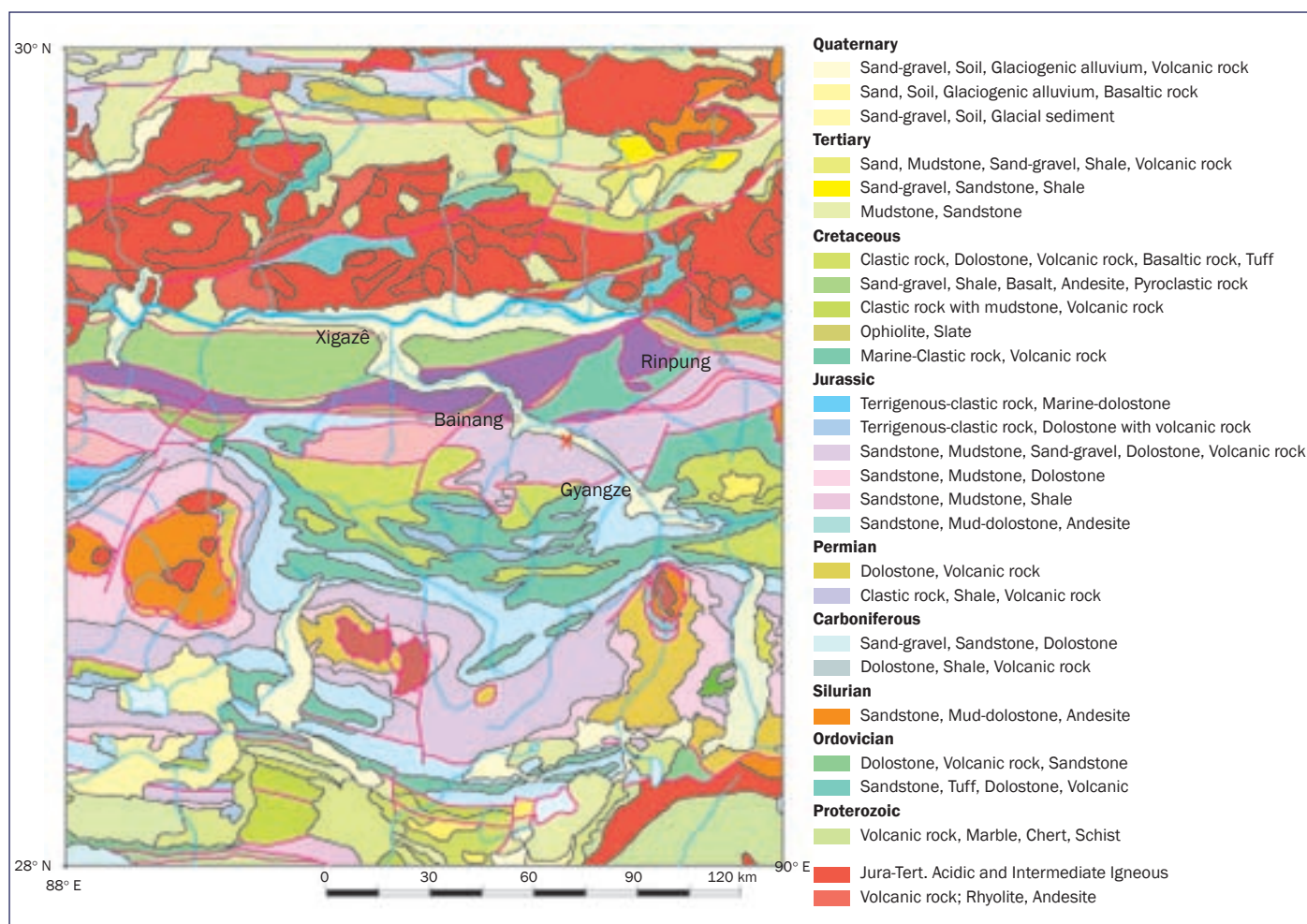


Figure 5: Geological sketch map of Bainang County (modified after 'Qin Zang Gau Yuan and Adjacent land Geological Map' made by the Chengdu Institute of Multipurpose Utilization of Mineral Resources, China Geological Survey, 2004). The Bainang deposit lies in alluvial rocks derived from various volcanic and clastic rocks.

several metres horizontally into the andesine-bearing horizons. These tunnels do not exceed 2–2.5 m² and 1–4 m depth. Local miners working in family groups use picks and shovels for extracting the gravel and searching for gems (Figure 7a, b and c). The andesine crystals are concentrated in clusters of up to 20 (100–200 g total) in a matrix of sand, gravel or soil (Figure 8a and b). The excavated material is placed on a hand-operated shaker screen to remove the soil and small pebbles and then the rough andesine is picked out by hand. In the northern mining area, a shaft was sunk several metres deep but mining there was discontinued after the devastating Chengdu earthquake in May 2008.

Alluvial transport has rounded the crystals, and although most were found as translucent to transparent stones that are

<1 cm in diameter (Figure 9), the largest pieces reached 4 cm. Approximately 80 percent of crystals are orangy red and the remainder are mostly deep red, but in the southern mining area there are a few red and green pleochroic crystals and bicoloured crystals; we did not see any andesines that were completely brown, yellow or colourless. The annual production from the region is estimated to be 700–800 kg, of which 4–6 percent crystals are top gem quality (T. Li and M. Wong, pers. comm., 2008). The cleaned rough crystals are pre-sorted into four grades; the finest rough will be faceted and the lower-grade stones will be fashioned as cabochons and beads in Guang Zhou, China (Figure 10).

Materials and methods

For the investigation, 210 pieces of reddish-orange and orange-red rough crystals of Tibetan natural andesine were collected by the author from the alluvial sediments in Bainang County. All samples (up to 34 ct; see e.g. Figure 11) from this region were polished with two parallel windows, and were cleaned with acetone and aqua regia in an ultrasonic bath to remove surface contamination. All were characterized using traditional gemmological methods, to determine their optical and physical properties, and the following instruments were used for spectra collection and other measurements:

1. SHIMATSU-2450 polarized UV-Vis-NIR spectrometer to record the 220–860 nm range, operating in absorption-mode, equipped with intergrating-sphere and tungsten lamp; all samples were measured.

The characteristics of red andesine from the Himalaya Highland, Tibet



Figure 7 (a,b,c): The andesine is recovered from a series of tunnels, with the local Tibetan miners using simple hand tools and hand picking. Photos by A. Abduriyim.



Figure 8 (a,b): Rounded crystals of red Tibetan andesine in a matrix of sand and gravel at the entrance to the pit and inside the pit. Photos by A. Abduriyim.



Figure 9: Most of the orangy red andesine crystals are generally <1 cm in diameter, but some of the largest pieces reach 4 cm. Photo by A. Abduriyim.

The characteristics of red andesine from the Himalaya Highland, Tibet

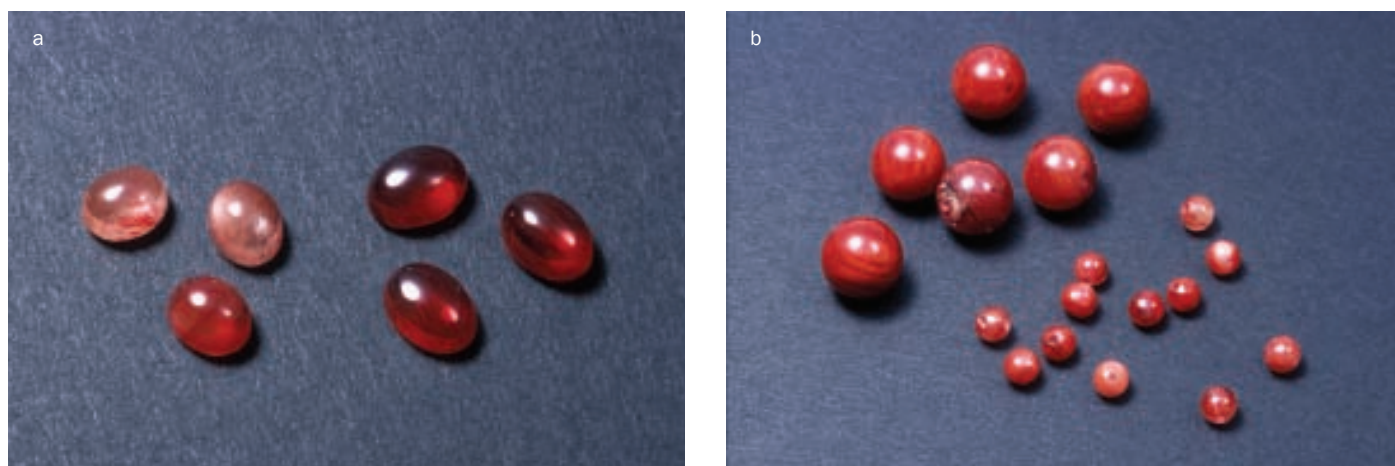


Figure 10: The Tibetan rough andesine is fashioned as cabochons (a) and beads (b) in China depending on its colour and transparency. Photo by M. Kobayashi. Courtesy of M.P. Gem Corp.

2. SHIMATSU Prestige-2000 spectrometer to record the $5000\text{--}400\text{ cm}^{-1}$ infrared range with a resolution of 4 cm^{-1} , operating in reflectance mode by a diffuse reflectance accessory, all samples were measured.
3. X-ray powder diffraction measurements were then carried out on ten samples from the Bainang region (TB-XRD-001-010), to calculate the lattice parameters of the andesine. Data collection was made using a Shimatsu LabX XRD-6000 X-ray powder diffractometer, using $\text{CuK}\alpha$ radiation ($\lambda=1.5406\text{\AA}$) and a beam of 40 kV, 30 mA. Diffraction data were collected over $3\text{--}70^\circ 2\theta$, with steps of $0.02^\circ 2\theta$, and a counting time of 1 sec/step. This has enabled the lattice (unit cell) parameters to be calculated by

the least-squares method using the CELLCalc software.

4. Chemical compositions of ten samples (TB-CH-R001-002 in deep red, TB-CH-OR001-004 in orange-red, TB-CH-RO001-003 reddish orange and TB-CH-RG001 bicoloured red-green) were obtained by electron probe microanalysis (EPMA) using a JEOL-8500 fitted with wavelength dispersive spectrometers (WDS), and using an accelerating voltage of 15 kV, a current of 7 nA, and counting times of 20 sec on peaks and 5 sec on backgrounds. Natural albite ($\text{NaAlSi}_3\text{O}_8$) for Na and Si, orthoclase (KAlSi_3O_8) for Al and K, wollastonite (CaSiO_3) for Ca, hematite (Fe_2O_3) for Fe, synthetic tenorite (CuO) for Cu and synthetic (SrTiO_3) for Sr were used as standards.
5. LA-ICP-MS trace element analyses of 56 samples (6 red TB-CH-R001-006, 30 orange-red TB-CH-OR001-030, 15 reddish-orange TB-CH-RO001-015, and 5 bicolour red-green TB-CH-RG001-005) were obtained using the laser ablation system NEWWAVE research UP-213 attached to an Inductively Coupled Plasma Mass Spectrometer (ICP-MS) Agilent 7500a series. Operating conditions were set as; 10 Hz repetition rate, 80 μm spot diameter, 25 second laser dwell time. Three spots were ablated on each sample. Calibration was done using NIST SRM 610, 612 multi-element glass as external element standard, with Al as the internal

Table I: Properties of gem-quality Tibetan andesine.

Colour	brownish-red, reddish-orange, orange-red and deep red bicoloured; red-green, red-colourless
Appearance	elongate habit with rounded faces, some cleavage surfaces, surface etching, melted glassy surface, transparent and translucent
RI	$\alpha=1.550\text{--}1.551$, $\beta=1.555\text{--}1.556$, $\gamma=1.560\text{--}1.561$
Birefringence	0.009–0.010
Optic sign	biaxial positive
SG	2.67–2.72
Pleochroism	weak
UV fluorescence	
long-wave	weak chalky orange
short-wave	dark red or inert
Chelsea Colour Filter	red
Spectroscope	broad absorption at 560 , very weak band at 630 nm
Internal characters	twin lamellae, lath-like hollow channels, pipe-like growth tubes, irregular dislocations, irregular colour patches, turbid milky granular clouds, fissures, discoid fractures, cleavage cracks, gas bubbles, negative crystals, tiny native-copper colloidal grains or platelets
Lattice parameters	$a_0=8.161\text{--}8.193(26)\text{ \AA}$, $b_0=12.849\text{--}12.919(16)\text{ \AA}$, $c_0=7.105\text{--}7.126(14)\text{ \AA}$, $\alpha=93.26^\circ\text{--}93.74^\circ$, $\beta=116.27^\circ\text{--}116.38^\circ$, $\gamma=89.93^\circ\text{--}90.16^\circ$.

The characteristics of red andesine from the Himalaya Highland, Tibet



Figure 11: A pile of andesine rough (behind) collected from the Bainang mine in Tibet. These untreated rough materials of various colours (2.4–34.42 ct), are rounded and have a water-worn appearance. Parallel 'windows' were polished on two sides of each crystal to enable thorough examination. Cut samples (3.52–4.95 ct) in the foreground were supplied by M. P. Gem Corp., Japan. Photo by M. Kobayashi.

standard element based on an average Al_2O_3 concentration of 27.7% (Al, 14.7 wt.%) which was determined by EPMA.

6. The nanostructure analysis of one sample (TB-TEM-001) was carried out using a high-voltage and high resolution transmission electron microscope (TEM), JEM-3200FSK, operated at 300 kV.

Characteristics of the Tibetan andesine

After cleaning with acetone and aqua regia in an ultrasonic bath, most rough andesine crystals exhibit a highly saturated body colour, ranging from brownish-red, through reddish-orange, orange-red to deep red. Bicoloured stones, green in the centre surrounded by a red rim, are very rare; the sharp boundary of green and red can be seen in *Figure 12a–d*. Most stones also have colourless zones that reach the crystal surface. The transparency of a crystal depends on the content and concentration of inclusions. None of the samples exhibit a good pinacoidal crystal form but have a water-worn appearance, generally elongated with rounded faces, a

few with broken cleavage surfaces, some andesines also have embayed areas that appear to have been created by chemical etching and some areas show a melted glassy surface (*Figure 12e*).

Refractive indices and specific gravities of all Tibetan samples fall in the range for plagioclase feldspar; $\alpha=1.550\text{--}1.551$, $\beta=1.555\text{--}1.556$, $\gamma=1.560\text{--}1.561$, and are consistent with the variety andesine ($\text{An}_{30\text{--}50}$); their birefringence is 0.009–0.010 and optic sign is biaxial positive. The SG was determined with a hydrostatic balance and ranges from 2.67–2.72. Pleochroism is weak. The andesines are weak chalky orange under long-wave UV, and dark red or inert under short-wave UV radiation. Under a Chelsea Colour Filter the andesine remains red. The gemmological properties of the Tibetan samples are summarized in *Table I*. Some red stones have a green hue on a white board in diffused light, and a red-green pleochroic stone appears red in white incident light.

Examination with a gemmological microscope revealed that most of the Tibetan samples contain prominent twin lamellae, parallel lath-like hollow channels and pipe-like tubes which are arranged

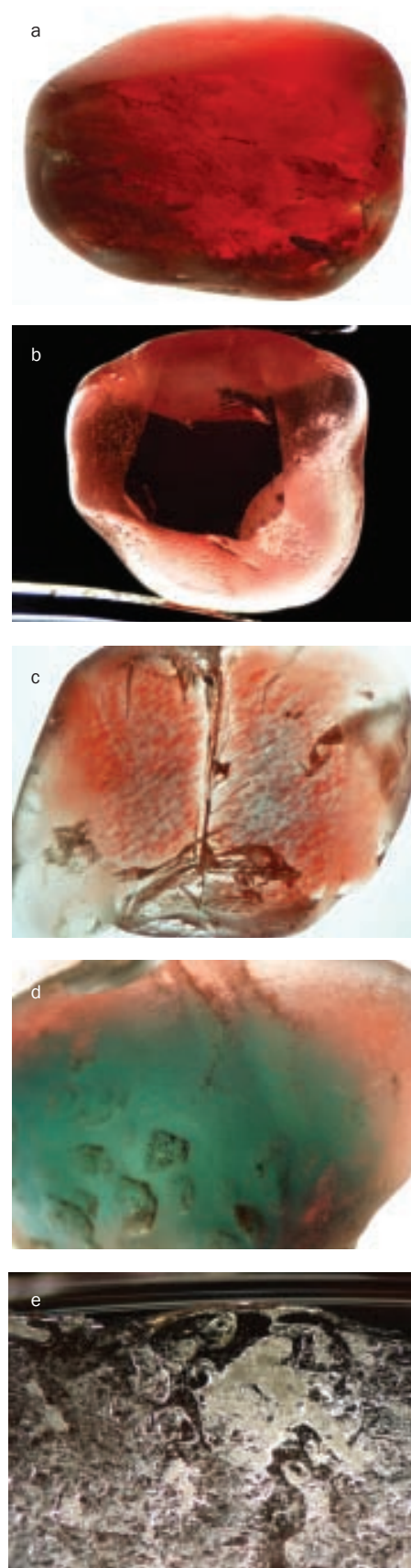


Figure 12: (a-d) Colours typical of Tibetan andesine water-worn crystals. (e) Surface etching and melted glassy surface of a Tibetan andesine crystal. Photos by A. Abduriyim; magnified 20 \times .

The characteristics of red andesine from the Himalaya Highland, Tibet



Figure 13: Characteristic inclusions in Tibetan andesine are (a) twin lamellae, (b) parallel lath-like hollow channels filled with a white solid substance, (c) dense concentrations of pipe-like growth tubes which are parallel to [010], (d) distinctive irregular dislocations, (e) concentrated turbid or milky uneven orange-red clouds composed of tiny granules, (f) leaf-like discoid fractures, cleavage cracks, gas bubbles and negative crystals, and (g) highly reflective small native-copper grains or platelets. Photomicrographs by A. Abduriyim; magnified 20–25×.

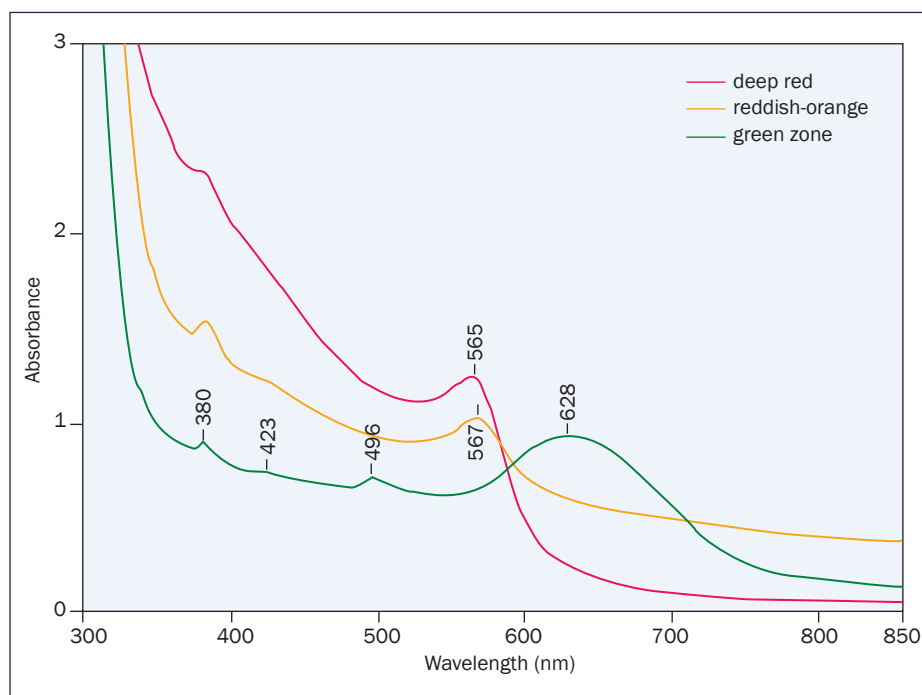
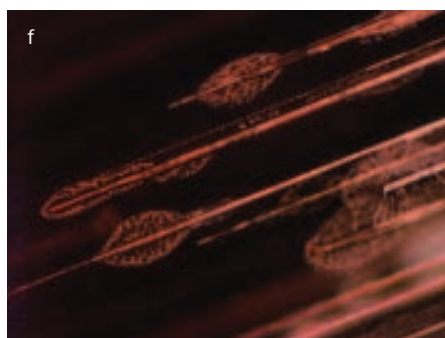
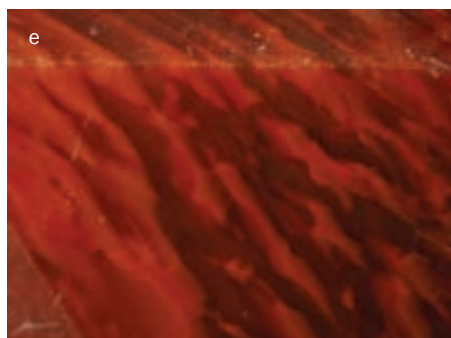
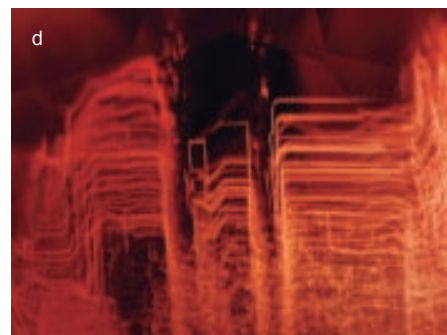


Figure 14: Polarized UV-Vis-NIR absorption spectra measured in the [010] direction (parallel to b axis) of representative reddish-orange, deep-red and bicoloured red-green Tibetan andesine. Reddish-orange and deep-red crystals show absorption bands at 565–567 nm attributed to colloidal copper (Cu⁰), as well as weak absorptions near 423 and 380 nm due to Fe³⁺. The absorption spectrum of a green zone in a bicoloured red-green crystal shows combination absorptions of 628, 496, 423 and 380 nm; strong absorption at 628 nm is attributed to Cu⁰-Cu⁺ and/or the size and shape of native copper particles.

The characteristics of red andesine from the Himalaya Highland, Tibet

parallel to the [010] direction (Figure 13a, b and c), irregular dislocations (Figure 13d), and irregular colour patches caused by milky turbidity from fine granular inclusions (Figure 13e), fissures, discoid fractures, cleavage cracks, gas bubbles and negative crystals (Figure 13f). One sample displayed reddish aventurescence caused by colloidal native-copper grains or platelets (Figure 13g).

Absorption spectra of three typical colours of Tibetan andesine are shown in Figure 14. The deep-red andesine exhibits increasing absorption from 320 nm toward shorter wavelengths and a prominent broad band near 565 nm. In the reddish-orange sample, the absorption is shifted to 567 nm. A weak peak near 380 nm and a very weak peak 423 nm were detected in all samples, but some samples also showed a very weak peak at 450 nm. Spectra obtained in the near-infrared region (800–2500 nm) show a strong broad absorption peak centred near 1260 nm (not shown). Green andesine shows weak absorptions at 380, 423, 450 and 496, and a very strong broad absorption centred at 628 nm (see again, Figure 14). Like the red andesine, a strong and broad absorption is also present near 1260 nm.

No OH- or H₂O-related absorptions in the range of 2800–3700 cm⁻¹ in the infrared spectra were detected in most of the samples, but some samples showed a small broad absorption band in the range 3000–3500 cm⁻¹ in some crystal orientations (Figure 15).

X-ray powder diffractograms of Tibetan andesine indicate a high-temperature disordered structure (see Figure 16 and discussion below). Lattice parameters were calculated in ten samples as; $a_0 = 8.161\text{--}8.193(26)$ Å, $b_0 = 12.849\text{--}12.919(16)$ Å, $c_0 = 7.105\text{--}7.126(14)$ Å, $\alpha = 93.26^\circ\text{--}93.74^\circ$, $\beta = 116.27^\circ\text{--}116.38^\circ$, $\gamma = 89.93^\circ\text{--}90.16^\circ$.

Electron probe microanalysis (EPMA) of ten samples, TB-CH-R001-002 (deep red), TB-CH-OR001-004 (orange-red), TB-CH-RO001-003 (reddish orange) and TB-CH-RG001 (bicoloured red-green) indicated compositions listed in Table II. Major amounts of Si, Al, Ca and Na were measured and there are minor contents of

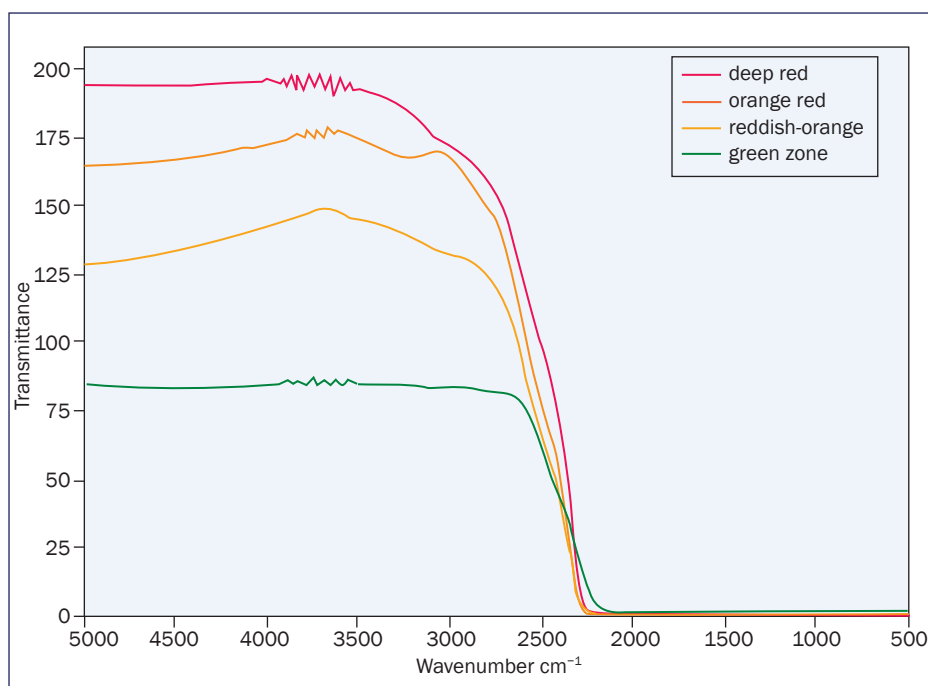


Figure 15: Representative infrared spectra of natural orange-red, reddish-orange, deep-red and bicoloured red-green Tibetan andesine from Baining.

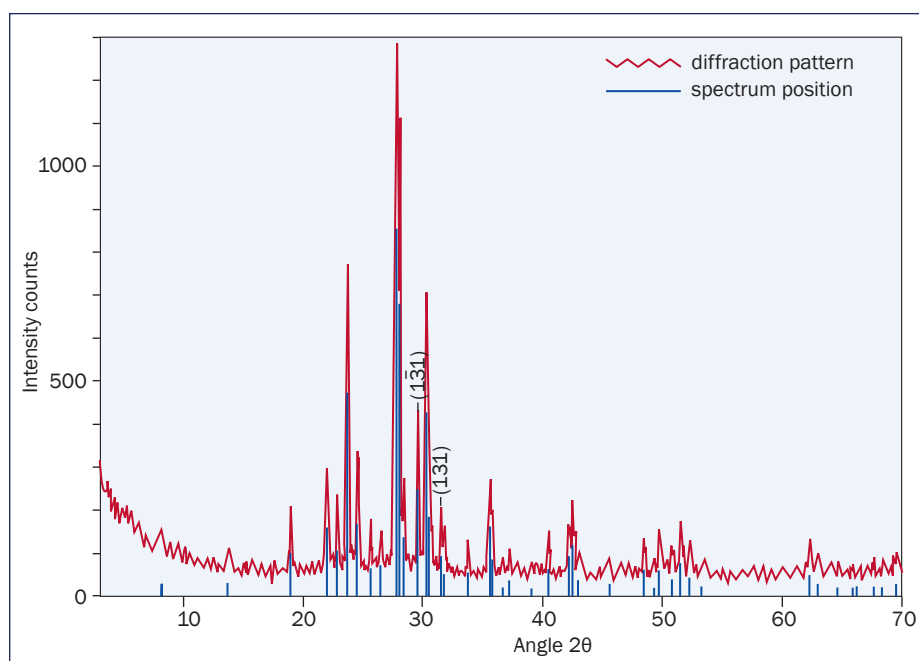


Figure 16: The X-ray powder diffraction pattern (3–70°) of Tibetan andesine from Bainang mine taken with CuK α radiation. (131) and (131) face indices in degrees 2 θ are indicated.

K, Fe, Cu and Sr. No significant difference in copper content was detected between red and green zones in the andesines. From the atomic proportions the ratio of albite:anorthite:orthoclase is calculated as $\text{Ab}_{46.96\text{--}49.79}:\text{An}_{46.72\text{--}49.94}:\text{Or}_{3.03\text{--}3.50}$, and the chemical formula as $(\text{K}_{0.03}\text{Na}_{0.46\text{--}0.49})_2\text{Ca}_{0.46\text{--}}$

$\text{Al}_{0.49}\text{Al}_{1.43\text{--}1.48}\text{Si}_{2.51\text{--}2.53}\text{O}_8$ (Figure 17).

The major, minor and trace elements of 56 samples analyzed by LA-ICP-MS are summarized in Table III. The major elements Al, Si and Ca and minor element Na were converted to oxide weight percent values for comparison with EPMA

The characteristics of red andesine from the Himalaya Highland, Tibet

Table II: Compositions of ten andesines from Bainang, Tibet.

Weight %	Deep-red TB-CH-R001-002	Orange red TB-CH-OR001-004	Reddish-orange TB-CH-RO001-003	Bicoloured TB-CH-RG001	
				red zone	green zone
Na ₂ O	5.49–5.56	5.29–5.52	5.50–5.61	5.54	5.53
Al ₂ O ₃	27.49–27.51	27.55–27.75	26.97–27.19	27.86	27.75
SiO ₂	55.90–55.92	55.80–55.99	56.54–56.72	55.5	55.65
K ₂ O	0.52–0.56	0.53–0.56	0.59–0.6	0.54	0.56
CaO	9.85–9.87	9.84–10.18	9.53–9.64	10	9.99
FeO	0.39–0.40	0.29–0.34	0.36–0.41	0.3	0.31
CuO	0.08–0.14	0.05–0.11	0.04–0.1	0.11	0.1
SrO	0.15–0.17	0.10–0.13	0.09–0.11	0.15	0.12
Atom					
Na	0.48	0.46–0.48	0.48–0.49	0.48	0.48
Al	1.48	1.46–1.47	1.43–1.44	1.48	1.48
Si	2.52	2.52–2.53	2.54–2.55	2.51	2.51
K	0.03	0.03	0.03	0.03	0.03
Ca	0.48	0.48–0.49	0.46	0.48	0.48
Fe	0.01	0.01	0.01	0.01	0.01
Cu	0	0	0	0	0
Sr	0	0	0	0	0
Total	5	4.99–5	4.98–4.99	5	5
Ab-An-Or composition					
Ab	48.59–48.96	46.96–48.73	49.05–49.79	48.5	48.43
An	48.00–48.17	48.01–49.94	46.72–47.47	48.42	48.36
Or	3.03–3.23	3.09–3.26	3.48–3.50	3.09	3.2

NB: EPMA chemical compositional data represent an average of 3–5 analyses per sample, and data show a range of values for a number of samples from each colour variety.

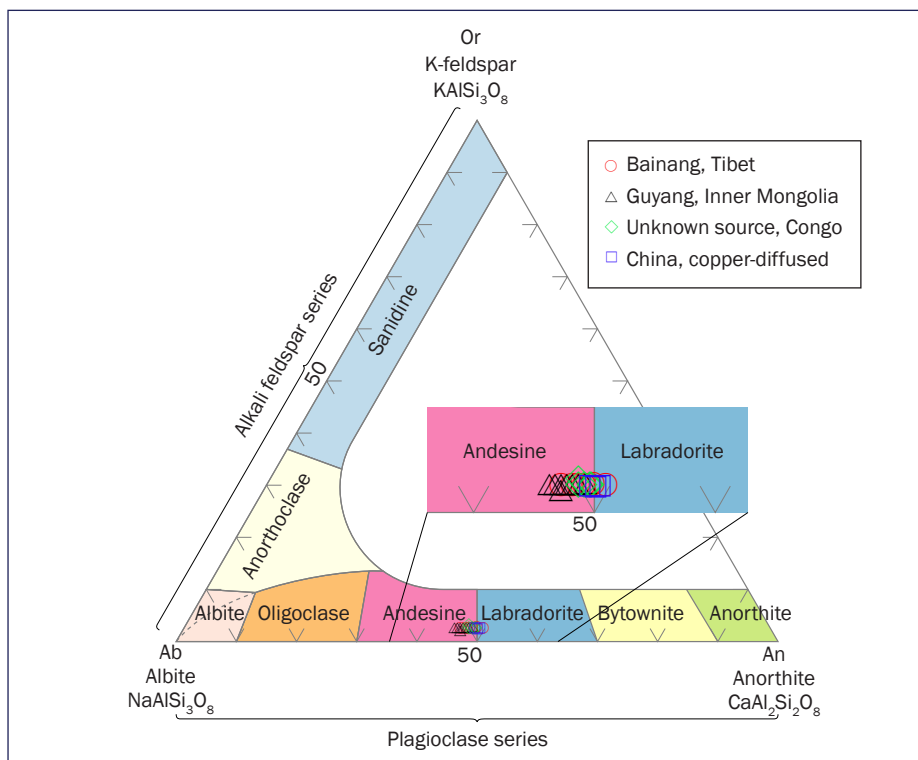


Figure 17: Compositions of Tibetan andesine from Bainang plotted in a ternary diagram of three end members orthoclase (Or), albite (Ab) and anorthite (An). EPMA data of ten samples from samples TB-CH-001 to 010 are indicated by circles. Feldspars from Inner Mongolia (10 samples, pale yellow), Democratic Republic of Congo (five samples, red) and copper-diffused stones from China (seven samples, red) are also plotted for comparison.

The characteristics of red andesine from the Himalaya Highland, Tibet

Table III: LA-ICP-MS analyses of 56 andesines from Bainang, Tibet.

Colour Sample nos.	Deep-red TB-CH-R001-006	Orange-red TB-CH-OR001-030	Reddish-orange TB-CH-RO001-015	Bicoloured crystals TB-CH-RG001-005	
				red zone	green zone
Major elements (ppm by weight)					
Na	38175–38341	37072–38222	38104–39650	36882–38320	36551–38780
Al	147000	147000	147000	147000	147000
Si	269637–271204	272301–280167	287513–291800	264540–280167	260740–283510
Ca	64900–69807	64756–70451	63174–68045	64956–71934	64900–71425
Trace elements					
Li	40–68	27–60	30–50	9–60	9–58
Mg	450–580	440–550	410–560	440–560	455–550
K	2230–4220	2340–3160	2280–3330	2320–3570	2390–3430
Sc	0.5–12	4–15	4–10	0.8–10	1–8
Ti	440–520	382–508	379–508	440–485	430–495
Mn	30–35	28–38	29–36	27–35	28–34
Fe	1000–3310	1969–2350	1891–2680	2010–4140	2030–4230
Cu	380–630	382–490	313–410	271–445	256–430
Ga	20–28	15–30	18–27	21–27	23–29
Sr	820–1000	756–960	761–950	807–970	792–960
Ba	100–150	99–140	104–143	117–143	116–147

NB: For LA-ICP-MS, external standard was NIST SRM 610, 612, internal standard was 27.7 wt.% Al_2O_3 (14.7 wt.% Al).

The values for each trace element are averages of three spots per sample, but not from the same position as the EPMA analysis. S, F, Cl were not measured in this study.

Operating conditions: Radio frequency power 1500w, Ablated particles and gas were carried to ICP by He gas at a rate of 1.0L/min, Nebulizer Ar gas flow 1.20L/min, Pulse frequency 10Hz, Laser spot 80 μm diameter, laser power 80%, Ablation time 25 sec.

data. The trace elements present are K (2230–4220 ppm), Fe (1000–4230 ppm), Sr (756–1000 ppm), Mg (410–580 ppm), Ti (379–520 ppm), Cu (270–630 ppm), Ba (99–150 ppm), Mn (27–38 ppm), Ga (15–30 ppm), Li (9–68 ppm) and Sc (0.5–15 ppm); B, V, Cr, Zn and Ce are <5.5 ppm each, and Be, Co, Ni, Ge, Rb, La, Pr, Nd, Eu, Gd and Pb occur in amounts less than 1.5 ppm or below the detection limits. The Cu contents tend to be higher in the redder colour zones.

Identification and discussion

The andesines from Bainang mine in Tibet show a RI range of 1.550–1.561 with birefringence 0.009, consistent with published values. These RI values overlap those of Inner Mongolian andesines from the Shuiquan and Haibozi mines in Guyang prefecture, China (Abduriyim, 2008), but are

significantly lower than those of labradorite from Oregon, USA, and Chihuahua, Mexico. In addition the inclusions in the Tibetan material such as the parallel lath-like hollow channels, pipe-like tubes, irregular dislocations and milky clouds, are also features enabling distinction from Oregon red labradorite. The native-copper grains in Tibetan material which cause some aventurescence are less extensive and smaller than those in the Oregon feldspars. However, similar inclusions have been reported in red and green labradorite from the Democratic Republic of Congo (Krzemnicki, 2004) but the source is unspecified. In our recent studies of copper-diffused red andesine, material from Inner Mongolia that featured a pipe and tube-like structure, discoid fractures, recrystallized white residue filling the lath-like hollow channels and cloud inclusions, had been used for treatment in China. These inclusions resemble those in the Tibetan andesines

(Figure 18) and may indicate that they were subject to a thermal event before eruption.

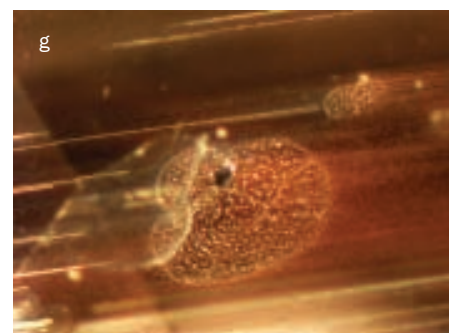
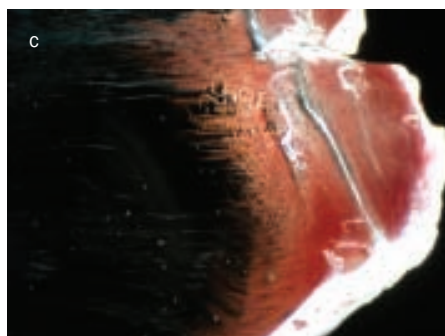
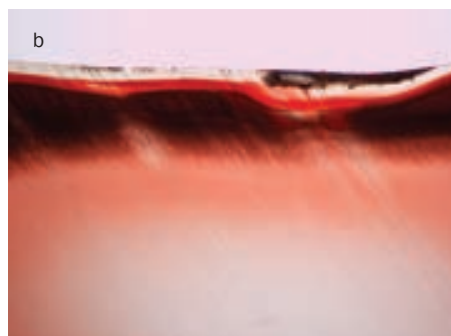
Recently, an experimental study has proved the viability of copper diffusion-treating such material (Roskin, 2008; Emmett and Douthit, 2009).

The depth of colour in Tibetan red andesine correlates with the concentration of copper. The highest content reaches 630 ppm Cu in deep-red andesine, whereas the reddish-orange variety only contains about 300 ppm. The absorption peak near 565 nm is caused by small particles of metallic copper (Cu^0) which are colloidal and less than 200 nm across according to data from a TEM (Figure 19). In the spectra, there are also several weak bands at 380 nm, 423 nm and 450 nm, due to Fe^{3+} and a broad absorption band centred at 1260 nm due to Fe^{2+} . This suggests that both Fe^{3+} and Fe^{2+} should be assigned to tetrahedral sites in the plagioclase structure.

The characteristics of red andesine from the Himalaya Highland, Tibet



Figure 18: (a) Copper-diffused rough andesine crystals from China. (b-g) Sections of a copper-diffused andesine: an induced orange-red colour layer penetrates from the rim towards the core (b), but a colourless zone remains at the surface of the stone; red pipe-tubes, discontinuous lath-like hollow channels, a pipe and tube-like structure, irregular dislocations, milky turbid cloud, discoid fractures, and a recrystallized white residue can be seen in one treated stone. These features resemble Tibetan untreated andesine. Photos by A. Abduriyim; magnified 20-25x.



On the other hand, the green zones in bicoloured stones show a broad absorption near 628 nm, produced by $\text{Cu}^0\text{-Cu}^+$ intervalence charge transfer. This model also explains the green colour of labradorite from Oregon and Congo (Hofmeister and Rossman, 1985; Krzemnicki, 2004). However, Nishida and Kimata (2002) have attributed the red and green coloration to the shape and size of the copper particles. When a dominant green has an added red component, the peak at 628 nm decreases. A weak absorption band at 496 nm has so far only been found in Tibetan green andesine;

this may be related to iron, as there is a slightly higher content of iron in the green zone compared to that in the red zone (2510 vs. 2420 ppm).

The detailed chemical study by EPMA showed that the feldspars from Tibet are poor in potassium and belong to the plagioclase series. The calculations of An and Ab proportions indicate a small range either side of the 50:50 Ab:An ratio, i.e. the stones fall into the high-Ca part of the andesine field in the ternary diagram and the low-Ca part of the labradorite field (Figure 17). Tibetan material can therefore be said to be largely calcic-andesine but

with a small amount of sodic-labradorite. Similar analyses of our mine collection of ten pieces of pale yellow andesine from Inner Mongolia, seven copper-diffused stones from China and five red stones from the Democratic Republic of Congo indicate a complete overlap with the Tibetan materials, very close to the boundary of andesine and labradorite, but not actually falling into the labradorite field. Stones from these three localities cannot be separated on the basis of chemical mapping.

Trace elements in the Tibetan andesines were discussed above, and one

The characteristics of red andesine from the Himalaya Highland, Tibet

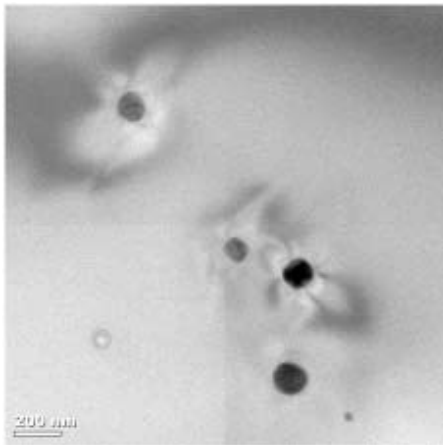


Figure 19: TEM image of round native copper grains in Tibetan red andesine. Photo by S.Toh, Kyushu University, Japan.

may add that the ratio of Ba/Sr and Ce/Nd in all the samples was rather constant, 0.12–0.13 and 2.15–2.85, respectively (Figure 20). This chemical homogeneity is consistent with the possibility that these plagioclases were formed from a single parent magma.

Recent analyses of 40 andesines from Inner Mongolia, 5 andesines reportedly from the Democratic Republic of Congo and 13 of Cu-diffused andesines from China have shown trace element contents similar to those in Tibetan stones, but the Li content of Inner Mongolian pale yellow stones and of the Chinese Cu-diffused red stones was lower and Ba was higher. To evaluate the usefulness of chemical data for separating the andesine from these localities, the ratios Ba/Sr and Ba/Li were plotted and are shown in Figure 21. Tibetan red andesines have ratios of Ba/Li < 9 and Ba/Sr ratios of 0.11–0.18, but bicoloured crystals tend to have lower Li contents and two samples showed a relatively high ratio of Ba/Li up to 12. The Inner Mongolian pale yellow andesines are characterized by Ba/Li ratios of > 11 and a more limited range of Ba/Sr of 0.14–0.18. Most of these andesines can be clearly differentiated from Tibetan stones on this basis. The Congo andesines show a distinct variation in their Ba/Li ratio. Three have ratios similar to those of Inner Mongolian stones, but two are similar to Tibetan stones. However, these ratios in the 13 copper-diffused samples do not lead to clear conclusions about

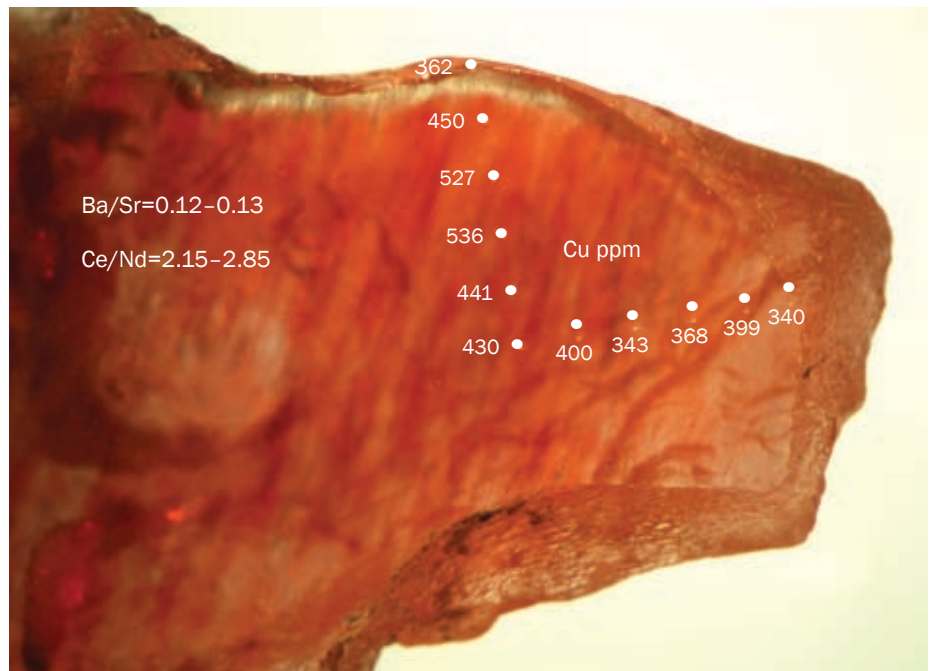


Figure 20: Two compositional traverses showing copper contents from rim to interior of an andesine crystal (TB-CH-001). The ranges of ratios Ba/Sr and Ce/Nd are also provided.

provenance and further work is needed.

In 1979, Trevena and Nash presented the compositions of hundreds of detrital plagioclases from various arkosic sandstones plotted on an An-Ab-Or ternary diagram and they defined seven provenance groups; volcanic, plutonic,

metamorphic, volcanic and plutonic, volcanic and granophyric, plutonic and metamorphic, and plutonic, metamorphic and authigenic (Figure 22). According to this diagram, the K₂O in plagioclase generally decreases from volcanic through plutonic to metamorphic

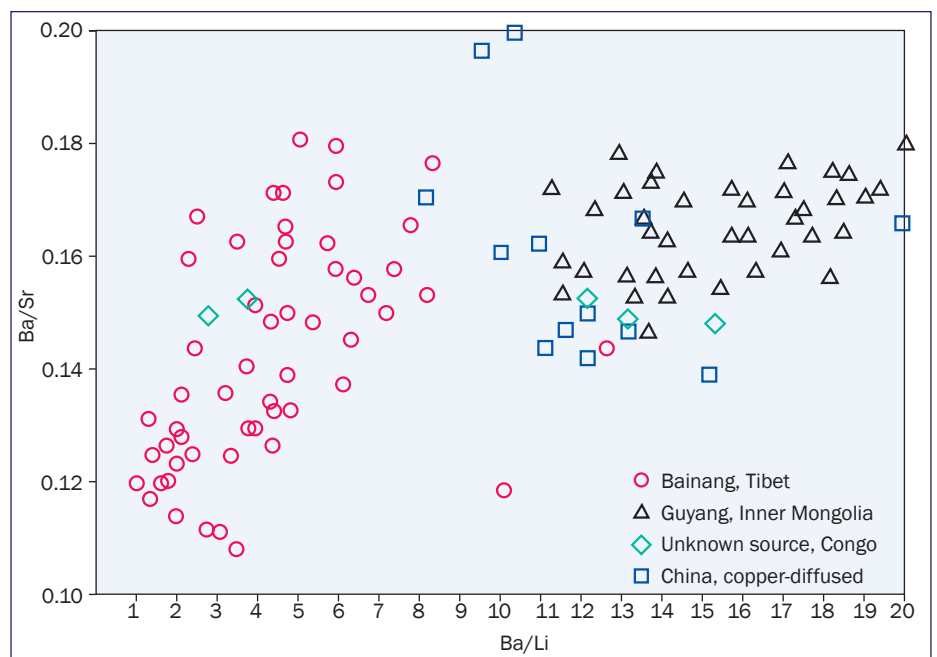


Figure 21: In this diagram, Ba/Sr and Ba/Li ratios obtained from LA-ICP-MS analyses of 56 samples from Tibet, 40 samples from Inner Mongolia, 13 copper-diffused samples from China and five samples from Democratic republic of Congo are shown. Most Tibetan andesine has low Ba/Li values and has a wide range of Ba/Sr. The Inner Mongolian andesine shows relatively high Ba/Li that enables distinction from Tibetan andesines.

The characteristics of red andesine from the Himalaya Highland, Tibet

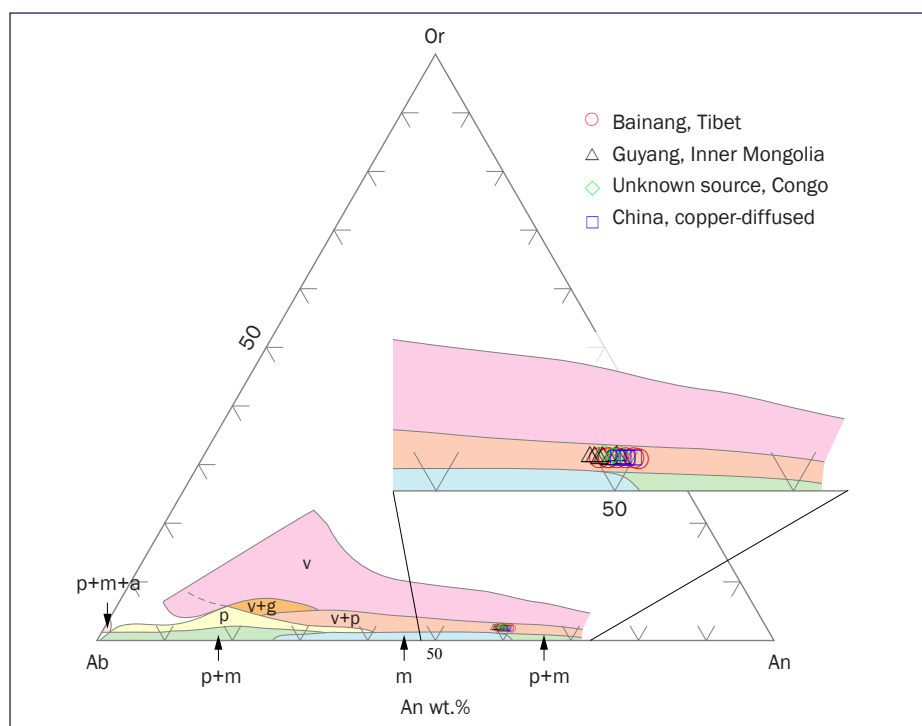


Figure 22: Plagioclase ternary diagram showing compositions of seven provenance groups: v=volcanic, p=plutonic, m=metamorphic, v+g=volcanic+granophyre, v+p=volcanic+plutonic, p+m=plutonic+metamorphic, p+m+a=plutonic+metamorphic+authigenic. Compositions of ten samples of Tibetan and Inner Mongolian andesine, seven copper-diffused samples from China and five samples of Congo andesine (wt.%) analysed by EPMA lie in the v+p field.

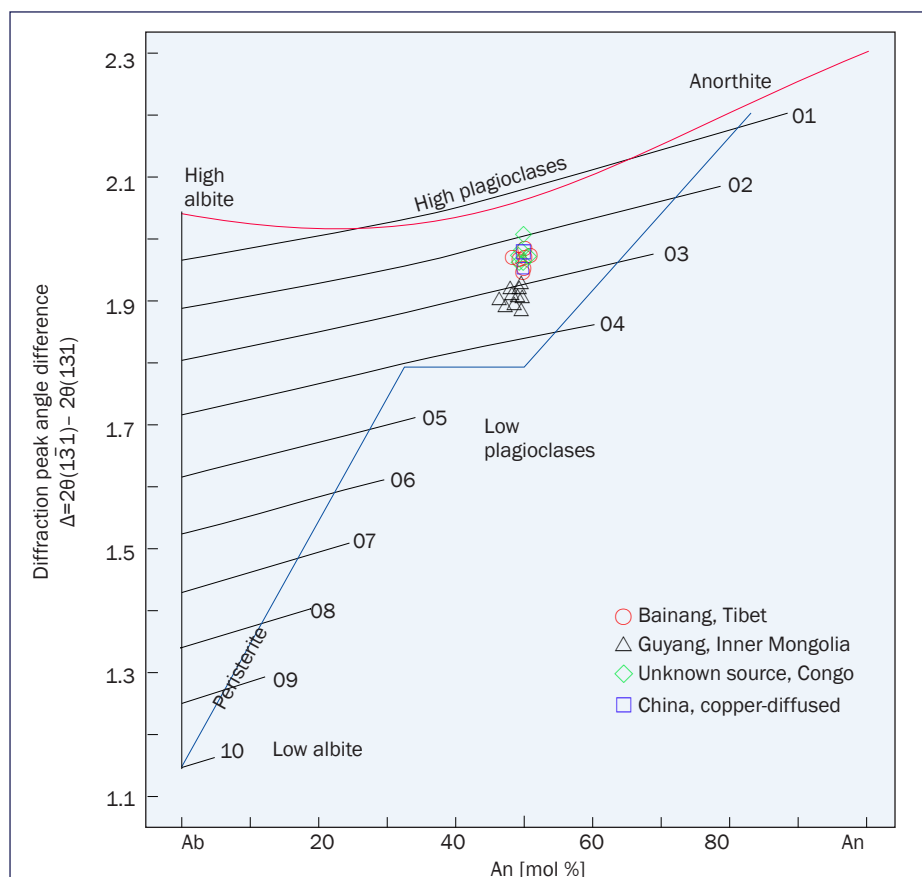


Figure 23: Diagram showing degree of ordering of Al in the plagioclase structure by means of contours 10 to 01 from low to high albite and anorthite. Andesines from Tibet, Mongolia and Congo are plotted. See text for discussion.

parageneses. Compositions of detrital plagioclase feldspar samples from Tertiary sedimentary deposits in Tibet are shown in part of the volcanic or plutonic field. The Tibetan material appears to consist almost entirely of plagioclase that is volcanic in origin.

Temperature is the most important factor that influences the degree of ordering of Al/Si in feldspar. Smith and Yoder (1956) introduced a simple method, based on measurement of the spacing between the $(1\bar{3}1)$ and (131) peaks of the X-ray power diffraction pattern, to estimate the differences of Al content in four non-equivalent tetrahedral sites: $T_1(o)$ and $\{T_1(m), T_2(o), T_2(m)\}$. In 1980, Kroll and Ribbe used the parameter of $\Delta=2\theta(1\bar{3}1) - 2\theta(131)$ and the lattice angle parameter γ , combined with the anorthite (An) content of plagioclase to determine the Al/Si distribution among the four tetrahedral sites in the plagioclase structure. This study mentioned that the γ plot gives more precise results for plagioclase. On the other hand, the well-known method of $\Delta=2\theta(1\bar{3}1) - 2\theta(131)$ can be used somewhat less precisely to determine structural states, but the value of Δ is comparable from one sample to the next.

In studies of synthetic plagioclase, Eberhard (1967) and Smith (1972) examined the relationship between formation temperature and the parameter $\Delta=2\theta(1\bar{3}1) - 2\theta(131)$. They presented a model in which Δ was plotted against An content and contours were drawn of the different degrees of Al/Si ordering in the tetrahedral sites of the feldspar structure (01–10 in Figure 23). Our TEM observations of the microstructure of Tibetan and Inner Mongolian andesines confirmed that they do not include any complex exsolution lamellae, which means that accurate measurement of $2\theta(131)$ can be obtained from a homogeneous matrix of feldspar by X-ray powder diffraction. The X-ray power diffraction data for ten Tibetan andesines gave values of $\Delta=1.9539-1.9668$, and of γ , values of $89.93^\circ-90.16^\circ$. The range of values measured for Δ indicate the degree of Al/Si ordering of 0.24–0.29 in Figure 23, and for γ the Al/Si degree of ordering

The characteristics of red andesine from the Himalaya Highland, Tibet

indicated is 0.22–0.28 (Figure 24), which indicates that 22–29% of aluminium moves into the tetrahedral site $T_1(o)$ from $T_1(m)$, $T_2(o)$, and $T_2(m)$. From a plot of the Δ data for Tibetan andesines, we estimate that the temperature at which this degree of Al/Si ordering is stable is about 800°C, consistent with temperatures in a volcanic environment at high crustal level (Figure 25). The ten samples of pale yellow andesine from Inner Mongolia have values of $\Delta=1.9161$ – 1.9487 , and $\gamma=89.69^\circ$ – 89.83° , an Al/Si degree of ordering range of 0.32–0.36, and lattice angle γ values of 0.30–0.38, which indicates that the Inner Mongolian feldspar is more structurally ordered on the tetrahedral site and that it probably formed close to 700°C (see again, Figures 23, 24 and 25). Our data are closely comparable with those from a recent study of andesine from Inner Mongolia by Dong *et al.*, 2009. Our more recent work on seven samples of copper-diffused red andesine gave values of $\Delta=1.9595$ – 2.0095 and $\gamma=89.83^\circ$ – 90.22° , and two Congolese samples gave $\Delta=1.9574$ – 1.9729 and $\gamma=89.99^\circ$ – 90.16° . These points lie in fields that almost completely overlap those of the Tibetan red andesines, so these parameters are not discriminatory.

Conclusions

The Bainang mine south-east of Xigazê in Tibet, is located in a volcanic-sedimentary deposit and produces gem-quality orange-red andesine feldspar. Simple hand-tool mining by local people currently yields several hundred kilograms of rough per year. Mining using heavy machinery could increase the productivity. Several new deposits have been discovered recently in Tibet in areas other than Bainang that produce andesine with such saturated colours (T. Li, pers. comm., 2009).

Figure 25: Shown is a plot of the parameter $\Delta=2\theta(1\bar{3}1) - 2\theta(131)$ versus An composition for various formation temperature isotherms for plagioclase. This provides information about the structural ordering of Al and Si that is produced when different compositions crystallize at various temperatures. The data from Tibetan, Congolese and copper-diffused Chinese andesines indicate that they had a higher formation temperature than Inner Mongolian material.

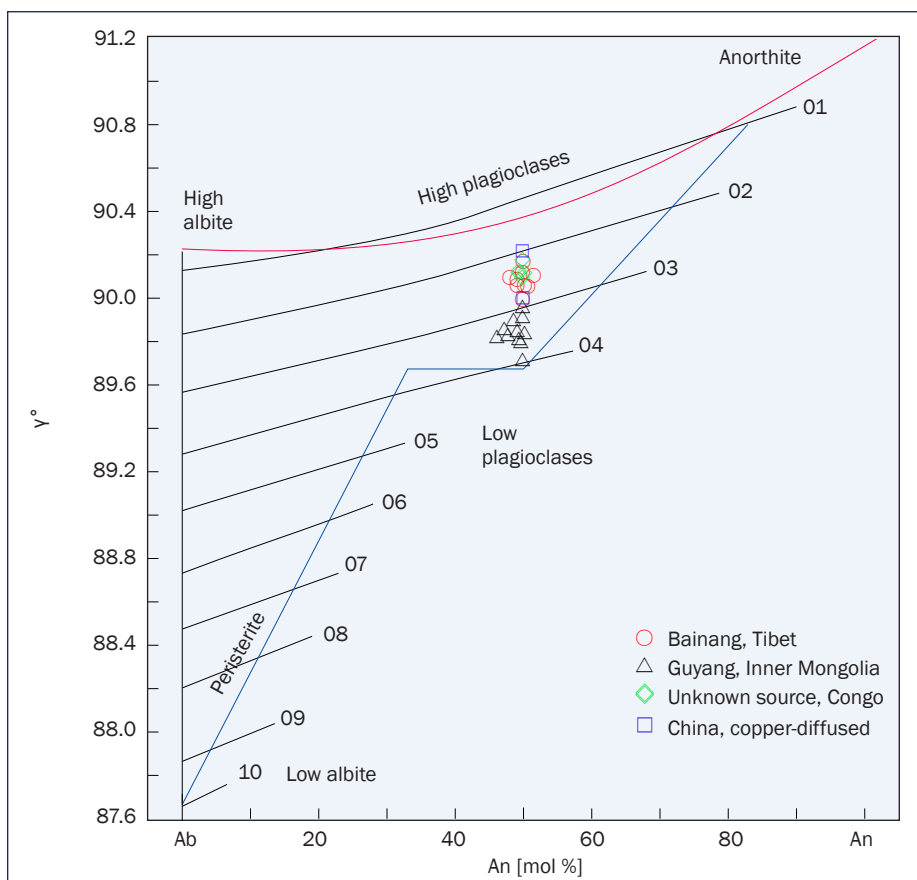
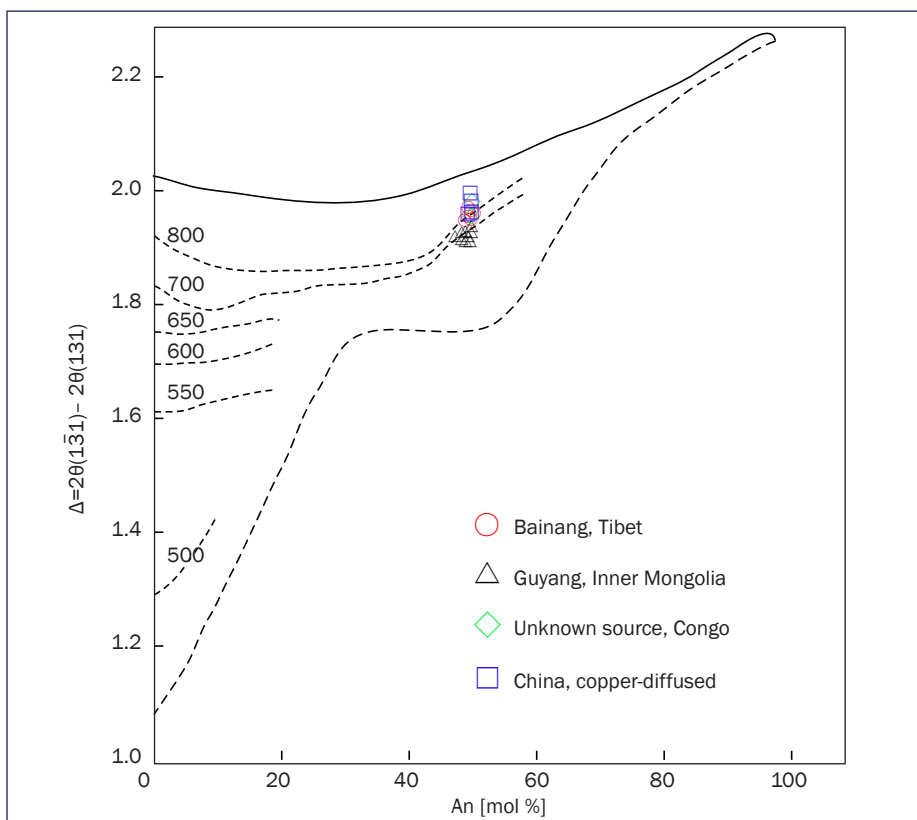


Figure 24: A diagram of lattice angle parameter γ (in degrees) as a function of anorthite in mole percent for low, high and intermediate structural states. Contours indicate the degree of ordering of Al in tetrahedral sites $T_1(o)$ - $T_1(m)$. These γ values of andesines from Tibet, Inner Mongolia and Congo, and of the copper-diffused China samples indicate similar degrees of order as does the parameter $\Delta=2\theta(1\bar{3}1) - 2\theta(131)$ (Figure 22).



The characteristics of red andesine from the Himalaya Highland, Tibet

Gemmological and chemical investigations indicate that the red colour results from clusters of tiny copper particles (Cu^0) and the green colour may result from Cu^0 - Cu^+ intervalence charge transfer or from differences in shape and size of the copper particles. RI and SG values and chemical data indicate an andesine composition of $\text{Ab}_{46.96-49.79}\text{An}_{46.72-49.94}\text{Or}_{3.03-3.50}$, i.e. an andesine near the andesine-labradorite border; its chemical formula is $(\text{K}_{0.03}\text{Na}_{0.46-0.49})_2\text{Ca}_{0.46-0.49}\text{Al}_{1.43-1.48}\text{Si}_{2.51-2.53}\text{O}_8$. The lattice parameters are ($a_0=8.161-8.193$ Å, $b_0=12.849-12.919$ Å, $c_0=7.105-7.126$ Å, $\alpha=93.26^\circ-93.74^\circ$, $\beta=116.27^\circ-116.38^\circ$, $\gamma=89.93^\circ-90.16^\circ$). The parameter $\Delta=2\theta(1\bar{3}1) - 2\theta(131)=1.9539-1.9668$, calculated from XRD measurements indicates that Tibetan andesine is in a low state of structural order with a value of 0.22–0.29, and that it formed at a minimum of 800°C in a volcanic environment.

Chemical analysis of Cu-bearing Tibetan and non-Cu-bearing Inner Mongolian andesines by EPMA has shown comparable contents of major and minor elements. But trace element analysis using LA-ICP-MS and the plot of Ba/Sr versus Ba/Li has been found useful for distinguishing Cu-bearing andesine from Tibet.

Acknowledgements

The author is grateful to Wong Ming (King Star Jewellery Co) and Christina Iu (M. P. Gem Corp.) for supporting and organizing the field trip and especially to the mine owner Li Ting in Tibet for allowing access to and for a guide to the mine. Special thanks to Prof. Detlef Günther from the Swiss Federal Institute of Technology, Zürich, for comparative study of chemical analysis by the LA-ICP-MS technique. Also Kousuke Kosuda from National Institute for Materials Science (NIMS) is thanked for his support on electron probe microanalysis. Dr Shoichi Toh from the Research Laboratory of High Voltage Electron Microscopy, Kyushu University, is thanked for supporting the TEM observations. Assistance from research colleagues Hiroshi Kitawaki, Dr Jun Kawano, Makoto Okano, Taisuke Kobayashi and Chihiro Fukuda at

GAAJ-ZENHOKYO Laboratory is much appreciated, and the author is also thankful to Prof. Masao Kitamura for critically reading this manuscript.

References

- Abduriyim, A., 2008. Gem News International: Visit to andesine mines in Tibet and Inner Mongolia, Gemmological properties of andesine collected in Tibet and Inner Mongolia. *Gems & Gemology*, **44**(4), 369–73
- Carpenter, M.A., and McConnell, J.D.C., 1984. Experimental bracketing of order/disorder transformations in plagioclase. *Progress in Experimental Petrology*, **6**, 186–9
- Dong X. Z., Qi L.J., and Zhong Z.Q., 2009. Preliminary study on gemmological characteristics and genesis of andesine from Guyang, Inner Mongolia. *Journal of Gems and Gemmology*, **11**(1), 20–4
- Eberhard, V.E., 1967. Zur synthese der plagioclase. *Schweizerische mineralogische und petrographische Mitteilungen*, **47**, 385–98
- Haifu Li, 1992. First study of gem-quality Inner Mongolian Labradorite moonstone. *Jewellery*, **1**(6), 45–7 [in Chinese]
- Hofmeister, A.N., and Rossman, G.R., 1985. Exsolution of metallic copper from Lake County labradorite. *Geology*, **13**, 644–7
- Kroll, H., and Ribbe, P.H., 1980. Determinative diagrams for Al, Si order in plagioclases. *American Mineralogist*, **65**, 449–57
- Krzemnicki, M.S., 2004. Red and green labradorite feldspar from Congo. *Journal of Gemmology*, **29**(1), 15–23
- Lauris, M.B., 2005. Gem News International: Gem plagioclase reportedly from Tibet. *Gems & Gemology*, **41**(4), 356–7
- Nishida N., and Kimata M., 2002. Identification of microinclusions in the nanometer dimension by electron microprobe analysis — the chromophores in colored sunstones. *Ganseki Kobutsu Kagaku*, **31**, 268–74
- Smith, J.R., and Yoder, H.S., 1956. Variation in X-ray powder diffraction patterns of plagioclase feldspars. *American Mineralogist*, **41**, 632–47
- Smith, J.R., 1972. Critical review of synthesis and occurrence of plagioclase feldspar and a possible phase diagram. *The Journal of Geology*, **80**(5), 505–25
- Trevena, A.S., and Nash, W.P., 1979. Chemistry and provenance of detrital plagioclase. *Geology*, **7**, 475–8
- Yue Cao, 2006. Study on the feldspar from Guyang County, Inner Mongolia, and their colour enhancement, Master's thesis, Beijing, Geological University of China

Web list

- Emmett, J., and Douthit, T. (2009). Copper diffusion in plagioclase. Presentation in GIA seminar on 21st Aug, <http://www.gia.edu/research-resources/news-from-research/special-issue-homepage.html>
- Roskin, G., 2008. "JCK web exclusive: The andesine report," posted November 12, <http://www.jckonline.com/article/CA6613857.html?desc=topstory>

The Author

Dr Ahmadjan Abduriyim

Chief Research Scientist, Research Laboratory, Gemmological Association of All Japan (GAAJ)-ZENHOKYO, 5-25-11 Uneo Taitoku, Tokyo, 110-0005 Japan
Email: Ahmadjan@gaaj-zenhokyo.co.jp

NEW!



Twist Portable Lamp

Flexible head twists to give maximum light exactly where you want it.

Now used in all Gem-A in-house diamond classes.



Gem-A

THE GEMMOLOGICAL ASSOCIATION
OF GREAT BRITAIN

- Ideal for examining diamonds and coloured stones
- Lightweight and foldable — take it with you wherever you go
- Low heat technology
- 13w Daylight™ energy-saving tube: Energy Grade A
- Runs on 220 volts

PRICE: £44.00* (Gem-A members and Gem-A registered students £39.60*)

* Prices exclude VAT, postage and packing

For further details or to order your Twist Portable Lamp, contact the Gem-A shop at shop@gem-a.com or call +44 (0)20 7404 3334.

Abstracts

Diamonds

The SEM and CCL-SEM study of graphitic inclusions in natural brown diamonds.

A.S. BIDNY, O.V. KONONOV, A.G. VERESOV and P.V. IVANNIKOV. *The Australian Gemmologist*, **23**(3), 2007, 126–30.

Plastic deformation, the supposed cause of colour in brown diamonds, closely parallels the high density of dislocations found in brown type I and type IIa diamonds. Using high-resolution Scanning Electron Microscopy (SEM) and Colour Cathodoluminescence Scanning Electron Microscopy (CCL-SEM) the characteristics of graphite inclusions in natural brown diamonds was researched. Graphite inclusions were found to lie along the {111} plane and of approximately 0.7 µm. Besides graphite, recrystallized micro-figures were visible with trigons on the octahedral surfaces. J.S.

Color variation and properties of johachidolite from Myanmar.

K.M. CHADWICK AND C.M. BREEDING. *Gems & Gemology*, **44**(3), 2009, 246–51.

Various analytical techniques were used to study 15 faceted examples of the rare gem material johachidolite from Myanmar showing a range of colours: saturated orange, orange, yellow, desaturated yellow and desaturated green. Both orange-yellow-hued and green samples showed various trends for Be, U, Th and Pb. Orange/yellow samples also showed relatively constant amounts of REE, though the green samples had higher REE values, particularly for the lighter REE. R.A.H.

'Fluorescence cage': visual identification of HPHT-treated type I diamonds.

I.A. DOBRNETS AND A.M. ZAITSEV. *Gems & Gemology*, **45**(3), 2009, 186–90.

High-pressure/high-temperature

diamonds of various colours may exhibit unusually intense fluorescence at the facet edges and junctions. This effect (here named the 'fluorescence cage') is observed with a fluorescence microscope as a luminous network on the surface of the diamond; it is not seen in untreated diamonds or colourless type IIa HPHT-treated diamonds. This fluorescence pattern is considered to result from a high concentration of HPHT-induced optical centres which remain on facet edges after repolishing. R.A.H.

The Wittelsbach Blue.

R. DRÖSCHEL, J. EVERS AND H. OTTOMEYERE. *Gems & Gemology*, **44**(4), 2008, 348–63.

The 55.56 ct Wittelsbach Blue is one of the largest historic, blue diamonds ever fashioned. Its chequered history is reviewed; it was most recently sold at Christie's in December 2008 to the London jeweller Laurence Graff for £16,393,250 (or just over \$683,000 per carat). R.A.H.

The French Blue and the Hope: new data from the discovery of a historical lead cast.

F. FARGES, S. SUCHER, H. HOROVITZ AND J.-M. FOURCAULT. *Gems & Gemology*, **45**(1), 2009, 4–19.

Models of a recently discovered lead cast of the French Blue diamond and of the Hope diamond confirm that the latter could have been recut from the French Blue. R.A.H.

Color grading 'C to Z' diamonds at the GIA Laboratory.

J.M. KING, R.H. GEURTS, A.M. GILBERTSON AND J.E. SHIGLEY. *Gems & Gemology*, **44**(4), 2008, 296–321.

The use of letter designations for diamond colour grades is virtually universal in the gem and jewellery industry but

the use of GIA colour grading standards and procedures is not. The history and ongoing development and application of this grading system is described. Important aspects of this system include a specific colour grading methodology for judging the absence of colour in diamonds, a standard illumination and viewing environment, and the use of colour reference diamonds ('masterstones') for the visual comparison of colour. R.A.H.

Gem News International.

B.M. LAURS (Ed.). *Gems & Gemology*, **45**(3), 2009, 214–32.

A brief description is given of a 1.02 ct greenish-yellow diamond which has had a glass filling and HPHT treatment. R.A.H.

Lab notes.

T.M. MOSES AND S.F. McCLURE (Eds.). *Gems & Gemology*, **44**(3), 2009, 252–60.

Notes are given on black diamonds coloured by hydrogen clouds and other diamond oddities. R.A.H.

Lab Notes.

T.M. MOSES AND S.F. McCLURE (Eds.). *Gems & Gemology*, **44**(4), 2008, 364–8.

Notes are given on a 3 ct fancy dark brown-yellow zoned type IIa/IIb diamond and a 0.21 ct CVD synthetic diamond which was found to have been HPHT treated. R.A.H.

Lab notes.

T.M. MOSES AND S.F. McCLURE (Eds.). *Gems & Gemology*, **45**(1), 2009, 53–8.

Notes include mention of a cut cubic zirconia coated with nanocrystalline synthetic diamond, and of a rare mixed type (Ia/IIb) diamond with nitrogen and boron centres. R.A.H.

Lab Notes.

T.M. MOSES AND S.F. McCLURE (Eds.). *Gems &*

Abstracts (continued)

Gemology, **45**(2), 2009, 134–40.

Items noted include a 1.79 ct cut bicoloured diamond (near colourless to orangy brown) and a 0.4 ct cut diamond graded as Fancy Black but which showed a deep violet colour when viewed through the pavilion. R.A.H.

Lab Notes.

T.M. MOSES and S.F. McCLURE (Eds). *Gems & Gemology*, **45**(3), 2009, 208–13.

Items noted include a treated 0.28 ct diamond graded as Fancy Red (a very rare colour grade) and a 12.01 ct Fancy Vivid Yellow diamond (type Ib) coloured by isolated nitrogen. R.A.H.

A crystallographic analysis of the Tavernier blue diamond.

S.D. SUCHER. *Gems & Gemology*, **45**(3), 2009, 178–85.

By correlating the facets on the Tavernier Blue (the 'grandparent' of the Hope diamond) with the facets of a diamond crystal, information has been obtained on the crystallography of the original rough. By using these data, the original drawings and a computer model of the French Blue diamond generated from a laser scan of a recently discovered lead cast, a computer model of the Tavernier Blue was obtained. This new model completely encloses the computer model of the French Blue, conforms to Tavernier's physical description and establishes the orientation of the finished diamond within the original diamond crystal. R.A.H.

Spectroscopic methods for the identification of natural yellow gem-quality diamonds.

L. TRETIAKOVA. *European Journal of Mineralogy*, **21**(1), 2009, 43–50.

The characteristic spectroscopic features and identification criteria for different types of yellow diamonds are presented, including varieties of naturally occurring yellow diamonds and varieties of artificially produced yellow diamonds. The spectroscopic techniques discussed include infrared spectroscopy, optical absorption spectroscopy and laser-induced photoluminescence spectroscopy. The latter technique is much more sensitive than optical absorption spectroscopy and can excite defects which have very low concentrations in diamonds: examples are

given of diamonds with high hydrogen contents or with high nitrogen and low hydrogen. R.A.H.

Gray-to-blue-to-violet hydrogen-rich diamonds from the Argyle mine, Australia.

C.H. VAN DER BOGERT, C.P. SMITH, T. HAINSCHWANG and S.F. McCLURE. *Gems & Gemology*, **45**(1), 2009, 20–37.

A study of 20 type IaB hydrogen- and nitrogen-rich grey to blue to violet diamonds from the Argyle mine showed that their unusual colour is the result of broad absorption bands centred at ~ 520–565 and 720–730 nm with a pronounced 551 nm band superimposed on the 520–565 nm feature. The photoluminescence spectra exhibit peaks associated with Ni-related defects which may be important in the more violet diamonds. R.A.H.

Gems and Minerals**Characterization of 'green amber' with infrared and nuclear magnetic resonance spectroscopy.**

A. ABDURIYIM, H. KIMURA, Y. YOKOYAMA, H. NAKAZONO, M. WAKASUKI, T. SHIMIZU, M. TANSHO and S. OHKI. *Gems & Gemology*, **45**(3), 2009, 158–77.

A peridot-like bright greenish yellow to green gem material is produced by treating natural resin (amber or copal) with heat and pressure in two stages in an autoclave. Differences in the molecular structure between the untreated materials and treated 'green amber' were studied by FTIR and ¹³C NMR, using powdered samples. Regardless of the starting material, the FTIR spectrum of 'green amber' showed an amber pattern but with a characteristic small absorption feature at 820 cm⁻¹. Solid-state ¹³C NMR of the treated material indicated a significantly lower volatile content than the untreated natural resin. A new absorption feature near 179 ppm in the NMR spectrum of all treated samples distinguished them from their natural-colour counterparts. R.A.H.

Characterization of peridot from Sardinia, Italy.

I. ADAMO, R. BOCCHIO, A. PAVESE and L. PROSPERI. *Gems & Gemology*, **45**(2), 2009, 130–33.

Olivine-rich nodules in basalts near

Pozzomaggiore, NW Sardinia, yield yellowish-green peridot crystals with gem quality potential and have α 1.650–1.652, β 1.669–1.670, γ 1.688–1.690, SG 3.32–3.36. Microprobe results give a composition of Fo₉₁Fa₉. R.A.H.

Aquamarine, maxixe-type beryl and hydrothermal synthetic blue beryl: analysis and identification.

I. ADAMO, A. PAVESE, L. PROSPERI, V. DIELLA, D. AJÒ, C.D. GATTA and C.P. SMITH. *Gems & Gemology*, **44**(3), 2009, 252–60.

An investigation is reported of aquamarine, maxixe-type (irradiated) beryl and two types of hydrothermally grown synthetic beryl, using standard gemmological methods, chemical analysis (microprobe results are reported), UV-Vis-NIR and mid-IR spectroscopy to identify these materials conclusively. The maxixe-type beryl (as for natural colour maxixe beryls) is distinguished by its unusual pleochroism, green UV fluorescence (if present), iron-free chemical composition and distinctive UV-Vis-NIR spectrum. The blue hydrothermal synthetic beryls can be discriminated from their natural equivalents by their microscopic features, chemical composition, and their visible and infrared spectroscopic features. R.A.H.

The Lac d'Amiante mine.

M. AMABILI, F. SPERTINI, M. AUGUSTE and G. BONIN. *Mineralogical Record*, **40**(4), 2009, 297–304.

Fine ornamental green fluorite is described from the Lac d'Amiante mine, in the town of Thetford, Quebec, Canada.

M.O'D.

Crystallization of biogenic Ca-carbonate within organo-mineral micro-domains.**Structure of the calcite prisms of the Pelecypod *Pinctada margaritifera* (Mollusca) at the submicron to nanometre ranges.**

A. BARONNET, J.P. CUIF, Y. DAUPHIN, B. FARRE and J. NOUET. *Mineralogical Magazine*, **72**(2), 2008, 617–26.

Atomic force microscopy (AFM) and TEM were used to investigate the fine structure of calcite prisms from the pearl-oyster shell *Pinctada margaritifera*. The AFM analysis showed that the prisms are made of densely packed circular micro-

Abstracts (continued)

domains (in the 0.1 μm range) surrounded by a dense cortex. The TEM images and diffraction patterns allow the internal structure of the micro-domains to be described: each of them is enriched in Ca-carbonate. Hosted in distinct regions of each prism, some are fully amorphous, and others are fully crystallized as sub-units of a large calcite single crystal. At the border separating the two regions, micro-domains display a crystallized core and an amorphous rim, probably marking out an arrested crystallization front having propagated through a previously bio-controlled architecture of the piling of amorphous micro-domains. Compared to recent data concerning the stepping mode of growth of the calcite prisms and the resulting layered organization at the μm -scale, these results give unexpected views regarding the modalities of biocrystallization. R.A.H.

Aquamarine from the Masino-Bregaglia Massif, Central Alps, Italy.

R. BOCCHIO, I. ADAMO and F. CAUCIA. *Gems & Gemology*, **45**(3), 2009, 204–7.

Pale, blue-green aquamarine crystals occur in granitic pegmatites of the Masino-Bregaglia massif in the Central Alps of northern Italy. They have yielded three cut and faceted stones, the largest being a 2.33 ct pale greenish-blue aquamarine. An 8.5 ct cabochon is also illustrated. The UV-Vis-NIR and mid-IR absorption spectra are shown, and trace elements determined by LA-ICP-MS are reported for six crystals. R.A.H.

Topaz from near El Chalten, Santa Cruz Province, Argentina.

R. BRANDSTETTER. *Mineralogical Record*, **40**(1), 2009, 1–15.

Topaz of ornamental or even gem quality is described from pegmatite pockets in a remote area of Patagonia, Argentina. Large white crystals of feldspar and milky quartz crystals accompany the topaz. M.O'D.

Edle Topase und Zepterquarze aus Patagonien.

R. BRANDSTETTER. *Lapis*, **34**(5), 2009, 13–24.

Transparent yellow topaz of apparent ornamental quality is described from Patagonia, Argentina, from where sceptre quartz is also reported. M.O'D.

Die Rogerley Mine.

R. BRANDSTETTER. *Lapis*, **35**(1), 2010, 13–26.

Fine, probably transparent, green fluorite crystals are described from the Rogerley mine in the northern Pennine orofield, England. M.O'D.

Fluorite from Riemvasmaak.

B. CAIRNCROSS. *Mineralogical Record*, **40**(4), 2009, 307–24.

Fine green ornamental to gem-quality fluorite is described from the Riemvasmaak area of Northern Cape Province, South Africa. M.O'D.

A study on the characteristics of some C- and CT-opals from Brazil.

F. CAUCIA, C. GHISOLI and I. ADAMO. *Neues Jahrbuch für Mineralogie, Abhandlungen*, **185**(3), 2009, 289–96.

The physical properties of blue and fire opals from Piauí State, Brazil, have been determined by optical analyses, specific gravity, X-ray diffraction and IR spectroscopy, with chemical compositions via LA-ICP-MS and SEM-EDS. The values obtained for specific gravity and refractive index are 1.98–2.28 and 1.420–1.461, respectively. The presence of cristobalite is confirmed. Trace amounts of chromophore elements are correlated with variation in colour. The particular 'coral islands' structure, built of microspherules of amorphous silica, is observed by SEM analyses, and could explain the particular effects of iridescence shown by some blue specimens. The LA-ICP-MS analyses confirm the presence of Fe as the principal cause of colour in the fire opals (perhaps present as an Fe-oxyhydroxide); only in the darkest specimens is Mn significant. R.A.H.

About mineral collecting. Part 5 of 5.

R. CURRIER. *Mineralogical Record*, **40**(3), 2009, 193–202.

The author describes the Tucson Gem and Mineral Show and gives advice to prospective exhibitors and visitors. Examples of some classic items are illustrated in colour. M.O'D.

The color durability of 'Chocolate pearls' by Ballerina Pearl Co.

G. DU TOIT, A.H. SHEN and C.M. BREEDING. *Gems & Gemology*, **44**(3), 2009, 234–41.

Seven colour-treated brown Tahitian

cultured pearls supplied by the Ballerina Pearl Co. and 12 untreated Tahitian cultured pearls were exposed to typical conditions of customer use (heat, household chemicals, daylight and some typical cosmetics) to determine their effects on the colour. Both groups gave similar largely negative results, but subtle changes were noticed after exposure to heat, with more significant changes observed when the samples were exposed to chemically reactive household cleaning solutions (bleaches). R.A.H.

Zur Flammenstruktur bei einigen porzellanartigen Perlen.

H.A. HÄNNI, 2009. *Gemmologie. Z.*

Dt. Gemmol. Ges., **58**(1/2), 47–52. 2 photographs, 5 photomicrographs, bibl.

The sheen displayed on nacreous pearls is due to the structure of stacked aragonite tablets in parallel superimposition. Non-nacreous pearls often show a flame structure that is due to a crosswise array of bundles of aragonite laths or fibres. Small bundles alternate in their orientation, so that some light is reflected and some absorbed, producing brighter and darker patches as in a flame structure. This is typical for the porcellaneous lining of marine gastropod shells and some bivalves, and their pearls produced by the same mantle tissue. Some of these bundles can also occasionally produce interference colours. E.S.

Beschädigungen an geschliffenen Edelsteinen.

H.A. HÄNNI. *Gemmologie. Z. Dt.*

Gemmol. Ges., **58**(3/4), 2009, 91–104. 22 photographs, bibl.

The article deals with the various factors that can influence a gem's durability. These can be caused during mining, manufacture and setting, cleaning or wearing. Damage to diamonds includes damage caused during cutting and setting or use, such as chipped girdle, worn facet edges, or abrasion by rubbing against other diamonds. More marked is damage to other gemstones, especially if in contact with diamonds. Naturally caused damage with time is the expansion of uranium-containing zircon inclusions and uraninite inclusions in sapphires, which can lead to chipping or fractures, especially during

Abstracts (continued)

repairs. During torch repairs diamonds are protected by coating with a borax compound; however, the same compound attacks rubies, sapphire and other gems during soldering. When borax is not used, diamond surfaces can be burned. Soldering can also cause heat stress and fracture in some set stones. An example shows a crater-shaped chip in a diamond caused by a soldering laser shot to a prong. Other examples show damage by removal of the polymer-filler in jade by ultrasonic cleaning and serious etching to peridot from acid cleaning after soldering. E.S.

Das neue Rubinorkommen von Montepuez, Mosambik.

H.A. HÄNNI and M.S. KRZEMNICKI. *Gemmologie. Z. Dt. Gemmol. Ges.*, **58**(3/4), 2009, 127–30. 6 photographs, bibl.

The new deposit is in the north-east of Mozambique and the first faceted stones from there were shown at the Hong Kong autumn Fair 2008. The rubies are found in an amphibolite, a metamorphic rock that also hosts the Winza deposit in Tanzania. Crystal habit is tabular to prismatic. The iron-containing rubies often show twin lamellae, contain minor rutile silk, corroded amphibolite grains, some zircons, fluids and secondary minerals in fissures. E.S.

Mit Kunstharz stabilisierter Seraphinit (Klinochlor).

U. HENN. *Gemmologie. Z. Dt. Gemmol. Ges.*, **57**(3/4), 2008, 143–5. 2 photographs, 1 graph, bibl.

Radial to fibrous aggregates of clinocllore are known in the trade as seraphinite. Material from Korshunovskoye in Siberia has been found to be polymer impregnated. Infrared spectra and density proved the material to have been treated. E.S.

Zirkone von Tansania: 'Malaya-Zirkon'.

U. HENN. *Gemmologie. Z. Dt. Gemmol. Ges.*, **58**(1/2), 2009, 67–72. 4 photographs, 2 graphs, 2 tables, bibl.

The zircons are found in the Tanga province in northern Tanzania. They are transparent and brown, yellow or red,

known in the trade as Malaya zircons. They are 'high crystalline', with high density and RI values, and with typical absorption spectra with narrow bands and fine lines of tetravalent uranium. All Malaya zircons fluoresce in brown or yellow-brown colours. E.S.

Sultanit — farbwechselnder diaspor aus der Türkei.

U. HENN. *Gemmologie. Z. Dt. Gemmol. Ges.*, **58**(1/2), 2009, 73. 1 photograph.

Diaspore from Mugla in Turkey shows an interesting colour change from greenish-brown in daylight to pink-brown in incandescent light. Material is called sultanate/zultanite. E.S.

Tiefgrüne Sphene aus Tansania.

J. HINTZE. *Lapis*, **34**(10), 2009, 29–30.

Specimens of green sphene, some translucent, are reported from Tanzania. M.O'D.

Vorkommen von Achaten in rhyolitischen bis dacitischen Vulkaniten Deutschlands und deren historische Gewinnung sowie Nutzung — Teil I.

G. HOLZHEY. *Gemmologie. Z. Dt. Gemmol. Ges.*, **57**(3/4), 2008, 77–102. 27 photographs, 1 map. Bibl.

The article deals with agates from rhyolitic to dacitic volcanic rocks with relatively little free silica, which are generally less known. In Freiburg these types of agates were already worked in the fifteenth to sixteenth centuries, while other agates from the Black Forest came into favour in the eighteenth to nineteenth centuries. In Thuringia rhyolite balls were well known in the seventeenth and eighteenth centuries, while about the same time Saxony produced many agate articles. E.S.

Vorkommen von Achaten in rhyolitischen bis dacitischen Vulkaniten Deutschlands und deren historische Gewinnung sowie Nutzung — Teil II (Sachsen).

G. HOLZHEY. *Gemmologie. Z. Dt. Gemmol. Ges.*, **58**(1/2), 2008, 3–46. 44 Photographs, 1 table.

The author deals in some detail with the locations and occurrences in Saxony. Mining first became important under

the reign of August I of Saxony in 1694 and gained popularity during the first half of the eighteenth century. Lapidary and goldsmiths' skills were developed in Dresden and master goldsmiths such as Taddel, Stiehl and Nueber produced beautiful pieces of hardstone mounted in gold, such as snuff boxes, table tops, fireplaces and cabochons for personal jewellery, mostly from banded jasper. E.S.

Fact or fiction: lessons from the history of gems.

D. HOOVER. *The Australian Gemmologist*, **23**(3), 2007, 117–25.

A transcribed lecture stating how erroneous, fabricated and misinterpreted information passed down through history has skewed information we perceive to be true today. As the lecturer quotes from Thomas Katz: "Frequent repetition can turn fictional breakthroughs into common lore." Without proper correction the future will continue to believe these stories as true. Several interesting examples are given to illustrate how false information has been handed down and what the correct information really is. (NB: A 'must read', if not for the information the author provides, then for the strength of character to believe not what others deem to be true, but what you do). J.S.

Magnetic susceptibility for gemstone discrimination.

D.B. HOOVER and B. WILLIAMS. *The Australian Gemmologist*, **23**(4), 2007, 146–59.

Delving into the past history, beginning with Pliny's writings of 2000 years ago, the author presents how magnets were used to aid in medicine, science and gemmology. Once calibrated, the presence and amount of a magnetic pull is an important indicator of the nature of growth and in differentiating between gem materials. For example, based on the amount of iron content in corundums, magnetic pull can differentiate between magmatic or metamorphic growth. In this example, the first of four magnetic principles is explored; the elemental make-up is magnetic (iron and magnesium). The other three are: diamagnetic (diamond and quartz),

Abstracts (continued)

paramagnetic (peridot and garnet) and ferromagnetic (inclusions in a diamond).
J.S.

Lune River petrified ferns: an overview.

R.E. JONES. *The Australian Gemmologist*, **23**(3), 2007, 131–5.

Tectonic movement led to volcanic activity creating the Lune River flora, an area of petrified plants in Tasmania. Dating zircon in the ash and sandstone in the area using Pb-U indicates that the specimens are from the Toarcian stage of the early mid-Jurassic period. Six genera are represented: *Cibotium tasmanense*, *Oguracaulis banksii*, *Osmundacaulis sp.*, *Lunea jonesii*, *Asbicaulis wrightii* and *Tasmanopteris richmondii*.
J.S.

Role of polyenes in the coloration of cultured freshwater pearls.

S. KARAMELAS, E. FRITSCH, J.-Y. MEVELLEC, S. SKLAVOUNOS and T. SOLDATOS. *European Journal of Mineralogy*, **21**(1), 2009, 85–7.

The examination of 21 untreated cultured freshwater pearls from *Hyriopsis* by diffuse reflectance UV-Vis-NIR and Raman scattering measurements at high resolution is reported. All natural colour samples show the two major Raman resonance features of unmethylated (unsubstituted) polyenes, not carotenoids. Their general formulae are $R-(CH=CH)_N-R'$ with $N = 6$ to 14, and they give absorptions from violet to yellow-green.
R.A.H.

Aquamarine, quartz and topaz in kimberlites: case studies from Minas Gerais State, Brazil.

J. KARFUNKEL, G.N.C. SGARBI, P.B. DE A. SGARBI, P.A.F. DE BROU, O.S. FRANCA, D.B. HOOVER and R. WEGNER. *Gemmologie. Z. Dt. Gemmol. Ges.*, **58**(3/4), 2009, 105–14. 10 photographs, 2 maps, bibl.

Most gems form in magmatic rock, with many coloured stones coming from pegmatites. Diamonds originate mainly from kimberlites. Recent finds of aquamarine, quartz and topaz in kimberlites from central-west Minas Gerais State apparently contradict accepted genetic aspects. The study from this region explains their occurrence in weathered pipes as 'hitchhikers'. Pegmatite fragments detached probably

many hundreds of metres below surface from their original rock were plucked and incorporated into the ascending magma and transported to the surface. The gems were released near the surface and tropical weathering processes did not affect them as much as some kimberlite minerals. These finds might be important for coloured gem prospectors in avoiding wrong interpretations.
E.S.

Identification of the endangered pink-to-red Stylaster corals by Raman spectroscopy.

S. KATAMELAS, E. FRITSCH, B. RONDEAU, A. ANDOUCHE and B. MÉTIVIER. *Gems & Gemology*, **45**(1), 2009, 48–52.

Raman scattering revealed that corals of the *Stylaster* genus (as opposed to those of the *Corallium* genus which include most pink-to-red corals used in jewellery) are made of aragonite and contain carotenoid pigments (polyenic pigments substituted with methyl groups), whereas those of the *Corallium* genus are coloured by unmethylated polyenic pigments and consist of calcite.
R.A.H.

Solution-generated pink color surrounding growth tubes and cracks in blue to blue-green copper-bearing tourmalines from Mozambique.

J.I. KOIVULA, K. NAGLE, A. H-T. SHEN and P. OWENS. *Gems & Gemology*, **45**(1), 2009, 44–7.

From the examination of several transparent, faceted, blue to blue-green copper-bearing tourmalines containing growth tubes and cracks surrounded by sleeves of pink colour, it is suggested that the probable cause of the pink colour is treatment with a radioactive solution. There was no visual evidence of heat treatment.
R.A.H.

Hackmanite/sodalite from Myanmar and Afghanistan.

D. KONDO and D. BEATON. *Gems & Gemology*, **45**(1), 2009, 38–43.

Many samples of sodalite from Myanmar and about half of those studied from Afghanistan showed the distinct tenebrescence characteristic of hackmanite, but a few saturated blue-to-purple Myanmar specimens and some very desaturated Afghan specimens showed little or no colour change on exposure to UV radiation or bright

white light. Such stones with no or only very weak tenebrescence may best be referred to as sodalite (despite containing sulphur). It is suggested that only sodalite with notable tenebrescence be called hackmanite.
R.A.H.

Gem news international.

B. LAURS (ED.). *Gems & Gemology*, **44**(3), 2009, 262–82.

Items mentioned include fluorite impersonating colour-change garnet, colourless cut forsterite from the Mogok area and from Tadjikistan, a tourmaline crystal within a crystal, a cluster of aquamarine crystals from Namibia showing trapiche structure and long crystals of spodumene extending from a matrix of K-feldspar reportedly from Afghanistan.
R.A.H.

Gem News International.

B.M. LAURS (ED.). *Gems & Gemology*, **44**(4), 2008, 369–79.

Items mentioned include a visit to andesine mines in Tibet and Inner Mongolia, a particularly vivid gem-quality kunzite from Pala, California, synthetic citrine with abundant nail-head spicules and a cobalt-blue synthetic quartz.
R.A.H.

Gem news international.

B. LAURS (ED.). *Gems & Gemology*, **45**(1), 2009, 59–75.

Items noted include opals from Ethiopia, gem-quality rhodochrosite from China, colour-zoned Moroccan amethyst, cabochons of intergrown malachite and azurite, kornepupine from Tanzania, crystals of pink zoisite from Afghanistan, gem-quality blue kyanite from Myanmar, Australian chrysoprase with dendritic inclusions and inclusions of ankangite and celsian in quartz from Brazil (for which analyses are given).
R.A.H.

Gem News International.

B.M. LAURS (ED.). *Gems & Gemology*, **45**(2), 2009, 142–55.

Items mentioned include the first occurrence of a star apatite, translucent bluish-green crystals from Bahia State, Brazil, of 'sugarcane emerald' with white mottled veins (some set as jewellery), distinctly orange kyanite crystals from Tanzania, and unusual colourless cut stones of petalite (14.98 ct) and pollucite (11.30

Abstracts (continued)

and 12.10 ct) reportedly from Laghman province, Afghanistan. A description is also given of mining in Cambodia for brownish zircons which yield blue crystals after heat treatment. R.A.H.

Gem News International.

B.M. LAURS (Ed.). *Gems & Gemology*, **45**(3), 2009, 214–32.

Brief descriptions are given of an 8 cm long aquamarine crystals with inclusions resembling seaweed, a phenakite from Madagascar exhibiting chatoyancy, garnets from Kenya showing a colour change from greenish in daylight to bluish violet in incandescent light, lilac-coloured Cu-bearing tourmaline from Nigeria, sapphires from the Vortex mine in Montana showing a uniform cornflower-blue colour and mabe pearls from Vietnam with seashell nuclei. R.A.H.

Polymer-filled aquamarine.

LI JIANJUN, S. YUAN, H. WANGJIAO, L. HAN, C. YOUFA, L. HUAIFENG, L. YING, Y. HONG and F. CHENGXING. *Gems & Gemology*, **45**(3), 2009, 197–9.

Polymer-filled aquamarines which have been appearing on the Chinese jewellery market can be identified readily using a standard gemmological microscope as this material shows a flash effect and relief lines. Some of the filled fractures fluoresce chalky white in long-wave UV radiation. FTIR spectroscopy reveals diagnostic features at ~ 3100–2850 cm^{-1} . R.A.H.

LED lightsources and gemmological instruments that analyse colour.

T. LINTON. *The Australian Gemmologist*, **23**(4), 2007, 177–9.

As the colour temperature of LEDs (light emitting diodes) can vary dramatically (from 5000 to 8000K), so does their effect on gemstones. The pleochroic and dichroic colours seen through a dichroscope have traditionally been obtained using tungsten lamps (2800K). Using the 'whiter' light of LEDs will alter these colours from what has hitherto been considered the standard. Three images show the different spectral absorptions of over 6000K LED, 6000K LED and 5000K daylight equivalent light, further showing how spectra can vary even within the close proximity of similar

temperature colour. The author suggests LEDs are very good for microscopic evaluations while a Solux 50W halogen lamp will better serve the purpose for a dichroscope and Chelsea colour filter. J.S.

Sanidin aus der Eifel-als wasserklarer Edelstein.

H. LOCKER. *Lapis*, **34**(6), 2009, 13–18.

Notably inclusion-free sanidine feldspar is described from the Eifel region of Germany. M.O'D.

Echte Edelsteine?

H. LOCKER. *Lapis*, **34**(9), 2009, 13–19.

It is suggested that a translucent to transparent blue volcanic glass from the Eifel region of Germany may have ornamental potential. M.O'D.

Mushroom elbaite from the Kat Chay mine, Momeik, near Mogok, Myanmar: II. Zoning and crystal growth.

A. J. LUSSIER, F. C. HAWTHORNE, S. HERWIG, Y. ABDU, P. M. AGUIAR, V. K. MICHAELIS and S. KROEKER. *Mineralogical Magazine*, **72**(5), 2008, 999–1010.

A variety of mushroom tourmaline from the Kat Chay mine, Myanmar, has a black-to-grey single-crystal core, the remaining 50% consists of extremely acicular, sub-parallel crystals that diverge towards the edge of the mushroom. These acicular crystals are dominantly colourless to white, and pale pink outside the black zone. Microprobe results confirm that both the crystal core at the base of the mushroom and the material near the top are elbaite, the principal substitutions being $\text{Li} + \text{Al} = 2 \text{Fe}$ and $\text{B} + \text{Al} = \text{Si} + \text{Fe}$. It is suggested that the changes in habit are driven in part by changes in external variables such as T and P . R.A.H.

Der Opal Jaspis von Tautenhain, Sachsen.

J. LÜTICH. *Lapis*, **34**(1), 2009, 40–4.

Jasper with an opal-like play-of-colour against a predominantly orange-brown background is described from Tautenhain, Saxony, Germany. M.O'D.

Famous mineral localities: Volodarsk-Volynski, Zhitomir Oblast, Ukraine.

P. LYCKBERG, V. CHORNOUSENKO and W.E. WILSON. *Mineralogical Record*, **40**(6), 2009, 473–506.

Green beryl and blue topaz, some with apparent gem potential, are described from a major pegmatite in north-central Ukraine. M.O'D.

The Sapó mine.

L. MENZES. *Mineralogical Record*, **40**(4), 2009, 273–96.

Attractive and ornamental-quality crystals of apatite and tourmaline are described from the Sapó mine, located in a pegmatite about 40 km NW of Conselheiro Pena, Minas Gerais, Brazil. M.O'D.

Gemmologie Aktuell.

C.C. MILISENDA and K. WEHR. *Gemmologie. Z. Dt. Gemmol. Ges.*, **58**(3/4), 2009, 77–89. 16 photographs.

Transparent to translucent orange-brown kyanite crystals were examined; these were found in the new spessartine garnet occurrence near Loliondo in north Tanzania. Two rectangular faceted stones of 0.30 ct and 0.80 ct were also received. Also from Tanzania (Longido) came some green oligoclase with an unusual mint-green colour; the transparent faceted stone weighed 8.64 ct. Also from Tanzania came two faceted green kornupines and some faceted light yellowish-green diopside.

Other stones described included a demantoid garnet from Madagascar, a sillimanite cat's-eye from Guinea in West Africa, a trapiche tourmaline from Zambia, and pink fire quartz from Brazil. The latter are rock crystals with aventurescent inclusions. Also mentioned were euclase from Colombia and colourless pollucite from Pakistan; also from Pakistan some green pargasite crystals and a brown-yellow sphene twin with a greenish tinge weighing 92.79 ct.

Also described are some scapolite cat's-eyes from Afghanistan; these are violet transparent cabochons weighing between 1.40 and 8.63 ct. Some greenish-brown rough and faceted stones were offered in the trade as dunilite. These were identified as olivines, originally described by Dunil P. Gunasekera, hence the name dunilite.

Opaque white stones were recently offered in the trade as howlites, but were

Abstracts (continued)

identified as a barium-sulphate ceramic. A transparent cushion-cut sapphire of unusual neon-blue colour weighing 0.89 ct was shown to be cobalt treated. E.S.

Edele Zirkone aus dem Sächsischen Vogtland.

W. MODALECK, G. SEIFERT and S. WEISS. *Lapis*, **34**(2), 2009, 13–27.

Zircon of gem quality is described from the Vogtland area, Saxony, Germany. Specimens of various colour are illustrated: yellow to reddish-brown colours appear to dominate and phantom specimens (zircon in zircon) are also illustrated. M.O'D.

Collector profile: John S. White, Jr., and his single crystal collection.

T.P. MOORE. *Mineralogical Record*, **40**(3), 2009, 215–23.

A biography of the former Curator-in-Chief of the mineralogical collection at the Smithsonian and founder of the *Mineralogical Record*. Some examples from his collection of single crystals and twins are illustrated in colour. M.O'D.

What's new in Minerals.

T.P. MOORE. *Mineralogical Record*, **40**(3), 2009, 239–58.

Vayrnenite of gem quality was exhibited at the 2009 Tucson show. The orange crystal came from Shengus, Shigar Valley, Skardu District, Northern Areas, Pakistan. The crystal was displayed alongside a faceted stone of 1.89 ct. In the same show was a green twinned crystal of titanite from Mpwapwa, Dodoma Province, Tanzania. M.O'D.

Mexico V.

T.P. MOORE, M. ORIGIERI, T.C. WALLACE and B.L. CROSS. *Mineralogical Record*, **39**(6), 2008, 13–26.

Beautifully illustrated survey of spectacular minerals found in Mexico. The text is well written. M.O'D.

Lab Notes.

T.M. MOSES and S.F. McCLURE (Eds). *Gems & Gemology*, **44**(3), 2009, 252–60.

Notes are given on a citrine with Brazil law twinning visible to the naked eye, a 74 mm long inclusion of emerald in quartz, a calcite 'melt' in a Tanzanian grossular and a rare yellow trapiche sapphire. R.A.H.

Lab Notes.

T.M. MOSES and S.F. McCLURE (Eds). *Gems & Gemology*, **44**(4), 2008, 364–8.

A note is given of induced copper contamination of two cut 'water-melon' tourmalines. R.A.H.

Lab Notes.

T.M. MOSES and S.F. McCLURE (Eds). *Gems & Gemology*, **45**(2), 2009, 134–40.

Items noted include a 22.21 ct peridot with a distinct four-rayed star and a 5.44 ct tourmaline double cabochon showing silver chatoyancy on one side and a golden eye on the other. R.A.H.

Lab Notes.

T.M. MOSES and S.F. McCLURE (Eds). *Gems & Gemology*, **45**(3), 2009, 208–13.

Items noted include a striking 6.64 ct polished quartz crystal coloured green by inclusions of pumpellyite and a 2.62 mm long, doubly terminated columbite crystal inclusion in colourless topaz from Pakistan. R.A.H.

Update on ammolite production from southern Alberta, Canada.

K.A. MYCHALUK. *Gems & Gemology*, **45**(3), 2009, 192–6.

Since 2001, the dominant supplier of ammolite (a gem material composed of aragonite in the shells of ammonites) from the area southwest of Lethbridge, Alberta, reports a 40% increase in finished stone production. 'Dinolite', in which ammolite is combined with siliceous dinosaur bone, is being produced as yet another use of ammolite. R.A.H.

Lapis lazuli and phlogopite paragenesis from Sar-e-Sang deposit (Badakhshan, Afghanistan).

L. NATKANIEC-NOWAK, W. HEFLIK and M. DUMAŃSKA-SŁOWIK. *Gemmologie. Z. Dt. Gemmol. Ges.*, **57**(3/4), 2008, 103–12. 9 photographs, 1 table, bibl.

From the investigations of the overgrowths of lapis lazuli on phlogopite flakes from the Sar-e-Sang deposit in Afghanistan, it can be concluded that the paragenesis is a product of postmagmatic and metasomatic activities. E.S.

'Cristalli' — Sonderschau die Sammlung Adalberto Giazotto in Florenz.

F. PEZZOTTA and G. PRATESI. *Lapis*, **34**(10), 2009, 61–4.

Gem quality minerals are a feature of the Florentian Adalberto Giazotto. M.O'D.

Gota de Aceite: nomenclature for the finest Colombian emeralds.

R. RINGSRUD. *Gems & Gemology*, **44**(3), 2009, 242–5.

The finest and rarest emeralds have been said to have an optical effect termed *gota de aceite*, used to describe a particular aspect of emerald clarity associated with Colombian emeralds. This phenomenon and the gemmological causes of it are described and illustrated. The term should be used only after a careful examination and an understanding of the growth structures that cause the effect. R.A.H.

Winza, ein neues Rubinorkommen in Tansania.

K. SCHMETZER, W. RADL and D. SCHWARZ. *Lapis*, **34**(5), 2009, 41–6.

Ruby of gem quality is described from Winza in central Tanzania where it occurs in amphibolite. Some well-formed crystals are described and illustrated. M.O'D.

Rubine und Saphir aus Winza-eine Ergänzung.

K. SCHMETZER, W. RADL and D. SCHWARZ. *Lapis*, **34**(6), 2009, 48.

Additional notes on ruby found at Winza, Tanzania. A table summarizing the morphologies of this material is given. M.O'D.

'Deutscher Lapis': Der Nunkircher Jaspis und seine Verwendung.

H. SCHMITT. *Lapis*, **34**(9), 2009, 20–4.

A bluish jasper thought to resemble lapis lazuli is reported from the Nunkircher area, Germany. M.O'D.

Rubies and sapphires from Winza, central Tanzania.

D. SCHWARZ, V. PARDIEU, J.M. SAUL, K. SCHMETZER, B.M. LAURS, G. GIULIANI, L. KLEMM, A.-K. MALSY, E. EREL, C. HAUZENBERGER, G. DU TOIT, A.E. FALICK and D. OHNENSTETTER. *Gems & Gemology*, **44**(4), 2008, 322–47.

Rubies and sapphires are being mined from both eluvial and primary deposits at Winza. The gem corundum is related to 'dykes' of Proterozoic amphibolitic rocks. Prismatic-tabular-rhombohedral and dipyrmidal types occur. In general, medium and dark red rubies are rhombohedral, whereas pink, purple

Abstracts (continued)

and blue sapphires are, for the most part, dipyrarnidal. The top-quality rubies are characterized by long tube-, fibre-, needle- or hair-like inclusions containing limonitic material. The lower-quality material generally contains a larger amount of solid inclusions (mostly amphibole crystals), fissures and growth features. The corundum from this area has bluish violet colour zones parallel to the prism and basal pinacoid. A relatively high Fe content (>2370 ppm) of Winza rubies distinguishes them from most other natural and almost all synthetic counterparts.

R.A.H.

Natural gamma radioactivity and exploration for precious opal in Australia.

B.R. SENIOR and L.T. CHADDERTON. *The Australian Gemmologist*, **23**(4), 2007, 160–76.

Through both spontaneous fissions, indicated by the high barium content, and radioactive decay of the trace elements uranium and thorium found in opals, there is a quantifiable amount of gamma ray emission. Utilizing the radioactive properties associated with opals and their surrounding environment it is possible using gamma ray logging to assess their location. Calibrated gamma ray logging can locate the host rock of opals, its quality and the relative depth.

J.S.

Structural characterization and chemical composition of aragonite and vaterite in freshwater cultured pearls.

A.L. SOLDATI, D.E. JACOB, U. WEHRMEISTER and W. HOFMEISTER. *Mineralogical Magazine*, **72**(2), 2008, 579–92.

Vaterite and aragonite in freshwater cultured pearls from mussels of the genus *Hyriopsis* (*Unionidae*) were structurally and compositionally characterized by Raman spectroscopy, micro computer tomography, high resolution field emission SEM and LA-ICP-MS. The appearance of vaterite in pearls is related to the initial stages of biomineralization, but vaterite cannot be a precursor to aragonite. Vaterite is not related to a particular crystal habit and therefore does not have a structural function in the pearls. Larger contents of such elements as P and S in vaterite, as well as larger total organic contents in vaterite as

opposed to aragonite, in conjunction with larger amounts of Mn²⁺ and Mg²⁺, imply a stabilizing role for organic molecules and X²⁺ ions for biological vaterite. Distribution coefficients between aragonite and vaterite for provenance-independent elements, such as Mn and Mg (0.27 and 0.04, respectively) agree very well with those observed in fish otoliths.

R.A.H.

The Miguel Romero collection of Mexican minerals.

T.C. WALLACE and others. Supplement to *Mineralogical Record*, **39**(6), 2008.

Overview in colour of the Romero collection of Mexican minerals formed by the late Miguero Sanchez. Many specimens are ornamental or gem quality; none of the items illustrated have been fashioned.

M.O'D.

Ruby suites from New South Wales.

G. WEBB. *The Australian Gemmologist*, **23**(3), 2007, 99–116.

Corundum samples were analyzed for their gemmological features, absorption spectra, fluorescence, inclusions and chemical composition from seven New South Wales localities. Some trace elements seem to be diagnostic for the determination of geographic and geologic origin in some of the localities. Rubies from Swan Brook, Bingara, and Macquarie and Cudgegong rivers contain Sn, an element common in tin-bearing granite locations. Rubies from Swan Brook showed higher amounts of Ga compared to the surrounding localities, indicating magmatic inception. Other areas studied are Barrington Tops, Tumbarumba and Yarrowitch Valley.

J.S.

Sammlersteine.

K. WEHR, C.C. MILISENDA and M. WILD. *Gemmologie. Z. Dt. Gemmol. Ges.*, **57**(3/4), 2008, 113–32. 20 photographs, 2 graphs, 1 table, bibl.

Collector stones are not commercially viable due to their low hardness, perfect cleavage, low resistance to heat, brittleness or solubility in water, which makes cutting and faceting difficult. Some of these rare gemstones have recently been examined by the DSEF German Gem Lab and are presented in this article together with photographs and physical and optical properties. They are anatase from Pakistan,

parisite from Colombia, anglesite from Morocco, charlesite from South Africa, rhodizite-londonite from Madagascar, powellite from India, montebrasite from Brazil, xenotime from Afghanistan, monazite from Brazil, lazulite from Brazil, triphylite-lithiophilite mixed crystal from Brazil, triplite from Afghanistan, kovdorskite from Russia, legrandite from Mexico, katapleite from Canada, hackmanite from Afghanistan and Canada, staurolite from Brazil, chromepidote (tawmawite) from Pakistan, vlasovite from Canada, leucite from Italy, enstatite from Tanzania, poldervaartite-olmiite mixed crystal from South Africa and whewellite from Saxony (Germany). Many reflection spectra are given. There is also an extensive table showing the chemical composition, colour, RI, DR, density, hardness and literary references for these stones.

E.S.

Photochromismus in Hackmaniten aus Afghanistan und Myanmar.

K. WEHR, C.C. MILISENDA and M. WILD. *Gemmologie. Z. Dt. Gemmol. Ges.*, **58**(3/4), 2009, 115–26. 10 photographs, 5 graphs, bibl.

Some gem-quality sodalites and hackmanites have recently appeared in the trade; they have been mined in the Badakhshan Province in Afghanistan and in the Mogok area in Myanmar. The term hackmanite has been used either for the sulphur-bearing and/or pink variety that shows tenebrescence (photochromism), i.e. they changed their colour commonly to an intense violet in response to either sunlight or UV exposure and faded when kept in the dark or by exposure to white light.

E.S.

Röntgen-Mikro-Computertomographie: Zerstörungsfreier Einblick in das Innere von Zuchtperlen.

U. WEHRMEISTER, A. SOLDATI, H. GOETZ, D.E. JACOB, W. XU, H. DUSCHNER and W. HOFMEISTER. *Gemmologie. Z. Dt. Gemmol. Ges.*, **58**(1/2), 2009, 53–66. 7 X-rays and tomographs, 1 table, bibl.

Computerized three-dimensional X-ray micro tomography is capable of revealing the internal structure and some of the material properties of pearls at high resolution, and is thus a more useful tool

Abstracts (continued)

in pearl testing than conventional X-ray radiography. Differences in transparency to X-rays (radiodensities) can be detected and speed up the process locating different CaCO₃ polymorphs. When combined with Raman spectroscopy, vaterite-containing areas can be identified. E.S.

Hyazinthe und 'Malakone' im Ofen: Zur Farbarsache und Fluoreszenz sächsisch/bayerischer Zirkone.

S. WEISS and S. MEIER. *Lapis*, **34**(2), 2009, 37–40.

The colour of zircon from different localities is described with notes on chemical composition and its possible influence on colour. M.O'D.

Neufund: Kupferhaltiger Aquamarin aus dem Binntal.

S. WEISS and A. GORSATT. *Lapis*, **34**(10), 2009, 54–60.

Aquamarine is reported from the Binntal area of Switzerland which may owe its colour to copper. M.O'D.

Wilensky fine materials.

W.E. WILSON. Supplement to *Mineralogical Record*, **40**(3), 2009.

Several mineral examples with possible ornamental quality are featured in this survey of some of the collection of Wilensky Fine Minerals. The survey includes very high-quality colour photographs. M.O'D.

Famous mineral localities: the Merelani tanzanite mines, Lelatema Mountains, Arusha Region, Tanzania.

W.E. WILSON, J.M. SAUL, V. PARDIEU and R.W. HUGHES. *The Mineralogical Record*, **40**(5), 2009, 346–408.

History of the discovery and development of the tanzanite mines at Merelani, Tanzania, with illustrations of major specimens retrieved and brief biographies of some of those engaged in the prospecting and marketing. M.O'D.

Pressures beyond rubies.

A. WRIGHT. *Geoscientist*, **19**(11), 2009, 16–17.

An exceptionally large specimen of ruby in zoisite is described from the Merkerstein area of northern Tanzania. M.O'D.

Gem-quality yellow-green h a yne from Oldoinyo Lengai volcano, northern Tanzania.

A.N. ZAITSEV, O.A. ZAITSEVA, A.K. BUYKO, J. KELLER, J. KLAUDIUS and A.A. ZOLOTAREV. (Ed.). *Gems & Gemology*, **45**(3), 2009, 200–3.

Yellow-green to green-yellow gem-quality h a yne is reported for the first time from an alkaline plutonic rock from the active Oldoinyo Lengai volcano. The h a yne has the typical optical and physical properties for sodalite-group minerals. Infrared and Raman spectroscopy showed that in addition to the (SO₄)²⁻ group, this mineral also contains (NO₃)⁻, (CO₃)²⁻, and water in the structure. The presence of Ca, Al, and Si as major cations, with minor K, was confirmed. A 1.53 ct brilliant cut yellow-green faceted stone is illustrated. R.A.H.

of fire opal marketed as 'Mexifire'. Some of its gemmological properties are similar to those of natural fire opal, though the low specific gravity of <1.77 offers strong evidence for a synthetic origin. Further indications of this include the relatively low refractive index of <1.40 and the presence of scattered pinpoint inclusions when examined at high magnification. R.A.H.

Identification of melee-size synthetic yellow diamonds in jewelry.

H. KITAWAKI, A. ABDURIYIM and M. OKANO. *Gems & Gemology*, **44**(3), 2009, 202–13.

Melee-sized (0.05–0.30 ct) yellow synthetic diamonds have been examined using infrared microspectroscopy in combination with cathodoluminescence imaging for rapid and accurate distinction between these sizes of natural and synthetic diamonds, based on their characteristic mid-IR absorption spectra and growth structures. It has been established that approximately 10% of loose and dozens of mounted yellow melee diamonds submitted recently were synthetic. R.A.H.

Instruments and Techniques

Application of the Vis-NIR Avaspec-2048 portable automatic spectrometer to distinguish gem-quality materials.

D. BERNINI, F. CAUCIA and M. BOIOCCHI. *S. Neues Jahrbuch f ur Mineralogie, Abhandlungen*, **185**(3), 2009, 281–8.

The use of the Avaspec-2048 fibre optic spectrometer to analyse the Vis-NIR spectra of cut gemstones is described. For each sample, however, the spectrum is influenced by such factors as the shape of the stone, the number of carats, the size of the exposed surface, and the intensity and tonality of the colour. An efficient use of this instrument to discriminate gemstones is only possible after a large and comprehensive database has been developed. R.A.H.

A new type of synthetic fire opal: Mexifire.

G. CHOUDHARY and R. BHANDARI. *Gems & Gemology*, **44**(3), 2009, 228–33.

A description is given of a new type

The TrueGemColor system: a new computer color imaging system based on a uniform CIELAB color space for color grading of gemstones.

Y. LIU and K.N. HURWIT. *Gemmologie. Z. Dt. Gemmol. Ges.*, **57**(3/4), 2008, 133–42. 6 charts, 3 graphs, bibl.

A computer colour imaging system has been developed that incorporates a Universal Colour Grading system based on a uniform CIELAB colour space with 22 hues, 7 lightness levels and 4 saturation intensities. This system gives a reference colour grade which matches the average colour of the gemstone to be graded under standard light conditions (CIE D65 light source and neutral surrounding background) and also provides a corresponding CIELAB colour coordinate. For coloured diamonds, it gives the colour grade using fancy colour diamond terminology. The colour is precisely profiled and can be calibrated by the user. E.S.

Abstractors

R.A. Howie – R.A.H.

M. O'Donoghue – M.O'D.

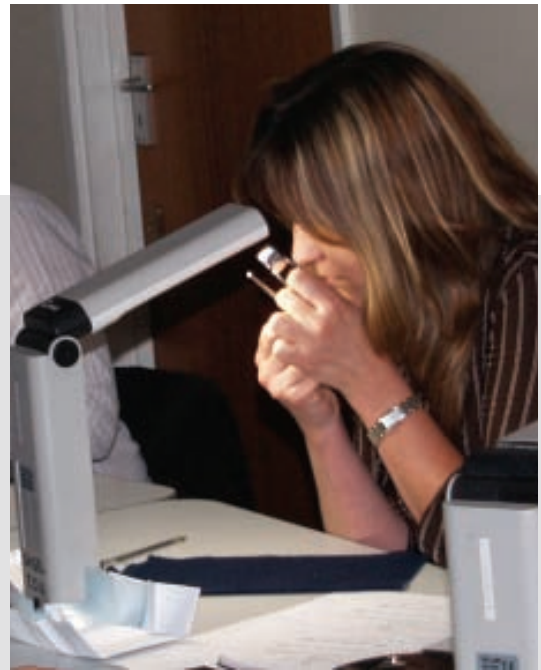
J. Sheby – J.S.

E. Stern – E.S.

Gem-A WORKSHOPS

Spring 2010

- Mon 8 March **ALLURE OF GEMS**
The perfect introduction to the world of gemstones.
£97.00. Gem-A members and students £79.00
- Mon 22 March **INTRODUCTION TO PRACTICAL GEMMOLOGY**
How to test gems with basic gemmological equipment. Ideal for anyone considering a more in-depth study of gemmology and would like a 'taster' or for those wanting to brush up on existing skills.
£97.00. Gem-A members and students £79.00
- Mon 12 April **DIAMOND BUYING GUIDE**
An introduction to the 4Cs, carat weight, colour, clarity and cut.
£97.00. Gem-A members and students £79.00
- Wed 28 April **BEAD STRINGING I**
An introduction to the techniques needed for basic bead stringing.
£156.00. Gem-A members and students £115.00
- Thurs 29 April **BEAD STRINGING II**
Gain an insight into the techniques needed for multi-strand and graduated beads, and some of the more complicated designs.
£156.00. Gem-A members and students £115.00
- Mon 26 April **RUBY, SAPPHIRE AND EMERALD**
A day dedicated these important gemstones and their treatments, imitations and synthetic counterparts.
£97.00. Gem-A members and students £79.00



From its headquarters in the Hatton Garden jewellery quarter, Gem-A provides a varied programme of workshops ranging from an introduction to the fascinating world of gemstones to information on the latest synthetic and treated gemstones.

For further information or to book for a workshop go to www.gem-a.com or call Paveet Amrit on +44 (0)20 7404 3334 email paveet.amrit@gem-a.com



Gem-A

THE GEMMOLOGICAL ASSOCIATION
OF GREAT BRITAIN

Gem-A Shop



Don't miss the monthly **SPECIAL OFFERS**
on books and instruments from the
Gem-A Shop

Log on to the Gem-A website at www.gem-a.com to discover what is on offer each month.

Book reviews

Laboratory-grown Diamonds. Information Guide to HPHT and CVD-grown Diamonds. Second edition.

BRANKO DELJANIN and DUSAN SIMIC, 2009. Gemology Headquarters International, Mumbai, India. pp 86. £15.00.

Attractively produced, well referenced and with many small but sharp colour photographs, this is a useful guide to the fast-changing diamond synthesis scene. HPHT and CVD-grown diamonds are highlighted. M.O'D.

Eifel. Die Mineralien der Vulkaneifel. extraLapis No. 34.

2008. Weise, Munich, Germany. pp 98, illus. in colour. €17.80.

Minerals, some of near-gem or ornamental quality, are described from the Eifel region of Germany. The area is noted for hauyne, a species of the forsterite-fayalite series, and for fine examples of bright orange hematite of micromount size. Details of the volcanic geology are described. M.O'D.

Freiberg. Mineralien, Bergbau und Museen. extraLapis No. 36.

2009. Weise, Munich, Germany. pp 100, illus. in colour. €17.80.

Survey, of the major mineral deposits, species and mineralogical museum collections of the Freiberg area of Germany. M.O'D.

The Immortal Stone: Chinese Jades from the Neolithic Period to the Twentieth Century.

JAMES C.S. LIN, 2009. Scala, London. pp 160. Illus. in colour. Hardcover, ISBN 978 1 85759 581 9 £29.95; paperback ISBN 9781857595949 £14.95.

This attractive and welcome survey is the first catalogue of the important collection of jades in the Fitzwilliam Museum, Cambridge. The collection consists largely of specimens bequested

by Oscar Raphael in 1946 and contains many items of high quality which are illustrated in colour in the book with a high standard of reproduction.

The book also includes an essay on the nature of the two jade minerals and on the use and significance of jade in different dynasties: there is a comprehensive bibliography and a table of Chinese characters to be found on the jade artefacts in the collection. Notes are given on the marketing of jade in and from the Song Dynasty of 960–1279, and from earlier dynasties. I have rarely seen a study in any field to equal this. M.O'D.

China: Mineralien, Fundstellen, Lagerstätten.

BERTHOLD OTTENS, 2008. Weise, Munich, Germany. pp 552, illus. in colour. Hardcover, €9.00. (In German.)

An English language version of this exhaustive survey of minerals of China would be most welcome. Many items depicted appear to be of ornamental quality. M.O'D.

Quartz. extraLapis No. 37.

2009. Weise, Munich, Germany. pp 100, illus. in colour. €7.80.

Well illustrated but lacking a bibliography, this survey of the quartz varieties is well up to the standard of this long-running series. M.O'D.

Emeralds: A Passionate Guide.

RONALD RINGSRUD, 2009. Green View press, Oxnard, California. pp 382. £75.00.

Most attractively illustrated overview of the nature of emerald, printed on heavy art paper which allows excellent reproduction of the colour photographs. As well as being a guide to the history, appreciation and grading of emeralds, it is a good read and invaluable to the gem dealer and appraiser. M.O'D.

American Mineral Treasures.

G. STAEBLER and W.E. WILSON, 2008. Lithographie LLC, East Hampton, Connecticut. pp 368. Hardcover, ISBN 9780979099823. Price US\$85.00.

This is a magnificent book, unequalled and a most welcome survey, beautifully illustrated with photographs of the highest quality. The page size is 33 x 24 cm and there are 368 of them. Every opening shows some colour. Due to the excellent paper and the solid binding, the book needs to be supported when consulted.

The arrangement of the text appears to be random but a clear index precedes the major descriptive section. A comprehensive bibliography and literature for further reading completes the book.

The aim of the book is to introduce and describe some of the major mineral deposits of the United States and to illustrate the finest specimens obtained from them. Very many of the sites described produce gem material and so the book is of especial value for the gemmologist. Naturally most of the alluvial deposits are not covered as site and product might be less visually arresting.

Historical notes are plentiful and their profusion shows the depth of the source material consulted for the book.

I cannot sufficiently praise the enterprise of the authors and their assistants. The book may perhaps provide a 'Tucson at home'. M.O'D.

Gems and Mines of Mogok.

T. THEMELIS, 2008. A & T Publishers, Bangkok. 352 pp. Over 800 colour figures, most of which are made up of several items. Hard cover. ISBN 0940-965-30-5. US\$ 129 plus postage and packing.

There is far more in this book than the title would suggest and it is a photographic feast. It covers the history of the area, its geological evolution, mineralogy and crystallography; it

Book reviews (continued)

provides a cornucopia of fine photographs of mines, minerals and gems, and local life, almost all taken by the author. He describes himself as a 'non-trained geologist', but he has enjoyed the co-operation of Burmese university geologists and several eminent geologist/gemmologists in the field during his nine visits between 1996 and 2004. He is an internationally recognized expert on the heat treatment of gemstones.

The book is divided into five wide-ranging chapters with six appendices and a bibliography of over 400 references. In Chapter I – Geology of Mogôk – he describes (with the aid of diagrams) the geological evolution of the area from the break-up of Gondwanaland to the collision of the Indian and Asian plates, and the major regional structural features. He provides a new geological map of the Mogôk area (a collaborative work with Burmese geologists). The local rocks are described under the following broad types: Igneous, Mantle and Metamorphic, with excellent photos of hand specimens, field outcrops, mines and photomicrographs (PPL and crossed polars) of thin sections.

In Chapter 2 – Genesis of Ruby, Spinel, Sapphire and Peridot – he discusses the classification of Mogôk gems and divides them, according to their mode of formation, into conveniently tabulated Metamorphic, Igneous and Skarn or Contact origins. There is a useful map showing mining areas where ruby, sapphire, spinel, peridot, pegmatite gems, mixed gems and alluvial gems respectively are dominant. The main part of the chapter deals in detail with the crystal form and habit, chemistry and inclusions of the above gems, with an excellent series of photos of gem minerals in matrices.

Chapter 3 – Gem Mining in Mogôk – starts with a short history outlining

mining developments from pre-history to 1886, under the British from 1886 to 1947 and then under various Burmese administrations after independence. He divides mining into primary workings (largely in syenites and marbles) and secondary (mainly alluvial workings). Mining methods include sinking shafts, sluicing, open-pit operations and recovery from twisted holes, cavity fillings and tunnelling. Sorting methods include washing by hand and in pulsating jigs, and recovery from discarded material – the 'kanase' tradition (largely carried out by women). There are maps of smuggling routes out of Burma and annual production tables. There is a detailed photographic coverage of these operations.

Chapter 4 – The Gem Mines of Mogôk – starts with a very useful map of the Mogôk area divided into ten sub-areas (running from East to West) showing the locations of the mines. Detailed maps of each area are accompanied by photos of mines showing working methods along with lists of the gem minerals recovered from them. There are excellent photos of crystals in matrix and cut stones from the mines.

Chapter 5 – Profiles of Mogôk Gems – is arranged alphabetically and gives details of some sixty gem species with their gemmological properties and lists the mines and rock assemblages in which the gems are found. Each species' description is accompanied by very good photos of cut stones showing colour varieties.

There are six appendices: (A) List of the Pain Collection of Mogôk gemstones in the Natural History Museum, London; (B) A short account of gem enhancement methods; (C) A brief description of gemstone identification techniques; (D) Tabulated properties of Mogôk gem minerals including colour; (E) List of Burmese gemmological jargon; and (F)

Detailed list of Mogôk gem mines.

This book is probably the most comprehensive account of the Mogôk Stone Tract so far produced and is claimed to be correct to 2007. This is a volume for gemmologists, geologists, lapidaries, jewellers and many others with an interest in the Burmese scene. The book is expensive, but worth the money for the photographic pleasure and detailed accounts of the mines.

E.A.J.

Minerals of Britain and Ireland.

A.G. TINDLE, 2008. Terra Publishing, Harpenden. pp viii, 616. ISBN 13-978-1-903544-22-8. £94.00.

Mineral species, many illustrated in colour, are described in alphabetical order in a larger book which effectively replaces Greg and Letsom's work of 1858. Particularly useful are the historical data provided as well as the expected notes on modes of occurrence which are supported by references to reliable sources. Both papers and monographs are included in a comprehensive bibliography and details of the mineral collections are noted.

This is a major work, long overdue to say the least, and reflects great credit on all who contributed to and worked on it.

M.O'D.

Private Mineral Collections in Texas.

WENDELL WILSON, WALLY MAN and GARY WHITE, 2009. Mineralogical Record, Tucson, USA. pp 180, illus. in colour. Hardcover, US\$ 60.00.

Drawing upon the resources of dedicated collectors, this survey includes examples of gem-quality crystals with at least one synthetic product. Specimens are arranged in alphabetical order of the collector's surname.

M.O'D.



Gems & Mines of Mogok

Special limited illustrated edition by Ted Themelis

Signed by the author

Available through the Gem-A shop. Details on application to shop@gem-a.com or call +44 (0)20 7404 3334.

Go to www.gem-a.com/shop.aspx for the latest details of books and equipment from Gem-A

Proceedings of the Gemmological Association of Great Britain and Notices

Gem-A Events

Gem-A Conference: Showing Colour

The 2009 annual Conference, held on Sunday 18 October at the Hilton London Kensington Hotel, celebrated the 75th anniversary of the introduction of the Chelsea Colour Filter with the theme 'showing Colour'.

Speakers included Brian Dunn, Thomas Hainschwang, John Harris, Alan Hodgkinson, Harry Levy, Antoinette Matlins, Dr Karl Schmetzer and Dr Menahem Sevdemish.

The conference was followed by a candlelit dinner at the hotel.

A programme of events and workshops arranged to coincide with the Conference was held on Monday 19 and Tuesday 20 October. These included the Graduation Ceremony at Goldsmiths' Hall (see below), and a guided tour of the Crown Jewels at the Tower of London with David Thomas. Following the theme 'Showing Colour', a half-day workshop on the practical use of the spectroscope with John Harris as guest tutor was held on the morning of Monday 19 October and the final event was Gem Discovery Club with guest speaker Beatrice Gimpel who demonstrated how gems and pearls can complement a person's colouring and also how to mix stones for best effect.

A report of the Conference was published in the October 2009 issue of *Gems & Jewellery*.

Graduation Ceremony

On Monday 19 October the Graduation Ceremony and Presentation of Awards was held at Goldsmiths' Hall in the City of London. Professor Andy Rankin, President of the Gemmological Association, presided and Alan Hodgkinson, President of the Scottish Gemmological Association presented the awards and gave the address.

Following the presentations to the graduates, it was announced that John Harris of Dudar, Cumbria, had been

Conference Sponsors and Supporters:

The Association is most grateful to the following for their support:

Major Sponsors

Marcus McCallum FGA, London

w: www.marcusmccallum.com

T.H. March, Insurance Brokers

w: www.thmarch.co.uk

Supporters

Benjamin Zucker

Precious Stones Company, New York, U.S.A.

Apsara

w: apsara.co.uk

Marcia Lanyon Ltd

w: www.marcialanyon.co.uk

Sponsorship of Leaflets and Badges

dg3 Diversified Global Graphics Group

w: www.dg3.com

awarded the R. Keith Mitchell Award for Excellence in the Field of Gemmological Spectroscopy, an award introduced in 2006 in honour of the late R. Keith Mitchell. A Gem-A gemmology tutor since 1986, John Harris is renowned for his work with the spectroscope and his outstanding photography of spectra.

During the ceremony it was also announced that E. Alan Jobbins and Michael J. O'Donoghue had been appointed Vice Presidents of the Association in appreciation of their commitment to gemmological education for many years.

In his address, Alan Hodgkinson stressed to the graduates the importance of taking every opportunity to improve and increase their gemmological knowledge and to 'go that extra mile'. He concluded: "Of all the careers that are on offer, I cannot imagine one which is so full

Proceedings of the Gemmological Association of Great Britain and Notices



Above: The Graduation Ceremony in the magnificent Livery Hall at Goldsmiths' Hall, London. Below: Guest speaker Alan Hodgkinson (right) speaking with Dominic Mok of Hong Kong who sponsored the new Dominic Mok Diamond Practical Prize. Photos © Photoshot.

of fascination and opportunity. So head back home full of gemmological commitment. Work as hard at building your career as you do at building friendships. Both need a good foundation and you now have that foundation by your award tonight. And finally realize this simple fact; if you enjoy your work, you will never have to work another day in your life. I wish you well." (Alan Hodgkinson's full address may be downloaded at www.gem-a.com/education/gem-a-graduation-and-awards.aspx)

The ceremony was followed by a reception for graduates and guests.

A report of the Graduation Ceremony was published in the October issue of *Gems & Jewellery*.

Nature's Treasures II: Minerals and Gems

A seminar organized jointly by Gem-A, the Mineralogical Society and the Russell Society, was held on Sunday 13 December 2009 at the Flett Theatre, Natural History Museum, London SW7.

Talks on a variety of subjects from mining the oceans to minerals in paints, were presented by Chris Carlon, Guy Clutterbuck, Alan Collins, John Faithfull, Martin Feely,



Norman Moles, Jolyon Ralph and Ruth Siddall.

During the lunch break, delegates had the opportunity to view displays by Gem-A, The Mineralogical Society, The Russell Society, Richard Tayler and the Mike Rumsey (Natural History Museum).

Proceedings of the Gemmological Association of Great Britain and Notices

Gem-A Awards

Gem-A Examinations were held worldwide in January and June 2009. In the Examinations in Gemmology 376 candidates sat for the Diploma Examination of whom 205 qualified, including two with Distinction and 31 with Merit. In the Foundation in Gemmology Examination, 434 candidates sat of whom 335 qualified. In the Gem Diamond Examination 178 candidates sat of whom 108 qualified, including eight with Distinction and 14 with Merit.

The **Christie's Prize for Gemmology** for the best candidate of the year in the Diploma Examination was awarded to **Noémie Georgy** of St Remy Les Chevreuse, France.

The **Anderson Bank Prize** for the best set of theory papers in the Diploma in Gemmology examination was awarded to **Yang Shuo** of Hubei, China.

In 2008 we awarded for the first time a Diploma Practical Prize for excellence in the Diploma Practical Examination. This has been named the **Read Practical Prize** in memory of Peter Read who sadly died earlier in the year. The prize was sponsored for 2009 by DeeDee Cunningham of Toronto, Canada, who also kindly donated a copy of her book *The Diamond Compendium*. The Read Practical Prize was awarded to **Amy Campbell-Jones** of Sheffield, Yorkshire.

In the Foundation Certificate in Gemmology examination, the **Anderson Medal** for the candidate who submitted the best set of answers which, in the opinion of the Examiners, were of sufficiently high standard, and the **Hirsh Foundation Award** for the best candidate of the year, were awarded to **Louise Dennis** of Halesowen, West Midlands.

In the Gem Diamond Diploma examination, the **Bruton Medal**, awarded for the best set of theory answer papers of the year, and the **Deeks Diamond Prize** for the best candidate of the year, were awarded to **Antonia Ross** of Fleet, Hampshire.

A new prize, the **Dominic Mok Diamond Practical Prize** for excellence in the Diamond Practical Examination, was awarded for the first time, sponsored by Dominic Mok from AGIL, Hong Kong. The Dominic Mok Diamond Practical Prize was awarded to **May Wai Ho** of Hong Kong

The Tully Medal was not awarded.

The names of the successful candidates are listed below.

Examinations in Gemmology

Gemmology Diploma

Qualified with Distinction

Georgy, Noémie, St Remy Les Chevreuse, France
Zhong Feng, Beijing, P.R. China

Qualified with Merit

Campbell-Jones, Amy V., Sheffield, Yorkshire
Cathelineau, Thierry, Les Breviaires, France
Chan Wai Sze, New Territories, Hong Kong
Chen Xi, Beijing, P.R. China
Cong Li, Wuhan, Hubei, P.R. China
Eastwood, Layla, Bellaire, Texas, U.S.A.
Gan, Cuiling, Guilin, Guangxi, P.R. China
Harris, Kay, Allendale, Northumberland
He Fei, Wuhan, Hubei, P.R. China
Hovi, Maria, Hyvinkää, Finland
Huby, Melanie, Liège, Belgium
Kong Jin, Wuhan, Hubei, P.R. China
Leavey, Harriet, Worcester

Li Yi, Guilin, Guanxi, P.R. China
Li Yujiao, Guilin, Guangxi, P.R. China
Li Xiao, Da Zu County, Ching Qing City, P.R. China
Liang Huan, Guilin, Guanxi, P.R. China
Liu Mei, Beijing, P.R. China
Ming Yan, Guilin, Guanxi, P.R. China
Ngan Yin Ying, Kowloon, Hong Kong
Pareek, Subhash, Gujarat, India
Parvela-Säde, Anu Liisa Johanna, Espoo, Finland
Qi Ming, Guilin, Guanxi, P.R. China
Rakotoharinavalona, Tahiana Lalaina, Antananarivo, Madagascar
Sugihara, Toshiyuki, Osaka, Japan
Versini, Valerie, Marseille, France
Wang Xia, Beijing, P.R. China
Xu Jiahui, Guilin, Guangxi, P.R. China
Yan Yaying, Guilin, Guanxi, P.R. China
Yang Shuo, Jingzhou City, Hubei, P.R. China
Zhan Zhanwen, Wuhan, Hubei, P.R. China

Proceedings of the Gemmological Association of Great Britain and Notices

Qualified

- Abey, Sara, London
 Aboosalih, Najeema Shahin, Colombo, Sri Lanka
 Amrit, Paveet, Northolt, Middlesex
 Au, Anita Suet Ki, Kowloon, Hong Kong
 Bahri, Sebastien, Feucherolles, France
 Baptiste, Karen Anne, Panadura, Sri Lanka
 Becquaert, Gregory Julien Pascal, Saint-Jans-Cappel, France
 Blagg, Natalie, London
 Burton, Estelle, Surbiton, Surrey
 Cai Min, Guilin, Guangxi, P.R. China
 Cao Juan, Shanghai, P.R. China
 Cao Weifeng, Guilin, Guanxi, P.R. China
 Cartier, Laurent E., Ribeaupillé, France
 Chan Kin Chung, Kowloon, Hong Kong
 Chatellain, Yannick, Bonneville, France
 Chen Anny Shin-Mien, Taipei, Taiwan R.O.C.
 Chen Ge, Guilin, Guangxi, P.R. China
 Chen Hsiang Ling, Taipei, Taiwan R.O.C.
 Chen Tianran, Guilin, Guangxi, P.R. China
 Chen Wenlong, Beijing, P.R. China
 Chen Ying, Guilin, Guangxi, P.R. China
 Chen Yuemei, Guilin, Guangxi, P.R. China
 Cheng Qi, Guilin, Guangxi, P.R. China
 Cheng Yu-Lin, Taipei, Taiwan R.O.C.
 Cheung Suk Wan, New Territories, Hong Kong
 Chien Hung-Dau, Wuhan, Hubei, P.R. China
 Chit Su Su Lin, Mogok, Myanmar
 Chou Mei-Lien, Taipei, Taiwan R.O.C.
 Christmas, Jacqueline, Godalming, Surrey,
 Chu Chanyuan, Beijing, P.R. China
 Chu Kong Ting, New Territories, Hong Kong
 Chung Tsz Bun, Kowloon, Hong Kong
 Coquel, Isabelle, Saint Germain Laprade, France
 de Josselin de Jong, J.P., Amsterdam, The Netherlands
 Donsin, Julie, Verviers, Belgium
 Evans, Natalie, London
 Feng Heng YI, Beijing, P.R. China
 Fu Kangyu, Guilin, Guanxi, P.R. China
 Gabay, Nicole, Montrouge, France
 Gonzalez, Olga, New York, U.S.A.
 Grounds, Camilla Sara, London
 Guo Haifeng, Shanghai, P.R. China
 Guo Hao, Guilin, Guanxi, P.R. China
 Guo Yingli, Guilin, Guanxi, P.R. China
 Guo Yunrong, Shanghai, Changning District, P.R. China
 Hara, Shintarou, Sasebo City, Nagasaki Pref., Japan
 Hartono, Djayani, Mount Tamborine, Queensland, Australia
 Häyry, Tiia, Hinthaara, Porroo, Finland
 Hirisy, Elisabeth, Ramboahangy Ranse, Madagascar
 Hollaar, Alexa, Bias, France
 Hong, Nabin, Shanghai, P.R. China
 Honour, Kevin J., Yeading, Middlesex
 Hu Jie, Guilin, Guangxi, P.R. China
 Huang Shanshan, Beijing, P.R. China
 Hughes, Kym Renaye, Nerang, Queensland, Australia
 Jain, Devesh, Delhi, India
 Jansch, Peter Alexander, Luxembourg
 Jeong, Eun Ah, Kofu City, Yamanashi Pref., Japan
 Johnston, Nanette LeTendre, Granite Bay, California, U.S.A.
 Johnstone, Isobel Phebe, Brisbane, Queensland, Australia
 Kagia, Georgia, Nikea, Greece
 Kambale, Sonia, Maharashtra, India
 Kettle, Georgina Elizabeth, Birmingham, West Midlands,
 Keung Wing Fun, Hong Kong
 Kovanovic, Milena, London
 Krska, Gemma, Durban, South Africa
 Kuchard, Monika, London
 Lepage, Anick, Mont Saint Hilaire, Quebec, Canada
 Leung Rakotovao, Anna, Antananarivo, Madagascar
 Li Chunlin, Wuhan, Hubei, P.R. China
 Li Geng, Beijing, P.R. China
 Li Jiakuan, Guilin, Guanxi, P.R. China
 Li Lin, Guilin, Guanxi, P.R. China
 Li Qian, Wuhan, Hubei, P.R. China
 Li Qianhui, Wuhan, Hubei, P.R. China
 Li Ruimin, Xi An City, Shanxi Province, P.R. China
 Li Zhuonan, Shanghai, P.R. China
 Lilley, Heather Jane, Newcastle-under-Lyme, Staffordshire,
 Liu Hailan, Shanghai, P.R. China
 Liu Jingna, Guilin, Guangxi, P.R. China
 Liu Liping, Guilin, Guangxi, P.R. China
 Liu Xianfeng, Shanghai, P.R. China
 Loke Hui Ying, Singapore
 Lu Yisha, Wuhan, Hubei, P.R. China
 Ma Hoi Shan, Kowloon, Hong Kong
 Ma Tsz Kwan, New Territories, Hong Kong
 Ma Xu, Guilin, Guanxi, P.R. China
 Maccaferri, Arianna, London
 Mclachlan, David, Woking, Surrey
 Man Sai Wing, Yuen Long, Hong Kong
 Matsukawa, Kent, Yokohama, Japan
 Mergalet, Caroline, Villefranche-sur-Mer, France
 Mithaiwala, Priyanka M., Surat, India
 Mizukami, Yusuke, Saitama City, Saitama Pref., Japan
 Mooney, Robert John, Cooroy, Queensland, Australia
 Muhamedjanova, Jelena, Tallinn, Estonia
 Muller, Paul, Antananarivo, Madagascar
 Murakami, Akiko, Tokyo, Japan

Proceedings of the Gemmological Association of Great Britain and Notices

Murray, Patricia A, Ottawa, Ontario, Canada
 Nay Lin Aung, Mogok Township, Myanmar
 Naylor, Peter D., Birmingham, West Midlands
 Ng Fei Yeung, Kowloon, Hong Kong
 O'Hagan, David Michael, Sutton Coldfield, West Midlands
 Oncina, Christelle, St Raphael, France
 Otterstrom, Camilla Anna, Bålsta, Sweden
 Ouchene, Linda, Paris, France
 Oxberry, Hannah Clare, Norwich, Norfolk
 Partner, Robert, Cropston, Leicestershire
 Patel, Maulika, London
 Petropoulou, Eleni, Athens, Greece
 Poore, Sarah, Worthing, West Sussex
 Possen, Armand, Soumagne, Belgium
 Preston, Paula, London
 Prince, Ronald Fisher, Richmond, Surrey
 Qin Qing, Guilin, Guanxi, P.R. China
 Quiros, Marylene, Bordeaux, France
 Qureshi, Erum Ali, Thane, India
 Ramampy, Pierrot, Antananarivo, Madagascar
 Raneke, Annamaria, Stockholm, Sweden
 Ribarevic, Ivanka, Montreal, Quebec, Canada
 Rousseville, Prisca, Nantes, France
 Santer, Kurt, Jersey, Channel Islands
 Share, Rebecca Louise, Birmingham, West Midlands
 Shen, Huanqun, Shanghai, P.R. China
 Shi, Hua Yan, Shanghai, P.R. China
 Siegan-Smith, Breige, London
 Soe Pa Pa, Yangon, Myanmar
 Song Lanlan, Guilin, Guangxi, P.R. China
 Song Liping, Beijing, P.R. China
 Su Chenmin, Wuhan, Hubei, P.R. China
 Sun, Norton, Central, Hong Kong
 Sung, Sophia, Tapei, Taiwan R.O.C.
 Szvath, Gabriella, Laukaa, Finland
 Tang Kit Yee, New Territories, Hong Kong
 Tian Mi, Guilin, Guanxi, P.R. China
 Tidd, Lauren Elizabeth, Churchdown, Gloucester
 Tissa, V.G. Samith Madhawa, Colombo, Sri Lanka
 Tran Vinh-Logez, Caroline, Paris, France
 Verma, Pragati, Delhi, India
 Vlemmix, Joost M.A, Ravenstein, The Netherlands
 Wan Qijuan, Wuhan City, Hubei Province, P.R. China
 Wang Mengqing, Guilin, Guangxi, P.R. China
 Wang Junyi, Guilin, Guanxi, P.R. China
 Wang Zongyu, Guilin, Guangxi, P.R. China
 Ward, Simon Francis, Leigh-on-Sea, Essex
 Wei, Qiaokun, Guangzhou, P.R. China
 Weng Chuxin, Guilin, Guangxi, P.R. China
 Wickramarathne, Hettiarachchi Keerthi, Thalawatugoda, Sri Lanka

Wiguna, Aland, Surabaya, Indonesia
 Wright, Lee Peter, Chaddesley Corbett, Worcestershire
 Wu Na, Guilin, Guanxi, P.R. China
 Xiang Tingyi, Wuhan, Hubei, P.R. China
 Xu Gengbo, Wuhan, Hubei, P.R. China
 Xu Zhao, Shanghai, P.R. China
 Yang Pei-Chi, Taipei, Taiwan R.O.C.
 Yang Yiwei, London
 Yang Zhuo, Guangzhou, P.R. China
 Yip Long Ching, Hong Kong
 Young, Stephanie Lynne, Chalfont St. Peter, Buckinghamshire
 Yu, Byron Kwai Sang, New Territories, Hong Kong
 Yu Zhiwei, Shanghai, P.R. China
 Yuan Yi, Guilin, Guangxi, P.R. China
 Zhang Fan, Wuhan, Hubei, P.R. China
 Zhang Li, Wuhan, Hubei, P.R. China
 Zhang Xiao Wen, Wuhan, Hubei, P.R. China
 Zhang Xiaohu, Guilin, Guanxi, P.R. China
 Zhao Chunji, Shanghai, P.R. China
 Zheng Wenting, Shanghai, P.R. China
 Zhou Die, Wuhan City, Hubei Province, P.R. China
 Zhou Jing, Wuhan, Hubei, P.R. China
 Zhou Mengji, Shanghai, P.R. China
 Zhou Xia, Shanghai, P.R. China

Foundation in Gemmology*Qualified*

Aarsaether, Anita Ronning, Sandvika, Norway
 Aderhold, Bryan Christopher, Ridgewood, New Jersey, U.S.A.
 Agrawal, Shriraj, Nagpur, India
 Åkerlund, Sophia, Lidingo, Sweden
 Akintayo, Olusegun James, London
 Allen, Amanda, Northampton
 Alokhin, Andriy, London
 An, Ran, London
 Andren Georgsen, Cecilia, Lund, Sweden
 Andriamanohisoa Axhel, Robert, Antananarivo, Madagascar
 Aung Ko Ko, Yangon, Myanmar
 Azema, Valerian, Le Val, France
 Bagriacik, Didem, London
 Bailey, Sarah, London
 Balakchiev, Ruslan, Marseille, France
 Beale, Sioned, Lapworth, Warwickshire
 Becquaert, Gregory Julien Pascal, Saint-Jans-Cappel, France
 Belanger, Jeannine, Quebec, Canada
 Bergeron, Marie Josee, Quebec, Canada
 Borenstein, Guy, Pardes-hana Karkur, Israel

Proceedings of the Gemmological Association of Great Britain and Notices

- Brenan, Amy, Dorchester, Dorset
 Brown, Sandra Jane, Birmingham, West Midlands
 Bryan, Daniel, London
 Burgoni, Eva Maria, Carnoux-en-Provence, France
 Butini, Enrico, Rome, Italy
 Butini, Flavio, Rome, Italy
 Byrne, Ruth, London
 Cai Jia, Beijing, P.R. China
 Caldwell, Neil Charles, Morningside, South Africa
 Cambray, Elinor, Salisbury, Wiltshire
 Cathelineau, Thierry, Les Breviaires, France
 Cederferm, Magdalena, Rosersberg, Sweden
 Cederqvist, Zarah, Lannavaara, Sweden
 Cerutti, Gabriella, Valenza, Italy
 Chan Kam Kong, Tseung Kwan O, Hong Kong
 Chan Pei Pei, Betty, Quarry Bay, Hong Kong
 Chan Pui Shan, Shatin, New Territories, Hong Kong
 Chan Sau Kwan, Hong Kong
 Chatagnier, Pierre Yves, Saint-Albin, Vareilles, France
 Chatellain, Yannick, Bonneville, France
 Chau Lai La, New Territories, Hong Kong
 Chen Ge, Guilin, Guangxi, P.R. China
 Chen Shan-Yi, Roquebrune Cap Martin, France
 Chen Shifeng, Guang Dong, P.R. China
 Chen Suoyi, Beijing, P.R. China
 Chen Tianran, Guilin, Guangxi, P.R. China
 Chen Ying, Guilin, Guangxi, P.R. China
 Chen Yuemei, Guilin, Guangxi, P.R. China
 Cheng Qi, Guilin, Guangxi, P.R. China
 Cherino, Edwin, London
 Cheung Yuk King, New Territories, Hong Kong
 Chit Su Su Lin, Mogok, Myanmar
 Chiu Po Yee, Lam Tin, Hong Kong
 Choi Chi Ho, Tuen Mun, Hong Kong
 Choi Wing Cheong, Chai Wan, Hong Kong
 Chow Chun Lok, New Territories, Hong Kong
 Chow Man Fai, Shatin, New Territories, Hong Kong
 Chow Wai Kei, North Point, Hong Kong
 Chu Yilin, Zhejiang Province, P.R. China
 Chui Wing Chung, Kowloon, Hong Kong
 Chung Chin Ying, Kowloon, Hong Kong
 Cirkot, Mark, New York, U.S.A.
 Clark, David, Lewes, East Sussex
 Comotto, Elisabetta, Genova-Sestri, Italy
 Cooper, Amy, Las Vegas, Nevada, U.S.A.
 Coquel, Isabelle, Saint Germain Laprade, France
 Darli Sein Win, Yangon, Myanmar
 De Mey, Inge, Shanghai, P.R. China
 de Nevi, Danilo, Genoa, Italy
 De Witt Sandstrom, Ida, Lunde, Sweden
 Delerholm, Peter, Enskede, Sweden
 Deng Xiansong, Guilin, Guangxi, P.R. China
 Dennis, Louise, Halesowen, West Midlands
 Donsin, Julie, Verviers, Belgium
 Du Liuyin, Beijing, P.R. China
 Dumas, Anne Catherine, London,
 Elliott, Marc, Birmingham, West Midlands
 Elmetto, Pamela, London
 Esteves, Catarina, Meudon, France
 Evans, Rachel, London
 Featherstone, Hazel, London,
 Feng Yan, Guangzhou, P.R. China
 Filipe, Muenga Ana Paula, Birmingham, West Midlands
 Fontaine, Marie, London
 Fung Sin Ting, Central, Hong Kong
 Gabay, Nicole, Montrouge, France
 Gamley, Alistair, Harare, Zimbabwe
 Gan Cuiling, Guilin, Guangxi, China
 Georgy, Noémie, St Remy Les Chevreuse, France
 Gilson, Karen Margaret, Wanstead, London
 Glendening, Sarah Louise, Eastbourne, East Sussex
 Gomez, Amanda, London
 Gorris, Tanja, Amsterdam, The Netherlands
 Graham, Lisa J., Tunbridge Wells, Kent
 Gram-Jensen, Margrethe, Vejle, Denmark
 Grocholska, Katherine, London
 Gu Ying, Shanghai, P.R. China
 Guez, Arielle, Aix-en-Provence, France
 Guo Fang Yu, Beijing, P.R. China
 Hall, Josephus, Birmingham, West Midlands
 Hammond, Ross, London
 Han, Byeo Ri, Geumjeong-Gu, Busan, Korea
 Han Yi, Beijing, P.R. China
 Harnois, Dominique, Paris, France
 Hart, Alan, London
 Herzog, Franz Adrian, Oltingen, Switzerland
 Hirisy, Elisabeth, Ramboahangy Ranse, Antananarivo,
 Madagascar
 Hoeksma, John, Surhuisterveen, The Netherlands
 Hollaar, Alexa, Bias, France
 Horak, Jana M., Cardiff, South Glamorgan, Wales
 Höstlöf, Catarina, Enskede Se, Sweden
 Hsiao Yu-Hsin, Taichung City, Taiwan R.O.C.
 Hu Jie, Guilin, Guangxi, P.R. China
 Huang Yi-Chia, Taipei, Taiwan R.O.C.
 Huang Hsiang-Ching, Taipei, Taiwan R.O.C.
 Hui Kei Chun, Aberdeen, Hong Kong
 Hui Marilyn Hang-Chung, Hong Kong
 Hui Wai Wai, New Territories, Hong Kong
 Jackson, Annie, Uxbridge, Middlesex
 Jacquier, Nathalie, Genthod, Switzerland
 Jefford, Alexandra, London

Proceedings of the Gemmological Association of Great Britain and Notices

- Jia Xiaodan, Tanjian, P.R. China
 Jonsson, Caroline, Uppsala, Sweden
 Joung Ki Park, Daejeon, South Korea
 Jubelin, Marion, Sanary-sur-Mer, France
 Jung-Lim Han, Busan, South Korea
 Kapoor, Kushagra, London
 Kauppinen, Paivi, Sunningdale, Berkshire
 Kedaria, Sujata, Amstelveen, The Netherlands
 Kim Hee Jung, Daegu, South Korea
 Kim Sae Bom, Gyeonggi-Do, South Korea
 Kintgen Gerez, Ingrid, Wasquehal, France
 Koutra, Ioanna, Agia Paraskeyi, Greece
 Kovanovic, Milena, London
 Krontira, Sofia, Marousi, Athens, Greece
 Kyaw Min Naing, Yangon, Myanmar
 Kyaw Myo Htet, Mogok, Myanmar
 Lai Chin Heng, Taipei, Taiwan R.O.C.
 Lai Hsin Ya, Taichung City, Taiwan R.O.C.
 Lai Ngating, London
 Lai Pui Ki, Emily, Kowloon, Hong Kong
 Lam King Fai, Kowloon, Hong Kong
 Lanza, Davide, Genoa, Italy
 Lau King Suen, Shau Kei Wan, Hong Kong
 Law Chun Him, Kwai Chung, Hong Kong
 Leavey, Harriet, Worcester
 Lee Hsiu-Ling, Taipei, Taiwan R.O.C.
 Lee Hun Ji, Seoul, Korea
 Lee Ji Hyun, Yeonje-Gu, Busan, Korea
 Lee Ka Chun, New Territories, Hong Kong
 Lee Ki Chan, Daejeon, Korea
 Lee Shih-Ping, Taipei, Taiwan R.O.C.
 Lee Yi Chen, New Territories, Hong Kong
 Leon, Virginie, Marseille, France
 Leung Man Nga, New Territories, Hong Kong
 Leung Rakotovao, Anna, Antananarivo, Madagascar
 Leza, Marianna, Ano Glyfada, Greece
 Li Mengfei, Shanghai, P.R. China
 Li Yujiao, Guilin, Guangxi, P.R. China
 Liang Zhe, Guilin, Guangxi, P.R. China
 Lin Yuk Ling, North Point, Hong Kong
 Lioe Yuk Fung, North Point, Hong Kong
 Liu Hong Jie, Beijing, P.R. China
 Liu Jingna, Guilin, Guangxi, P.R. China
 Liu Liping, Guilin, Guangxi, P.R. China
 Liu Sui Chung, New Territories, Hong Kong
 Liu Zhichao, Guilin, Guangxi, P.R. China
 Lo King Shan, Hong Kong
 Logan, Peter, Coventry, West Midlands
 Loosvelt, Bart, Kortrijk, Belgium
 Lundin, Emelie, Akersstyckebruk, Sweden
 Lung Mei Ting, May, Shatin, Hong Kong
 Lungley, Charlotte, Repton, Derbyshire
 McIntosh, Emma Jayne, Newcastle-upon-Tyne, Tyne and Wear
 Maclean, Victoria Elizabeth Frances, London
 McKeown, Julia, Oldbury, West Midlands
 Mclachlan, David, Woking, Surrey
 Mayer, Melanie, St. Helier, Jersey, Channel Islands
 Meikle, Alastair Murray Scott, Cambridge
 Meng Yan, Yunan Province, P.R. China
 Mi Ruiyun, Birmingham, West Midlands
 Michaelides, Emma, Enfield, Middlesex
 Midwinter-Porter, Holly, London
 Minassian Bardehshahi, Odett, Mykonos, Greece
 Misme, Eric, Lyon, France
 Mohammad, Aamir, Oldham, Lancashire
 Mullan, Bronagh, Birmingham, West Midlands
 Muller, Paul, Antananarivo, Madagascar
 Mulrooney, Rosalyn, London
 Muntz, Jennifer Louise, London
 Murakami, Akiko, Tokyo, Japan
 Myint Htun Yan, Stephen, Yangon, Myanmar
 Nambovera, Annet, Entebbe, Uganda
 Navarro, Gloria, London
 Nay Hlaing Oo, Yangon, Myanmar
 Nay Lin Aung, Mogok Township, Myanmar
 Neslen, Lewis, London
 Ng Lit Kwan, Kowloon, Hong Kong
 Ng Siu May, Sai Wan Ho, Hong Kong
 Ng Wing Yan, New Territories, Hong Kong
 Ngan Lai Shan, Ann, Kowloon, Hong Kong
 Nicolai, Namaste, Cardiff, South Glamorgan, Wales
 Nilsson, Jeanette Karin Madeleine, Lannavaara, Sweden
 Ning, Charles, Loughborough, Leicestershire
 Noble, Frances, Wendover, Buckinghamshire
 O'Neill, Helen, Berkhamsted, Hertfordshire
 O'Neill, Sarah Louise, Leeds, West Yorkshire
 Or Ting Ting, Tammy, Causeway Bay, Hong Kong
 Orsini, Paolo, Alessandria, Italy
 Otterstrom, Camilla Anna, Bålsta, Sweden
 Oudy, Myriam, London
 Paige, Denise, London
 Palo, Markus, Malmberget, Sweden
 Parkes, Matthew, Dublin, Ireland
 Parnpuu, Rao, Harku Vald, Estonia
 Patel, Maulika, London
 Patenaude, Lizanne, Westmount, Quebec, Canada
 Perosino, Lorenzo, Novi Ligure AL, Italy
 Piper, Valerie, Birmingham, West Midlands
 Poilane, Nadji, Paris, France
 Poon Pak Kei, New Territories, Hong Kong
 Possen, Armand, Soumagne, Belgium



Gem-A

THE GEMMOLOGICAL ASSOCIATION
OF GREAT BRITAIN

Exclusive to Gem-A members:

NEW GEMMOLOGY COURSE NOTES

These new full-colour notes combining both the Foundation and Diploma sections, are the perfect gemmological reference tool for members and students alike.

Updates: Members will be able to download from our website additional and updated pages should new information on major gemstone sources, treatments or synthetics become available. The notes are supplied in loose-leaf ringbinders enabling the additional pages to be easily inserted in the correct sequence.



USUAL PRICE :

£199 + postage and packing

INTRODUCTORY OFFER:

£135.00 + postage and packing

(offer available to the end of March 2010 only)

To order your set of Gemmology Course Notes
(available *only* to current Gem-A members and students)
email info@gem-a.com or call us on +44 (0)20 7404 3334

Proceedings of the Gemmological Association of Great Britain and Notices

- Pradat, Thierry, Francheville, France
 Prokopenko, Vera, Kallithea, Greece
 Prus, Emilia, London
 Quiros, Marylene, Bordeaux, France
 Rabary-Ranovona, Haga, Antananarivo, Madagascar
 Rakotoharinaivalona, Tahiana Lalaina, Antananarivo, Madagascar
 Ramampy, Pierrot, Antananarivo, Madagascar
 Ramaromisa, Naina, Antananarivo, Madagascar
 Ramsen, Jan Hakan, Halmstad, Sweden
 Rann, Evelina Birgitta, Övre Soppero, Sweden
 Ravaioni, Camilla, Genova, Italy
 Reeves, Emma, Sunninghill, Berkshire
 Regala, Benjamin, Alea, Hawaii, U.S.A.
 Renaud, Eric, London
 Richbourg, Carole, Las Altos, California, U.S.A.
 Rocchiero, Loredana, Genova, Italy
 Roelofse, Frederick, Die Wilgers, South Africa
 Rowe Rawlence, Emily, London
 Rutter, Anna, Edinburgh, Scotland
 Ryu, Hyunjung, Seoul, Korea
 Sanders, Esmee Elice, Amsterdam, The Netherlands
 Schutte, Maryke, London
 Seidenbinder, Arnaud, Ville-d'Avray, France
 Shen Yi, Shanghai, P.R. China
 Shih Chih Wen, Taipei, Taiwan R.O.C.
 Sibley, Christopher, St Albans, Hertfordshire
 Simm, Charlotte, London
 Smookler, Deborah, London
 So Kin On, Kowloon, Hong Kong
 Song Lanlan, Guilin, Guangxi, P.R. China
 Spofforth, Kristian David, London
 Srinivasa, Deepa, Ras al Khaimah, U.A.E.
 Tan, Fiona Jing, Calgary, Alberta, Canada
 Tejima, Yuko, Ichikawa City, Chiba Pref., Japan
 Tereszczuk, Stasia-Mae, London
 Thilakarathne, Kanishka Lalith, Birmingham, West Midlands
 Thomas, Craig Arthur, Sandton, Gauteng, South Africa
 To Ka Lun, New Territories, Hong Kong
 Tong Siu-Kuen, Ma On Shan, Hong Kong
 Tong Po Sang Cindy, Tsing Yi Island, Hong Kong
 Tsai Min-Chieh, Taipei, Taiwan R.O.C.
 Tsai Su-Fen, Shanghai, Zhabei District, P.R. China
 Tsai Yi-han Emma, Barcelona, Spain
 Tsang Hing Cheung, Tuen Mun, Hong Kong
 Vaessen, Servaas, Amsterdam, The Netherlands
 Valentini, Francesca, London
 Van der Lint, Roos, AB Haaften, The Netherlands
 van Elderen, Colin Nico, Schoonhoven, The Netherlands
 Van Minsel, Eefje Eva, West Drayton, Middlesex
 Verret, Jean-Michel, Montreal, Quebec, Canada
 Versini, Valerie, Marseille, France
 Viksten, Fanny Catarina Ariane, Umeå, Sweden
 Vodyanova Hitzi, Elena, Athens, Greece
 Wan Ching Yi, New Territories, Hong Kong
 Wang Jingjing, Guilin, Guangxi, China
 Wang Lei, Shanghai, P.R. China
 Wang Mengqing, Guilin, Guangxi, P.R. China
 Wang Shang Bai, Beijing, P.R. China
 Wang Xiawen, Guilin, Guangxi, P.R. China
 Wang Xu, Shanghai, P.R. China
 Waugh, Andrew D., Braintree, Essex
 Wei Qiaokun, Guangzhou, P.R. China
 Welsh, Simon Ian, Dawlish, Devon
 Wen Huashan, Guilin, Guangxi, P.R. China
 Weng Annlu Yu, Shanghai, P.R. China
 Westley, Penny, Hagley, Worcestershire
 Whiffin, Andrew Stafford, Meopham, Kent
 Whittaker, Laura Victoria, Pedmore, West Midlands
 Williams, Samantha, Birmingham, West Midlands
 Wilson, Maria, Rugby, Warwickshire
 Wong, Phyllis, Greenwich, London
 Wong Fung Ha, Hong Kong
 Wong Tsz Shing Milton, Kowloon, Hong Kong
 Wong Wan Kam Jean Vele, Junk Bay, Hong Kong
 Wong Wing Suet, Kowloon, Hong Kong
 Wong Yee Man, Quarry Bay, Hong Kong
 Wright, Hayley, Wolverhampton, West Midlands
 Wu Di, Beijing, P.R. China
 Wu Tsung-Jen, Taipei City, Taiwan R.O.C.
 Xia Xiyue, Guilin, Guangxi, P.R. China
 Xie Tian Qi, Da Qing City, Hei Long Jiang Province, P.R. China
 Xie Yan, Shanghai, P.R. China
 Xu Jiahui, Guilin, Guangxi, P.R. China
 Xu Zhao, Shanghai, P.R. China
 Xu Zhenxiu, Guangzhou, P.R. China
 Yang Pei-Chi, Taipei, Taiwan R.O.C.
 Yang Yiwei, London
 Yang Zhuo, Guangzhou, P.R. China
 Yao Qiong, Shanghai, P.R. China
 Yapa Abeywardena, Jayani Madhavi, Colombo, Sri Lanka
 Yau Chui Shan, Yuen Long, Hong Kong
 Ye Jiandong, Wenzhou City, Zhejiang Province, P.R. China
 Yeh Chun-Hau, Taichung, Taiwan R.O.C.
 Yin Yiqing, Shanghai, P.R. China
 Yip Wing Man Kennis, Kowloon, Hong Kong
 Young, Stephanie Lynne, Chalfont St Peter, Buckinghamshire

Proceedings of the Gemmological Association of Great Britain and Notices

Youssef, Raewin, Melbourne, Victoria, Australia
 Yu Nordgren, Pia, Arsta, Sweden
 Yu Pei-Shang, Wellingborough, Northamptonshire
 Yu Tao, Guilin, Guangxi, P.R. China
 Yuan Heng Yi, Guangdong, China
 Yuan Yi, Guilin, Guangxi, P.R. China
 Zachou, Maria, Papagou, Greece
 Zahid, Asiya, Nairobi, Kenya
 Zerillo, Jocelyn, Marseille, France

Zhang Jingwen, Birmingham, West Midlands
 Zhang Kai, Shanghai, P.R. China
 Zhang Rui, Taiyuan Shanxi, P.R. China
 Zhang Yi, Da Qing City, Hei Long Jiang, P.R. China
 Zhao Xin, Guilin, Guangxi, P.R. China
 Zhou Xia, Shanghai, P.R. China
 Zhou Xing, Shanghai, P.R. China
 Zhu Jiachen, Zhenjiang, P.R. China

Gem Diamond Diploma Examination

Qualified with Distinction

Cheung Yuk King, New Territories, Hong Kong
 Diamond, Marcia, London
 Gleave, Elizabeth, London
 Gong Sheng Wei, Zhujiang New Town, P.R. China
 Korejwo, David A., Quantico, Virginia, U.S.A.
 Leavey, Harriet, Worcester
 Liang, Weizhang, Guangzhou, P.R. China
 Ross, Antonia, Fleet, Hampshire

Qualified with Merit

Bigford, Julie Claire, Malvern Wells, Worcestershire,
 Jensen, Annalisa, London,
 Lee Chi-Ju, Taipei, Taiwan R.O.C.
 Lin Chun Hsien, Taipei, Taiwan R.O.C.
 Lin Xin, Beijing, P.R. China
 Liu Siyang, Beijing, P.R. China
 Lu Jia, Wuhan, Hubei, P.R. China
 Maclellan, Kiki, Nr Southam, Warwickshire
 Peng Hsiang Chieh, Taipei, Taiwan R.O.C.
 Rufus, Simon, London
 Shaw, Heather Catherine, Barnsley, West Yorkshire
 Spencer, Jason, Birmingham, West Midlands
 Xu Juan, Beijing, P.R. China
 Zhai Shanshan, Beijing, P.R. China

Qualified

Brunstrom, Isabella, Älvsjö, Sweden
 Cai Hongxiang, Beijing, P.R. China
 Chan Chun Wai, Kowloon, Hong Kong
 Chan Ho Yin, Henry, Kowloon, Hong Kong
 Chan Man Tao, New Territories, Hong Kong
 Chan Shun Heng, Champaign, Illinois, U.S.A.
 Chan Wai Ming, Jerry, Kowloon, Hong Kong
 Chan Yuen Yi, Kowloon, Hong Kong
 Chen Hsiu-Chuan, Taipei, Taiwan R.O.C.
 Chen Min, Wuhan, Hubei, P.R. China

Chen Yanni, Wuhan, Hubei, P.R. China
 Cheng Cheuk Yu, New Territories Hong Kong
 Cheng Wing Yan, New Territories, Hong Kong
 Cheng Yee Ha, Joyce, Kowloon, Hong Kong
 Cheung, Siu Lui Sharon, Kowloon, Hong Kong
 Choi Wing Cheong, Eric, Chai Wan, Hong Kong
 Clifford, Ellen, Kirkella, East Yorkshire
 Dalton, Alan, Dungarvan, Co. Waterford, Ireland
 Efthymiadis, Avraam, Parga, Greece
 Elliott, Marc, Birmingham, West Midlands
 Evans, Natalie, London
 Fumagalli, Laura, Brentford, Middlesex
 Gibbard, Penelope, Marlow, Buckinghamshire
 Gu Rui, Beijing, P.R. China
 Guo Haihong, Beijing, P.R. China
 Haymes, Richard, Caterham, Surrey
 He Wan Ying, Wuhan, Hubei, P.R. China
 Hou Yu, Beijing, P.R. China
 Huang Ya Yao, Kowloon, Hong Kong
 Karkouli, Elpida, Drossia, Greece
 Kotlarska, Patrycja, London
 Lam Pui Pik, Kowloon, Hong Kong
 Lam Tan Ly, Kowloon, Hong Kong
 Laow Chun Yim, New Territories, Hong Kong
 Lau Yuen Yee Simmy, Kowloon, Hong Kong
 Lee Shan Shan, New Territories, Hong Kong
 Leung Ka Wai, Hong Kong
 Leung Pui Shan, Sandra, Kowloon, Hong Kong
 Li Ching Tung, New Territories, Hong Kong
 Li Liu Fen, Kowloon, Hong Kong
 Liang Yue, Wuhan, Hubei, P.R. China
 Lin Ling, Beijing, P.R. China
 Lo Yi Ting, Kowloon, Hong Kong
 Ma Yu, London
 McLoughlin, Emma, Dublin, Ireland
 Mai Zhiqiang, Zhujiang New Town, P.R. China

Proceedings of the Gemmological Association of Great Britain and Notices

Meninno, Marco, London
Muddyman, Jennifer Ruth Sarah, Birmingham, West Midlands
Murakami, Akiko, Tokyo, Japan
O'Doherty, Brigid Isobel, Belfast, Northern Ireland
O'Hagan, David Michael, Sutton Coldfield, West Midlands
Owen, Cheryl, Birmingham, West Midlands
Pan Hong, Wuhan, Hubei, P.R. China
Patel, Maulika, London
Platis, George, Athens, Greece
Poon King Hong, Kowloon Bay, Hong Kong
Poon Wai Man, Sheung Wan, Hong Kong
Poon Yuen Yan, Kowloon, Hong Kong
Smith-Bingham, Cassia, London
Starkey, Imogen, Shanklin, Isle of Wight
Stevens, Laura Ann, Bewdley, Worcestershire
Stöt, Linda, Stockholm, Sweden
Su Chenmin, Wuhan, Hubei, P.R. China
Tachiveyi, Brian, Birmingham, West Midlands
Tang Yalong, Wuhan, Hubei, P.R. China
To, Matthew Ka Ho, Taipo, Hong Kong
To Ka Wing, Kowloon, Hong Kong
Tse Vivian Wai Yin, Hong Kong
Walsh, Antonio, Bilston, West Midlands
Wang Bo, Wuhan, Hubei, P.R. China
Webster, Rebecca, Birmingham, West Midlands
Whittaker, Laura Victoria, West Midlands
Wong Kam Yan, Kowloon Tong, Hong Kong
Wong Yin Kwan, Angela, Tin Shui Wai, Hong Kong
Wu Shih-Ying, Taipei, Taiwan R.O.C.
Xiaoyan, Yu, Wuhan, Hubei, P.R. China
Yeung Kwok Li, Kowloon, Hong Kong
Yeung Man Yee, New Territories, Hong Kong
Yu Mingxia, Beijing, P.R. China
Yuan Ye, Beijing, P.R. China
Yuen Kim-Yu, Kowloon Bay, Hong Kong
Zhang Pingting, Wuhan, Hubei, P.R. China
Zhao Yuan, Beijing, P.R. China
Zhao Yunmiao, Beijing, P.R. China
Zheng Chen, Wuhan, Hubei, P.R. China
Zou Yi, Beijing, P.R. China

Membership

During 2009, the Council approved the election to Membership of the following:

Fellowship and Diamond membership (FGA DGA)

Kettle, Georgina Elizabeth, Birmingham, West Midlands.

2009/2008

Khaing, Win Win, Yangon, Myanmar. 2004/2008

Lau, Ho, Sandra, Kowloon, Hong Kong. 2008/2006

Meninno, Marco, London. 2008/2009

O'Hagan, David, Sutton Coldfield, West Midlands.

2009/2009

Taylor, Roger, Walsall, West Midlands. 1986/1994

Fellowship (FGA)

Bai Feng, Beijing, P.R. China. 2008

Barrows, Mark, Hunnington, West Midlands. 1973

Benson, Jillian Rose, Ontario, Canada. 2008

Bove, Bertrand, Vitry-sur-Seine, France. 2007

Burton, Estelle, Surbiton, Surrey. 2009

Campbell-Jones, Amy Victoria, Sheffield, South Yorkshire.

2009

Cartier, Laurent E., Ribeaupillé, France. 2009

Cathelineau, Thierry, Les Breviaires, France. 2009

Chen, Anny Shin-Mien, Taipei, Taiwan R.O.C. 2009

Cheung Suk Wan, New Territories, Hong Kong. 2009

Christmas, Jacqueline, Godalming, Surrey. 2009

Chu, Sin-Yi, Christine, Sheungwan, Hong Kong. 1990

De Josselin De Jong, J.P., Amsterdam, The Netherlands.
2009

Fontaine, Josee, St-Basile-le-Grand, Quebec, Canada. 2009

Foran, Amelia Luetta, Toronto, Ontario, Canada. 2008

Forsberg, Conny, Kisa, Sweden. 1987

Goldman, Lucy, London. 2008

Han, Fen, London. 2007

Hartono, Djayani, Mt Tamborine, Queensland, Australia.
2009

Hirst, Catherine, Harborne, West Midlands. 2004

Honour, Kevin J., Yeading, Middlesex. 2009

Hughes, Kym Renaye, Nerang, Queensland, Australia. 2009

Jaugeat, Blaise, Vanves, France. 2008

Johnston, Nanette LeTendre, Granite Bay, California,
U.S.A. 2009

Kamoune Ndemanga, Yannick, Pierrefitte-sur-Seine,
France, 2009

Larsson, Alf Christian, Finland. 1982

Lee, Marian Hui Min, Taipei, Taiwan R.O.C. 2007

Lek Chin Kwang, Singapore. 2009

Li Geng, Beijing, P.R. China. 2009

Liang Jie, Beijing, P.R. China. 2008

Matsukawa, Kent, Yokohama, Japan. 2009

Menekodathu Remanan Amarnath, New Delhi, India. 2007

Meraly, Afsana, Antananarivo, Madagascar. 2008

View *The Journal* online

Exclusive to Gem-A Members

New to the Gem-A website is the 'Members only' area, where paid-up Gem-A members are able to access searchable downloads of the latest issues of *The Journal* and our magazine *Gems & Jewellery*, and view current articles to be published in the *The Journal* at a later date. Fellows and Diamond Members are able to download the Gem-A Coat of Arms for use on their business stationery and websites. Members are also able to update their contact details and pay their membership subscription online.



Logging into the Members Only area

Step 1:

From the Home page, click on [Login/Register](#) in the top right-hand corner.

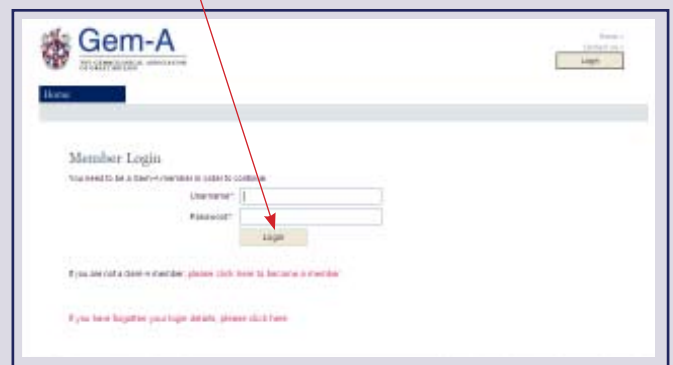


To access the latest issues and upcoming articles of *The Journal*, click on the [Publications](#) tag, then go to [The Journal of Gemmology](#) in Publications, and [The Journal online](#).

Step 2:

This takes you to the Login screen. Enter your username, which is your surname (or family name) only, and your password which is your six-digit membership number.

Click on the [Login](#) button which will take you to the Members only area.



To update your contact details or to change your password, click on [Member area](#) in the top right-hand corner, then go to [My Details](#).

If you would like to add the name of your workplace, go to [My organization](#).



Proceedings of the Gemmological Association of Great Britain and Notices

- Mooney, Robert John, Cooroy, Queensland, Australia. 2009
 Muhhamedjanova, Jelena, Tallinn, Estonia. 2009
 Otterstrom, Camilla Anna, Bålsta, Sweden. 2009
 Ouchene, Linda, Paris, France. 2009
 Oxberry, Hannah Clare, Norwich, Norfolk. 2009
 Partner, Robert, Cropston, Leicestershire. 2009
 Poore, Sarah, Worthing, West Sussex. 2009
 Ranasinghe, Liyanage Daya Somaratna, Kadawatha, Sri Lanka. 1995
 Raneke, AnnaMaria, Stockholm, Sweden. 2009
 Ranoroso, Nadine Joelle, Antananarivo, Madagascar. 2008
 Ribarevic, Ivanka, Montreal, Quebec, Canada. 2009
 Samaratunge, Punyadevi, Horana, Sri Lanka. 2008
 Share, Rebecca Louise, Birmingham, West Midlands. 2009
 Sun, Norton, Central, Hong Kong. 2009
 Sung, Sophia, Taipei, Taiwan R.O.C. 2009
 Szvath, Gabriella, Laukaa, Finland. 2009
 Tang, Kit Yee, New Territories, Hong Kong. 2009
 Tran Vinh-Logez, Caroline, Paris, France. 2009
 Veenhoven, Taletta W., Amsterdam, The Netherlands. 2008
 Vlemmix, Joost, Ravenstein, The Netherlands. 2009
 Ward, Simon Francis, Leigh-on-Sea, Essex. 1979
 Watson, Timothy, Johannesburg, South Africa. 2009
 Wickramaratne, Hettiarachchi Keerthi, Thalawatugoda, Sri Lanka. 2008
 Wright, Lee Peter, Chaddesley Corbett, Worcestershire. 2009
 Wu, Benson Hon Wa, Toronto, Ontario, Canada. 2007
 Yu, Byron Kwai Sang, Beijing, P.R. China. 2009
 Yu, Xiaoyan, New Territories, Hong Kong. 2008
- Diamond Membership (DGA)**
 Bresson, Wan, Bussy Saint Georges, France. 2008
 Brunstrom, Isabella, Älvsjö, Sweden. 2009
 Chan, Shun Heng, Champaign, U.S.A. 2009
 Gibbard, Penelope, Marlow, Buckinghamshire. 2009
 Lai Siu Kwong, New Territories, Hong Kong. 2006
 Monogyios, John, Athens, Greece. 2008
 Platis, George, Rhodes, Greece. 2009
 Shaw, Bianca, Wanchai, Hong Kong. 2008
 Shaw, Martin Mackenzie, Wanchai, Hong Kong. 2008
 Starkey, Imogen, Shanklin, Isle of White. 2009
 Yuen, Kim-Yu, Kowloon Bay, Hong Kong. 2009
- Associate Membership**
 Alcantara, Regina, London
 Algaay, Khaled, London
 Bailey, Anneabell, Althorpe, Essex
 Baker, Carol, London
 Bayliss, Catherine, Tamworth, Staffordshire
 Bhatia, Naresh Satram, Pune, India
 Birchall, Alana, Victoria, Australia
 Borenstein, Guy, Pardes-hana Karkur, Israel
- Chang, Cheng, Taipei, Taiwan R.O.C.
 Chia, Simon, Singapore
 Davis, Fitzroy, Godmanchester, Cambridgeshire
 Dayaratne, Rohan Pushpakumara Dayaratn, Kohuwala, Sri Lanka
 Delerholm, Peter, Enskede, Sweden
 Fleming, Emanuel, Lewisham, London
 Gibson, David, Scarborough, North Yorkshire
 Graham, Lisa, Tunbridge Wells, Kent
 Grocholska, Katherine Rose, London
 Henderson, Elizabeth, Altrincham, Cheshire
 Hikel, Jerry, Stamford, Connecticut, U.S.A.
 Hunt, Glynis, Andover, Hampshire
 Hussein, Batcha, London
 Jefford, Alexandra, London
 Joshi, Radhika, Hounslow, Middlesex
 Kaneko, Midori, Tokyo, Japan
 Kapoor, Kushagra, New Delhi, India
 Kaye, Charlotte, Hungerford, Berkshire
 Langeslag, Leone, Bussum, The Netherlands
 Liu Shih-Chieh, Edinburgh, Scotland
 Loosvelt, Bart, Kortrijk, Belgium
 MacMillan, Margaret-Anne, Grangemouth, Stirlingshire, Scotland
 Matsumoto, Itsufumi, Nakatsu City, Japan
 Meikle, Alastair, Cambridge
 Mowbray, Caroline, London
 Norris, Eddi, London
 O'Connell, Angela, Edgbaston, West Midlands
 Ono, Kouichi, Kurume City, Fukuoka Pref., Japan
 Patel, Farzin, Gloucester
 Ring, L. G., Christchurch, Dorset
 Risdon, Jennifer Leigh, Bethesda, Maryland, U.S.A.
 Robbins, Laurie, San Leandro, California, U.S.A.
 Sakaguchi, Saori, Kumamoto-si, Kumamoto Ken, Japan
 Sakakibara, Kenichi, Oita City, Japan
 Sansom, Henry, Hove, East Sussex
 Smart, Jacqui, Cupar, Fife, Scotland
 Van Minsel, Eva Eefje, West Drayton, Middlesex
 Wetherall, Alan, Hitchin, Hertfordshire
 Wilson, Claire, Bristol, Avon
 Wong, Phyllis, London
 Yu Ling-Yu, Danville, California, U.S.A.
 Zazai, Rahem Khoshal, Barking, Essex

Transfers

Fellowship to Fellowship and Diamond Membership (FGA DGA)

- Bigford, Julie Claire, Malvern Wells, Worcestershire. 2009
 Gleave, Elizabeth, London. 2009
 Jensen, Annalisa, London. 2009
 Lau Yuen Yee Simmy, Kowloon, Hong Kong. 2009
 Lin Chun Hsien, Chung Ho, Taiwan R.O.C. 209

Gifts and Donations to the Association

The Association is most grateful to the following for their gifts and donations for research and teaching purposes:

Apsara Gems, London, for faceted and rough sapphires, and ruby rough before and after 'glass filling'.

Edwin Vincent Cherino, London, for a pyrite crystal from the Congo.

Cyrille Djankoff, London, for three pieces of morganite (one natural colourless, one greyish after irradiation and one pinkish after irradiation and heating) from the Marropino Mine, Zambezi province Mozambique; also for a piece of lapis from Tadjikistan, Pamir Region.

Makhmout Douman, Arzawa Mineralogical Inc., New York, U.S.A., for a demantoid garnet crystal from Kerman Province, South East Iran.

Luella Woods Dykhuis, Tucson, Arizona, U.S.A., for a selection of coral branches, a star garnet rough from India, heat treated rough Montana sapphires, faceted amethysts and tumbled olivines from Hawaii.

Gemfields PLC, London, for three pieces of emerald rough from the Kagem mine, Zambia.

Lisa Graham, Tunbridge Wells, Kent, for a carved ivory puzzle ball.

Marcia Lanyon, London, a selection of small faceted emeralds and sapphires, and some cut natural and synthetic gemstones.

Graham and Anthony Mitchell, Kent, for a collection 35 mm slides depicting gems and jewellery from the estate of their late father R. Keith Mitchell.

Emma Mouawad, West Hampstead, London, for a nephrite jade cylinder with fern leaf design finials.

So Pa Pa, Yangon, Myanmar, for a quartz crystal with rutile inclusions and mica crystals in matrix.

Jason Williams, G.F. Williams & Co., London for selections of synthetic and natural cut gemstones.

Monetary donations were gratefully received from:

Raed Al-Hadad, Abu Dhabi, U.A.E.

Alexander Armati, Reading, Berkshire

Burton A. Burnstein, Los Angeles, California, U.S.A.

Joseph A. Cassarino, Rochester, New York, U.S.A.

Susan Deacon, London

James C. Finlayson, Stoke-on-Trent, Staffordshire,

Bernice M. Gay, Romsey, Hampshire

Masao Kaneko, Tokyo, Japan

Sandra Lear, Morpeth, Northumberland

Cherie Leigh, Canterbury, Kent

Torbjorn Lindwall, Lannavaara, Sweden

Caroline E. Maclachlan, Edinburgh, Scotland

Anton S. Mayer, Jersey, Channel Islands

Ernest Mindry, Chesham, Buckinghamshire

Sara Naudi, London

Jamie B. Nelson, London

Daniel Novak, Amarillo, Texas, U.S.A.

Bebs Roper, Howrah, Tasmania, Australia

Thomas C. Roper, Howrah, Tasmania, Australia

Robert L. Rosenblatt, Salt Lake City, Utah, U.S.A.

David J. Sayer, Wells, Somerset

Moe Moe Shwe, Singapore

Paul L. Siegel, Rocky Point, New York, U.S.A.

Joseph W. Tenhagen, Miami, Florida, U.S.A.

U Myint Tun, Lulea, Sweden

Veronica Wetten, Hounslow, Middlesex

MacLellan, Kiki, London. 2009

Ross, Antonia, Fleet, Hampshire. 2009

Rufus, Simon, London. 2009

Shaw, Heather Catherine, Barnsley, Yorkshire. 2009

Spencer, Jason, Birmingham, West Midlands. 2009

Diamond Membership to Fellowship and Diamond Membership (FGA DGA)

Naylor, Peter D., Birmingham, West Midlands. 2009

Patel, Maulika, London. 2009

Prince, Ronald F., Richmond, Surrey. 2009

Yang, Yiwei, London. 2009

Shen, Huanqun, Shanghai, P.R. China. 2009

Associate Membership to Fellowship (FGA)

Abey, Sara, London. 2009

Amrit, Paveet, London. 2009

Chen, Anny Shin-Mien, Taipei, Taiwan R.O.C. 2009

Eastwood, Layla, Madeira Beach, Florida, U.S.A. 2009

Gonzalez, Olga, New York, U.S.A. 2009

Hara, Shintarou, Sasebo City, Nagasaki Pref., Japan. 2009

Harris, Kay, Allendale, Northumberland. 2009

Hartono, Djayani, Mt Tamborine, Queensland, Australia. 2009

Häyry, Tiia Marjut, Hintaara/Porvoo, Finland. 2009

Jeong, Eun Ah, Yamanashi Pref., Japan. 2009

Johnstone, Isobel, Brisbane, Queensland, Australia. 2009

Kovanovic, Milena, London. 2009

Proceedings of the Gemmological Association of Great Britain and Notices

Lepage, Anick, Mont Saint Hilaire, Quebec, Canada. 2009
Maccaferri, Arianna, London. 2009
Mclachlan, David, Woking, Surrey. 2009
Mergalet, Caroline, Villefranche-sur-Mer, France. 2009
Mizukami, Yusuke, Saitama City, Saitama Pref, Japan. 2009
Mooney, Robert, Cooroy, Queensland, Australia. 2009
Oxberry, Hannah Clare, Norwich, Norfolk. 2009
Parvela-Säde, Anu, Espoo, Finland. 2009
Preston, Paula, London. 2009
Santer, Kurt, Jersey, Channel Islands. 2009
Sugihara, Toshiyuki, Osaka, Japan. 2009
Sung, Sophia, Taipei, Taiwan R.O.C. 2009
Young, Stephanie, Chalfont St. Peter, Buckinghamshire.
2009

Associate Membership to Diamond membership (DGA)

Diamond, Marcia, London, 2009
Efthymiadis, Avraam, Parga, Greece. 2009
O'Doherty, Brigid, Belfast, Northern Ireland. 2009
Patel, Maulika, London, 2009
Stöt, Linda, Stockholm, Sweden. 2009

Associate Membership to Fellowship and Diamond Membership (FGA DGA)

Leavey, Harriet, Worcester. 2009
Murakami, Akiko, Tokyo, Japan. 2009

Corporate Membership

Cherie Leigh Antique Jewellery, Canterbury, Kent
HPJ Retailing Limited (head office), Congleton, Cheshire
Landsberg and Son Antiques, London
Otley Jewellers, Leeds, South Yorkshire
Van Molendorff Diamonds Ltd, Woking, Surrey

Gold Corporate membership

BKT Rings Ltd, London
Marcus McCallum, London
S.P. Green & Co. Ltd, Hockley, West Midlands

Subscriptions 2010

The membership subscriptions for 2010 are £85.00 for UK members and £90 for those in Europe and overseas.

Annual General Meeting

The Annual General Meeting was held at the National Liberal Club, Whitehall Place, London SW1, on Monday 22 June. The meeting was chaired by James Riley the newly appointed Chairman of the Council. The Annual Report and Accounts were approved. Professor Alan Collins was re-elected and Steven Collins, Brian Jackson, and Cally Oldershaw elected to serve on the Council. Dr Tony Allnutt was re-elected and Janice Kalischer elected to serve on the Membership Liaison Committee. David Lancaster retired in rotation from the Membership Liaison Committee and did not seek re-election. Hazlems Fenton were re-appointed as auditors for the year.

A presentation by Rui Galopim de Carvalho of the Gemological Laboratory in Portugal (LABGEM), entitled 'Lalique's gems: as seen in the collections of the Calouste Gulbenkian Foundation' followed the AGM.

Enrol now for the Spring 2010 course held at Gem-A's London headquarters

Gem-A Diploma in Gemmology



The course that prepares you for the realities of the gem world and for decision making when buying and selling, whether for business or hobby.

Eight-Month Gemmology Daytime Course

28 September 2010 to June 2011. Fee: £7425.00
Three days a week (Tues, Wed and Thurs*), combining the Foundation and Diploma courses and exams.

* Supported study day

For further information or to enrol go to
www.gem-a.com/education/gemmology-courses.aspx
or call our Education team on +44 (0)20 7404 3334



Gem-A
THE GEMMOLOGICAL ASSOCIATION
OF GREAT BRITAIN

Obituary

Peter George Read 1927-2009



Born in London in 1927, Peter passed away quietly on 15 January 2009 after a brave fight with cancer: he will be sadly missed by his family and all his friends and colleagues who knew him as a most congenial, friendly and talented person.

Peter's education led him to become a Chartered Engineer with a strong background knowledge of electronics. He qualified as

a Fellow of the Gemmological Association and also held the Diamond Certificate of the Association.

Peter held a number of professional positions during his working life in a diverse range of companies including GEC, Iliffe the publishers and Johnson Matthey & Co. Ltd, the bullion refiners, where he was the senior Development Engineer. Later he became Technical Manager of the Diamond Trading Company (Pty) Ltd. (part of the De Beers organization).

During his time with De Beers Peter spent some time in Namibia, where he was involved in the development of a diamond-sorting machine. Whilst in South Africa, he was able to visit many of the major diamond producing areas including the famous Premier mine near Pretoria, the Dutoitspan and Bultfontein at Kimberley and the Consolidated Diamond Mines coastal operation at Oranjemund in South West Africa.

As a technical author, Peter excelled and he produced a number of books, which included *Gemmology*, *Gemmological Instruments* and *Dictionary of Gemmology*. He also edited the 5th edition of Webster's *Gems*. Peter was also known to some of us as an author of several

novels, including *The Phantom Diamond*, *Diamond Mine* and *The Peking Diamonds*; these were based on his experiences in the gemmological world.

Peter gave many talks on gemmological matters both in the UK and abroad. For many years he was a tutor for the Gem-A courses. Since 1994 he was an Assistant Editor of The Journal, and wrote many book reviews. For a number of years he was a Member of the Council of the Association and latterly he sat on the Members' Council.

All the foregoing was still not enough for Peter. He became very involved in designing gemmological instruments, one of which was Gem Data, a computer-aided programme for gem identification. The most recent instrument that he designed was the Brewster Angle Meter for Gem-A, which is now in use worldwide.

Although retired, Peter kept in close touch with his gem friends and colleagues in both the UK and abroad. He was a gentleman in every respect, quiet, helpful, modest and with a great sense of humour. He will be greatly missed by all.

Noel W. Deeks

Alain A.M. van Acker FGA (D.1990), Tilburg, The Netherlands, died on 30 March 2009.

Bruno Bolli FGA (D.1976), St Gallen, Switzerland, died on 16 December 2008.

Leslie Punchihewa FGA (D.1983), Colombo, Sri Lanka, died on 26 April 2009.

Leonard Sanitt FGA (D.1949), London, died in 2009.

Richard A.F. Will FGA (D.1974), Peterborough, Cambridgeshire, died on 21 May 2009.

Wilhelm J.E. Van Deijl, FGA (D.1969), Bellville, South Africa, died on 23 July 2009.

Patricia J. Walker FGA DGA (D.1969 and 1970), London, died in 2009.

Daniel Taylor FGA DGA (D.2005 and 2004), Leeds, Yorkshire, died on 29 October 2009.

Gem-A Events 2010

- Friday 26 February **MIDLANDS BRANCH**
Emeralds: formation, treatment, manufacturing and identification by DOUG GARROD
Venue: The Earth Science Building, University of Birmingham, Edgbaston
- Tuesday 2 March **GEM DISCOVERY CLUB**
Gemmology on the Job - identifying set gemstones with KERRY GREGORY
Venue: Gem-A, 27 Greville Street (Saffron Hill entrance), London EC1N 8TN
- Tuesday 2 March **SCOTTISH GEMMOLOGICAL ASSOCIATION**
Members' Night: Tales from Tucson
Venue: British Geological Survey, West Mains Road, Edinburgh
- Friday 26 March **MIDLANDS BRANCH**
A practical and hands-on look at some rare stones and inclusions in quartz with MARCUS McCALLUM
Venue: The Earth Science Building, University of Birmingham, Edgbaston
- Tuesday 30 March **SCOTTISH GEMMOLOGICAL ASSOCIATION**
Wine and cheese reception and SGA AGM followed by Piteiras emeralds with PADRAIC LAVIN
Venue: British Geological Survey, W Mains Road, Edinburgh
- Friday 30 April **MIDLANDS BRANCH**
Jewellery of the Great Exhibition of 1851 by DAVID LANCASTER
Venue: The Earth Science Building, University of Birmingham, Edgbaston
- Friday 30 April to
Monday 3 May **SCOTTISH GEMMOLOGICAL CONFERENCE**
Venue: The Queens Hotel, Perth
For further information see page 180
- Sunday 7 November **GEM-A CONFERENCE**
Venue: The Hilton London Kensington Hotel
- Monday 8 November **GRADUATION CEREMONY AND PRESENTATION OF AWARDS**
Venue: Goldsmiths' Hall, London
- Sunday 12 December **NATURE'S TREASURES III: MINERALS AND GEMS**
A seminar organized jointly by Gem-A, The Mineralogical Society, The Russell Society and Rockwatch
Venue: Flett Theatre, Natural History Museum, London

Contact details

Gem-A Headquarters:	Arianna Maccaferri on 020 7404 3334 email arianna.maccaferri@gem-a.com
Midlands Branch:	Paul Phillips on 02476 758940 email phillips10@sky.com
North East Branch:	Mark Houghton on 01904 639761 email markhoughton1@hotmail.co.uk
North West Branch:	James Riley on 01565 734184 or 07931 744139 email jameshriley@btinternet.com
South East Branch:	Veronica Wetten on 020 8577 9074 email veronica@wetten.co.uk
South West Branch:	Richard Slater on 07810 097408 email RichardS@fellows.co.uk
Scottish Gemmological Association:	Email info@scotgem.co.uk; website www.scotgem.co.uk

For up-to-the minute information on Gem-A Events visit our website at www.gem-a.com



Gem-A

THE GEMMOLOGICAL ASSOCIATION
OF GREAT BRITAIN

Supercharge your career



New Open Distance Learning Courses in Gemmology enrolling now

A strong knowledge of gemstones and diamonds will increase customer confidence and boost your sales. Gain that knowledge by studying with the world's longest established educator in gemmology. Graduates may apply for Fellowship of the Association enabling them to use the initials FGA after their name.

Study gemmology from your own home or workplace with comprehensive course notes, and online coursework and study groups*. You will also receive a selection of instruments and stones to help you with your studies. Additional instruments and books can be purchased from Gem-A's extensive range.

* Access to a computer with an internet connection essential.

Foundation Certificate in Gemmology

Start date: 15 March 2010 (nine-month programme)

Course fees: £1500 (or £1800 to include the London practical workshop) payable in instalments

Diploma in Gemmology (open only to Foundation Certificate holders)

Start date: 15 March 2010 (nine-month programme)

Course fees: £1695 (or £2295 to include the London practical workshop) payable in instalments

Full details at www.gem-a.com/education.aspx or call 020 7404 3334

The Gemmological Association of Great Britain

27 Greville Street (Saffron Hill entrance), London EC1N 8TN

tel: 020 7404 3334 fax: 020 7404 8843 email: information@gem-a.com

UK Registered Charity No. 1109555

Contents

- 153** A signature for nephrite jade using its strontium isotopic composition: some Pacific Rim examples
C.J. Adams and R.J. Beck
- 163** Jaspilite — the gemstone of Ukraine
P. Baranov, S. Shevchenko, W. Heflik, L. Natkaniec-Nowak and M. Dumańska-Słowik
- 171** Ruby and sapphire from Marosely, Madagascar
L.E. Cartier
- 181** Identification of dyed jadeite using visible reflection spectra
Yan Liu, Taijin Lu, Manjun Wang, Hua Chen, Meidong Shen, Jie Ke and Beili Zhang
- 185** Jadeite jade from Myanmar: its texture and gemmological implications
Guanghai Shi, Xia Wang, Bingbing Chu and Wenyuan Cui
- 196** A description and history of one of the largest nacreous pearls in the world
J.C. Zwaan and H.A. Dommissie
- 203** Geographic typing of gem corundum: a test case from Australia
F.L. Sutherland and A. Abduriyim
- 211** Dickite: a gem material for carving from Thailand
S. Saminpanya, C. Dharmgrongartama and N. Susawee
- 226** Application of mineralogical methods to the investigation of some gem-quality corals
L. Natkaniec-Nowak, M. Dumańska-Słowik, J. Fijał and A. Krawczyk
- 235** Colour-change garnets from Madagascar: variation of chemical, spectroscopic and colorimetric properties
K. Schmetzer, H.-J. Bernhardt, G. Bosshart and T. Hainschwang
- 283** The characteristics of red andesine from the Himalaya Highland, Tibet
A. Abduriyim
- 300** Abstracts
- 310** Book Reviews
- 312** Proceedings of The Gemmological Association of Great Britain and Notices
- 328** Gem-A Events 2010

Cover Picture: A large nacreous pearl (estimated weight 2385 grains) surrounded by golden 'stamens' decorated with ruby, sapphire and emerald beads, and mounted on a pedestal of lapis lazuli. Photo © Amsterdam Pearl Society. (See A description and history of one of the largest nacreous pearls in the world, page 196.)

The Gemmological Association of Great Britain

27 Greville Street, London EC1N 8TN

T: +44 (0)20 7404 3334 **F:** +44 (0)20 7404 8843

E: information@gem-a.com **W:** www.gem-a.com

